THE JOURNAL OF PHYSICAL CHEMISTRY

VOLUME 67, NUMBER 5 MAY, 1963

NOTES

COMMUNICATION TO THE EDITOR

AUTHOR INDEX

THE JOURNAL OF
PHYSICAL CHEMISTRY

VOLUME 67, NUMBER 5 MAY 13, 1963

THE HYDROLYSIS OF β-DIETHYLAMINOETHYL ACETATE

BY J. A. ZASLOWSKY AND E. FISHER[1]

Olin Mathieson Chemical Corporation, New Haven, Connecticut, and Niagara University, Niagara Falls, New York

Received May 21, 1962

The hydrolysis of β-diethylaminoethyl acetate was investigated over the pH range of 5.5 to 8.4. The data indicate that the hydrolysis proceeds by the interaction of the acid salt of the amine with hydroxyl ion rather than the kinetically equivalent mechanism involving the amine with water. This is explained on the basis of the polarization of the carbonyl bond of the ester by the favorably located positive charge.

Introduction

The physiological activity of β-aminoethyl carboxylates has prompted this investigation of the kinetics of

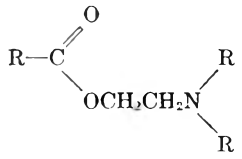

hydrolysis of a simple prototype at physiologically significant pH values.

Davis and Ross[2] compared the rates of hydrolysis of ethyl acetate, dimethylaminoethyl acetate, and acetylcholine in acidic and basic 80% aqueous acetone solutions at 50°. The marked increase in rate noted in basic solution for acetylcholine was attributed to the positive charge on the β-nitrogen atom. The formation of a sterically favorable activated complex was postulated.

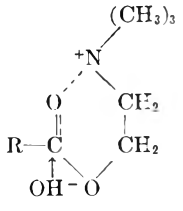

The increased rate of hydrolysis of dimethylaminoethyl acetate (relative to ethyl acetate) was attributed to activation of the carbonyl bond by the β-nitrogen atom electrons.

The present research deals with a study of the comparative kinetics of hydrolysis of β-diethylaminoethyl acetate, acetylcholine, and ethyl acetate over the pH range 5.5–8.4 at 50–65°.

Experimental

1. **Preparation of β-Diethylaminoethyl Acetate Hydrochloride (DEA·HCl).**—The material was prepared by the method of Gilman[3] from acetyl chloride and β-diethylaminoethanol in ether. A 5–10% excess of acetyl chloride was employed. The crude product was washed with ether, recrystallized from dry acetone, and dried *in vacuo*. The m.p. was 113–114°, literature 116–117°[3]; Cl^- analysis: 18.26%; theor.: 18.12%.

2. **Kinetic Studies with Diethylaminoethyl Acetate and its Hydrochloride Salt.**—The rates of hydrolysis were determined at constant pH with a Model K Beckman automatic titrimeter. The pH was effectively controlled to the nearest 0.05 pH unit. The temperature of the reaction was maintained to ±0.1° by means of a conventional thermoregulated water bath.

A weighed sample of DEA·HCl (0.3 mmole) was added to about 100 ml. of distilled water at the reaction temperature. The pH was rapidly adjusted with 0.05 *N* NaOH (from the titrimeter). The hydrolyses were conducted at pH 5.5, 7.5, 7.9, and 8.4 at 60° and at pH 8.0 at 50, 55, and 65°. The initial value for kinetic evaluation purposes was determined from the terminal base consumption. The data were treated on the basis of pseudo-first-order kinetics. First-order constants were determined by the method of least squares. There was no significant deviation over the entire range of reaction.

3. **Determination of the K_a of DEA·HCl.**—The partial titration curve was determined for weighed quantities of DEA·HCl (0.003 *M* solutions) at 50, 55, 60, and 65°. From the per cent titrated at each pH the K_a was calculated.

The values of K_a at the various temperatures permitted a calculation of the fraction of the total amine present as the free base and as the amine salt at the experimental pH values.[4]

T, °C.	pH	K_a	BH^+/B_0
50	8.0	5.2×10^{-9}	0.658
55	8.0	6.4×10^{-9}	.614
60	5.5	7.9×10^{-9}	.997
60	7.5		.799
60	7.9		.613
60	8.4		.334
65	8.0	9.9×10^{-9}	.502

BH^+ = acid salt. B_0 = total ester.

4. **Determination of Hydrolysis Rates of DEA·HCl in Deuterium Oxide.**—The same procedure was employed as in water.

(1) In partial fulfillment of the requirements for the Master of Science Degree at Niagara University, 1960. Presented at the 137th National Meeting of the American Chemical Society, Cleveland, Ohio, 1960.

(2) W. Davis and W. C. J. Ross, *J. Chem. Soc.*, 3056 (1950); 2706 (1951).

(3) H. Gilman, L. C. Heckert, and R. McCracken, *J. Am. Chem. Soc.*, **50**, 437 (1928).

(4) J. W. Churchill, M. Lapkin, F. Martinez, and J. A. Zaslowsky, *ibid.*, **80**, 1944 (1958).

The pH meter readings were however corrected by the method of Long as described by Bender[5]

$$pD = pH + 0.4$$

The calculated pseudo-first-order reaction rate constants at 60° and pD 8.4 were 1.57×10^{-3} sec.$^{-1}$ and 1.66×10^{-3} sec.$^{-1}$ in duplicate experiments.

The K_a (at 60°) of DEA·HCl in D_2O was determined using the relationship between pD and the measured pH.

$$K_a(D_2O) = 4.09 \times 10^{-9}$$

5. The Hydrolysis of Acetylcholine Chloride.—Acetylcholine chloride (Matheson, Coleman and Bell) was recrystallized from acetone. The dry hygroscopic salt had a melting point of 150–151° in agreement with Jones and Major.[6]

The hydrolyses were conducted in a manner similar to that described for DEA·HCl. The kinetic data, at 60°, are summarized

pH	k_1, sec.$^{-1}$ (pseudo-first-order)	k_2, l. mole sec.$^{-1}$
6.0	2.53×10^{-6}	26.4
6.9	2.13×10^{-5}	28.0
6.9	2.24×10^{-5}	29.4
7.8	1.77×10^{-4}	29.2
	Av. k_2:	28.2

6. The Hydrolysis of Ethyl Acetate.—The reaction was studied at 60° employing the same general technique which has been described, provision being made to operate in a closed system to prevent evaporation losses.

The data are summarized

pH	k_1, sec.$^{-1}$	k_2, l. mole sec.$^{-1}$
6.0	$1.0 \pm 0.08 \times 10^{-7}$	1.04
7.0	$1.1 \pm 0.1 \times 10^{-6}$	1.18
	Av. k_2:	1.1

7. The Determination of the Presence (or Absence) of the Ethyleneimmonium Ion during the Hydrolysis of DEA.—The rapid reaction of ethyleneimmonium ion with sodium thiosulfate suggested that the presence of thiosulfate ion in the hydrolysis solution of DEA would monitor (at least qualitatively) the formation of the cyclic ion. A known excess of sodium thiosulfate was added to a hydrolysis solution at pH 8. After approximately 60% reaction, an aliquot of the solution was titrated with standard iodine for thiosulfate assay. There was no consumption of thiosulfate during the hydrolysis.

Discussion

Although the rate of hydrolysis over the entire pH range can be expressed by the summation

$k_1(B) + k_2(BH^+) + k_3(B)(H^+) + k_4(B)(OH^-) + k_5(BH^+)(OH^-) + k_6(BH^+)(H^+)$ (where B is the concentration of the free base of the ester and BH^+ is the acid salt)

the relationships

$$f = B/B_0$$

$$f^1 = BH^+/B_0$$

permit all the terms to be converted to linear functions of B_0 (total ester concentration). The following equation results after rearrangement of the terms

$$V = (k_1 f + k_2 f^1 + k_3 f(H^+) + k_4 f(OH^-) + k_5 f^1(OH^-) + k_6 f^1(H^+))B_0$$

First-order constants were calculated at four different pH values (5.5–8.4) at 60°. The data are presented in Table I. Assuming the important kinetic term to be $k_1(B)$, the autohydrolysis of the free base, the pseudo first-order constant could be converted to a true first-order constant by dividing the experimental value by the fraction of free amine present at each pH value (f). The results are given in columns 3 and 4 of Table I.

TABLE I

HYDROLYSIS OF DEA·HCl (60°)

pH	k exp. (pseudo-first-order constant), sec.$^{-1}$	f	k_1, sec.$^{-1}$
8.4	4.11×10^{-3}	0.666	6.17×10^{-3}
8.4	4.25×10^{-3}	.666	6.39×10^{-3}
8.4	4.24×10^{-3}	.666	6.39×10^{-3}
7.9	2.27×10^{-3}	.387	5.87×10^{-3}
7.9	2.15×10^{-3}	.387	5.55×10^{-3}
7.9	2.09×10^{-3}	.387	5.40×10^{-3}
7.5	1.18×10^{-3}	.201	5.89×10^{-3}
7.5	1.24×10^{-3}	.201	6.17×10^{-3}
5.5	1.64×10^{-5}	.0025	6.54×10^{-3}
		Av.:	6.04×10^{-3}
		Least squares value:	6.23×10^{-3}

The constancy of the results over the 1000-fold range of hydrogen ion concentration suggest that the assumption was valid. A statistical treatment confirmed the fact that within the precision of the experiments the equation

$$k \text{ exp.} = fk_1$$

represents the data to high degree of confidence (>95%).

The equilibrium

$$B + H_2O \rightleftarrows BH^+ + OH^-$$

$$K_b = \frac{(BH^+)(OH^-)}{(B)} = \frac{K_w}{K_a}$$

permits an alternate kinetically equivalent interpretation

$$k_1(B) = \frac{k_1(BH^+)(OH^-)}{K_b} = k_5(BH^+)(OH^-)$$

The value of k_5 was calculated directly from k_1 assuming the latter to be the significant contributor. K_w at 60° was taken as 9.6×10^{-14}.[7] The least square value of k_5 (at 60°) was 516 l. mole^{-1} sec.$^{-1}$. This value has the same statistical significance as the first-order constant k_1 previously developed. The following alternate kinetic terms were determined at each temperature

T, °C.	k_1, sec.$^{-1}$	k_5, l. mole^{-1} sec.$^{-1}$
50	2.71×10^{-3}	259
55	4.80×10^{-3}	413
60	6.23×10^{-3}	516
65	9.17×10^{-3}	715
60 (D_2O)	3.18×10^{-3}	785

The data fit the equation: $k_5 = 1.73 \times 10^{10} e^{\frac{-15,480}{RT}}$ l. mole^{-1} sec.$^{-1}$ (for water).

The value of $K_w(D_2O)$ necessary for the determination of $k_5(D_2O)$ was obtained from the data of Abel and co-workers[8] and the variation of $K_w(D_2O)$ with

(5) M. L. Bender, E. J. Pollock, and M. C. Neveu, *J. Am. Chem. Soc.*, **84**, 595 (1962).

(6) L. W. Jones and R. T. Major, *ibid.*, **69**, 200 (1947).

(7) H. S. Harned and R. A. Robinson, *Trans. Faraday Soc.*, **36**, 973 (1940).

(8) E. Abel, E. Brateau, and O. Redlich, *Z. physik. Chem.*, **173**, 353 (1935).

temperature reported by Wynne-Jones.[9] $K_w(D_2O)$ at 60° is 1.7×10^{-14}; $K_w(D_2O)$ at 25° is 1.6×10^{-15}.

The ratio $k_1(D_2O)/k_1(H_2O)$ is 0.51; the ratio $k_5(D_2O)/k_5(H_2O)$ is 1.52. The data of Laughton[10a] and Reitz[10b] for a series of solvolysis reactions indicated a ratio of slightly less than unity for $k(D_2O)/k(H_2O)$. The value for k_5 was in accord with the work of Long and co-workers[11] and Wiberg[12] on the expected isotope effect for OH^- catalyzed reactions, *e.g.*, ethyl acetate, 1.33; methyl acetate, 1.60. Since recent work[13] has shed considerable doubt as to the utility of the deuterium isotope criterion for unequivocal mechanism assignment, no attempt will be made to utilize this criterion for distinguishing the two possible mechanisms.

A cyclic mechanism can participate in hydrolysis reactions of β-aminoethyl esters.[2,14,15] The question to be resolved is then that of deciding which of the following is the probable reaction path

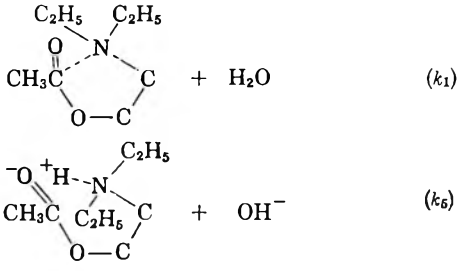

The latter alternative (k_5) is chosen on the basis of the work of Davis and Ross[2] and this research. The former have shown that acetylcholine hydrolyzes in basic solution about 150 times faster than ethyl acetate and 32 times faster than dimethylaminoethyl acetate at the same concentrations. In the present research at relatively neutral pH values the second-order reaction rate constants were

DEA·HCl	516 l. mole^{-1} sec.$^{-1}$
acetylcholine	28.2 l. mole^{-1} sec.$^{-1}$ (ref. 2 at 50° in 80% aq. acetone is 27)
ethyl acetate	1.1 l. mole^{-1} sec.$^{-1}$

If the plausible assumption that DEA and dimethylaminoethyl acetate are similar substrates is accepted than the order of reactivity of Davis and Ross[2] must be reversed and the hydrochloride of the amine is found to be about 20 times as reactive to (OH^-) catalyzed hydrolysis as acetylcholine. These data indicate that a positive charge on the nitrogen atom has a markedly accelerating effect on the hydrolysis of β-amino esters; it is reasonable to expect the effect to be more marked when the positive charge is carried by a labile proton rather than by a quaternary nitrogen atom. It appears that the electrically neutral β-nitrogen atom is not a particularly effective activating group.

It should be noted that at complete hydrolysis of DEA the theoretical quantity of acid was not liberated. Although this did not interfere with the kinetic interpretation, it was of interest to correlate this "missing" acid with the base strength of the formed alcohol (diethylaminoethanol).

For example at pH 8.4, 33.4% of the original ester was present as the acid salt; only 54% of the theoretical quantity of acid was liberated at the conclusion of the reaction. These data indicate that 46% of the formed acid was bound as the acid salt of the alcohol. The calculated K_a, at 60° of diethylaminoethanol is 1.0×10^{-9} (K_a of DEA is 7.9×10^{-9}). This value was reproducible at different pH values. At pH 5.5 the theoretical quantity of acid was not liberated for a different reason. Although essentially all the amine remained bound as the acid salt only 83% of the acid was neutralized at this pH.

To avoid possible interference of a significant salt effect in the interpretation of the kinetics the solutions were maintained as dilute as believed practical. Since the reaction solutions were prepared from 0.003 *M* solutions of DEA·HCl, the ionic strength of the initial solutions were all about 3×10^{-3}. At the termination of the reaction the ionic strengths had increased to 6×10^{-3}. The primary salt effect involves the expression (for a critical complex involving a positive and a negative ion)

$$\log \frac{k}{k_0} = -2Az^+z^-\sqrt{u}$$

where A is the Debye–Hückel constant (0.54 at 60° in water), z^+ and z^- are the valences of the ions participating in the rate-determining step, and k_0 is the rate constant for the infinitely dilute solution. This equation permits a calculation to be made of the expected change in rate constant as the reaction progresses. The initial rate constant was $0.872k_0$, the final was $0.825k_0$. This small gradual change was not detectable in the present experiments.

Conclusion

The labile hydrolysis of β-aminoesters at physiologically significant pH values is probably caused by the interaction of a β-nitrogen atom carrying a positive charge with the carbonyl oxygen of the ester. The activated carbonyl linkage is rendered particularly susceptible to hydroxyl ion attack.

(9) W. F. K. Wynne-Jones, *Trans. Faraday Soc.*, **32**, 1397 (1936).

(10) (a) P. M. Laughton and R. E. Robertson, *Can. J. Chem.*, **34**, 1714 (1956); (b) O. Reitz, "Handbuch der Katalyse," Vol. II, Vienna, Austria, Julius Springer, 1940, p. 273.

(11) J. G. Pritchard and F. A. Long, *J. Am. Chem. Soc.*, **78**, 6008 (1956); P. Ballinger and F. A. Long, *ibid.*, **81**, 2347 (1959).

(12) K. Wiberg, *Chem. Rev.*, **55**, 713 (1955).

(13) M. L. Bender, E. J. Pollock, and M. C. Neveu, *J. Am. Chem. Soc.*, **84**, 595 (1962).

(14) G. F. Holland, R. C. Durant, S. L. Fries, and B. Witkop, *ibid.*, **80**, 6031 (1958).

(15) E. R. Garrett, *ibid.*, **80**, 4049 (1958).

THE DEUTERIUM ISOTOPE EFFECT IN THE HYDROGEN BONDING OF IMIDAZOLE IN NAPHTHALENE SOLUTIONS

BY ALEC GRIMISON

Chemistry Department, University of Puerto Rico, Río Piedras, P. R.

Received June 15, 1962

A study has been made of the self-association of imidazole and 1-*d*-imidazole in naphthalene solution at 80°. Under these conditions imidazole forms linear oligomers through N–H–N hydrogen bonding. The deuterium compound is found to be less associated, by about 8%, than the hydrogen analog. This difference is analyzed in terms of the equilibrium constants and free-energy changes for the various association equilibria. For, *e.g.*, dimerization the results give a ΔF^0 of −1100 cal./mole for imidazole, and a ΔF^0 of −1020 cal./mole for 1-*d*-imidazole. This implies weaker hydrogen bonding by deuterium.

Introduction

The question of the relative strengths of the hydrogen and deuterium bonds is one which has been discussed recently in several papers,[1-10] without any general conclusion being reached. This problem is of interest in fields varying from purely chemical kinetic and mechanistic studies, where deuterium substitution in solute or solvent is often used to aid interpretation, to biological studies of the inhibition of mitosis by deuterium oxide.[5-10] Some of the most important recent evidence of quantitative significance is that of Potter, Bender, and Ritter,[2] Dahlgren and Long,[3] and Plourde.[4] These data will be discussed later.

The technique used by Potter, Bender, and Ritter was to study, by means of vapor density measurements, the relative extent of dimerization of acetic acid and deuterated acetic acid (actually acetic-d_3 acid-*d*). The major difficulty lies in the small magnitude of the effect for the systems studied, often of the same order as the experimental error. It was felt that a more effective approach to the problem was through the study of the relative self-association of a highly associated system, forming oligomers through hydrogen bonding. It was preferable for the mathematical analysis of results that the model system should show a linear increase of association with increasing concentration, indicating that linear, rather than cyclic, polymers are being formed. Further, the protons other than those involved in hydrogen bonding should be resistant to exchange by deuterium, or internal deuterium exchange may necessitate the study of a completely deuterated compound, as in the work of Potter, Bender, and Ritter.[2] According to the work of Halevi,[11] this introduces the possibility of changes in the acid or base strength of the compound (and thus in the strength of the hydrogen bonding), although the existence of this effect has been disputed.

A system satisfying these requirements was imidazole and 1-*d*-imidazole, as it is known that imidazole is highly associated through N–H–N bonds in solvents which do not compete effectively for hydrogen bonding,[12] and a careful spectroscopic study of the association of imidazole in carbon tetrachloride[13] has recently proved that linear oligomers are formed, as would be indicated on steric grounds, and as previous cryoscopic work in naphthalene[14] has suggested. Also, it is known that while deuterium exchange of the 1-position is extremely rapid, as expected for an N–H proton, the exchange rates of the remaining C–H protons are very slow, particularly in neutral solution.[15] The possibility of internal exchange can therefore be ignored. The association of imidazole and 1-*d*-imidazole was therefore studied in naphthalene solution by a cryoscopic method, which satisfies the dual requirements of simplicity and accuracy, in the concentration range used.

Experimental

Molecular weights were measured by an adaptation of the Beckmann f. pt. depression technique, but with certain alterations, specifically designed to exclude moisture. Stirring was found to be best accomplished manually, the spiral glass stirrer being raised and lowered by a nichrome wire passing through a closely fitting polythene seal. A Beckman f. pt. thermometer was used, passing through a rubber bung, and capable of being read to 0.002°. The freezing point cell was surrounded by an air jacket, this being immersed in an oil bath, which was thermostated to within 0.05° by a Sunvic unit and intermittent heater. The use of a large (1.5 kw.) main heater through a rheostat allowed rapid changes in the thermostating temperature of the bath.

The stoppered freezing point cell, containing a weighed amount of naphthalene, was quickly heated to about 10° above the melting point of naphthalene by a small auxiliary oil bath, then the thermometer and stirrer assembly replaced, and the whole placed in the air jacket in the bath, which was thermostated at about 1.5° below the freezing point of naphthalene. The naphthalene was allowed to cool while stirring gently, until a supercooling of about 0.02° had occurred, when slightly more vigorous stirring produced crystallization, and the highest steady temperature reached under stirring was recorded as the freezing point. No supercooling difficulties or correction proved necessary as is found for certain other solvents, particularly sulfuric acid. Subsequent measurements could be effected simply by warming up the cell in the auxiliary oil bath, then replacing in the air jacket in the thermostated bath, and were generally reproducible to ±0.002°. This procedure is much more rapid and rigorous than the alternative of raising the cell temperature by means of the main bath, then re-equilibrating the bath and cell at the correct thermostating temperature. Solid samples were introduced through a stoppered glass tube passing into the cell, by means of a specially designed weight bottle and glass tube.

(1) J. H. Wang, *J. Am. Chem. Soc.*, **73**, 510 (1951).
(2) A. E. Potter, Jr., P. Bender, and H. L. Ritter, *J. Phys. Chem.*, **59**, 250 (1955).
(3) G. Dahlgren, Jr., and F. A. Long, *J. Am. Chem. Soc.*, **82**, 1303 (1960).
(4) G. R. Plourde, *Dissertation Abstr.*, **22**, 1400 (1961).
(5) J. Hermans, Jr., and H. A. Scheraga, *Biochim. Biophys. Acta*, **36**, 534 (1959); see also M. Calvin, J. Hermans, Jr., and H. A. Scheraga, *J. Am. Chem. Soc.*, **81**, 5048 (1959).
(6) A. M. Hughes, B. M. Tolbert, K. Lonberg-Holm, and M. Calvin, *Biochim. Biophys. Acta*, **28**, 58 (1958).
(7) V. Moses, O. Holm-Hansen, and M. Calvin, *ibid.*, **28**, 62 (1958).
(8) A. M. Hughes and M. Calvin, *Science*, **127**, 1445 (1958).
(9) A. M. Hughes, E. L. Bennett, and M. Calvin, *Proc. Natl. Acad. Sci.*, **45**, 581 (1959).
(10) See, *e.g.*, P. R. Gross and W. Spindel, *Ann. N. Y. Acad. Sci.*, **90**, Second Conference on the Mechanisms of Cell Division (1960), p. 500.
(11) E. A. Halevi, *Tetrahedron*, **1**, 174 (1957).
(12) K. Hofmann, "Imidazole and its Derivatives," Pt. I, Interscience Publishers, New York, N. Y., 1953, p. 24.
(13) D. M. W. Anderson, J. L. Duncan, and F. J. C. Rossotti, *J. Chem. Soc.*, 2165 (1961).
(14) L. Hunter and J. A. Marriott, *ibid.*, 777 (1941).
(15) R. J. Gillespie, A. Grimison, J. H. Ridd, and R. F. M. White, *ibid.*, 3228 (1958); A. Grimison, Ph.D. Thesis, London, 1958.

Materials.—Deuterium oxide was >99.8%, obtained from Bio-Rad Labs.

B. D. H. cryoscopic naphthalene was dried by resubliming twice over phosphorus pentoxide *in vacuo* at 60° and was stored over P_2O_5 in a vacuum desiccator. The freezing point of the pure naphthalene provided a purity check, being usually constant to within ±0.005°. Samples varying more than 0.01° from the mean were discarded, or resublimed.

Imidazole was purified by a preliminary recrystallization from benzene, followed by vacuum sublimation at *ca.* 60°.

1-*d*-Imidazole was prepared by equilibrating 2 g. of imidazole with two 15-ml. portions of 99.8% D_2O, removing the solvent by means of a vacuum oil pump at room temperature each time, then subliming the product to purify, without transfer from the original vessel. This technique and associated apparatus has previously been described.[15]

Analysis of the Data.—The data from experimental cryoscopic measurements consists initially of a series of values for the apparent molecular weight of the solute at different solute concentrations. This is customarily expressed in terms of an association factor given by $f = Q/N$, where Q = stoichiometric concentration of single molecules, *i.e.*, in terms of formula weights, and N = apparent concentration from measurement of any colligative property, both expressed in the same units. The first step of an analysis of the data is a calculation of the equilibrium constants, K_L for the self-association reactions $LA \rightleftharpoons A_L$, where A = monomer, A_L = polymer of order L, and $K_L = A_L/A_L$. Also of interest may be the equilibrium constant K_L' for the addition of a monomer unit to a polymer of order L; *i.e.*, the association reaction $A_L + A \rightleftharpoons A_{L+1}$, given by $K_L' = K_{L+1}/K_L$. From these equilibrium constants the free-energy changes for the above reactions can be calculated. The basic assumption necessary for a calculation of the equilibrium constants is that all deviations from ideality are due to the presence of associated molecules. This is certainly not strictly correct at the concentrations normally used in cryoscopic work, and precautions need to be taken when making precise calculations.[16] However, the deviations will be of no significance in a relative study on two closely similar molecules as reported here, *i.e.*, it is assumed that the solute–solvent interactions are not significantly changed by the substitution of deuterium for hydrogen in this system. It is appropriate to mention here that no assumptions are made that some very weak hydrogen bonds are not formed with the solvent naphthalene, but only that these interactions are so weak in comparison with the predominant solute–solute hydrogen bonding that any changes in this solute–solvent bonding by substitution of deuterium for hydrogen must be negligible.

As demonstrated in the work of Martin and Kilpatrick,[16] the first essential step is the establishment of a relationship between f and N or Q. Three somewhat different methods of calculating the equilibrium constants are those of Lassettre,[17,18] Dunken,[19,20] and Bjerrum and Fronaeus.[21,22] See also Rossotti and Rossotti.[23] The method of Lassettre, although less generally applicable than the others, is accurate and convenient for suitable systems, and has been shown to give good results for compounds with a similar type of association behavior to imidazole,[16] it was therefore used exclusively.

Lassettre considered a general equation for association behavior

$$f = 1 + \alpha Q + \beta N$$

where α and β are constants. It is obvious that in the limit $\beta = 0$ the equation describes a compound in which f is a linear function of Q. It can be seen from Fig. 1 that this is true for imidazole, so that α is easily determined from the slope of the straight line plot. Lassettre goes on to prove that the equilibrium constants K_L are given by $K_L = (\alpha L)^{L-1}/L!$, and the equilibrium constants K_L' by $K_L' = \alpha(L+1)^{L-1}/L$ for the limiting case with $\beta = 0$.

Equilibrium constants K_L and K_L' were therefore determined from the slope of a plot of f against Q as above. The free energy changes involved in the more physically meaningful reaction $A + A_L \rightleftharpoons A_{L+1}$, $\Delta F_L^{0'}$, for both normal and 1-*d*-imidazole were calculated from the relation $\Delta F_L^{0'} = -RT \ln \alpha - RT (L-1) \ln (L+1)/L$.

Results and Discussion

The results for the association of imidazole are shown in Table I and plotted in Fig. 1. The slope of the graph agrees very well with the results of Hunter and Marriott[14] (1.5% diff.), although their graph was displaced slightly to the right, and in fact failed to extrapolate to the point $f = 1$, $Q = 0$. This might be due to the neglect of drying the naphthalene used, resulting in some competition for hydrogen bonding by water.

TABLE I

ASSOCIATION OF IMIDAZOLE[a]

Run no.	Concn. (m)	ΔT_f, °C.	Assn. factor
H. 2	0.0612	0.337	1.25
H. 2	.1174	.531	1.53
H. 1	.1300	.567	1.58
H. 2	.1625	.645	1.74
H. 3	.3705	.915	2.79
H. 4	.3960	.940	2.91
H. 3	.4781	1.014	3.25
H. 5	.6117	1.095	3.86

[a] K_f for naphthalene = 6.90 throughout.

In Table II is shown the association behavior of 1-*d*-imidazole, and these results are also plotted in Fig. 1. Qualitatively, it is immediately obvious that the deuterium compound is less associated at all concentrations than the hydrogen compound; and the benefit of working with a higher extent of association is immediately seen by the spread of the two plots at higher concentrations. It is worth noting that it is in this very region that the precision of molecular weight measurement is greatest, since the observed depressions are large.

TABLE II

ASSOCIATION OF 1-*d*-IMIDAZOLE

Run no.	Concn. (m)	ΔT_f, °C.	Assn. factor
D. 8	0.0347	0.224	1.07
D. 9	.1177	.550	1.48
D. 2	.1481	.618	1.65
D. 8	.1486	.622	1.65
D. 9	.2545	.862	2.04
D. 8	.2827	.859	2.27
D. 8	.4246	1.032	2.84
D. 8	.5459	1.125	3.35
D. 6	.6331	1.167	3.74
D. 1	.6767	1.178	3.96
D. 4	.7417	1.218	4.20
D. 5	.7450	1.227	4.19

TABLE III

	α	K_2	K_3	K_4	K_5
H CMPD	4.79	4.79	34.4	293.0	2741
Other workers	4.86				
D CMPD	4.29	4.29	27.6	210.0	1758

The results, then, indicate that the deuterium bond is weaker than the hydrogen bond, by 80 cal./mole in 1000 for the free energy of self-association, or roughly 8%. This is in agreement both in direction and magnitude with results obtained by Grimison and Long from a study of the effects of deuterium substitution on some keto–enol equilibria involving internally hydro-

(16) N. E. White and M. Kilpatrick, *J. Phys. Chem.*, **59**, 1044 (1955).
(17) E. N. Lassettre, *Chem. Rev.*, **20**, 259 (1937).
(18) E. N. Lassettre, *J. Am. Chem. Soc.*, **59**, 1383 (1937).
(19) H. Dunken, *Z. physik. Chem.*, **45B**, 201 (1940).
(20) K. L. Wolf, H. Dunken, and K. Merkel, *ibid.*, **46B**, 287 (1940).
(21) J. Bjerrum, *Kem. Maanedsblad*, **24**, 121 (1943).
(22) S. Fronaeus, Dissertation, "Komplexsystem hos Koppar," Lund, 1948.
(23) F. J. C. Rossotti and N. Rossotti, *J. Phys. Chem.*, **85**, 1376 (1961).

TABLE IV

						Kcal. (mole)				
	α	K'_1	K'_2	K'_3	K'_4	$-\Delta F'_1{}^0$	$-\Delta F'_2{}^0$	$-\Delta F'_3{}^0$	$-\Delta F'_4{}^0$	$\Delta\Delta F'^0$, cal./mole
H CMPD	4.79	4.79	7.18	8.51	9.35	1.10	1.39	1.50	1.57	78 ± 1 cal.
D CMPD	4.29	4.29	6.43	7.62	8.37	1.02	1.31	1.43	1.49	

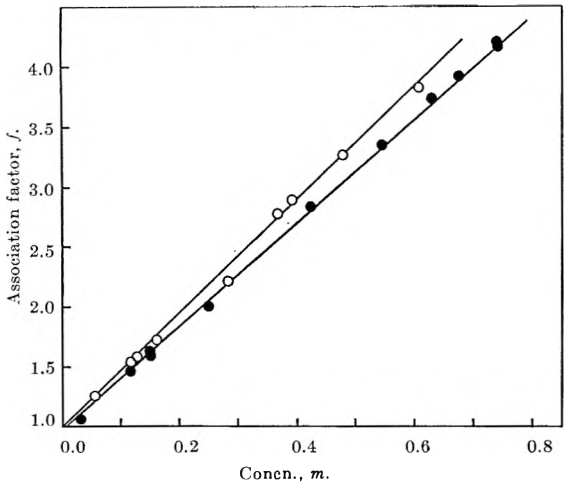

Fig. 1.—Association behavior of imidazole (O) and 1-^{2}H-imidazole (●).

gen bonded enols.[24] The results also agree well with the recent findings of Plourde[4] on the dimerization of phenol-*h* and phenol-*d*, although the effect was reversed for the very weak association of phenol-*h* and phenol-*d* with added compounds.

The conclusion of Potter, Bender, and Ritter[2] from their work on acetic acid was a difference of 300 cal. in 1400 cal. in the enthalpy of dimerization, with the deuterium bond stronger than the hydrogen bond. However, a survey of the measurements on acetic acid and other carboxylic acids,[25] indicates that observed differences are usually within the experimental error for carboxylic acid systems, and formic acid shows a lower extent of dimerization for the deuterium compound, *i.e.*, an effect in the opposite direction to that of Potter, Bender, and Ritter. Most of these results stem from work in the gas phase. Pimentel and McClellan[25] have concluded from these results that $-\Delta H^0$ is essentially constant, regardless of deuterium substitution in the cases studied, and that the data do not support the postulate of a stronger deuterium bond.

The work of Dahlgren and Long on the ionization constants of maleic and fumaric acids and their monoethyl esters in H_2O and D_2O[3] showed that there was less H bonding of the deuteriobimaleate ion in deuterium oxide than the corresponding hydrogen analog. As was pointed out, there is a considerable body of evidence[26-28] to suggest a smaller amount of H bonding for deuterium in deuterium oxide than for hydrogen in water, although this permits of two interpretations. One is that in fact the relative hydrogen bonding of deuterium would be weaker for the isolated molecules, but the other is that the H bonding of the solvent H_2O is greater than that for D_2O.

The implication of the present work is that the relative hydrogen bonding of deuterium is weaker for molecules associating in a non-H bonding solvent, although the second effect may also be important in aqueous solutions. Plourde's work suggests that the entropy effect can be significant, at least for very weak hydrogen bonds, and it is planned to ascertain if this effect is at all appreciable for the association of imidazole.

Acknowledgment.—This work was carried out at the Chemistry Department, University College of the West Indies, Kingston, Jamaica, W. I. The author wishes to thank Mr. G. O. Henry for carrying out some of the determinations reproduced in Table I.

(24) A. Grimison and F. A. Long, unpublished work.

(25) "The Hydrogen Bond," G. C. Pimentel and A. L. McClellan, W. H. Freemann and Co., 1960, p. 210.

(26) S. Korman and V. K. Lamer, *J. Am. Chem. Soc.*, **58**, 1396 (1936).

(27) F. C. Nachod, *Z. physik. Chem.*, **182A**, 193 (1938).

(28) F. A. Long and D. Watson, *J. Chem. Soc.*, 2019 (1958).

OXYGEN EXCHANGE BETWEEN CHROMATE AND WATER[1]

BY MICHAEL R. BALOGA AND JOSEPH E. EARLEY

Chemistry Department, Georgetown University, Washington, D. C.

Received June 21, 1962

The rate of oxygen exchange between chromate and water in moderately alkaline solution is first order in $[CrO_4^{-2}]$ and independent of pH. The first-order rate constant at 25° in *M* $LiClO_4$ is $(6.9 \pm 0.1) \times 10^{-4}$ min.$^{-1}$. Below pH 9.7 the rate is dependent on pH. At pH 7.2 the rate is second order in [Cr(VI)], indicating a mechanism involving $Cr_2O_7^{-2}$.

Several investigators[2] have observed that oxygen exchange between chromate(VI) ions and solvent water is subject to acid catalysis. Mechanisms involving formation of dichromate have been suggested. Mills[3] has rejected these mechanisms in favor of a monomolecular dehydration similar to that suggested for some other oxyions.[4] No data are available as to the effect of Cr(VI) concentration on the rate of oxygen exchange of chromates. The aim of this study was to obtain such data as a test of the proposed mechanism.

Experimental

Reagents were prepared and purified by standards methods. CO_2-free solutions were employed. Solid enriched Li_2CrO_4 (2.68 atom % O^{18}) was dissolved in normal water containing sufficient $HClO_4$ or LiOH to give the desired pH and having a

(1) Taken from part II of the thesis to be submitted by Michael R. Baloga to the Graduate School of Georgetown University in partial fulfillment of the requirements for the Ph.D. degree, 1963.

(2) (a) E. R. S. Winter, M. Carlton, and H. V. A. Briscoe, *J. Chem. Soc.*, 131 (1940); (b) N. F. Hall and O. R. Alexander, *J. Am. Chem. Soc.*, **62**, 3455 (1940); (c) A. I. Brodskii and E. I. Dontsova, *Dapovidi Akad. Nauk, URSS*, 3 (1940); *Chem. Abstr.*, **37**, 4957 (1943).

(3) G. A. Mills, *J. Am. Chem. Soc.*, **62**, 2833 (1940).

(4) G. A. Mills and H. C. Urey, *ibid.*, **62**, 1019 (1940).

concentration of $LiClO_4$ calculated to bring the total, nominal ionic strength to 1 M. The pH of the solution was measured and, if necessary, readjusted after Li_2CrO_4 was dissolved. Reaction mixtures were thermostated at 25.0 ± 0.1°. Aliquots were quenched with $Ba(ClO_4)_2$ solution.[5] The resulting mixture was centrifuged and the precipitate was washed with water and vacuum dried. A Bendix time-of-flight mass spectrometer was used to determine the isotopic composition of O_2 obtained by heating $BaCrO_4$ at 500° for 2 hr.

Rates, R, were evaluated using eq. 1

$$\log \frac{C_\infty' - C'}{C_\infty' - C_0'} = \log F = \frac{R(W + C)}{2.3WC}\, t \quad (1)$$

where C is the total concentration of oxygen in Cr(VI) and C' is the concentration O^{18} in Cr(VI). W is the total concentration of oxygen in water. C_0' was checked by analysis of O_2 obtained by decomposing Li_2CrO_4 at 1000°. C_∞' was obtained after ten half-times. Both C_0' and C_∞' agreed well with expected values. Rates are reproducible to 3%.

Results

Table I shows rates of oxygen exchange between CrO_4^{-2} and solvent water measured under various concentration conditions at 25.0°. Above pH 9.7 the rate is independent of pH and first order in total Cr(VI) concentration (thereafter [Cr(VI)]). This is indicated by the constant values of k (ratio of rate to [Cr(VI)]) found in experiments one to four. Experiments four to six show the expected acid catalysis below pH 9.7.

TABLE I

RATE OF OXYGEN EXCHANGE BETWEEN CrO_4^{-2} AND H_2O AT 25.0° ($LiClO_4$)

Expt.	pH	[Cr(VI)] × 10, M	[$LiClO_4$] × 10, M	$t_{1/2}$, min.	Rate × 10^4, M min.$^{-1}$	$k \times 10^4$, min.$^{-1}$[a]	$k_2 \times 10$, M^{-1} min.$^{-1}$[b]
1	12.03	1.26	6.12	4080	0.849	6.79[c]	
2	10.90	1.64	5.05	4040	1.12	6.82[c]	
3	10.90	1.57	5.26	3900	1.12	7.06[c]	
4	9.71	3.31		3850	2.34	7.04[c]	
5	8.22	0.467	8.60	1600	0.808	(17.3)	
6	7.20	.140	9.58	538	0.539	(38.5)	2.7
7	7.20	.195	9.42	481	1.12		2.7
8	7.20	.240	9.28	405	1.64		2.8
9	7.20	.274	9.18	318	2.39		3.2
10	7.20	.746	7.76	125	16.5		3.0
11	7.20	1.46	5.62	34	118		(5.5)
12	7.20	1.83	4.45	26	193		(5.7)
13	7.20	1.92	4.24	19	275		(7.4)

[a] Rate/[Cr(VI)]. [b] Rate/[Cr(VI)]^2. [c] Average (6.9 ± 0.1) × 10^{-4} min.$^{-1}$.

(5) More easily handled precipitates were obtained when less than equivalent quantities of $Ba(ClO_4)_2$ were used.

King and Tong have studied[6] the formation of $Cr_2O_7^{-2}$ from $HCrO_4^-$ in M $LiClO_4$. The acidity constant of $HCrO_4^-$ in this medium was not determined. Studies in more dilute[7] and more concentrated[8] media indicate that pK_a is about 5.9. This indicates that at pH 7.2 most (>90%) of the Cr(VI) is present as CrO_4^{-2} rather than as $HCrO_4^-$ or $Cr_2O_7^{-2}$. Therefore, the equilibrium concentration of $Cr_2O_7^{-2}$ is approximately proportional to [Cr(VI)]^2.

Experiments six to ten show that the rate of oxygen exchange is proportional to [Cr(VI)]^2 at low [Cr(VI)]. This indicates the presence of a term in $Cr_2O_7^{-2}$ in the rate law. The results of experiments eleven to thirteen might be thought to indicate a higher order term in Cr(VI). It is more probable that these results reflect variations in total ionic strength among these experiments.

The rate law for oxygen exchange involves several terms.

$$\text{Rate} = k[CrO_4^{-2}] + k_D[Cr_2O_7^{-2}] + \ldots$$

In order to compute a meaningful value for k_D or assess the importance of terms in $HCrO_4^-$,[9] it is necessary to have exchange and equilibrium data measured in the same medium.

The observed second order constant k_2 (Table I) could be related to k_D if these data were available. The rate constant for $Cr_2O_7^{-2}$ hydrolyses measured by Lipshitz and Perlmutter-Hayman,[10] using flow techniques, should be comparable to k_D. Several hazardous approximations are involved in the comparison of their results with our measured k_2, but the sets of data do not seem to be incompatible.

The experiments in basic solution show that exchange occurs without polymerization: the experiments at pH 7.2 indicate that exchange occurs in neutral solution by a mechanism involving $Cr_2O_7^{-2}$.

Acknowledgment.—This work was supported by the United States Atomic Energy Commission.

(6) E. L. King and Y. P. Tong, *J. Am. Chem. Soc.*, **75**, 6180 (1953).

(7) J. D. Nuess and W. Rieman, *ibid.*, **56**, 2238 (1934).

(8) Y. Sasaki, *Acta Chem. Scand.*, **16**, 719 (1962).

(9) Professor H. W. Baldwin (University of Western Ontario) and Mr. R. Holyer are conducting a thorough investigation of this exchange and have data on these terms.

(10) A. Lipshitz and B. Perlmutter-Hayman, *J. Phys. Chem.*, **65**, 2098 (1961).

ELECTRON SPIN RESONANCE STUDIES OF IRRADIATED SINGLE CRYSTALS OF D-FRUCTOSE AND L-SORBOSE[1]

BY HISASHI UEDA[2]

Department of Physics, Duke University, Durham, North Carolina

Received July 9, 1962

Among the polycrystalline sugars, only D-fructose and L-sorbose, when irradiated, are known to give an e.s.r. spectrum of four lines. When irradiated polycrystalline L-sorbose was heated to 100°, it gave a spectrum identical with that of irradiated D-fructose which had not been heated. In the present work, the results obtained from polycrystalline materials were studied in more detail using single crystals. Irradiation at 77°K. followed by heating revealed that a radical transformation occurs in these sugars, which is caused by the deformation of the pyranose ring. The free radical produced is $-CH(OH)-\dot{C}(OH)-CH_2-O-$.

Introduction

The author and his co-workers found that irradiated polycrystalline fructose and sorbose yield well resolved e.s.r. spectra, while most other irradiated sugars give broad asymmetric spectra.[3] When irradiated single crystals of sucrose were studied, it was found that the broadening of the lines is caused by some kind of anisotropy.[4] It was also found that, if polycrystalline L-sorbose irradiated at 20° is heated at 100°, the e.s.r. spectrum thus obtained coincides with that of D-fructose which had been irradiated at 20° but not heated.

The present work was planned to illustrate these points by studies on single crystals.

Experimental

Single crystals of D-fructose were obtained by slow evaporation of an aqueous solution. These crystals are orthorhombic[5] and conventional coördinate axes were selected as shown in Fig. 1. Single crystals of L-sorbose, obtained by slow evaporation of a methanol solution, are also orthorhombic[5] and conventional coördinate axes were selected as shown in Fig. 1. By slow evaporation of a 1:1 mixed solution of D-fructose and L-sorbose a single crystal having a different crystal structure from either fructose or sorbose and with an apparent density of 1.60 (L-sorbose; 1.5 and D-fructose; 1.8) was obtained. However, the melting point of this crystal was the same as that of L-sorbose, which is less soluble in water than D-fructose.

These single crystals were irradiated at 77 and 293°K., and e.s.r. measurements were made at both of these temperatures at a frequency of 9400 Mc./sec.

Results

1. Irradiation at 77°K.—The e.s.r. spectra, observed at 77°K., of these crystals are shown in Fig. 2. The spectra of both sorbose and fructose consist of a doublet with a splitting of 18 gauss at a certain orientation of the crystal in the magnetic field. This doublet, the spacing of which is isotropic, further splits at other orientations into a pair of doublets, whose splitting is less than 2.5 gauss. Therefore there are two kinds of protons interacting with the unpaired electron. The spectral lines of sorbose are broader and more deformed than those of fructose, but are of the same nature.

When these crystals were warmed to 193°K., cooled again to 77°K., and the e.s.r. spectra again measured, the spectra obtained were as shown in Fig. 2. The isotropic spacing increased from 18 gauss to 23 gauss.

When these crystals were further warmed to 293°K., they gave spectra identical to those obtained from the sugars irradiated at 293° K.

2. Irradiation at 293°K. A. D-Fructose.—On irradiation at 293°K., a quartet e.s.r. spectrum is observed as shown in Fig. 3. The spacing of the quartet, which is independent of crystal orientation, is 15 gauss. However, the intensity ratios of these four lines depend upon the orientation of the crystal in the magnetic field. A quartet having equal spacings can be obtained by nuclear spin coupling with two protons (splitting factors 1:2) or three protons with equal coupling.

When this crystal is cooled to 77°K. and the spectra taken, broadened lines are observed at the same positions as those observed at 293°K.

B. L-Sorbose.—At this temperature, the spectra from the irradiated sorbose are significantly different from those of fructose. They consist of a doublet and a quartet, as shown in Fig. 4. The quartet becomes relatively stronger in intensity when the microwave power is decreased. When the crystal is heated to 100° for ten minutes the intensity of the doublet decreases and that of the quartet increases, as shown in Fig. 4. Therefore, the free radical which gives rise to the doublet changes to the other radical, which gives rise to the quartet. The spacings of the quartet are all 15 gauss, the same as those in the spectrum of fructose.

The power dependence of the intensity ratio, defined by l_2/l_1 of Fig. 4, is shown in Fig. 5. The change of this intensity ratio with the orientation of the crystal in the magnetic field is shown in Table I.

TABLE I

THE ORIENTATION DEPENDENCE OF THE INTENSITY RATIO

Angle: $<H$ Incident power	0°	30°	60°	90°	120°	150°
1 mw.	1.0	1.0	1.2	1.4	1.3	2.1
30 mw.	6.3	9.5	7.3	6.5	9.2	4.7
30 mw./1 mw.[a]	6.3	9.5	6.1	4.6	7.1	2.2

[a] This line shows the ratio of the values in the second and the first lines. The z-axis was kept perpendicular to the direction of the magnetic field.

Discussion

Although the intensity of the quartet cannot be used to decide the number of protons interacting with the unpaired electron in the irradiated fructose and sorbose at 293°K., it may be concluded that there are three protons interacting equally with the unpaired electron for the following reason. Among the various hexoses, only these ketohexoses have a pyranose ring with a methylene group in it. And since only these

(1) This work was supported by the Air Force Office of Scientific Research, Air Research and Development Command.

(2) Nishina Memorial Fellow.

(3) H. Ueda, Z. Kuri, and S. Shida, *Nippon Kagaku Zasshi*, **82**, 8 (1961).

(4) H. Ueda, Z. Kuri, and S. Shida, *J. Chem. Phys.*, **35**, 2145 (1961).

(5) P. Groth, "Chemische Crystallographie," Vol. 3, Leipzig, 1912, p. 440.

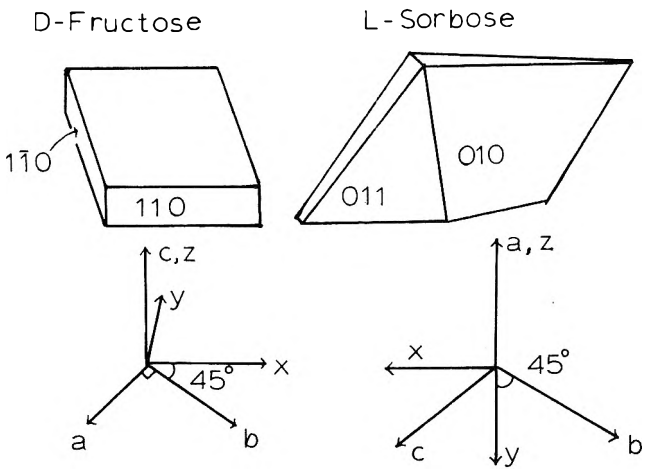

Fig. 1.—Single crystals of D-fructose and L-sorbose.

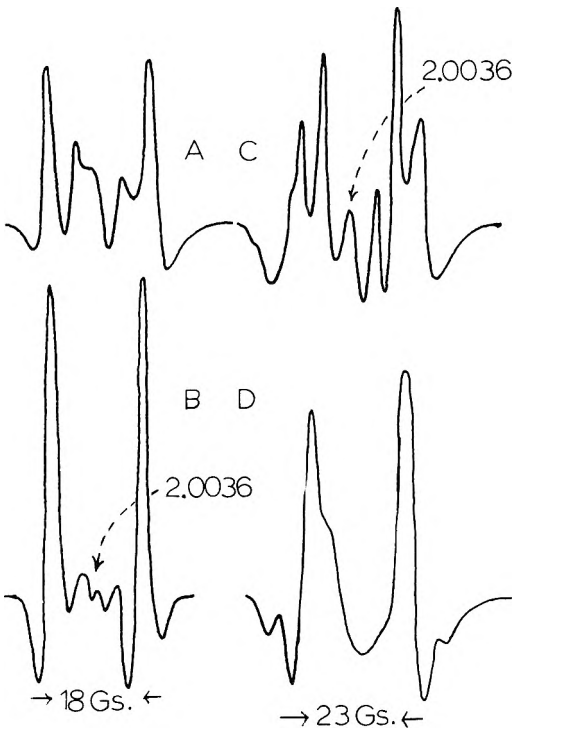

Fig. 2.—E.s.r. spectra of D-fructose irradiated at 77°K. A: ∠xH = 90°, ∠yH = 75°, and ∠zH = 165°. B: ∠xH = 90°, ∠yH = 30°, and ∠zH = 120°. Both A and B were measured at 77°K. C: H//y. D: ∠xH = 90°, ∠yH = 120°, and ∠zH = 30°. Both C and D were observed after the crystal was warmed to 193°K. and cooled again to 77°K.

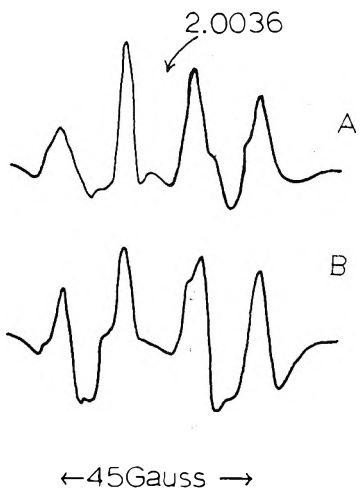

Fig. 3.—E.s.r. spectra of D-fructose irradiated at 293°K. A: ∠xH = 90°, ∠yH = 60°, and ∠zH = 150° at the microwave power of 20 mw. B: ∠xH = 90°, ∠yH = 105°, and ∠zH = 15° at the microwave power of 2 mw.

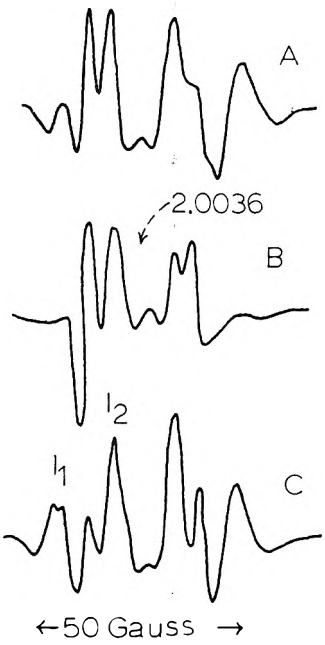

Fig. 4.—E.s.r. spectra of L-sorbose irradiated and measured at 293°K. A, at the microwave power of 2 mw. and at y // H; B, in the same orientation in the magnetic field and at the microwave power of 20 mw.; C, after the crystal was heated to 373°K. for ten minutes. The microwave power was 2 mw. and the orientation was the same as in the above two cases.

ketohexoses, upon irradiation give rise to a quartet, these methylene protons may be interacting with the unpaired electron. The isotropic character of the spacing of the doublet suggests that the structure of the free radical is not RĊH—R′. Therefore, the structure of the free radical, in which the H atoms in the methylene group are interacting with the unpaired electron, is as shown in Fig. 6. If H_1 and H_1' are interacting with the unpaired electron, H_3 should also be interacting. The configuration in which the three protons are interacting equally with the unpaired electron is that in which $C_1C_2C_3$ are in the same plane, as shown in Fig. 6C.

In the original configuration, Fig. 6A, however, $C_1C_2C_3$ are not in the same plane. In the configuration shown in Fig. 6B, the p_z orbital of the unpaired electron is nearly parallel to the axial bond. Therefore, $S \cdot I$ interaction is observed only with H_1 in this case. The doublet observed at 77°K. in the crystal of both fructose and sorbose, and also at 293°K. in the crystals of sorbose, is explained by this configuration. In the crystals of sorbose irradiated at room temperature, most of the free radicals are in the configuration B. After heating, the configuration of most of the free radicals changes to configuration C. However, in the crystals of fructose irradiated at room temperature, all the free radicals have taken the configuration C. The difference of melting point between these two sugars may account for this difference. The melting point of L-sorbose is 160°, while that of D-fructose is 95°. The thermal change of configuration which can only be accomplished at 100° in L-sorbose has occurred in D-fructose even at 20°.

The spin densities calculated from the formula $\rho = A/2Q\cos^2\theta$ are listed in Table II.

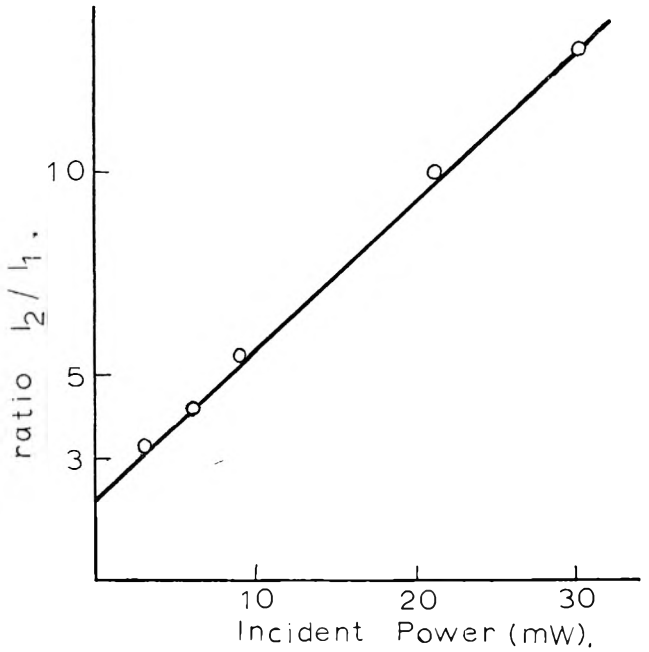

Fig. 5.—The power dependence of the intensity ratio I_2/I_1 in Fig. 4, which is supposed to be 3.0 in an ideal case.

TABLE II
THE FREE RADICALS IN D-FRUCTOSE AND L-SORBOSE

Crystals	Irradiation, °K.	Heating, °K.	Measurement, °K.	$\cos^2\theta$	Spin density
D-Fructose	77	..	77	0.9	0.4
	77	193	77	.9	.5
	293	..	293	.9	.4
L-Sorbose	293	..	293	.7[a]	.5
	293	..	293	.9[b]	.6

[a] For the quartet. [b] For the doublet.

In Table II, almost all the spin densities observed appear too small. However, the unpaired electron may find its spin density on the oxygen atom of the OH group attached to C_3, and perhaps on the oxygen atom in the ring. On the other hand, $\cos^2\theta$ is not precisely estimated for such deformed configuration.

The small splitting of 2.5 gauss, as seen in Fig. 2, may be attributed to the interaction with the proton of OH group attached to C_2.

Ogawa irradiated polycrystalline cyclohexanediol-1,4 and obtained a well resolved triple triplet.[6] This spectrum could be interpreted in terms of a free radical whose structure is R—$\dot{C}$—OH. In this compound, however, the power saturation phenomenon was not so strong as with the sugars and the spectrum appeared as well separated lines. The result shows the cyclohexyl ring is still present in the free radical.

(6) S. Ogawa, *J. Phys. Soc. Japan*, **16**, 1488 (1960).

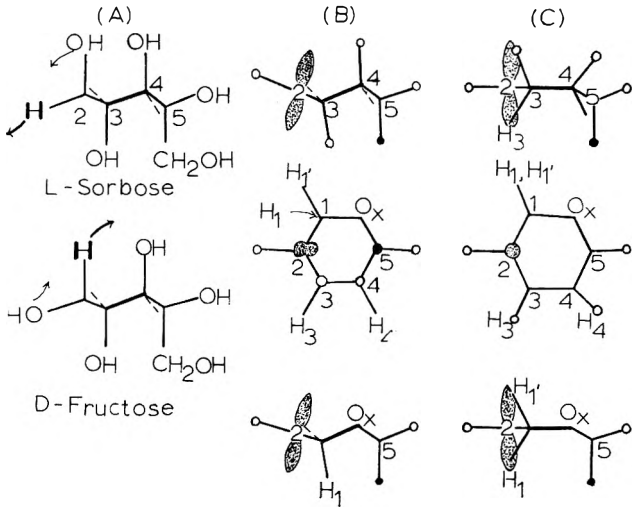

Fig. 6.—The structure of the produced free radical. A: the original molecules. The bold faced hydrogens are knocked off. B: the free radical at lower temperatures. The top figure is a side view of the radical from this side. The bottom figure is another side view from the other side. The middle one is the upper view. The dotted lobe shows the spin cloud. C: the free radical after deformation at higher temperatures. O denotes hydroxyl groups, ● denotes —CH_2OH groups, O_x denotes oxygen atoms.

The stability of the pyranose ring is not so high as that of the cyclohexyl ring. The former ring can be disintegrated in an aqueous solution by hydrolysis. This small stability of the ring explains the radical transition process in these sugars.

The saturation factor[7] is expressed by the formula

$$Z = \frac{n_s}{n_0} = \frac{1}{1 + {}^1/_4\gamma^2 H_1^2 T_1 T_2}$$

where n_s or n_0 is the difference in number of the unpaired electrons between ground and excited energy levels, n_0 is for thermal equilibrium, n_s is for the saturated state, γ is the gyromagnetic ratio, H_1 is the strength of the microwave magnetic field, T_1 is the spin–spin relaxation time, and T_2 is the spin lattice relaxation time. The irregularity of the intensity ratio of the quartet, when the crystal is placed in various orientation in the magnetic field, may be intepreted by an anisotropy of the spin lattice relaxation time T_2.

Acknowledgment.—The author thanks Prof. Walter Gordy for his interest in this study. He also thanks Dr. D. J. Ward who read his manuscript.

(7) D. J. B. Ingram, "Free Radicals as Studied by Electron Spin Resonance," Butterworth, London, 1958, p. 130.

CONTACT ANGLES AND ADSORPTION ON SOLIDS[1,2]

BY E. H. LUCASSEN-REYNDERS

Unilever Research Laboratorium, Vlaardingen, The Netherlands

Received July 19, 1962

Contact angles and surfactant adsorptions have been measured in three-phase systems containing glyceryl tristearate crystals, water, and either paraffin oil or air. The addition of either oil-soluble or water-soluble surfactants, in concentrations up to 80% of the critical micelle concentration, has no effect on the contact angle when the second liquid phase is paraffin oil, and results in a decreasing contact angle when air is present. The results, as interpreted with the equations of Young and Gibbs, indicate that the surfactant adsorptions at the three interfaces are proportional to one another over the whole concentration range. This proportionality of the adsorptions at different interfaces appeared to be generally valid for three-phase systems containing hydrophobic solids and yielded a new equation for the influence of adsorption on the contact angle in such systems. The constant contact angle, observed in several systems hydrophobic solid–water–hydrocarbon liquid represents a special case of this equation. It is suggested that a general relation exists between the adsorption at different interfaces for a constant surfactant activity and the interfacial tensions of the different interfaces when no surfactant is present. Knowledge of this relation will reveal the conditions necessary to obtain contact angles which are insensitive to surfactant adsorption.

Introduction

The contact angle, ϑ, of a fluid–fluid interface against a solid surface is determined by the three interfacial tensions, γ, in the system by means of Young's equation

$$\gamma_{SO} - \gamma_{SW} = \gamma_{OW} \times \cos \vartheta \qquad (1)$$

where S denotes the solid phase and O and W denote oil and water, standing for any pair of immiscible fluids.

The convention is followed here to measure the contact angle in the water phase or, if no water phase is present, in the fluid phase with the higher density. Any of the interfacial tensions in eq. 1 can be affected by surfactant absorption by virtue of Gibbs' law

$$\frac{d\gamma_i}{d \ln a} = - RT\Gamma_i \qquad (2)$$

$$i = SO, SW, \text{ and } OW$$

a being the activity of the surfactant and Γ_i its surface excess at any interface. The activity a in any of the phases may be used in eq. 2, because the changes in ln a upon addition of surfactant are constant over the whole system. These adsorptions can only influence the contact angle if they affect the ratio between $\gamma_{SO} - \gamma_{SW}$ and γ_{OW}. Therefore changes in contact angle may be represented conveniently in terms of $\gamma_{SO} - \gamma_{SW}$ as a function of the liquid–liquid interfacial tension γ_{OW}.

In such a plot any straight line through the origin is the locus for a particular ϑ-value, from 0° up to 180° for points on the +45° line and the −45° line, respectively.

The advantage of this representation over the usual types is that it directly yields a relation between the adsorptions at the three interfaces. From eq. 1 and 2 the slope of the above type of curve is found to be

$$\frac{d(\gamma_{SO} - \gamma_{SW})}{d\gamma_{OW}} = \frac{\Gamma_{SO} - \Gamma_{SW}}{\Gamma_{OW}} \qquad (3)$$

Contact angle measurements can thus be used to calculate surfactant adsorption at an interface between bulk phases not containing measurable amounts of surfactant, if the adsorptions at the two other interfaces are measured separately.

Contact angles and surfactant adsorption were investigated in this way for triglyceride crystals in contact with water and air or hydrocarbon liquid, in the presence of various amounts of surface-active agents.

Experimental

Materials.—Glyceryltristearate (fully hardened linseed oil, recrystallized 5× from acetone and treated with alumina); Paraffin oil (Brocades); Glyceryl α-monoöleate (purity 98% by weight as determined by oxidation with periodic acid; iodine value 71.5; melting point 35°); Sodium diethylhexylsulfosuccinate (Aerosol OT, American Cyanamid Company; purity 96% by weight as found from titration with a cationic soap, standardized with highly purified sodium dodecylsulfate). Glyceryl monoöleate dissolves almost completely in the oil phase and Aerosol OT in the water phase.

The critical micelle concentration of both surfactants is at about 1.6×10^{-6} moles cm.$^{-3}$.

Methods. Measurement of Contact Angle.—Contact angles were determined with Bartell's method,[3] which measures the capillary pressure across a liquid–liquid interface in a plug of a powdered solid by compensation with a known external pressure. The capillary pressure ΔP (going from water to oil) in the pores formed by solid bodies of arbitrary shape is related to the contact angle ϑ by

$$\Delta P = \frac{\gamma_{OW} \times \cos \vartheta}{m} \qquad (4)$$

m being the mean hydraulic radius of the plug, defined as the ratio between liquid volume and solid surface of the pores. This mean hydraulic radius was found from the permeability of the plug.[4]

The apparatus used for the measurement of the permeability and the capillary pressure consisted of a plug holder, both ends of which could be connected with a pressure device and an indicator tube with liquid to measure the rate of flow. In most cases a simple glass tube, carrying a glass filter at the lower end to support the plug, could be used as a plug holder; a more complicated metal apparatus[3] was only necessary in some cases where the pressure to be applied during a measurement exceeded one atmosphere. In each type of apparatus plugs could be prepared from a slurry of coarse crystals in equilibrium with the liquid phase containing the surfactant in the higher concentration. Crystals were used with a specific surface area between 1 and 4 m.^{2}/cm.^{3}, as obtained by crystallization either from paraffin oil under specified conditions or from acetone. Slurries of the latter type of crystals were consolidated under a pressure of several atmospheres. The resulting plugs were homogeneous and did not show compression during the subsequent measure-

(1) Unilever Symposium, Surface Phenomena in Disperse Systems, Noordwijk, September, 1961.

(2) The contents of this paper are part of a thesis prepared under the supervision of Prof. Dr. J. Th. G. Overbeek of Utrecht University.

(3) (a) F. E. Bartell and H. J. Osterhof, *Ind. Eng. Chem.*, **19**, 1277 (1927); (b) F. E. Bartell and F. C. Benner, *J. Phys. Chem.*, **46**, 846 (1942).

(4) P. C. Carman, *Trans. Inst. Chem. Engr.*, **15**, 150 (1937).

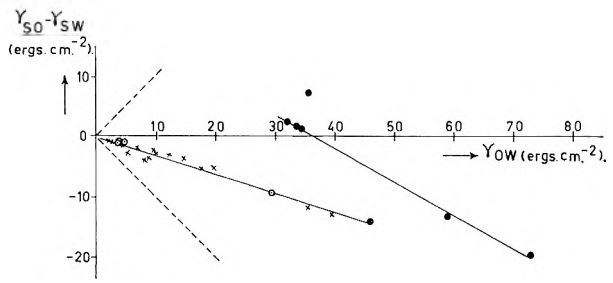

Fig. 1.—Wetting of glyceryl tristearate: by paraffin oil and water upon addition of glyceryl mono-oleate (×) and Aerosol OT, (⊙); by air and water upon addition of Aerosol OT (●).

ments of permeability and capillary pressure; the porosity ranged between 0.3 and 0.6 and the mean hydraulic radii between 0.2 and 1 μ.

After a determination of the permeability of a plug with an amount of the equilibrated liquid, the second liquid was introduced in the plug for the measurement of the capillary pressure ΔP.

The rate of flow of this liquid in the plug was measured as a function of the external pressure, both for the advancement and for the recession of the displacing liquid. Usually no movement was observed in a certain range of pressure values, separating the branches for advancing and receding flow in the flow-pressure curve; this indicates contact angle hysteresis. The external pressures found by extrapolation (from the lowest measurable rates of flow, about 10 Å. sec.$^{-1}$) of the two branches to zero rate of flow were used to calculate the advancing and receding contact angles from eq. 4. The interfacial tension γ_{OW} necessary for this calculation was measured with the drop weight method,[5] using the equilibrated liquid from the consolidated crystal slurry, and pure water or oil as the second liquid.

Measurement of the Adsorptions.—The adsorption of surfactant at the liquid–liquid interface was found by applying Gibbs' law to interfacial tension measurements at known surfactant concentrations. The adsorption at the interface between the solid and the liquid containing the higher concentration of the surfactant was found from the difference between the initial concentration in a plug and the equilibrium concentration, and the solid area available for adsorption. The surface area of the solid in a unit volume of liquid is, by definition, equal to the reciprocal value of the mean hydraulic radius m of the solid–liquid mixture. Consequently the adsorption simply amounts to $\Gamma = m\Delta c$, where Δc represents the decrease in surfactant concentration in moles cm.$^{-3}$. The equilibrium surfactant concentration was determined either by titration with a cationic soap (in the case of Aerosol OT) or by comparing the interfacial tension of the equilibrated solution with the interfacial tensions at known concentrations (in the case of monoglyceride).

The third adsorption (at the interface between the solid and the liquid not containing measurable amounts of surfactant) was obtained by applying eq. 3 to the experimentally determined contact angles, interfacial tensions, and adsorptions at the two other interfaces.

Results

Results of advancing *contact angle* measurements in the system tristearate–water–paraffin oil are given for various concentrations of glyceryl monoöleate and of Aerosol OT in both cases up to about 80% of the c.m.c. (Fig. 1, left hand curve).

The remarkable result of these measurements was that the contact angle did not change on varying the nature or the amount of the surfactant added. For 24 out of 27 experiments a mean value of 108° was found, with nonsystematic deviations up to 10°. This surprisingly constant contact angle should correspond with a straight line pointing to the origin in Fig. 1. Such a straight line does result from the method of the least squares, giving an equation in which the intercept on the ordinate of Fig. 1 is negligibly small

$$\gamma_{SO} - \gamma_{SW} = -0.31\gamma_{OW} - 0.2 \qquad (5)$$

Similar results were also obtained in some additional measurements with cetyl alcohol, soluble in oil, and sodium dodecylsulfate, soluble in water. The slight deviation from a zero value of the additional constant in eq. 5 corresponds with a systematic increase in the contact angle of only 2° over the whole range of surfactant concentrations. This slight variation is far within experimental error.

The receding contact angles in all cases were about 90°, except at very high concentrations where they approached the values of the advancing contact angles. For contact angles of about 90° the experimental error in the displacement measurements is very high; within this error there was no difference in the contact angles found for the oil-soluble and the water-soluble surfactants.

Finally similar measurements were performed with Aerosol OT as a surfactant and air as second fluid phase, instead of paraffin oil. Results from advancing *contact angles* (Fig. 1) can be represented again by a straight line, which, however, does not point to the origin in this case

$$\gamma_{SA} - \gamma_{SW} = -0.56\gamma_{WA} + 21 \qquad (6)$$

In this case the high value of the additional constant signifies a decrease in contact angle from 106° at zero concentration to 82° at 80% of the c.m.c. of the surfactant. Again receding angles of about 90° were observed at low concentrations; this hysteresis started to decrease as soon as the advancing angles had decreased to below 90°.

The adsorption measurements showed saturation adsorption (given in Table I) for concentrations higher than about 0.5×10^{-6} mole cm.$^{-3}$, for both surfactants and at all interfaces.

TABLE I

AREA PER MOLECULE (IN Å.^{2}) AT SATURATION ADSORPTION FOR VARIOUS SURFACTANTS AT DIFFERENT INTERFACES

	Interface				
	Oil	Solid	Solid	Water	Solid
	Surfactant				
	Water	Oil	Water	Air	Air
Glyceryl monoöleate	38	2000	115		
Aerosol OT	106	116	88	106	159

Discussion

The Accuracy of the Permeability Method.—It is realized that this method, used for the determination of mean hydraulic radius and specific surface area, is not very accurate. This is not believed to be serious for the contact angle measurements, because it can be shown that the same average capillary radius determines both the permeability and the capillary pressure. Possible errors may thus cancel out largely. The adsorption values at the solid–liquid interfaces, however, are surely affected by any uncertainty in the solid surface areas. These values must therefore be regarded as approximate. The error is assumed to be not larger than about 20%, as judged by comparison with surface areas estimated microscopically.

The Hysteresis of the Contact Angle.—Of the known mechanisms of contact angle hysteresis, neither rough-

(5) A. Weissberger, "Physical Methods of Organic Chemistry," Vol. I. Interscience Publishers, Inc., New York, N. Y., 1945, p. 167.

ness of the solid surface nor slow establishment of adsorption equilibrium seem to be relevant in the present measurements. Roughness hysteresis would not vanish at high surfactant concentrations, and the second-type hysteresis might be expected to be different for oil-soluble and water-soluble surfactants, a difference which was not found experimentally. Maybe different orientations of the solid phase molecules, dependent on which liquid has been present on the solid surface, are responsible here.

This gives no information about which angle is more representative for the system. In agreement with common use,[6] the advancing angle has been chosen here for two reasons: first, at high concentrations the receding angle values approached those of the advancing angles, second, the advancing angle values were more accurate and reproducible. The advancing angle will therefore be assumed to be more probably an equilibrium angle. If only the last-mentioned mechanism contributes to the hysteresis, both angles might represent a kind of equilibrium, and the interpretation to be given for the advancing contact angles could be used in the same way for the receding angles.

Contact Angles and Adsorptions.—The contact angle measurements given in Fig. 1 show two remarkable features: first in all cases the slope of the plots given by eq. 3 is independent of surfactant concentration, from zero up to the c.m.c., and even of the type of surfactant; second the straight lines point to the origin (indicating a constant contact angle) if paraffin oil is used as second fluid phase.

The constant slope means that the difference $\Gamma_{SO} - \Gamma_{SW}$ is proportional to Γ_{OW} over the whole concentration range. Such a proportionality has not been reported before, but nevertheless appears to occur generally in three-phase systems containing hydrophobic solids. Some typical examples are shown in Fig. 2, calculated from the contact angle data of the authors indicated.[7-9] (It will be noticed that also in the measurements on solid paraffin the slope is independent of the type of surfactant, like in Fig. 1.) This linear relation corresponds with a linear relation between cos ϑ and $1/\gamma_{OW}$, whereas a linear relation between cos ϑ and γ_{OW} has been suggested by several authors, for example Fowkes[8] and Zisman.[10] The latter, empirical relation, however, only gives a good fit to the experiments plotted in Fig. 2 over a rather small range of high concentrations, whereas the linear relation between $\gamma_{SO} - \gamma_{SW}$ and γ_{OW} holds for the whole range from zero to the c.m.c.

The present linearity is most simply explained by assuming that the three adsorptions remain proportional to each other over the whole concentration range. It should be possible to prove this by careful measurements of two of the adsorption isotherms, which should then show an identical shape. Present adsorption measurements below saturation adsorption were not accurate enough to allow such a proof. From the literature data only Smolders' investigation[9] contains

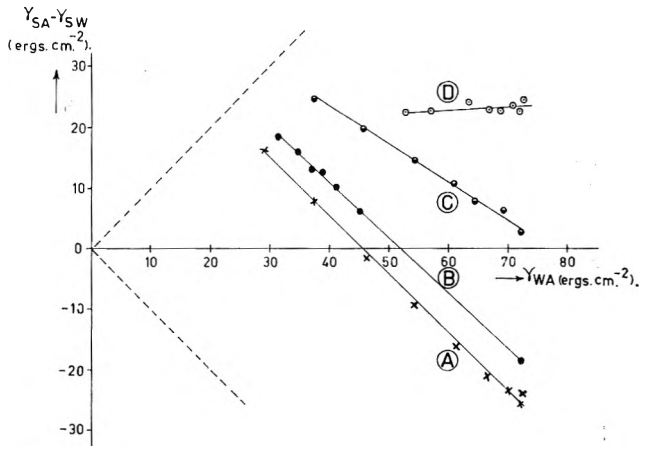

Fig. 2.—Wetting of solid paraffin by air and water upon addition of butyl alcohol (curve A) from data of Fowkes and Harkins[7] upon addition of Aerosol OT (curve B) from data of Fowkes[8]; wetting of talc upon addition of butyl alcohol (curve C) from data of Fowkes and Harkins[7]; wetting of mercury at the electrocapillary maximum by hydrogen gas and water upon addition of sodium decyl sulphonate (curve D) from data of Smolders.[9]

sufficient information for this check, because in the case of mercury as a "solid" all interfacial tensions are accessible to measurement. Proportionality of adsorptions is equivalent with a linear relation between the interfacial tensions; such linear relations do result from his γ-measurements. It will be supposed that also in the other systems with a constant slope the adsorptions separately are proportional. These proportionalities are not unexpected for the low concentration range, by virtue of Traube's rule, nor for the high concentrations, where the adsorptions no longer change. Surprising is only that in systems with hydrophobic solids the proportionality factors for the two concentration regions are equal, and that they are also observed at intermediate concentrations. No explanation can be given for this, by lack of a theory which predicts the influence of both surfactant concentration and nature of the interface on adsorption. Knowledge of the latter influence is also necessary to predict the actual value of the constant slope, which determines whether ϑ increases or decreases upon surfactant addition.

In special cases, as a second remarkable result, the straight line discussed above points to the origin, so that ϑ is not affected by the surfactant

$$\frac{\gamma_{SO} - \gamma_{SW}}{\gamma_{OW}} = \frac{\Gamma_{SO} - \Gamma_{SW}}{\Gamma_{OW}} = \text{constant}$$

This was found for tristearate in contact with paraffin oil and water (Fig. 1). An effect of surfactant addition on the contact angle could only be obtained by replacing the hydrocarbon liquid by air; then the system behaves like all hydrophobic solids in contact with air and water. A similar difference has been found by Schulman and Leja[11] for the wetting of artificially hydrophobic $BaSO_4$: a decrease of the contact angle to zero was found on using air and a constant obtuse contact angle when benzene was used instead of air. The most simple explanation of this behavior would assume a direct proportionality of the adsorption at any interface with the interfacial tension of that interface in the absence of surfactant, γ^0. This cannot be correct,

(6) (a) L. A. Girifalco and R. J. Good, *J. Phys. Chem.*, **64**, 561 (1960); (b) G. A. H. Elton, *J. Colloid Sci.*, **7**, 450 (1952); (c) F. M. Fowkes and W. M. Sawyer, *J. Chem. Phys.*, **20**, 1650 (1952).

(7) F. M. Fowkes and W. D. Harkins, *J. Am. Chem. Soc.*, **62**, 3377 (1940).

(8) F. M. Fowkes, *J. Phys. Chem.*, **57**, 98 (1953).

(9) C. A. Smolders, *Rec. trav. chim.*, **80**, 699 (1961).

(10) M. K. Bernett and W. A. Zisman, *J. Phys. Chem.*, **63**, 1241 (1959).

(11) J. H. Schulman and J. Leja, *Trans. Faraday Soc.*, **50**, 598 (1954).

however, since the data of Fig. 1 and Table I then would give values for γ^0_{SO} and γ^0_{SW} which are not only improbable in view of the estimated value $\gamma^0_{SO} \approx 10$ ergs cm.$^{-2}$, but moreover differ for the systems containing monoöleate and AOT.

For oil–water and air–water interfaces, Bartell and Davis[12] found a general increase of the adsorptions of aliphatic alcohols with increasing γ^0, except for the air–water interface, which showed lower adsorption values than would correspond with $\gamma^0 = 72$ ergs cm.$^{-2}$. To account for this, they introduced the concept of the "available free surface energy," which is only about 50 ergs cm.$^{-2}$ for air–water because surface tensions of aqueous surfactant solutions can never be decreased to below 20 ergs cm.$^{-2}$. Quantitatively, however, the relation between Γ and γ^0, or the available fraction of γ^0, is not even known for these fluid–fluid interfaces.

(12) F. E. Bartell and J. K. Davis, *J. Phys. Chem.*, **45**, 1321 (1941).

Still more difficulties may be expected on extending such a relation to interfaces with solids. Quantitative prediction of contact angles as influenced by surfactant adsorption is therefore not possible at present.

Qualitatively, the concept of the available free surface energy might explain why a constant angle is generally not obtained in systems solid–air–water, as these systems contain at least one interface for which the available free surface energy is not given by the total surface tension, which determines the contact angle.

Further research will be necessary in order to elucidate the factors determining the relation between adsorption and interfacial tension, and thus the influence of surfactant adsorption on contact angles.

Acknowledgment.—The author is indebted to Mr. H. Dekker, who performed all of the measurements.

REACTION KINETICS IN SOLUTION BY A DIFFERENTIAL CALORIMETRIC METHOD

BY C. H. LUECK, L. F. BESTE, AND H. K. HALL, JR.

Pioneering Research Division, Textile Fibers Department, E. I. du Pont de Nemours & Company (Inc.), Wilmington, Delaware

Received July 20, 1962

A method was developed for following reaction kinetics in solution. The temperature difference between a reaction calorimeter cell and a reference calorimeter cell, both immersed in a constant temperature bath, was measured. The area swept out by the temperature–time curve was related to the heat formed by the reaction and was used to calculate the rate constant. The method is useful for reactions with half-lives of 0.5–10 minutes and over a range of temperatures. As a test of the method the hydrolysis rates of tetramethyldiamidophosphorochloridate over the range 10–40° were determined and found to agree well with earlier data.

We have developed a method for determining moderately rapid reaction rates in solution by measuring the heat evolved as a function of time, using a pair of simple twin calorimeters.[1] Related methods have been described independently by a number of other investigators.[2] We compare our method with these and other methods below.

General Description.—Our equipment resembles that described by Borchardt and Daniels[3] although our studies are performed at almost constant temperature. Briefly, in a constant temperature bath are immersed two identical glass reaction vessels, each equipped with an efficient stirrer and a thermistor. Each cell contains the same amount of reagent solution. One cell serves as the reaction calorimeter cell and the other as a reference calorimeter cell. The thermistors are connected through an amplifier and a bridge to a recording potentiometer, providing a measure of the temperature difference between the two calorimeter cells as the reaction proceeds. The reaction proceeds at essentially constant temperature as far as the rate constant is concerned, since the largest temperature rise is about 0.1°.

When the reagent is injected into the reaction calorimeter cell, a plot of temperature difference against time resembles curve A of Fig. 1. The initial sharp rise in temperature at time zero when the reagent is injected is caused by (a) the difference in temperature of the added reagent reaction from that in the cell, and (b) the heat of mixing of the reagent with the solvent. The reaction begins and heat is generated, causing a further rise in temperature. However, heat is also being lost from the reaction cell to the bath. After a maximum temperature is reached, a gradual decline of ΔT_t, the temperature difference between reaction and reference cells at any time t, to zero occurs. (This cooling process can be observed separately in curve B in Fig. 1, obtained by adding a drop of warm solvent to the reaction calorimeter cell after the reaction is ended.)

Calculation of the First-Order Rate Constant.—The exact form of curve A will clearly depend on k_1, the rate constant of the chemical reaction, and on the rate of cooling. We now show how the former can be extricated from the data given by curve A. At any time, t, the following heat balance equation holds

$$C_p \Delta T_t = Q_m + Q_r - Q_d \qquad (1)$$

where

C_p is the heat capacity of the reaction cell and contents in cal. per temperature unit. It is taken as constant during the run.
ΔT_t is the temp. difference between the reaction and reference cells in appropriate units at any time.
Q_m is that heat in cal. which would be just sufficient to cause the rapid temperature rise, ΔT_i, which is observed when the given quantity of reagent at any temperature is mixed with the solution, in given amount and concentration, at the particular bath temperature.
ΔT_i is the value of ΔT_t reached almost instantly after injection of the reagent.
Q_r is the heat in cal. evolved by the reaction of the given amount of reagent by time t.
Q_d is the heat in cal. which has been dissipated from the reaction cell into the bath by time t.

(1) See J. M. Sturtevant in "Physical Methods of Organic Chemistry," Interscience Publishers, New York, N. Y., 1945, Vol. I, pp. 342–344.

(2) (a) V. Kamenik and H. Hruby, *Chem. Prumysyl*, **5**, 510 (1955); (b) F. Becker, *Z. physik. Chem.*, **26**, 1 (1960); (c) P. Baumgartner and P. Duhaut, *Bull. soc. chim. France*, 1187 (1960); (d) Z. Manyasek and A. Rezabek, *J. Polymer Sci.*, **56**, 47 (1962).

(3) H. Borchardt and F. Daniels, *J. Am. Chem. Soc.*, **79**, 41 (1957). See also C. Kitzinger and T. Benzinger, *Z. Naturforsch.*, **10b**, 375 (1955); "Principle and Method of Heatburst Calorimetry and the Determination of Free Energy, Enthalpy, and Entropy Changes" in "Methods of Biochemical Analysis," Vol. VIII, edited by D. Glick, Interscience Publishers, New York, N. Y., 1960, p. 309.

Heat is being lost to the bath throughout the run, and if Newtonian behavior is followed the heat lost will be expressed as

$$-\frac{1}{C_p}\frac{dQ_d}{dt} = K\Delta T_t = -\frac{d\ \Delta T_t}{dt} \qquad (2)$$

where K, in reciprocal minutes, is a constant characteristic of the particular cell, stirrer, and cell contents. That Newtonian behavior is indeed followed in our equipment was demonstrated by plotting the data represented by curve B, Fig. 1, according to the equation

$$\Delta T_t = \Delta T_i\, e^{-Kt} \qquad (3)$$

A semilogarithmic plot of ΔT_t against time was linear and K was evaluated numerically from the slope.

Integrating equation 2 gives 4

$$-\int_0^t dQ_d = -Q_d = KC_p \int_0^t \Delta T_t dt \qquad (4)$$

The term Q_m can be evaluated from the value of ΔT_i (see Fig. 1, curve A or B)

$$Q_m = C_p \Delta T_i \qquad (5)$$

Replacing terms in equation 1 with their equivalents from equations 4 and 5 rearranging, we obtain

$$Q_r = C_p\Delta T_t - C_p\Delta T_i + KC_p \int_{t=0}^t \Delta T_t dt \qquad (6)$$

Now, Q_r is proportional to the concentration of product, $(P)_t$, formed at time t

$$\frac{Q_r}{Q_{r(\infty)}} = \frac{(P)_t}{(M)_0} \qquad (7)$$

in which $Q_{r(\infty)}$ is the total heat in calories formed by the complete reaction of the added reagent under the specified conditions and $(M)_0$ is the initial concentration of reagent. By eliminating Q_r between equations 6 and 7, we show this explicitly

$$(P)_t = \frac{C_p(M)_0}{Q_{r(\infty)}} \times \left\{\Delta T_t - \Delta T_i + K\int_{t=0}^t \Delta T_t dt\right\} \qquad (8)$$

Here the bracketed term involving experimentally accessible quantities is directly proportional to the product concentration. The values of ΔT_t and ΔT_i are read directly from the potentiometer tracing at various times and just after injection, respectively, K is evaluated from curve B as described above, and the integrals under the curve are evaluated at various times by either planimetric, weighing, or computer methods.

The form of equation 8 allows the calculation of the first-order rate constant k_1 by the mathematical method of Guggenheim[4] or, preferably, the more recent one of Swinbourne.[5] The procedure of the latter led to equation 9

$$\left\{\Delta T_t + K\int_0^t \Delta T_t dt\right\} = e^{k_1\tau}\left\{\Delta T_{(t+\tau)} + K\int_0^{t+\tau} \Delta T_t dt\right\} + C \qquad (9)$$

where τ is a fixed time interval between two sets of readings. A plot of the left side of equation 9 against

(4) See A. A. Frost and R. G. Pearson, "Kinetics and Mechanism," John Wiley and Sons, Inc., New York, N. Y., 1953, pp. 48–49.

(5) E. S. Swinbourne, *J. Chem. Soc.*, 2371 (1960).

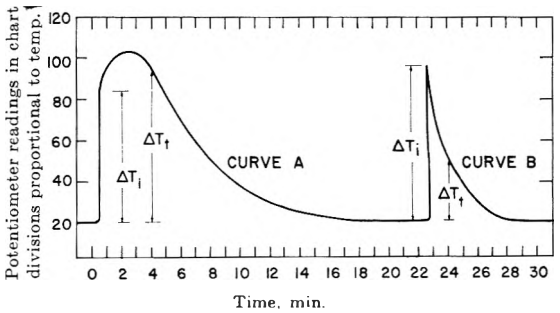

Fig. 1.—Potentiometer tracings for a first-order reaction and for a cooling curve.

the bracketed term on the right gives a straight line with slope $e^{k_1\tau}$, from which the rate constant, k_1, can be evaluated. The Guggenheim procedure gives analogous results.

We might also have proceeded to calculate the fraction reacted, x, at any time as follows. Letting $t = \infty$ in equation 8 gives 10

$$(P)_\infty = \frac{C_p(M)_0}{Q_{r(\infty)}}\left\{0 - \Delta T_i + K\int_{t=0}^{\infty} \Delta T_t dt\right\} \qquad (10)$$

Dividing (8) by (10) and letting $x = (P)_t/(P)_\infty$, we obtain (11)

$$x = \frac{\Delta T_t - \Delta T_i + K\int_{t=0}^t \Delta T_t dt}{-\Delta T_i + K\int_{t=0}^{\infty} \Delta T_t dt} \qquad (11)$$

The rate constant k_1 could then be evaluated by conventional means. This is less satisfactory than the Swinbourne method. The total area under the curve is difficult to evaluate precisely because of the asymptotic approach of the curve to the time axis.

Comparison of Present Calculation Method with Those of Previous Investigations.—In the above treatment of the data we have worked with the relationship of heat to time. A number of earlier investigations have focused attention on the relationship of temperature to time.[6] We can show that our equation is consistent with their treatment as follows. Differentiating equation 8 and letting

$$x = \frac{(P)_t}{(M)_0}$$

we obtain

$$\frac{dx}{dt} = \frac{C_p}{Q_{r(\infty)}}\left\{\frac{d\ \Delta T_t}{dt} + K\Delta T_t\right\} \qquad (12)$$

For a first-order reaction equation 13 holds

$$\frac{dx}{dt} = k_1 e^{-k_1 t} \qquad (13)$$

Eliminating dx/dt between (12) and (13), integrating, and evaluating the integration constant by letting $\Delta T_t = \Delta T_i$ at $t = 0$ provides equation 14

(6) (a) R. P. Bell and J. C. Clunie, *Proc. Roy. Soc.* (London), **212**, 16 (1952), and later articles; (b) V. Gold and J. Hilton, *J. Chem. Soc.*, 838 (1955); (c) R. P. Bell, V. Gold, J. Hilton, and M. H. Rand, *Discussions Faraday Soc.*, **17**, 151 (1954); (d) N. H. Ray, *ibid.*, 4023 (1960); (e) P. A. H. Wyatt, *J. Chem. Soc.*, 2299 (1960); (f) W. J. Albery and R. P. Bell, *Trans. Faraday Soc.*, **57**, 1942 (1961).

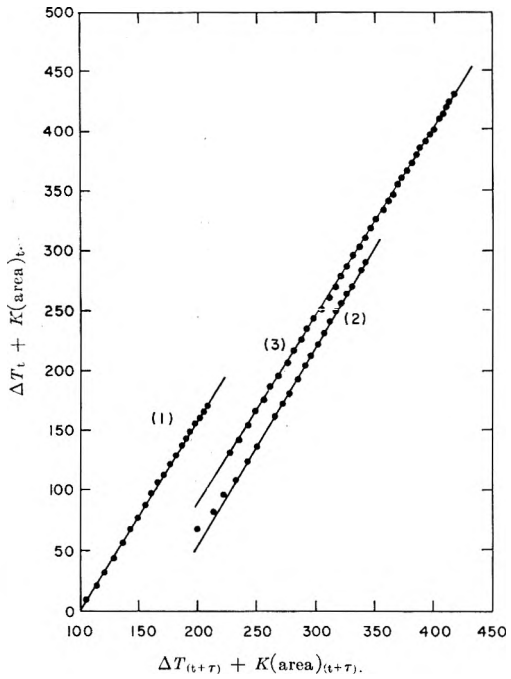

Fig. 2.—Representative Swinbourne first-order rate plots for the hydrolysis of tetramethyldiamidophosphorochloridate in water: 1, 10°; 2, 20°; 3, 30° (100 was subtracted from each observed abscissa point). ΔT's are in chart divisions, K in min.$^{-1}$, and area in chart divisions × min.

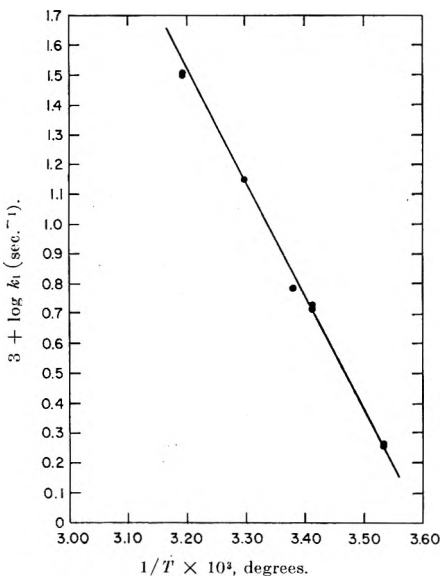

Fig. 3.—Arrhenius plot of the first-order rate constants for the hydrolysis of tetramethyldiamidophosphorochloridate in water. The line was drawn from the data given in ref. 8.

$$(K - k_1)\Delta T_t = \frac{Q_{r(\infty)}}{C_p} k_1 e^{-k_1 t} + \left\{ K\Delta T_i - k_1 \Delta T_i - \frac{Q_{r(\infty)}}{C_p} k_1 \right\} e^{-Kt} \quad (14)$$

The quantity $Q_{r(\infty)}/C_p$ is the temperature rise which would be observed under adiabatic conditions. Equation 14 is identical with the one derived by Bell and Clunie,[6a] who treated the problem as a case of two consecutive first-order reactions, with temperature playing the role of the intermediate compound.

We considered the possibility that a simple plot of the logarithm of ΔT_t against time might be linear with a slope equal to $-0.434k_1$. Analysis of the required conditions revealed that, under our experimental conditions, such a plot would not give reliable values of k_1.

Test of the Method.—It was advisable to test the method on a reaction of known rate. The hydrolysis of tetramethyldiamidophosphorochloridate[7] was selected

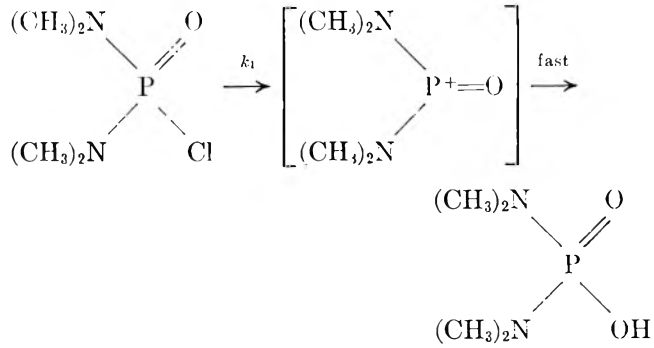

Reactions were followed to 90% completion. Swinbourne plots of the data obtained are given in Fig. 2. They appeared to be satisfactorily linear. The rate constants calculated from the slope of these lines are given in Table I. They agree to within 5% of each other with the exception of the two values at 60° (which are commented on below) and with the values determined independently by a potentiometric method. This precision is about as high as this method provides in general. The data were also treated by Guggenheim's method and yielded results consistent with those recorded in Table I. The data are plotted in Fig. 3 according to the Arrhenius equation.

TABLE I

FIRST-ORDER RATE CONSTANTS[a] FOR THE HYDROLYSIS OF TETRAMETHYLDIAMIDOPHOSPHOROCHLORIDATE IN WATER SOLUTION

Temp., °C.	Initial concn. of halide, $M \times 10^3$	$k_1 \times 10^3$, sec.$^{-1}$	Lit.[7] $k_1 \times 10^3$, sec.$^{-1}$
10.0	23	1.8	1.75
10.0	23	1.9	1.75
20.0	16	5.2	5.20
20.0	16	5.4	5.20
22.6	37	6.1	6.80
30.0	14	14	14.2
40.0	11	32	36.5[b]
40.0	9	32	36.5[b]
60.0	7	(87)	180[b]
60.0	9	(25)	180[b]

[a] Calculated by method of Swinbourne.[5] [b] Extrapolated value.

Advantages of the Differential Calorimetric Method.—Like all thermal methods the present method is applicable to a variety of reactions which for one or another reason cannot be followed by other more commonly used means. Conversely, since it is nonspecific to a particular reagent in the solution, one must be sure that the course of the reaction under study is definitely established. Although only exothermic reactions have been explicitly considered, the method should also apply to endothermic ones.

The advantages over the thermal maximum method[6a] are: (1) the adiabatic temperature rise is not required; (2) any heat of mixing, either positive or negative, is conveniently handled in the calculations and need not be compensated experimentally; (3) a series of kinetic

(7) H. K. Hall, Jr., *J. Org. Chem.*, **21**, 248 (1956).

points is obtained throughout the reaction rather than a single value; (4) the essential equipment is commonplace and can easily be assembled for short-term studies; (5) no calibration of the cell by a reaction of known heat is required. The differential calorimetric method is roughly comparable to the adiabatic method of Wyatt[6e,f] in these advantages.

The advantages over the method of Becker[2b] reside chiefly in points 2 and 4 and perhaps in the calculations, since no slopes are required. The use of a reference cell favors our method over that of Baumgartner and Duhaut[2c] only in point 2.

Limitations and Possible Sources of Error.—The present equipment did not permit the determination of rates of reactions whose half-lives are less than 30 sec. If these more rapid reactions are attempted, deceptively straight first-order plots with slopes which differ from run to run, may be obtained as in the two runs at 60°. Here the extrapolated half-life is about 20 sec., which is too fast for our equipment. In this it compares unfavorably to the thermal maximum method. The time–temperature curve swells up toward the ordinate axis and becomes indistinguishable from the cooling curve as the reaction becomes progressively faster. The cooling rate half-life in our equipment was 0.5–0.7 min.

In the direction of slower reactions, potentiometer drift was found to be negligible during the course of an experiment. However, the potentiometer often did not return exactly to the original base line, falling either slightly above or below it. Acceptable runs displayed a deviation of not more than 1–2% of the maximum height during the run. One possible cause is a non-Newtonian dissipation of heat at small values of ΔT_t. Another contributing factor may be an inevitable slight mismatching of the two cells. As stirring continues, a slight buildup of heat in one relative to the other may take place. This occurs even though stirring in the cells is allowed to proceed for a while before the start of the reaction. The deviations are most appreciable toward the end of the run (which is another reason for not placing too much confidence in the approximate method of calculation of Appendix I) and set an upper limit to the half-life of about 10 min. Viscous liquids also fail to give satisfactory kinetic data, because the heat is not properly dissipated from the reaction cell.

Although the rate constants for second-order reactions can be calculated from the extent of reaction, x, we preferred to study such reactions by using a large excess of one reagent and measuring the pseudo first-order disappearance of the other. Since the accessible half-lives vary from 0.5–10 min. and the reagent concentration can be varied from 0.01–1.0 M, the accessible second-order rate constants at a single temperature are in the range of 1×10^{-3} to 2.5 M^{-1} sec.$^{-1}$. Since the temperature can be varied considerably, depending on the solvent, a wide variety of reactions can be studied by this calorimetric method.

In practice, one will obtain a curve of the form B, Fig. 1, if the reaction with reagent R is too fast to measure and also if it is too slow to measure; the curve in the latter case stems merely from the heat of mixing. These can be distinguished through use of an added control reagent of moderate reactivity in the solution. If the rate of reaction with S alone is measurable and the reaction curve for a mixture of R and S is of the form of curve B, this suggests that R is reacting too quickly to measure. One must be sure that neither R nor S catalyzes the reaction of the other.

Experimental

Apparatus.—Two Pyrex tubes 3.05 cm. in diameter, 14 cm. long, topped by a 34/28 outer joint were used as cells. Each had a capacity of approximately 65 ml. Two machined "Teflon"[8] resin stoppers approximately 2.54 cm. thick equipped with insert holes for the stirrers, thermistors, and for addition of sample, enclosed the cells. In later experiments creased cells were used to ensure rapid dissolution. The cells were supported in a constant temperature bath by inserting them through close fitting holes drilled through a 0.64 cm. piece of "Lucite"[9] sheeting which covered the bath. Both the reference and reaction solutions were stirred with identical stirrers driven from the same stirring motor by means of a pulley arrangement. The stirrers consisted of 0.16 cm. diameter stainless steel rods equipped with identical "Teflon" stirring blades. The stirring shafts fitted through holes in the "Teflon" stopper which served to center and lubricate the stirrers.

The differential temperature was measured with two glass-enclosed thermistors 11.4 cm. long which protruded through holes in the stopper and dipped into the reaction and reference solutions. The output of the thermistors was fed to a bridge and thence through a Leeds and Northrup d.c. amplifier (Model 9835A) into a recording potentiometer (L. & N. Model G, 12 mv., without standardization). Chart speeds varying from 2.54 to 10.2 cm. per minute were used. For temperatures below approximately 40°, 2000-ohm thermistors (Veco 32A30 U-9) were used; 10,000- or 100,000-ohm thermistors (Veco t × 929; t × 928) were used for higher temperatures. The bridge circuit was conventional. Amounts of reactant ranging from 0.01 to 0.07 ml. were added to the reaction cell by means of a Gilmont Ultramicroburet (the Emil Greiner Co.). The tip of the buret was elongated and bent at a 60° angle so it could be readily inserted through the addition port of the reaction cell.

Procedure.—In a typical run 30 ml. of reaction solution was pipetted into each cell. The "Teflon" stoppers containing the stirring shafts and thermistors were inserted into each cell and the constant temperature bath adjusted to the desired temperature. The contents of the cells were vigorously stirred. When thermal equilibrium was established between the two cells, as indicated by a horizontal differential base line free of drift, the reactant, 0.05 ml., was rapidly added to the reaction cell by means of a Gilmont Ultramicroburet. The completion of the reaction was indicated by the return of the differential plot to the original base line, ample time being allowed.

After each run the cell dissipation constant was determined by adding a drop of solvent to the reaction mixture. If this added solvent is at a slightly higher temperature than that of the reaction mixture, curve B is obtained.

Above 60° condensation of water on the "Teflon" stoppers and subsequent dripping back into the solution caused appreciable irregularities in the temperature–time curve.

Calculations.—The recorder chart paper was Leeds and Northrup No. 951, 120 ARV. Along the time axis the scale is in inches, while the transverse (temperature) axis is in arbitrary units (one chart division ~2.19 mm.). As equation 9 shows, it is not necessary to evaluate ΔT_t in degrees, but only a quantity proportional to it. We have, therefore, retained the temperature readings in these chart divisions (C.D.) and made no attempt to calibrate the temperature scale. In most runs the zero line was set at 20 C.D. and, by adjusting the amount of reagent added, the maximum reading during the run was ~100, so that ΔT_t varied from 0 to ~80 C.D. For use in equation 9, ΔT_t and ΔT_i were read from the potentiometer tracing at a series of times in arbitrary units. If ΔT_i was negative, it was added algebraically. The base line reading was taken as that at zero time. The integral $\int_0^t \Delta T_t dt$ was read for each time with a planimeter or calculated with a computer. If negative, as at the beginning of many runs, it was added algebraically.

As noted the Swinbourne equation took the form

(8) Trademark for Du Pont's TFE-fluorocarbon resin.

(9) Trademark for Du Pont's acrylic resin.

$$\{\Delta T_t + K(\text{area})_t\} = e^{k_1\tau}\{\Delta T_{(t+\tau)} + K(\text{area})_{(t+\tau)}\} + C \quad (9)$$

where K is the cooling curve constant, k_1 is the first-order rate constant, t is the time, and ΔT_t is the height of the differential temperature plot from the base line. Reactions were followed to 90% completion and τ was the time at which $x = 0.40$, as established by a preliminary conventional first-order calculation using the observed total area.

The Guggenheim equation was

$$k_1 t + \ln [\Delta T_{(t+\tau)} + K(\text{area})_{(t+\tau)} - \Delta T_t - K(\text{area})_{(t)}] = C \quad (15)$$

The data to 90% completion were used and τ equaled the time for 70% completion.

Acknowledgments.—We are deeply indebted to Mrs. Nancy Abbadini, Mrs. Janet Willoughby, and Mr. John Bair for excellent technical assistance.

RECOIL PARTICLE LOSS IN HOT ATOM CHEMISTRY EXPERIMENTS; THE DISTRIBUTION OF PATH LENGTHS IN A RIGHT CIRCULAR CYLINDER

BY WILLIAM J. ARGERSINGER, JR.

Chemical Laboratory of the University of Kansas, Lawrence, Kansas

Received August 6, 1962

The geometrical problem of the distribution of distances from random sources to the wall in a right circular cylinder is completely solved. The distribution function is used to determine the recoil loss in hot atom chemistry experiments. The cylinder shape for minimum recoil loss is determined for conditions of fixed sample volume and particle range; the recoil loss is compared with that for a spherical sample.

Introduction

Reactions involving hydrogen atoms of high kinetic energy have been extensively studied with the use of tritons produced by the nuclear process $He^3(n,p)T$.[1-8] The tritons produced in this process recoil with a specified range r in the given reaction system. Some tritons escape into the container walls before they have had opportunity to dissipate all of their energy to molecules of the gas. The calculation of this recoil loss, a geometrical problem, is of importance in such studies. We shall investigate first the distribution of path lengths in the container, then the recoil loss, and finally the shape considerations for minimum recoil loss.

Distribution of Path Lengths.—The helium is generally contained in an ampoule of the shape of a right circular cylinder of radius R and length L. Tritons are produced uniformly throughout its volume and recoil in random directions from the site of production. The path length, or flight, is the distance to the wall, and we wish to find $P(l)$, where $P(l)dl$ is the probability of a path length between l and $l + dl$. Appropriate variables are shown in Fig. 1.

The probability that a flight originates at (ρ, ξ) and travels in the direction (θ, ϕ) is

$$d^3P(l)dl = \frac{2\rho d\rho}{R^2}\frac{d\xi}{L}\frac{d\phi}{2\pi}\frac{\sin\theta d\theta}{2} \quad (1)$$

and

$$l = \xi \sec\theta \text{ for } 0 \leqslant \theta \leqslant \tan^{-1}\frac{\sigma}{\xi}$$

$$l = \sigma \sec\theta \text{ for } \tan^{-1}\frac{\sigma}{\xi} < \theta < \tan^{-1}\frac{\sigma}{\xi - L} \quad (2)$$

$$l = (\xi - L)\sec\theta \text{ for } \tan^{-1}\frac{\sigma}{\xi - L} \leqslant \theta \leqslant \pi$$

$$R^2 = \rho^2 + \sigma^2 + 2\rho\sigma\cos\phi$$

We define $S'(\rho,\xi,l)$ by

$$d^2P(l) = \frac{2\rho d\rho}{R^2}\frac{d\xi}{L}S'(\rho,\xi,l) \quad (3)$$

so that

$$dS'(\rho,\xi,l)\,dl = \frac{d\phi}{2\pi}\frac{\sin\theta d\theta}{2} \quad (4)$$

Now let $S_1(\rho,\xi,l)$ refer to flights terminating in the upper cylinder end, and $S_2(\rho,\xi,l)$ to flights terminating in the cylinder wall from the upper end to the depth ξ. It is evident that

$$S'(\rho,\xi,l) = S_1(\rho,\xi,l) + S_2(\rho,\xi,l) + S_2(\rho,L-\xi,l) + S_1(\rho,L-\xi,l) \quad (5)$$

Equation 3 may be integrated to yield

$$P(l) = \frac{4}{R^2L}\int_0^R \rho d\rho \int_0^L S(\rho,\xi,l)d\xi \quad (6)$$

in which $S(\rho,\xi,l) = S_1(\rho,\xi,l) + S_2(\rho,\xi,l)$.

Evaluation of $S(p,\xi,l)$ and $P(l)$.—From equations 2 and 4 we find

$$dS_1 = \frac{\xi}{2l^2}\frac{d\phi}{2\pi} \qquad dS_2 = \frac{\sigma^2}{2l^2\sqrt{l^2-\sigma^2}}\frac{d\phi}{2\pi} \quad (7)$$

which are to be integrated over appropriate ranges of ϕ consistent with the given values of p, ξ, and l. The results are not given explicitly here, there being eight different functional expressions for $S(\rho,\xi,l)$ corresponding to different ranges of the arguments. When the results for $S(\rho,\xi,l)$ are incorporated in equation 6 to give $P(l)$ and the several integrals evaluated, however, the cases

(1) M. Amr El-Sayed, P. J. Estrup, and R. Wolfgang, *J. Phys. Chem.*, **62**, 1356 (1958).
(2) M. Amr El-Sayed and R. Wolfgang, *J. Am. Chem. Soc.*, **79**, 3286 (1957).
(3) A. Gordus, M. Sauer, and J. Willard, *ibid.*, **79**, 3284 (1957).
(4) M. Amr El-Sayed, Ph.D. Thesis, Florida State University, 1959.
(5) P. J. Estrup and R. Wolfgang, *J. Am. Chem. Soc.*, **82**, 2661, 2665 (1960).
(6) J. Evans, J. Quinlan, M. Sauer, and J. Willard, *J. Phys. Chem.*, **62**, 1351 (1958).
(7) M. Sauer and J. Willard, *ibid.*, **64**, 359 (1960).
(8) J. K. Lee, B. Musgrave, and F. S. Rowland, *J. Chem. Phys.*, **32**, 1268 (1960); *J. Phys. Chem.*, **64**, 1950 (1960).

reduce to five. We convert the results to non-dimensional form by the substitutions

$$l = 2uR \quad L = 2\lambda R \quad P(l)\mathrm{d}l = Q(u)\mathrm{d}u \qquad (8)$$

The distribution functions are given formally by the relations

$$Q_A = \frac{J(u,u) - J(0,u)}{\lambda} + H(u,u) - H(0,u) \qquad u < \lambda, u < 1$$

$$Q_B = \frac{J(\lambda,u) - J(0,u)}{\lambda} + H(\lambda,u) - H(0,u) \qquad \lambda < u < 1$$

$$Q_C = \frac{J(u,u) - J(\sqrt{u^2-1},u)}{\lambda} + H(u,u) - H(\sqrt{u^2-1},u) \qquad 1 < u < \lambda \qquad (9)$$

$$Q_D = -Q_A + Q_B + Q_C \qquad 1 < u, \lambda < u < \sqrt{1+\lambda^2}$$

$$Q_E = 0 \qquad \sqrt{1+\lambda^2} < u$$

$$J(\lambda,u) = \frac{\lambda^2}{2u^2} - \frac{(3 + 2\lambda^2 - 18u^2)\sqrt{u^2-\lambda^2}\sqrt{1+\lambda^2-u^2}}{12\pi u^2} + \frac{(1 - 4\lambda^2 + 4u^2)\sin^{-1}\sqrt{u^2-\lambda^2}}{4\pi u^2}$$

$$H(\lambda,u) = \frac{4}{3\pi u^2}\left[(1-2u^2)E\left(u, \cos^{-1}\frac{\lambda}{u}\right) - (1-u^2)F\left(u, \cos^{-1}\frac{\lambda}{u}\right)\right]$$

Here $F(k,\phi)$ and $E(k,\phi)$ are elliptic integrals of the first and second kinds, respectively.

Figure 2 shows a typical distribution curve, that for $\lambda = 2$, for a cylinder of length twice its diameter. As would be expected, short flights are highly probable and long flights are relatively unlikely. The most probable path length is zero and the average path length approximately $u = 0.45$.

Recoil Loss.—Every triton which follows a flight of length l (defined as above) less than the range r is lost from the system. In terms of the relative range $\gamma = r/2R$ the total recoil loss $W(\lambda,\gamma)$ is therefore given by

$$W(\lambda,\gamma) = \int_0^\gamma Q(\lambda,u)\mathrm{d}u \qquad (10)$$

The results for $W(\lambda,\gamma)$, the recoil loss functions, may be defined formally by the expressions

$$W_A = \frac{U(\gamma,\gamma) - U(0,\gamma)}{\lambda} + V(\gamma,\gamma) - V(0,\gamma) + \frac{\gamma}{2\lambda} \qquad \gamma < \lambda, \gamma < 1$$

$$W_B = \frac{U(\lambda,\gamma) - U(0,\gamma)}{\lambda} + V(\lambda,\gamma) - V(0,\gamma) + 1 - \frac{\lambda}{2\gamma} \qquad \lambda < \gamma < 1$$

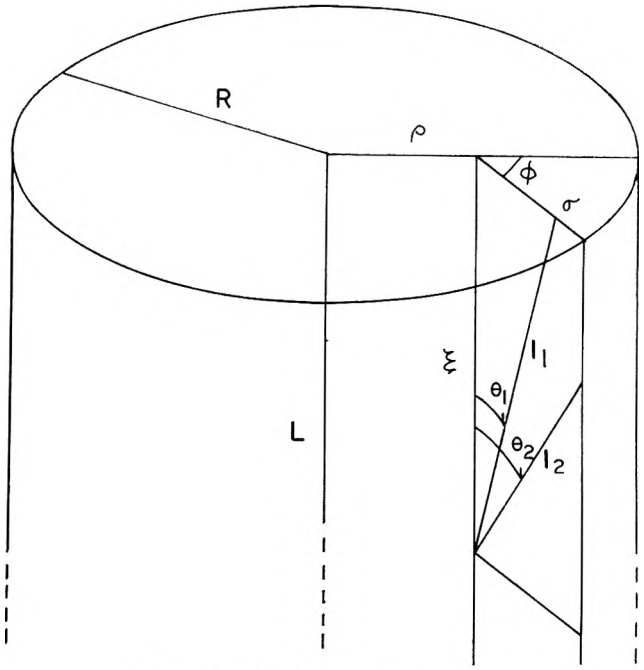

Fig. 1.—Idealized irradiation ampoule.

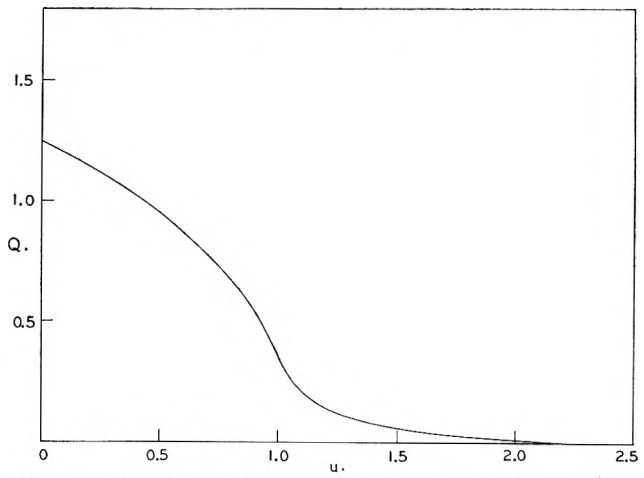

Fig. 2.—Path length distribution function $Q(\lambda,u)$ for $\lambda = 2$.

$$W_C = \frac{U(\gamma,\gamma) - U(\sqrt{\gamma^2-1},\gamma)}{\lambda} + V(\gamma,\gamma) - V(\sqrt{\gamma^2-1},\gamma) + \frac{\gamma}{\lambda} - \frac{1}{2\lambda\gamma} \qquad 1 < \gamma < \lambda \qquad (11)$$

$$W_D = -W_A + W_B + W_C \qquad 1 < \gamma, \lambda < \gamma < \sqrt{1+\lambda^2}$$

$$W_E = 1 \qquad \sqrt{1+\lambda^2} < \gamma$$

$$U(\lambda,\gamma) = \frac{1}{12\pi\gamma}\left[(3 + 2\lambda^2 + 6\gamma^2)\sqrt{\gamma^2-\lambda^2}\times\sqrt{1+\lambda^2-\gamma^2} - 3(1 - 4\lambda^2 - 4\gamma^2)\sin^{-1}\sqrt{\gamma^2-\lambda^2}\right]$$

$$V(\lambda,\gamma) = \frac{4}{3\pi\gamma}\left[(1-\gamma^2)F\left(\gamma, \cos^{-1}\frac{\lambda}{\gamma}\right) - (1+\gamma^2)E\left(\gamma, \cos^{-1}\frac{\lambda}{\gamma}\right)\right]$$

The limits of W_A and W_C as $\lambda \to \infty$, that is, the functions $-V(0,\gamma)$ and $-V(\sqrt{\gamma^2-1}, \gamma)$ (which is $-\gamma$

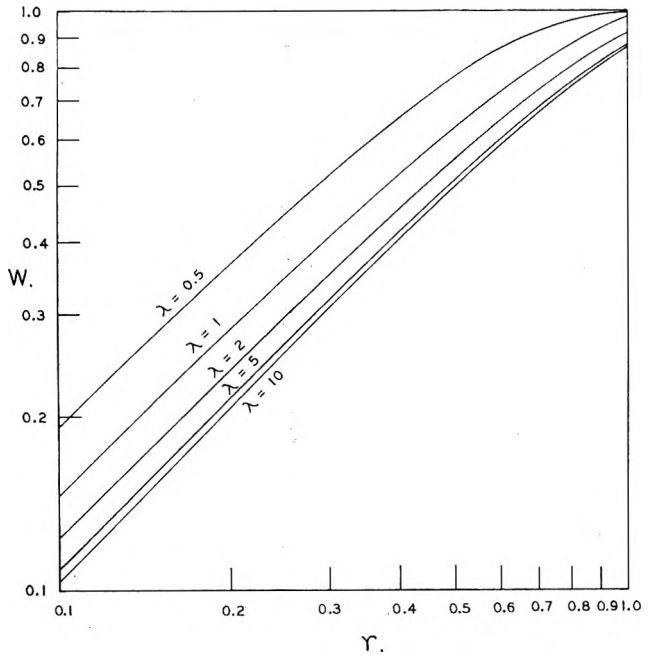

Fig. 3.—Recoil loss W as function of reduced range γ and shape factor λ.

$V(0,1/\gamma)$), appropriate for infinitely long cylinders, have been reported by Estrup and Wolfgang.[5]

Some illustrative results of computation of recoil loss are given in Table I and shown in Fig. 3. The entries in the last column of Table I, for $\lambda \to \infty$, indicate the error introduced by using the Estrup–Wolfgang approximation without correction.

TABLE I

RECOIL LOSS W AS A FUNCTION OF REDUCED RANGE γ AND SHAPE FACTOR λ

γ	λ = 0.5	1.0	2.0	5.0	10.0	∞
0.1000	0.1914	0.1456	0.1228	0.1090	0.1045	0.0999
.1414	.2655	.2033	.1722	.1535	.1473	.1411
.2000	.3652	.2821	.2405	.2156	.2073	.1990
.2828	.4955	.3877	.3339	.3015	.2908	.2800
.3742	.6245	.4960	.4318	.3932	.3803	.3675
.4472	.7165	.5762	.5060	.4638	.4498	.4357
.5477	.8238	.6768	.6016	.5564	.5414	.5263
.6325		.7526	.6758	.6297	.6144	.5990
.7071	.9253	.8122	.7359	.6901	.6749	.6596
.7746		.8601	.7856	.7408	.7259	.7110
.8367		.8990	.8270	.7837	.7693	.7549
.8602	.9769	.9123	.8415	.7990	.7848	.7706
.9055		.9358	.8675	.8264	.8128	.7991
.9487		.9552	.8895	.8500	.8369	.8237
1.0000		.9738	.9113	.8738	.8613	.8488
1.0541			.9276	.8920	.8801	.8683
1.1043		.9925	.9391	.9051	.8938	.8825
1.1180	1.0000		.9418	.9082	.8971	.8859
1.1471			.9471	.9144	.9035	.8926
1.1952			.9546	.9232	.9128	.9023
1.2910			.9663	.9373	.9276	.9179
1.4142		1.0000	.9770	.9505	.9416	.9328
1.5811			.9866	.9629	.9550	.9471
1.8258			.9952	.9746	.9678	.9609
2.2361			1.0000	.9855	.9799	.9743
2.6726				.9915	.9869	.9822
3.5355				.9970	.9934	.9899
5.0000				1.0000	.9975	.9950
7.0711					.9993	.9975
10.0000					1.0000	.9987

Minimum Recoil Loss.—We seek that value of the shape factor λ ($= L/2R$) which gives a minimum recoil loss under the conditions of fixed range r and fixed sample volume V ($= \pi R^2 L$). Under these conditions we have

$$\frac{\lambda}{\gamma^3} = \frac{4V}{\pi r^3} = K \quad \text{or} \quad \lambda = K\gamma^3 \qquad (12)$$

in which the volume factor K is fixed.

We consider only cases W_A and W_C, for $\lambda \geq \gamma$, which are of the form

$$W(\lambda,\gamma) = \frac{A(\gamma)}{\lambda} + B(\gamma) \qquad (13)$$

We determine the minimum in W by the conditions

$$\frac{dW}{d\gamma} = 0 \qquad \frac{d^2W}{d\gamma^2} > 0 \qquad (14)$$

Thus we obtain the relationship between volume factor K and shape factor for minimum recoil loss, λ^*, in parametric form with γ viewed now merely as a convenient parameter. The recoil loss is a minimum, W^*, for

$$K = \frac{3A(\gamma) - \gamma A'(\gamma)}{\gamma^4 B'(\gamma)} \qquad \lambda^* = K\gamma^3 \qquad (15)$$

provided that

$$\gamma B''(\gamma)[3A(\gamma) - \gamma A'(\gamma)] + B'(\gamma)[\gamma^2 A''(\gamma) - 6\gamma A'(\gamma) + 12A(\gamma)] > 0 \qquad (16)$$

In these equations the prime indicates differentiation with respect to γ, and $A(\gamma)$ and $B(\gamma)$ are defined by reference to equations 13 and 11.

TABLE II

MINIMUM RECOIL LOSS W^* AND SHAPE FACTOR FOR MINIMUM LOSS, λ^*, AS FUNCTIONS OF VOLUME FACTOR K, WITH CORRESPONDING VALUES OF RECOIL LOSS W_S FOR SPHERICAL SAMPLE

K	λ^*	W^*	W_S	K	λ^*	W^*	W_S
0	....	1.0000		1.1957	0.9871	0.9525	0.9558
0.0200	19.950	0.9994		1.3109	.9380	.9394	.9430
.0398	14.071	.9987		1.4350	.9135	.9258	.9294
.0596	11.460	.9981		1.5382	.9008	.9148	.9185
.0792	9.899	.9975		1.8906	.8787	.8807	.8834
.0987	8.831	.9969		2.4503	.8663	.8358	.8359
.1182	8.040	.9963		3.406	.8616	.7773	.7730
.1567	6.927	.9950		4.162	.8619	.7416	.7345
.1949	6.163	.9938		5.258	.8640	.7005	.6902
.2326	5.595	.9925		6.945	.8682	.6527	.6388
.2699	5.152	.9913		9.780	.8747	.5963	.5786
.3067	4.792	.9900		13.784	.8822	.5428	.5223
.3790	4.238	.9875		16.931	.8869	.5124	.4906
.4668	3.734	.9844		21.467	.8924	.4788	.4560
.5515	3.357	.9813		28.424	.8988	.4414	.4177
.6331	3.058	.9783		40.068	.9066	.3988	.3746
.7113	2.812	.9752	0.9993	62.345	.9163	.3491	.3252
.8567	2.423	.9693	.9906	82.474	.9221	.3206	.2970
.9858	2.121	.9636	.9785	116.10	.9288	.2885	.2657
1.0952	1.870	.9582	.9668	180.30	.9369	.2514	.2301
				334.81	.9470	.2068	.1877
				961.13	.9611	.1475	.1325
				∞	....	0	0

In Table II are shown computed values of λ^*, the shape factor for minimum recoil loss, as a function of the volume factor K, along with the values of the minimum recoil loss. Between K values of approximately 1.144 and 1.231, the recoil loss curve as a function of γ at fixed K exhibits two minima and an intermediate maximum; for the smaller K values the lower minimum is that at the larger value of γ, hence for the larger value of λ^*, and for the larger K values the reverse is true. In this range of K values, however, the recoil loss

is so great that it is unlikely that many investigators will be concerned with the choice.

For reasonably large values of K the recoil loss may be made fairly small, and there is then, for $\lambda \geq \gamma$, but a single extremum, a minimum as listed.

In general, we note that small recoil loss corresponds to large values of K, as would be expected. As K increases above about 4, λ^* approaches unity, because for large K the loss becomes proportional to the surface area, and this is a minimum for $\lambda = 1$. On the other hand, if one must use small sample volumes and long ranges, so that K is quite small, then minimum recoil loss results from choice of long, thin cylinders, as again would be predicted, and as $K \to 0$, $\lambda^* \to \infty$. The actual minimum recoil loss under these conditions, however, is very large.

It is interesting that for most of the range of K values commonly encountered, the minimizing value of λ is significantly less than unity. The ampoules used, however, generally have lengths greater than their diameters, that is, possess shape factors λ larger than unity.

Comparison with Spherical Case.—The distribution and recoil loss functions for a spherical sample are very easily found to be

$$Q(u) = \frac{3}{2}(1 - u^2) \qquad 0 \leq u \leq 1 \qquad \text{and } Q(u) = 0 \qquad 1 < u$$

$$W(\gamma) = \frac{\gamma}{2}(3 - \gamma) \qquad 0 \leq \gamma \leq 1 \qquad \text{and } W(\gamma) = 1 \qquad 1 < \gamma \quad (17)$$

where u and γ are as defined earlier. Table II also contains values of W_s, the recoil loss for a spherical sample. It may be seen that for values of the volume factor K greater than approximately 2.45, that is, sample volumes greater than approximately 1.92 (range),[3] a spherical sample gives smaller recoil loss than any cylindrical sample. In many experiments, however, reactor designs or other experimental considerations require a cylindrical sample. For very small values of K, of course, spherical samples may have an exorbitant recoil loss.

Acknowledgments.—The author is indebted to Professor F. S. Rowland who suggested this problem, to Mr. David K. Anderson who performed some preliminary computations of recoil loss, and to the National Science Foundation which supported Mr. Anderson as an undergraduate research assistant under grant NSF-G8154.

ANION EXCHANGE OF METAL COMPLEXES. VIII.[1] THE EFFECT OF THE SECONDARY CATION. THE ZINC–CHLORIDE SYSTEM

BY Y. MARCUS AND D. MAYDAN[2]

Israel Atomic Energy Commission, Soreq Research Establishment, Radiochemistry Department, Rehovoth, Israel

Received August 17, 1962

Distribution measurements were made of tracer radioactive zinc ions between Dowex-1, quaternary ammonium anion exchange resin, cross-linked by various amounts (2, 4, 8, 10, and 16%) of divinylbenzene, and aqueous solutions of chlorides of lithium, sodium, ammonium, potassium, and cesium, and hydrochloric acid. The invasion of the various electrolytes into the resins has also been measured. Expressing the electrolyte concentrations in terms of activity functions $a = m\gamma_{\pm}$, and correcting the distribution coefficients for the electrolyte invasion, yielded parallel curves for the variously cross-linked resins. These may be described by a single set of complex formation parameters for the aqueous solutions, the same for all alkali metal chlorides, and one parameter dependent on the cross linking.

Introduction

Most distribution studies of trace metal ions between anion exchangers in chloride form and aqueous solutions were conducted with hydrochloric acid, but a few give data also for other chlorides as the macro electrolyte. It was found earlier[3] that the distribution coefficients vary from salt to salt. What was at first believed to be a "LiCl effect"[3] was later shown to be an "HCl effect," since lithium chloride behaves as the other alkali metal chlorides, whereas hydrochloric acid behaves differently. The "HCl effect" was explained in terms of weak chloro-metallic acid formation in the aqueous phase[4,5] and in terms of differences in activity coefficients[3] and of ion pairing in the resin phase.[6,7] No quantitative correlation of the results of the alkali metal chlorides in general has been given, although they[6] as well as substituted ammonium ions[8,9] have been studied. The following investigation attempts the application of a general approach to this problem to the zinc–chloride system. This system has been previously studied by many workers[4,6,9-11] giving scattered data for different electrolytes and cross linkings. The present work[2] is a systematic study of these factors.

First it should be noted that the salts display in the concentration range studied, 0.1 M to a few molar,

(1) Previous paper in series: Y. Marcus and I. Abrahamer, *J. Inorg. Nuclear Chem.*, **22**, 141 (1961).

(2) Taken from part of a Ph.D. thesis submitted by (Mrs.) D. Maydan to the Hebrew University, Jerusalem, March, 1962. Preliminary communications: D. Paritzky and Y. Marcus, *Bull. Res. Council Israel*, **8A**, 133 (1959); D. Maydan, *ibid.*, **9A**, 246 (1960); Y. Marcus and D. Maydan, *ibid.*, **10A**, 102 (1961). *Cf.* Israel A.E.C. Report IA-764 (1962).

(3) (a) Y. Marcus, *Bull. Res. Council Israel*, **4**, 326 (1954); (b) K. A. Kraus, F. Nelson, F. B. Clough, and R. C. Carlston, *J. Am. Chem. Soc.*, **77**, 1391 (1955).

(4) K. A. Kraus and F. Nelson, *Proc. 1st. Intl. Conf. Peaceful Uses At. Energy, United Nations, Geneva*, **7**, 113 (1956).

(5) Y. Marcus, *J. Phys. Chem.*, **63**, 1000 (1959).

(6) R. A. Horne, *ibid.*, **61**, 1651 (1957).

(7) B. Chu and R. M. Diamond, *ibid.*, **63**, 2021 (1959).

(8) R. A. Horne, *ibid.*, **62**, 873 (1958).

(9) B. Chu, Ph.D. Thesis, Cornell University, 1959.

(10) U. Schindewolf, *Z. Elektrochem.*, **62**, 335 (1958).

(11) Y. Marcus and C. D. Coryell, *Bull. Res. Council Israel*, **8A**, 1 (1959).

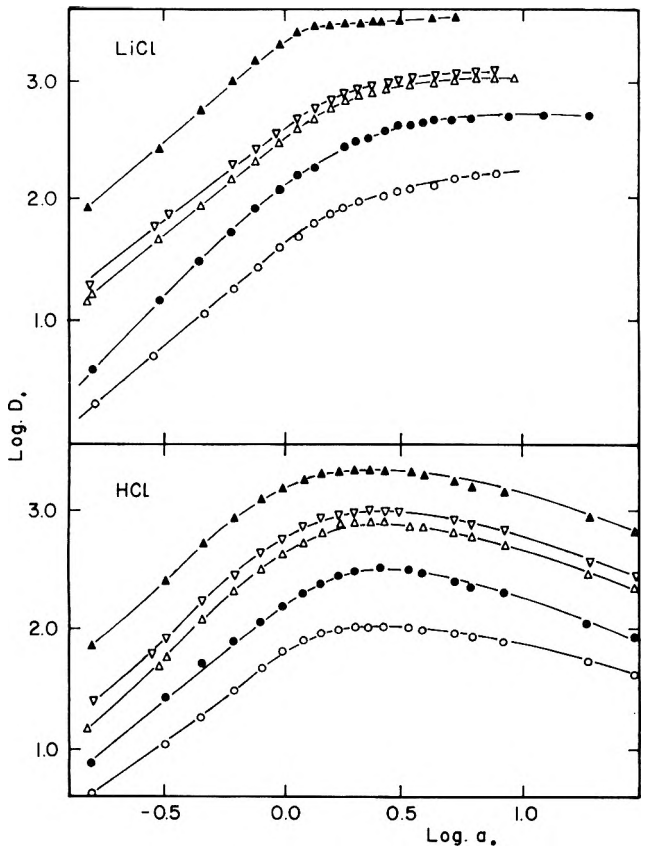

Fig. 1.—Zinc distribution coefficients, log D, *vs.* solution activity function, log a, for lithium chloride (upper part) and hydrochloric acid (lower part). Resin cross linking: O, 2%; ●, 4%; △, 8%; ▽, 10%, ▲, 16%.

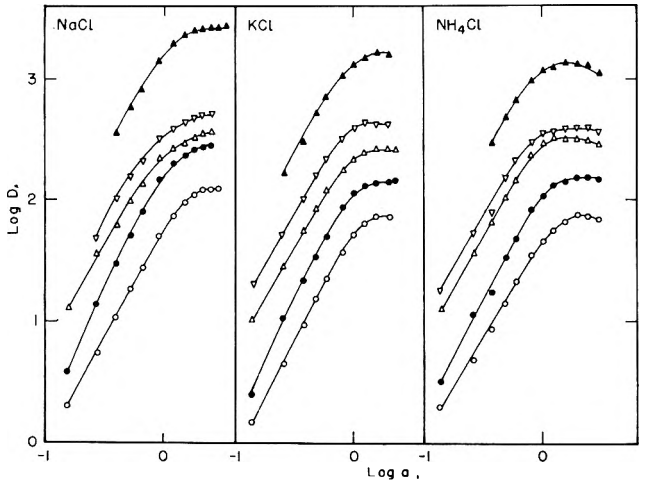

Fig. 2.—Zinc distribution coefficients, log D, *vs.* solution activity function, log a, for sodium (left), potassium (middle), and ammonium (right) chlorides. Symbols as in Fig. 1.

non-ideal behavior specific for every salt. Comparison of salts should take these differences into account. This was found to be best made using activity functions, defined as $a = a_{CCl} = m_{CCl}\gamma_{\pm CCl} = M_{CCl}\, y_{\pm CCl}$. The activity function extending the Guggenheim convention to high concentrations, describes what may be termed an "effective" activity of the ligand in the given solution. Different concentrations of electrolytes are required to produce a given "effective" activity, according to their activity coefficients. This concept was used by Bjerrum[12] and by Gamlen and Jordan[13] to explain spectrophotometric measurements of the chloride complexes of copper and iron, by Poskanzer[14] for solvent extraction and by Marcus and Coryell[11] for anion-exchange studies of complex formation in chloride solutions.

Another point is the different resin-invasion properties exhibited by the various electrolytes. At equilibrium with concentrated solutions, the ligand in the resin consists mainly of invading electrolyte. Hence again, in order to obtain a given ligand activity function in the resin, $\bar{a}$, different concentrations of the various electrolytes are required, according to their invasion characteristics. Invasion measurements are, therefore, needed for the same resin samples and electrolyte solutions, as used for the tracer metal distribution experiments.

Experimental

Materials.—Dowex-1 anion-exchange resins, either Bio-Rad AG or Fluka purified grade, were used after additional cycles of washing with acid and base, conversion to the chloride form, washing with water, and final drying over Anhydrone.

The alkali metal chlorides and other reagents were of analytical grade.

The zinc tracer used, $Zn^{65}Cl_2$, was supplied by O.R.N.L. Its half-life, 245 days, and γ-radiation make it well suited for measurement in solution with the continuous flow method employed. The zinc concentration in the solutions, was kept within 10^{-5} to 10^{-6} M, and loading of the resin below 0.1%. Iodide 131 tracer was supplied by C.E.A., France, and wasp ractically carrier-free.

Measurement of Invasion.—Invasion of electrolyte into the resin was measured by the centrifugation method.[15] Resin samples were shaken with the solutions overnight at room temperature (20–25°) to ensure equilibrium. The decrease of chloride concentration in the solution and the change in volume served to calculate the amount of chloride invasion per gram of dry resin. The concentration of invading cations $\bar{m}_{C^+}$ was calculated from this quantity and the water content of the resin, and the total concentration of chloride ions $\bar{m}_{Cl^-}$ is the sum of it and the capacity of the resin. The ligand activity function in the resin is defined as $\bar{a} = \bar{m}_{Cl^-}\bar{\gamma}_{\pm}$ and may be obtained from the expression[11]

$$\bar{a} = a\bar{m}_{Cl^-}{}^{1/2}\bar{m}_{C^+}{}^{-1/2} \qquad (1)$$

where values of $a = m_{CCl}\gamma_{\pm CCl}$ were calculated using density data from[16] and activity coefficients from Robinson and Stokes.[17]

Zinc Distribution Measurements.—A continuous flow method was used, described previously by Aveston, Everest, and Wells.[18] Because of its advantages over the usually used batch methods it merits more widespread consideration. The main advantages are the necessity of fewer weighing and pipetting operations, reducing random errors, a check by observation on the recorder that equilibrium has been reached, elimination of effects of absorption on the walls of vessels, easy thermostating, and a reduction in the work necessary for the accumulation of a large quantity of distribution data. The distribution coefficients were calculated from the equation

$$D = \frac{(h_0 - h)/(\text{weight of resin})}{h/(\text{weight of solvent})} \qquad (2)$$

where h_0 is the count rate shown on the recorder for the solution of the tracer without resin and salt, and h is the rate in the presence of the resin and at a molality m of salt. The increase in volume of the solution with the addition of weighed amounts

(12) J. Bjerrum, *Kgl. Danske Videnskab. Selskab. Mat.-Fys. Medd.*, **22**, 18 (1946).

(13) G. A. Gamlen and D. O. Jordan, *J. Chem. Soc.*, 1435 (1953).

(14) A. M. Poskanzer, Ph.D. Thesis, M.I.T., Cambridge, Mass., 1957.

(15) K. W. Pepper, D. Reichenberg, and D. K. Hale, *J. Chem. Soc.*, 3129 (1952).

(16) C. N. Hodgman, Editor, "Handbook of Chemistry and Physics," Chemical Rubber Publ. Co., Cleveland, Ohio, 1959, p. 1970.

(17) R. A. Robinson and R. H. Stokes, "Electrolyte Solutions," Butterworths, London, 1955.

(18) J. Aveston, D. A. Everest, and R. A. Wells, *J. Chem. Soc.*, 231 (1958).

of salt to a given volume of water must be taken into account since the counter "sees" a constant volume of solution. The relative increase in volume was found to be approximately $(1 + 0.022\ m)$ for all salts. The distribution coefficients reported are $(1 + 0.022\ m)^2$ times higher than published values, which are related to the volume of solution. The average deviation of experimental points is 0.02 log units of D. Distribution curves were determined from at least two runs. The temperature was kept constant at 25 ± 1°.

Iodide Distribution Measurements.—These were made as above for zinc.

Results

The resin ligand activity function a was found in the invasion measurements to be almost independent of cross linking for hydrochloric acid, but to increase somewhat with cross linking for the alkali metal salts. Except for hydrochloric acid, double logarithmic graphs were linear over the range investigated, the slope of the line decreasing slightly with increasing cross linking.

The distribution coefficients for zinc are shown in Fig. 1 and 2. There is seen to be a considerable spread in the curves with varying cross linking for all electrolytes studied, the distribution coefficients increasing with the cross linking. Data for cesium were obtained only with 8% cross-linked resin, and they are shown in Fig. 3, A and B, where the distribution coefficients for zinc, and the resin activity function, respectively, are compared for all electrolytes studied with this cross linking. Similar curves are obtained for the other resins.

The distribution of iodide tracer between 8% cross-linked resin and sodium and cesium chloride solutions was measured, with results shown in Fig. 4. According to Marcus and Coryell,[11] a singly charged anion such as iodide should obey the relationship

$$\log D_I = \log K_I + \log \bar{a} - \log a \qquad (3)$$

hence a plot of $\log D_I - \log \bar{a}$ *vs.* $\log a$ should give a straight line with slope −1, independent of the nature of the cation of the macro electrolyte. This is shown to be true in this case in Fig. 4, the agreement being an independent check of the values of $\bar{a}$.

Similarly, Marcus and Coryell[11] showed that the distribution coefficient of zinc should obey the relationship

$$\log D_{Zn} = \log K_{Zn} + p \log \bar{a} - \log \sum_{-2}^{N} \beta_i^{*\prime}\, a^i \qquad (4)$$

where $-p$ is the average charge of the zinc species in the resin and K_{Zn} and $\beta_i^{*\prime}$ are parameters independent of a. The value of p may be taken as 2, as Horne, Holm, and Myers have shown at high loading.[19] This is confirmed by the dependence of the distribution coefficients on the cross linking[20] for tracer loading. The function $\log D_{Zn} - 2 \log \bar{a}$, according to Marcus and Coryell's theory, should be independent of the cation of the macroelectrolyte, and the dependence on the resin should be determined by the value of the parameter K_{Zn}. The curves were normalized to 8% cross linking, using the differences $\Delta = \log K_{Zn}(X\%) - \log K_{Zn}(8\%) = -0.38$ for $X = 2$, -0.12 for $X = 4$, $+0.11$ for $X = 10$, and $+0.64$ for $X = 16$. Plots of the normalized functions $\log D - 2 \log \bar{a} - \Delta$ *vs.* $\log a$ for all the electrolytes and resins studied are shown in Fig. 5. For the sake of clarity, only about one fifth of all experimental points are shown.

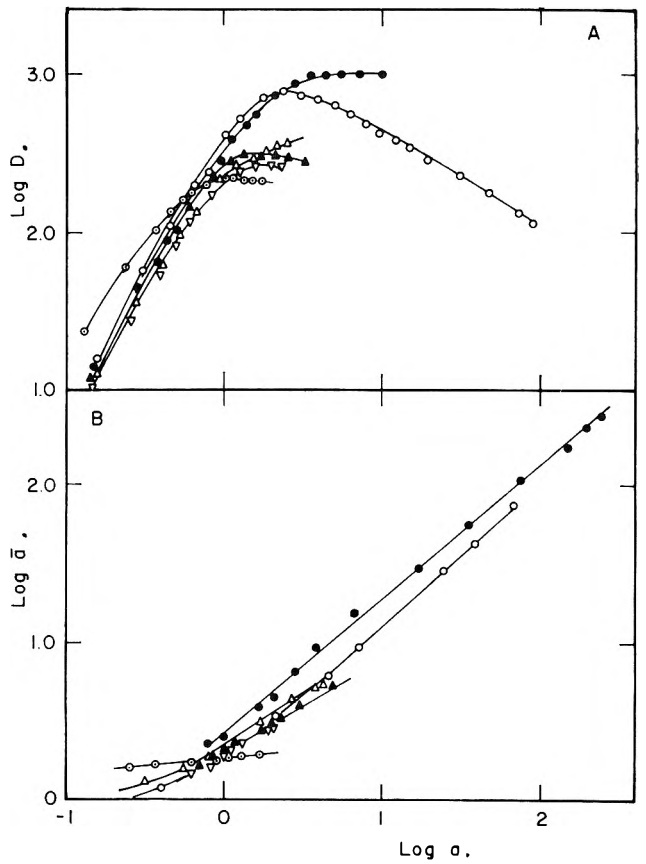

Fig. 3.—(A) Comparison of zinc distribution curves, log D *vs.* log a, for various electrolytes and 8% cross-linked resin: ○, HCl; ●, LiCl; △, NaCl; ▽, KCl; ▲, NH_4Cl; ⊙, CsCl. (B) Comparison of resin activity function curves, log $\bar{a}$ *vs.* log a, for various electrolytes and 8% cross-linked resin. Symbols as in Fig. 3A.

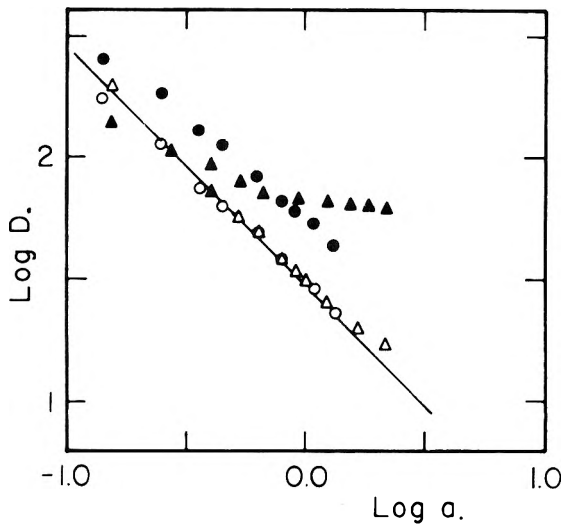

Fig. 4.—Iodide distribution coefficients, log D. *vs.* solution activity function, log a, for 8% cross-linked resin and ● CsCl, ▲ NaCl. Full symbols: log D, open symbols: log D − log $\bar{a}$; line has slope −1.00.

Discussion

Figure 5 shows that the predictions of the theory are confirmed, all the data falling on a single curve.[21]

(19) R. A. Horne, R. H. Holm, and M. D. Myers, *J. Phys. Chem.*, **61**, 1655 (1957).

(20) Y. Marcus and D. Maydan, *ibid.*, **67**, 983 (1963).

(21) It should be noted that it is important to use D and $\bar{a}$ values pertaining to the same resin sample and the same concentration units. A failure to do so (such as using $\bar{a}$ values from Marcus[11] and D values from Horne[6] led to erroneous results in a previous treatment of the zinc–chloride system[11]).

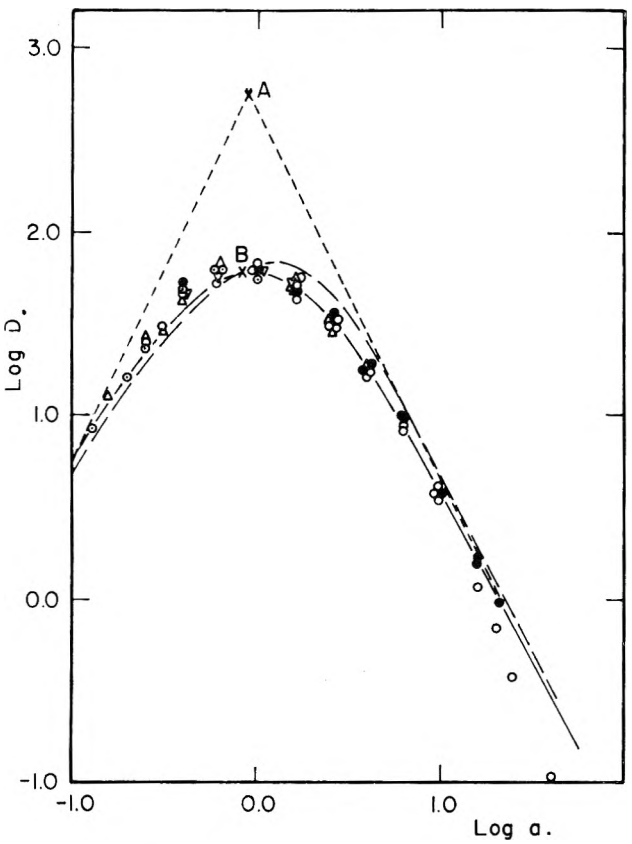

Fig. 5.—Corrected and normalized distribution curve for zinc, $\log D - 2 \log \bar{a} - \Delta$ *vs.* $\log a$. Symbols correspond to these in Fig. 3. Asymptotes are drawn with slopes +2.00 and −2.00, meeting at A; point B is on data curve with same abscissa as A. Dashed curve calculated from constants given by Short and Morris[22]; solid curve calculated from constants obtained by the two parameter method in this work.

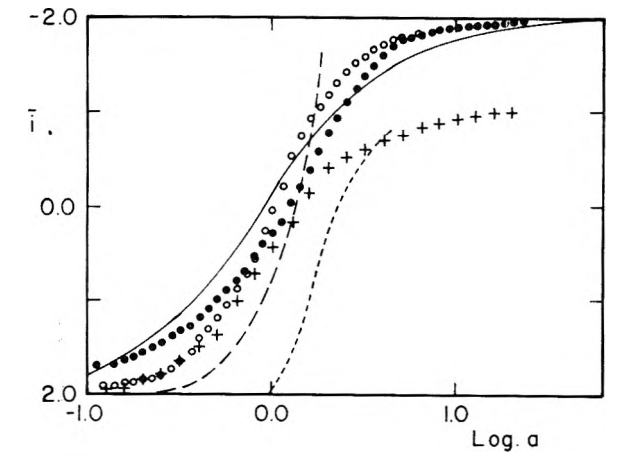

Fig. 6.—Charge number (average charge) of zinc chloride complexes, $\bar{\imath}$, *vs.* solution activity function, $\log a$. Solid line, this work; short dashes, Kraus and Nelson[31] with Debye–Hückel correction; long dashes, same with additional linear term in activity coefficient; ●, calculated from Short and Morris[22]; ○, from Shchukarev, Lilich, and Latysheva[23]; +, from Kivalo and Luoto.[25]

This shows that the secondary cation effect is due mainly to differences in the invasion of the various electrolytes. An exception to this are the data for high concentrations of hydrochloric acid, the well known "HCl effect," where an additional explanation is necessary.

The normalized data can be analyzed according to eq. 4 to give values of K_{Zn} and of the over-all stability constants, referred to the neutral complex, β_i^*. The higher zinc chloride complexes have been studied by a number of authors, who gave stability constants. The constants given by Short and Morris,[22] inserted in eq. 4 with an adjusted value of K_{Zn}, describe the data fairly well (dashed curve in Fig. 5); those of Shchukarev, Lilich, and Latysheva[23] do so somewhat less well. It is clearly seen that a doubly charged anionic complex becomes important at higher concentrations of chloride so that the sets of three constants given by Sillén and Liljequist,[24] and by Kivalo and Luoto[25] are inadequate.

The data are not sufficiently accurate to permit the calculation of four independent complexity constants and may be best described by the two parameter method of Dyrssen and Sillén.[26] These authors define an "average complexity constant" y and a "spreading factor" x, which for the case of the zinc chloride complexes become

$$y = {}^1/_4 (\log \beta_2' - \log \beta_{-2}') \quad (5)$$

$$x = \log \beta_i' - {}^1/_2 (\log \beta_{i+1}' - \log \beta_{i-1}') \quad (6)$$

so that the complex formation constants may be expressed as[27]

$$\log \beta_i' = iy - i^2x \quad (7)$$

According to the two parameter method,[26] the asymptotes to the experimental curve with slopes +2.00 and −2.00 meet at the point A (Fig. 5), the coördinates of which are given by

$$\log a_A = -y = -0.05$$

$$\log D_A = \log K_{Zn} + 4x = 2.77 \quad (8, 8a)$$

The point B on the data curve directly below this has the ordinate value

$$\log D_B = \log K_{Zn} + 4x - \log [2 + (2 \times 10^{-3x}) + 10^{-4x}] \quad (9)$$

From eq. 8, 8a, and 9, the three parameters K_{Zn}, y, and x may be obtained by curve fitting.[28] The values so obtained are $\log K_{Zn}$ (8% cross linking) = 2.26, $y = 0.05$, $x = 0.127$ (all ±0.05).[29] The two parameter approach does not permit a decision to be made on which of the intermediate complexes $ZnCl^+$, $ZnCl_2$, and $ZnCl_3^-$, is relatively more important. As pointed out, among others, by Wormser,[30] data such as those presented here may be interpreted in terms of only some of all possible intermediate species.

Another approach, adopted by Kraus and Nelson, is to calculate the charge number $\bar{\imath}$

$$\bar{\imath} = \mathrm{d} (\log D - 2 \log \bar{a})/\mathrm{d} \log a \quad (10)$$

The results are shown in Fig. 6, compared with the

(22) E. L. Short and D. F. C. Morris, *J. Inorg. Nuclear Chem.*, **18**, 192 (1961).

(23) S. A. Shchukarev, L. S. Lilich, and V. A. Latysheva, *Zh. Neorgan. Khim.*, **1**, 225 (1956).

(24) L. G. Sillén and B. Liljequist, *Svensk Kem. Tidskr.*, **56**, 85 (1944).

(25) P. Kivalo and R. Luoto, *Suomen Kemistilehti*, **30B**, 163 (1957).

(26) D. Dyrssen and L. G. Sillén, *Acta Chem. Scand.*, **7**, 663 (1953).

(27) In this series of papers unprimed constants refer to ligand numbers n, primed constants to charge numbers i. For the zinc chloride system $i = n - 2$, $\beta_i' = \beta_n/\beta_2$.

(28) L. G. Sillén, *Acta Chem. Scand.*, **10**, 186 (1956).

(29) For comparison, the values of $\log \beta_n$ calculated from (7) and those given by Short and Morris[22] are: $\log \beta_1$: 0.43, 0.73; $\log \beta_2$: 0.61, 0.49; $\log \beta_3$: 0.53, −0.20; $\log \beta_4$: 0.20, 0.18. The present data indicate $ZnCl_3^-$ to be more important than Short and Morris suggest.

(30) Y. Wormser, *Bull. soc. chim. France*, 387 (1954).

average charge obtained by Kraus and Nelson,[31] from their anion-exchange data. The latter authors consider the invasion of the resin as negligible, hence they obtain results which bear little resemblance to those of other authors who studied the zinc chloride complexes. One of their curves, which uses the Debye–Hückel correction for the aqueous phase has charges more positive than +2 at low concentrations, the other, which adds a linear term to the activity coefficient correction, tends towards infinite negative charge at higher concentrations. The anion-exchange data obtained in the present work yield charges in line with those calculated from the publications which consider $ZnCl_4^{-2}$ [22,23] but not with those calculated with $ZnCl_3^-$ as the highest complex.[25]

The agreement of the data for the various alkali chlorides shows that the use of the activity function a is reasonable. Difficulties are encountered when polyvalent macro electrolytes are considered,[32] since the mean ionic activity coefficient may not be the best approximation to the ligand single ion activity coefficient. Ryan[33] has criticized the use of the activity function, finding that the absorbance of plutonium(VI) solutions at 948 mμ was not the same for various nitrates at given values of a. Since there are no other data available at present and in view of the success with chloride solutions found also by other workers,[12,14] no comment on the failure in nitrate solutions can now be made.

Concerning the "HCl effect," the position is still not clear. If the hypothesis of Chu and Diamond[7,9] were correct, *i.e.*, if hydrochloric acid formed ion pairs to a much larger extent than lithium chloride in the resin phase, the invasion curves for these two electrolytes should have shown larger differences than they actually do. A large part of the observed effect is explained when the activity function and invasion are considered. However above 5 M hydrochloric acid, the corrected curve for hydrochloric acid becomes steeper than that for lithium chloride. As noted previously, the point of divergence is different for different trace metals, being 0.2 M for cadmium,[5] 9 M for iron(III),[34] and 12 M for silver.[35] An explanation in terms of specific interactions, such as formation of non-absorbable, non-dissociated chloro-metallic acids, may hold after all.

Acknowledgments.—The authors thank Miss S. Yitshaki and Mrs. N. Bauman for technical help in carrying out the experiments. D. M. thanks Prof. G. Stein of the Hebrew University, Jerusalem, and the Scientific Director, Israel Atomic Energy Commission, for making possible the use of the work as part of a Ph.D. thesis.

(31) K. A. Kraus and F. Nelson, "Anion Exchange Studies of Metal Complexes," in "The Structure of Electrolyte Solutions," W. J. Hamer, Editor, John Wiley and Sons, New York, N. Y., 1959.
(32) Y. Marcus, *Acta Chem. Scand.*, **11**, 619 (1957).
(33) J. L. Ryan, *J. Phys. Chem.*, **65**, 1099 (1961).
(34) Y. Marcus, *J. Inorg. Nuclear Chem.*, **12**, 287 (1960).
(35) Y. Marcus, *Bull. Res. Council Israel*, **8A**, 17 (1959).

ANION EXCHANGE OF METAL COMPLEXES. IX.[1] THE EFFECT OF CROSS LINKING

BY Y. MARCUS AND D. MAYDAN[2]

Israel Atomic Energy Commission, Soreq Research Establishment, Radiochemistry Department, Rehovoth, Israel

Received August 17, 1962

Distribution coefficients for zinc, indium, iridium(III), and iodide tracers between sodium chloride solutions and 2, 4, 8, 10, 16, and 24% cross-linked Dowex-1 quaternary ammonium anion-exchange resins have been obtained. The data, corrected for resin invasion and complex formation in solution, yield parameters for the various resins, independent of the chloride concentration. The dependence of these parameters on the cross linking is much higher for the doubly charged zinc complex in the resin than for the singly charged resin species obtained with indium, iridium(III), and iodide. This dependence is explained on the basis of ion pair formation in the resin, using for the effective dielectric constant quantities calculated from the water contents of the various resins.

Introduction

The general increase in selectivity of ion-exchange resins with the cross linking is well known. Anionic metal complexes have also been found to show higher distribution coefficients for anion exchangers, the higher the cross linking of the resin.[1,3-5] One reason for this is the higher concentration of ligand generally obtained in the more highly cross-linked resin. Account of this can be taken by normalizing to a constant value of the resin ligand activity function $\bar{a}$.[1,6] It was found that even after this correction has been applied there remains a cross-linking effect, which is different, for various anions. This work gives a systematic study of this effect, with an attempt to explain it in terms of ion pairing in the resin phase.

Experimental

Materials.—The properties of the anion-exchange resins used, Dowex-1, poly-(styrene(methylene trimethylammonium)), cross-linked by divinylbenzene(DVB), have been determined and are shown in Table I.

The zinc and iodide tracers used were the same as described previously.[1] Indium-115 tracer was obtained from R.C.C., Amersham, England, and Ir-192 was obtained by irradiating $(NH_4)_3IrCl_6$ in the Israel Research Reactor. The iridium tracer was purified from Ir(IV) on an anion-exchange column.

Distribution Measurements.—These measurements were made as described previously.[1]

(1) Previous paper in series: Y. Marcus and D. Maydan, *J. Phys. Chem.*, **67**, 979 (1963). *Cf.* Israel A.E.C. Report IA-779 (1962).
(2) Taken from part of a Ph.D. thesis submitted by (Mrs.) D. Maydan to the Hebrew University, Jerusalem, March, 1962.
(3) R. H. Herber, K. Tongue, and J. W. Irvine, Jr., *J. Am. Chem. Soc.*, **77**, 5840 (1955).
(4) J. Aveston, D. A. Everest, and R. A. Wells, *J. Chem. Soc.*, 231 (1958).
(5) B. Chu, Ph.D. Thesis, Cornell University, 1959.
(6) Y. Marcus and C. D. Coryell, *Bull. Res. Council Israel*, **8A**, 1 (1959).

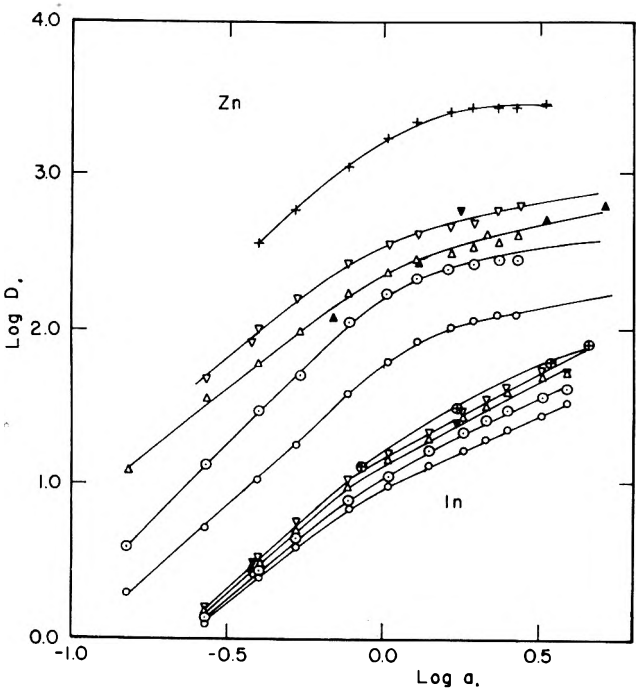

Fig. 1.—Distribution coefficients for zinc and indium, log D, *vs.* solution activity function of sodium chloride, log a. Resin cross linking: ○, 2%; ⊙, 4%; △, 8%; ▽, 10%; +, 16%. Filled points and surrounded crosses are from Chu.[5]

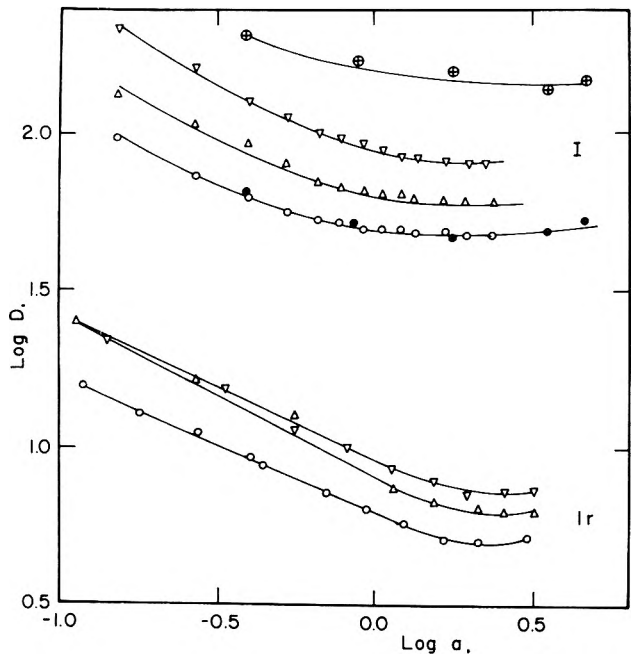

Fig. 2.—Distribution coefficients for iodide and iridium(III), log D, *vs.* solution activity function of sodium chloride, log a. Symbols as in Fig. 1.

Results

The distribution coefficients of zinc, indium, iodide, and irridium between the various resins and sodium chloride solutions are shown in Fig. 1 and 2. The few values available from the work of Chu[5] for these tracers and sodium chloride solutions are also shown. Distribution curves for indium and zinc tracers and 24% cross-linked resin were obtained, but because of the low capacity of the resin are not comparable with the other results.

It has been shown previously,[1,6] that the distribution coefficient D_j for a given tracer j may be expressed as

TABLE I

Cross linking nominal % DVB	Dry capacity, meq./g. air dried resin Cl^-	Wet capacity, meq./g. water swollen resin Cl^-	Water content, wt. % H_2O in water swollen resin Cl^-	Equiv. vol. ml./equiv. water swollen resin Cl^-	Resin ligand activity function log $\bar{a}$ (a_{NaCl} = 1)
2	3.3	1.11	78.0	900	0.19
4	3.5	1.85	66.0	540	.30
8	3.2	1.90	58.5	525	.33
10	3.0	2.04	55.0	490	.36
16	..	2.00	48.0	500	.35
24[a]	..	1.10	20.0	905	(0.09)[b]

[a] A gift of resin sample by Dr. Wheaton of the Dow Chemical Corporation is gratefully acknowledged. [b] Estimated from an extrapolation of the relation between $\bar{a}$ and the wet capacity for the other resins. The invasion of this resin by electrolyte, even in concentrated sodium chloride solutions, has been found to be below the amount measurable.

function of the ligand activity function in the solution $a = m_{NaCl}\,\gamma_{\pm NaCl}$ as

$$\log D_j = \log K_j + p_j \log \bar{a} - \log \sum_{-m}^{N-m} \beta_i'^* a^i \quad (1)$$

In this expression K_j is a parameter specific for the tracer and the resin, but independent of a, p_j is the charge of the predominant species of the tracer in the resin, and $\bar{a}$ is the resin ligand activity function. In the case of anionic complexes, $\beta_i'^*$ are over-all complex formation constants, referred to the neutral complex MCl_m, whereas for a stable anion B^{p-} like iodide, log $\Sigma\beta_i'^* a^i$ is replaced by $p \log a$.

The value of p for iodide is 1, for the zinc complex it is 2[1] and for the indium complex it is 1.[7] Kraus, Nelson, and Smith[8] assumed that iridium(III) is present as $IrCl_6^{3-}$ in chloride solutions, and would pass as such into the resin, although only to a negligible extent, because the resin prefers mononegative species. Contrary to their findings, however, Berman and McBryde[9] found appreciable (log D up to 3.0) absorption of Ir(III) from dilute hydrochloric acid, and in the present work, too, considerable absorption was found from sodium chloride solutions. Blasius, Preetz, and Schmitt[10] showed that in dilute chloride solutions iridium(III) is largely present as $Ir(H_2O)_2Cl_4^-$. It has been found[11] that in general, many anions tend to exist in the resin phase, which have a low effective dielectric constant, not as the most highly charged anionic complex, if they can easily shed off the last one or two ligands. Hence is assumed that for Ir(III) $p = 1$, and this asssumption leads also to the reasonable result that $Ir(H_2O)_2Cl_4^-$ is the main species in solution over the concentration range studied, as will be seen below.

Using values of log $\beta_i'^*$ for zinc and of log $\bar{a}$ for sodium chloride solutions obtained in the previous paper,[1] values of log $\beta_i'^*$ for indium from the next paper,[7] the values of p_j given above and the experimental log D_j data, the expressions

$$\log K_{Zn} = \log D_{Zn} - 2 \log \bar{a} + \log \sum_{-2}^{2} \beta_{i(Zn)}'^* a^i \quad (2)$$

(7) D. Maydan and Y. Marcus, *J. Phys. Chem.*, **67**, 987 (1963).
(8) K. A. Kraus, F. Nelson, and G. W. Smith, *ibid.*, **58**, 11 (1954).
(9) S. S. Berman and W. A. E. McBryde, *Can. J. Chem.*, **36**, 835 (1958).
(10) E. Blasius, W. Preetz, and R. Schmitt, *J. Inorg. Nuclear Chem.*, **19**, 115 (1961).
(11) Y. Marcus, unpublished results. *Cf. Acta Chem. Scand.*, **11**, 619 (1957); *Bull. Res. Council Israel*, **8A**, 17 (1959); Israel A.E.C. Report R-20 (1959); A. Soneson, *Acta Chem. Scand.*, **15**, 1 (1961).

$$\log K_{\mathrm{I}} = \log D_{\mathrm{I}} - \log \bar{a} + \log a \qquad (3)$$

$$\log K_{\mathrm{In}} = \log D_{\mathrm{In}} - \log \bar{a} + \log \sum_{-3}^{1} \beta_{i(\mathrm{In})}{}'^{*}\, a^{i} \qquad (4)$$

$$\log K_{\mathrm{Ir}} = \log D_{\mathrm{Ir}} - \log \bar{a} + \log a \qquad (5)$$

were calculated, and are shown in Fig. 3. It is seen that, by and large, K_j is independent of a, as expected from the theory of Marcus and Coryell.[6] It is further seen that, indeed, iodide and iridium(III) behave as simple mononegative anions in the solutions. The behavior of zinc and indium is discussed elsewhere.[1,7] Last, it is seen that the dependence of the parameters K_j (*i.e.*, the distribution coefficients corrected for changes in resin ligand activities, complex formation in the solution, and competition for the ligand) on the cross linking is slight for indium and iridium(III), somewhat higher for iodide, and very appreciable for zinc.

Discussion

To explain the behavior shown by the various anions and resins in Fig. 4, let us first consider the differences exhibited by the resins (Table I). The variation in capacity, leading to a variation of $\bar{a}$, has already been taken into account by eq. 2–5. The differences in equivalent volume, V_{eq}, of the fully swollen resins, although considerable, are related to only slight differences in the distances between exchange sites. The average distance $\bar{d}$, expressed in Å., is given by

$$\bar{d} = 10^{8}(6V_{eq}/N_0)^{1/3} = 1.47V_{eq}{}^{1/3}\ \text{Å}. \qquad (6)$$

and varies at most by 20%, and not in the same direction as the cross linking changes from low to high. The distances, which are 12–14 Å., are similar to the sum of the diameters of the tracer anions and the (methylene trimethyl) ammonium groups of the exchange sites, or even slightly smaller, so that the inter-site distance does not determine the distance of approach of the anions to the positive charges of the sites. Thus, the effect of cross linking is not due to differences in the equivalent volume. Much larger variations in the distances, as obtainable with low capacity resins, or partly protonated weakly basis resins,[4] are necessary for this factor to be of importance.

The water content of the resin, on the other hand, or more precisely the average composition of the resin in terms of organic matter and water, seems to play a major role. A number of authors have explained in a qualitative manner various phenomena in the resin phase in terms of ion-pair formation, depending on the low effective dielectric constant in the resin.[5,12–14] An estimate of this dielectric constant can be made by comparison to mixed solvents, like water–dioxane mixtures. Over not too short distances, such as those characteristic of Bjerrum's treatment of ion pairing, the mixture of resin matrix and water is no less homogeneous than a dioxane–water solution. Equating the effective dielectric constants of the resins to those of dioxane–water mixtures of the same water content on a weight basis, the estimates in Table II were obtained. These values are in the range where association reactions

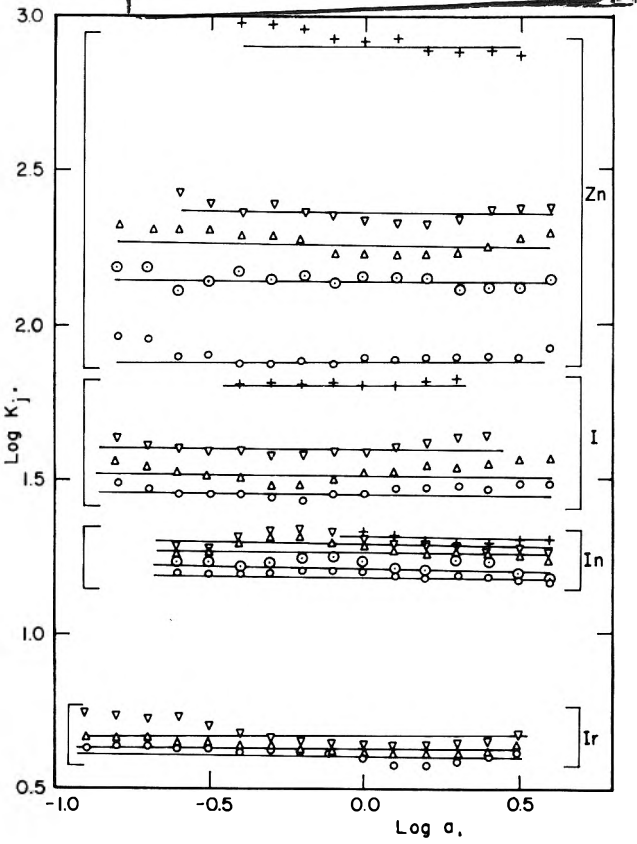

Fig. 3.—The parameter log K_j for zinc, iodide, indium, and iridium(III) tracers *vs.* solution activity function of sodium chloride, log a. Symbols as in Fig. 1. Lines are average values.

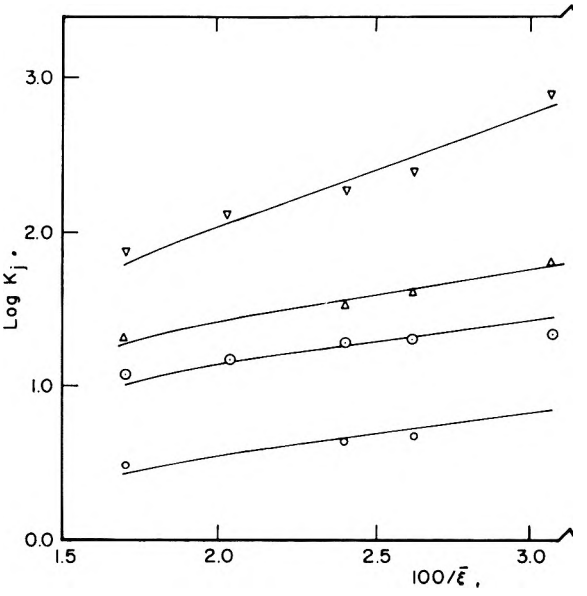

Fig. 4.—The parameter log K_j for zinc, ▽; iodide, △; indium, ⊙; and iridium(III), ○, tracers *vs.* the reciprocal of the effective dielectric constants of the resins, $100/\bar{\epsilon}$. Points are average values from Fig. 4; lines are calculated from eq. 9a.

leading to ion-pair formation have been studied. Denison and Ramsay,[15] found for instance that for tetraisoamylammonium nitrate, which is similar to the ions involved in the present study, the logarithm of the association constant shows a simple inverse proportionality to the dielectric constant of the medium. It is thus likely that the association in the resin may be similarly described.

(12) S. A. Rice and F. E. Harris, *Z. physik. Chem.* (Frankfurt), **8**, 314 (1956).

(13) S. Lindenbaum, C. F. Jumper, and G. G. Boyd, *J. Phys. Chem.*, **63**, 1924 (1959).

(14) R. A. Horne, R. H. Holm, and M. D. Myers, *ibid.*, **61**, 1661 (1957).

(15) J. T. Denison and J. B. Ramsay, *J. Am. Chem. Soc.*, **77**, 2615 (1955).

TABLE II
ESTIMATES OF THE DIELECTRIC CONSTANTS OF ANION-EXCHANGE RESINS

Cross linking nominal % DVB	Water content, wt. %	Effective dielectric constant	Effective radius of chloride $\bar{r}_{Cl}$, Å.	Effective radius of iodide $\bar{r}_I$, Å.
2	78.0	59	3.20	3.22
4	66.0	49	3.11	3.16
8	58.5	42	3.07	3.13
10	55.0	38	3.04	3.10
16	48.0	33	3.98	3.06
24	20.0	10	..	..

Another phenomenon connected with the changes in the water content of the resin is the dehydration of highly hydrated ions. Anions, with which the present work is concerned, are less prone to dehydration; still it should be observable with chloride and, somewhat less with iodide ions. As a rough approximation, it may be assumed that the volume of the hydration shell is proportional to the relative water content of the resin. Hence the radius of the ion in the resin will be given by the expression $\bar{r} = r_{cryst} + (\%\text{ water content}/100)^{1/3} \times (r^0_{hyd} - r_{cryst})$. The values calculated for chloride and iodide, using radii r^0_{hyd} reported by Nightingale,[16] are shown in Table II.

Consider now the reactions leading to the distribution of the tracer anion

$$B^{p-} + p\,\overline{Cl} \rightleftarrows \overline{B}^{p-} + p\,\overline{Cl}^- \quad K_E \qquad (7)$$

$$\overline{B}^{p-} + p\,\overline{R}^+ \rightleftarrows \overline{R_pB} \quad K_P \qquad (8)$$

where B^{p-} is either a stable anion such as I^- or the anionic complex predominant in the resin, MCl^{p-}_{m+p}, and K_E and K_P are the equilibrium constants for the exchange and ion-pairing reactions, respectively. According to Marcus and Coryell,[6] the parameter K_j is proportional to $K_E K_P$. The constant K_E may be calculated using a process in which B^{p-} is transfered in a Born cycle through the gas phase from a medium (water) of dielectric constant ϵ to a medium of dielectric constant $\bar{\epsilon}$, and p chloride ions are transfered in the opposite direction, taking changes in the radii into account.[17] The constant K_P may be calculated from Fuoss' extension[18] of Denison and Ramsay's[15] derivation. The expression obtained is

$$\log K_j = \text{const.} + \log K_E + \log K_P = \log K_E^0 - \frac{0.4343 \cdot 10^8 e^2 p}{2kT}\left[\left(\frac{1}{\epsilon}\left(\frac{p}{r_B} - \frac{1}{r_{Cl}}\right) - \frac{1}{\bar{\epsilon}}\left(\frac{p}{\bar{r}_B} - \frac{1}{\bar{r}_{Cl}}\right)\right] + \log K_p^0 + \frac{0.4343 \cdot 10^8 e^2 p}{kT} \times \frac{1}{\mathring{a}\bar{\epsilon}} \qquad (9)$$

$$\log K_j = \log K_j^0 + \left(\frac{1}{\mathring{a}} - \tfrac{1}{2}\left[\frac{\bar{\epsilon}}{\epsilon}\left(\frac{p}{r_B} - \frac{1}{r_{Cl}}\right) - \left(\frac{p}{\bar{r}_B} - \frac{1}{\bar{r}_{Cl}}\right)\right]\right)\frac{242p}{\bar{\epsilon}} \qquad (9a)$$

where $\log K_j^0$ consists of terms independent of the radii and dielectric constants, $\mathring{a}$ is the closest distance of approach of anion and cation, and r_B, r_{Cl}, $\bar{r}_B$, and $\bar{r}_{Cl}$ the hydrated and partly dehydrated radii of the anions, all in Å. The second term in the brackets in eq. 9a is a relatively small correction term to $1/\mathring{a}$. Values of $r_{Cl} = 3.32$ Å. and $r_I = 3.31$ Å. were taken from Nightingale,[16] values of $\bar{r}_{Cl}$ and $\bar{r}_I$ from Table II. Approximate values for $\bar{r}_B$, assumed equal to r_B for non-hydrated complex anions, were calculated from the tetrahedral radii, and are 3.4 Å. for indium and iridium and 3.3 Å. for zinc, and values of $\mathring{a}$ were obtained by adding the radius of the tetramethylammonium cation, 2.8 Å., to these radii.

The values of $\log K_j$ obtained from eq. 2–5 are plotted *vs.* the reciprocal effective dielectric constant in the resin, $1/\bar{\epsilon}$, in Fig. 4. Curves calculated from eq. 9a are also shown, using arbitrary values for $\log K^0_j$. The slopes of the calculated curves are found to agree with the experimental points. Even in view of the many approximations made, the agreement means that the effects of dehydration, and in particular ion pairing in the resin medium of low effective dielectric constant, can explain the cross-linking effect quantitatively.

The value of p influences the slope of the lines in Fig. 4 considerably. In fact, the above considerations should permit one to decide on its value from the spread in the log D *vs.* log a curves for various cross linkings, since the differences in the (hydrated, or partly dehydrated) radii of the various anions are not so large as to confuse the picture. On this basis, too, the predominant complex for iridium(III) in the resin should be mononegative.

Acknowledgments.—The authors thank Miss S. Yitshaki and Mrs. N. Bauman for technical help in carrying out the experiments. D. M. thanks Prof. G. Stein of the Hebrew University, Jerusalem, and the Scientific Director, Israel Atomic Energy Commission for making possible the use of the work as part of a Ph.D. thesis.

(16) E. R. Nightingale, Jr., *J. Phys. Chem.*, **63**, 1381 (1959).
(17) C. B. Monk, "Electrolytic Dissociation," Academic Press, London and New York, 1961, p. 259.
(18) R. M. Fuoss, *J. Am. Chem. Soc.*, **79**, 3301 (1957).

ANION EXCHANGE OF METAL COMPLEXES. X.[1] THE INDIUM–CHLORIDE SYSTEM. COMPARISON OF RESIN AND LIQUID ANION EXCHANGE

BY D. MAYDAN[2] AND Y. MARCUS

Israel Atomic Energy Commission, Soreq Research Establishment, Radiochemistry Department, Rehovoth, Israel

Received August 7, 1962

Distribution measurements were made of tracer indium ions between Dowex-1, quaternary ammonium anion-exchange resin chloride, and aqueous solutions of sodium chloride. Correcting the distribution data for electrolyte invasion permitted calculation of complex formation parameters for the indium–chloride system. The same set of parameters describes also the liquid distribution data obtained with triisoöctylammonium chloride in xylene and sodium chloride and dilute hydrochloric acid solutions. The species predominant in the resin phase is $InCl_4^-$, those in the liquid amine phase are $RInCl_4$ and R_3InCl_6, dependent on concentration; the difference is attributed to differences in the effective dielectric constants of the media.

Introduction

The indium chloride complex system shows interesting features that make the study of the anionic species formed of special importance. Although it is formally similar to, *e.g.*, the iron(III) and gallium systems, indium shows much lower distribution coefficients both in anion exchange[3] and solvent extraction.[4,5] This may be due to a tendency to form anionic complexes higher than $InCl_4^-$, the species involved in the extraction by ether or similar solvents, or in anion exchange.[3] Indeed, Woodward and Taylor[6] found that the Raman spectrum of concentrated aqueous solutions of indium chloride, containing up to 15 *M* hydrochloric acid, indicates the absence of significant quantities of $InCl_4^-$ in these solutions. They suggested that $InCl_5^{2-}$ and $InCl_6^{3-}$ should be the predominant species. Solvent extraction measurements,[7,8] however, gave such small values for the formation constants of $InCl_3$ and $InCl_4^-$, that the probability for higher complexes would be negligible. An alternative explanation of the low distribution coefficients and the Raman results would be a possible tendency of indium to retain octahedral coördination, so that the probability of the reaction

$$MCl_3(H_2O)_3 + Cl^- \rightleftarrows MCl_4^- + 3H_2O \qquad (1)$$

which is very high for, *e.g.*, gold or gallium, and high for iron(III), would be low for indium (and iridium-(III)[1]), having to compete with the reaction

$$MCl_3(H_2O)_3 + Cl^- \rightleftarrows MCl_4(H_2O)_2^- + H_2O \quad (2)$$

where the octahedral, hydrated species, show preference for the aqueous phase, interacting with the water much more than the tetrahedral MCl_4^-.

Published anion-exchange data for indium are scant,[3,9,10] and do not permit detailed analysis in terms of the species involved. Additional data are therefore desirable. Another fruitful approach to the study of the higher chloride complexes is extraction by liquid anion exchangers, *i.e.*, long chain amines. Their use has been shown to yield information on the species in both the organic and aqueous phases.[11,12] Some amine extraction data were found also for indium chloride.[13,14] The present work is a detailed study of the formation of the higher indium chloride complexes using anion exchange[15] and amine extraction techniques.

Experimental

Materials.—The resins and In^{114} tracers used have been described previously.[16] The triisoöctylamine, (TIOA, R_3N) kindly furnished by Dr. Kertes of the Hebrew University, Jerusalem, was purified by distillation, and was found by titration to be 98% pure. The amine was neutralized with 2 *M* hydrochloric acid, washed with water, and pre-equilibrated with the solution used for the indium distribution measurements.

Methods.—Anion-exchange distribution measurements were made by the continuous flow method previously described.[16] Amine extraction measurements were made by batch equilibration for 24 hr. of the amine at a given concentration in xylene, with aqueous solutions of hydrochloric acid or sodium chloride containing the indium tracer. Aliquots of both phases were counted in a well scintillation counter after phase separation by centrifugation. Loading experiments were made by determining the gain of weight of a resin column after percolating through a large excess of indium chloride solutions in dilute hydrochloric acid, correcting for interstitial and imbibed solution.

Results

The distribution data for indium between sodium chloride solutions and anion-exchange resins of various cross linkings have been given in the previous paper.[1] Distribution coefficients given by Sudèn[10] for sodium chloride solutions were obtained with the resin Amberlite IRA-400 for which no invasion data are available, so that no comparison can be made. The few data given by Chu[17] are in good agreement with ours.

The distribution data for indium between TIOA hydrochloride in xylene and hydrochloric acid and sodium chloride solutions are shown in Fig. 1 and 2, respectively, as function of amine concentration, and in Fig. 3 as function of the chloride activity function *a*. Data by White, Kelly, and Li for tri-*n*-octylamine are shown for comparison; they agree well with the present data. Values obtained by Nakagawa[13] for

(1) Previous paper in series: IX. Y. Marcus and D. Maydan, *J. Phys. Chem.*, **67**, 983 (1963). Preliminary communication: D. Maydan, *Bull. Res. Council Israel*, **10A**, 91 (1961). *Cf.* Israel AEC Report IA-780 (1962).

(2) Taken from a part of a Ph.D. thesis submitted by (Mrs.) D. Maydan to the Hebrew University, Jerusalem, March, 1962.

(3) K. A. Kraus, F. Nelson, and G. W. Smith, *J. Phys. Chem.*, **58**, 11 (1954).

(4) R. M. Diamond, *ibid.*, **61**, 1522 (1957).

(5) H. Irving and F. J. C. Rossotti, *J. Chem. Soc.*, 1946 (1955).

(6) L. A. Woodward and M. J. Taylor, *ibid.*, 4473 (1960).

(7) R. J. Dietz, Jr., Ph.D. Thesis, M.I.T., 1958.

(8) J. S. Mendez, Ph.D. Thesis, M.I.T., 1959.

(9) E. P. Tsintsevich, I. P. Alimarin, and L. I. Nikolaeva, *Vestn. Moskov. Univ. Ser. Mat., Mekh., Astron., Fis. i Khim.*, **14**, No. 2, 189 (1959).

(10) N. Sundèn, *Svensk Kem. Tidskr.*, **66**, 173 (1954).

(11) U. Schindewolf, *Z. Elektrochem.*, **62**, 335 (1958).

(12) K. A. Allen, *J. Am. Chem. Soc.*, **80**, 4133 (1958).

(13) G. Nakagawa, *J. Chem. Soc. Japan, Pure Chem. Sect.*, **81**, 1533 (1960).

(14) J. M. White, P. Kelly, and N. C. Li, *J. Inorg. Nuclear Chem.*, **16**, 337 (1961).

(15) Y. Marcus and C. D. Coryell, *Bull. Res. Council Israel*, **8A**, 1 (1959).

(16) Y. Marcus and D. Maydan, *J. Phys. Chem.*, **67**, 979 (1963).

(17) B. Chu, Ph.D. Thesis, Cornell University, 1959.

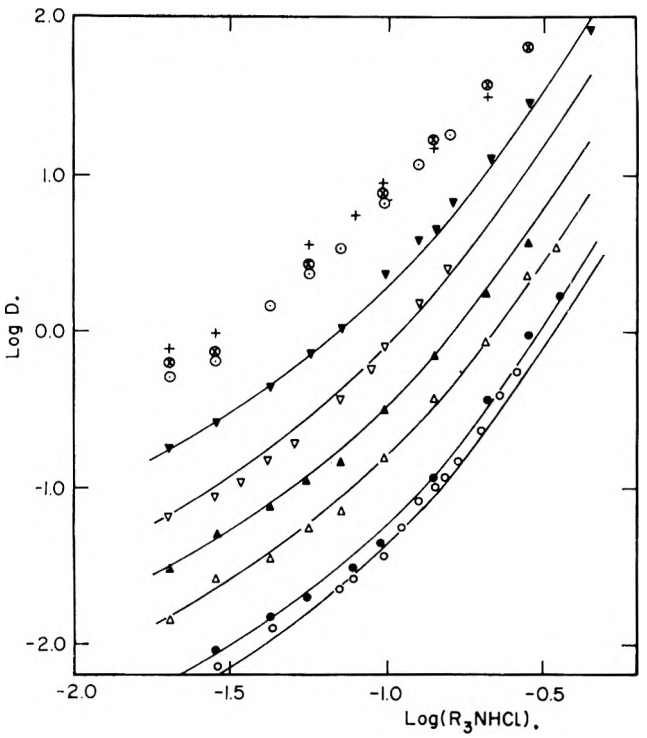

Fig. 1.—Distribution of indium tracer between triisoöctylammonium chloride in xylene and hydrochloric acid, as function of molar amine concentration. Concentration of HCl: ○, 0.075 *M*; ●, 0.10 *M*; △, 0.25 *M*; ▲, 0.50 *M*; ▽, 0.75 *M*; ▼, 1.85 *M*; ⊙, 3.0 *M*; ⊗, 4.0 *M*; + 9.0 *M*. Curves are calculated from eq. 10.

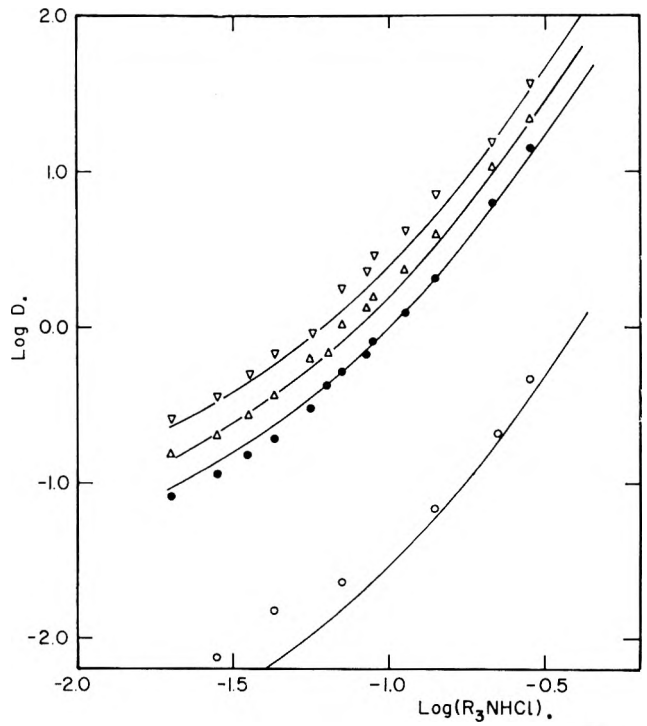

Fig. 2.—Distribution of indium tracer between triisoöctylammonium chloride in xylene and sodium chloride solutions, as function of molar amine concentration. Concentration of NaCl: ○, 0.10 *M*; ●, 2.0 *M*; △, 3.0 *M*; ▽, 4.0 *M*. Curves are calculated from eq. 10.

the secondary amine Amberlite LA-1 (not shown) differ considerably.

Loading experiments with 0.1, 0.2, and 0.5 *M* indium chloride in equimolar hydrochloric acid showed 1.23, 1.07, and 0.86 equivalents of resin per mole of indium chloride, respectively, *i.e.*, formation of $R^+InCl_4^-$.

It has been shown[15] that the anion-exchange distribution coefficients D may be expressed as a function of the ligand activity function $a = m_{NaCl}\gamma_{\pm NaCl}$ as

$$\log D = \log K + p \log \bar{a} - \log \sum_{-3}^{N-3} \beta_i'^* a^i \quad (3)$$

K is a parameter independent of a and characteristic of the tracer and the resin, $-p$ is the charge of the predominant species of the tracer in the resin, and $\bar{a}$ is the resin ligand activity function. The parameters $\beta_i'^*$ are over-all complex formation constants, referred to the neutral complex $InCl_3$.

The value of p at high loading and macro concentrations of indium was found to be one, and it is assumed that the same value holds also at tracer concentrations of indium. Taking values of $\log \bar{a}$ from previous work,[16] and correcting for changes in cross linking by normalizing to 8% cross-linked resin,[1,16] values of

$$\log D - \log \bar{a} - \Delta = \log K \text{ (8\% cross linking)} - \log \sum_{-3}^{N-3} \beta_i'^* a^i \quad (4)$$

as function of $\log a$ were obtained, and are shown in Fig. 4. The points are seen to fall on a single curve, which may be analyzed in terms of the parameters K and $\beta_i'^*$. The initial and final slopes of the curve in the range of measurement are +1.5 and −0.7, indicating the presence of the complexes $InCl^{2+}$, $InCl_2^+$, $InCl_3$, and $InCl_4^-$ (neglecting possible coördinatively bound water), with no free In^{3+} ions. Use of iterative curve fitting[15] gave the following values of the parameters

$$\log K \text{ (8\%)} = 1.00 \pm 0.02$$

$$\log \beta_{-2}'^* = -0.50 \pm 0.05;$$

$$\log \beta_{-1}'^* = -0.45 \pm 0.05; \ (\log \beta_0'^* = 0.00);$$

$$\log \beta_{+1}'^* = -1.6 \pm 0.1$$

and a curve calculated with them is seen in Fig. 4 to describe the data adequately.

The amine extraction data can be described by considering the reaction

$$InCl_3 + q\ RCl_{or} \rightleftharpoons Rq\ InCl_{3+q\ or} \quad (5)$$

in a way formally similar to the one used in anion exchange.[15] Neglecting as a first approximation nonideality of the organic phase, the distribution coefficient for indium may be expressed as

$$\log D' = \log K' + q \log (RCl) - \log \sum_{-3}^{N-3} \beta_i'^* a^i \quad (6)$$

With this assumption, $\partial \log K' (RCl)^q / \partial \log a = 0$, and hence D' will be the same function of a at a given value of (RCl) as $\log D - \log \bar{a}$, given in eq. 4. Using the parameters calculated from the anion-exchange data, and in addition $\log \beta_{-3}'^* \sim -3$, the curve drawn in Fig. 3 is obtained, in reasonable agreement with the data, except at very high concentrations of sodium chloride and in particular hydrochloric acid. The assumption $\partial \log (RCl)/\partial \log a = 0$ is no doubt not valid at these concentrations, since it has been shown that additional hydrochloric acid above the amount

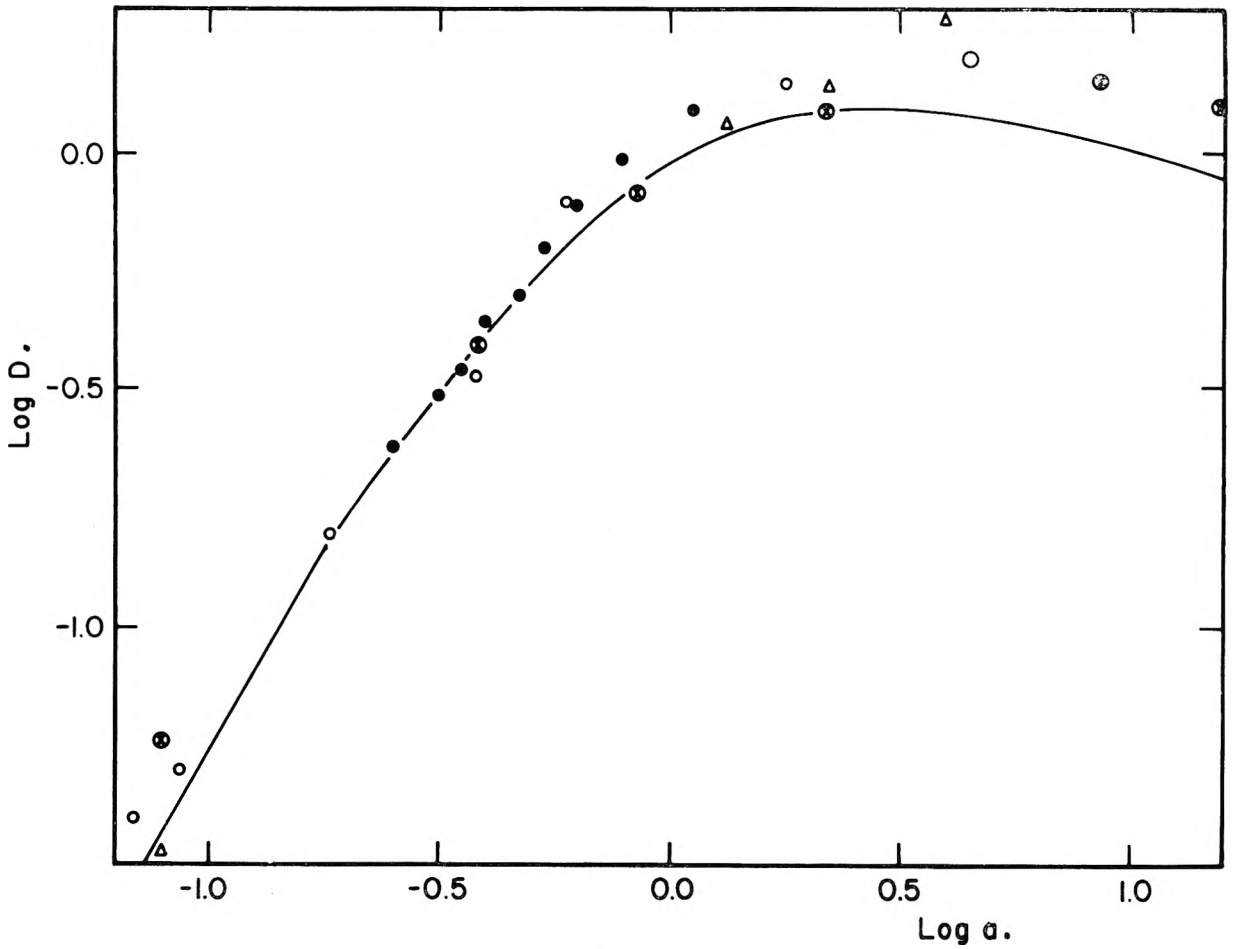

Fig. 3.—Distribution of indium tracer between 0.10 M triisooctylammonium chloride in xylene and sodium chloride △ and hydrochloric acid ○ solutions, as function of chloride activity function a. ●, data from White, Kelly, and Li[14]; ⊗, points derived from polarographic data of Schufle, Stubbs, and Witman[22] according to eq. 11, with const. = 3.50. Curve calculated from eq. 10.

required for neutralization, reacts with the amine, above about 3 M hydrochloric acid.[18]

On the other hand, the differentiation

$$\left(\frac{\partial \log D'}{\partial \log (\mathrm{RCl})}\right)_a = q \qquad (7)$$

will yield the number of amine hydrochloride molecules reacting with one indium chloride molecule. Figures 1 and 2 show that this quantity is not constant. Over a certain range, q approximates 2, as White, Kelly and Li[14] concluded from rather few experimental points. However, it is seen that q tends toward the limiting values 1 and 3 as the concentration of amine hydrochloride tends towards very small or very large values. Thus, depending on the amine hydrochloride concentration the two following reactions take place

$$\mathrm{InCl_3} + \mathrm{RCl_{or}} \rightleftarrows \mathrm{RInCl_{4\,or}} \quad K_1' \qquad (8)$$

$$\mathrm{InCl_3} + 3\mathrm{RCl_{or}} \rightleftarrows \mathrm{R_3InCl_{6\,or}} \quad K_3' \qquad (9)$$

with the distribution coefficient obeying the relationship

$$\log D = \log K_1' + \log (\mathrm{RCl}) + \log\left(1 + \frac{K_3'}{K_1'}(\mathrm{RCl})^2\right) - \log \sum_{-3}^{N-3} \beta_i'^* a^i \qquad (10)$$

The values obtained by extrapolation are log K_1' = 1.0 ± 0.1 and log K_3' = 3.1 ± 0.1. Curves calculated with these two constants and the $\beta_i'^*$ constants reported above are seen in Fig. 1 and 2 to agree with the data. At high hydrochloric acid concentrations the slope q becomes smaller, and does not reach an upper limiting value of three. This may be attributed to formation of species such as R_2HInCl_6 and RH_2InCl_6, in addition to the non-ideality of the solutions.

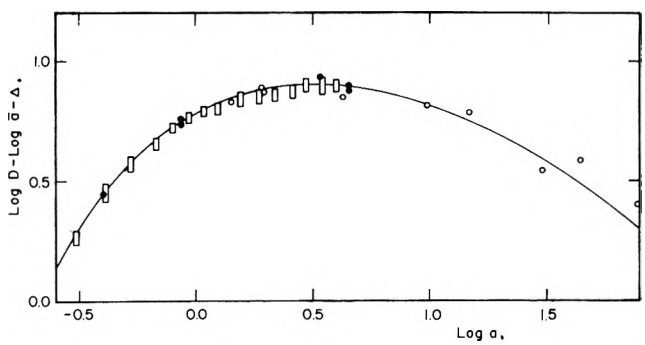

Fig. 4.—Distribution of indium tracer between anion-exchange resins and alkali chloride solutions, corrected for resin invasion and differences in cross linking, as function of chloride activity function. □, data[1] indicating range of points for various cross-linking. Data from Chu[17]: ●, for NaCl, ○, for LiCl. Curve calculated from eq. 10.

Discussion

Both the anion exchange and the extraction data indicate that in the range of concentrations studied, *i.e.*, up to *ca.* 6 M lithium chloride, no anionic species higher than $InCl_4^-$ are formed in the aqueous phase.

(18) U. Bertocci and G. Rolandi, *J. Inorg. Nuclear Chem.*, **23**, 323 (1961).

The stability of the complexes found in this work may be compared to the findings of other workers in Table I. A critical survey by Carleson and Irving[19] showed

TABLE I

Author	Method, conditions	log β_{-2}'*	log β_{-1}'*	log β_1'*
Carleson[20]	Cation exchange, 20°, 0.69 *M* H(ClO_4 + Cl) medium, pH 0.16	−1.82	−0.43	
Dietz[7]	Ether extraction, varying HCl medium		.53	−1.26
Mendez[8]	Nitrobenzene extraction, varying HCl medium		.32	−1.12
This work	Anion exchange, amine extraction, varying HCl and NaCl media	−0.50	− .45	−1.6

that earlier values of constants for formation of $InCl_2^+$ and $InCl_3$ probably are incorrect. In particular, the polarographic work of Schufle, Stubbs, and Witman[22] may be reevaluated, taking account of the irreversibility of the wave in absence of chloride.[23] Referring the half wave potentials $E_{1/2}$, in mv., to the extrapolated value for zero hydrochloric acid concentration[23] instead of to the perchlorate solution,[22] permits the calculation of the left side of the eq.

$$-\log \Sigma\beta_i'^* a^i = \text{const.} + 3\log a - 3(E_{1/2} - E_{1/2}^0)/0.059 \quad (11)$$

as function of log a, giving values agreeing with those obtained in the present work (Fig. 3). The present work leads to the conclusion that $InCl_2^+$ is relatively less important than found by Carleson, while $InCl_3$ is more important than found by Dietz and Mendez. In any case, this work agrees with previous work in showing the absence of $InCl_5^{2-}$ and $InCl_6^{3-}$ in aqueous solutions.

If in aqueous solutions higher anionic complexes are not formed, it is reasonable that this would also be the case in the anion-exchange resin phase, with its lower effective dielectric constant, because of the repulsion of the negative charges. This argument holds, however, only if the species are ionic, as they probably are at the dielectric constants encountered in the resin and aqueous solutions. In xylene solutions of triisoöctylammonium chloride, however, the dielectric constant is presumably so low that no ionic dissociation occurs. Under such conditions it is conceivable that amine hydrochloride molecules react with neutral indium chloride molecules to give neutral species with more than four chloride ligands. If indeed indium tends to retain hexacoördination, the species $RIn(H_2O)_2Cl_4$ and R_3InCl_6 are likely in the organic phase (with possibly some of the intermediate $R_2In(H_2O)Cl_5$, although the present results do not require its consideration). The important point here is, that contrary to former belief,[11,24] it is not possible to conclude from the species found in the organic phase in amine extraction experiments on the species predominant in the resin in the corresponding anion-exchange experiments. The different mechanisms of distribution, due to great differences in the effective dielectric constant, would make such a direct comparison generally invalid.

Acknowledgments.—The authors thank Miss S. Yitshaki and Mrs. N. Bauman for technical help in carrying out the experiments. D. M. thanks Prof. G. Stein of the Hebrew University, Jerusalem, and the Scientific Director, Israel Atomic Energy Commission, for making possible the use of the work as part of a Ph.D. thesis.

(19) B. G. F. Carleson and H. Irving, *J. Chem. Soc.*, 4390 (1954).

(20) The values reported by Carleson[19] are valid for constant ionic strength, and hence are not truly β_i'* values. To convert them, $-i$ log $\gamma_{\pm HCl}$ at ionic strength 0.69 was added to the constants.[21]

(21) G. P. Haigt, Jr., J. Zoltevicz, and W. Evans, *Acta Chem. Scand.*, **16**, 311 (1962).

(22) J. A. Schufle, M. F. Stubbs, and R. E. Witman, *J. Am. Chem. Soc.*, **73**, 1013 (1951).

(23) E. D. Moorhead and W. M. MacNevin, *Anal. Chem.*, **34**, 269 (1962).

(24) Y. Marcus, *Bull. Res. Council Israel*, **8A**, 17 (1959).

ION EXCLUSION AND SALT FILTERING WITH POROUS ION-EXCHANGE MATERIALS[1]

BY LAWRENCE DRESNER AND KURT A. KRAUS

Oak Ridge National Laboratory, Oak Ridge, Tennessee

Received August 20, 1962

A theoretical analysis is given of the salt filtering properties of microporous bodies composed of particles with ion-exchange active surfaces. The computations are based on solutions of the Poisson–Boltzmann equation for uniformly charged cylindrical micropores and for a regular lattice of charged rods; point charges are assumed for the interstitial solution. The results are discussed in terms of anticipated salt rejection as a function of effective pore radius.

Ion-exchange materials have long been known to have the property of excluding electrolytes. In general, the concentration of invading electrolyte in an ion exchanger is less than in the surrounding aqueous phase provided the concentration of the latter is not too high. The ability of exchangers to exclude electrolytes forms the basis of the ion exclusion process[2] and of the electrodialysis method for desalination. It should also be useable for desalination in a hyperfiltration (reverse osmosis) method, since the relative transport of water and salts through an exchanger membrane should be closely related to their relative amounts in the membrane. Salt filtration by ion-exchange membranes was discussed in considerable detail, and with good coverage of the earlier literature, by McKelvey,

(1) Work performed for the Office of Saline Water, U. S. Department of the Interior, at the Oak Ridge National Laboratory, Oak Ridge, Tennessee, operated by Union Carbide Corporation for the U. S. Atomic Energy Commission.

(2) See *e.g.*, R. M. Wheaton and W. C. Bauman, *Ind. Eng. Chem.*, **45**, 228 (1953); *Ann. N. Y. Acad. Sci.*, **57**, 159 (1953).

Spiegler, and Wyllie.[3] These authors studied filtration of NaCl solutions (0.01 to 1 M) and $CaCl_2$ solutions (1 M) with commercial membranes of the type used in electrodialysis equipment. They found reasonably good salt rejection but extremely low flow rates at pressures of 1000 p.s.i.

It thus appeared of interest to examine the principles of salt screening by somewhat more "porous" materials and, in particular, to evaluate the properties of microporous bodies consisting of small surface-charged (ion-exchange active) particles. Such a configuration may be expected to act as a "salt filter" which combines reasonable salt rejection with good flow. Even a relatively small increase in the effective pore size of a "salt filter" compared with the effective pore size of an ion-exchange membrane should cause considerable increase in flow, since, for example, according to Poisseuille's law, laminar flow varies with the fourth power of the pore radius.

1. Thermodynamic Considerations.—The exclusion of electrolytes from ion-exchange materials can readily be understood by considering the condition of equilibrium for any component J

$$\mu_J = \mu_{J(r)} \tag{1}$$

where μ is the chemical potential and the subscript (r) designates the resin phase. When the reference states of J in both phases are the same, eq. 1 yields

$$a_J = a_{J(r)} \tag{2}$$

where a is the activity of J.

Equation 2 holds point by point in each phase and across the phase boundary. When J is a 1–1 electrolyte, then

$$m_1 m_2 \gamma_\pm^2 = m_{1(r)}' m_{2(r)}' \gamma_{\pm(r)}'^2 \tag{3}$$

where m denotes concentration in grams per kg. of water, $\gamma_\pm$ denotes the mean activity coefficient, and the subscripts 1 and 2 denote counter- and co-ions, respectively. The primes on $m_{1(r)}'$ and $m_{2(r)}'$ are to remind the reader that the actual ionic concentrations in the exchanger phase may be strongly non-uniform functions of position. Associated with the actual concentrations is a mean activity coefficient $\gamma_{\pm(r)}'$ assumed space-independent. A more convenient formulation of the equilibrium condition (2) entirely in terms of space-independent (stoichiometric) quantities is

$$m_1 m_2 \gamma_\pm^2 = m_{1(r)} m_{2(r)} \gamma_{\pm(r)}^2 \tag{4}$$

where the unprimed concentrations $m_{1(r)}$ and $m_{2(r)}$ are spatial averages of $m_{1(r)}'$ and $m_{2(r)}'$ over the liquid-filled volume of the exchanger phase or porous body and $\gamma_{\pm(r)}$ is the associated mean activity coefficient.

In addition to eq. 4, the average concentrations in the two phases satisfy the electroneutrality requirements

$$m_1 = m_2 = m_J \tag{5a}$$

$$m_{1(r)} = m_{2(r)} + m_{0(r)} \tag{5b}$$

where $m_{0(r)}$ is the average concentration of fixed ions in the exchanger and is equal to its capacity. Equations 4 and 5 can be solved for the ionic concentrations in the resin and yield[4]

$$m_{1(r)} = (1/2)m_{0(r)} + \sqrt{((1/2)m_{0(r)})^2 + m_J^2(\gamma_\pm^2/\gamma_{\pm(r)}^2)} \tag{6a}$$

$$m_{2(r)} = -(1/2)m_{0(r)} + \sqrt{((1/2)m_{0(r)})^2 + m_J^2(\gamma_\pm^2/\gamma_{\pm(r)}^2)} \tag{6b}$$

When the capacity of the exchanger $m_{0(r)}$ is high enough or the external electrolyte concentration m_J is low enough, the second term in the square root of eq. 6 will be small compared to the first, and eq. 6 may be written with good accuracy as

$$m_{1(r)} = m_{0(r)} \tag{7a}$$

$$m_{2(r)} = \frac{m_J^2}{m_{0(r)}}\left(\frac{\gamma_\pm^2}{\gamma_{\pm(r)}^2}\right) \tag{7b}$$

Another form of the condition of validity of eq. 7 is $m_{2(r)} << m_{0(r)}$. Since $m_{2(r)}$, the co-ion concentration, measures electrolyte invasion relative to water, it follows from eq. 6 or 7 that membranes of high capacity should be the most effective in desalination.

The exclusion of ions from a microporous "salt filter" is also described by eq. 6 or 7. However, in this case, the ratio $\gamma_\pm^2/\gamma_{\pm(r)}^2$ may be much larger than unity if the interstitial pores have radii somewhat greater than the thickness of the diffuse counterion layer near the surface of bed particles. (However, if the pore radius is very much larger or very much smaller than the thickness of the diffuse layer, $\gamma_\pm^2/\gamma_{\pm(r)}^2$ is near unity.) This increase in the ratio $\gamma_\pm^2/\gamma_{\pm(r)}^2$ is due to a decrease in the mean activity coefficient $\gamma_{\pm(r)}$ caused by the strong spatial non-uniformity of the counterion concentration.

The spatial non-uniformity of the counterion distribution will be assumed to be electrostatic in origin, *i.e.*, to arise from the balance of the electrostatic attraction of the counterions to the bed particles and the tendency of the counterions to diffuse away from regions of high concentration. The electrostatic contribution to the mean activity coefficient $\gamma_{\pm(r)}$ for point-ions can be calculated by well known techniques using the Poisson–Boltzmann equation, if the distribution of fixed charges $m_{0(r)}$ is known. In sections 2, 3, 4, and 5 of this paper two charge distributions (cylindrical charged pores and a lattice of charged rods) are analyzed and explicit formulas found for the electrostatic contribution to $\gamma_{\pm(r)}^2$. It is hoped that these computations also characterize porous beds of comparable surface-to-volume ratio. In section 6 these calculations are used to establish the parameters of suitable "salt filters."

2. Equations for the Ion Distribution in a Porous Exchanger.—The spatial variations of the mobile co- and counterion concentrations are related to the electric potential ϕ by Boltzmann's relation, which can be written in a suitably normalized form as

$$m_{i(r)}' = m_{i(r)} \frac{e^{-z_i e\phi/kT}}{\langle e^{-z_i e\phi/kT} \rangle} \qquad i = 1, 2 \tag{8}$$

(3) J. G. McKelvey, K. S. Spiegler, and M. R. J. Wyllie, *Chem. Eng. Progr. Symposium Ser.*, **55**, No. 24, 199 (1959).

(4) K. H. Meyer and J. F. Sievers, *Helv. Chim. Acta*, **19**, 649 (1936); T. Teorell, *Proc. Soc. Exper. Biol. Med.*, **33**, 282 (1935), *Trans. Faraday Soc.*, **33**, 1053 (1937), *Z. Elektrochem.*, **55**, 460 (1951).

where z_i is the valence of ions of type i ($= \pm 1$), k is Boltzmann's constant, T is the absolute temperature, and the braces denote a spatial average over the liquid-filled volume of the microporous bed. According to eq. 8

$$m_{1(r)}'m_{2(r)}' = \frac{m_{1(r)}m_{2(r)}}{\langle e^{-z_1e\phi/kT}\rangle\langle e^{-z_2e\phi/kT}\rangle} \qquad (9)$$

From eq. 3, 4, 8, and 9 it follows that

$$\gamma_{\pm(r)}'^2/\gamma_{\pm(r)}^2 = \langle e^{-z_1e\phi/kT}\rangle\langle e^{-z_2e\phi/kT}\rangle \qquad (10)$$

A similar expression has been derived by Marcus[5] in an analysis of thermodynamic properties of polyelectrolytes. He shows furthermore that since $z_1 = -z_2$, the product of averages on the right hand side of eq. 10 must always be $\geqq 1$. In effect this means that the departure of the mobile ion spatial distributions from uniformity always abets the invasion of the bed by co-ions, since when ϕ is spatially uniform, $\gamma_{\pm(r)}'^2/\gamma_{\pm(r)}^2 = 1$.

The electric potential ϕ is related to the ionic concentrations by Poisson's law[6]

$$\nabla^2\phi = \frac{-z_1e\rho}{\epsilon}(m_{1(r)}' - m_{2(r)}') + \frac{z_1e\rho}{\epsilon}m_{0(r)}' \qquad (11)$$

where ρ is the local density of the water, ϵ is the dielectric constant, and $m_{0(r)}'$ is the local fixed charge concentration. If we introduce the variable $\psi = -z_1e\phi/kT$ for convenience, and combine eq. 6, 8, and 10 with eq. 11, we find the following form of the Poisson–Boltzmann equation for ψ

$$\nabla^2\psi = \frac{e^2m_{0(r)}\rho}{2kT\epsilon} \times \left[\left(1 + \sqrt{1 + \left(\frac{2m_J\gamma_\pm}{m_{0(r)}\gamma_{\pm(r)}'}\right)^2\langle e^{-\psi}\rangle\langle e^{\psi}\rangle}\right)\frac{e^{\psi}}{\langle e^{\psi}\rangle} + \left(1 - \sqrt{1 + \left(\frac{2m_J\gamma_\pm}{m_{0(r)}\gamma_{\pm(r)}'}\right)^2\langle e^{-\psi}\rangle\langle e^{\psi}\rangle}\right)\frac{e^{-\psi}}{\langle e^{-\psi}\rangle} - \frac{2m_{0(r)}'}{m_{0(r)}}\right] \qquad (12)$$

The solution of eq. 12 for ψ and the calculation of the important product $\langle e^{\psi}\rangle\langle e^{-\psi}\rangle$ in general is difficult. In the case of good co-ion exclusion from the microporous bed, simple results are accessible.

3. The Case of Good Exclusion.—In the case of good exclusion $m_{2(r)} << m_{0(r)}$. It follows from eq. 5 and 10 then that the quantity $(2m_J\gamma_\pm/m_{0(r)}\gamma_{\pm(r)}')^2\langle e^{\psi}\rangle\langle e^{-\psi}\rangle$ must be $<< 1$. If we neglect this quantity in eq. 12, it simplifies greatly to

$$\nabla^2\psi = \frac{e^2m_{0(r)}\rho}{kT\epsilon}\left(\frac{e^{\psi}}{\langle e^{\psi}\rangle} - \frac{m_{0(r)}'}{m_{0(r)}}\right) \qquad (13)$$

If we introduce the variables

$$\zeta = \psi - \ln\langle e^{\psi}\rangle \qquad (14a)$$

$$\xi^2 = \frac{e^2m_{0(r)}\rho}{kT\epsilon}r^2 \qquad (14b)$$

where r is the radius vector, eq. 13 becomes

$$\nabla_\xi^2\zeta = e^{\zeta} - \frac{m_{0(r)}'}{m_{0(r)}} \qquad (15)$$

ζ has the properties

$$\langle e^{\zeta}\rangle = 1 \qquad (16a)$$

$$\langle e^{-\zeta}\rangle = \langle e^{\psi}\rangle\langle e^{-\psi}\rangle = \gamma_{\pm(r)}'^2/\gamma_{\pm(r)}^2 \qquad (16b)$$

In order to solve eq. 15 explicitly, the distribution $m_{0(r)}'$ of fixed charges in the bed must be specified. All interesting distributions have the common feature that the fixed charges are localized in or on the bed particles and are not present in the interstitial pores. In such cases, ζ obeys the source-free equation

$$\nabla_\xi^2\zeta = e^{\zeta} \qquad (17)$$

in the interstitial pores, the source $m_{0(r)}'$ being introduced through an appropriately chosen boundary condition.

The earliest and most general solution known to eq. 17 is due to Liouville.[7]

Liouville's solution applies to two dimensions and has the form

$$e^{\zeta} = -8\frac{\left(\frac{\partial u}{\partial x}\right)^2 + \left(\frac{\partial u}{\partial y}\right)^2}{(u^2 + v^2 + 1)^2} \qquad (18)$$

where $u + iv = f(x + iy)$, $\xi^2 = x^2 + y^2$, and f is an arbitrary analytic function. In the case of cylindrical symmetry, Walker[8] has shown that this solution can be written

$$\zeta = -2\ln(a^{-1}\xi^{\beta} + a\xi^{2-\beta}) + \ln[-8(\beta - 1)^2] \qquad (19)$$

where a and β are arbitrary constants. Lemke,[9] Fuoss, *et al.*,[10] and Alfrey, *et al.*,[11] have obtained the same solution by solving eq. 17 directly in cylindrical coördinates.

In view of the accessibility of the cylindrically symmetric solution eq. 19, we shall analyze in detail the following two cylindrically symmetric models of the fixed charge distribution:

(i) The fixed charges are confined to a surface layer of density σ on the inner surface of cylindrical pores of radius R. Solution can only penetrate the interior of the pores; the rest of the bed is impenetrable.

(ii) The fixed charges are disposed in a square lattice of cylindrical charges of density λ per unit length and spacing $R\sqrt{\pi}$, and solution can penetrate all of the bed between them. This model is on the face of it not cylindrically symmetric. By making a Wigner–Seitz type of approximation explained in detail in section 5, a truly cylindrically symmetric problem can be obtained to which the solution eq. 19 can be directly applied. The model then becomes similar to that used by Fuoss, *et al.*,[10] and by Alfrey, *et al.*,[11] in their studies of counterion distributions around rod-shaped polyelectrolytes.

4. The Pore Model.—The boundary conditions determining the constants a and β in the pore model

(5) R. A. Marcus, *J. Chem. Phys.*, **23**, 1057 (1955).

(6) The electrical units are the rationalized meter-kilogram-second-coulomb units described by J. A. Stratton, "Electromagnetic Theory," McGraw–Hill Book Co., New York, N. Y., 1941.

(7) J. Liouville, *J. de Mathem.* [1], **18**, 71 (1853).

(8) G. W. Walker, *Proc. Roy. Soc.* (London), **A41**, 410 (1915).

(9) H. Lemke, *J. Math.*, **142**, No. 2, 118 (1913).

(10) R. M. Fuoss, A. Katchalsky, and S. Lifson, *Proc. Natl. Acad. Sci.*, **37**, 579 (1951).

(11) T. Alfrey, P. W. Berg, and H. Morawetz, *J. Polymer Sci.*, **7**, 543 (1951).

are these: (a) ζ is regular everywhere inside the pore, and (b) $(d\zeta/d\xi)_{\xi=\xi_R} = (1/2)\xi_R$, where ξ_R is the value of ξ corresponding to $r = R$. The boundary condition (b) can be obtained as follows: Outside the pore the electric field vanishes by a simple application of Gauss's law; just inside the pore surface the electric field is equal to $(\sigma/\epsilon)\mathbf{n}$ where $\mathbf{n}$ is the inward normal to the pore surface. Thus $(\partial\phi/\partial r)_{r=R} = \sigma/\epsilon$, from which (b) easily follows by noting that $m_{0(r)}\rho = 2|\sigma|/eR$.

From (a) it follows by integrating eq. 17 over an infinitesimal cylinder of radius ξ around $\xi = 0$ that

$$0 = \left(\frac{d\zeta}{d\xi}\right)_{\xi=0} = \lim_{\xi \to 0}\left[-2\,\frac{\beta a^{-1}\xi^{\beta-1} + (2-\beta)a\xi^{1-\beta}}{a^{-1}\xi^{\beta} + a\xi^{2-\beta}}\right] \quad (20)$$

Only if $\beta = 2$ or 0 is the limit on the right zero. Using either of these values and redefining the arbitrary constant a for convenience by $b\sqrt{-8}$ or $(b\sqrt{-8})^{-1}$, respectively, we can write

$$\zeta = -2\ln\left(b - \frac{\xi^2}{8b}\right) \quad (21)$$

By application of condition (b) we find that

$$b^2 = 1 + (1/8)\xi_R^2 \quad (22)$$

A simple integration shows that

$$\langle e^{-\zeta}\rangle = \frac{1 + (1/8)\xi_R^2 + (1/3)((1/8)\xi_R^2)^2}{1 + (1/8)\xi_R^2} \quad (23)$$

5. The Lattice Model.—The charge lattice can be decomposed into identical, non-overlapping squares of side $R\sqrt{\pi}$, each centered on a charged cylinder. At corresponding points in each of these squares ζ is the same. If we integrate (15) over any such square, we find that the surface integral of the normal derivative of ζ must vanish. If we now make the Wigner–Seitz assumption[12] that replacing this square by a circle of equal area (radius R) will affect the results of our calculation only slightly, we arrive at the boundary condition

$$\left(\frac{d\zeta}{d\xi}\right)_{\xi=\xi_R} = 0 \quad (24a)$$

For simplicity we first treat the case in which the radius of the charged cylinder is zero, *i.e.*, the case of line charges. In this case application of Gauss's law gives

$$\lim_{\xi \to 0}\left(\xi\frac{d\zeta}{d\xi}\right) = -(1/2)\xi_R^2 \quad (24b)$$

The coefficient a in eq. 19 may be determined in terms of β using the boundary condition (24a)

$$a^{-2} = \frac{\beta - 2}{\beta}\,\xi_R^{2(1-\beta)} \quad (25)$$

With this value $\langle e^{-\zeta}\rangle$ can be found in terms of β by simple integration, *viz.*

$$\langle e^{-\zeta}\rangle = \frac{\xi_R^2}{8} \times \frac{12 + 2\beta - \beta^2}{\beta(1+\beta)(2-\beta)(3-\beta)} \quad (26)$$

(12) F. Seitz and E. P. Wigner, *Phys. Rev.*, **43**, 804 (1933).

β can be determined from eq. 24b. To begin with

$$\xi\frac{d\zeta}{d\xi} = -2\beta(2-\beta)\,\frac{(\xi/\xi_R)^{\beta} - (\xi/\xi_R)^{2-\beta}}{(2-\beta)(\xi/\xi_R)^{\beta} - \beta(\xi/\xi_R)^{2-\beta}} \quad (27)$$

so that

$$-(1/2)\xi_R^2 = \lim_{\xi \to 0}\left(\xi\frac{d\zeta}{d\xi}\right) = -2\beta \quad \mathrm{Re}\,\beta < 1 \quad (28a)$$

$$= -2(2-\beta) \quad \mathrm{Re}\,\beta > 1 \quad (28b)$$

Since the extreme left hand side of eq. 28 is real, β is real if $\mathrm{Re}\,\beta \gtrless 1$. In fact

$$\beta = \frac{\xi_R^2}{4} \quad \mathrm{Re}\,\beta < 1 \quad (29a)$$

$$= 2 - \frac{\xi_R^2}{4} \quad \mathrm{Re}\,\beta > 1 \quad (29b)$$

In either case ξ_R must be ≤ 2. Since eq. 26 is invariant to the substitution $\beta \to 2 - \beta$, when $\xi_R \leq 2$

$$\langle e^{-\zeta}\rangle = \frac{\xi_R^2}{8}\left[\frac{12 + 2\beta - \beta^2}{\beta(1+\beta)(2-\beta)(3-\beta)}\right]_{\beta=\xi_R^2/4} \quad \xi_R \leq 2 \quad (30)$$

When $\xi_R > 2$, the only value for $\mathrm{Re}\,\beta$ is unity; thus at most $\beta = 1 + i\omega$, where ω is real. In this case

$$\langle e^{-\zeta}\rangle = \frac{\xi_R^2}{8} \times \frac{13 + \omega^2}{(1+\omega^2)(4+\omega^2)} \quad (31)$$

and

$$-(1/2)\xi_R^2 = \lim_{\xi \to 0}\left(\xi\frac{d\zeta}{d\xi}\right) = \lim_{\xi \to 0}\left[-2(1+\omega^2) \times \frac{(\xi/\xi_R)^{1+i\omega} - (\xi/\xi_R)^{1-i\omega}}{(1-i\omega)(\xi/\xi_R)^{1+i\omega} - (1+i\omega)(\xi/\xi_R)^{1-i\omega}}\right] \quad (32)$$

By substituting

$$x = \ln\left(\frac{\xi_R}{\xi}\right) \quad (33)$$

equation 32 for determining ω can be written

$$\frac{\xi_R^2}{4} = \lim_{x \to \infty}\left(\frac{1+\omega^2}{1 + \omega\cot\omega x}\right) \quad (34)$$

Now for every finite x there is a value of $\omega x < \pi$ such that the bracketed quantity on the right hand side of eq. 34 equals $\xi_R^2/4$.[13] As x becomes larger but remains finite, this value of ω draws closer and closer from below to ω_0, the smallest value of ω at which $1 + \omega\cot\omega x$ vanishes. The larger x is, the closer $\omega_0 x$ is to π. Thus as x grows without bound, ω_0 and therefore ω approach zero but in such a way as to satisfy eq. 34. Thus finally

$$\langle e^{-\zeta}\rangle = \frac{13\xi_R^2}{32} \quad \xi_R > 2 \quad (35)$$

When $\xi_R = 2$, expressions 30 and 35 coincide.

The procedure just outlined for the calculation of $\langle e^{-\zeta}\rangle$ can also be used when the charged cylinders

(13) The restriction of ωx to value $< \pi$ is to ensure that the argument of the logarithm in eq. 19 never vanishes, *i.e.*, that ζ is never singular.

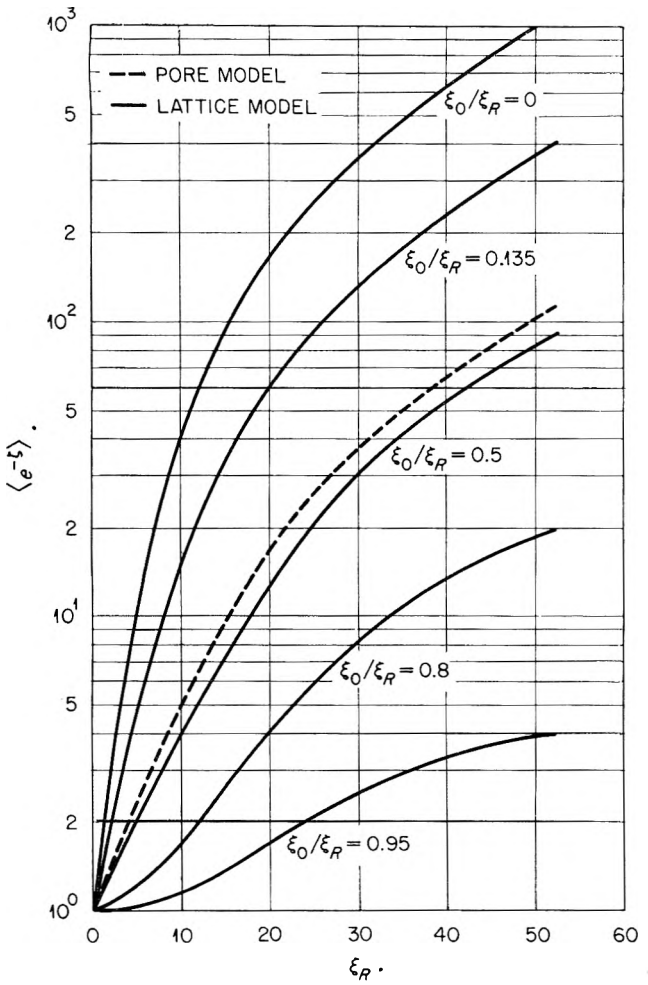

Fig. 1.—The factor $\langle e^{-\zeta} \rangle$ which corrects the square of the salt concentration in the exterior solution for the non-uniform counterion distribution plotted against ξ_R, the dimensionless pore or cell radius. The ratios ξ_0/ξ_R attached to the lattice model curves are the ratios of the dimensionless charge-cylinder radii ξ_0 to the dimensionless cell radii ξ_R.

have a finite radius R_0, although the resulting formulas are more complicated. Equation 28b must now be written

$$\left(\xi \frac{d\zeta}{d\xi}\right)_{\xi = \xi_0} = -(1/2)(\xi_R^2 - \xi_0^2) \qquad (24b')$$

where ξ_0 is the value of ξ corresponding to R_0. When $R_0 \neq 0$, it is convenient to take $\beta = 1 + i\omega$; in terms of ω

$$\langle e^{-\zeta} \rangle = \frac{\xi_R^4}{8(\xi_R^2 - \xi_0^2)} \left[\frac{13 + \omega^2}{(1 + \omega^2)(4 + \omega^2)} - \frac{\xi_0^4}{\xi_R^4 \omega^2} \times \left(1 - 2 \frac{(2 - 4\omega^2) \cos(2\omega x') + (\omega^3 - 5\omega) \sin(2\omega x')}{(1 + \omega^2)(4 + \omega^2)} \right) \right] \qquad (35')$$

where ω now satisfies the equation

$$(1/4)(\xi_R^2 - \xi_0^2) = \frac{1 + \omega^2}{1 + \omega \cot \omega x'} \qquad (34')$$

and x' is defined as

$$x' = \ln\left(\frac{\xi_R}{\xi_0}\right) = \ln\left(\frac{R}{R_0}\right) \qquad (33')$$

In the preceding equations $\omega x'$ is real and $< \pi$ as long as the left hand side of eq. 34′ is $> x'/(x' + 1)$; otherwise it is pure imaginary. The results given in eq. 30, 35, and 35′ for $\langle e^{-\zeta} \rangle$ have been given previously by Marcus.[5]

6. Discussion and Numerical Examples.—The quantity $e^2 m_{0(r)} \rho / kT\epsilon$ is the square of Debye's reciprocal length for the relevant average fixed ion concentration. At 15° and *in vacuo* ($\epsilon = \epsilon_0 = 8.854 \times 10^{-12}$ farad/meter)

$$\frac{e^2}{kT\epsilon_0} = 7292 \text{ Å.} \qquad (36a)$$

so that for the typical conditions $\epsilon/\epsilon_0 = 80$ and $m_{0(r)}\rho = 10$ moles/liter

$$\frac{e^2 m_{0(r)} \rho}{kT\epsilon} = 0.549 \text{ Å.}^{-2} \qquad (36b)$$

Since in what follows interest will mainly be focused on pore and cell radii in the 10 to 100 Å. range, only values of ξ_R up to 50 will be considered. Shown in Fig. 1 are values of $\langle e^{-\zeta} \rangle$ plotted *vs.* ξ_R for both the pore and lattice models. The general trend of these curves can be understood as follows: For small values of ξ_R in either the pore or lattice models or for values of ξ_0/ξ_R near unity in the lattice model, $\langle e^{-\zeta} \rangle$ is near unity. This behavior is a reflection of the fact that the scale of distance over which appreciable changes in ζ can occur is about one unit of ζ. Thus for ξ_R or $\xi_R - \xi_0 << 1$, ζ must be nearly uniform. Furthermore, the more spread out the fixed charge distribution, the lower $\langle e^{-\zeta} \rangle$ will be in general. Thus for large ξ_R, the value of $\langle e^{-\zeta} \rangle$ for the line-charge lattice model ($\xi_0 = 0$) exceeds that for the pore model by about an order of magnitude because the former refers to a line charge whereas in the latter the same charge is spread over the pore surface. By the same token $\langle e^{-\zeta} \rangle$ is doubtless larger in a cubic lattice of point charges than in a square lattice of line charges with the same $m_{0(r)}\rho$ and the same lattice spacing.

The curve marked "Pore Model" in Fig. 1 lies very close to the curve of the lattice model marked "$\xi_0/\xi_R = 0.5$." If ξ_0/ξ_R were about 0.46, the lattice and pore model curves would nearly coincide. This example is only one drawn from the following rule of equivalence between the pore and lattice models: For any given value of ξ_0/ξ_R there is a nearly linear relation between ξ_R and $\xi_{R'}$, where $\xi_{R'}$ is the value of ξ_R for the capillary with the same value of $\langle e^{-\zeta} \rangle$ as the cell considered (see Fig. 2). Shown in Fig. 3 is the ratio $\xi_{R'}/\xi_R$ plotted against ξ_0/ξ_R. In addition three other curves are shown in Fig. 3 based on (i) equal volume-to-surface ratios for the cell and its equivalent pore

$$\xi_{R'}/\xi_R = (\xi_R/\xi_0) - (\xi_0/\xi_R) \qquad (37)$$

(ii) equal volumes, and (iii) equal surfaces. For $\xi_0/\xi_R \gtrsim 0.8$ (which corresponds to a void fraction of 36% or less in the cell) the value of $\xi_{R'}/\xi_R$ obtained from eq. 37 (equal volume-to-surface ratios) agrees well with the exact value. This is fortunate, because a cell and a capillary with the same volume-to-surface ratio have similar fluid flow properties.

The results of the pore model in the case of good exclusion can be expressed in a particularly useful way as follows: eq. 7b can be written with the help of eq. 16b as

$$\frac{m_{0(r)}m_{2(r)}}{\gamma_{\pm}^2 m_J^2} = \langle e^{-\zeta} \rangle \qquad (38)$$

if, as is henceforth assumed, $\gamma_{\pm(r)}'^2 = 1$. For convenience, let us introduce the distance R_∞ defined by

$$\frac{\xi^2_{R\infty}}{24} = \frac{m_{0(r)}m_{2(r)}}{\gamma_{\pm}^2 m_J^2} \qquad (39)$$

In terms of R_∞ the pore radius R may be written as

$$\frac{R}{R_\infty} = \frac{\xi_R}{\xi_{R\infty}} = \sqrt{\frac{\xi_R^2/24}{\langle e^{-\zeta} \rangle}} \qquad (40)$$

From (39) it follows that R_∞ is given by

$$R_\infty^2 = \frac{24kT\epsilon}{e^2} \frac{m_{2(r)}}{\gamma_{\pm}^2 m_J^2 \rho} \qquad (41a)$$

and is independent of $m_{0(r)}$ and a function only of $\gamma_{\pm}^2 m_J^2/m_{2(r)}$. When $\rho = 1$ g./cm.^{3}, $T = 15°$, $\epsilon/\epsilon_0 = 80$, and $m_{2(r)}$ and m_J are expressed in moles/kg. water, eq. 41a can be written

$$R_\infty = 20.9 \, (\gamma_{\pm}^2 m_J^2/m_{2(r)})^{-1/2} \text{ Å.} \qquad (41b)$$

According to eq. 38 and 40 to each value of ξ_R there correspond unique values of $m_{0(r)}m_{2(r)}/\gamma_{\pm}^2 m_J^2$ and R/R_∞. Thus these latter quantities are connected by a unique relationship which is shown in Fig. 4.

One interesting conclusion which Fig. 4 shows clearly is that it is futile to increase $m_{0(r)}$ once it has reached a value several times the quantity $\gamma_{\pm}^2 m_J^2/m_{2(r)}$. On the other hand, if it is not as large as $\gamma_{\pm}^2 m_J^2/m_{2(r)}$, the desired degree of exclusion can never be achieved. Finally, Fig. 4 shows that given $\gamma_{\pm} m_J$ and $m_{2(r)}$, the quantity R_∞ represents the largest pore radius compatible with the desired salt exclusion.

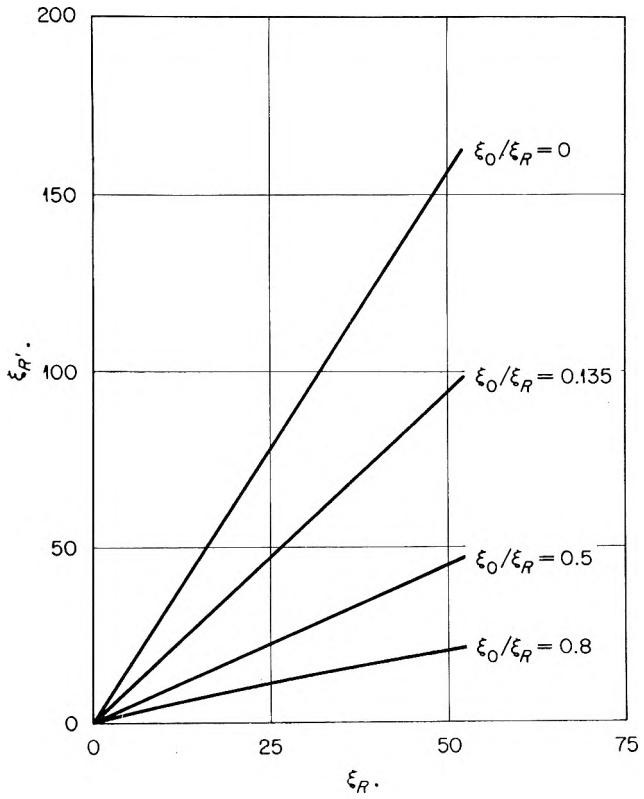

Fig. 2.—The effective dimensionless pore radius ξ_R' of the pore having the same value of $\langle e^{-\zeta} \rangle$ as a lattice cell with a dimensionless charge-cylinder radius ξ_0 and a dimensionless cell radius ξ_R plotted against ξ_R.

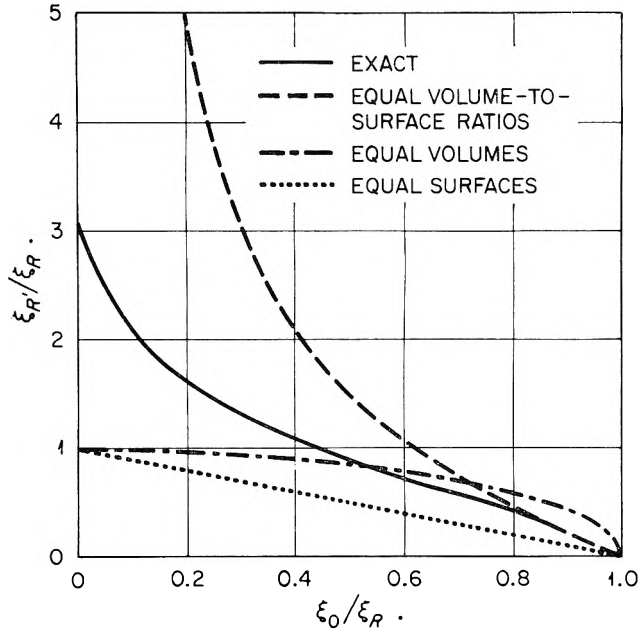

Fig. 3.—The ratio ξ_R'/ξ_R plotted against the ratio ξ_0/ξ_R, where ξ_R' is the effective dimensionless pore radius of the pore having the same value of certain quantities as a lattice cell with a dimensionless charge-cylinder radius ξ_0 and a dimensionless cell radius ξ_R. The curve marked "exact" refers to equal values of the correction factor $\langle e^{-\zeta} \rangle$.

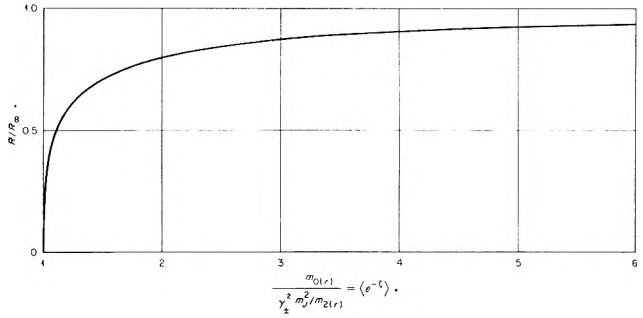

Fig. 4.—The ratio of the pore radius R to the limiting pore radius R_∞ defined in eq. 41 plotted against $\langle e^{-\zeta} \rangle$ in the case of good exclusion. The abscissa also equals the ratio of the capacity $m_{0(r)}$ to the limiting capacity $\gamma_{\pm}^2 m_J^2/m_{2(r)}$.

Using Fig. 4, the following kind of typical design problem can easily be solved. Given a feed water of salinity $\gamma_{\pm} m_J$ and a bed material of surface charge density σ (unit charges/cm.^{2}), what must the pore size R be to maintain a salt concentration $m_{2(r)}$ in the porous bed? For right cylindrical pores, $m_{0(r)}$, σ, and R are related by the equation

$$m_{0(r)}\rho = \frac{2\sigma}{R} \qquad (42a)$$

or its equivalent

$$\frac{R}{R_\infty} \times \frac{m_{0(r)}}{[\gamma_{\pm}^2 m_J^2/m_{2(r)}]} = \frac{2\sigma/R_\infty}{[\rho\gamma_{\pm}^2 m_J^2/m_{2(r)}]} \qquad (42b)$$

The intersection of the hyperbola (42b) with the curve in Fig. 4 gives the desired pore radius R and fixed ion concentration $m_{0(r)}$.

Shown in Table I are some results for the typical cases $\sigma = 0.04$ Å.$^{-2}$, $m_{2(r)} = 0.01$ mole/kg. water, and $\gamma_{\pm} m_J = 0.025$, 0.05, 0.1, and 0.5 mole/kg. water (ρ has been taken as 1 g./cm.^{3}). It is clear from these

results that porous bed salt filters will only be useful for treating waters of low original salinity. It is interesting to note that in all these cases R is quite close to R_∞.

TABLE I

PARAMETERS OF POROUS BED SALT FILTERS FOR WHICH σ = 0.04 Å.$^{-2}$, T = 15°, ρ = 1 G./CM.^{3}, ϵ/ϵ_0 = 80, AND $m_{2(r)}$ = 0.01 MOLE/KG. WATER ACCORDING TO THE PORE MODEL

These results are based on a Donnan exclusion in which the only departures from ideality considered are the electrostatic interactions of the point counterions.

$\gamma_\pm m_J$, mole/kg.	R_∞, Å.	R, Å.	$m_{0(r)}$, mole/kg.
0.025	84	83	1.7
.05	42	41	3.3
.1	21	20	6.7
.5	4.2	3.2	43

Consider next the energy W consumed in viscous flow per unit volume of water traversing the filter, which can be estimated as follows. W is equal to the pressure drop P across the filter. In the pore model, if we assume Poisseuille flow in the pores purely for the sake of argument, W can be written

$$W = \frac{8\eta q d}{\pi R^4} \tag{43}$$

where η is viscosity of the water, d the filter thickness, and q the volume of water put through the filter in unit time. If we use R_∞ in place of R, eq. 43 can be written

$$W \propto \eta d q \rho^2 \frac{\gamma_\pm{}^4 m_J{}^4}{m_{2(r)}{}^2} \tag{44}$$

the factor of proportionality being a combination of various physical constants. Thus for fixed $m_{2(r)}$, the energy consumed per unit throughput varies as the fourth power of the mean activity of the salt in the feed water. (An integration over the parabolic velocity profile characteristic of Poisseuille flow shows the product water salinity to be $(^3/_2)m_{2(r)}$ when $\xi_R \gg 1$).

These conclusions apply to lattice cells with a void fraction of about 36% or less if the relation

$$\frac{R'}{R} = \frac{R}{R_0} - \frac{R_0}{R} \tag{45}$$

is used between the equivalent capillary radius R', the cell radius R, and the charge radius R_0, and if the fixed charge in the lattice model arises from a surface density σ on the cylinder of radius R_0. This can be shown as follows: In the lattice model, $m_{0(r)}\rho$ is given by the equation

$$m_{0(r)}\rho = \frac{2\pi\sigma R_0}{\pi(R^2 - R_0{}^2)} = \frac{2\sigma}{(R^2/R_0) - R_0} = \frac{2\sigma}{R'} \tag{46}$$

Thus $m_{0(r)}\rho$ is the same as in the related capillary. In such a case, eq. 45 becomes identical with eq. 37 and the lattice cell and the equivalent capillary have the same value of $\langle e^{-\zeta}\rangle$. Thus when R'/R_∞ calculated from eq. 45 and 41 is plotted against $\langle e^{-\zeta}\rangle$ for the lattice cell, the curve of Fig. 4 is again obtained. Secondly, the geometric relation (46) between $m_{0(r)}\rho$ and the radius R' from eq. 45 is identical with eq. 42. Thus to each capillary radius R' determined by a given σ and $\gamma_\pm{}^2 m_J{}^2/m_{2(r)}$ there corresponds a manifold of lattice cells (with void fractions not exceeding 36%) whose parameters R and R_0 must satisfy eq. 45.

This is a very satisfactory state of affairs, first because the lattice model is presumably a much better replica of a porous bed than the capillary model, and second because a good way to compare these two dissimilar models is through eq. 45 which says that the volume-to-surface ratio is the same in both models. It is plausible to expect that to every capillary radius R' determined by a σ and a ratio $\gamma_\pm{}^2 m_J{}^2/m_{2(r)}$ there corresponds a porous bed with a volume-to-surface ratio equal to $R'/2$.

Acknowledgment.—We wish to extend our heartfelt gratitude to Prof. George Scatchard for a series of illuminating discussions.

THE STRUCTURE OF ACTIVE CENTERS IN NICKEL CATALYST. II.

BY ITURO UHARA, SHOZO KISHIMOTO, TADASHI HIKINO, YOICHI KAGEYAMA, HIDEBUMI HAMADA, AND YOSHIHIKO NUMATA

Chemistry Department, Faculty of Science, Kobe University, Mikage, Kobe, Japan

Received August 20, 1962

When slightly cold-worked nickel is annealed, the disappearance of vacancies and dislocations takes place at different temperature ranges, T_V and T_D, respectively, and the influence of the degree of cold-working and the existence of impurities on T_D is considerable. The change of the catalytic activities of cold-worked nickel due to annealing at various temperatures was measured for the following reactions: (A) hydrogenation of cinnamic acid, (B) dehydrogenation of ethanol, (C) decomposition of hydrogen peroxide, (D) para-ortho conversion of hydrogen, and (E) electrolytic generation of hydrogen (overvoltage). The activities decreased in two steps at temperature ranges, T_{A1} and T_{A2}, and these temperatures coincided approximately with T_V and T_D, respectively, when specimens of the same material were employed for the measurements of both physical properties and catalytic activities. It was concluded that the active centers annealed at T_{A1} are point defects at the surface which coexist and vanish together with vacancies in the bulk metal, and that those annealed at T_{A2} are the terminations of dislocations at the surface.

Introduction

The structure and the temperature of disappearance of lattice defects in metals which were subjected to cold-working, etc., have been studied in recent years by measuring the rate of release of defect energy (ΔP),[1] changes of density (D), extra-resistivity ($\Delta\rho$), and hardness (H) on annealing.[1] Typical behavior of twisted

(1) L. M. Clarebrough, M. E. Hargreaves, and G. W. West, *Proc. Roy. Soc.* (London), **A232**, 252 (1955); *Phil. Mag.*, **1**, 528 (1956); W. Boas, "Defects in Crystalline Solids," The Physical Society, 1955, p. 212.

nickel (only the $\Delta P'$ curve is that of a ground specimen) is shown in Fig. 1. Changes on annealing take place in two (or three) temperature ranges, *i.e.*, T_v (*ca.* 200–330°) and T_D (~400–750°), differing sample by sample) and the range centered at 100°, which was suggested to be due to the disappearance of interstitials.[2-4] Nothing is known of the relation between these defects and catalysis. A gradual decrease in the breadth of X-ray diffraction line is observed between room temperature–300° and a sudden change at 515–550°, and the hardness of cold-worked nickel was reported to decrease at 550–750°.[5]

The change at T_v is believed to be due to the disappearance of vacancies.[1,6] At T_D recrystallization and a sudden decrease in hardness are noted and these changes have been attributed to the disappearance of dislocations.

As the concentration of defects increases with the degree of cold-working, stronger interactions among them are naturally expected, *i.e.*, the formation of divacancies, clusters, vacancy-dislocation complexes and dislocation networks. These give rise to the depression of T_D as follows:

Cu.—Discussed in a previous paper.[7]

Pt.—T_D found by Kishimoto[8] from the measurement of the thermoelectric force is centered at 530 and 450° for 68 and 88% compressed specimens, respectively.

Ni.—The rate of release of defect energy, ΔP for a specimen deformed in torsion to $nd/l = 1.87$, where n = number of turns, d = diameter of wire or cylinder, and l = gage length, and $\Delta P'$ for a powder specimen of equal purity prepared by grinding, and recovery of density of specimens subjected to various degrees of working are shown in Fig. 1. On the other hand, T_D is elevated remarkably by the existence of impurities as shown in Table I.

TABLE I

THE TEMPERATURE CORRESPONDING TO THE MAXIMUM OF ΔP AS THE FUNCTION OF THE DEGREE OF COLD-WORKING AND THE CONTENT OF IMPURITIES

Purity (%)	99.6	99.85	99.96
Cold-working	Pulverized: 500° ($\Delta P'$) Twisted nd/l = 2.34: 610° nd/l = 1.87: 630–660° (ΔP)	70% Compressed: 520° Twisted nd/l = 2.01: 450° (ΔP_0)	70% Compressed: 325°

T_v remains nearly constant irrespective of the method of preparation or the degree of working.[6,8] Depression of T_D results in an unavoidable overlapping of T_v and T_D as seen in Table I and Fig. 1, especially in the density recovery curve. (In the lower part of T_D, rearrangement of dislocations may also occur.)

In order to establish unquestionably the relation between lattice defects and active centers in metal catalysts, therefore, it is necessary to employ the identical specimens or at least specimens of the same material slightly cold-worked for the measurements of both physical properties and catalytic activities.

The thermoelectric force, S, also is sensitive to the presence and disappearance of lattice defects. Since the measurement of S can be performed easily with small quantities of specimens, it offers a convenient and effective method for studies of this field as shown by Kishimoto.[8,9] In Fig. 2 and 3, the temperature ranges corresponding to T_v and T_D for sudden changes

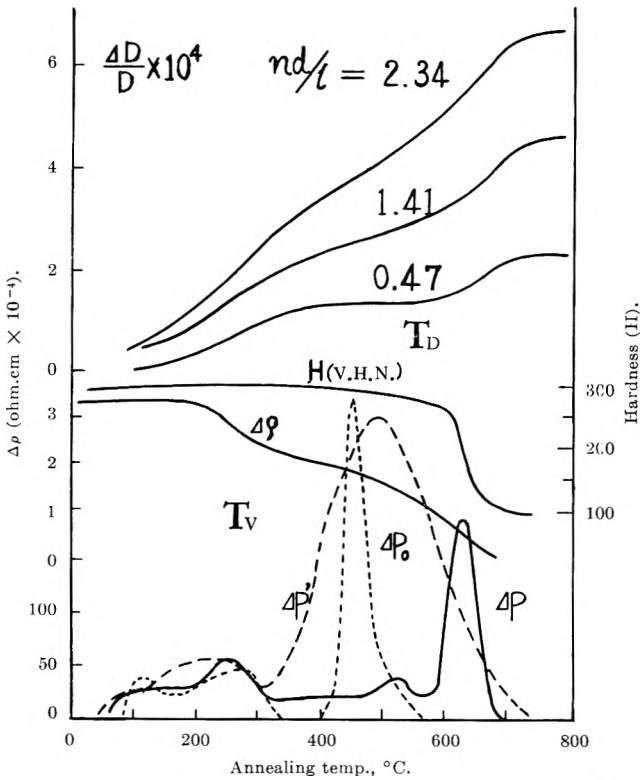

Fig. 1.—The rate of release of strain energy (ΔP), changes of density (D), extra-resistivity ($\Delta\rho$), and hardness (H) as functions of annealing temp. for Ni (99.6%) deformed in torsion to nd/l = 1.87 (Clarebrough, *et al.*[1]). ΔP = the rate of release of strain energy for Ni powder (Mitchell, *et al.*[2]). ΔP_0 = that of twisted Ni (99.85%, nd/l = 2.01) (Clarebrough, *et al.*[3]).

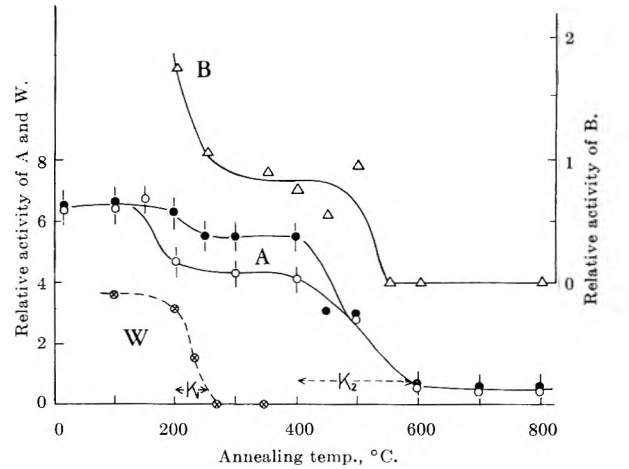

Fig. 2.—Catalytic activities (scales being arbitrary) of cold-worked Ni(I) as functions of annealing temps. A = hydrogenation of cinnamic acid by twisted (●) and compressed (○) Ni. E = dehydrogenation of ethanol (Δ). W = hydrogenation of C_2H_4 by Ni foil (Eckell)[18] (⊗). K_1 and K_2 = temp. ranges for sudden decrease of thermoelectric force of Ni(I), corresponding to T_v and T_D, respectively.[9]

(2) D. Mitchell and F. D. Haig, *Phil. Mag.*, **2**, 15 (1957).

(3) L. M. Clarebrough, M. E. Hargreaves, M. H. Loretto, and G. W. West, *Acta Met.*, **8**, 797 (1960).

(4) A. Sosin and J. A. Brinkman, *ibid.*, **7**, 478 (1959).

(5) J. E. Wilson and L. Thomassen, *Trans. AIME*, **22**, 769 (1934).

(6) "Vacancies and Other Point Defects in Metals and Alloys," The Institute of Metals, London, 1958.

(7) I. Uhara, S. Yanagimoto, K. Tani, G. Adachi, and S. Teratani, *J. Phys. Chem.*, **66**, 2691 (1962).

(8) S. Kishimoto, to be published.

(9) S. Kishimoto, *J. Phys. Chem.*, **66**, 2694 (1962).

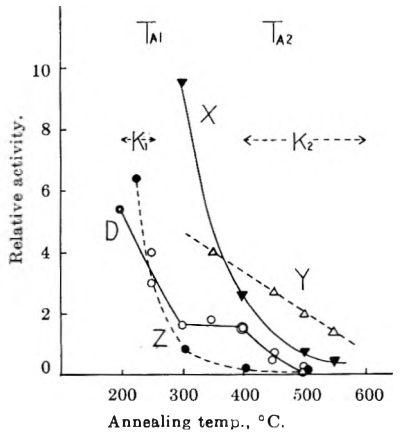

Fig. 3.—Catalytic activities (scales being arbitrary) of Ni for p–o conversion of H_2 as functions of annealing temps. D = slightly cold-worked Ni(I) (O . ⓪ means two measurements). Z = heavily cold-worked foil (●).[20] X[28] and Y[29] = ordinary reduced catalysts (▼ and Δ, respectively). $K_1 = T_V$, $K_2 = T_D$.

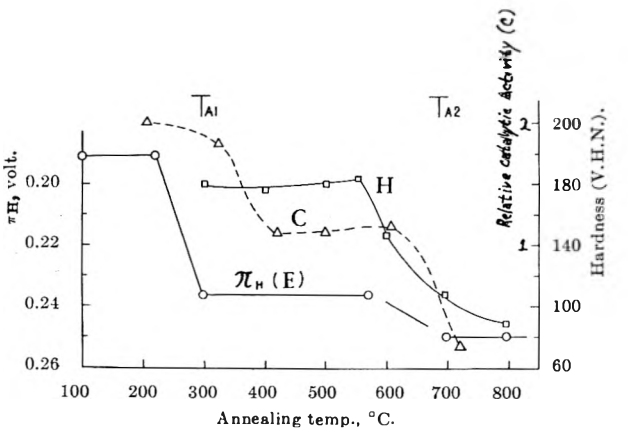

Fig. 4.—Catalytic activity for the decomposition of H_2O_2 (C, Δ), hydrogen overvoltage (π_H(E), O), and hardness (H, □) of cold-worked Ni(II) as functions of annealing temps.

in S on annealing cold-worked nickel (sample I) determined by Kishimoto are represented with the horizontal lines, K_1 and K_2. For sample II which is less pure than (I), no reliable data on S can be obtained because of large fluctuations probably owing to non-uniform distribution of impurities. It is, therefore, necessary to employ samples of high purity for this method.

Instead, T_D of sample II was determined from the change of hardness on annealing (measured by K. Iwasaki with a micro-Vickers hardness tester) as shown in Fig. 4, H.

Uhara and co-workers[10] have studied the relation between lattice defects and active centers in metallic catalysts and established experimentally that the ends of dislocations at the surface are the active centers of copper catalyst for the decomposition of diazonium salt[7,10] and the dehydrogenation of ethanol.[7] They also reported preliminarily that in the case of nickel catalysts the active centers are surface point defects for some reactions and these are both point defects and ends of dislocations at the surface for some other reactions.[11] In this paper, details of experimental evidence for the conclusion concerning the structure of active centers in nickel are given.

(10) I. Uhara, S. Yanagimoto, K. Tani, and G. Adachi, *Nature*, **192**, 867 (1961).

(11) I. Uhara, T. Hikino, Y. Numata, H. Hamada, and Y. Kageyama, *J. Phys. Chem.*, **66**, 1374 (1962).

Experimental

Two samples of nickel wire containing the following impurities (in per cent) were employed. Ni(I): 0.009 C, 0.011 Si, 0.001 S, 0.092 Mn, 0.022 Cu, and 0.033 Fe. Ni(II): 0.023 C, 0.07 Si, and 0.006 P, other elements being unknown. Wire was annealed at 800° in hydrogen atmosphere for 1 hr. and twisted or rolled in air slowly so as to prevent temperature elevation; the degree of working being represented by nd/l or by the degree of compression defined by $100(d-\delta)/d$, where δ = the thickness of the resulting plate. The change of catalytic activity of cold-worked metals due to annealing at various temperatures[12] may be studied by the following methods: (i) pieces of specimens cold-worked under conditions as identical as possible are divided into several groups and each group is annealed at different temperatures. (ii) a group of pieces is employed throughout a series of experiments by repeating annealing at increasing temperatures followed by the activity measurement. Although the latter is excellent in avoiding fluctuations of data (see below) and in keeping the experimental conditions constant, it is applicable only when poisoning is absent or at least recovery from it is easy on repeated catalytic reactions. A large number of pieces of cold-worked catalysts must be employed to avoid the fluctuation of activity due to non-uniformity of cold-working and of distribution of impurity, since their influence on the generation and disappearance of lattice defects cannot be neglected. The activity of catalysts employed in our research was much less than that of the usual catalyst; therefore, special devices are frequently necessary for determining the yield and for the selection of experimental conditions. The reproducibility of results was ascertained for reactions (A), (B), and (C).

(A) Hydrogenation of *trans*-Cinnamic acid.—Ni(I) was (a) twisted (nd/l = 0.21) or (b) 78% compressed (the apparent surface area = 3.65 cm.²) and then polished with emery paper in water. One cc. of 0.45 N alcoholic solution of cinnamic acid (extra pure) was put in Warburg's apparatus and the hydrogen uptake was measured at 25°.

(B) Dehydrogenation of Ethanol.—Ni(I) wire (total surface area = 15.7 cm.²) was twisted (nd/l = 0.25) without previous annealing, washed with pure alcohol, dried and put in hydrogen at 200° over 1 hr. to remove the oxide layer at the surface. Pure nitrogen saturated with ethanol vapor free from aldehyde at 30° was sent on the catalyst at 200° at the rate of 1 l./hr. for 2 hr. Aldehyde produced was dissolved in cold water and the yield was determined colorimetrically with *m*-phenylenediamine.[13] After the reaction the catalyst was annealed in a flow of nitrogen at a higher temperature for 1 hr., put in hydrogen overnight and then the activity measured again, etc. The catalyst was not exposed to air throughout the experiment.

(C) Decomposition of Hydrogen Peroxide.—Nickel(II) wire (the surface area = 3.22 sq. cm.) was twisted (nd/l = 0.41) and thrown into 30% hydrogen peroxide solution in Warburg's apparatus at 20°.

(D) Para–ortho Conversion of Hydrogen.—Seventy-four per cent compressed nickel(I) (the apparent surface area = 15 cm.²) was polished with emery paper in acetone, washed with alcohol and acetone and dried by evacuation to 10^{-5} mm. at 150°. Hydrogen purified by passing through a palladium tube was adsorbed at liquid nitrogen temperature on active carbon which had been degassed at 300° to 10^{-5} mm. The resulting hydrogen contains 50.4% of the para-form. The rate of conversion to the ortho-form was measured at 150°, where the equilibrium content of para-hydrogen is 25.0%, with a Pirani gage with platinum wire in a bath maintained at −110°. The catalyst was annealed in the reaction vessel without contact with air. Hydrogen (15–19 mm.) was circulated constantly in the vessel with a mercury pump.

(E) Electrolytic Generation of Hydrogen.—Hydrogen overvoltage (π_H) was measured at 25° in 0.12 N HCl solution and compared at a current density of 10^{-4} amp./cm.². A twisted specimen of nickel(II)(nd/l = 0.217) was employed as the cathode. Even when it was brought in contact with air a constant value of π_H was obtained after flowing a weak current by which adsorbed oxygen was probably removed.

Results

The catalytic activity of nickel (I or II) cold-worked

(12) Cooling after annealing must be slow to avoid the generation of lattice defects due to quenching.

(13) B. Richard, *Anal. Chem.*, **20**, 922 (1948); J. Bailey, *Ind. Eng. Chem., Anal. Ed.*, **13**, 834 (1941).

and annealed at various temperatures is shown in Fig. 2, 3, and 4 on arbitrary scales together with K_1 and K_2 for S measured with sample I and H for sample II.

(A) $C_6H_5CH{=}CHCO_2H + H_2 = C_6H_5CH_2CH_2CO_2H$, (Fig. 2, A). About 0.6 μl. of hydrogen was absorbed in min. when the catalyst was not annealed.

(B) $C_2H_5OH = CH_3CHO + H_2$, (Fig. 2, B).—At 200° the formation of ethylene and ether is negligible and the decomposition of aldehyde to carbon monoxide was also not detected. The reproducibility of the activity was shown as follows:

Experiment	Relative activity	Treatment after catalytic reacn.
1	0.50	Put in hydrogen flow overnight
2	.48	Put in hydrogen flow overnight
3	.50	Immediately after 3rd experiment without sending hydrogen
4	.10 (poisoning by aldehyde ?)	Put in hydrogen flow overnight
5	0.52	Put in hydrogen flow for 2 days
6	.72	

The activity observed after putting in hydrogen flow overnight was compared. By the catalyst not annealed 2.4×10^{-6} mole of aldehyde was formed, about half at the point defects and another half at the ends of dislocations at the surface as discussed below.

(C) $2H_2O_2 = 2H_2O + O_2$, (Fig. 4, C). About 10 μl. of oxygen was evolved in 40 min. by the catalyst not annealed

(D) Para-H_2 = ortho-H_2, (Fig. 3, D)- This reaction proceeded according to a first-order rate equation and the rate constant was 0.13 when the catalyst annealed at 200° was employed.

(E) $2H^+aq \rightarrow H_2$, (Fig. 4, E).—Lowering of π_H due to mechanical working such as grinding has been explained in terms of increase of the surface area, and consequently, of depression of the current density. But we know that even the surface area of reduced nickel (powder) does not change on annealing over T_v,[14] while π_H of cold-worked metal with far less roughness of the surface increases suddenly on annealing at this temperature. Since the change at the cathode is also a sort of catalytic reaction, it may be most rational to explain it in an analogous manner as in cases (A) ~ (D).

TABLE II

THE SINTERING TEMPERATURE (T_{A1} AND T_{A2}) OF COLD-WORKED NICKEL (SAMPLES I AND II)

Reaction	Sample	T_{A1} (°C.)	T_{A2} (°C.)
A	I	150–270	400–600
B	I	200–300	460–540
C	II	300–400	630–720
D	I	~200–300	400–500
E	II	220–300	570–*ca.* 700
Physical properties		T_v	T_D
S	I	200–250 (K_1)	400–*ca.* 600 (K_2)
H	II		500–*ca.* 800

Discussion

The comparison of these results with Fig. 1 indicates that the decrease of catalytic activities generally takes place in two temperature ranges, *i.e.*, T_{A1} and T_{A2}, in concurrent with the disappearance of vacancies and dislocations at T_v and T_D, respectively, in the bulk metal. The coincidence of T_{A1} with T_v, and T_{A2} with T_D is fairly good when they are measured with an identical specimen or at least specimens of the same material, as seen in the Table II and Fig. 2, 3, and 4. It has frequently been assumed that the surface of nickel catalyst is perfect and the only heterogeneity comes from the variety of appearing crystal faces, and that sintering is explained only in terms of the decrease of the surface area. But the change of the area due to annealing over T_v and in some cases at T_D was shown to be quite small compared with the decrease of activities even for ordinary catalysts with the highly developed surface so long as they are non-porous, *e.g.*, the van der Waals adsorption area of reduced nickel does not decrease on annealing at 380°,[14] and that of deposited copper is almost invariable on annealing over T_D.[10] The concurrent change of the catalytic activity with various physical properties of the bulk metal indicates that the sintering of catalysts is not a mere shrinkage of the area but a qualitative and structural change given rise by the disappearance of (surface) lattice defects. The stepwise decrease of the activities demonstrates this most clearly.[15] Accordingly, we may conclude that the active centers annealed at T_{A2} are the terminations of dislocations at the surface.

The approximate coincidence of T_{A1} and T_v indicates that T_{A1} is substantially concerned with the disappearance of point defects. Since the active centers of the catalyst exist, of course, at the surface they must be surface point defects(P), although nothing is known of the physical nature of them so far. Of P in the catalyst with a slightly deformed structure and with low concentration of the lattice defects as studied in our research, the simplest type, *i.e.*, a surface vacancy (Sv) with one atomic size, and a projecting atom (Pr) may predominate over other complex types of defects. It has been considered that at T_v vacancies begin to migrate to dislocations, to grain boundaries or to the surface, where they are absorbed or disappear. When a vacancy comes to a plane surface it will form Sv. If a considerable part of the surface is covered with Sv, the remaining part of the surface will form Pr in a dispersed state, hence vacancies in the bulk and P at the surface are not independent and various types of interaction including mutual annihilation are conceivable. At the temperature where the surface migration of P become possible, 1:1 annihilation of Sv and Pr resulting in the formation of a plane surface, or agglomeration of Sv (or Pr) only or combination with dislocations may occur. This temperature may probably correspond to T_{A1}. It may be supposed that the surface migration is easier than the bulk migration of vacancies, hence that T_{A1} is somewhat lower than T_v. If so, catalysts must lose all of their activity originating from P when they are annealed at the temperature range between T_{A1} and T_v, then the

(14) S. Iijima, *Rev. Phys. Chem. Japan*, **14**, 128 (1940).

(15) Crystalline nickel powder prepared by complete evaporation of amalgam is perfectly inactive for the hydrogenation of benzene, indicating the essential importance of the presence of surface defects.[16] Heterogeneity of the surface of nickel catalyst was demonstrated also from the analysis of the data of hydrogen adsorption.[17]

(16) P. Zemsch and F. Lihl, *Z. Elektrochem.*, **56**, 985 (1952).

(17) (a) H. S. Taylor, *Advan. Catalysis*, **I**, 1 (1948); A. Eucken and W. Hunsmann, *Z. physik. Chem.*, **B44**, 163 (1939); (b) T. Takaishi, *ibid.*, **14**, **3/4**, 164 (1958).

activities will be partly recovered by the migration of vacancies to the surface on heating to T_v. As a matter of fact, however, no example of catalysts which behave in such a way when they are sintered is known. In our research, also, no distinct difference between T_{A1} and T_v is observable. Consequently, we may conclude that T_{A1} is practically equal to T_v, and that the active centers annealed at T_{A1} are the surface point defects which coexist and vanish together with vacancies in the bulk metal. A method of assigning Sv or Pr to the active center for individual reaction may be shortly reported.

According to Eckell,[18] rolled nickel (foil) lost most of the activity for the hydrogenation of ethylene on annealing at 275° and completely at 300° (Fig. 2, W). This may be interpreted to mean that the active center for this reaction is some kind of P, contrary to Cratty and Granato's postulate[19] which attributed it to a dislocation.

Contribution of the normal surface to the activities of nickel is almost negligible or at most only a few per cent in every case so far studied.

With the increasing degree of cold-working, separation of T_v and T_D (hence that of T_{A1} and T_{A2}) becomes diffuse resulting in only continuous decrease of activity with increasing temperature of annealing, as observed in the case of nickel foil, which is, of course, prepared by heavy rolling, for para–ortho conversion of hydrogen-(*ca.* 200–500°)[20] (Fig. 3, Z).

Generation of Active Centers

Various procedures other than the mechanical one are known to generate active centers in metals.

(i) **Irradiation.**—When annealed nickel is irradiated with thermal neutrons (1.5×10^{16}/cm.^{2}) it gained catalytic activity of nearly the same magnitude as that of the cold-worked one for the decomposition of hydrogen peroxide. If the annealing experiment is performed the sort of the active center generated may be determined.

(ii) **Electrodeposition.**—By means of electrolysis under high current density (>0.1 amp./cm.^{2}) catalytically active metals are obtained. They contain impurities as oxide, hydroxide, etc., and distortion of the structure is shown by means of the X-ray method.[21] The existence of dislocations is estimated from their high hardness and was ascertained in the case of copper from the catalytic activity characteristic of dislocations.[7] The generation of point defects during electrolysis can be demonstrated by the catalytic activity of electro-deposited nickel for the hydrogenation of ethylene observed by Umemura.[22]

(iii) **Reduction of Salt with Base Metals.**—Copper powder containing many dislocations can be obtained by means of the reaction of copper sulfate solution with zinc dust.[7] Urushibara, *et al.*,[23] prepared a nickel catalyst with a high activity by means of the reaction of nickel chloride solution with zinc dust. It can be utilized for many catalytic reactions, hence it is certain that it contains both P and dislocations.

(iv) **Quenching.**—In the study of the catalytic decomposition of formic acid by nickel Duell and Robertson[24] found the generation of very high activities after flashing them at high temperature and attributed it to surface vacancies acting as active catalytic sites. It is well known that vacancies are generated during quenching (including radiation quenching), hence the formation of P (Pr and Sv) also is quite conceivable.

(v) **Purely Chemical Method (Ordinary Catalysts).**—Ordinary catalysts are prepared chemically and display much higher activity than the cold-worked metals. They are considered to have highly distorted structures analogous to that of the extremely cold-worked specimens discussed above, in view of the diffuseness of X-ray diffraction pattern, abnormally high chemical activity (pyrophoricity, etc.), energy content and heat of adsorption, and low density. For example, density of copper twisted to $nd/l = 1.8$ is less than that of the normal one (8.93) by 0.025%,[1] whereas that of a sample of reduced copper is less by 2.5%,[25] and even a value, as low as 7.6 was reported.[26] The density of nickel twisted ($nd/l = 1.41$) is less than that of the normal metal (8.90) by 0.045% (Fig. 1), whereas that of reduced catalyst is sometimes less than 8.0, although the existence of macroscopic voids may be suspected, too.[27] Clustering of lattice defects and strong interactions among them result in overlapping of T_v and T_D, or T_{A1} and T_{A2}, and consequently a continuous sintering (at T_s) curve as shown by curves X (nickel catalyst reduced at 300°)[28] and Y (catalyst reduced at 340°)[29] in Fig. 3 for para–ortho conversion of hydrogen. Their active centers may substantially be the same as those generated at the surface of metals by cold-working, considering the approximate coincidence of T_s with T_{A1} (or T_v) and T_{A2} (or T_D), although the possibility cannot be denied that two or more lattice defects combine to form complex active centers with new functions when the concentration of defects is high. Estimation of the structure of active centers is possible from T_s value for some reaction, *e.g.*, since nickel catalyst loses most of the activity for the hydrogenation of benzene at *ca.* 350°,[30] the active center may be P.

If the distortion of the crystal lattice is extreme as in the case of Raney nickel, the structure becomes nearly amorphous and hence the terms, vacancy and dislocation, which have been defined for defects in a nearly perfect crystal, lose their strict sense, and their properties may be different from those of isolated ones. In such a case, assignment of active centers to individual lattice defects is difficult. Although it was also found in some cases that the activity remains after annealing at temperatures higher than T_v or T_D, especially when the catalyst is supported, their physical conditions are too complex to be explained now.

At the present stage of our knowledge, we must, first of all, assign active centers to individual surface defects for each reaction employing slightly distorted crystals, though experimental difficulties owing to

(18) J. Eckell, *Z. Elektrochem.*, **39**, 433 (1933).
(19) L. E. Cratty, Jr., and A. V. Granato, *J. Chem. Phys.*, **26**, 96 (1957).
(20) E. Cremer and R. Kerber, *Advan. Catalysis*, **VII**, 82 (1955).
(21) W. Blum and C. Kasper, *Discussions Faraday Soc.*, **31**, 1203 (1935); C. H. Desch, *ibid.*, **31**, 1043 (1935); D. J. Macnaughtan and A. W. Hothersall, *ibid.*, **31**, 1168 (1935).
(22) K. Umemura, *Bull. Univ. Osaka Pref.*, **A9**, 91 (1960).
(23) Y. Urushibara and S. Nishimura, *Bull. Chem. Soc. Japan*, **27**, 480 (1954); Y. Urushibara, S. Nishimura, and H. Uehara, *ibid.*, **28**, 446 (1955).
(24) M. J. Duell and A. J. Robertson, *Trans. Faraday Soc.*, **56**, 1416 (1960).
(25) R. N. Pease, *J. Am. Chem. Soc.*, **45**, 2296 (1923).
(26) É. Audibert and A. Raineau, *Compt. rend.*, **197**, 596 (1933).
(27) J. W. Mellor, "A Comprehensive Treatise on Inorganic and Theoretical Chemistry," Vol. XV, London, 1936, pp. 52, 53.
(28) E. Fajans, *Z. physik. Chem.*, **B28**, 252 (1935).
(29) G. Tammann, *Z. anorg. allgem. Chem.*, **224**, 25 (1935).
(30) F. Lihl and P. Zemsch, *Z. Elektrochem.*, **56**, 979 (1952).

their low catalytic activity are sometimes unavoidable. Our present circumstance is quite analogous to the study of the solution, in which a dilute solution was studied at first with success because of the simplicity of the physical condition of the state treated.

Acknowledgment.—We wish to express hearty thanks to Dr. H. Takegoshi, Mr. M. Hasegawa, Mr. S. Taniguchi, Mr. K. Iwasaki, and Mr. N. Murakami for their helpful assistance, and to Prof. T. Iida and Dr. A. Saika for their kind advice.

THE SURFACE CONDUCTANCE OF SODIUM CHLORIDE CRYSTALS AS A FUNCTION OF WATER VAPOR PARTIAL PRESSURE

BY GEORGE SIMKOVICH

Max-Planck-Institut für physikalische Chemie, Göttingen, Germany

Received August 21, 1962

Surface conduction of a NaCl crystal in H_2O vapor may be due to (1) individual adsorbed semi-hydrated ions, and/or (2) saturated NaCl solution formed by virtue of capillary condensations in grooves on the surface of the crystal. In the latter case, the conductance is supposed to be decreased by the presence of a detergent, *e.g.*, 1-hexanol. Samples having a low conductance show no appreciable effect of the presence of hexanol. So conduction through adsorbed semi-hydrated ions seems to prevail. Samples having a higher conductance show an effect of the presence of hexanol supposedly due to conduction in grooves. Formulating the law of mass action for the formation of adsorbed semi-hydrated ions, one may calculate the average number of H_2O molecules of adsorbed semi-hydrated cations and anions. A value of 3 is found at low humidities, whereas a value of about 10 corresponding to a second hydration shell is found at high humidities.

Theoretical

It is well known that the resistance of a solid insulator, *e.g.*, glass, decreases markedly with increasing humidity of the surrounding atmosphere.[1-7] This is usually ascribed to the occurrence of conduction along the surface of the solid. It is the objective of this paper to try to clarify the nature of this kind of surface conduction. To this end, it seems expedient to investigate a simple salt, *e.g.*, NaCl, rather than glass whose structure is rather involved and where hysteresis phenomena prevail.

In the absence of H_2O, surface conduction may occur by the movement of individual adsorbed ions, or ion vacancies in the outermost lattice plane. At room temperature, such defects are supposedly very rare because of their high energy content and accordingly surface conductance in a dry atmosphere is very low. In the presence of H_2O vapor, two limiting mechanisms of surface conduction may be anticipated, *viz.*, (1) conduction due to the formation of individual adsorbed semi-hydrated ions schematically shown in Fig. 1 with an energy content much lower than that of adsorbed non-hydrated ions and (2) conduction through a saturated NaCl solution formed by virtue of capillary condensation of water vapor in sufficiently narrow grooves shown schematically in Fig. 2. In what follows the characteristics of each limiting case are discussed. Intermediate conditions are considered below.

(1) The formation of adsorbed semi-hydrated ions may be described by the equation

$$NaCl(s) + (m_1 + m_2)H_2O(g) = Na(OH_2)_{m_1}^{+}(ad) + Cl(H_2O)_{m_2}^{-}(ad) \quad (1)$$

where m_1 and m_2, respectively, are the numbers of H_2O molecules associated with individual cations and anions sitting on the surface of the bulk crystal shown schematically in Fig. 1. In general, one has to expect simultaneous formation of adsorbed ions involving a variety of hydration numbers, *i.e.*, $m_1 = 1,2,3\ldots$ and $m_2 = 1,2,3\ldots$ For the sake of simplicity, one may tentatively assume that ions with particular hydration numbers m_1^* and m_2^* prevail. Then nearly equal numbers of adsorbed cations with $m_1^*H_2O$ molecules and adsorbed anions with $m_2^*H_2O$ molecules are formed in accord with eq. 1. Denoting their concentrations in mole per unit surface area by Γ, assuming low surface coverage of the adsorbed ions, and applying the ideal law of mass action to the reaction stated in eq. 1, one has

$$\Gamma^2/p^{m_1^* + m_2^*} = K \quad (2)$$

where p is the H_2O partial pressure and K is a constant.

In the case of low surface coverage, one may assume constant mobilities of the adsorbed ions so that the conductance becomes essentially proportional to the surface concentration Γ. Thus, under conditions where the volume conductance can be neglected, the conductance of a sample of given dimensions, *i.e.*, the reciprocal of the resistance R is expected to be proportional to Γ, whereupon it follows with the help of eq. 2 that

$$1/R = \text{const } p^m \quad (3)$$

where

$$m = {}^1/_2(m_1^* + m_2^*) \quad (4)$$

is the average number of water molecules found in the hydration shells of adsorbed cations and anions. Taking logarithms of both sides of eq. 3, one has

$$\log (1/R) = m \log p + \text{const} \quad (5)$$

Thus, measuring the resistance of a NaCl crystal at different water vapor partial pressures and plotting log $1/R$ *vs.* log p, one may expect a straight line. Actually, deviations from a straight line may occur because of the occurrence of a variety of adsorbed ionic species with different numbers of H_2O molecules in the hydration shell, in particular because of the occurrence of a second

(1) J. S. Dryden and P. T. Wilson, *Austral. J. Appl. Sci.*, **1**, 97 (1950).
(2) M. Kantzer, *Bull. inst. verre*, No. 5, 11 (1946).
(3) P. Le Clerc, *Silicates Ind.*, **19**, 237 (1954).
(4) K. Kawasaki, K. Kanou, and Y. Sekita, *J. Phys. Soc. Japan*, **2**, 222 (1958).
(5) N. Chirkov, *Russ. J. Phys. Chem.*, **21**, 1303 (1947).
(6) W. A. Yager and S. O. Morgan, *J. Phys. Chem.*, **35**, 2026 (1931).
(7) A. Ya. Kuznetsov, *Zh. Fiz. Khim.*, **27**, 657 (1953).

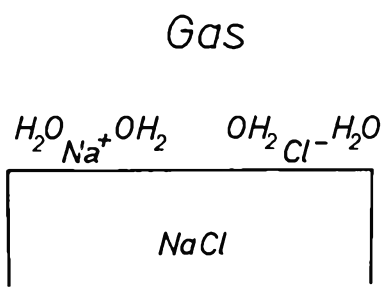

Fig. 1.—NaCl crystal with adsorbed semi-hydrated Na^+ and Cl^- ions.

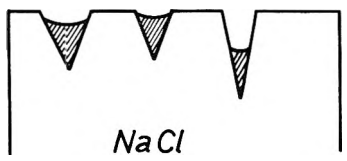

Fig. 2 —NaCl crystal with grooves partially filled with saturated NaCl solution.

hydration shell when the H_2O partial pressure approaches the value over a saturated NaCl solution as is discussed below. Even if a plot log $(1/R)$ *vs.* log p may be fitted by a straight line within a certain range, the model underlying eq. 1 to 5 is not necessarily confirmed, since other models may also be compatible with the experimental results.

(2) On the other hand, one may assume that conduction along the surface takes place mainly through grooves containing saturated NaCl solution as shown schematically in Fig. 2. The higher the H_2O partial pressure, the greater is the radius of curvature of a liquid coexisting with the gas phase according to the Gibbs–Thomson formula. Consequently, upon increasing the H_2O partial pressure, grooves become filled to a greater height with saturated NaCl solution and the conductance increases accordingly. Under these conditions, the relation between conductance and H_2O partial pressure is not a simple function involving only thermodynamic quantities but depends decisively on the roughness of the surface on a quasi-molecular scale. Thus a dependence of the conductance on the kind of surface preparation of a sample is to be expected.

To test the occurrence of surface conduction through grooves partially filled with saturated NaCl solution, one may investigate the effect resulting from the presence of a detergent added to the gas phase which lowers the surface tension of the liquid phase, *e.g.*, hexanol.[8] According to the Gibbs–Thomson formula, one has for a surface concave toward the gas phase[9]

$$\ln\left(\frac{p}{p^0}\right) = -\left(\frac{1}{r_1} + \frac{1}{r_2}\right)\frac{\sigma V}{\mathbf{R}T} \qquad (6)$$

where p is the H_2O partial pressure over a saturated NaCl solution with r_1 and r_2 as the principal radii of curvature of the surface, p^0 the vapor pressure for a plane surface, σ the surface tension of the solution, V the partial molar volume of H_2O in the solution, $\mathbf{R}$ the gas constant, and T the temperature. From eq. 6 it follows, that the sum of the reciprocals of the principal radii of curvature of the liquid phase coexisting with the gas phase of given humidity is

$$\frac{1}{r_1} + \frac{1}{r_2} = \frac{2.30y\,\mathbf{R}T}{\sigma V} \qquad (7)$$

where the humidity exponent, y, is defined by

$$y = -\frac{1}{230}\ln(p/p^0) = -\log(p/p^0) \qquad (8)$$

with the inverse relation

$$p = p^0 \times 10^{-y} \qquad (9)$$

For the same value of the right-hand member of eq. 7 without and with a detergent such as hexanol, one has equal values of $(1/r_1 + 1/r_2)$ corresponding to equal fractions of grooves filled with saturated NaCl solution and accordingly equal conductances without and with detergent, if effects resulting from changes in the contact angle and from changes in the specific conductivity of the liquid are ignored. Hence, upon decreasing the surface tension of a saturated NaCl solution from σ to σ' by the presence of a detergent, the value of y' with detergent and the value y without detergent for the same conductance of the sample are supposed to obey the relation

$$\left(\frac{y'}{y}\right)_{R=\text{const}} = \frac{\sigma'}{\sigma} \qquad (10)$$

Assume that without detergent one has measured a certain resistance R for $p/p^0 = 0.5$ corresponding to $y = 0.3$. Then, upon adding detergent and lowering the surface tension to $\sigma' = {}^1/_2\sigma$ one may expect to measure the same resistance R at $y = 0.15$ corresponding to $p/p^0 = 0.71$, *i.e.*, at a considerably higher relative humidity. A test of this prediction provides a possibility to check whether conductance in grooves filled with saturated NaCl solution is significant. The actual difference between y and y' may be even greater because for $y = 0.3$, *i.e.*, $p/p^0 = 0.5$ and $r_1 \cong \infty$ the radius r_2 is as low as 7×10^{-8} cm., *i.e.*, of the order of atomic dimensions and, therefore, a considerable fraction of the liquid in a groove may consist of detergent and may practically not contribute to the conductance.

Apart from experimental difficulties it must be realized that at high relative humidities corresponding to the presence of large numbers of adsorbed ions the conceptual difference between the two mechanisms formulated as limiting cases tends to vanish. Thus it may not be possible to distinguish unambiguously between the two mechanisms outlined above.

Experimental

For the resistance measurements NaCl bars of nearly quadratic cross section with four loops of silver wire as leads were used. The outer leads carried the current provided by a battery passing a calibrated resistor of appropriate seize, 10^8, 10^9, 10^{10}, or 10^{11} ohms, in series. The voltages between the inner leads and across the calibrated resistor were measured with the help of a potentiometer and a fiber electrometer as a null instrument.

Single crystals of NaCl were obtained from Ernst Leitz, G.m.b.H., Wetzlar, Germany. All samples were prepared as:

(1) Bars, 1 × 1 × 2 cm., were cleaved from the supplied crystals.

(2) Grooves for the silver leads were cut in the bars.

(3) The bars were polished on wet silk cloth, rinsed with H_2O, and then with ethanol.

(4) Silver wires as leads were wrapped around the crystals and the samples were wiped clean with tissue paper.

(5) Samples were dried for about 12 hr. at 115°.

(8) C. C. Addison, *J. Chem. Soc.*, 98 (1945).

(9) G. N. Lewis and M. Randall, "Thermodynamics," revised by K. S. Pitzer and L. Brewer, Second Edition, McGraw-Hill Book Co., New York, N. Y., 1961, p. 482.

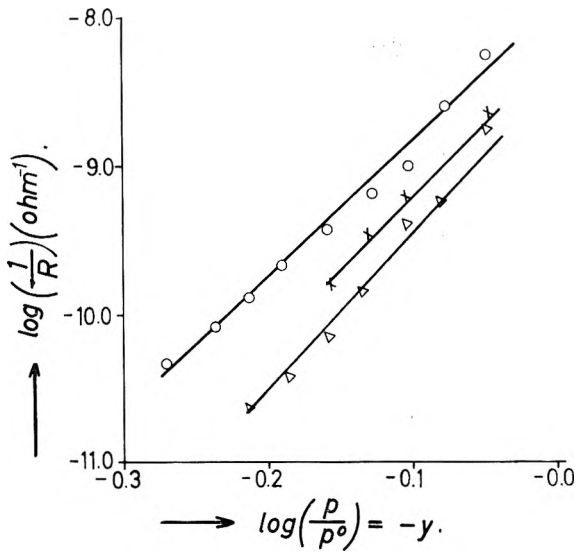

Fig. 3.—Log $(1/R)$ *vs.* log (p/p^0) for 3 NaCl samples in static atmosphere at high humidities and 22.4°.

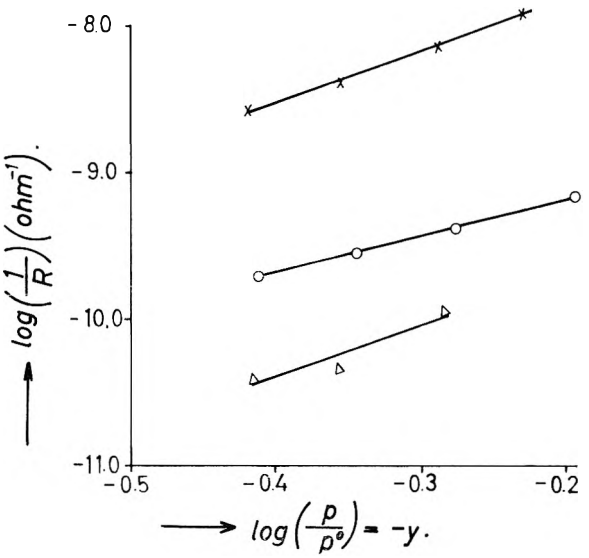

Fig. 4.—Log $(1/R)$ *vs.* log (p/p^0) for 3 NaCl samples in dynamic atmosphere at low humidities at 9.8°.

To provide definite H_2O partial pressures, first a static method was used. The sample with leads was installed at the top of an evacuated vessel kept at 22.4°, whereas the lower end of the vessel containing liquid water was kept at predetermined lower temperatures ranging from 9 to 15°. Further runs were made with a dynamic method by passing mixtures of dry nitrogen and nitrogen saturated with water at 20.3° along the sample having a temperature of 9.8°. Upon passing mixtures of dry nitrogen, nitrogen saturated with water, and nitrogen saturated with 1-hexanol, measurements in the presence of a detergent were made. In these runs the ratio of the partial pressures of water and 1-hexanol was about 18 as found over a saturated solution of 1-hexanol in H_2O with a surface tension of 30 dynes/cm.[8]

Discussion

Figures 3 and 4 show representative results obtained for different samples with the help of the static and the dynamic method, respectively. The observed points of plots $\log(1/R)$ *vs.* $\log\ (p/p^0)$ may be fitted by straight lines. For the range $y = 0$ to 0.25 covered in runs with the static method shown in Fig. 3, one has

$$\frac{\mathrm{d}\ \log\ (1/R)}{\mathrm{d}\ \log\ (p/p^0)} \cong 10 \qquad (11)$$

In contrast, runs for the range $y = 0.2$ to 0.45 made with the help of the dynamic method and shown in Fig. 4 yield

$$\frac{\mathrm{d}\ \log\ (1/R)}{\mathrm{d}\ \log\ (p/p^0)} \cong 3 \qquad (12)$$

Results obtained with the dynamic method for a relatively wide range of humidity are plotted in Fig. 5 and

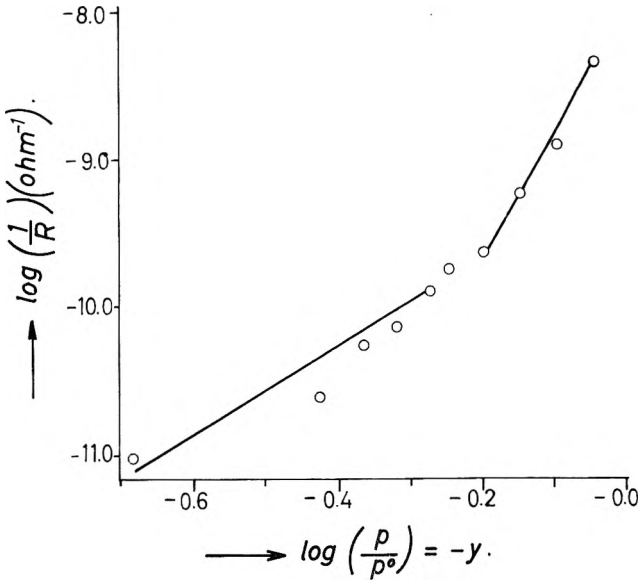

Fig. 5.—Log $(1/R)$ *vs.* log (p/p^0) for a NaCl sample in dynamic atmosphere covering a large humidity range at 9.8°.

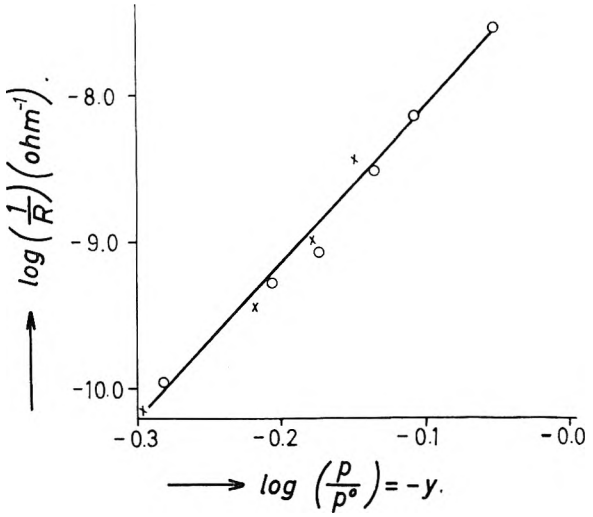

Fig. 6.—Log $(1/R)$ *vs* log (p/p^0) for NaCl sample I in H_2O (○) and H_2O + 1-hexanol (×) vapor at 9.8°.

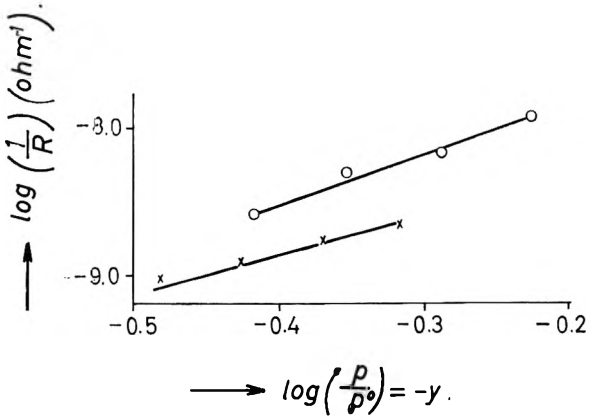

Fig. 7.—Log $(1/R)$ *vs* log (p/p^0) for NaCl sample II in H_2O (○) and H_2O + 1-hexanol (×) vapor at 9.8°.

show the change in slope with increasing H_2O partial pressure for one particular sample.

Results for two different samples without and with 1-hexanol as detergent are shown in Fig. 6 and 7. The log $(1/R)$ *vs.* (p/p^0) curve for the first sample shown in Fig. 6 is practically not shifted by the presence of 1-hexanol in contradistinction to the prediction in eq. 10, whereas a shift qualitatively in accord with eq. 10 is found for the second sample, see Fig. 7. Thus surface conduction in grooves partially filled with saturated NaCl solution is seemingly insignificant for the first sample but significant for the second sample. This is in accord with the fact that for equal H_2O partial pressures the conductance of the second sample was about 10^2 times greater than that of the first sample. Likewise differences between the results for different samples shown in Fig. 3 and 4 and differences in the results for repolished samples suggest that in addition to surface conduction *via* adsorbed ions, conduction was due in part to a second mechanism involving conduction in grooves whose contribution is supposed to depend on details of the surface preparation beyond the control exercised in the present research.

Disregarding the contribution of conduction in grooves for samples having a high resistance, one may tentatively identify the values of d log $(1/R)$/d log (p/p^0) reported in eq. 11 and 12 with the average number m of H_2O molecules present in the hydration shell of adsorbed cations and anions in accord with eq. 5. The value of $m \cong 3$ found for the low-humidity range ($y = 0.2$ to 0.45) is essentially in accord with the concept of adsorbed ions with a hydration shell only on the outer side where the individual hydration number m_1^* and m_2^* of cations and anions, respectively, may be 3 and 3, or 4 and 2, or 2 and 4, etc. The value of about 10 found for high humidities ($y = 0$ to 0.2) indicates the presence of a second hydration shell.

The foregoing calculations are based on the presupposition that the surface coverage of adsorbed ions is low. This can be confirmed by the following estimate. The surface conductance $1/R$ may be written as

$$\frac{1}{R} = \frac{nuec}{L}$$

where n is the number of adsorbed ions per unit area (cm.^{2}), u is the mobility supposedly about equal to that of ions in aqueous solution ($\cong 5 \times 10^{-4}$ cm.^{2}/volt sec.), $e = 1.6 \times 10^{-19}$ coulomb is the electronic charge, $C = 4$ is the circumference of the sample, and $L = 0.5$ is the distance between the probes. Thus n is found to be of the order of 1.5×10^{11} ions per cm.^{2} for $R = 10^{10}$ ohms, or 1.5×10^{12} ions per cm.^{2} for $R = 10^9$ ohms, which is much less than the number of ions on a close-packed 100 plane of a NaCl crystal ($= 1.3 \times 10^{15}$ ions/cm.^{2}). Assuming a higher mobility of adsorbed ions, one obtains an even lower surface coverage.

Although surface conduction of glass is a more involved phenomenon, as has been mentioned above, it is noteworthy that plots log $(1/R)$ *vs.* log (p/p^0) of results reported by various investigators[4,6] also yield essentially straight lines with slopes corresponding to values of d log $(1/R)$/d log (p/p^0) between 9 and 18.

Acknowledgments.—Sincere thanks are extended to Professor C. Wagner, who suggested this research and discussed the results with the author.

METHYL RADICAL PRODUCTION IN THE RADIOLYSIS OF HYDROCARBONS[1]

BY ROBERT H. SCHULER AND ROBERT R. KUNTZ

Radiation Research Laboratories, Mellon Institute, Pittsburgh, Pa.

Received September 10, 1962

Radioiodine scavenging methods have been employed in the radiolysis of liquid hydrocarbons to examine details of the production and reaction of methyl radicals. Carrier-free chromatographic separation of the radio-methyl iodide has enabled studies to be carried out at iodine concentrations down to 5×10^{-7} M. In the radiolysis of 2,2,4-trimethylpentane–iodine solutions at room temperature the methyl iodide yield is shown to be independent of iodine concentration above 10^{-5} M. Competition between the scavenging reaction and abstraction of hydrogen from the solvent by the methyl radicals is observed in the region of 10^{-6} M. In the absence of iodine the methane yield is shown to be dependent on absorbed dose rate in the region of 10^7 rads/hr. At this dose rate the abstraction process competes effectively with the reaction between methyl radicals and other alkyl radicals. Measurement of the competition rates of the above reactions, together with rate information from paramagnetic resonance experiments, allows an estimate to be made of the absolute second-order rate constant for the reaction of methyl radicals with molecular iodine. This rate constant is shown to be of the same order of magnitude as that for reaction of free radicals with one another. A survey of methyl radical production from various hydrocarbons has shown that carbon–methyl bond rupture deviates substantially from that predicted by a simple model involving only a statistical consideration of the number of methyl groups in the molecule. The yields are found to be very markedly dependent on specific details of the structure of the species being irradiated. For individual homologous series the methyl radical yields are observed to be decreasing monotonic functions of the chain length of the hydrocarbon. For the paraffins and isoparaffins the yield is proportional to the inverse square of the number of carbon–carbon bonds in the molecule. By a generalization of this relationship, an empirical rule has been developed which allows reasonable quantitative estimates to be made for the methyl radical yields from even highly branched hydrocarbons.

Introduction

Extensive studies have previously been carried out in which iodine has been used to scavenge radicals produced in hydrocarbons by ionizing radiations. This work has been summarized in a previous review.[2] These studies have shown in general that about five radicals are produced in liquid aliphatic hydrocarbons per 100 e.v. of absorbed energy. Except for the very

(1) Supported, in part, by the U. S. Atomic Energy Commission. Presented at the 139th National Meeting of the American Chemical Society, St. Louis, Missouri, March, 1961.

(2) R. H. Schuler, *J. Phys. Chem.*, **62**, 37 (1958).

early work of Gevantman and Williams[3] and a number of more recent studies[4-7] little attention has been paid to the identity of the individual iodide products.[8] Most of this work has been carried out at relatively high iodine concentrations. Currently available gas chromatographic methods provide an extremely attractive means of separating organic iodides and allow attention to be focused on details of the reactions of the individual radicals. The incorporation of radioiodine tracer methodology makes it possible to carry out studies at very low scavenger concentrations. The present investigation shows that direct measurements of the competition between reactions of the radicals with the scavenger and with the organic substrate is feasible even though this competition occurs at scavenger concentrations of the order of 10^{-6} M. Attention is focused here on the production and reactions of methyl radicals in the radiolysis of the simpler aliphatic hydrocarbons.

Experimental

Hydrocarbons.—Hydrocarbons used were either Phillips Research Grade or, where indicated in Table II, samples from the American Petroleum Institute collection. The Phillips hydrocarbons were passed through a silica gel column to remove possible olefinic impurities. Before irradiation the samples were frozen and degassed at least three times to remove dissolved air (oxygen). The concentration of dissolved air was less than the detectability limit of the gas analysis apparatus (10^{-6} M). Butane was handled on a vacuum line and was irradiated as a liquid at room temperature under its own vapor pressure.

Radioiodine.—Iodine-131, obtained as the iodide from Oak Ridge National Laboratory, was evaporated to dryness and exchanged with an appropriate amount of molecular iodine. The resultant radioiodine was sublimed to storage ampoules on a vacuum line. The specific activity of the iodine was adjusted so that it would be convenient for counting at the concentrations employed in the individual experiments. The maximum specific activity, which was used only in the case of the most dilute solutions, was approximately 50 mc./mmole of iodine. Even at this high a specific activity the background reaction due to self-radiolysis was only of the order of 1% per day and was considered negligible for the short contact times used.

Samples of a known concentration of iodine in the desired hydrocarbon were prepared from weighed amounts of the radioiodine with appropriate dilutions being made for work at lower concentrations. Where there was question of the loss of iodine due to adsorption on the walls of the vessel, the concentration of iodine was determined by comparison of the measured activity with samples where additional carrier was added before dilution. Dilutions were conveniently made for the small volumes employed with calibrated micropipets. The experiments with API hydrocarbons (and liquid butane) were accomplished with a minimum amount of sample by dissolving 0.5–1.0 mg. of iodine of known specific activity in 1 cc. of the hydrocarbon. The iodine concentration was then determined from measurement of the activity of the sample. The concentration in these cases ($2 - 4 \times 10^{-3}$ M) is somewhat higher than in the experiments on the more readily available hydrocarbons.

Irradiations.—The majority of irradiations were carried out at room temperature with cobalt-60 γ-radiations inside an annular source at an absorbed dose rate of 250,000 rads/hr. In the experiments on very dilute solutions of iodine in 2,2,4-trimethylpentane, where the total dose was as little as 30 rads, irradiations were carried out either in a cobalt source at a dose rate of 50,000 rads/hr. or with 3-mev. X-rays from a Van de Graaff accelerator at dose rates of from 5000 to 50,000 rads/hr. Absorbed dose rates in the various geometries were measured with the Fricke (ferrous sulfate) dosimeter. In calculating the energy absorbed in the individual hydrocarbons it was assumed that absorbed dose was proportional to the electron density of the hydrocarbon. Radiation yields are given in terms of G, *i.e.*, molecules per 100 e.v. of absorbed energy.

Methane production measurements were carried out with the above sources and in addition at lower dose rates with a 100-curie cobalt-60 point source (in one instance at 110 rads/hr.) and at higher dose rates with 2.38 mev. electrons from the Van de Graaff accelerator. In the latter case absolute yields were measured by the charge-input method.[9] The absorbed dose was $\sim 8 \times 10^{18}$ e.v./cc. for each of the fast electron experiments (electron currents were from 10^{-5} to 10^{-9} amp. and the corresponding irradiation periods from 1 to 10,000 sec.).

Methyl Iodide Measurements.—After irradiation samples were chromatographed at room temperature on a 250-cm. column packed with fire brick impregnated with 25% of its weight of silicone grease. A known volume of the sample (usually 0.5 cc.) was injected into a fore-column (50 cm.) which served to retain the unreacted iodine and the high boiling iodine-containing components produced as a result of the radiolysis. This stripping column was repacked between runs. Since only the lower alkyl iodides (up through the butyl iodides) were normally passed by this short section of column during the periods used for elution, the main chromatographic column was never subjected to contamination with samples which might contribute to the background in later runs. Blank runs carried out in this way were always negative. The radio-methyl iodide in the effluent stream was trapped in a tube containing 3 cc. of 2,2,4-trimethylpentane chilled to Dry Ice temperature. It was shown, by placing two such tubes in sequence, that none of the active sample passed the first trap.

Methyl iodide is the lowest boiling organic iodide and the first one expected to come off the column. A typical example of the separation attainable is illustrated in Fig. 1 taken from an experiment in which a partially eluted column was scanned with a scintillation probe. Under the conditions employed here the elution times of methyl, vinyl, and ethyl iodides were 17, 30, and 47 min., respectively. Fractionation experiments in which separate methyl and vinyl iodide fractions were collected showed that except for certain cases where the methyl iodide component was extremely low, *i.e.*, cyclopentane and cyclohexane, the vinyl iodide contribution was entirely negligible. In the majority of the experiments elution was carried out for a period of 33 min. which was shown in conventional chromatographic equipment to be sufficient to collect all of the methyl iodide. Since methyl iodide tends to tail quite badly when large samples of hydrocarbon are employed, this radiochemical procedure has a significant advantage over standard chromatographic detection methods in that the accumulated activity gives a direct quantitative measure of the total amount of the component under study. There is no base line ambiguity. In addition the method is, of course, highly sensitive as is illustrated by the fact that in one case (at the lowest concentration reported here) measurements were made on a sample which contained only 5×10^{-12} mole of methyl iodide and which received a total dose of only 30 rads.

In a number of preliminary experiments attempts were made to separate the unreacted iodine from the sample by thiosulfate extraction and by treatment with mercury. The results were, however, somewhat erratic due to the solubility of methyl iodide in water in the first case and due to the formation of a suspension of mercuric iodide in the hydrocarbon in the second case. Experiments in which carrier methyl iodide was added before separation also gave erratic results due to exchange of activity between the unreacted iodine and the carrier. Separation of methyl iodide without the addition of inactive carrier, as described here, appears to be free from difficulties.

The collection tubes in which the samples were trapped could be placed directly in a well-type scintillation counter. The amount of methyl iodide formed was determined from the activity of the trapped sample and the known specific activity of the iodine used in the experiment. In a number of cases the irradiated samples were washed with sodium thiosulfate solution and the total yield of organic iodide was also determined.

Methane Measurements.—Methane yields were determined

(3) L. Gevantman and R. R. Williams, Jr., *J. Phys. Chem.*, **56**, 569 (1952).

(4) C. E. McCauley and R. H. Schuler, *J. Am. Chem. Soc.*, **79**, 4008 (1957).

(5) G. A. Muccini and R. H. Schuler, *J. Phys. Chem.*, **64**, 1436 (1960).

(6) H. A. Dewhurst, *ibid.*, **62**, 15 (1958); *J. Am. Chem. Soc.*, **80**, 5607 (1958).

(7) K. H. Napier and J. H. Green, *Proc. Australasian Conf. Radiation Biol.*, **2**, 87 (1959); J. Dauphin, *Proc. Conf. Use Radioisotopes Physical Sci. Ind.*, **III**, 471 (1962).

(8) Holroyd and Klein have very recently developed a method for the identification of the various radicals formed using ethylene-C^{14} as a scavenger; *cf.* R. A. Holroyd and G. W. Klein, *J. Am. Chem. Soc.*, **84**, 4000 (1962).

(9) R. H. Schuler and A. O. Allen, *J. Chem. Phys.*, **24**, 56 (1956).

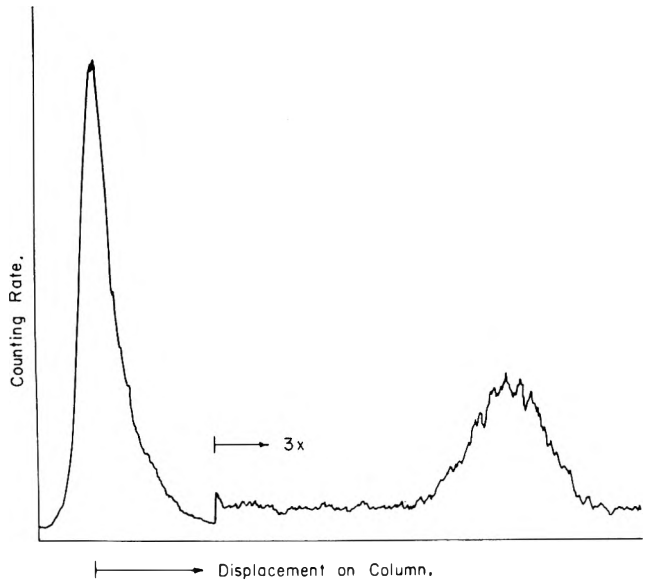

Fig. 1.—Scan of partially eluted chromatographic column showing separation of the methyl iodide component from the higher alkyl iodides for an irradiated solution of iodine in 2,2,4-trimethylpentane. Area under methyl iodide peak is 13% of total.

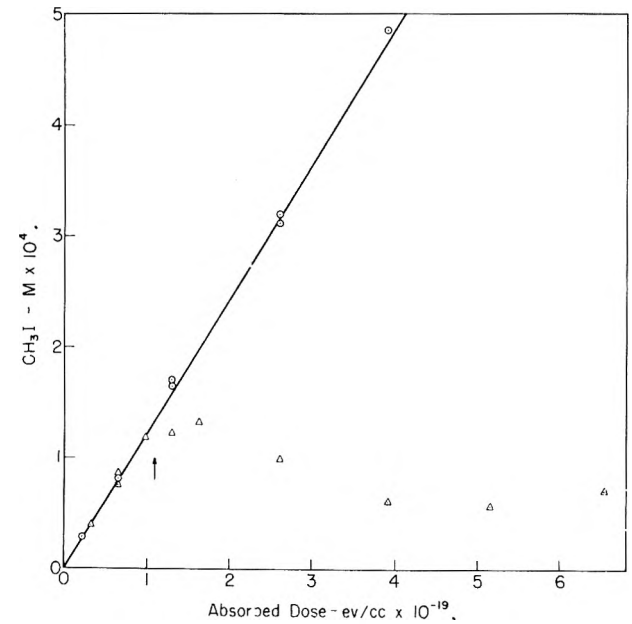

Fig. 2.—Methyl iodide production in 2,2,4-trimethylpentane containing (△), 5×10^{-4} M I_2 and (⊙), 5×10^{-3} M I_2. The arrow indicates the dose at which iodine is depleted in the more dilute solution.

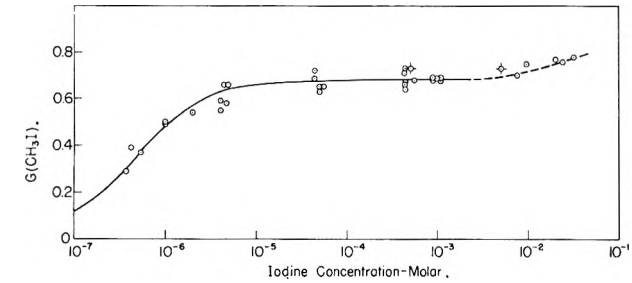

Fig. 3.—The dependence of methyl iodide yield on iodine concentration. The flagged circles represent the yields from the data of Fig. 2. Solid curve is calculated on the assumption that $G(CH_3\cdot) = 0.69$ and that $k_1/k_2 = 7 \times 10^{-8}$.

by conventional vacuum line techniques.[10] The hydrogen-methane fraction was pumped from the sample at −196° and analyzed by combustion on copper oxide at 575°. These combustion analyses were supplemented by mass spectrometry in a number of cases. A total of five degassings were employed in the removal of methane (approximately 80% of the residual methane was recovered in each degassing). In the case of 2,2,4-trimethylpentane, 1 to 5 micromoles of methane were collected from a sample volume of 10 cc. in the case of the γ-ray experiments and 20 cc. in the fast electron experiments. This methane was in the presence of about twice its volume of hydrogen. The amount of methane obtained from most of the other hydrocarbons was even smaller and the proportion of hydrogen greater.

Competitive Reactions of Methyl Radicals

Scavenging by Iodine.—Because a reasonably large methyl radical yield was expected from previous experiments on 2,2,4-trimethylpentane,[2] this substance was chosen for the detailed studies reported here. A number of experiments were carried out at iodine concentrations of 5×10^{-4} and 5×10^{-3} M. These show, as is indicated in Fig. 2, that methyl iodide builds up with a constant yield until the iodine is nearly exhausted. This is then followed by a decrease in the methyl iodide concentration, as expected from previous work on methyl iodide solutions.[11] All subsequent irradiations were adjusted so that no more than 75% of the iodine would react during the experiment and usually considerably less. The observed yields of methyl iodide are given in Fig. 3 as a function of iodine concentration. The yield is independent of concentration from 10^{-5} to 10^{-2} M. At higher concentrations a very slight rise is noted. This rise is, however, much less than was observed for the total organic iodide formed in the cyclohexane system[12] but is consistent with the work on butane[4] where an analogous increase was found to be due to the production of high molecular weight iodine-containing products. One conventional determination of the amount of methyl iodide formed was made at 4×10^{-2} M with chromatographic apparatus employing thermal conductivity detection. The observed yield, 0.77, agrees well with that expected from the curve of Fig. 3.

The decrease in methyl iodide yield at iodine concentrations below 10^{-5} M is very probably due to the competition of the hydrogen abstraction reaction[13]

$$CH_3\cdot + RH \longrightarrow CH_4 + R\cdot \qquad (1)$$

with the scavenging reaction

$$CH_3\cdot + I_2 \longrightarrow CH_3I + I\cdot \qquad (2)$$

The solid curve in Fig. 3 is that calculated for a simple competition with the ratio k_1/k_2 being taken as 7×10^{-8}, the 2,2,4-trimethylpentane concentration as 6.0 M and the yield of methyl iodide at high concentrations as 0.69. The correspondence between the experimental yields and the calculated sigmoidal curve shows reasonable consistency with the assump-

(10) *Cf.* R. H. Schuler and C. T. Chmiel, *J. Am. Chem. Soc.*, **75**, 3792 (1953).

(11) R. H. Schuler, *J. Phys. Chem.*, **61**, 1472 (1957).

(12) R. W. Fessenden and R. H. Schuler, *J. Am. Chem. Soc.*, **79**, 273 (1957).

(13) Szwarc and co-workers in recent years have studied the competition for thermally produced methyl radicals between the abstraction of hydrogen from liquid 2,2,4-trimethylpentane and reaction with olefins. See, for example, R. P. Buckley and M. Szwarc, *Proc. Roy. Soc.* (London), **A240**, 396 (1957). In general they find that olefins are relatively unreactive as methyl radical scavengers and compete with the abstraction process only at quite high concentrations.

tion of a simple competition. Since reaction 1 results only in the change of the identity of the radicals and not in the total number, the organic iodide yield should be independent of the occurrence of this reaction.[12] No decrease was observed in the total yield even at the lowest iodine concentration so that reaction of the radicals with possible residual oxygen does not seem to be important. The reaction competing with scavenging might, however, involve impurities rather than the solvent proper. In fact, measurements given in Table I show a very slight induction period for methane formation in the absence of iodine. If this is the case then the 7×10^{-8} value given above will only be an upper limit to the ratio k_1/k_2. The discussion below indicates that the actual value cannot be very much lower.

A number of experiments were also carried out at 75° with iodine concentrations in the region of 5×10^{-7} to 5×10^{-5} M. The results scatter considerably more than the data given in Fig. 2 but do show a drop in the methyl iodide yield in the region of 1.5×10^{-6} M iodine, *i.e.*, at about a threefold higher concentration than at room temperature. Unfortunately the rate constant ratio cannot be determined with sufficient accuracy over the fairly narrow temperature range available to measure directly the activation energy difference between reactions 1 and 2.

Scavenging by Hydrocarbon Radicals.—Elementary considerations of the steady state radical concentrations maintained during radiolysis[14] indicate that at readily available absorbed dose rates these concentrations are of the order of magnitude at which scavenging of methyl radicals is observed with iodine. It is expected then that in the absence of scavenger one should be able to observe the competition between reaction 1 and reaction of methyl radicals with other radicals, *i.e.*

$$CH_3\cdot + R\cdot \longrightarrow RCH_3 \qquad (3a)$$

To illustrate this, detailed studies of the dose rate dependence of the formation of methane from 2,2,4-trimethylpentane have been carried out with cobalt-60 γ-radiations and with Van de Graaff electrons.[15] The observed yields are reported in Fig. 4 as a function of the dose rate and of the corresponding steady state radical concentration. This radical concentration is calculated from the known rate of radical production ($10DG/N$ moles $l.^{-1}$ $sec.^{-1}$ where D is rate of energy absorption in e.v. $cc.^{-1}$ $sec.^{-1}$ and G is taken as 5) and a second-order rate constant (k_R) of 10^9 l. $mole^{-1}$ $sec.^{-1}$ for the bimolecular disappearance of radicals as estimated from e.s.r. steady state experiments.[16] In calculating the radical concentrations for the fast

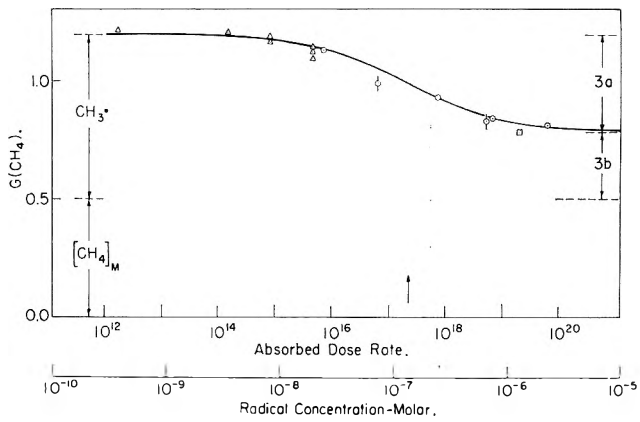

Fig. 4.—Methane production in the radiolysis of 2,2,4-trimethylpentane: ⊙, 2.38 mev. electrons; ⊙, same, sample stirred during irradiation; ⊡, 36.8 mev. helium ions; △, cobalt-60 γ-rays. The radical concentration is taken as $2.9 \times 10^{-16} D^{1/2}$ (D in e.v. $cc.^{-1}$ $sec.^{-1}$) and the solid curve is calculated as described in the text.

TABLE I

EFFECT OF IODINE ON METHANE AND HYDROGEN PRODUCTION FROM 2,2,4-TRIMETHYLPENTANE

I_2 concn.	Irradiation period,[a] min.	$G(H_2)$[b]	$G(CH_4)$
0	45	2.39	1.09
0	88.5	2.29	1.12
0	1420	1.93	1.14
10^{-3} M	46	1.85	0.49
10^{-3} M	80	1.88	.50
10^{-2} M	196	1.37	.51

[a] At an absorbed dose rate of $\sim 2 \times 10^{17}$ e.v. $cc.^{-1}$ $min.^{-1}$. [b] A hydrogen yield of 2.45 was observed in the γ-ray experiment at 110 rads/hr. The average of the hydrogen yields from the Van de Graaff determinations was 2.42 at an absorbed dose of 8×10^{18} e.v./cc. The hydrogen yield observed in the helium ion experiment was 2.44 at an absorbed dose of 3×10^{19} e.v./cc.

electron experiments the dose rate has been averaged over the irradiation zone (1.8 cc.). Because of the square root dependence of the radical concentration on dose rate, minor variations in the dose rate have only a very small effect on the averaging of the concentration. At the dose rates employed in these experiments the mean lifetime of the radicals is of the order of milliseconds[14] so that a major fraction of the reaction occurs in the irradiation zone before diffusion or stirring can distribute the radicals over the bulk of the sample. A small fraction of the reaction will of course occur in a fringe zone at lower concentration. The energy dissipated here is however quite small and it is assumed that the contribution to the methane production in this region is not significant.

At very low dose rates, where abstraction predominates, the observed methane yield is expected to be equal to the sum of the methyl radical yield (which produces methane by reaction 1) and the molecular methane formed by non-radical processes. This latter quantity was determined to be 0.50 from measurement of the methane yield in the presence of iodine (*cf.* Table I). At high dose rates methane is expected to decrease to the molecular yield if all methyl radicals disappear by reaction 3a. A considerably higher yield of methane is however observed at the highest absorbed dose rate employed (6×10^9 rads/hr.) indicating that methyl radicals in part disproportionate upon reaction with the other radicals present. An approximate ex-

(14) R. W. Fessenden and R. H. Schuler, *J. Chem. Phys.*, **33**, 935 (1960).

(15) H. A. Dewhurst, *J. Am. Chem. Soc.*, **80**, 5607 (1958), reports $G(CH_4) = 0.7$ for fast electrons and Knight, *et al.* (J. A. Knight, R. L. McDaniel, R. C. Palmer, and F. Sicilio, *J. Phys. Chem.*, **65**, 2109 (1961)) report $G(CH_4) = 1.1$ for X-rays at 10^6 rads/hr.

(16) No e.s.r. absorption signals were observed in 2,2,4-trimethylpentane at room temperature in experiments similar to but at somewhat lower sensitivity than those reported in reference 14. At −40° signals due predominantly to *t*-butyl and neopentyl radicals were found. Although it is not possible, for various reasons, to determine accurately the total radical concentration in this case, an estimate of 10^9 l. $mole^{-1}$ $sec.^{-1}$ for the rate constant at room temperature is reasonably in accord with the above qualitative e.s.r. observations. The calculated radical concentrations are, of course, inversely proportional to the square root of this assumed rate constant. The various possible competitive reactions of methyl radicals presumably do not affect this average rate constant to any significant extent.

$$CH_3\cdot + R\cdot \longrightarrow CH_4 + R(-H) \qquad (3b)$$

trapolation of the data at high dose rates indicates that the sum of the molecular yield and that due to (3b) is 0.78. By difference the yield for (3b) is estimated as 0.28 and for (3a) as $0.69 - 0.28 = 0.41$. The ratio of rate constants of disproportionation to recombination, 0.68, is reasonable in view of the fact that methyl radicals react to a large extent with secondary and tertiary radicals. The production of methane by disproportionation of methyl and *t*-butyl radicals has been noted in studies of the radiolysis of liquid neopentane.[17]

With the low dose rate limit being set at 1.19 and the high dose rate limit being set at 0.78 by the above arguments, the yields in the transitional region must be given by a sigmoidal curve which describes the competition between reactions 1 and 3. It is seen that the expected transition occurs in the region of 2×10^{17} e.v. cc.$^{-1}$ sec.$^{-1}$ (2×10^7 rads/hr.) at which the steady state radical concentration is estimated to be 1.4×10^{-7} *M*. The curve given in Fig. 4 is that calculated from the above limits with k_1/k_3 being taken as 2.4×10^{-8} (or $k_1 k_R^{1/2}/k_3 = 7.6 \times 10^{-4}$ (l. mole^{-1} sec^{-1})$^{1/2}$; k_R is assumed to be constant).

The measurement of the competitive rates of both reactions 2 and 3 with respect to reaction 1 allows us in turn to interrelate their rate constants

$$k_2 k_R^{1/2}/k_3 = 1.1 \times 10^4 \text{ (l. mole}^{-1} \text{ sec.}^{-1})^{1/2}$$

or based on $k_R = 10^9$ l. mole^{-1} sec^{-1}

$$k_2/k_3 = 0.3$$

If we assume that k_3 is similar to the second-order rate constant for the larger radicals, as is very probably the case since the e.s.r. experiments indicate that all reactions are diffusion controlled, then the rate constant for the reaction of methyl radicals with iodine molecules may be estimated as 3×10^8 l. mole^{-1} sec.$^{-1}$ at room temperature in liquid 2,2,4-trimethylpentane. Because of the possible influence of impurities on the measurement of k_1/k_2, as mentioned above, this value of k_2 must be regarded as a lower limit.

Both reactions 2 and 3 are diffusion controlled. Comparison of the significance of the relative rate constants involves consideration of the encounter frequencies for the reacting species; methyl radicals and iodine atoms in the first instance and methyl radicals and larger alkyl radicals (*e.g.*, *t*-butyl radicals) in the second instance. However, these frequencies should be quite similar since the burden of the diffusion is largely carried by the methyl radicals. If one assumes that the diffusion coefficients for the various species under consideration are proportional to the reciprocal square root of the reduced mass of the solute–solvent system then reaction 3 should be favored over 2 by only 10%. While the indicated difference between k_2 and k_3 is somewhat larger the efficiency of reaction per encounter seems to be well within a factor of ten of unity and probably in fact is very close to unity. Little or no activation energy or entropy seems to be involved in (2) although a small term from this source would be masked by the larger activation energy for diffusion of the reactants (~2 kcal./mole[18]).

(17) R. Holroyd, *J. Phys. Chem.*, **65**, 1352 (1961).

From the above-measured competitive rates (and again an assumed value of 10^9 l. mole^{-1} sec.$^{-1}$ for k_3) an absolute rate constant of 20 l. mole^{-1} sec.$^{-1}$ can be given for the abstraction of hydrogen by methyl radicals from 2,2,4-trimethylpentane at room temperature. This reaction involves the reaction of methyl radicals with the surrounding solvent molecules and is therefore not diffusion controlled. If we take the appropriate frequency here to be 2×10^{11} l. mole^{-1} sec.$^{-1}$ then a collision efficiency of 10^{-10} is estimated for (1). This value is quite reasonable for the abstraction of hydrogen from a branched chain hydrocarbon by methyl radicals.[19] If the steric factor is assumed to be 2×10^{-4} then this corresponds to an activation energy of 8.5 kcal./mole.

Since reaction 2 is diffusion controlled while reaction 1 is not the temperature coefficient of their competition is somewhat smaller than that expected if one considers only the large difference in activation energies involved in the reactions themselves. Actually the temperature coefficient should correspond to an effective activation energy difference of about 6 kcal./mole. Thus an increase in temperature from 25 to 75° should lead to an increase of the iodine concentration at which (1) and (2) are found to compete by a factor of about 4. This is approximately as found within the relatively large error involved in measuring this difference.

Methyl Radical Yields

The results of a survey of the methyl radical yields from a large number of liquid hydrocarbons are given in Tables II and III. For the Phillips hydrocarbons measurements were made at both 0.5×10^{-3} *M* and 1.0×10^{-3} *M* with, for the most part, excellent internal agreement. Typical results obtained were, for example, for 2-methylbutane $G(CH_3I) = 0.387$ and 0.396, for 2-methylpentane $G(CH_3I) = 0.272$ and 0.263 and for 3-methylpentane $G(CH_3I) = 0.156$ and 0.151. A yield of 0.278 was obtained in two experiments on liquid butane. This is somewhat smaller than the previous estimate of 0.4[4] but is regarded as being considerably more significant since carriers were not used here. It will be noted that a large scatter in the methyl iodide determinations, presumably because of a relatively rapid exchange between radioiodine present and the added carrier methyl iodide, was observed in the previous work. The higher alkyl iodides are apparently not as subject to this troublesome exchange. For the API samples a single determination was made at an iodine concentration in the region of $2\text{–}4 \times 10^{-3}$ *M*. Since the work on 2,2,4-trimethylpentane shows that competing reactions occur in the pure material only at much lower scavenger concentrations there appears to be little reason to question the efficacy of the scavenging in any of the cases under study here.

For a number of hydrocarbons methane measurements were made both in the absence and in the presence of 10^{-3} *M* iodine (*cf.* Table IV). At this concentration the iodine is used up rapidly and only

(18) D. C. Douglass and D. W. McCall, *ibid.*, **62**, 1102 (1958); D. W. McCall, D. C. Douglass, and E. A. Anderson, *J. Chem. Phys.*, **31**, 1555 (1959).

(19) *Cf.*, for example, the summary by S. W. Benson, "The Foundations of Chemical Kinetics," McGraw-Hill Book Co., Inc., New York, N. Y., 1960, p. 296.

TABLE II

METHYL RADICAL YIELDS FROM PARAFFINS

		$G(CH_3\cdot)$ Empirical[a]	$G(CH_3\cdot)$ Experimental
C_4H_{10}	Butane	0.227	0.278
C_5H_{12}	Pentane	.128	.139
	2-Methylbutane	.412	.392
C_6H_{14}	Hexane	.082	.077
	2-Methylpentane	.264	.268
	3-Methylpentane	.122[d]	.154
	2,2-Dimethylbutane	.987	.987
	2,3-Dimethylbutane	.446[d]	.344
C_7H_{16}	Heptane	.057	.054
	2-Methylhexane[b]	.183	.181
	2,4-Dimethylpentane	.310[d]	.284
	3,3-Dimethylpentane[b]	.212[d]	.343
C_8H_{18}	Octane	.042	.042
	2-Methylheptane[b]	.135	.135
	3-Methylheptane[b]	.063[d]	.071
	4-Methylheptane[b]	.063[d]	.064
	2,2,4-Trimethylpentane	.597[d]	.686[c]
	2,3,4-Trimethylpentane	.248[d]	.187
C_9H_{20}	Nonane	.032	.032
	2,2,5-Trimethylhexane	.458[d]	.485
	2,2,4,4-Tetramethylpentane[b]	.740[d]	.712
	2,3,3,4-Tetramethylpentane[b]	.261[d]	.243
$C_{10}H_{22}$	Decane	.025	.026
$C_{11}H_{24}$	Undecane	.020	.019
	2-Methyldecane[b]	.066	.074
$C_{12}H_{26}$	2,2,4,6,6-Pentamethylheptane[b]	.400[d]	.425
$C_{13}H_{28}$	Tridecane	.014	.016
$C_{14}H_{30}$	Tetradecane[b]	.012	.014
$C_{16}H_{34}$	Hexadecane[b]	.009	.014

[a] From eq. IV. [b] American Petroleum Institute sample; iodine concentration 2–4 $\times 10^{-3}$ M; all others the average of determinations at 0.5 and 1.0 $\times 10^{-3}$ M. [c] From Fig. 3. [d] Empirical estimates independent of eq. I, II, and III.

TABLE III

METHYL RADICAL YIELDS FROM CYCLOPARAFFINS

		$G(CH_3\cdot)$ Empirical[a]	$G(CH_3\cdot)$ Experimental
Cyclopentane	(0.015; 0.021; .019; .017; .021[c])[b]	0	0.019
Methylcyclopentane	(.057; .062)	0.041	.060
Cyclohexane	(.003; .005)	0	.004
Methylcyclohexane	.037; .038)	.028	.038
cis-1,2-Dimethylcyclohexane	(.049)	.042	.049
trans-1,2-Dimethylcyclohexane	(.044)	.042	.044
1,1,3-Trimethylcyclopentane[c]	(.117; 0.131)	.135	.124

[a] From eq. IV. [b] Results of individual experiments. [c] American Petroleum Institute sample.

limited exposures (<250,000 rads) are possible. The analytical accuracy is correspondingly poor. With careful degassing the inherent error involved in the measurement of $G(CH_4)$ is of the order of 0.02 to 0.04. In many cases this is a relatively large fraction of the observed yield and particularly of the difference between the measurements made in the presence and in the absence of iodine. Hydrogen determinations, which were made incidental to the methane measurements, are also given in the table. It will be noted that in the majority of cases the presence of 10^{-3} M iodine during the irradiation reduces the hydrogen yield by only 10–20%.

It is evident from the data of Table IV that 40–50% of the methane production is not affected by the presence of iodine and is presumably formed in non-

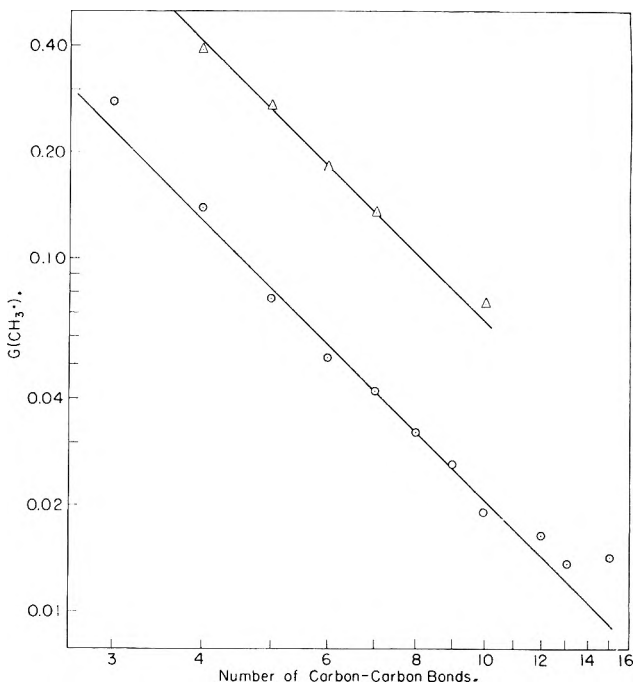

Fig. 5.—Methyl radical yields from the normal paraffins (⊙) and isoparaffins (△) as a function of the number of carbon–carbon bonds in the hydrocarbon. Lines are of slope −2.

TABLE IV

HYDROGEN AND METHANE YIELDS[a]

	$G(H_2)$ I_2 absent	$G(H_2)$ I_2 present[b]	$G(CH_4)$ I_2 absent	$G(CH_4)$ I_2 present[b]	$\Delta(CH_4)$	$G(CH_3\cdot)$[c]
Pentane	5.04	[d]	0.25	[d]	..	0.14
2-Methylbutane	3.86	3.40	0.75	0.36	0.39	0.39
2,2-Dimethylpropane	2.40[e]	1.05[e]	3.76[e]	1.66[e]	2.10[e]	2.3[e]
2-Methylpentane	4.02	3.77	0.33	0.14	0.19	0.27
3-Methylpentane	3.87	3.50	0.26	.10	.16	.15
2,2-Dimethylbutane	2.58	1.64	1.56	.76	.80	.99
2,3-Dimethylbutane	3.26	2.87	0.43	.23	.20	.34
2,4-Dimethylpentane	3.74	2.85	.54	.28	.26	.28
Octane	4.59[a]	[d]	.08[a]	[d]	..	.04
2,2,4-Trimethylpentane	2.34	1.88	1.12	0.50	.62	.69
2,3,4-Trimethylpentane	2.72	2.40	0.30	.17	.13	.19
2,2,5-Trimethylhexane	2.43	2.18	0.89	.40	.49	.49

[a] Measurements made at doses of ~150,000 rads (9 $\times 10^{18}$ e.v./g.) and at a dose rate of 250,000 rads/hr. except for octane where the dose was 4 $\times 10^6$ rads. [b] At an iodine concentration of ~1.0 $\times 10^{-3}$ M. [c] From Table II. [d] Not determined. [e] From ref. 17.

radical processes. The methane yields measured in the absence of iodine are correspondingly larger than the methyl radical yields determined in the scavenging experiments. In general the ratio of the yield of molecular methane to that of methyl radidals is in the range of 0.6 to 0.9 and is not dependent on the structure of the parent molecule in any obvious fashion. As expected from the more extensive studies on 2,2,4-trimethylpentane, the difference between the methane yields in the absence and in the presence of iodine at the absorbed dose rates employed here is, within experimental error, similar to (and presumably slightly smaller than) the methyl radical yields measured in the scavenging experiments.

One of the objectives of the present study was the examination of possible correlations of the radiation chemical yields of methyl radicals with the detailed structure of the parent hydrocarbon. It should be pointed out that since, except for neopentane, the methyl radical production represents only a small

fraction of the total radical production (<20%) any correlation of frequency of bond rupture with structure, if it exists, should become readily observable experimentally. An examination of the data of Table II shows that the methyl radical yields from the normal and 2-methyl paraffins decrease monotonically as the carbon chain is lengthened. This is qualitatively in accord with the early suggestion of Burton[20] that the frequency of rupture of the end groups in the normal alkanes should correspond to the fractional importance of these bonds in the molecule. A more detailed study of the data, however, shows that the yields drop off somewhat more rapidly than would be indicated by direct proportionality. The logarithmic plot of the methyl radical yield against the number of carbon–carbon bonds $(n - 1)$ given in Fig. 5 shows that the slope of the dependence has the interesting value of -2. For these two series of hydrocarbons, therefore, the methyl radical yields can be expressed by the empirical relationships

$$G(CH_3\cdot)_{\text{normal paraffins}} = \frac{2.04}{(n-1)^2} \qquad \text{(I)}$$

and

$$G(CH_3\cdot)_{\text{2-methyl paraffins}} = \frac{6.60}{(n-1)^2} \qquad \text{(II)}$$

where n is the carbon number of the parent molecule. Except for butane (and for what appears to be an anomalously high observation on hexadecane) the measured yields correspond to those given by I and II quite well, *i.e.*, within 10%. Even in the case of butane, which might well be expected to be atypical because of its small size, the indicated difference is only 20%.

A more generalized empirical relationship can be developed from the above if we assume that the various branched hydrocarbons contain three types of methyl groups: type A where no other methyl groups are attached to the same carbon atom, type B where one other methyl group and type C where two other methyl groups are attached. Thus the normal paraffins contain two type A methyl groups to each of which may be assigned a yield of $1.02/(n-1)^2$. If we assume that this yield applies to the omega methyl group in the case of the 2-methyl paraffins then we obtain a contribution of $2.79/(n-1)^2$ for each of the type B methyl groups present. If we further assume that the $(n-1)^{-2}$ dependence applies to the 2,2-dimethyl paraffins then we can give

$$G(CH_3\cdot)_{\text{2,2-dimethyl paraffins}} = \frac{24.69}{(n-1)^2} \qquad \text{(III)}$$

from the measurement on 2,2-dimethylbutane. Equation III indicates a contribution of $7.89/(n-1)^2$ for type C methyl groups. For whatever significance it might be it is interesting to note that the ratio of type C to type A coefficients is very nearly the square of the ratio of type B to type A coefficients. Neopentane (2,2-dimethylpropane) is of course the singular example of a tetramethyl substituted carbon. Here the contribution assigned to each methyl group may be expressed as $9.2/(n-1)^2$. A slight increase of the coefficient over type C methyl groups is noted although the effect of increased substitution is seen to be saturating due to the fact that methyl radical formation represents the predominant mode of rupture in this case.

The methyl radical yields obtained from the various hydrocarbons can be summarized by a single empirical relationship of the form

$$G(CH_3\cdot) = \frac{1}{(n-1)^2}[1.02a + 2.79b + 7.89c] \qquad \text{(IV)}$$

where a, b, and c are the numbers of type A, B, and C methyl groups, respectively present. The yields predicted by IV are given in Tables II and III and are seen to correspond rather well to the experimental measurements. The agreement for the normal and 2-methyl paraffins and for 2,2-dimethylbutane of course only again reflects relations I, II, and III given above. Twelve of the branched hydrocarbons (indicated by superscript d in the table) may however be regarded as independent checks on the estimates made from IV. Of these twelve seven agree within 15% and of these seven three agree within 5%. The major discrepancy noted is with 3,3-dimethylpentane where the yield is 62% larger than predicted. This, together with the fact that the experimental yield for 3-methylpentane is similarly high by 26%, suggests that additional small terms should be added to IV to cover cases where ethyl groups are attached to the same carbon atom as the methyl groups under consideration. The experimental values for 2,3-dimethylbutane and for 2,3,4-trimethylpentane are lower than the predicted ones by about 25%. Embarrassingly the next most important discrepancy (16%) occurs with the much-studied 2,2,4-trimethylpentane. It will be noted however that the difference for 2,2,5-trimethylhexane, which has a methyl configuration similar to 2,2,4-trimethylpentane, is only 6%.

It is seen from the above that where more than one methyl group is attached to a particular carbon atom each influences the others in such a way as to mutually enhance the total production of methyl radicals. The effect is very pronounced. Thus 2,2,4,4-tetramethylpentane, which has six type C methyl groups, has an approximately threefold greater methyl radical yield than 2,3,3,4-tetramethylpentane, which has six type B methyl groups. In a similar fashion the yield from 2,3-dimethylbutane is found to be considerably lower than that from 2,2-dimethylbutane. Comparisons of the yields from 2-methylpentane and 3-methylpentane and from the series, 2-methylheptane, 3-methylheptane and 4-methylheptane, illustrate the relative importance of type B and type A methyl groups in otherwise similar systems. It will be particularly noted that in the case of 4-methylheptane, where the branch is very well isolated from the other ends of the molecule, that the correspondence between the measurement and the value predicted for three type A methyl groups is excellent.

One other interesting feature of equation IV is the very rapid decrease in yield expected with increased molecular size. Thus while in the absence of such a generalization a very high yield of methyl radicals might be predicted for 2,2,4,6,6-pentamethylheptane the yield is actually relatively small. The moderate yield observed corresponds very nicely with that ex-

(20) M. Burton, *J. Phys. Colloid Chem.*, **51**, 786 (1947).

pected from IV because of the large size of the molecule. One additional comparison which is extremely interesting involves the methyl radical yields from 2,4-dimethylpentane and 2,3,4-trimethylpentane. One would at first think that the yield from the latter molecule would be the greater. It is seen however that the fractional increase expected to be produced by the additional methyl group (12.52/11.52 = 1.09) is more than balanced by the decrease due to the increased molecular size (36/49 = 0.74). A net decrease is therefore expected and is observed.

As indicated in Table III, the methyl radical yields predicted by IV also seem to apply reasonably well to the methyl substituted cyclopentanes and cyclohexanes. No methyl radicals are expected from cyclopentane and cyclohexane themselves. Small yields are in fact observed. It was shown by collecting separate fractions that these yields are not attributable to contaminating vinyl iodide. In the case of cyclopentane one experiment was carried out with an API sample and gave a methyl iodide yield quite similar to that with the Research Grade material. It would therefore seem that these methyl radicals probably do not result from impurities but rather that a certain amount of rearrangement may be possible. The methyl radical yield from methyl cyclopentane is higher than predicted to about the same extent as the yield from cyclopentane alone.

The theoretical foundation for equation IV is not obvious at the moment. It would seem that such a foundation awaits the detailed application of the more general treatments of energy flow within the molecule before bond dissociation occurs. Apropos of this the $(n - 1)^{-2}$ dependence of the yield on molecular size indicates very strongly that energy must be exchanged between various degrees of freedom. In the absence of such energy flow one would expect that the yields would be more nearly proportional to the frequency of occurrence of the methyl groups. A related manifestation would seem to be the large influence of adjacent methyl groups on the probability of rupture of a given C–CH_3 bond.

Acknowledgment.—The authors wish to express their appreciation to Mr. Gerald Buzzard for his aid with many of the methyl iodide determinations reported here.

ANALYSIS OF LIQUID DIFFUSIVITY MEASUREMENTS TO ACCOUNT FOR VOLUME CHANGES ON MIXING—THE DIAPHRAGM CELL

By Donald R. Olander

Department of Nuclear Engineering and Inorganic Materials Research Division, Lawrence Radiation Laboratory, University of California, Berkeley, California

Received September 11, 1962

The method of computing differential diffusion coefficients in liquids from diaphragm cell data has been re-examined to allow for volume changes upon mixing. The diffusion coefficient upon which the new calculational method is based is of greater theoretical interest than the common Fick diffusivity. The difference between the two is usually small in diaphragm cell work, but deviations as large as 6% have been found for the ethanol–water system.

Most experimental liquid phase diffusion work is based upon a diffusion coefficient defined by Fick's law (in the sense originally used by Fick)

$$\mathbf{N} \equiv -D_{\text{Fick}}\nabla C \qquad (1)$$

However, a more satisfactory definition of the mutual diffusion coefficient for binary systems is

$$\mathbf{n} \equiv -\rho_t D\nabla W + W(\mathbf{n} + \mathbf{n}_s) \qquad (2a)$$

$$\mathbf{N} \equiv -C_t D\nabla x + x(\mathbf{N} + \mathbf{N}_s) \qquad (2b)$$

$$\mathbf{N} \equiv -D\nabla C + C(\mathbf{N}\bar{V} + \mathbf{N}_s\bar{V}_s) \qquad (2c)$$

In eq. 2, the subscript s denotes the component chosen as solvent, and no subscript denotes the solute. W and x are the solute mass and mole fractions, respectively; D is the mutual diffusion coefficient; $\mathbf{n}$ and $\mathbf{N}$ the mass and molar fluxes of solute relative to a stationary observer; ρ_t and C_t the total mass and molar density, respectively; $\bar{V}$ and $\bar{V}_s$ denote the partial molal volumes of the solute and solvent, respectively. The quantities in the parentheses of eq. 2 are: (a) the total density times the mass average velocity, (b) the total concentration times mole average velocity, and (c) the volume average velocity. Each of eq. 2 is an equivalent definition of the same diffusion coefficient.[1,2] The derivation of eq. 2c from 2b is shown in the appendix.

The quantity defined by eq. 2 has numerous advantages over the Fick diffusion coefficient: (1) The diffusivity is defined in the same way for liquids and gases; eq. 2b is the Stephan–Maxwell equation for a binary gas.

(2) The Fick diffusion coefficient depends upon the component in terms of which concentrations are measured (*i.e.*, $D_{AB} \neq D_{BA}$). The coefficient defined by eq. 2 characterizes the system, and is independent of the method of measurement.

(3) Eq. 2 defines the diffusion coefficient to which all theoretical interpretation of transport phenomena in liquids refer (*e.g.*, it is the D^V of Hartley and Crank[3]).

(4) The convective term in eq. 2 is essential if a diffusion equation is to be coupled with the hydrodynamic equations, as in the analysis of mass transfer in laminar flow systems.[4]

(5) Unless the last terms of eq. 2 are included in the definition of D, experimentally measured diffusivities

(1) R. B. Bird, W. E. Stewart, and E. N. Lightfoot, "Transport Phenomena," John Wiley and Sons, New York, N. Y., 1960, pp. 502, 518.
(2) I. Prigogine, *Bull. Acad. Roy. Sci. Belg.*, [5], **34**, 930 (1948).
(3) G. S. Hartley and J. Crank, *Trans. Faraday Soc.*, **45**, 801 (1949).
(4) D. R. Olander, *Intern. J. Heat Mass Transfer*, **5**, 765 (1962).

will differ according to the geometry and convective flow conditions of the measuring device. Gross fluid motion need not be the result of "forced" or "natural" convection; some sort of average motion is inevitably present as a result of the diffusive movement of the two components of the mixture.

The Fick diffusion coefficient and that defined by eq. 2 are identical if the volume average velocity in the experimental device is zero at all points of the diffusion path. This condition is precisely fulfilled for diaphragm and capillary cells only if there is no volume change on mixing (*i.e.*, if the partial molal volumes of each component are constant in the range of concentration over which the experiment is conducted). The following discussion will develop the means by which volume change effects can be incorporated into the treatment of the data obtained from a typical diffusion cell. For simplicity, the diaphragm cell will be investigated, although a similar analysis should be applied to all experimental diffusivity devices.

Descriptions and analyses of diaphragm cells for systems with no volume change on mixing are given in detail elsewhere.[5,6] Two compartments (usually of equal volume) are separated by a porous glass diaphragm, through which transfer occurs solely by molecular diffusion. To minimize natural convection effects, the diaphragm is mounted in a horizontal position, with the denser solution beneath the disk and the less dense one above it. The lower compartment is completely filled with liquid, while the upper one contains a small free volume open to the atmosphere to accommodate the small volume changes which may occur.[7]

An analysis of volume change effects upon diaphragm cell measurement has recently been presented by Dullien and Shemilt.[8,9] However, their derivation contains an error; even if it were rigorous, the problem of extracting differential diffusivities from cell measurements is so complex a task that the authors did not even apply it to their own experimental data.[10]

(5) R. H. Stokes, *J. Am. Chem. Soc.*, **72**, 763, 2243 (1950).

(6) A. R. Gordon, *Ann. N. Y. Acad. Sci.*, **46**, 285 (1945).

(7) In principle it is possible to avoid volume changes by sealing off the top compartment. However, this will lead to a large pressure buildup in the cell which (if it does not rupture the apparatus) will affect the diffusion coefficient.

(8) F. A. L. Dullien and L. W. Shemilt, *Trans. Faraday Soc.*, **58**, 244 (1962).

(9) F. A. L. Dullien and L. W. Shemilt, *Can. J. Chem. Eng.*, **39**, 242 (1961).

(10) Equation 21 of ref. 8 can be written (in the nomenclature of the reference) as

$$X\beta d\theta = \frac{\rho_A''}{\Delta\rho_A}\frac{dV''}{V''} + d \ln \Delta\rho_A$$

where the symbol X is

$$X = {}^1/_2 \bar{D}_{AB}(\omega_A{}^+ r_{BA} + \omega_B{}^+)^{-1}(1 + K)$$

K and β are defined by eq. 22 and 23 of the same reference. Integrating eq. 21 from the initial to final conditions yields

$$\int_0^\theta X\beta d\theta = -(\ln R + I)$$

where I and R are defined by eq. 25 and 26.

Eq. 24 reads

$$\bar{\beta}\int_0^\theta X d\theta = -(\ln R + I)$$

For both of the preceding equations to be valid, $\bar{\beta}$ must be the X-weighted time average

$$\bar{\beta} = \int_0^\theta X\beta d\theta \Big/ \int_0^\theta X d\theta$$

Despite the considerable mathematical difficulties which the problem in its completely rigorous form poses, the generally small perturbation of the common Fick coefficients caused by volume change effects permits an approximate correction factor to be calculated.

Since the perturbation from Fick's Law is caused in part by non-equi-volume flow conditions, eq. 2c has been chosen as the most convenient starting point.

Diffusion through the diaphragm is assumed to be one dimensional and quasi-steady state. From eq. (2c), the flux is

$$N = -\frac{D}{1 - C\bar{V}_s\left[\frac{\bar{V}}{\bar{V}_s} + \frac{N_s}{N}\right]}\frac{dC}{dy} \qquad (3)$$

where y is measured perpendicular to the plane of the

Now rewrite eq. 21 as

$$\beta d\theta = \frac{1}{X}\left[\frac{\rho_A''}{\Delta\rho_A}\frac{dV''}{V''} + d \ln \Delta\rho_A\right]$$

Integration from the initial to the final conditions yields

$$\int_0^\theta \beta d\theta = \int_0^f \frac{1}{X}\left[\frac{\rho_A''}{\Delta\rho_A}\frac{dV''}{V''} + d \ln \Delta\rho_A\right]$$

Eq. 30 reads

$$\bar{\beta}\theta = \int_0^f \frac{1}{X}\left[\frac{\rho_A''}{\Delta\rho_A}\frac{dV''}{V''} + d \ln \Delta\rho_A\right]$$

For both of the preceding equations to be valid, $\bar{\beta}$ must be the simple time average

$$\bar{\beta} = \int_0^\theta \beta d\theta \Big/ \int_0^\theta d\theta$$

Thus, Dullien and Shemilt have erroneously employed two values of $\bar{\beta}$, neither of which is equal to their eq. 27. The simple average definition reduces to eq. 27 if β is assumed to be a linear function of θ. Equations 24 and 30 are simply two different definitions of $\bar{\beta}$, and since they are not equal, the combination of eq. 29 (which is based upon the first $\bar{\beta}$) and eq. 30 (which is based upon the second) cannot be performed to yield eq. 31. Equation 33, therefore, is not a rigorous formulation of the problem; the error incurred by its use will depend upon the difference between the simple time average and the X-weighted time average of β as derived above. In addition, since $\bar{\beta}$ appears in eq. 29, the difference between the X-weighted $\bar{\beta}$ and the $\bar{\beta}$ of eq. 27 will influence the result.

Even if eq. 33 were rigorous, calculation of differential diffusivities from it presents a formidable problem. If values of ρ_{A0}', ρ_{A0}'', V_0', V_0'' and the density–composition curves are specified, over-all and one component material balances provide V'', ρ_A'', ρ', ρ'', ω_A', and ω_A'' as functions of ρ_A'. A value of r_{BA} is then computed from eq. 8 (with ρ and ρ_A primed). If a D_{AB}–composition variation is assumed, F can be computed as a function of ρ_A' from eq. 34 (by numerical integration, unless the density–composition curve is amenable to analytic approximation. A series of $F(\rho_A')$ values must be computed for $\rho_{A0}' \leq \rho_A' \leq \rho_{Af}'$, which then permits the two integrals in the denominator of eq. 33 to be integrated numerically. The parameter I is then evaluated by numerical integration of eq. 25. This yields a single value of $\bar{D}_{AB}$ for a single run and for an assumed D_{AB}–composition variation. These calculations must be repeated for as many assumed D_{AB}–composition curves (each time for all experiments involved) as are required for all of the computed $\bar{D}_{AB}$ from eq. 33 to agree with those obtained from the data and by eq. 29 (there is an obvious misplacement of I and R here). However, the previous discussion has indicated that the $\bar{\beta}$ which should appear in eq. 29 (the X-weighted average) is not that used by Dullien and Shemilt.

In any case, the authors never performed these calculations for their own data on the ethanol–water system. Instead, they computed the effect of volume changes for a single hypothetical run, found it to be small, and interpreted their own experimental data by the conventional constant volume methods. The reason that the volume change effect was small in the example treated by Dullien and Shemilt (in addition to possible errors associated with an incorrect treatment of $\bar{\beta}$) is that the concentration range considered (0–60 g. EtOH/100 ml.) was not in the region of the most drastic volume change effects. According to Fig. 1 of this paper the region from ~65–78.5 g./100 ml. (~14–17 moles/l.) is the most serious in this regard. They explained the 7% discrepancy between their value of the limiting diffusivity at 100% ethanol and that of Hammond and Stokes[12] as due to the increased number of data points and a minor improvement in the conventional graphical method of Stokes. It will be shown in the paper that a discrepancy of this order is due to volume change effects in the work of Hammond and Stokes.

diaphragm, with $y = 0$ at the lower face. A material balance on the lower or fixed volume compartment shows that the molar flux ratio in eq. 3 equals $-(\bar{V}_0/\bar{V}_{s0})$, where the subscript 0 denotes the lower or fixed volume compartment. Since the right-hand term in the denominator of eq. 3 is zero for ideal solutions and is small even when volume changes on mixing are substantial, the following approximation will be made: the denominator will be written as $1/(1 - x) \approx 1 + x$; the solvent molal volume in the correction term will be taken as the average value in the concentration range between the upper and lower compartments ($\bar{V}_{savg}$); the ratio of the solute and solvent partial molal volumes will be assumed linear in solute concentration over the same interval

$$\bar{V}/\bar{V}_s = L + rC, \qquad C_1^i \leq C \leq C_0^i \qquad (4)$$

where the superscript i denotes initial conditions, and the subscript 1 denotes the variable volume (top) compartment. L and r are constants determined from the best linear fit of the partial molal volume ratio–concentration curve. Only a numerical value of r is required for this analysis. With these simplifications and the material balance relation for the bottom compartment, eq. 3 can be integrated to yield

$$-\frac{2}{\beta}\frac{1}{C_0 - C_1}\frac{dC_0}{dt} = \frac{1}{C_0 - C_1} \times \int_{C_1}^{C_0} D[1 - r\bar{V}_{savg}\, C(C_0 - C)]dC \qquad (5)$$

Here t is the time and β the cell constant, which for equal volumes of both compartments is twice the effective pore area divided by the product of the cell volume and the effective pore length. Further treatment of eq. 5 requires a material balance relation between the concentrations in each compartment.

If the initial volumes in each compartment are equal to v_0, and the pore volume denoted by v_p, material balances on both the solute and solvent yield

$$\frac{v_1/v_0 + v_p/2v_0}{1 + v_p/2v_0} = \frac{C_0^i + C_1^i - C_0}{C_1} = \frac{C_{s0}^i + C_{s1}^i - C_{s0}}{C_{s1}} \qquad (6)$$

where v_1 is the variable volume of the solution in the top compartment. The solvent concentration in the above expression can be eliminated by the relation $C\bar{V} + C_s\bar{V}_s = 1$. The reciprocal partial molar volume of the solvent will be approximated by a linear relation in solute concentration

$$1/\bar{V}_s = 1/\bar{V}_{sb} + QC \qquad (7)$$

The constants for the region $C_0^i \geq C \geq C_1^i$ are obtained from the partial molal volume data. The desired relation between C_0 and C_1 can be written as

$$C_1 = (C_0^i + C_1^i - C_0)(1 + F) \qquad (8)$$

where, for small volume changes[11]

$$F = \left\{\frac{r\bar{V}_{sb}(C_0^i - C_0)}{2(C_0^i + C_1^i - C_0)^2[1 + r\bar{V}_{sb}(C_1^i)^2]}\right\} \times \left\{4(C_1^i)^2(C_0 - C_1^i) + {}^1/_2(C_0^i - C_0)\left[(C_0^i + C_0)^2 - \frac{\{4C_1^i + 2(C_0^i - C_0) - [1 - r\bar{V}_{sb}(C_1^i)^2](C_0^i + C_0)\}^2}{[1 + r\bar{V}_{sb}(C_1^i)^2]^2}\right]\right\} \qquad (9)$$

Two special cases of eq. 9 are applicable to most diaphragm cell work

(1) Pure solvent is initially placed in the upper compartment, of $C_1^i = 0$.

(2) The upper compartment is pre-loaded with solute to reduce the total concentration driving force. Since the factor F (which represents the fractional volume change of the upper compartment) is zero initially, and at its maximum at the end of the run, replacement of C_0 in the denominator of the first bracketed term in eq. 9 by the final concentration in the lower compartment, C_0^f, is a justifiable simplification. Furthermore, since volume changes are small, $C_0^i + C_1^i - C_0^f \backsimeq C_1^f$. The last term in the second bracket is multiplied by $(C_0^i - C_0)$, which is usually kept small compared to the driving force in high concentration experiments. In addition, the two components of this term are of opposite sign and tend to cancel. Neglecting the last term in the second bracket will only introduce a small error into what is already a small correction factor.

In both of these cases, eq. 9 reduces to

$$F = 2A(C_0^i - C_0)(C_0 - C_1^i) \qquad (10)$$

where in the first case ($C_1^i = 0$)

$$A = r\bar{V}_{sb} \qquad (11)$$

and in the second case ($C_1^i \neq 0$)

$$A = \frac{r\bar{V}_{sb}}{1 + r\bar{V}_{sb}(C_1^i)^2}\left(\frac{C_1^i}{C_1^f}\right)^2 \qquad (12)$$

Utilizing the smallness of F compared to unity and approximating C_0 in eq. 10 by its equivalent for the constant volume case, the left-hand side of eq. 5 can be written in terms of the driving force $\theta = C_0 - C_1$. Gordon[6] and Stokes[5] have shown for $r = 0$, the right-hand side of the eq. 5 can be considered constant at $C_0 = C_0^m$ and $C_1 = C_1^m$, where $C^m = {}^1/_2(C^i + C^f)$. Since the partial molal volume changes introduce a small correction to the integrand, it will be assumed that the same approximation is valid for the entire integral of eq. 5. Expanding the differential diffusion coefficient is a power series in C

$$D = D_0 + \sum_{j=1} a_j C^j \qquad (13)$$

the integration of (5) yields

$$\bar{D}\left[\frac{1 - AG}{1 - r\bar{V}_{savg}\delta_0}\right] = D_0 + \sum_{j=1} \xi_j \left[\frac{1 - r\bar{V}_{savo}\delta_j/\xi_j}{1 - r\bar{V}_{savg}\delta_0}\right] a_j \qquad (14)$$

where $\bar{D}$ is the measured integral coefficient

(11) Equation 9 is correct to the extent that $\sqrt{1 + x} \approx 1 + {}^1/_2x - {}^1/_8x^2$, where $x = \frac{2r\bar{V}_{sb}(C_0^i - C_0)}{[1 + r\bar{V}_{sb}(C_1^i)^2]^2}\{4C_1^i + 2(C_0^i - C_0)[1 + {}^1/_4r\bar{V}_{so}(C_0^i + C_0)^2] - [1 - r\bar{V}_{sb}(C_1^i)^2](C_0^i + C_0)\}$

Since r and $(C_0^i - C_0)$ are usually both small, this approximation is quite satisfactory.

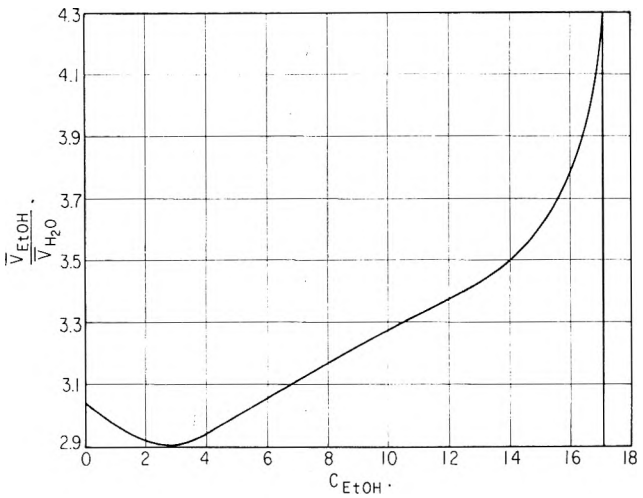

Fig. 1.—Partial molal volume ratio for the ethanol-water system at 25°—From "Thermodynamics," 2nd Ed., by K. S. Pitzer, L. Brewer, G. N. Lewis, and M. Randall, McGraw-Hill Book Co., New York, N. Y., 1961, p. 209.

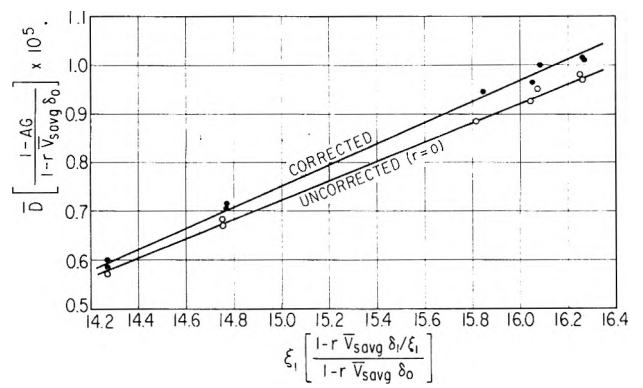

Fig. 2.—Method of obtaining the constants describing the diffusivity of the ethanol–water system—with and without consideration of volume changes.

$$\bar{D} \equiv \frac{1}{\beta t} \ln\left(\frac{\theta_i}{\theta_f}\right) \tag{15}$$

$$G = \frac{2(C_0^i + C_1^i)(\theta_i - \theta_f) - {}^3/_2(\theta_i^2 - \theta_f^2) + \theta_i^2 \ln\left(\frac{\theta_i}{\theta_f}\right)}{4 \ln\left(\frac{\theta_i}{\theta_f}\right)} \tag{16}$$

$$\xi_j = \frac{(C_0^m)^{j+1} - (C_1^m)^{j+1}}{(j+1)(C_0^m - C_1^m)} \tag{17}$$

$$\delta_j = C_0^m \xi_{j+1} - \xi_{j+2} \tag{18}$$

Equation 14 is the basic relation from which the constants D_0 and a_j can be obtained from the data. The AG term accounts for volume changes in the upper compartment, and the terms containing $r\bar{V}_{savg}$ reflect the definition of the diffusion coefficient by eq. 2. If $r = 0$, eq. 14 reduces to the relation which has been derived previously by Hammond and Stokes[12] and its solution is equivalent to the usual graphical techniques.[5,6] Non-integer values of j are permitted, and may be quite useful for solutions of electrolytes. If D_0 is known (as a Nernst limiting value), eq. 14 is divided by D_0 and used as with non-electrolytes.

(12) B. R. Hammond and R. H. Stokes, *Trans. Faraday Soc.*, **49**, 890 (1953).

Whether or not the precision of the experimental measurements warrants full scale computation of the usually small difference between the Fick diffusion coefficient and that of eq. 2 can be readily determined from eq. 14. The bracketed terms in eq. 14 can be evaluated for the experiment which involves the largest driving force in the region of largest r. If these terms differ from unity by the same order as the experimental precision, then the correction for volume changes will just barely be significant.

It may prove inconvenient to fit the data with a polynomial of a reasonable number of terms, and the graphical method may be easier to employ if r is assumed to be zero. In this case, eq. 14 can be used to provide a correction to the Fick coefficients. The experimental data are fitted to eq. 14 for $r = 0$ and for the true values.[13] This yields two sets of coefficients, D_0^* and a_j^* for $r = 0$, and D_0 and a_j for r from partial molal volume data. The correction to the graphically determined Fick diffusion coefficient is then

$$\frac{D}{D_{Fick}} = \frac{D_0 + \sum_{j=1} a_j C_j}{D_0^* + \sum_{j=1} a_j^* C_j} \tag{19}$$

Application to the Ethanol–Water System.—The system ethanol–water exhibits rather large volume changes on mixing, as indicated by the partial molal volume ratio–concentration curve shown in Fig. 1. Since Hammond and Stokes[12] have employed the diaphragm cell technique to measure the diffusivity of this system without accounting for volume changes, the methods derived above will be used to correct their values. These authors attempted to minimize the effects of volume changes by dividing the concentration range into three groups, 0–6.5 moles EtOH/l., 6.5–13, and 13 to 17 (pure ethanol). It is obvious from Fig. 1 that the last of these groups was most severely subjected to volume change effects; therefore, the analysis was applied to these data (reported in Table I of ref. 12).

TABLE I

DIFFERENTIAL DIFFUSION COEFFICIENT IN THE ETHANOL–WATER SYSTEM

G. EtOH/100 ml. soln.	Diffusion coefficient, cm.²/sec. × 10⁵	
	No volume changes[b]	With volume changes
65	0.551	0.561
70	.766	0.797
75	.981	1.034
78.51[a]	1.132	1.200

[a] Pure ethanol. [b] From Table II, ref. 12.

Complete accounting for volume change effects requires the initial and final concentrations in each compartment, the integral diffusion coefficient, and r, $\bar{V}_{savg}$, and $\bar{V}_{sb}$ for each run. Hammond and Stokes, however, have reported only the mean concentrations (C_0^m and C_1^m) and the integral coefficients. They stated that the initial ethanol-rich solutions in their group 3 ranged from 70 to 78 g. EtOH/100 ml. solution. On this basis, the data can be divided into three subgroups, according to estimated initial ethanol contents of the top compartment: (a) two runs with $C_1^i = 15.19$ (70 g./100 ml.); (b) two runs with $C_1^i =$

(13) Since the ratio D/D_{Fick} will usually be close to unity, only an approximate fit is required to yield a satisfactory correction factor.

16.28 (75 g./100 ml.); (c) five runs with $C_1^i = 17.04$ (pure ethanol). With C_0^m, C_1^m and the assumed values of C_1^i, all of the required concentrations can be computed by use of eq. 8, 10, and 12 and the definitions of C_0^m and C_1^m. Values of r, $\bar{V}_{savg}$, and $\bar{V}_{sb}$ are then computed for each of the subgroups from the partial molal volume data and Figure 1. They are[14]

(a) $13.4 \leq C \leq 15.2$, $r \approx 0.11$, $\bar{V}_{savg} \approx 0.0164$, $\bar{V}_{sb} \approx 0.0252$

(b) $13.4 \leq C \leq 16.3$, $r \approx 0.16$, $\bar{V}_{savg} \approx 0.0161$, $\bar{V}_{sb} \approx 0.0314$

(c) $15.0 \leq C \leq 17.0$, $r \approx 0.39$, $\bar{V}_{savg} \approx 0.0149$, $\bar{V}_{sb} \approx -0.0294$

Since the differential diffusivities were found to be linear in ethanol concentration, the calculations were performed using only the first term of the series of eq. 14. The results are shown in Fig. 2; the lower line essentially reproduces the calculations of Hammond and Stokes, and the constants are $D_0^* = -2.230 \times 10^{-5}$ and $a_1^* = 0.197 \times 10^{-5}$. The upper line shows the effect of including volume changes; its constants are $D_0 = -2.503 \times 10^{-5}$ and $a_1 = 0.217 \times 10^{-5}$. The effect on the differential diffusion coefficients caused by this change in the constants is shown in Table I. The maximum change occurs for pure ethanol, where a 6% error in the diffusion coefficient is introduced if volume change effects are neglected. This deviation is substantially greater than the reported experimental precision of 0.5%. These results are subject to the errors involved in approximating the partial molal volume ratio curve by straight lines and in the estimate of the initial concentrations associated with the data of Hammond and Stokes. The major source of the 6% error at 100% ethanol is due to Hammond and Stokes' choice of ethanol as the solute (the component whose concentration appears in Fick's law) for all experiments. This accentuates the discrepancies resulting from volume changes in the high ethanol content runs. If the computation had been based on water as the solute, the deviations from Fick's law would have been much less prominent. The volume change effect is practically negligible in the low ethanol experiments. Considerable cancellation of the effects due to volume changes of the top component (the AG term of eq. 14) and the use of a diffusion coefficient defined by eq. 2 (the $rV_{savg}\delta_0$ term on the left of eq. 14) rendered the net effect of volume changes less pronounced than it would have been if only one of the two effects had been considered.

In recent experimental work on the $CuSO_4$–H_2O system,[15] by contrast, the r values were considerably larger than in the ethanol–water case. However, the solute ($CuSO_4$) was always at a molar concentration an order of magnitude smaller than the ethanol concentrations in the experiments of Hammond and Stokes. As a result, the deviations from Fick's law were found by the method described in the paper to be far smaller than the experimental precision. The small value of r for the system *n*-butyl alcohol–water rendered volume change effects negligible as well.

(14) r, $\bar{V}_{savg}$, and $\bar{V}_{sb}$ are in liters per mole.

(15) A. Emanuel and D. R. Olander, *J. Chem. Eng. Data*, **8**, 31 (1963).

Conclusion

For most binary liquids, the effects of volume changes on mixing are too small to alter appreciably the diffusion coefficients measured in diaphragm cells. However, for systems such as ethanol–water, $HClO_4$–water, H_2SO_4–water, and HNO_3–water, volume changes may be of sufficient magnitude to warrant treatment of diaphragm cell data by the method outlined here. Although the treatment here has been limited to the diaphragm cell, interpretation of data from all types of diffusivity measuring devices should be based upon eq. 2 rather than Fick's law.

Appendix

Equation 2b can be written as

$$C(\mathbf{u} - \mathbf{V}^*) = -C_t D \nabla x \qquad \text{(A-1)}$$

where $\mathbf{V}^*$ is the mole average velocity, $\mathbf{V}^* \equiv x\mathbf{u} + x_s\mathbf{u}_s$. $\mathbf{u}_s$ and $\mathbf{u}$ are the velocities of the solute and solvent, respectively, defined by their relation to the molar fluxes in the lab system, $\mathbf{N} = C\mathbf{u}$ and $\mathbf{N}_s = C_s\mathbf{u}_s$. The solute velocity relative to the mole average velocity can be written as

$$\mathbf{u} - \mathbf{V}^* = \frac{C_s}{C_t}(\mathbf{u} - \mathbf{u}_s) \qquad \text{(A-2)}$$

Similarly, the solute velocity relative to the volume average velocity is

$$\mathbf{u} - \mathbf{V}^+ = C_s\bar{V}_s(\mathbf{u} - \mathbf{u}_s) \qquad \text{(A-3)}$$

where $\mathbf{V}^+$ is the volume average velocity, $\mathbf{V}^+ = C\bar{V}\mathbf{u} + C_s\bar{V}_s\mathbf{u}_s$.

For a binary system at constant pressure and temperature

$$\bar{V}C + \bar{V}_sC_s = 1 \qquad \text{(A-4)}$$

$$\bar{V}dC + \bar{V}_sdC_s = 0 \qquad \text{(A-5)}$$

Using eq. A-4 and A-5, and the relation $x = C/C_t$, $x_s = C_s/C_t$, $C_t = C + C_s$, the following relation between mole fraction and molar concentration gradients can be derived

$$\nabla C = C_t^2\bar{V}_s\nabla x \qquad \text{(A-6)}$$

Substituting eq. A-2, A-3, and A-6 into A-1, there results

$$C(\mathbf{u} - \mathbf{V}^+) = -D\nabla C \qquad \text{(A-7)}$$

This is equivalent to eq. 2c.

RADIATION INDUCED POLYMERIZATION OF PROPYLENE AT HIGH PRESSURE[1]

BY DANIEL W. BROWN AND LEO A. WALL

National Bureau of Standards, Washington 25, D. C.

Received September 22, 1962

The polymerization of propylene was investigated at temperatures of 21, 48, and 83°, and at pressures between 5000 and 16,000 atmospheres. The effect of reaction conditions on the rate of polymerization and the molecular weight suggests that the polymerization proceeds by a radical mechanism with a large monomer transfer constant. The degree of polymerization was equal to the ratio of propagation rate to transfer rate. It varied from 25 to 75, decreasing with temperature increases or pressure decreases. The rate of polymerization increased by a factor of 100 at room temperature between pressures of 5000 and 16,000 atmospheres. The activation energy was 8 kcal./mole at 5000 and 12,000 atmospheres pressure.

Introduction

A technique has been developed whereby materials can be exposed to ionizing radiation at pressures at least as high as 16,000 atmospheres. Such pressures substantially affect the rate constants in vinyl polymerizations. Propylene, for example, was found to polymerize readily with high values for the number, $G(-M)$, of monomer units converted to polymer per 100 e.v. of energy absorbed. The kinetics of the polymerization are described herein.

Experimental

The pressure vessels were described previously.[2] Degassed propylene (10–12 g., Matheson, Reagent Grade) is condensed into the pre-evacuated, precooled bomb. A plug bearing a Bridgeman seal is inserted in the bore without admitting air. Enough force is applied to a piston bearing on the seal to prevent leakage of propylene. The vessel is brought to temperature and the contents then are brought to the desired pressure by forcing the sealing plug into the cylinder. The vessel is exposed to radiation from cobalt-60, cooled, and opened. The unconverted propylene is measured by passing it through a wet test meter. The polymer is dissolved in benzene, and weighed after removing the solvent under vacuum. The polymerization rate is calculated by dividing conversion by time. The maximum conversion was 20%.

The values of pressure are believed to be within 400 atmospheres of the true values; they have been corrected for deformation of the cylinder under load, packing friction, and the change in pressure that occurs when the bomb is removed from the hydraulic press.

Heat is applied by use of an electrical winding around the bomb. The temperature is controlled to 0.5°, by using a signal from a thermocouple located between wall and winding to operate the heaters. A relation at atmospheric pressure was established between the temperature inside the bomb and the regulating temperature. This relation was assumed to hold when the contents of the bomb were under pressure.

Dose rates in the bombs were established through use of cobalt blue glass plates obtained from Bausch and Lomb Optical Co. Number average molecular weights were determined with a Mechrolab vapor pressure osmometer.

Results

The essential kinetic data are presented in Table I and Fig. 1. Quantities listed in Table I are: R_p, the fraction of monomer converted to polymer per hour, the dose rate in Mrad/hr., the square root of the dose rate, and $(DP_N)^{-1}$, the reciprocal of the number average degree of polymerization. The results in this table were obtained from experiments performed at constant pressure (14,600 atm.) and temperature (21°). Figure 1 is a plot of log 10^5R_p and log (DP_N) *vs.* pressure. Experiments were performed at 83, 48, and 21° and at constant dose rate (0.0031 Mrad/hr.). The thermal rate of polymerization (not shown) was measured at 12,200 atmospheres pressure at 83°; log 10^5R_p was (-0.102). Each rate given in Table I or plotted in Fig. 1 was determined from the result of a single experiment.

The inherent viscosities of many of the samples were measured in decalin at 135°. The viscosity average degree of polymerization (DP_V) was calculated using the relation of Chiang.[3] The maximum inherent viscosity of our samples was 0.11 whereas the minimum value in his calibration is 1.5. Qualitatively, the changes in DP_V with reaction conditons parallel those in DP_N, but the calculated DP_V is as much as four times DP_N. This ratio is not firmly fixed owing to the uncertainty of the extrapolation.

TABLE I

EFFECT OF RADIATION INTENSITY ON DP_N AND R_p AT 21° AND 14,600 ATMOSPHERES PRESSURE

$R_p \times 10^2$, hr.$^{-1}$	DP_N^{-1}	$I \times 10^2$ (Mrad/hr.)	$(I)^{1/2} \times 10^2$ (Mrad/hr.)$^{1/2}$
0.015	...	0[a]	0
.32	0.015	0.31	5.6
.68	.016	1.08	10.4
1.08	.014	13.0	36.0

[a] Thermal polymerization.

Infrared spectra of the polymers are more like those of molten Ziegler–Natta polypropylene than the product of the low temperature halide-catalyzed polymerization.[4] There is evidence, however that propyl groups and vinyl groups are present in small amounts. This presumably reflects the relatively low molecular weights of our polymers. Terminal ethyl groups do not seem to be present.

The polymers range from faintly colored materials with flow properties like those of low molecular weight polyisobutylene to opalescent gums so viscous that they show impressions for several days. The latter have higher molecular weights than the less viscous materials. All are soluble in benzene at room temperature; sometimes the solutions are opalescent but they pass through coarse frits without loss of polymer or opalescence.

The specific volume of propylene was measured at pressures between 1,000 and 15,000 atmospheres at 21, 48, and 83°. The values are accurate to 0.01 cc./g. and sensitive to about 0.002 cc./g. The accuracy of the pressure measurements was given above; the sensitivity was ±100 atm. The PVT data are in Table II. They

(1) Based on research supported by the U. S. Army Research Office, Durham, North Carolina. Presented at 142nd National Meeting of the American Chemical Society, Atlantic City, N. J., September, 1962. Division of Polymer Chemistry.

(2) L. A. Wall, D. W. Brown, and R. E. Florin, American Chemical Society National Meeting, Chicago, Illinois, September, 1961, Division of Polymer Chemistry, preprint booklet p. 366.

(3) R. Chiang, *J. Polymer Sci.*, **28**, 235 (1958).

(4) A. D. Ketley and M. C. Harvey, *J. Org. Chem.*, **26**, 4649 (1961).

were used to get rates at constant volume by interpolation of observed rates.

TABLE II

PVT DATA FOR PROPYLENE

Pressure, atm.	21°	48°	83°
	Specific vol., cc./g.		
15,000	1.164	1.166	1.175
14,000	1.175	1.178	1.187
13,000	1.186	1.190	1.198
12,000	1.199	1.203	1.213
11,000	1.214	1.219	1.232
10,000	1.234	1.238	1.251
9,000	1.255	1.258	1.271
8,000	1.276	1.281	1.296
7,000	1.301	1.307	1.325
6,000	1.333	1.339	1.357
5,000	1.364	1.375	1.396
4,000	1.406	1.420	1.439
3,000	1.460	1.475	1.500
2,000	1.537	1.558	1.588
1,000	1.659	1.688	1.725

Discussion

Mechanism.—The kinetic data will be discussed in terms of the free radical mechanism

Step	Reaction	Rate
1. Initiation	$M \xrightarrow{\gamma} 2R$	$\frac{dR}{dt} = k_i' I$
2. Propagation	$R_n + M \longrightarrow R_{n+1}$	$\frac{-dM}{dt} = k_2 M \sum_1^\infty R_n$
3. Transfer	$R_n + M \longrightarrow P_n + R$	$\frac{dP}{dt} = k_3 M \sum_1^\infty R_n$
4. Termination	$R_n + R_m \longrightarrow P_n + P_m$	$\frac{-dR}{dt} = 2k_t \left[\sum_1^\infty R_n\right]^2$

In these equations the concentrations of monomer, radicals, and polymer are M, R, and P, respectively. The quantities I and t are radiation intensity and time, respectively. The k's are rate constants.

If the steady-state assumption is applied to the over-all radical concentration, expressions can be obtained for the fractional rate of polymerization (R_p) and DP_N^{-1}. These expressions at constant temperature and pressure are

$$R_p = \frac{-dM}{Mdt} = \left(\frac{k_i'}{2k_4}\right)^{1/2} I^{1/2} k_2 \qquad (1)$$

$$DP_N^{-1} = \frac{2k_4}{k_2^2 M}(R_p) + (k_3/k_2) \qquad (2)$$

The measured thermal rate is so low that it can be ignored in comparison to the radiation-induced rate. Values of $G(-M)$, which can be calculated from information in Fig. 1 and Table I, range from 570 to 108,000. Such large G values indicate that the polymerization proceeds by a chain mechanism. That it is a free radical as opposed to an ionic mechanism is indicated by the approximate square root dependence of rate on intensity below 0.01 Mrad/hr. (see Table I), and by the increase in rate with temperature (Fig. 1). Additional evidence against an ionic mechanism is the lack of infrared absorption attributable to ethyl groups. Such absorption was present in the product of the halide-catalyzed polymerization at low temperature which presumably follows an ionic mechanism.[4]

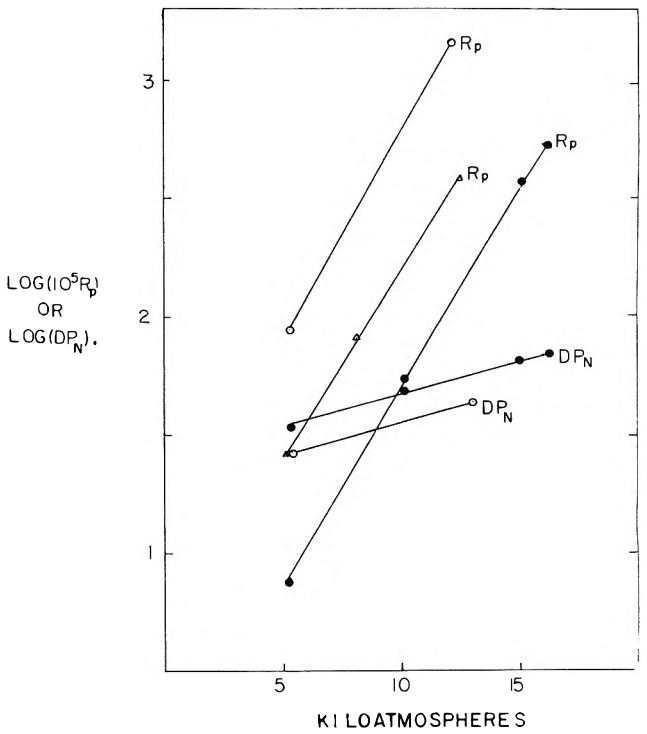

Fig. 1.—Dependence of polymerization rate and number average degree of polymerization on pressure; radiation dose rate = 0.0031 Mrad/hr.; ○, 83°; △, 48°; ●, 21°.

The low values of DP_N and high values of $G(-M)$ suggest that transfer is an important part of this mechanism. Equation 2 offers a means of evaluting transfer relative to propagation. The quantity DP_N^{-1} should vary linearly with R_p. In fact DP_N^{-1} does not vary significantly with R_p. In terms of equation 2 this means that $(2k_4/k_2^2M)(R_p)$ is much less than k_3/k_2. Qualitatively, the DP_N is regarded as being determined by the ratio k_3/k_2. Therefore equation 2 can be replaced by equation 3

$$DP_N = \frac{k_2}{k_3} \qquad (3)$$

The ratio has a maximum value of 72 in this work; molecular weights are 3,000 or less.

At intensities above 0.01 Mrad/hr. the rate of polymerization increases less rapidly than the square-root of intensity. This effect is observed with other monomers and is attributed to termination of an appreciable portion of the initiating radicals by other initiating radicals and by polymeric radicals; it is discussed by Chapiro and Magat.[5] A referee has commented that PD_N at this intensity should be less than at intensities at which the kinetics follow the square-root relation. A calculation by us indicates that the observable effect would be about 10% if the G-value for formation of radicals is 10 and about 1% if this G value is 1, since about 60 mole % of the polymeric products from the two reactions suggested above and all polymer formed by transfer reactions of the specific radicals formed by radiation would evaporate with the monomer. The sensitivity of individual DP_N measurements is ±5% so no effect need be observed.

The large ratio of DP_V to DP_N may indicate that there is transfer of radical activity to polymer. We do

(5) A. Chapiro and M. Magat, "Actions Chimiques at Biologiques Des Radiations," Masson et Cie, 1958, p. 90.

not consider this type of transfer since it does not affect DP_N or R_p. Moreover, the exponent in the relation between inherent viscosity and molecular weight need only to be changed by 7% to make DP_V/DP_N less than 2. A value less than 2 is compatible with the proposed mechanism.

Equations 1 and 3 are applicable at 14,600 atmospheres pressure and 21° at dose rates up to 0.01 Mrad/hr. If temperature and pressure are changed, do these equations still apply? The activation energy for propagation is greater than that for termination in vinyl polymerization. With propylene that for transfer is greater than that for propagation since DP_N decreases as temperature increases (see Fig. 1). Therefore, increases in temperature at constant pressure should extend the applicability of both equations. Decreases in pressure at constant temperature decrease DP_N (see Fig. 1) and so suggest that equation 3 applies. Since R_p decreases as the pressure is reduced, some reduction probably occurs in the range of equation 1. It is not known whether it is sufficient to affect interpretation of results obtained at 5,000 atmospheres pressure at 0.0031 Mrad/hr. We have assumed that equation 1 applies under such conditions.

Effect of Pressure.—Absolute rate theory offers the most straightforward interpretation of the effects of temperature and pressure on R_p and DP_N. If each rate constant is formulated in terms of this theory, *i.e.*, $k_j = VAT \exp(-\Delta F_j^*/RT)$ where V is the molar volume, A is the ratio of the Boltzmann to Planck constant and the other terms are defined below, and the constants are combined in accord with equation 3, the result for a reaction at constant pressure is

$$DP_N = \exp\left(\frac{-\Delta F_2^* + \Delta F_3^*}{RT}\right) \qquad (3')$$

In this equation ΔF^* is the change in free energy in forming the transition complex from the reactants, the subscripts refer to the steps in the mechanism, R is the gas constant, and T is the absolute temperature.

The variation of log DP_N with pressure at constant temperature can be shown to be[6]

$$\log DP_N = \frac{(-\Delta V_2^* + \Delta V_3^*)P}{2.3RT} + C_1 \qquad (3'')$$

In this equation P is the pressure, C_1 is an integration constant, and the ΔV^*'s are volume changes that occur in forming the transition states. In getting this integrated form the sum of the ΔV^*'s is assumed to be independent of pressure. In accord with this assumption log DP_N varies linearly with pressure (see Fig. 1). The algebraic sums $(\Delta V_2^* - \Delta V_3^*)$ are -1.57 and -1.67 cc./mole at 21° and 83°, respectively.

In arriving at analogous expressions for R_p an additional assumption is useful because it eliminates a molar volume term from the final equations. It is that the G-value for radical formation, $G(R)$, is independent of temperature and pressure. This seems a reasonable assumption in view of the low activation energy exhibited by radiation-induced reactions that do not proceed by a chain mechanism. The expressions for R_p analogous to 3′ and 3″ are, respectively

$$R_p = (k_i)^{1/2}\left(\frac{kT}{2h}\right)^{1/2} \exp\left(\frac{-\Delta F_2^* + \Delta F_4^*/2}{RT}\right) \qquad (1')$$

$$\log 10^5 R_p = \left[\frac{(-\Delta V_2^* + \Delta V_4^*/2)}{2.3RT}\right] P + C_2 \qquad (1'')$$

In these equations the quantities not previously defined are: k_i, the fractional rate of initiation, k, the Boltzmann constant; h, Planck's constant. The quantity log $10^5 R_p$ varies linearly with pressure (see Fig. 1). The sum $(\Delta V_2^* - \Delta V_4^*/2)$ in cc./mole is: -9.62 at 21°, -9.64 at 48°, and -12.22 at 83°. The value at 48° should probably be more nearly intermediate between the others. It certainly seems unlikely that the slope of the line at 48° should be less than at 21° or at 83°.

Effect of Temperature.—The variation in log $10^5 R_p$ with temperature at constant pressure can be shown to be

$$\log 10^5 R_p = {}^1/_2 \log T + \frac{(\Delta H_4^*/2) - \Delta H_2^*}{2.3RT} + C_3 \qquad (1''')$$

In this equation ΔH^* is the change in enthalpy that occurs when the transition complex is formed. If the temperature is varied and the volume is kept constant, the expression for log $10^5 R_p$ is identical with 1‴ except that the ΔH^* is replaced by ΔE^*, the change in internal energy. Thus the ΔH^* term in equation (1‴) can be calculated from the slope of isobars of (log $10^5 R_p$ − 1/2 log T) *vs.* T^{-1}. Similarly, ΔE^* terms may be calculated if values of R_p at constant volume are used. These were obtained by interpolating ordinates in Fig. 1 by use of the PVT data in Table II. Since the pressure increases with temperature at constant volume the slope of the latter isobars is greater than at constant pressure. Consequently, values of the ΔE^* term are greater than those of the ΔH^* term. This is in accord with the negative ΔV^* since $\Delta H^* = \Delta E^* + P\Delta V^*$.

Table III lists representative values of the ΔE^* and ΔH^* terms. They are both rather small compared with over-all activation energies observed in thermal polymerizations; this suggests that the initiation is temperature independent as assumed. Both terms increase slightly with pressure. Since the rate increases with pressure the over-all ΔF^* must decrease and as ΔH^* increases with pressure the over-all ΔF^* must decrease and as ΔH^* increases slightly all the decrease in the over-all ΔF^* comes from the increase in the entropy terms.

Effect of Pressure on Entropy Change.—This can be put on a quantitative basis in several ways. We assume a value of $G(R)$; this enables us to calculate k_i and therefore $\exp(-\Delta F_2^* + \Delta F_4^*/2)/RT$ by equation 1. From this can be calculated $(\Delta F_2^* - \Delta F_4^*/2)$. Values of $(\Delta S_2^* - \Delta S_4^*/2)$ can be calculated from the relation $\Delta F = \Delta H - T\Delta S$. Results of these calculations for $G(R) = 1$, $G(R) = 10$, and $T = 294$°K. are in Table III. Between 5,000 and 16,400 atmospheres the quantity $(\Delta F_2^* - \Delta F_4^*/2)$ decreases by about 2,500 cal./mole. All the decrease must result from the increase in $(\Delta S_2^* - \Delta S_4^*/2)$ since $(\Delta H_2^* - \Delta H_4^*/2)$ increases slightly. Changes with pressure of the ΔF^* and ΔS^* terms are not affected by the value assumed for

(6) S. D. Hamann, "Physico-Chemical Effects of Pressure," Academic Press, New York, N. Y., 1957, p. 162.

TABLE III

THERMODYNAMIC QUANTITIES IN RATE EXPRESSIONS AT 21°

SUMS OF TERMS IN RATE EXPRESSION

Pressure (k atm.)	Form of sum[a]	ΔF^*, cal./mole	ΔH^*, cal./mole	ΔS^*, cal./mole deg.	ΔE^*, cal./mole	$\Delta H^* - \Delta E^*$, cal./mole	$P\Delta V^*$, cal./mole
5.0	$\Delta_2^* - \Delta_4^*/2$	15,860[b]	7800	−27.3	9050	−1250	−1160
12.0	$\Delta_2^* - \Delta_4^*/2$	14,450[b]	8160	−21.4	9860	−1700	−2770
16.4	$\Delta_2^* - \Delta_4^*/2$	13,270[b]	8400[d]	−16.6			
5.0	$\Delta_2^* - \Delta_4^*/2$	16,540[c]	7800	−29.7			
12.0	$\Delta_2^* - \Delta_4^*/2$	15,150[c]	8160	−23.8			
16.4	$\Delta_2^* - \Delta_4^*/2$	13,960[c]	8400[d]	−18.8			
5.0	$\Delta_2^* - \Delta_3^*$	−2,070	−855	4.13	−676	−179	−190
12.0	$\Delta_2^* - \Delta_3^*$	−2,330	−760	5.34	−544	−216	−453
16.4	$\Delta_2^* - \Delta_3^*$	−2,500	−700[d]	6.12			

[a] Each thermodynamic function to the right is made up of elements having the form defined in this column. [b] Assumed that $G(R) = 1$. [c] Assumed that $G(R) = 10$. [d] By extrapolation of values at 5 and 12 katm.

$G(R)$. Assuming $G(R)$ enables us to calculate the absolute value of the ΔF^* and ΔS^*. Indeed, the changes in the sums of the ΔF^* and ΔS^* terms could have been calculated from any two rate constants.

An alternative way of calculating the change in $(\Delta S_2^* - \Delta S_4^*/2)$ is of some interest. Thermodynamically $(\partial S/\partial P)_T$ equals $-(\partial V/\partial T)_P$. If we approximate

$$\left(\frac{\partial(\Delta V_2^* - \Delta V_4^*/2)}{\partial T}\right)_P \text{ by } \frac{(\Delta V_2^* - \Delta V_4^*/2)_{83°} - (\Delta V_2^* - \Delta V_4^*/2)_{21°}}{83 - 21}$$

we obtain -0.0419×10^{-3} liter/mole deg. from values of the ΔV^* terms given previously. According to our data this figure is independent of pressure. Direct integration is possible and gives $\Delta(\Delta S_2^* - \Delta S_4^*/2) = 11.5$ cal./mole deg. between pressures of 5,000 and 16,400 atmospheres. From Table III by subtraction of ΔS^* terms one obtains the value 10.8 cal./mole deg.

Difference between ΔH^* Term and ΔE^*.—The difference between the ΔH^* term and ΔE^* term should equal $P(\Delta V_2^* - \Delta V_4^*/2)$ since pressure is constant during formation of the transition complexes. Values of the difference between the enthalpy and internal energy terms and also $P(\Delta V_2^* - \Delta V_4^*/2)$ are in Table III. The agreement is good at 5,000 atmospheres but the volume term becomes larger than the other term at higher pressure. Probably the error is in the difference between enthalpy and internal energy since the data from which these were calculated scatter considerably.

Thermodynamic Quantities from DP_N.—The lower portion of Table III gives results calculated from the variation of DP_N with temperature and pressure. Smaller changes are obtained throughout since DP_N changes relatively less than does R_p. The negative ΔF^* term indicates that propagation is faster than transfer, as it must be if polymer is obtained. The negative ΔH^* term and positive ΔS^* term show that propagation is favored by both enthalpy and entropy sums in the rate expression.

PVT **Data.**—Consideration of the data in Table II indicates that propylene becomes more difficult to compress as the pressure is raised or the temperature is lowered. There are apparent point to point exceptions to this generalization, but they are not significant under the precision limits given in the Results section. At atmospheric pressure and room temperature isotactic polypropylene has a specific volume of 1.09 cc./g.[7] This is less than the lowest specific volume of the monomer that we obtained. This indicates that the average intermolecular distance in the monomer at 15,000 atmospheres pressure is still considerably greater than normal bond lengths.

Acknowledgment.—The authors thank Mr. Edward P. Regalis, Department of Agriculture, for the use of the Mechrolab vapor pressure osmometer.

(7) G. Natta, *Angew. Chem.*, **68**, 393 (1956).

THERMAL STUDIES OF COOL-FLAME OXIDATIONS

BY G. H. MEGUERIAN

Research and Development, American Oil Co., Whiting, Indiana

Received September 24, 1962

A thermal method for the study of cool-flame oxidations in laminar-flow systems has been developed. The empirical equation $\Delta T_m = B[F]_i\{[O_2]_i - [O_2]_0\}$ relates the maximum temperature-rise to oxygen and fuel concentrations in terms of two constants: the exothermicity constant, B, and the minimum oxygen requirement, $[O_2]_0$. The value of B varies directly with the residence time. The value of $[O_2]_0$ changes slightly or remains constant depending whether the residence time is varied by changing the gas flow-rate or by moving the thermocouple along the axis of the reactor. The cool-flame oxidation of isoöctane is enhanced by *n*-heptane and inhibited by propionaldehyde and aromatic amines. Initiation is suggested to result from the activation of oxygen molecules on the surface of the reactor through formation of π-complexes with the carbonaceous layer. The latter forms during aging of the reactor and is replenished during the oxidation.

Introduction

Despite the large amount of work done and several elementary reactions proven possible,[1,2] the over-all mechanism of hydrocarbon oxidation in the cool-flame region, between 250 and 450°, is still not clear. For this reason, interpretation of results obtained by different methods under various conditions is very difficult. The task is even more difficult with comparative results of hydrocarbon reactivities, the order of which sometimes changes with experimental conditions. Further studies are needed to elucidate the effects of surfaces, temperatures, and other experimental variables upon the various steps of oxidation.

The gas-phase oxidation of hydrocarbons proceeds by a series of chain reactions of the degenerate-branching type.[3] The over-all reaction is highly exothermic, and may produce cool flames and explosions. This exothermicity puts restrictions on the kinetic methods used. In the static method, to assure isothermal conditions or avoid explosions, oxidations must be carried out at sub-atmospheric pressures, low concentrations, or low temperatures. Under these conditions the kinetics of the reaction can be conveniently determined from pressure rise, but the analysis of the reaction mixture is very difficult. Also, hydrocarbons of greatly different reactivities often must be studied at different temperatures[4] and pressures. Because the relative importance of the various steps of oxidation to the over-all reaction may change with pressure and especially with temperature, this procedure may lead to inaccurate comparisons. These difficulties can be alleviated by use of the flow method. By varying the residence time, the extent of oxidation can be kept low and, therefore, wider ranges of pressures, concentrations, and temperatures can be used. This flexibility may also make it possible to exaggerate and study the various steps of oxidation.

Cool-flame oxidations in flow systems have been followed by measuring consumption of reactants or formation of products, such as CO.[5,6] Because of inherent difficulties, the most direct method, namely the measurement of temperature rise, has attracted little attention. However, it has been applied with some success to kinetic studies in static systems[7,8] and recently, in this Laboratory, to the comparative study of hydrocarbon reactivities.[9]

This method has now been refined and adapted to more precise studies of cool-flame oxidations. A cylindrical reactor was modified to give laminar flow and to minimize heat losses. An empirical expression for the maximum temperature rise was derived in terms of initial oxygen and fuel concentrations. Although this expression can be used to compare reactivities of various hydrocarbons, in this study only results with isoöctane were used to demonstrate the method and to suggest a mechanism for the thermal initiation of cool-flame oxidations on the reactor surface.

Experimental

Isoöctane and *n*-heptane, both ASTM grade (Phillips) were further purified by percolation through silica gel and Al_2O_3 before use. Propionaldehyde (Eastman) was similarly purified. Aniline, N-methylaniline, and N,N-dimethylaniline (all Eastman) were distilled under reduced pressure, and a middle fraction of each amine boiling at constant temperature was collected and stored under nitrogen. Fresh mixtures were made as they were needed. Cylinder oxygen and nitrogen of high purity were used without further purification.

The apparatus consists of fuel measuring and delivery systems, a preheater-reactor assembly, a furnace, instrumentation for controlling and measuring temperatures, and the conventional system for handling and metering gases. The final choice of design was based upon trial and error to achieve maximum reproducibility and the greatest ease of operation.

By means of a Rideal Microdoser[10] submerged in a constant-temperature bath the fuel is metered and, through a capillary tubing, delivered to the upper bulb of a vertical carburetor. The two bulbs of the carburetor, which can be heated separately, assure the complete evaporation of the fuel and its better mixing with the stream of nitrogen. To obtain a constant and regular flow of fuel, the bath temperature is kept constant within 0.005° at 25°, and the carburetor temperatures are adjusted so that the fuel evaporates completely without causing bubbles to form in the capillary side arm of the carburetor.

From the carburetor, the fuel–nitrogen mixture enters the outer chamber of the 70 cm.-long preheater and flows to the mixing tip, as shown in Fig. 1. Metered oxygen flows through the inner chamber. The gases, mixed by the reversal of the oxygen flow, enter the reactor through three slots, which are cut into the tip and are 1 mm. wide and 3 mm. long. The gases are released into the air through an exhaust tube. The preheater and the reactor are connected by means of tightly fitting standard tapered (14/35) ground joints. To minimize heat losses through the walls, the reaction chamber is enclosed in a jacket which is

(1) A. S. Sokolik, "Autoignition, Flames, and Detonation in Gases," Academy of Sciences, U.S.S.R., Moscow, 1960; C. F. H. Tipper, *Quart. Rev.*, **11**, 313 (1957).

(2) N. N. Semenov, "Some Problems in Chemical Kinetics and Reactivity," Academy of Sciences, U.S.S.R., Moscow, 1954.

(3) N. N. Semenov, "Chemical Kinetics and Chain Reactions," Oxford Univ. Press, 1935.

(4) C. F. Cullis and C. N. Hinshelwood, *Discussions Faraday Soc.*, **2**, 117 (1947).

(5) M. B. Neĭman and A. F. Likovnikov, "Chain Reactions of Hydrocarbon Oxidation in the Gas Phase," Academy of Sciences, U.S.S.R., Moscow, 1955, p. 140.

(6) K. C. Salooja, *Combustion and Flame*, **4**, 193 (1960).

(7) M. Vanpeé, *Bull. soc. chim. Belg.*, **64**, 235 (1955).

(8) R. H. Burgess and J. C. Robb, *Trans. Faraday Soc.*, **54**, 1015 (1958).

(9) J. F. Bussert, *Combust. Flame*, **6**, 245 (1962).

(10) R. O. King and R. R. Davidson, *Can. J. Res.*, **21A**, 65 (1943).

silvered from the inside, evacuated, and sealed. To minimize heat losses through the mixing tip, it is placed just outside the chamber. To prevent reactions from occurring before gases enter the chamber, the clearance between the tip and the reactor wall is made less than 1 mm. Temperatures of reactant mixture and exhaust gases are sensed by thermocouples T_M and T_E and recorded continuously by a duplex recorder. Chromel–alumel thermocouples with bare junctions, about 1 mm. in diameter, are used; sheating of the junctions with Pyrex glass gave identical results.

The preheater-reactor assembly is placed in an electrically heated cylindrical furnace. A program controller provides a constant rise of 5° per minute over the entire temperature range studied.

The operating procedure was carefully standardized for maximum reproducibility. With the rates of nitrogen and oxygen flows adjusted, the furnace is heated to about 150° and kept there until equilibrium between mixture and exhaust temperatures is established. The program controller is then activated, the fuel is turned on, and the run is continued until the mixture temperature reaches 450°. The reactor is cooled by blowing air from the outside while a slow flow of nitrogen is maintained through it, and the procedure is repeated for the next run. From the tracings of mixture and exhaust temperatures, the temperature rise, ΔT, due to the oxidation of the fuel, is easily determined at any mixture temperature.

Irregular fuel-flows due either to wide fluctuations of the bath temperature or to badly adjusted carburetor-temperatures give wavy traces of exhaust temperatures; they are poorly reproducible and may lead to erroneous conclusions. With good operative conditions smooth traces are obtained which give reaction temperatures reproducible within 3° and maximum temperature rises, within 1°.

Because of breakage, three reactors with volumes of 11, 13, and 14 ml. were used. All three had about the same inside diameter of 22 mm. but, because of the tapered construction on both ends of the reactor, the surface to volume ratios were not the same. No attempt was made to determine these ratios precisely. All new reactors were washed with nitric acid and thoroughly rinsed with distilled water before use. Freshly cleansed reactors gave, at first, weak exothermic reactions. The intensities increased with subsequent runs, but reproducible results were obtained only after 4 hours of continuous oxidation of isoöctane at 350°. During "aging," the reactor surface was coated with an invisible carbonaceous material that could be removed by oxidation with oxygen rapidly above 350°, but only slowly at lower temperatures. Washing with nitric acid or acetone also destroyed the coating.

Results

A typical plot of temperature rise, ΔT, at various mixture temperatures is shown in Fig. 2 for isoöctane. This plot, the thermal profile[11] of the cool-flame region, shows that the highly exothermic cool-flame reactions begin at temperature T_i and reach maximum intensity at T_m. Beyond this temperature their intensity gradually decreases to zero. The steep S-shape of the low-temperature half of the thermal profile also shows that the rate of temperature change increases with temperature and passes through a maximum; the maximum temperature rise, ΔT_m, is attained at $d(\Delta T)/dT = 0$. Although any ΔT or $d(\Delta T)/dT$ on the thermal profile can be used to study cool-flame reactions, ΔT_m has been preferred because of the greater reproducibility of both T_m and ΔT_m.

Effect of Concentrations of Reactants.—The thermal properties of cool-flame reactions for several series of runs at various oxygen and isoöctane concentrations are given in Table I. Nitrogen was used as diluent to bring the total gas flow to 512 cc. per minute at 25°. Although increasing oxygen concentrations reduces the temperature, T_i, at which exothermic reactions begin, the effect is small; the difference between the highest and the lowest temperatures being only 15°. The effect of isoöctane concentration on T_i seems to be within the experimental error. The maximum temperature rise, ΔT_m, occurs over a temperature range of 5 to 6°. Values of T_m vary in general with the size of ΔT_m, the highest ΔT_m occurring at the lowest mixture temperatures.

(11) G. H. Meguerian and J. F. Bussert, *J. Chem. Eng. Data*, **7**, 127 1962)

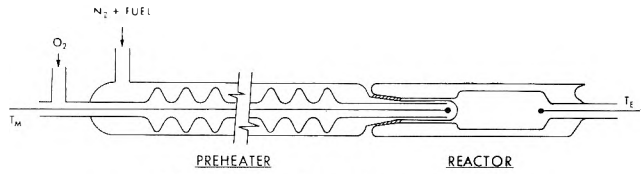

Fig. 1.—The thermal apparatus.

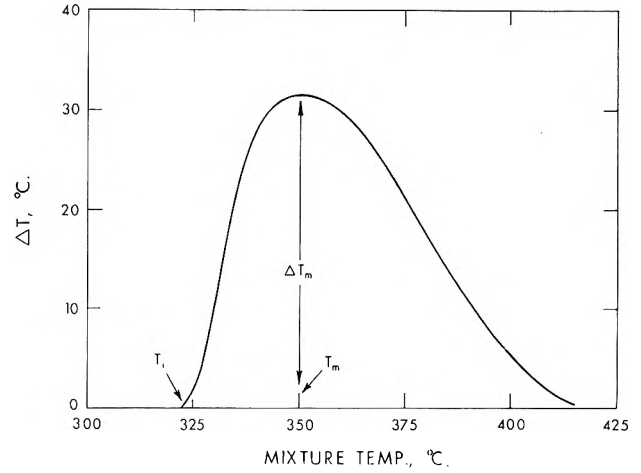

Fig. 2.—Thermal properties of cool-flame reactions.

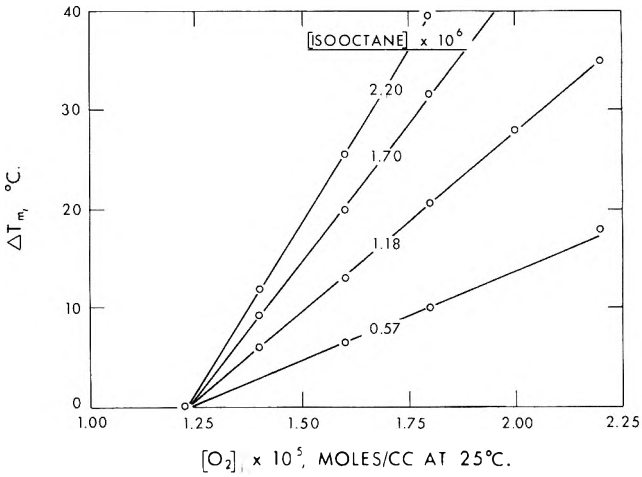

Fig. 3.—Effect of oxygen concentration.

The maximum temperature rise, ΔT_m, depends on the first power of either reactant concentration when the other is kept constant. Figure 3 shows the existence of a limiting value for the oxygen concentration, $[O_2]_0$, given by the intercept, below which no exothermic reactions occur regardless of the isoöctane concentration in the mixture. However, no such limit exists for the isoöctane concentration, since all the lines pass through the origin. These relations can be expressed mathematically

$$\Delta T_m = B[F]_i\{[O_2]_i - [O_2]_0\} \qquad (1)$$

where $[F]_i$ and $[O_2]_i$ are the initial concentrations of isoöctane and oxygen, and B is a proportionality constant, called the "exothermicity" constant. An average

value of 3.15 ± 0.08 × 10^{12} deg. cc.²/moles² was obtained for B at 4 isoöctane and 5 oxygen concentrations.

TABLE I

EFFECT OF OXYGEN AND ISOÖCTANE CONCENTRATIONS ON COOL-FLAME REACTIONS

Isoöctane, moles/cc. × 10^6	Oxygen moles/cc. × 10^5	T_i, °C.	T_m, °C.	ΔT_m, °C.
0.57	1.60	330	360–365	6.5
.57	1.80	327	360–365	10
.57	2.20	324	360–365	18
.57	2.40	324	355–360	21
1.18	1.40	335	355–360	6
1.18	1.60	328	355–360	13
1.18	1.80	324	352–357	20.5
1.18	2.00	323	355–360	28
1.18	2.20	322	355–360	35
1.70	1.40	330	353–358	9.5
1.70	1.60	327	350–360	20
1.70	1.80	326	348–354	31.5
1.70	2.00	326	348–352	42.5
2.22	1.40	330	353–357	12
2.22	1.60	330	353–357	25.5
2.22	1.80	324	348–352	39.5
2.22	2.00	320	345–350	53

Effect of Residence Time.—The effect of residence time was studied by varying (a) the total flow rate of the gases through the reactor, and (b) the position of the thermocouple along the axis of the reactor. The last method was based on the assumption that under the laminar-flow conditions used there was little or no longitudinal mixing within the reactor. When the flow rate was varied, the thermocouple position was held at its usual position—1 cm. from end of reactor—and when the thermocouple position was varied, the flow rate was held constant at 512 cc. per minute. The residence time, Δt, was defined as the ratio of reactor volume to total flow rate per second at 25°. The reactor volume was estimated from the position of the thermocouple: a position of 4 cm. from the tip of the preheater being equivalent to 12.6 ml.

Results at six different flow rates giving residence times from 0.74 to 2.52 seconds show that the oxygen requirement varies inversely with the residence time, but the effect is not pronounced: about 3-fold increase in the flow rate increases the value of $[O_2]_0$ by only 20%. The exothermicity constant, on the other hand, increases linearly with the residence time according to the relation

$$B = k_e(\Delta t) \qquad (2)$$

Substitution of this expression for B in equation 1 gives, after rearrangement

$$\left(\frac{\Delta T}{\Delta t}\right)_m = k_e[F]_i\{[O_2]_i - [O_2]_0\} \qquad (3)$$

where k_e is an empirical constant related to the over-all rate constant for exothermic reactions at the peak temperature. A value of 2.04 × 10^{12} deg. cc.²/moles² sec. for k_e has been determined from equation 2.

Results for four different positions of thermocouple show that the oxygen requirement appears to be independent of the thermocouple position, the variations being within the experimental error. The exothermicity constant, on the other hand, increases as the thermocouple is moved farther away from the preheater tip, or as the effective length, L, of the reactor is increased according to the expression

$$B = CL \text{ or } B = k_e(\Delta t)$$

since L determines the effective volume of the reactor and hence, the residence time. From results at four different locations, k_e is calculated to be 2.22 × 10^{12} deg. cc.²/moles² sec., which compares very well with that obtained by varying the flow rate.

Mixtures of Isoöctane with Various Compounds.—Compounds, such as *n*-heptane and propionaldehyde, that undergo intense cool-flame reactions should enhance the reactivity of isoöctane. The minimum oxygen requirement and the exothermicity constant for isoöctane are compared with those of isoöctane containing 2.5, 5.0, and 10 mole % *n*-heptane in Table II. Two different fuel concentrations of the 5 mole % *n*-heptane mixture, like pure isoöctane, give the same value for $[O_2]_0$. Although the value of B increases with the amount of *n*-heptane in the mixture, the effect is much larger on $[O_2]_0$: with only 10 mole % *n*-heptane, the value of $[O_2]_0$ was reduced by about 50%.

TABLE II

EFFECT OF *n*-HEPTANE ON COOL-FLAME REACTIONS OF ISOOCTANE

n-Heptane in mixture, mole %	Total fuel concn., moles/cc. × 10^6	$[O_2]_0$, moles/cc. × 10^5	B × 10^{-12}, deg. cc.²/moles²
None	1.182	1.12	3.02
2.5	0.654	0.93	3.34
5.0	1.182	.70	3.94
5.0	0.654	.71	3.92
10.0	0.654	.48	4.63

Propionaldehyde, on the other hand, inhibits the initiation of the exothermic reactions and enhances their intensity only slightly. Five and 20 mole % propionaldehyde in isoöctane increase the minimum O_2 requirement from 1.23 × 10^{-5} mole/cc. to 1.43 × 10^{-5} and 1.59 × 10^{-5} and the constant B, from 3.17 × 10^{12} deg. cc.²/moles² to 3.24 × 10^{12} and 3.60 × 10^{12}. Furthermore, a run with isoöctane alone immediately following this series gave a low ΔT_m. The correct value for ΔT_m was obtained only after re-aging the reactor with isoöctane for about one hour.

Oxidation inhibitors, such as aromatic amines, raise the minimum oxygen requirement and lower the value of B. Results of experiments with isoöctane containing various amounts of aniline, N-methylaniline (NMA), and N,N-dimethylaniline (DMA) are given in Table III. Both aniline and NMA reduce the exothermicity constant, by 20% at 1 mole % concentration. But DMA is relatively ineffective, reducing the value of B by only 7% at 4 mole % concentration. Beyond 1 mole %, adding more amines to isoöctane appears to affect B only slightly. The minimum oxygen requirement increases linearly with the concentration of the amines. Again the inhibitory effect of DMA is very weak; but NMA seems to be slightly more effective than aniline.

Discussion

The reactor assembly was designed and flow rates were chosen to assure essentially a laminar flow within the entire length of the reactor. That this was achieved is shown by the same values of the constant k_e deter-

TABLE III

EFFECT OF AROMATIC AMINES ON COOL-FLAME REACTIONS

Amine in isooctane, moles %	$[O_2]_0$, moles/cc. × 10^5	$B \times 10^{-12}$, deg. cc.²/moles²
0.00	1.24	3.08
	A. Aniline	
0.94	1.55	2.47
1.94	1.80	2.50
3.02	2.12	2.49
	B. N-methylaniline	
0.51	1.51	2.72
1.01	1.68	2.48
1.49	1.92	2.65
1.95	2.16	2.24
2.46	2.52	2.57
	C. N,N-Dimethylaniline	
2.03	1.34	2.88
5.0	1.40	2.86

mined by the two methods used to vary the residence time. Under good laminar conditions, the hydrocarbon–oxygen mixture within a small volume of gas flowing through the reactor probably reacts independently of the rest, so that the heat generated increases the temperature of the gas only within this same volume. With the temperature of the mixture entering the reactor held constant, a steady-state temperature gradient is soon established along the axis of the reactor. Figure 4 shows several examples of this gradient in terms of temperature rises at various positions along the axis of the reactor at four different inlet temperatures. Plotting temperature rise at any position as a function of the inlet temperature should give the thermal profile for that position. However, the profiles used in this study were obtained by continuously increasing the inlet mixture temperature. Nevertheless, because this rate was slow compared with the halflife for the establishment of thermal equilibrium[7,12] the resulting profiles are also considered to be for steady-state conditions.

Figure 4 also shows that exothermic reactions begin at the reactor entrance. Thus, temperature rises making up the thermal profile results from the exothermic reactions occurring throughout the entire residence time. If during this time Δn moles of oxygen, or hydrocarbon, are consumed causing a temperature rise of ΔT, the two quantities are related by

$$\Delta n \cdot \Delta H = C_p \Delta T + K \Delta T' \cdot \Delta t \qquad (4)$$

where ΔH is the heat of the reaction per mole of reactant consumed; C_p, the heat capacity of the system; K, the heat transfer coefficient; $\Delta T'$, the difference between the temperatures of the gas and the surrounding, and Δt, the residence time.

In setting up equation 4, ΔH and C_p are assumed to be independent of temperature and concentration changes and Δt is assumed constant. These assumptions are justified because ΔT_m is kept below 40°, which corresponds to about 15% conversion at an isooctane concentration of 1.2×10^{-6} mole/cc. Heat loss by radiation through the silvered walls is negligible and has been omitted. $K\Delta T' \cdot \Delta t$ represents the heat lost by conduction and, because of the vacuum jacket, must be small; furthermore, at constant Δt and under

(12) S. W. Benson, *J. Chem. Phys.*, **22**, 46 (1954).

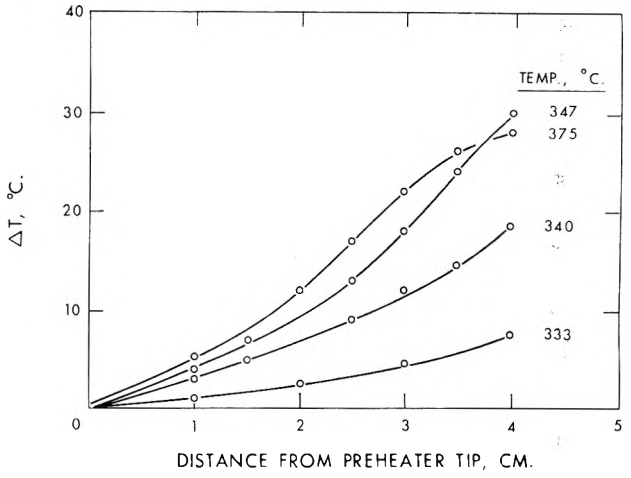

Fig. 4.—Reaction along the reactor.

rigidly controlled conditions, it is assumed to be proportional to ΔT

$$K\Delta T' \cdot \Delta t = K'\Delta T$$

Substitution of this expression in equation 4 gives, after rearrangement

$$\Delta n = \left(\frac{C_p + K'}{\Delta H}\right) \Delta T$$

The average rates of reactant consumption and temperature rise are then related by

$$\frac{\Delta n}{\Delta t} = \left(\frac{C_p + K'}{\Delta H}\right) \frac{\Delta T}{\Delta t} \qquad (5)$$

Because at constant residence time $\Delta T/\Delta t$ is proportional to ΔT, the thermal profile is similar in shape with curves obtained by plotting average rates of consumption against temperatures.[13]

An empirical expression for the maximum average rate is obtained from equations 3 and 5

$$\left(\frac{\Delta n}{\Delta t}\right)_m = k_e \left(\frac{C_p + K'}{\Delta H}\right) [F]_i \{[O_2]_i - [O_2]_0\}$$

Thus, k_e, determined by the thermal method, depends not only on the reaction rate but also on the thermal properties of the system. When they are held constant, k_e can be used to measure the relative reactivities of hydrocarbons with respect to their exothermic reactions.

Calculations show that the thermal properties change little with the kind and concentration of fuels if nitrogen is used as diluent gas and the reactions are carried out in the same reactor. A 4-fold change in isooctane concentration from 0.567×10^{-6} to 2.215×10^{-6} mole/cc. results in about 20% change in the thermal capacity of the gaseous mixture. The change should be smaller for the value of $(C_p + K')$ since the reactor also contributes to it, so that the effect on the value of k_e, or of B at constant Δt, could be within the experimental error. Actually, the values of B determined at the two extreme concentrations differ by only 7%.

The Minimum Oxygen Requirement.—Although the lower limit for the oxygen concentration may arise from the effect of oxygen either upon the reactions or the formation of the degenerate-branching agent, the experimental results argue in favor of the latter. These

(13) B. V. Alvazov and M. B. Neiman, *Zhur. Fiz. Khim.*, **8**, 88 (1936).

results are: the value of $[O_2]_0$ (a) is independent of isooctane concentration (b) is greatly affected by surface conditions; (c) is independent of residence time at constant surface to volume ratios but varies slightly with the linear velocity of the gas; and (d) increases linearly with the concentration of inhibitors. Furthermore, exothermic reactions appear to start always at the entrance to the reactor.

A plausible mechanism for the oxygen effect may result from the special role played by the reactor surface in cool-flame reactions. This surface can both initiate and break chains.[14] If the onset of the branching reactions depends upon the formation of a critical concentration of the degenerate-branching agent, and if the rate of formation of this agent is determined by the balance between initiation and termination reactions, then the balance must be in favor of chain initiation from the very beginning of the laminar-flow reactor for branching reactions to occur. Otherwise no branching agent will be formed, and exothermic reactions will not occur at any other position within the reactor. The carbonaceous material produced during aging and adsorbed on the surface may inhibit termination reactions on the surface and/or, most importantly, may enhance the initiation of chains. The former effect may result from covering the Pyrex surface, which is a relatively good chain breaker[15]; the latter effect may arise from the interaction of oxygen with the carbonaceous material. Because of its mode of formation, this material should contain unsaturated bonds that can activate oxygen molecules through the formation of complexes

$$S + O_2 \underset{k_{-i}}{\overset{k_i}{\rightleftarrows}} S\text{–}O_2^*$$

$$RH + S\text{–}O_2^* \xrightarrow{\text{fast}} R\cdot + S\text{–}O_2H \qquad (6)$$

The rate of initiation is given by

$$R_i = \frac{d[R\cdot]}{dt} = \frac{k_6 k_i [S][O_2][RH]}{k_{-i} + k_6 [RH]}$$

or, with $k_6 >> k_{-i}$

$$R_i = k_i[S][O_2]$$

In static systems degenerate branching is assumed to begin after a critical concentration of the branching agent is formed during the induction period. In the laminar-flow reactor, this critical concentration must be attained as soon as the reactants enter the reactor. This requirement sets a lower limit to the rate of formation of the branching agent. If, for simplicity, this agent is an aldehyde formed by the sequence

$$R\cdot + O_2 \longrightarrow RO_2\cdot \qquad (7)$$

$$RO_2\cdot \longrightarrow R'CHO + R'O\cdot \qquad (8)$$

$$R''O\cdot + RH \longrightarrow R\cdot + R''OH \qquad (9)$$

$$RO_2\cdot \longrightarrow \text{products} \qquad (10)$$

$$RO\cdot \longrightarrow \text{products} \qquad (11)$$

then with $k_9 >> k_{11}$

$$\frac{d[R'CHO]}{dt} = \frac{k_9}{k_{10}} R_i = \frac{k_9 k_i}{k_{10}} [S][O_2] \qquad (12)$$

or, at the limit

$$\left[\frac{d[R'CHO]}{dt}\right]_c = \frac{k_9 k_i}{k_{10}} [S][O_2]_0$$

which is in agreement with the experimental results.

Effect of Various Compounds.—The effects of *n*-heptane and aromatic amines on the constants B and $[O_2]_0$ are as expected. *n*-Heptane, being very active in the cool-flame region,[12] should enhance the reactivity of isooctane. Aromatic amines, on the other hand are well known to slow down the vapor-phase oxidation of hydrocarbons.[16] Aniline and methylaniline, because of their reactive amino-hydrogens, can react more effectively than dimethylaniline with radicals that are essential for the initiation and acceleration of cool-flame reactions. Dimethylaniline may deactivate these radicals either by reacting through its methyl-hydrogens or by forming π-complexes.[17] Amines may also increase $[O_2]_0$ by favorably competing for the complex in reaction 6

$$S\text{–}O_2^* + ArNHR \longrightarrow ArNR + S\text{–}O_2H\cdot \qquad (13)$$

If $k_{13} >> k_6$, the rate of initiation becomes

$$R_i = \frac{k_6 k_i [S][O_2][RH]}{k_{13}[ArNHR]}$$

Substitution of this expression in equation 12 leads, at constant hydrocarbon concentration, to the general relation

$$\frac{[O_2]_0}{[ArNHR]} = \text{constant}$$

which confirms the linear dependence of $[O_2]_0$ upon amine concentration.

Although propionaldehyde greatly enhances the initiation of cool-flame reactions in static systems,[18] the opposite effect is obtained in the flow system. This inhibitory effect appears to result from the deactivation of the reactor surface by the highly polar propionaldehyde. Details of this deactivation are being further studied.

Conclusion

The thermal method gives simultaneous information on both the activity and initiation of exothermic oxidation of hydrocarbons in terms of two empirical constants: the exothermicity constant and the minimum oxygen requirement. The exothermicity constant affords a simple and convenient means of determining the relative reactivities of hydrocarbons and the effects of inhibitors and accelerators. The existence of an oxygen limit and its independence of fuel concentration strongly suggest initiation of chains on the surface. The flow system appears to accentuate surface effects upon the initiation step and could be a suitable tool for their study.

Acknowledgment.—The valuable help of Mr. George Hajduk in setting up the apparatus and carrying out the experiments is greatly appreciated.

(14) M. V. Polyakov, *Usp. Khim.*, **7**, 351 (1948).
(15) J. H. Knox, *Trans. Faraday Soc.*, **55**, 1362 (1959).
(16) G. H. N. Chamberlain and A. D. Walsh, *ibid.*, **45**, 1032 (1949); K. U. Ingold and E. I. Paddington, *Can. J. Chem.*, **37**, 1376 (1959).
(17) G. S. Hammond, *et al.*, *J. Am. Chem. Soc.*, **77**, 3238 (1955).
(18) J. H. Knox, "Seventh Symposium (International) on Combustion," Butterworths, London, 1959, p. 122.

THE EFFECT OF SEVERAL OXY-ACIDS ON THE RATE OF ELECTRON TRANSFER BETWEEN IRON(II) AND IRON(III) IONS IN PERCHLORIC ACID

BY JOHN C. SHEPPARD[1a] AND LARRY C. BROWN[1b]

Department of Chemistry, San Diego State College, San Diego, California

Received October 5, 1962

The specific rate constants for the iron(II)–iron(III) sulfate, acid phosphate, and oxalate paths for electron transfer between these ions in perchloric acid have been determined. Assuming that these reactions are between iron(III) complexes and iron(II) ions and the heats of formation of the iron(III) complexes of these anions are negligible, the specific rate constants at 0° for these paths are: sulfate ion, $100 \pm 20\ M^{-1}$ sec.$^{-1}$; acid phosphate ion, $520 \pm 50\ M^{-1}$ sec.$^{-1}$; and oxalate ion, $250 \pm 20\ M^{-1}$ sec.$^{-1}$. The formal activation energies for these paths are 13.5 ± 2, 15 ± 3, and 21 ± 2 kcal./mole, respectively.

The effect of several anions on the rate of electron transfer between iron(II) and iron(III) ion has been extensively studied[2-5] with the purpose of elucidating the mechanism of the oxidation–reduction process. Since the energies and entropies of activation as well as the specific rate constants for most paths of these reactions are similar, suggestions[6-8] have been made that a common path exists.

The purpose of this research was the investigation of the influence of several large oxygenated anions on the rate of electron transfer between iron(II) and iron(III) ions. Sulfate and acid phosphate ions were chosen for this study because these ions are large, symmetrical, and about the same size. The results may be compared to the effects observed for other anions. Oxalate ion catalysis is of interest because this ion has a different geometry relative to phosphate and sulfate ions.

Experimental

Iron Tracer.—Iron-59, obtained from the Oak Ridge National Laboratory, was used in these experiments. The tracer contained less than 0.2% cobalt-60 at the time it was received and was further purified by the following method. The tracer, along with a few milligrams of cobalt(II) chloride, was added to a few ml. of concentrated hydrochloric acid and was absorbed on an IRA-400 anion-exchange resin column, previously washed with concentrated hydrochloric acid. After the iron(III) and cobalt(II) were absorbed on the column, the cobalt(II) ion was eluted with a 4 *M* hydrochloric acid and discarded. The iron-59 tracer was then eluted with 1 *M* hydrochloric acid and the eluate was evaporated to dryness with concentrated perchloric acid to remove any chloride ion present. The residue containing the tracer was then taken up in 6 *M* perchloric acid and small aliquots of the resulting solution were used in the exchange experiments. Radiochemical purity of the tracer was established by the fact that it decayed over a period of several months with a 45 day half-life. Also, comparison of the gamma spectrum of this tracer with an iron-59 standard indicated that its radiochemical purity was greater than 98%. Exchange experiments under conditions used by Silverman and Dodson[2a] as well as Hudis and Wahl[2b] gave essentially identical results and this was taken as additional proof of radiochemical purity of the tracer.

Reagents.—All reagents used in this study were reagent grade and were used without further purification.

Exchange Procedure.—The reaction vessel used in these experiments was a pear-shaped, three-necked flask. The flask, along with its contents, was maintained at the desired temperature by immersing it in a refrigerated, constant temperature bath. It is estimated that the temperature of the reaction solution varied not more than 0.1° during these experiments.

To 100 ml. of the solution containing the desired concentration of the anion of interest as well as 0.53 *M* perchloric acid, enough iron(II) and iron(III) perchlorate were added to make the total iron concentration about 1.0×10^{-4} to 2.5×10^{-4} *M*. The exchange reaction was initiated by injecting a small aliquot of the iron(III) tracer into the reaction mixture and mixing was accomplished by the use of a small electric motor-driven glass stirrer. During the course of the reaction about eight 5-ml. aliquots were removed at appropriate time intervals by means of an automatic pipet and injected into the quenching solution. Two of the aliquots were infinite time samples. The quenching solution consisted of 5 ml. saturated sodium acetate, 5 ml. 0.1% bipyridyl, and 1 ml. of 0.1 *M* lanthanum nitrate. One ml. of 15 *M* ammonium hydroxide was then added to precipitate lanthanum hydroxide which coprecipitates any iron(III) hydroxide present. The quenched reaction solutions were allowed to stand a few minutes to permit the formation of lanthanum hydroxide and then centrifuged. Five ml. of the supernatant solution, containing only the iron(II) bipyridyl complex, was transferred to a counting tube and counted in a well-type scintillation counter until the counting error was about one per cent

Results

Under the conditions used in these experiments, this reaction obeyed the exponential exchange law. Assuming that the reaction is first order with respect to the iron(II) and iron(III) ion concentrations as found by the other investigators,[2,4] the specific rate constant, 'k', for some experimental condition is related to the half-time $t_{1/2}$ of the exchange by

$$'k' = \frac{0.693}{t_{1/2}\{[\mathrm{Fe(II)}] + [\mathrm{Fe(III)}]\}} \qquad (1)$$

The data found in Fig. 1, 2, and 3 were obtained using this equation. Analysis of the exchange curves having half-times greater than 0.75 minute indicates that the error in the specific rate constants was less than 5%. Those runs with half-times of less than 0.75 minute had errors of not more than 10%.

It is interesting to note that the 10 and 20° oxalate ion data are in agreement with those of Horne[4] but the 0° data are not. In an effort to resolve this discrepancy the following were done: Two different sources of oxalate ion, oxalic acid, and ammonium oxalate were used. The reaction was initiated in a different way by having the tracer present in the iron(III) solution before mixing with the iron(II) solution. Both investigators ran exchange experiments. Within the experimental error of 5% the results of the experiments described above agreed with Horne's[4] data at 10 and 20° but not at 0°. The experimental errors reported by Horne[4] for the data at these temperatures are large, especially at

(1) (a) Now with General Electric Company, Hanford Laboratories, Richland, Washington; (b) National Science Foundation undergraduate research participant, 1960 and 1961.

(2) (a) J. Silverman and R. W. Dodson, *J. Phys. Chem.*, **56**, 846 (1952); (b) J. Hudis and A. C. Wahl, *J. Am. Chem. Soc.*, **75**, 4153 (1953).

(3) G. S. Laurence, *Trans. Faraday Soc.*, **53**, 1326 (1957).

(4) R. A. Horne, *J. Phys. Chem.*, **64**, 1512 (1960).

(5) D. Bunn and F. S. Dainton, *Trans. Faraday Soc.*, **55**, 1267 (1959).

(6) R. W. Dodson and N. Davidson, *J. Phys. Chem.*, **56**, 866 (1952).

(7) W. L. Reynolds and R. W. Lumry, *J. Chem. Phys.*, **23**, 2460 (1955).

(8) D. R. Stranks, "Modern Co-ordination Chemistry," J. Lewis and R. G. Wilkins, editors, Interscience Publishers, Inc., New York, N. Y., 1960, p. 154.

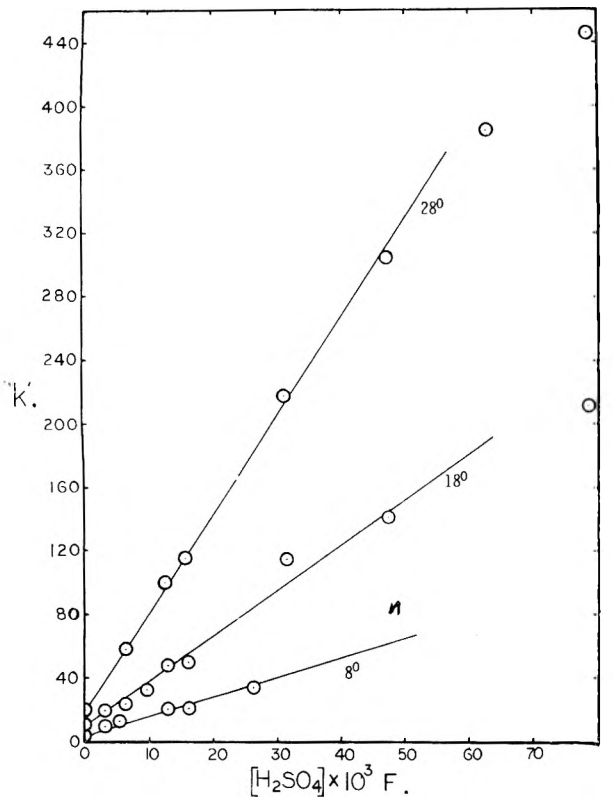

Fig. 1.—The effect of sulfuric acid on the rate of electron transfer between iron(II) and iron(III) ions in 0.81 formal perchloric acid and at an ionic strength of 1.0 ionic strength adjusted with sodium perchlorate.

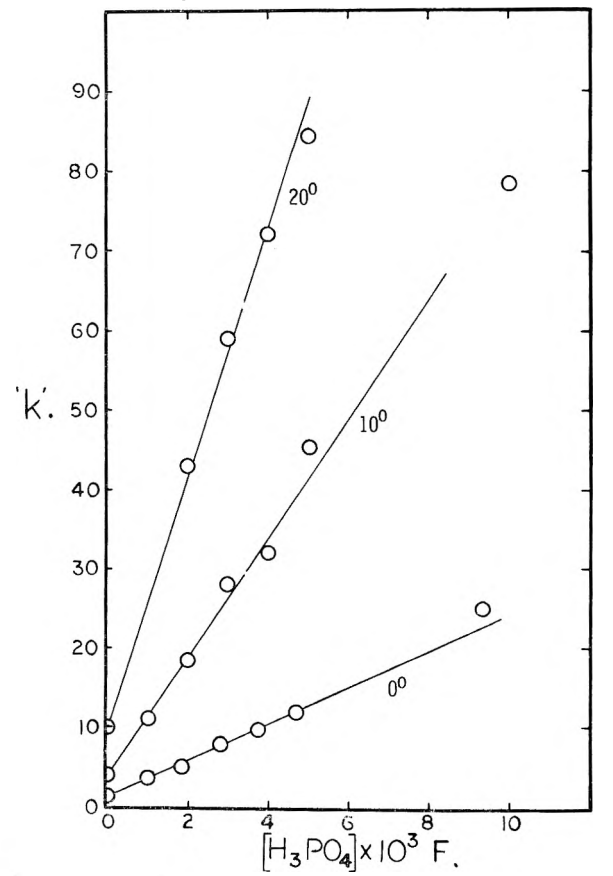

Fig. 2.—The effect of phosphoric acid on the rate of electron transfer between iron(II) and iron(III) ions in 0.53 formal perchloric acid.

0°. When these errors are considered in the interpretation of the data, widely different results and conclusions can be obtained.

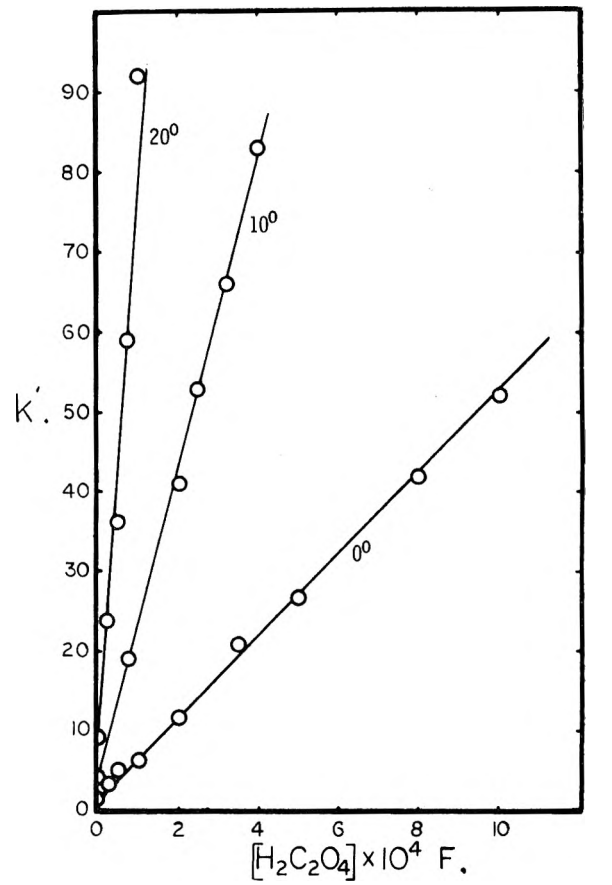

Fig. 3.—The effect of oxalic acid on the rate of electron transfer between iron(II) and iron(III) ions in 0.53 formal perchloric acid.

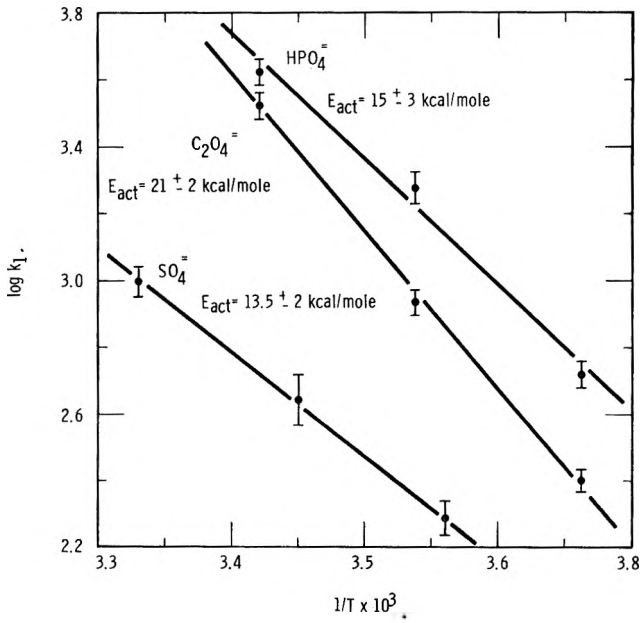

Fig. 4.—An Arrhenius plot of log k against $1/T$, yielding the formal activation energies for oxalic, phosphoric, and sulfuric acid paths of the iron(II)–iron(III) exchange reaction.

Discussion

Most investigators[2-5] who have studied the influence of anions on the rate of electron-transfer between iron(II) and iron(III) ions have assumed that complexes of iron(III) bring the anion into the transition state. Accordingly, entropies and energies were calculated for these paths, and proposals[6-8] concerning the nature of the electron-transfer process itself or the geometry of

the transition state were made. Some proposals have been made on the basis of even less kinetic data.[9]

As Taube[10] has pointed out, it is not possible from rate law studies to establish either the geometry or the mode of formation of the transition state for electron-transfer reactions involving substitution labile reactants and products. Iron(II) and iron(III) ions fall into this category, consequently there is an indeterminacy associated with the interpretation of the catalytic effect of anions on the rate of electron transfer between iron(II) and iron(III) ions. Therefore, it is not possible at the present state of the art to specify that iron(III) complexes react with uncomplexed iron(II) ions or iron(II) complexes react with uncomplexed iron(III) ions. It can only be argued that certain paths are more probable on the basis of relative abundances of the various complexes in solution,[2b] favorable considerations of coulombic repulsion, and by analogy. With respect to arguments of analogy it is of interest to note the observation[11] made on the chloride ion catalysis of the chromium(II)–iron(III) reaction. It is chromium(II) that brings the anion into the activated state at $-50°$. This suggests that the iron(II)–iron(III) reaction procedes by a similar mechanism. But, as pointed out by these investigators, this does not mean that the iron(III) complex cannot contribute significantly at higher temperatures. The same argument holds for the iron(II)–iron(III) reaction.

With the understanding that other anion catalyzed paths are available and possible, the rate data were analyzed assuming that the iron(III) complexes, which predominate in these reaction solutions, bring the anion into the activated state. At least under these conditions the results can be compared on the same basis used by earlier investigators.[2-5] The second assumption is that the heats of formation of the sulfate, oxalate, and acid phosphate complexes are negligible, and is made because of lack of data concerning the heats of formation of the sulfate, oxalate, and acid phosphate complexes of iron(III). There is, however, evidence to the effect that the heat of formation of the iron(III) sulfate complex may be less than one kcal./mole. Three values reported[12-14] for the first iron(III) sulfate complex were essentially the same for a ten degree temperature range. The situations with respect to heats of formation of the oxalate and acid phosphate complexes of iron(III) are less firm, however Horne[4] gives evidence in support of a small value for the former.

At low anion and constant hydrogen ion concentrations the data for the iron(II)–iron(III) reaction can be represented by the equation

$$'k' = \frac{k_1 + k_1K_3[\text{anion}]}{1 + K_3[\text{anion}]} \qquad (2)$$

which is the form used by previous investigators. $'k'$, k_0, k_1, and K_3 are, respectively, the observed rate constant in the absence of the complexing anion, the rate constant for the anion catalyzed path, and the formation constant for the iron(III) complex. At even lower anion concentrations data of this type can be fit to the equation

$$'k' = k_0 + k_1K_3[\text{anion}] \qquad (3)$$

The data shown in Fig. 1, 2, and 3 yielded straight lines when $'k'$ was plotted against the anion concentrations; however deviations were observed at higher anion concentrations. From the slopes, k_1K_3, of these lines and by use of the appropriate K_3 the values for k_1 were obtained. Table I includes the values for k_1 as well as the K_3's used to obtain them. Also included in this table are the respective energies and entropies of activation. Arrhenius plots for the data found in Table I are shown in Fig. 4. The ionization constants for the acids which were used to obtain the free anion concentration are listed in Table II. Fukushima and Reynolds[15] recently reported a rate constant for the iron(II)–iron(III) sulfate path of 680 M^{-1} sec.$^{-1}$ at 25° and an ionic strength of 0.25. When differences of ionic strength are considered, this value is in good agreement with 760 M^{-1} sec.$^{-1}$ calculated from the data in Table I.

TABLE I

SUMMARY OF RATE DATA FOR THE SULFATE, ACID PHOSPHATE, OXALATE ION CATALYSIS OF THE IRON(II)–IRON(III) EXCHANGE REACTION

Anion	Temp., °C.	K_3, M^{-1}	k_1, M^{-1} sec.$^{-1}$	E_{act}, kcal. M^{-1}	ΔS^*, e.u.
SO_4^{-2}	28.0°	25[a]	980 ± 90	13.5 ± 2	−2 ± 1[d]
	18.0		440 ± 80		
	8.0		190 ± 30		
	0.0		100 ± 20 (calcd.)		
HPO_4^{-2}	30.0	2.2×10^{9}[b]			
	20.0		4180 ± 400	15 ± 3	6 ± 1
	10.0		1850 ± 200		
	0.0		520 ± 50		
$C_2O_4^{-2}$	20.00	3.7×10^{5}[c]	3300 ± 300	21 ± 2	28 ± 1
	10.0		860 ± 80		
	0.0		250 ± 20		

[a] A recalculated formation constant for the iron(III) sulfate complex using Whitaker and Davidson's data[12] and the bisulfate ionization constant found by Kerker.[16] [b] The formation constant for the iron(III)–acid phosphate complex found by Langford and Kiehl.[17] [c] The formation constant for iron(III) oxalate complex found by Lambling[18] and corrected for an ionic strength of 0.5 by Horne.[4] [d] These errors show the effect of a plus or minus 3 kcal. M^{-1} heat of formation on the entropy of activation.

TABLE II

IONIZATION CONSTANTS USED TO FIND FREE ANION CONCENTRATIONS

Temp., °C.	Oxalic acid[19] K_1	Oxalic acid[19] K_1	Bisulfate ion[16] K	Phosphoric acid[20] K_1	Phosphoric acid[20] K_2
0	0.59	7.0×10^{-4}	0.37	1.0×10^{-2}	5.5×10^{-8}
10	.43	7.3×10^{-4}	.37	9.0×10^{-3}	5.8×10^{-8}
20	.32	7.6×10^{-4}	.37	8.0×10^{-3}	6.1×10^{-8}

These data indicate that the oxyanions studied are better electron mediators than the halides or thiocyanate ion. The order of effectiveness, acid phosphate > oxalate > sulfate, is not significantly altered by the

(9) K. H. Lieser and H. Schroeder, *J. Inorg. Nuclear Chem.*, **14**, 98 (1960).
(10) H. Taube, *Advan. Inorg. Chem. Radiochem.*, **3**, 1 (1959).
(11) M. Ardon, J. Levitan, and H. Taube, *J. Am. Chem. Soc.*, **84**, 872 (1962).
(12) R. A. Whitaker and N. Davidson, *ibid.*, **75**, 3081 (1953).
(13) B. N. Mattoo, *Z. physik. Chem.* (Frankfurt), **19**, 156 (1959).
(14) K. W. Sykes, *J. Chem. Soc.*, Spec. Publ. No. 1, 64 (1954).
(15) S. Fukushima and W. L. Reynolds, Abstr., 142nd National Meeting of the American Chemical Society, Atlantic City, N. J., Sept., 1962.
(16) M. Kerker, *J. Am. Chem. Soc.*, **79**, 3664 (1957).
(17) O. E. Langford and S. J. Kiehl, *ibid.*, **64**, 292 (1942).
(18) J. Lambling, *Bull. soc. chim. France*, 495 (1949).
(19) L. S. Darken, *J. Am. Chem. Soc.*, **63**, 1007 (1941).
(20) K. S. Pitzer, *ibid.*, **59**, 2365 (1937).

assumption of reasonable heats of formation (±3 kcal./mole) for the iron(III) complexes. However, the true order depends upon the determination of which complex, iron(III) or iron(II), brings the anion into the activated state.

The large energies and entropies of activation observed for the paths involving sulfate, oxalate, and acid phosphate ions suggest that the process of electron transfer for these ions may be different from that for the halide paths. Newton[21] has suggested that systematic differences in entropies of activation for reactions involving substitution labile reactants and products may be a criterion for differentiating between bridging and non-bridging mechanisms. Dainton[22] has gone further and has postulated on the basis of a positive entropy of activation for the azide ion catalyzed path of the iron(II)–iron(III) reaction that a symmetrical intermediate, $[Fe–N_3–Fe^{4+}]$, accounts for this difference. It is possible that the sulfate, oxalate, and acid phosphate also belong in this class; however there still remains the uncertainty of mechanism that cannot be resolved by this type of experiment.[23]

(21) T. W. Newton, private communication to A. Zwickel and H. Taube,[11] *J. Am. Chem. Soc.*, **83**, 793 (1961).

(22) F. S. Dainton, *Discussions Faraday Soc.*, **29**, 125 (1960).

(23) NOTE ADDED IN PROOF.—Reynolds and Fukushima (*Inorg. Chem.*, **2**, 76 (1963)) have reported their results on the sulfate ion catalysis of the iron(II)–iron(III) reactions in detail. It is interesting to note that essentially the same value for the rate constant for the iron(II)–iron(III) sulfate path was obtained by two sets of investigators using different bisulfate ion ionization quotients to calculate the free sulfate ion concentration.

Under identical reaction conditions and in the limiting case where $k' = k_0 + k_1K_3[SO_4^{=}]$ it can be shown that if two investigators, A and B, use different bisulfate ion ionization quotients that ratio of the slopes from which k_1 will be found is equal to

$$\frac{\text{slope A}}{\text{slope B}} = \frac{k_{1A}K_{3A}}{k_{1B}K_{3B}} = \frac{\dfrac{\Delta' k'}{\Delta[SO_4^{=}]_A}}{\dfrac{\Delta' k'}{\Delta[SO_4^{=}]_B}} = \frac{\left\{1 + \dfrac{[H^+]}{K_{iB}}\right\}}{\left\{1 + \dfrac{[H^+]}{K_{iA}}\right\}}$$

If $K_3 = \dfrac{\Delta Q}{\Delta[SO_4^{=}]}$ and Q is some measure of the formation constant, K_3, then

$$\frac{K_{3A}}{K_{3B}} = \frac{\left\{1 + \dfrac{[H^+]}{K_{iB}}\right\}}{\left\{1 + \dfrac{[H^+]}{K_{iA}}\right\}}$$

When this ratio is inserted above, it is found that $k_{1A} = k_{1B}$ which is the observed result.

Acknowledgments.—We wish to acknowledge support of this research by the Research Corporation and the National Science Foundation. We appreciate the valuable comments of Professors Henry Taube and Arthur C. Wahl who discussed with us various aspects of this type of reaction. Donald Holmes performed some of the experiments involving sulfate ion catalysis.

FORMATION AND EXCHANGE RATES OF SOME COMPLEXES OF BORON FLUORIDE WITH AMINES AND ETHERS[1]

BY S. BROWNSTEIN, A. M. EASTHAM, AND G. A. LATREMOUILLE

Division of Applied Chemistry, National Research Council, Ottawa, Canada

Received October 6, 1962

The fluorine magnetic resonance of mixtures of boron fluoride with a number of amines and ethers has been examined in toluene solution at low temperatures. Rates and enthalpies for the exchange of boron fluoride with the 1:1 complexes have been determined and a mechanism proposed. Only with pyridine was evidence obtained for the existence in solution of a complex of the type base·$2BF_3$, and then only at temperatures below about −50°. Triethylamine, dimethyl ether, anisole, and tetrahydrofuran do not appear to form such complexes in solution above about −100°.

Boron fluoride readily forms strong 1:1 complexes with most amines and ethers and has been reported in some cases to form also complexes of the type $R_3N \cdot 2BF_3$ both in the crystal and in solution.[2] Because the 2:1 complexes might be the nitrogen analogs of the reactive intermediates in certain Friedel–Crafts catalyzed isomerizations,[3] an examination of these systems by fluorine magnetic resonance spectroscopy was undertaken in an effort to get more information about them.

In order to distinguish separate resonance lines from fluorine nuclei in different chemical species it is necessary for the lifetime of the fluorine nuclei in such species to be longer than the difference in magnetic environment between the species. This condition is not always found in boron fluoride complexes but Diehl and Ogg were able to obtain separate signals from some alcohol·BF_3 complexes by working at low temperatures.[4] We therefore have examined toluene solutions of mixtures of boron fluoride with a number of amines and ethers down to temperatures as low as 165°K. Toluene was the only low melting solvent found which did not interact strongly with boron fluoride and which was a reasonable solvent for the complexes at low temperatures. Chloroform interacts strongly with boron fluoride as seen from the line widths listed in Table I, while fluorotrichloromethane is a poor solvent.

TABLE I

LINE WIDTHS IN CYCLES/SEC. OF BF_3 IN SOLUTION

T, °K.	Toluene	$CHCl_3$
184	5.2	
207	5.1	49
242	3.7	47
282	6.8	12
300	5.6	6.2

In no case could separate peaks corresponding to 1:1 and 2:1 complexes be detected, either because the 2:1 complex was not present in significant amounts or because the exchange rate was too rapid even at the lowest temperatures. However with all of the bases except dimethyl ether it was possible to slow the exchange rate sufficiently to observe the separate signals

(1) Issued as National Research Council bulletin No. 7316.

(2) H. C. Brown, P. F. Stehle, and P. A. Tierney, *J. Am. Chem. Soc.*, **79**, 2020 (1957).

(3) J. M. Clayton and A. M. Eastham, *Can. J. Chem.*, **39**, 138 (1961).

(4) P. Diehl and R. A. Ogg *Nature*, **180**, 1114 (1957).

from complexed and uncomplexed boron fluoride. With the amines coalescence of these peaks did not occur even at room temperature. From the relative intensity of these peaks and from the exchange rates of boron fluoride between the complexed and uncomplexed species it has been possible to reach some conclusions about the exchange mechanism and about the existence of a complex containing two molecules of boron fluoride in spite of the absence of any signal corresponding to the 2:1 complex.

The peak positions for free and complexed boron fluoride in solution with the various bases are listed in Table II. The chemical shift is given in p.p.m. to high field of $CFCl_3$ as an external standard, without correction for magnetic susceptibility differences since such corrections would probably be smaller than changes due to solvent effects at the various temperatures and, in any event, negligible compared to the large chemical shifts observed. Only in the boron fluoride–triethylamine complex was boron fluorine spin coupling observed. Therefore only in this complex is the boron–nitrogen bond sufficiently strong to allow the electric field about the boron nucleus to approach spherical symmetry and hence to reduce the contribution to relaxation by the boron quadrupole moment to a sufficient extent that the spin coupling can be observed. In the pyridine complex no spin coupling could be observed even at those temperatures where the exchange rate was sufficiently slow, clearly indicating the weaker boron–nitrogen bond. With the ether complexes the exchange rate could not be reduced sufficiently to determine whether exchange or quadrupole relaxation was responsible for the lack of observable spin coupling.

TABLE II

CHEMICAL SHIFTS OF FREE AND COMPLEXED BF_3

Base	Free BF_3	Complexed BF_3	
Pyridine	128.5	149.4	
Triethylamine	129.0	148.8	J B–F = 18.3 cycles/sec.
Tetrahydrofuran	128.7	154.2	
Anisole	128.8	152.8	

In the absence of separate peaks for the different complexes, information about the composition of the solutions must be obtained from the relative intensities of the existing peaks, by using them as a measure of the amount of boron fluoride in the free and complexed forms. Clearly, any area in the peak for complexed boron fluoride over and above that expected for the 1:1 complex can be attributed to the 2:1 complex and should be accompanied by a corresponding decrease in the area of the peak for free boron fluoride. The apparatus was therefore calibrated with solutions containing known amounts of boron fluoride and of 1:1 complex. In calibrating for free boron fluoride it was necessary to determine the solubility of the gas over the temperature range to be examined. This was done by enclosing in the sample tube a capillary tube containing $CFCl_3$, and measuring the relative areas of the resonance lines from $CFCl_3$ and from dissolved BF_3 over a range of temperatures. The relative areas were found to reach a constant value below 211°K., indicating that solution of the boron fluoride was essentially complete by this temperature, so the solubilities at higher temperatures could then be calculated. These

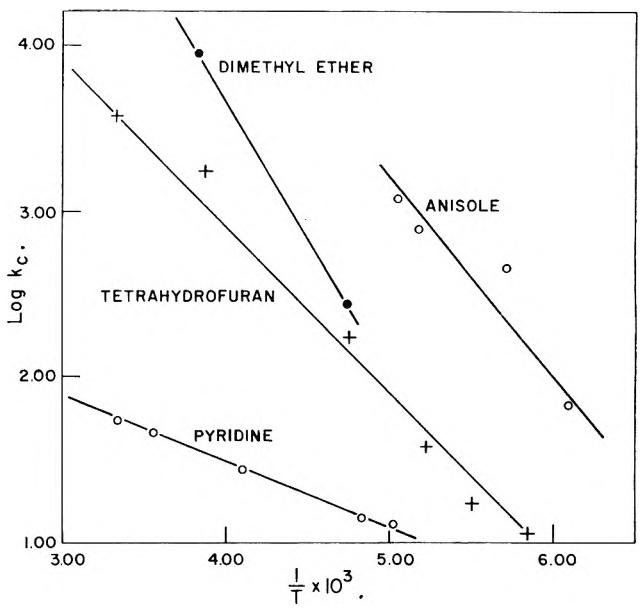

Fig. 1.—Rate constants for exchange of complexed boron fluoride.

solubilities were required in determining some of the rate constants for exchange but not for the equilibrium constants since the latter were obtained at temperatures below 211°K. where complete solution could be assumed.

For each base, samples were studied in which the mole ratio BF_3/base were 1.5, 2.0, and 2.5, but only in the case of pyridine was evidence obtained for a 2:1 complex and then only at temperatures well below those reported by Brown, *et al.*[2] The values of the equilibrium constant, $K_{2:1}$, are given in Table III.[5-7] From our observations it seems unlikely that any significant amount of 2:1 complex is formed with amines or ethers in solution at ordinary temperatures but in some cases when the amine–boron fluoride complex precipitates on cooling the concentration of free boron fluoride in solution is considerably reduced from its expected level. These results tend to confirm the results of Brown[2] that a complex containing more than one molecule of boron fluoride per molecule of amine exists as a solid at low temperatures.

As the rate of exchange between different magnetic environments increases, the resonance lines from the nuclei in the separate environments first broaden, then coalesce to a single broad line which finally narrows. From a quantitative treatment of this behavior the rates of exchange of the nuclei between the two environments may be calculated.[8] For those rates of exchange where two separate but broadened lines are observed, the lifetime of the species in each environment may be calculated but when only a single line is observed, an average lifetime is obtained from which the individual lifetimes may be calculated if the mole fraction of the two species is known.

Let k_F be the inverse of the average lifetime for exchange of free BF_3.

Let k_c be the inverse of the average lifetime for exchange of complexed BF_3.

(5) P. A. Van der Muelen and H. A. Heller, *J. Am. Chem. Soc.*, **54**, 4404 (1932).

(6) H. C. Brown and R. M. Adams, *ibid.*, **64**, 2557 (1942).

(7) A. Palko, R. Healy, and L. Landau, *J. Chem. Phys.*, **28**, 214 (1958).

(8) J. A. Pople, W. G. Schneider, and H. J. Bernstein, "High Resolution Nuclear Magnetic Resonance," McGraw-Hill Book Co., New York, N. Y., 1959, p. 218.

TABLE III

EQUILIBRIUM AND ENTHALPIES FOR BORON TRIFLUORIDE COMPLEXES

Base	$K_{2:1}$		k_F			k_c	
Pyridine	0.40 ± 0.07 at 196°K.	T, °K.	1.5:1	2:1	2.5:1	1.5:1	2:1
	0.35 ± 0.05 at 207°K.	196	11			13	
	0.03 ± 0.05 at 214°K.	207	16	20	16	15	16
		244	22	26	34	21	20
		282	38	58	66	25	38
		300	44	86	65	22	46
Triethylamine	0.00 ± 0.05 at 173°K.	Too slow to measure					
Pyrrole	Polymerizes						
N,N-Dimethylaniline	Insoluble						
Furan	Polymerizes						
Tetrahydrofuran	0.03 ± 0.05 at 182°K.	T,°K.	1.5:1	2:1	2.5:1	1.5:1	2:1
	0.04 ± 0.05 at 191°K.	171			26		
		181		40	32		34
		191		74	54	70	71
		210			460		
		258	3.7×10^3	3.4×10^3	2.4×10^3	1.7×10^3	2.1×10^3
		300	8.5×10^3	6.4×10^3	7.9×10^3	1.3×10^3	1.8×10^3
Dimethyl ether	Insoluble below 211°K.	T,°K.	1.5:1	2:1	2.5:1	1.5:1	2:1
		211		600	470		600
		261	1.9×10^4	2.4×10^4	1.1×10^4	6.8×10^3	1.5×10^4
Anisole	0.00 ± 0.05 at 164°K.	T,°K.	1.5:1	2:1	2.5:1	1.5:1	2:1
		164		163	97		163
		175			900		
		193	2.5×10^3	1.4×10^3	700	1.5×10^3	1.4×10^3
		198	3.1×10^3	1.5×10^3		1.8×10^3	1.5×10^3

Let k_F' be the exchange rate of free BF_3.
Let k_c' be the exchange rate of complexed BF_3.

Then

$$k_F' = k_F[BF_3] \qquad k_c' = k_c\,[S{:}BF_3]$$

where S represents a base. In order to convert the rate of exchange into rate constants, an assumption must be made about the mechanism of the exchange. Two plausible mechanisms for exchange of free boron fluoride with the 1:1 complex are shown in the schemes below.

(1) Exchange by dissociation

$$S{:}BF_3 \rightleftharpoons BF_3 + S$$

$$k_F' = k_c' = k_1[S{:}BF_3]$$

$$\therefore k_F = \frac{k_1[S{:}BF_3]}{[BF_3]} \qquad k_c = k_1$$

(2) Exchange by collision

$$BF_3{}^* + S{:}BF_3 \rightleftharpoons BF_3 + S{:}BF_3{}^*$$

$$k_F' = k_c' = k_2\,[BF_3][S{:}BF_3]$$

$$\therefore k_F = k_2\,[S{:}BF_3] \qquad k_c = k_2\,[BF_3]$$

It is found that k_2 varies randomly with increasing BF_3 concentration while k_1 increases, with pyridine as base. Because of the more rapid exchange with the ethers rate data were mostly obtained from a single broadened line with a resultant greater uncertainty in k_F and k_c. The experimental and calculated results are shown in Table III. They tend to show that the exchange occurs through interaction of free and complexed BF_3 rather than by dissociation of the BF_3 base complex. The values of k_2 have been plotted against $1/T$ (Fig. 1) to obtain the values of $\Delta H_2{}^*$ shown in Table III. These are much smaller than the heats of formation of the 1:1 complex. If exchange were to occur by dissociation the enthalpy of activation would have to be greater than the heat of formation.[9]

The enthalpies of activation for exchange of free and complexed BF_3 are, except in the case of dimethyl ether, inversely proportional to the strength of the complex. The large uncertainty in the value for dimethyl ether arises because, for solubility reasons, the rate measurements with this base could not be made at a sufficiently low temperature to slow down the exchange rate to the point where separate peaks could be observed for free and complexed boron fluoride. To calculate the exchange rates the average of the chemical shifts with anisole and tetrahydrofuran were used. It may be, therefore, that the enthalpy of activation for dimethyl ether is not actually inconsistent with those for the other bases.

Experimental

The fluorine resonance spectra were obtained with a Varian high resolution nuclear magnetic resonance spectrometer operating at a frequency of 56.44 Mc. Calibration of the spectra was obtained from side bands generated by modulation of the radiofrequency transmitter. The modulating frequency was determined with a Hewlett Packard Model 521C frequency counter. The thermostated probe assembly has been described previously.[10]

The quantities of reagents condensed in the sample tubes were determined by pressure measurements using standard vacuum line techniques. All reagents and solvent were distilled and carefully dried before introduction into the vacuum system.

(9) A referee suggested this point.
(10) S. Brownstein, *Can. J. Chem.*, **37**, 1119 (1959).

k_2 av.				k_1 from k_F			ΔH_2^*, kcal./mole	$\Delta H_{1:1}$ (ref.)
2.5:1	1.5:1	2:1	2.5:1	1.5:1	2:1	2.5:1		
	13			7.3				−50.6 (5)
23	16	14	13	11	23	27	1.8 ± 0.3	
55	27	21	33	11	22	43		
52	32	48	55	9.5	29	50		
63	37	72	54	7.3	31	33		
2.5:1	1.5:1	2:1	2.5:1	1.5:1	2:1	2.5:1		
26			11			14		−13.4 (6)
44		19	16		40	48	4.6 ± 0.3	
75	64	37	26		74	81		
361			175			690		
2.2×10^3	2.2×10^3	1.8×10^3	1.2×10^3	1.2×10^3	2.0×10^3	2.2×10^3		
3.4×10^3	4.3×10^3	3.2×10^3	4.0×10^3	1.3×10^3	1.8×10^3	3.4×10^3		
2.5:1	1.5:1	2:1	2.5:1	1.5:1	2:1	2.5:1	7.7 ± 2	
700		300	230		600	705		−13.3 (6)
9.8×10^3	9.1×10^3	1.3×10^4	5.5×10^3		1.4×10^4	1.0×10^4		
2.5:1	1.5:1	2:1	2.5:1	1.5:1	2:1	2.5:1		
166		82	52		163	146	5.5 ± 0.3	−12 (7)
1.4×10^3			460			1.4×10^3		
1.1×10^3	1.4×10^3	700	360	1.4×10^3	1.4×10^3	1.1×10^3		
	1.6×10^3	750		1.8×10^3	1.5×10^3			

FREE VOLUME AND VISCOSITY OF LIQUIDS: EFFECTS OF TEMPERATURE

By A. A. Miller

General Electric Research Laboratory, Schenectady, New York

Received October 10, 1962

The Doolittle free volume–viscosity equation, $\eta = A' \exp(B'v_0/v_f)$, for n-alkanes can be improved to include the low temperature region near the melting points. This improvement is based on a comparison with a modified Arrhenius (M.A.) equation, $\eta = A \exp[B/(T - T_0)]$. For the n-alkane $C_{13}H_{28}$, $T_0 = 73°K.$, $B = 965°$, and $\ln A = -8.35$. As the first step in transforming the M.A. temperature parameters into free volume parameters, a concept derived recently by Cohen and Turnbull[8] is used: $v_f \propto (T - T_0)$, in which T_0 is the theoretical zero-point for the free volume. The transformation of the parameters then depends upon the liquid expansion model used. One model, in which the free volume fraction, $f = v_f/v_1$, is made linear in temperature, leads to the following simple relationships: $f = (T - T_0)/B$ and $\eta = A \exp(1/f)$. For $C_{13}H_{28}$, this model gives an "occupied volume" which has a negative temperature coefficient. For an alternate model, in which v_f itself is made linear in temperature, the "occupied volume" increases non-linearly with temperature. Auxiliary considerations of liquid structure, which are required to establish the proper model, are mentioned.

Introduction

Several authors have reviewed liquid viscosity theories and have compiled empirical and semi-empirical equations relating viscosity with molecular structure, temperature, "free-volume," and, in the case of polymers, with molecular weight.[1-3] The temperature dependence has often been expressed by a simple Arrhenius equation, $\eta = A \exp(B/T)$. However, to describe adequately liquid processes, such as viscous flow and dielectric relaxation, over broad temperature ranges including low temperatures, a modified form, $\eta = A \exp[B/(T - T_0)]$, has been shown to be more appropriate.[4,5] Henceforth in this paper, this will be referred to as the M.A. (modified Arrhenius) equation. Recently, the M. A. equation has been applied to melt viscosities of polystyrene and polyisobutylene fractions and has been suggested as a basis for η–T–M relationships in polymers.[6]

The evolution of empirical viscosity–volume equations culminated in the exponential free volume relation, $\eta = A \exp(Bv_0/v_f)$, suggested in 1951 by Doolittle for n-alkane viscosities (see later discussion and references). The Doolittle equation has been used as the basis for correlating the temperature dependence of viscosity, and other liquid relaxation processes, with volume parameters.[7]

More recently, from fundamental considerations of liquid transport based on a "hard-sphere" model, Cohen and Turnbull[8] derived the approximate relation: $v_f \propto (T - T_0)$, in which T_0 is the theoretical zero-point for free volume. This concept appears to unify the M.A. and the Doolittle equations. However, in both

(1) A. Bondi, *Ann. N. Y. Acad. Sci.*, **53**, 870 (1951).

(2) A. K. Doolittle, "The Technology of Solvents and Plasticizers," John Wiley and Sons, New York, N. Y., 1954, Chap. 13.

(3) T. G Fox, S. Gratch, and S. Loshaek, Chap. 12 in "Rheology," Vol. 1, F. R. Eirich, Ed., Academic Press, N. Y., 1956.

(4) D. W. Davidson and R. H. Cole, *J. Chem. Phys.*, **19**, 148 (1951).

(5) See R. H. Cole, *Ann. Rev. Phys. Chem.*, **11**, 161 (1960).

(6) A. A. Miller, *J. Polymer Sci.*, in press.

(7) See J. D. Ferry, "Viscoelastic Properties of Polymers," John Wiley and Sons, New York, N. Y., 1961, Chap. 11.

(8) M. H. Cohen and D. Turnbull, *J. Chem. Phys.*, **31**, 1164 (1959).

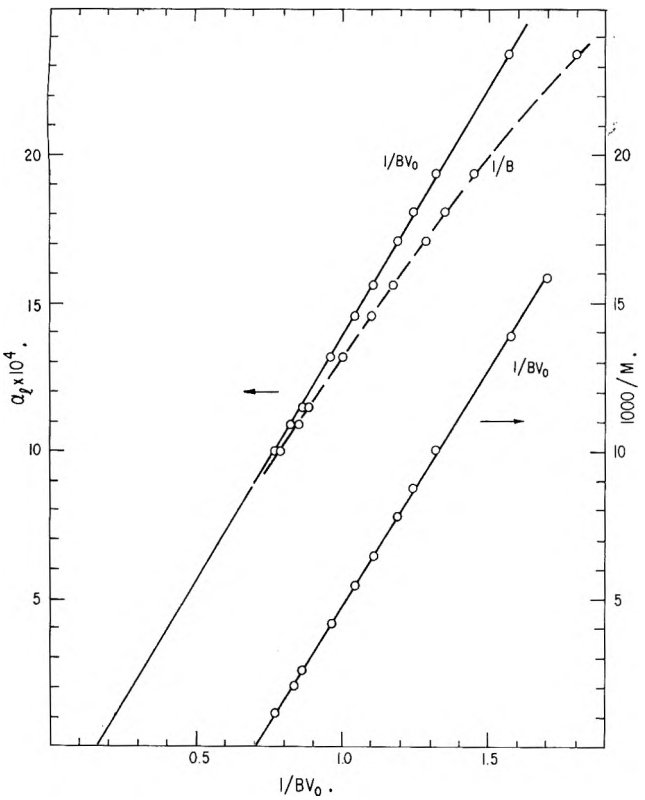

Fig. 1.—Relationship of Doolittle B and Bv_0 to molecular weight, M, and average thermal expansion coefficients,[11] α_l, for n-alkanes.

the Doolittle and in the Cohen and Turnbull approaches, the "occupied" volume is considered to be independent of temperature. While this premise may be reasonable for a "hard-sphere" model, its validity for more complex, linear molecules, such as the n-alkanes, is certainly questionable.

In this paper, the Doolittle free volume interpretation is re-examined and it is shown that the Doolittle equation does indeed require a temperature dependence of the occupied volume in order to conform properly to the viscosity data for the n-alkanes. The data for one n-alkane, $C_{13}H_{28}$, are treated in detail. These data are expressed by the M.A. equation and relationships between the M.A. parameters and free volume parameters are suggested.

The Doolittle Equation and Parameters.—Doolittle and Peterson[9] measured viscosities and densities of ten n-alkanes from C_5H_{12} to $C_{64}H_{130}$ between −5 and 300°. It was found that simple Arrhenius plots (ln η *vs.* $1/T$) were non-linear, with the slopes usually decreasing with increasing temperature. To express these viscosity data in terms of free volume, Doolittle[10a-e] showed that an exponential relationship was required and he suggested the equation: $\eta = A \exp(Bv_0/v_f)$, where A, B, and v_0 are temperature-independent parameters. The free volume was defined as $v_f = v - v_0$, in which v is the liquid specific volume at the measurement temperature. The "occupied" volume, v_0, was obtained by a special extrapolation of the liquid v–T data to 0°K. without change in phase.[10b] This extrapolation method gave $v_0 = e^{18/M}$, where M is the molecular weight of the n-alkane. Doolittle mentioned that at lower temperatures, approaching the melting points, the viscosity data tended to diverge from his free volume equation.[10b,e] The nature of this divergence and its implications will be described later.

Fox and Loshaek[11] have expressed the Doolittle specific volume data by the following empirical equation: $v = 0.900 + \alpha_l T$, in which the liquid expansion coefficient is given by $\alpha_l = 10^{-4}(8.8 + 1060/M)$. This linear v–T relation shows small deviations from the non-linear v–T data actually observed over the 200–300° temperature range. Also, this relation extrapolates to v(0°K.) = 0.900 ml./g. for all of the n-alkanes, independent of molecular weight.

Correlations between the Doolittle B and v_0 values and the Fox and Loshaek parameters are shown in Table I and Fig. 1.

TABLE I

VISCOSITY[10b,e] AND VOLUME[11] PARAMETERS FOR C_nH_{2n+2}

n	M	v_0, ml./g.	B	$\alpha_l \times 10^4$	$B(v_0 - 0.900)$
5	72	1.149	0.555	23.5	0.139
7	100	1.105	.688	19.4	.141
8	114	1.092	.740	18.1	.141
9	128	1.081	.778	17.0	.141
11	156	1.066	.852	15.6	.141
13	184	1.056	.912	14.6	.141
17	240	1.043	1.00	13.2	.142
28	395	1.026	1.129	11.5	.142
36	507	1.020	1.177	10.9	.142
64	900	1.011	1.285	10.0	.142

The reciprocal of Bv_0 is exactly linear in α_l and in $1/M$. However, $1/B$ itself becomes linear only at the higher M values, where the Doolittle v_0 approaches unity. The empirical equations derived from Fig. 1 are: $Bv_0 = 0.016/(1/M + 0.0112) = 17 \times 10^{-4}/(\alpha_l + 3 \times 10^{-4})$. The limiting values for $M = \infty$ are $Bv_0 = B = 1.43$. Also, as shown in Table I, $B(v_0 - 0.900)$ changes only slightly over the entire n-alkane range.

On the basis of the Fox and Loshaek linear v–T equation, the Doolittle free volume can be represented approximately as $v_f \simeq \alpha_l T - (v_0 - 0.900)$, the term in brackets being the difference in the "limiting specific volumes" at 0°K. according to the two extrapolation methods. From this equation, the temperature at which v_f becomes zero is given by $T_0' \simeq (v_0 - 0.900)/\alpha_l$. At 0°K., a negative value for v_f is obtained.

The Modified Arrhenius (M.A.) Equation.—Some time ago, Gutmann and Simmons[12] reported that viscosity data for a number of liquids, including some of the n-alkanes, conformed to the modified Arrhenius (M.A.) equation. In Fig. 2, the M.A. and the Doolittle free volume interpretations are compared for the n-alkane, $C_{13}H_{28}$. The Doolittle[10a] data were plotted as ln η *vs.* $1/(T - T_0)$, with trial values of T_0 until a straight line was obtained at $T_0 = 73$°K. (For $T_0 =$ 63 and 83°K., not shown in Fig. 2, the plots curved upward and downward, respectively). For the linear plot with $T_0 = 73$°K., the derived M.A. parameters are ln $A = -8.35$ and $B = 965$°, confirming the values reported by Gutmann and Simmons.[12]

For the Doolittle free volume interpretation, the straight line is drawn according to the parameters[10c]:

(9) A. K. Doolittle and R. H. Peterson, *J. Am. Chem. Soc.*, **73**, 2145 (1951).

(10) A. K. Doolittle, *J. Appl. Phys.*, (a) **22**, 1031 (1951); (b) **22**, 1471 (1951); (c) **23**, 236 (1952); (c) **23**, 418 (1952); (e) with D. B. Doolittle, **28**, 901 (1957).

(11) T. G Fox and S. Loshaek, *J. Polymer Sci.*, **15**, 371 (1955).

(12) F. Gutmann and L. M. Simmons, *J. Appl. Phys.*, **23**, 977 (1952).

B(slope) = 0.912 and ln A (intercept) = −7.68, and the points are the Doolittle v_0/v_f values.[10b] The divergence, increasing in the direction of lower temperature (higher v_0/v_f), is apparent. Indeed, for v_0/v_f to remain linear with the observed ln η data, it is necessary that the value of v_0 increase continuously as the temperature decreases.

The remaining n-alkanes of the Doolittle series follow a similar pattern. This is readily shown by calculations of the ratio $\Delta \ln \eta/\Delta(v_0/v_f)$ for all of the temperature intervals.[10b] This ratio, which should remain constant at the value B, actually decreases with increasing temperature for each alkane. Also, it appears that in all cases, the B values reported by Doolittle[10c] correspond to the slopes of the ln η *vs.* v_0/v_f curves only at the higher temperatures, as is indicated in Fig. 2 for $C_{13}H_{28}$.

These observations force the conclusion that while the exponential *form* of the free volume equation may be correct, the Doolittle premises regarding the "occupied" volume, v_0, cannot be valid. A more satisfactory approach, *via* the M.A. parameters, will be suggested later in this paper.

Further M.A. Relationships.—By differentiating the M.A. equation we obtain $d \ln \eta/d(1/T) = B_T = B \cdot [T/(T - T_0)]^2$, in which B_T is the temperature-dependent slope of the ordinary Arrhenius plot. The activation energies are $E = RB$ and $E_T = RB_T$ cal./mole. The apparent activation energy, E_T, approaches the true, temperature-independent value, E, as T approaches infinity. As the measurement temperature is decreased toward T_0, E_T increases exponentially.

Fox and co-authors[3] have reported an empirical E_T–temperature equation appying to several types of linear polymer chains. For $C_{13}H_{28}$ of the Doolittle n-alkane series, their equation gives log E_T = 4.762 − 0.5 log T. As shown below in Table II, the values of E_T calculated from this equation agree well with values calculated from the differentiated M.A. equation, in which E = 2(965) = 1930 cal./mole and T_0 = 73°K.

TABLE II

APPARENT ACTIVATION ENERGIES FOR $C_{13}H_{28}$

T, °K.	E_T, kcal./mole.[a]	E_T, kcal./mole[b]
263	3.57	3.70
293	3.37	3.44
323	3.22	3.22
373	2.99	2.98
423	2.81	2.82
473	2.66	2.70

[a] By the empirical equation of Fox and co-authors.[3] [b] By the differentiated M.A. equation.

By rearrangement of the differentiated M.A. equation: $T = E^{1/2}T/E_T^{1/2} + T_0$. A plot of $T/E_T^{1/2}$ against T should be linear, with $E^{1/2}$ as the slope and T_0 as the intercept. This provides a method for estimating the M.A. parameters from B_T or E_T values which, in turn, are derived from the slopes of the ordinary Arrhenius curves at several temperatures or from empirical E_T–T equations,[3] respectively.

The simple Arrhenius equation (T_0 = 0°K.) has often been used to express the viscosity data for n-alkanes[13,14] and other fluids on the basis of measurements over limited temperature ranges. The values for activation energies and for the pre-exponential A terms obtained from these *pseudo*-linear plots are significantly higher than those obtained from a linear M.A. plot and this divergence can be expected to increase as the n-alkane series is ascended, *i.e.*, as T_0 increases.

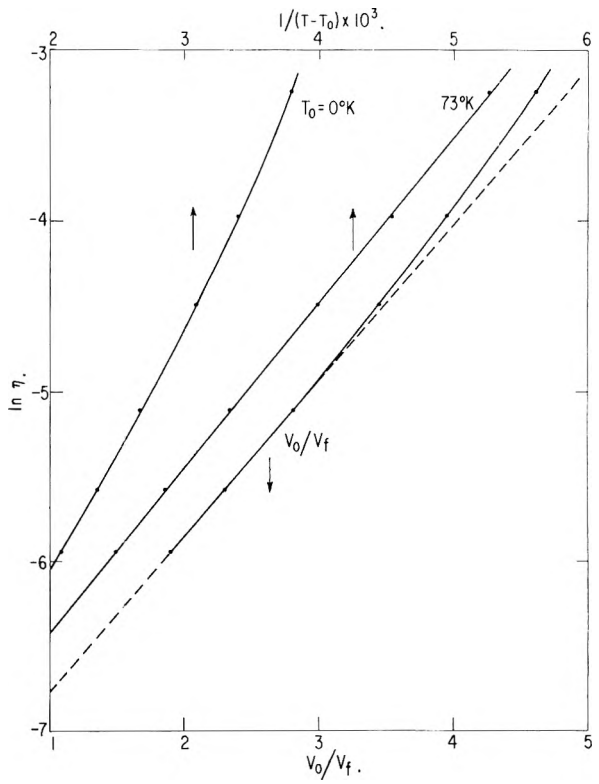

Fig. 2.—Normal (T_0 = 0°K.) and modified (T_0 = 73°K.) Arrhenius plots of viscosity for $C_{13}H_{28}$, compared with Doolittle v_0/v_f plot.

In the M.A. equation, the temperature-dependence occurs only in the exponential term. However, molecular theories of liquid transport appear to require an additional temperature factor. For example, the Cohen–Turnbull[8] derivation, relating viscosity to the self-diffusion constant, D, suggests that $\eta \propto T/D$ and $D \propto T^{1/2}$, leading to $\eta = A'T^{1/2} \exp[B/(T - T_0)]$. For such a relationship, the temperature dependence is still governed predominantly by the exponential term. Thus for the present case, $C_{13}H_{28}$, over the 263° to 473°K. measurement range, the $T^{1/2}$ term changes by a factor of only 1.34, while the exponential term changes by a factor of 14.6. A plot of ln $(\eta/T^{1/2})$ *vs.* $1/(T - T_0)$ shows, for T_0 = 0°K., somewhat less upward curvature than the corresponding plot in Fig. 2, indicating a decrease in the value of T_0 if the $T^{1/2}$ term is included. In this case, the plot becomes linear at $T_0 \simeq 63$°K., giving $B \simeq 1150$°. However, the $B/(T - T_0)$ term, which is to be related to free volume, is thus increased by less than 15%, compared to values using the original parameters, T_0 = 73°K. and B = 965.

Apparently, the M.A. equation can be readily adapted to include a pre-exponential temperature term, if required by theoretical considerations. The B and T_0 parameters can still be derived by the proper plots, as indicated above. Since the following discussion, relating to free volume, depends primarily on the exponential term, only the simpler M.A. form, $\eta = A \exp[B/(T - T_0)]$, will be considered.

Free Volume Considerations.—The dependence of viscosity on free volume will be expressed by an expo-

(13) W. Kauzmann and H. Eyring, *J. Am. Chem. Soc.*, **62**, 3113 (1940).
(14) K. Ueberreiter and H. J. Orthmann, *Kolloid Z.*, **126**, 140 (1952).

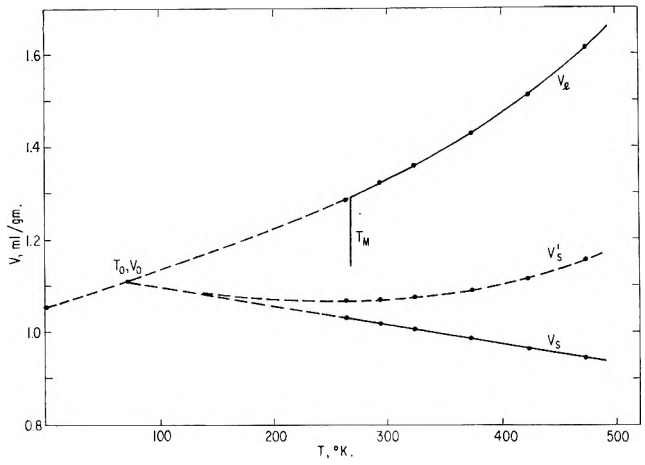

Fig. 3.—Occupied volumes derived from M.A. parameters for $C_{13}H_{28}$: $v_s = v_l[1 - (T - T_0)/B]$; $v_s' = v_l - v_0(T - T_0)/B$.

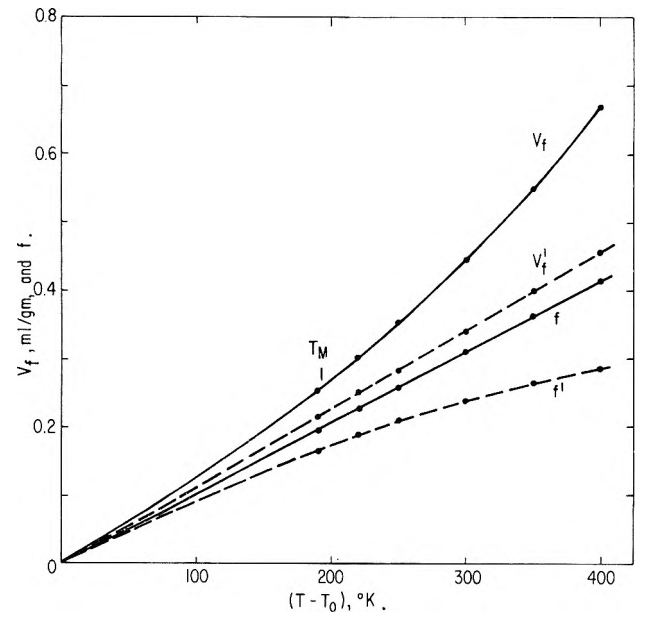

Fig. 4.—Free volumes, v_f, and v_f', and free volume fractions, f and f', corresponding to the two cases in Fig. 3. (T_0 = 73° K.).

nential equation of the form suggested empirically by Doolittle[10] and derived theoretically by Cohen and Turnbull[8]: $\eta = A \exp(v/v_f)$, in which the volume v remains to be specified. Comparison with the M.A. equation shows that v_f becomes zero at T_0, and that above T_0 some function of free volume is linear in temperature. One such function, which is suggested by past work,[7,15] is the free volume fraction, $f = v_f/v_l$. Thus, the viscosity equation becomes simply $\eta = A \exp(1/f)$, where $f = (T - T_0)/B$, or $v_f = v_l(T - T_0)/B$. On this basis, the volume parameters were derived for $C_{13}H_{28}$ and are listed in Table III. The liquid specific volumes, v_l, are the Doolittle values[10b] and the "occupied" volumes are given by $v_s = v_l - v_f$.

These volume–temperature values are plotted in Fig. 3. The liquid curve, v_l, is extrapolated to Doolittle's value of 1.056 ml./g. at 0°K.[10b] The occupied volume, v_s, decreases almost linearly with temperature, with a slope $dv_s/dT = -4.2 \times 10^{-4}$ ml./g./deg. Also, the v_s and v_l curves intersect at T_0, the theoretical zero-point for the free volume.

(15) F. Bueche, *J. Chem. Phys.*, **24**, 418 (1956).

Table III

Volume Parameters for n-$C_{13}H_{28}$

T, °K.	$T - T_0$	f	v_l, ml./g.	v_f, ml./g.	v_s, ml./g.
263	190	0.198	1.286	0.254	1.032
293	220	.228	1.322	.302	1.020
323	250	.260	1.361	.353	1.008
373	300	.310	1.432	.445	0.987
423	350	.363	1.514	.550	.964
473	400	.415	1.613	.670	.943

An alternate case may be considered briefly. If the free volume itself, rather than the free volume fraction, is made linear in temperature, we have $v_f = v_0(T - T_0)/B$, in which v_0 = 1.10 ml./g., obtained from the v_l curve at T_0. (Here v_0 must remain constant in order that v_f be linear in temperature.) The resulting occupied volume, represented by v_s' in Fig. 3, now *increases* non-linearly with temperature. Since $dv_f/dT = v_0/B$, we have: $dv_s/dT = dv_l/dT - V_0/B$, where $v_0/B = 11.4 \times 10^{-4}$ ml./g./deg.

The free volumes and free volume fractions are shown as functions of temperature in Fig. 4 for the two cases just described. It may be noted that values, according to the two models, differ markedly at the higher temperatures but converge as T_0 is approached.

It appears that a rigorous choice between these and other possible free volume models cannot be made on the basis of the M.A. treatment alone. An independent molecular approach, which can relate free volume, as manifested by liquid relaxation processes, to the liquid *structure*, is required. For example, in a discussion of "free volumes" in liquids, Bondi[16] has described the linear $\rightleftarrows$ coiled equilibrium in n-alkane melts as functions of temperature and molecular weight. In n-$C_{16}H_{34}$, which is similar to the $C_{13}H_{28}$ alkane being considered here, the estimated fraction of coiling is < 1% at 263°K., 5% at 373°, and 30% at 473° With respect to viscous flow, the model corresponding to v_s in Fig. 3 would imply that coiling decreases the occupied volume, while the model corresponding to v_s' leads to the opposite conclusion. Another structural factor is the possible alignment of the linear n-alkane molecules parallel to the direction of flow, suggested by Douglass and McCall[17] on the basis of self-diffusion studies. Finally, varying degrees of molecular association, depending upon temperature and chemical composition, may be expected to influence free and occupied volumes.

Free Volumes at Transition Points.—If the free volume fraction in liquids increases linearly with temperature, the resulting expression, $f = (T - T_0)/B$, may be used to estimate this fraction at any temperature. On this basis, $f_M = 0.20$ for $C_{13}H_{28}$ at the melting point (T_m = 268°K). The possibility that, within this homologous series, the melting point is an "iso-free volume fraction" state could be tested by derivation of the M.A. parameters from relaxation measurements on other n-alkanes.

Conversely, if an "iso-free volume fraction" condition at a transition point has been demonstrated, the transition temperature itself can be estimated. Thus, Williams, Landel, and Ferry[7] have shown that for a variety of liquids the free volume fraction at the glass point, T_g, is approximately constant, $f_g \simeq 0.025$.

(16) A. Bondi, *J. Phys. Chem.*, **58**, 929 (1954).
(17) D. C. Douglass and D. W. McCall, *ibid.*, **62**, 1102 (1958).

Assuming that this also applies to *n*-alkanes, we find $T_g \simeq 97°K.$ for $C_{13}H_{28}$.

Conclusions

This work provides further evidence that the temperature dependence of liquid relaxation processes, such as viscous flow, can be represented generally by the M.A. equation, $\eta = A \exp[B/(T - T_0)]$. For certain conditions (*i.e.*, narrow temperature ranges, $T >> T_0$, or $T_0 \rightarrow 0°K.$), this equation reduces to, or is experimentally indistinguishable from, the simple Arrhenius form: $\eta = A \exp(B/T)$. The M.A. equation can be converted directly into the empirical W.L.F. (Williams–Landel–Ferry) relationship, which has been applied to a variety of liquids near their glass transition temperatures.[7] For T_g as the reference temperature in the W.L.F. equation, the parameters transform as follows: $T_g - T_0 = C_2^g$ and $B = C_1^g C_2^g$. In the W.L.F. approach, $f_g = 1/C_1^g$, which is identical with $f_g = (T_g - T_0)/B$, the expression used earlier in this paper.

From a free volume viewpoint, the exponential Doolittle equation $\eta = A \exp(Bv_0/v_f)$, has been generally accepted. However, the Doolittle interpretation, with the occupied volume v_0 remaining temperature-independent, gives the same type of deviation at low temperatures as does the simple Arrhenius equation. To correct this, a change in the occupied volume with temperature must be allowed. In principle, this temperature dependence can be derived from the parameters of the M.A. equation.

The present M.A. approach adopts the viewpoint that the theoretical origin of the free volume is not 0°K. but T_0, as suggested by Cohen and Turnbull. The temperature dependence of the free volume is related to $1/B$. However, the transformation of the M.A. temperature parameters into true free volume parameters depends upon the choice of the liquid relaxation model. The model described here, in which the free volume *fraction* increases linearly with temperature, leads to $f = v_f/v_l = (T - T_0)/B$ and $\eta = A \exp(1/f)$.

This model, although a reasonable one, must be considered as tentative, pending auxiliary information from theory and measurements of liquid structure. Conversely, once the proper model is firmly established, information on liquid structure (*i.e.*, v_f and v_s) may be derived from liquid relaxation measurements *via* the M.A. parameters.

If the occupied volume in the liquid is determined by the liquid structure and molecular configurations, then v_s and its expansion coefficient, α_s, should have no direct relationship to the crystal or glass volumes and their expansion coefficients, except in the region of T_M or T_g, where the structure of the liquid most closely resembles that of the solid.

Acknowledgment.—Appreciation is expressed to D. Turnbull for stimulating and encouraging discussions in the early phases of this work.

THE INVESTIGATION OF THE BEHAVIOR OF SOME POLYSULFONATES IN CONCENTRATED AQUEOUS SOLUTIONS[1,2]

BY O. D. BONNER AND JAMES R. OVERTON

Department of Chemistry, University of South Carolina, Columbia, South Carolina

Received October 18, 1962

Osmotic coefficients, and in some instances activity coefficients, for two series of polymeric compounds having toluenesulfonate and ethylbenzenesulfonate as the monomeric unit have been determined by isopiestic comparison of solutions of these compounds with reference solutions of lithium chloride. It was observed that the osmotic coefficients of compounds of all degrees of polymerization were dependent upon the hydrocarbon content of the sulfonate, the coefficient being smaller for molecules of greater equivalent weight. It was further observed that, within the same "family" of polymers, the water activity of the solution was *primarily* a function of the concentration of ionic *groups* and not of the ional concentration. An "end-group effect" was also noted for polystyrene polymers. The osmotic coefficients of loosely cross-linked polystyrenesulfonates were higher than those of the linear compounds which would not be expected to have as many polar end-groups resulting from chain terminating steps.

The ion-exchange process has been recognized by many investigators to be a partition of ions between a resin phase and an aqueous phase which is governed by a Donnan membrane equilibrium. Myers and Boyd,[3] as well as others, have shown that if the same standard reference state is taken for both phases the thermodynamic equilibrium constant must be unity and the resin selectivity in the exchange of *singly* charged ions is given by the equation

$$\log D = P(\bar{V}_{B^+} - \bar{V}_{A^+})/2.3RT + \log (\gamma_{B^+}/\gamma_{A^+})_i - \log (\gamma_{B^+}/\gamma_{A^+})_o \quad (1)$$

where i refers to the resin phase and o refers to the dilute phase. The second term is known to make the largest contribution to log D since the molar volumes of the two exchangeable ions appearing in the first term are usually not too different and since the third term is small for dilute solutions and vanishes completely in the limiting case of an infinitely dilute solution. Although the value of the second term may be estimated from equilibrium experiments, it cannot be measured by *independent* means since ion-exchange resins are not susceptible to electromotive force measurements and infinitely dilute solutions are not attainable because of the divinylbenzene cross linking.

An alternative method for the estimation of the value of the second term of equation 1 is the use of solutions of soluble "model" compounds which are

(1) Presented at the 141st National Meeting of the American Chemical Society, Washington, D. C., March, 1962.

(2) This work was supported by the Atomic Energy Commission under Contract No. AT-(40-1)-1437.

(3) G. E. Myers and G. E. Boyd, *J. Phys. Chem.*, **60**, 521 (1956).

similar in structure to the monomer units of which ion exchangers are comprised. Activity coefficient ratios may then be calculated from measurements of water activities of solutions of varying concentrations.

Rice[4] and co-workers have noted that although an examination of the literature reveals that certain differences between polyelectrolytes and simple electrolytes are universally recognized, no studies have been made of the transition from one to the other.

It would appear that justification for the use of soluble "model" compounds in the interpretation of ion-exchange equilibria would involve the experimental substantiation of certain behavioral relationships. For example, it should be demonstrated that the structure of these aromatic sulfonates affects the osmotic properties of their aqueous solutions and also that sulfonates of different degree of polymerization but having the same recurring monomer unit should have similar osmotic properties. The effect of structure on the properties of solutions of sulfonates has been observed in previous work. In the case of monosulfonates for example, it has been observed[5] that the magnitude of the values of the osmotic coefficients have the order Li > H > Na for the benzene sulfonates and Li > Na > H for the dimethyl and trimethylbenzenesulfonates. The osmotic and activity coefficients of toluenesulfonates have the same order as the higher molecular weight sulfonates in dilute solutions but change to the order of the benzenesulfonates in more concentrated solutions. It was also observed that the osmotic and activity coefficients of any particular cation are greatest for the benzenesulfonate and decrease with increasing molecular weight of the sulfonate. These results indicate that there is more ion pair formation in salts of the higher molecular weight sulfonates where the organic portion of the molecule, with its low dielectric constant, constitutes a larger fraction of the total volume. In concentrated solutions of these electrolytes the volume occupied by the hydrocarbon portion of the molecule approaches that of the solvent. The more rapid decrease of the osmotic coefficients of the acids with increasing molecular weight when compared with the corresponding salts indicates that the acids are probably incompletely ionized in concentrated solutions.

This effect of structure on properties has also been observed in ion exchangers. Boyd and co-workers[6] studied the effect of capacity on ion-exchange equilibria by successive desulfonations of an exchanger until its equivalent weight was twice that of the original resin. The results are completely compatible with those of soluble monosulfonates.

The above observations concerning the monosulfonates have been substantiated by the results obtained from investigations of certain disulfonates.[7] The values of the osmotic and activity coefficients of the lithium, hydrogen, and sodium sulfonates have the same order as for the monosulfonates of corresponding equivalent weights. It was further noted that the osmotic coefficients of the *m*-benzenedisulfonates, in which the organic content of the molecule per equivalent of electrolyte is less than would be possible for any aromatic monosulfonate, is H > Li > Na.

The consistancy of the results obtained from the investigations of mono- and disulfonates suggests that additional work might be profitable using higher molecular weight polyelectrolytes as models to elucidate further the effect of polymerization on the properties of electrolytes in concentrated solutions.

It should be noted that at least two previous attempts have been made to evaluate this activity coefficient ratio by the use of model compounds. Myers and Boyd[3] used a 0.5% DVB resin as the model but in this instance the most dilute solutions obtainable contained about one equivalent of resin per 1000 g. of water. Bonner and co-workers[8] used *p*-toluenesulfonates and dimethylbenzenesulfonates as models. As stated above subsequent data have indicated that the structure of sulfonates has a substantial effect on their properties and thus monomers of slightly greater equivalent weight would have been preferrable as model compounds.

Experimental

Preparation and Purification of Compounds.—The osmotic properties of the acids and lithium and sodium salts of two "families" of sulfonates have been investigated. In one family having *p*-toluenesulfonic acid as the monomeric model the mono-,[5] di-,[7] and trimeric compounds have been investigated. The trimeric hydrocarbon, 1,2,3-triphenylpropane, was prepared by the reduction of phenyldibenzylcarbinol with red phosphorus and hydriodic acid according to the method of Klages and Heilmann.[9] The phenyldibenzylcarbinol was obtained by the Grignard reaction involving ethyl benzoate and benzyl chloride.[10]

The trisulfonation of the hydrocarbon was achieved by the dropwise addition of liquid SO_3, dissolved in CCl_4, to a solution of 1,2,3-triphenylpropane in CCl_4.[11] In addition to the normal preference for *para* sulfonation, steric considerations indicate that, in this compound, sulfonation must be essentially 100% in the *para* position.

In the second family, having ethylbenzene as the monomeric model, the mono-[3] and trimeric compounds have been synthesized and investigated. The synthesis of the parent triphenyl hydrocarbon was similar to that of the triphenylpropane described above. In this instance, the carbinol was obtained from the reaction of ethyl benzoate with a Grignard reagent prepared from 2-phenylethyl bromide. The reduction was performed as described above. It is to be noted that the trimeric compound, resulting from the synthesis described above, is 1,3,5-triphenylpentane rather than 1,3,5-triphenylhexane which would be the true trimer of ethylbenzene.

It was also possible in the case of the ethylbenzene family to obtain compounds of higher degree of polymerization, since polystyrenes contain this repeating structure. Samples of linear polystyrene sulfonates having hydrocarbon molecular weights averaging ten thousand,[12] seventy thousand,[12] and four hundred thousand[13] were purified and investigated. The samples as received were contaminated with sodium sulfate which was removed by recrystallization of the sulfonates from concentrated hydrochloric acid. The HCl and water were then removed by vacuum drying.

The loosely cross-linked co-polymer, Dowex 50 X-1, which may also be considered as belonging to the ethylbenzene family, was given the usual pre-treatment of alternate elutions with 6 *N* hydrochloric acid and water to remove traces of iron and washing with ethanol to remove organic contaminants.

Anisole sulfonic acid was prepared by the sulfonation of anisole according to the procedure described previously.[5] This procedure results in the production of predominantly *para*-sulfonates.

(4) S. Lapanje, J. Haebig, H. T. Davis, and S. A. Rice, *J. Am. Chem. Soc.*, **83**, 1590 (1961).
(5) O. D. Bonner and O. C. Rogers, *J. Phys. Chem.*, **64**, 1499 (1960).
(6) G. E. Boyd, B. A. Soldano, and O. D. Bonner, *ibid.*, **58**, 456 (1954).
(7) O. D. Bonner and O. C. Rogers, *ibid.*, **65**, 981 (1961).
(8) O. D. Bonner, V. F. Holland, and L. L. Smith, *ibid.*, **60**, 1102 (1956).
(9) A. Klages and S. Heilmann, *Ber.*, **37**, 1447 (1904).
(10) R. C. Fuson, *J. Am. Chem. Soc.*, **48**, 2937 (1926).
(11) H. H. Roth, *Ind. Eng. Chem.*, **46**, 2435 (1954).
(12) The authors are indebted to the Monsanto Chemical Company for the samples of 10,000 and 70,000 molecular weight polystyrene sulfonates.
(13) The authors are indebted to the Dow Chemical Company for the sample of 400,000 molecular weight polystyrene sulfonate.

Isopiestic Equilibration.—Water activities and osmotic coefficients of all acids and salts were determined by isopiestic comparison of solutions of these electrolytes with solutions of lithium chloride which served as standards. Values of the osmotic coefficients of lithium chloride are tabulated by Robinson and Stokes.[14] In the case of ethylbenzenesulfonic acid and the anisolesulfonates where dilute solution data are available, the activity coefficients were calculated using activity coefficient data for lithium chloride solutions taken from the same source.

Results and Discussion

The 1,2,3-triphenylpropanetrisulfonates are interesting compounds in several respects. The acid is quite soluble but concentrated aqueous solutions are not viscous as might be expected. The reason is apparent, when upon construction of models of the compounds, it is found that the trimer is not linear but probably exists in the form of a disk having a diameter of approximately 20 Å. This shape eliminates much of the resistance to flow in solution. Solubilities of the salts are also somewhat greater than might be expected. The solubilities of the sodium salts, for example, of the mono-, di-, and trisulfonates in this series, in equivalents per 1000 g. of water, are 4.0, 0.9, and 6.5, respectively. The dimer appears, thus, to represent a solubility minimum.

Osmotic coefficients have been calculated for this trimeric acid and its lithium and sodium salts and these data are presented in Table I. It may be noted that in solutions more dilute than 1.7 *m* the order of these coefficients is Li > H > Na. This is the same sequence observed for the *p*-toluenesulfonates and bibenzyldisulfonates. In solutions more concentrated than 1.7 *m* the osmotic coefficients of the acid become greater than those of the lithium salt. This behavior was not observed for the corresponding mono- and disulfonates due to solubility limitations although it may be noted that the osmotic coefficients of the acid and lithium salt are in each instance approaching the same value.

TABLE I

TABLE OF OSMOTIC COEFFICIENTS[a]

m	1	2	3	4	5	6
0.5	0.909	0.811	0.699	0.838	0.744	0.699
.6	.935	.845	.704	.867	.773	.671
.7	.964	.882	.711	.906	.811	.684
.8	.994	.921	.720	.947	.852	.702
.9	1.026	.963	.732	.990	.895	.722
1.0	1.061	1.005	.746	1.034	.935	.741
1.1	1.100	1.052	.760	1.079	.975	.759
1.2	1.140	1.100	.777	1.124	1.016	.777
1.3	1.181	1.142	.795	1.172	1.056	.794
1.4	1.223	1.191	.813	1.219	1.098	.811
1.5	1.268	1.244	.832	1.263	1.141	.828
1.6	1.313	1.298	.851	1.306	1.184	.848
1.7	1.357	1.350	.871	1.348	1.229	.867
1.8	1.398	1.398	.890	1.387	1.273	.886
1.9	1.439	1.448		1.425	1.318	.904
2.0	1.479	1.500		1.464	1.364	.922
2.1	1.518	1.550		1.505	1.410	
2.2		1.599			1.458	
2.3		1.648			1.508	
2.4		1.701			1.560	
2.5		1.757			1.613	

[a] 1, lithium 1,2,3-triphenylpropanetrisulfonate; 2, 1,2,3-triphenylpropanetrisulfonic acid; 3, sodium 1,2,3-triphenylpropanetrisulfonate; 4, lithium 1,3,5-triphenylpentanetrisulfonate; 5, 1,3,5-triphenylpentanetrisulfonic acid; 6, sodium 1,3,5-triphenylpentanetrisulfonate.

(14) R. A. Robinson and R. H. Stokes, *Trans. Faraday Soc.*, **45**, 612 (1949).

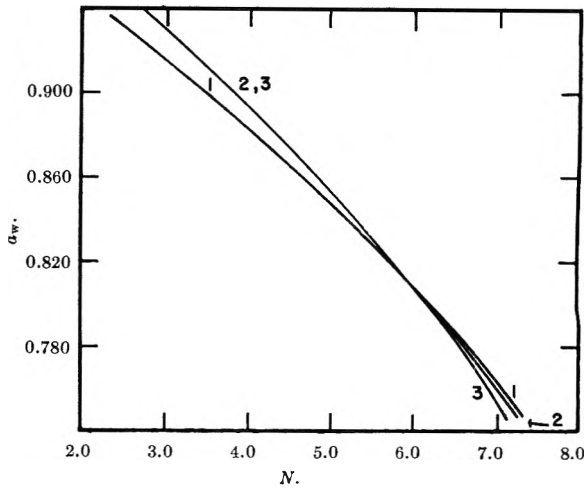

Fig. 1.—Water activity at 25° as a function of the concentration expressed in equivalents per 1000 g. of solvent: 1, *p*-toluenesulfonic acid; 2, bibenzyldisulfonic acid; 3, 1,2,3-triphenylpropanetrisulfonic acid.

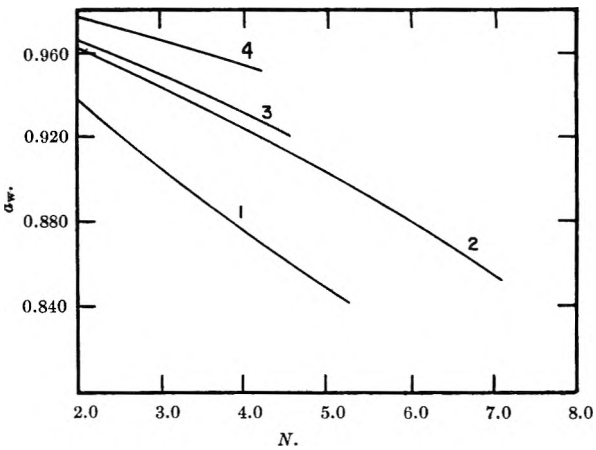

Fig. 2.—Water activity at 25° as a function of the concentration expressed in equivalents per 1000 g. of solvent: 1, KCNS; 2, K_2CrO_4; 3, K_2FeCN_6; 4, K_4FeCN_6.

A comparison of the effects of the mono-, di-, and trisulfonates on the solvent activity in concentrated solutions is probably of greater significance than the above mentioned considerations. A plot of water activities of solutions of the acids as a function of the concentration expressed in equivalents per 1000 g. of water is shown in Fig. 1. The results for the lithium and sodium salts are quite similar. It is apparent that, in concentrated solutions where the distances of separation of the ionic groups are virtually independent of the degree of polymerization, the lowering of the water activity is *primarily* a function of the concentration of ionic groups and not of the number of ions present.

The behavior of this family of polyelectrolytes may be contrasted with that of several "normal" polyvalent electrolytes for which data are available.[14,15] When water activities are plotted as a function of the number of equivalents of electrolyte per 1000 g. of water (Fig. 2) the salts of lower valence type appear to be more effective in lowering the vapor pressure. Plots of water activity as a function of *ion concentration* (Fig. 3) are quite similar, however, indicating that the ional concentration is in this instance *primarily* responsible for the vapor pressure lowering.

(15) R. A. Robinson and R. H. Stokes, "Electrolyte Solutions," 2nd Ed., Academic Press, London, 1959, pp. 485, 488.

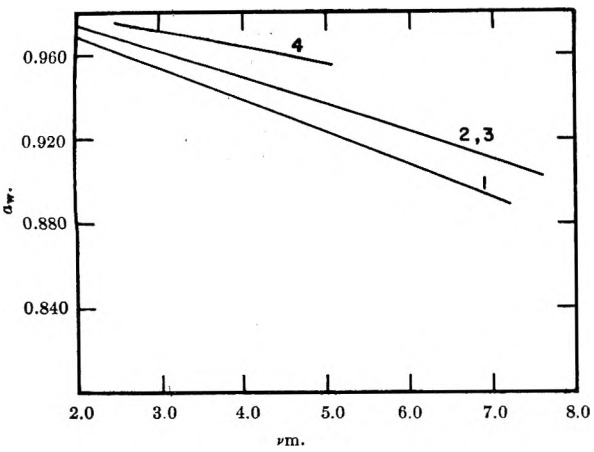

Fig. 3.—Water activity at 25° as a function of the ionic concentration: 1, KCNS; 2, K_2CrO_4; 3, K_3FeCN_6; 4, K_4FeCN_6.

For more direct comparison of "model compounds" with sulfonate type cation exchangers, compounds in the polystyrene series, having ethylbenzenesulfonic acid as the monomeric compound, should be used. Osmotic and activity coefficient data have already been reported for the ethylbenzenesulfonates in dilute and moderately concentrated solutions. These data for the acid have now been extended to solutions more concentrated than 5.0 *m* for comparison with the polyelectrolyte data (Table II). Osmotic coefficients have also been calculated for the trimer (Table I) in this series.

TABLE II

TABLE OF OSMOTIC AND ACTIVITY COEFFICIENTS FOR *p*-ETHYLBENZENESULFONIC ACID AT 25°

m	ϕ	γ
4.0	0.734	0.289
4.5	.774	.292
5.0	.823	.300
5.5	.870	.316
6.0	.916	.327
6.5	.964	.337
7.0	1.008	.352
7.5	1.055	.371
8.0	1.100	.389
8.5	1.143	.420

In order to extend these measurements to polyelectrolytes of higher degrees of polymerization solutions of three samples of linear polystyrenesulfonates and one sample of lightly cross-linked resin (1% DVB) have also been isopiestically compared with lithium chloride solutions. Although these are not compounds of known structure, in that their molecular weight is an average value and is only approximately known, osmotic coefficients may nevertheless be calculated. The function ($m\phi$) is known from water activity data and for polymers of high molecular weight the number of equivalents per 1000 g. of water, N, equals $(\nu - 1)m$ and this quantity is essentially identical with νm. Osmotic coefficient data for these compounds are listed in Table III. These data are roughly comparable with those of Myers and Boyd[3] and Gregor[16,17] for similar substances. Exact comparison is not possible though since Myers and Boyd did not state the capacity of the 0.5% DVB resin and Gregor's value of 6.85 meq./g. for 0.4% DVB resin corresponds to an equivalent weight of 146. This value is either in error or it indicates the presence of carboxyl or other exchange sites in addition to the sulfonate sites. The equivalent weights listed by Gregor for the linear polystyrenesulfonates are reasonable but no molecular weight data are given.

(16) B. R. Sundheim, M. H. Waxman, and H. P. Gregor, *J. Phys. Chem.*, **57**, 974 (1953).

(17) M. H. Waxman, B. R. Sundheim, and H. P. Gregor, *ibid.*, **57**, 969 (1953).

TABLE IIIA

TABLE OF OSMOTIC COEFFICIENTS[a] AT 25°

Weight normality	1	2[b]	3	4	5[c]	6
2.0	0.831	0.675	0.471	0.778	0.666	0.516
2.5	.933	.772	.511	.876	.756	.560
3.0	1.018	.875	.548	.966	.841	.597
3.5	1.101	.983	.589	1.051	.936	.632
4.0	1.180	1.085	.629	1.129	1.026	.663
4.5	1.262	1.190	.673	1.214	1.112	.690
5.0	1.347	1.300	.723	1.297	1.195	.718
5.5	1.431	1.421	.784	1.386	1.282	.753
6.0	1.518	1.547	.857	1.473	1.370	.791
6.5	1.608	1.682	.945	1.560	1.456	.828
7.0	1.695	1.831	1.046	1.646	1.542	.877
7.5	1.788	1.984		1.735	1.630	.931
8.0	1.880	2.146		1.823	1.726	.998

[a] 1, Sulfonated 10,000 mol. wt. polystyrene, lithium salt; 2, sulfonated 10,000 mol. wt. polystyrene, acid; 3, sulfonated 10,000 mol. wt. polystyrene, sodium salt; 4, sulfonated 70,000 mol. wt. polystyrene, lithium salt; 5, sulfonated 70,000 mol. wt. polystyrene, acid; 6, sulfonated 70,000 mol. wt. polystyrene, sodium salt. [b] Equivalent wt., 211. [c] Equivalent wt., 206.

TABLE IIIB

TABLE OF OSMOTIC COEFFICIENTS[a] AT 25°

Weight normality	1	2[b]	3	4	5[c]	6
2.0	0.827	0.729	0.667	0.657	0.651	
2.5	.905	.814	.711	.771	.767	0.490
3.0	.965	.887	.755	.868	.870	.538
3.5	1.021	.956	.786	.955	.972	.578
4.0	1.077	1.026	.816	1.034	1.079	.620
4.5	1.139	1.101	.844	1.114	1.199	.665
5.0	1.208	1.186	.876	1.195	1.324	.711
5.5	1.280	1.266	.900	1.280	1.461	.762
6.0	1.356	1.350	.936	1.370	1.590	.813
6.5	1.436	1.433	.974	1.466	1.717	.870
7.0	1.515	1.519	1.011	1.571	1.841	.933
7.5	1.599	1.612		1.677	1.961	.996
8.0	1.676	1.706		1.792	2.077	1.076

[a] 1, Sulfonated 400,000 mol. wt. polystyrene, lithium salt; 2, sulfonated 400,000 mol. wt. polystyrene, acid; 3, sulfonated 400,000 mol. wt. polystyrene, sodium salt; 4, Dowex 50 X-1, lithium salt; 5, Dowex 50 X-1, acid; 6, Dowex 50 X-1, sodium salt. [b] Equivalent wt., 188. [c] Equivalent wt., 196.

It would be expected that the cross-linked resin and the linear polymers would have essentially identical osmotic coefficients if they were identical in structure. Equivalent weights given in Table IV indicate, however, that there are appreciable differences in the completeness of sulfonation of these compounds and this is known to affect their properties.[5,6]

It is probable that there is also a second effect of at least equal importance. The polymerization and subsequent sulfonation of these polymers undoubtedly results in the presence of polar end groups. The linear polymers of lower molecular weight would contain more of these end groups per equivalent of sulfonate exchange sites than those of higher molecular weight. From an analogy with non-electrolytes such as sucrose, the presence of a polar group would be expected to increase

TABLE IV

TABLE OF OSMOTIC AND ACTIVITY COEFFICIENTS FOR ANISOLESULFONATES AT 25°

	Lithium salt		Acid		Sodium salt	
m	ϕ	γ	ϕ	γ	ϕ	γ
0.1	0.927	0.772	0.906	0.739	0.920	0.761
.2	.916	.723	.879	.668	.904	.705
.3	.911	.694	.860	.623	.892	.668
.4	.905	.673	.848	.590	.881	.640
.5	.901	.656	.840	.564	.872	.617
.6	.898	.642	.832	.544	.864	.597
.7	.896	.630	.826	.527	.856	.581
.8	.894	.621	.821	.511	.851	.566
.9	.893	.613	.816	.498	.846	.554
1.0	.892	.606	.813	.487	.841	.542
1.2	.893	.594	.806	.468	.833	.523
1.4	.895	.585	.805	.453	.826	.505
1.6	.897	.579	.806	.442	.820	.491
1.8	.901	.575	.808	.433	.814	.477
2.0	.907	.572	.811	.425	.808	.465
2.5	.920	.569	.822	.413	.799	.441
3.0	.935	.570	.840	.408	.795	.424
3.5			.865	.408		
4.0			.894	.413		
4.5			.926	.422		
5.0			.960	.435		
5.5			.996	.450		
6.0			1.033	.468		
6.5			1.069	.487		
7.0			1.106	.508		
7.5			1.141	.532		
8.0			1.175	.555		
			1.209	.580		

the osmotic coefficient. It may be noted in Fig. 4 that the linear polymers fall into a somewhat regular pattern. The position of the cross-linked polymer is of interest in that lower water activities indicate a larger number of polar end groups for this *branched chain* compound than for the linear polymer, even though it has an extremely high molecular weight.

In order to substantiate this "end group effect" on water activities, anisolesulfonic acid was prepared and purified as described above. The osmotic coefficients for the anisolesulfonates (Table IV) are, in fact, higher than those of the *p*-ethylbenzenesulfonates which have almost identical molecular weights. The behavior of anisolesulfonic acid in very concentrated solutions indicates some hydrogen bonding between the ether group oxygen and the hydrogen of the undissociated sulfonic acid groups.

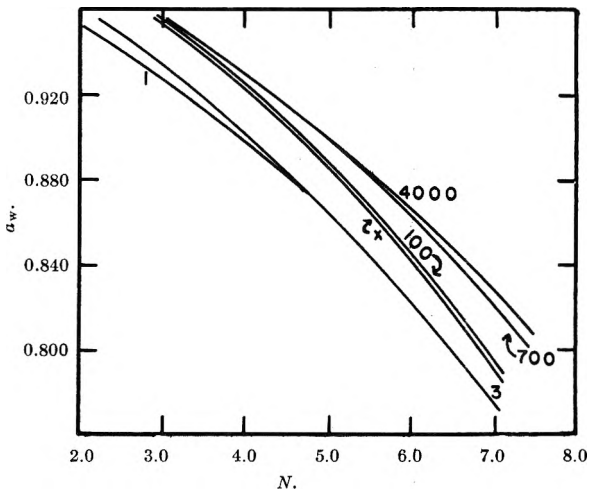

Fig. 4.—Water activity at 25° as a function of the concentration expressed in equivalents per 1000 g. of solvent for compounds in the polystyrene series. Degree of polymerization is approximately as noted. The symbol × refers to 1% cross-linked resin.

The water activity data of Fig. 4 indicate that, after the "end group effect" is considered, the styrenesulfonates ranging from the monomer to the cross-linked polymer exhibit quite similar osmotic properties. In this family of polyelectrolytes, as in the *p*-toluenesulfonate family, it appears that the lowering of the water activity in *concentrated* solutions is *primarily* a function of the concentration of ionic groups present. It may be also noted that similar relationships exist between the osmotic coefficients of the acids and lithium and sodium salts for sulfonates of all degrees of polymerization. In moderately concentrated solutions the order of osmotic coefficients is Li > H > Na. This order changes to H > Li > Na for more concentrated solutions in all instances in which the lithium salt has sufficient solubility. It would appear, on the basis of these results, that further work involving solutions of mixed sulfonates would be profitable in the comparison of the behavior of soluble "model" compounds and cross-linked ion exchangers.

VAPOR PRESSURES OF TIN SELENIDE AND TIN TELLURIDE

BY CHIKARA HIRAYAMA, YOSHIO ICHIKAWA, AND ANTHONY M. DEROO

Westinghouse Research Laboratories, Pittsburgh 35, Pennsylvania

Received October 18, 1962

The vapor pressures of SnSe and SnTe are given, respectively, by $\log p = 7.318 - (10{,}495 \pm 151)1/T$ between 773 and 898°K., and by $\log p = 7.672 - (11{,}211 \pm 258)1/T$ between 792 and 933°K. The heats of sublimation at 298°K. are 52.4 ± 1 for SnSe and 53.1 ± 1 kcal./mole for SnTe. The dissociation energies calculated from thermodynamic data are 85.5 and 80 kcal./mole for SnSe and SnTe, respectively.

The diatomic compounds formed between elements of groups IVB and VIB are characterized by high dissociation energies, with values ranging from 51.4 kcal./mole for PbTe[1] to 256 kcal./mole for CO.[2] Aside from the compounds of carbon and silicon, and GeO, these solid diatomic compounds are all stable in air at room temperatures and slightly higher. Because of the high dissociation energies these solids are expected to vaporize predominantly as the molecular species. Lead telluride,[1] for example, has been shown to have low dissociation constants at temperatures below its

(1) R. F. Porter, *J. Chem. Phys.*, **34**, 583 (1961).

(2) A. G. Gaydon, "Dissociation Energies and Spectra of Diatomic Molecules," 2nd Ed., Chapman and Hall, Ltd., London, 1953.

melting point, so that the vapor composition in the Knudsen cell is essentially PbTe(g).

The vapor pressures of all of these semiconducting solids, except SnSe and SnTe, have been measured and reported in the literature. We presently report the vapor pressures of SnSe and SnTe to complete the data on the volatility characteristics of the IVB–VIB binary compounds.

Both the tin–selenium and the tin–tellurium systems form binary compounds[3] of melting points 860 and 790°, respectively.

Experimental

Both SnSe and SnTe were prepared from semiconductor grade materials of assay 99.999% purity. The tin was obtained from Alpha Metals, Inc., while the selenium and tellurium were obtained from American Smelting and Refining Company. Seventy-five-gram batches were made by weighing stoichiometric quantities of the respective metals into a 75-mm. diameter Vycor tube. The latter then was evacuated to 10^{-5} torr and subsequently sealed. The sealed tube was then placed in an electric rocking furnace and heated to 890° for the preparation of SnSe, and to 820° for the preparation of SnTe. The tubes were allowed to rock at the above temperatures for 2 hr.; then they were removed and quenched in cold water. The compounds thus obtained were polycrystalline ingots. The X-ray powder diffraction pattern of SnSe gave crystal parameters a = 4.46 Å., b = 4.19 Å., and c = 11.57 Å., which agree identically with those reported by Okazaki and Ueda.[4] An extremely weak X-ray diffraction pattern for Se also appeared to be present. The chemical analysis showed Se = 40.5% (theoretical = 40.0%). The X-ray powder diffraction pattern for the SnTe showed only the lines belonging to this compound, with crystal parameter a = 6.320 Å. Chemical analysis gave 52.1% Te and 47.9% Sn (theoretical = 51.8% Te and 48.1% Sn). According to Mazelsky and Lubell,[5] the crystal parameter obtained corresponds to the composition $Sn_{0.992}Te$.

The apparatus and method have been described previously.[6] Graphite Knudsen cells of orifice diameters 0.125 and 0.0625 in., and lengths 0.177 and 0.185 in., respectively, were used in the SnSe measurements. The graphite cells used for the SnTe measurements were of lengths 0.267 and 0.261 in., respectively. The Clausing[7] correction was applied in computing the effective orifice area. A single sample of approximately 1 g. was used to make all of the measurements in the cell of 0.125-in. orifice; similarly, a single sample was used for all of the measurements in the other cell. In the SnSe measurements approximately 15 mg. of the sample was allowed to vaporize initially from each cell to remove any excess Se. The condensate from this evaporation showed a very weak X-ray powder diffraction pattern for Se, besides the strong pattern for SnSe. However, the condensate from subsequent evaporations showed no uncombined Se in the X-ray pattern.

Separate samples of SnTe were volatilized, and the X-ray pattern of the condensate showed only the SnTe pattern. Chemical analyses of the residue also showed the atom ratio of Sn:Te to be unity. A similar ratio was shown for the SnSe residue.

Results

The vapor pressures of SnSe and SnTe were calculated from the equation

$$p = 0.02255(m/At)(T/M)^{1/2} \qquad (1)$$

where p is the vapor pressure in atmospheres, m the weight loss in grams after effusion time t, A the effective orifice area, T the absolute temperature, and M the molecular weight of SnSe or SnTe. In the absence of mass spectroscopic data we assumed the monomolecular species. The results are summarized in Tables I and II in the order of determinations.

Least squares treatments of the data in Tables I and II gave the equations

$$\log p = 7.318 - (10{,}495 \pm 151)1/T \qquad (2)$$

for SnSe between 773 and 898°K., and

$$\log p = 7.672 - (11{,}211 \pm 258)1/T \qquad (3)$$

for SnTe between 792 and 933°K. The good linear relationships obtained with the cells of two different effective orifice areas suggest that the evaporation and condensation coefficients are close to unity.

TABLE I

VAPOR PRESSURE OF SnSe

T, °K.	Time, sec.	Weight loss, mg.	Eff. orifice area, cm.² × 10³	p, atm. × 10⁶
853	5370	6.0	5.61	9.33
837	7170	4.9	5.61	5.65
873	3700	9.0	5.61	20.6
898	3050	16.6	5.61	46.6
888	4110	15.1	5.61	31.3
822	10490	4.3	5.61	3.36
823	3560	9.8	34.5	3.67
833	2610	10.8	34.5	5.55
809	5390	8.7	34.5	2.13
773	13000	6.1	34.5	0.606
788	9160	6.7	34.5	0.954
793	7140	6.9	34.5	1.26

TABLE II

VAPOR PRESSURE OF SnTe

T, °K.	Time, sec.	Weight loss, mg.	Eff. orifice area, cm.² × 10³	p atm. × 10⁶
820	8200	5.6	27.51	1.02
867	6720	22.9	27.51	5.25
844	6300	9.7	27.51	2.34
792	11700	2.7	27.51	0.338
885	4920	25.8	27.51	8.12
918	3930	11.1	4.44	27.75
888	4320	5.2	4.44	11.32
874	7080	5.9	4.44	7.96
894	8070	11.2	4.44	13.43
933	1800	9.6	4.44	52.5

SnSe.—The heat of sublimation at 298°K. was computed by the third law method by using the entropy, 60.8 e.u.,[8] and thermodynamic functions given by Kelley[9] for SnSe(g), and by assuming that the heat capacity of SnSe(s) is identical with that of the isomorphous SnS(s).[9] The entropy of SnSe(s) is estimated in the Landolt-Bornstein Tabellen[10] as 20.6 e.u. Table III summarizes the third law calculations. The heat of sublimation thus obtaned is ΔH_{298}^0 = 52.4 ± 1 kcal./mole. The second law calculation for the heat of sublimation at 298°K., based on the high temperature value ΔH_{836} = 48.03 from eq. 2 and the heat capacity for SnS(s), yields ΔH_{298}^0 = 50.35 ± 1 kcal./mole, which is in good agreement with the third law calculation.

SnTe.—Since the heat capacity data for SnTe(s) are not available, the heat capacity of PbS(s),[9] which has the identical crystal structure, belongs to the same

(3) M. Hansen, "Constitution of Binary Alloys," 2nd Ed., McGraw-Hill Book Co., New York, N. Y., 1958.

(4) A. Okazaki and I. Ueda, *J. Phys. Soc. Japan*, **11**, 420 (1956).

(5) R. Mazelsky and M. S. Lubell, *Inorg. Chem.*, in press.

(6) C. Hirayama, *J. Phys. Chem.*, **66**, 1563 (1962).

(7) S. Dushman, "Scientific Foundations of Vacuum Technique," John Wiley and Sons, Inc., New York, N. Y., 1949, p. 99.

(8) K. K. Kelley and E. G. King, "Contributions to the Data on Theoretical Metallurgy," U. S. Bur. Mines, Bull. No. 592, 1961.

(9) K. K. Kelley, U. S. Bur. Mines, Bull. No. 584, 1960.

(10) Landolt-Bornstein Tabellen, Sechste Auflage, Band II, "Eigenschaften der Materie in Ihren Aggregatzustanden," Teil 4, Kalorische Zustandgrossen, 1961.

TABLE III

FREE ENERGY FUNCTIONS AND HEAT OF SUBLIMATION OF SnSe AT 298°K.

T, °K.	$-R \ln p$	$\left(\frac{F^0 - H_{298}^0}{T}\right)_{SnSe(g)}$	$\left(\frac{F^0 - H_{298}^0}{T}\right)_{SnSe(s)}$	ΔH_{298}^0, kcal./mole
853	23.02	64.30	25.58	52.66
837	24.01	64.19	25.41	52.56
873	21.45	64.44	25.78	52.48
898	19.82	64.61	26.02	52.45
888	20.61	64.53	25.93	52.58
822	25.04	64.09	25.26	52.50
823	24.87	64.09	25.28	52.41
833	24.05	64.17	25.38	52.35
809	25.95	64.00	25.14	52.43
773	28.45	63.75	24.77	52.12
788	27.55	63.86	24.93	52.39
793	26.99	63.89	24.98	52.26
			Av. =	52.43

group of binary compounds, and has a molecular weight not too different from that of SnTe, was used to calculate the free energy function. The entropy of SnTe(s) at 298°K. is reported[11] as 24.2 ± 1 e.u. The free energy function for SnTe(g) was computed from the data given by Kelley[9] and from the entropy of 62.92 e.u. at 298°K. for this species. The latter value was obtained by applying Badger's rule, which gave an interatomic distance of 2.55 Å., and by using the spectroscopic data given by Herzberg.[12] Table IV records the free energy functions and the heat of sublimation at 298°K. The average value of the latter computed by the third law method is $\Delta H_{298}^0 = 53.13 \pm 1$ kcal./mole. The heat of sublimation at 298°K., calculated by the second law method, is 53.9 ± 1.2 kcal./mole, in excellent agreement with that calculated by the third law method.

TABLE IV

FREE ENERGY FUNCTIONS AND HEAT OF SUBLIMATION OF SnTe AT 298°K.

T, °K.	$-R \ln p$	$\left(\frac{F^0 - H_{298}^0}{T}\right)_{SnTe(g)}$	$\left(\frac{F^0 - H_{298}^0}{T}\right)_{SnTe(s)}$	ΔH_{298}^0, kcal./mole
792	29.61	66.02	28.56	53.12
820	27.43	66.21	28.84	53.13
844	25.77	66.37	29.07	53.23
867	24.16	66.53	29.30	53.22
874	23.34	66.58	29.36	52.93
885	23.29	66.65	29.47	53.52
888	22.58	66.67	29.50	53.06
894	22.29	66.71	29.56	53.14
918	20.86	66.87	29.80	53.18
933	19.58	66.96	29.95	52.80
			Av. =	53.13

(11) J. H. McAteer and H. Seltz, *J. Am. Chem. Soc.*, **58**, 2081 (1936).

(12) G. Herzberg, "Molecular Spectra and Molecular Structure I, Spectra of Diatomic Molecules," 2nd Edition, D. Van Nostrand, New York, N. Y., 1950.

Discussion

The validity of assuming negligible contribution of the partial pressures of the elements may be inferred from the results obtained by Porter[1] for PbTe. The SnSe and SnTe are expected to have higher stability toward dissociation into the elements than does PbTe. Since mass spectroscopic data are not available, the exact concentrations of all the species in the vapor phases are not known. However, the ratio of the partial pressures of SnTe(g) to Sn(g) may be readily estimated from the thermodynamic properties of SnTe and the elements. We consider the equilibria

$$\mathrm{SnTe(s)} = \mathrm{SnTe(g)} \qquad (4)$$

The standard heat of formation of SnTe is −14.65 kcal./mole.[11] We use the enthalpy and entropy functions of PbS(s)[9] for that of SnTe(s), the thermodynamic functions for Sn(g) and Te(g) given by Stull and Sinke,[13] and the thermodynamic functions given by Kelley for SnTe(g). The heat of sublimation of SnTe is taken as 53.1 kcal./mole at 298°K., a reasonable value by comparison with those of GeTe[6] and PbTe.[14] Then at 900°K. for the system under equilibrium the ratio p_{SnTe}/p_{Sn} is approximately 10^5, showing negligible partial pressure of the elements in the measured temperature range. Similar calculation for SnSe is expected also to show negligible elemental partial pressures.

The dissociation energies of both SnSe and SnTe have been estimated by Gaydon to be 69 kcal./mole, and that of SnS as 69.5 kcal./mole. However, it is indicated that the spectroscopic data show considerable uncertainty. More recently[15] the dissociation energy of SnS has been calculated to be 111 kcal./mole. We herewith calculate the heat of dissociation of SnTe(g) and SnSe(g) from the heats of sublimation determined for the compounds, the heats of sublimation of the elements,[13] and the heats of formation of SnTe(s)[11] and SnSe(s).[16] The thermochemical cycles are

$\mathrm{SnTe(g)} = \mathrm{SnTe(s)}$	$\Delta H = -53.1 \pm 1$ kcal./mole	(5)
$\mathrm{SnTe(s)} = \mathrm{Sn(s)} + \mathrm{Te(s)}$	$\Delta H = 14.6 \pm 0.3$	(6)
$\mathrm{Sn(s)} = \mathrm{Sn(g)}$	$\Delta H = 72.0 \pm 2$	(7)
$\mathrm{Te(s)} = \mathrm{Te(g)}$	$\Delta H = 46.5$	(8)
$\mathrm{SnTe(g)} = \mathrm{Sn(g)} + \mathrm{Te(g)}$	$\Delta H = 80.0 \pm 2$ kcal./mole	(9)
$\mathrm{SnSe(g)} = \mathrm{SnSe(s)}$	$\Delta H = -52.4 \pm 1$ kcal./mole	(10)
$\mathrm{SnSe(s)} = \mathrm{Sn(s)} + \mathrm{Se(s)}$	$\Delta H = 16.5 \pm 2$	(11)
$\mathrm{Sn(s)} = \mathrm{Sn(g)}$	$\Delta H = 72.0 \pm 2$	(12)
$\mathrm{Se(s)} = \mathrm{Se(g)}$	$\Delta H = 49.4$	(13)
$\mathrm{SnSe(g)} = \mathrm{Sn(g)} + \mathrm{Se(g)}$	$\Delta H = 85.5 \pm 2$ kcal./mole	(14)

(13) D. R. Stull and G. C. Sinke, "Thermodynamic Properties of the Elements," Advances in Chemistry Series, No. 18, 1956.

(14) A. S. Pashinkin and A. V. Novoselova, *Russ. J. Inorg. Chem.*, **4**, 1229 (1959). English translation by the Chemical Society, London.

(15) R. Colin and J. Drowart, Technical Documentary Report No. WADD 60-782, Part VII, Wright-Patterson Air Force Base, April, 1962.

(16) O. Kubaschewski and E. L. Evans, "Metallurgical Thermochemistry," 2nd Ed., Pergamon Press Ltd., London, 1955.

The dissociation energies calculated for SnSe and SnTe are significantly higher than the 69 kcal./mole estimated by Gaydon. The present values, however, are more consistent with the dissociation energies of the other IVB–VIB binary compounds. Thus, there is a decreasing dissociation energy in the order 127, 111, 86, and 80 kcal./mole, respectively, for SnO, SnS, SnSe, and SnTe. The similar series of dissociation energies for the germanium compounds[2] is 150, 130, 115, and 94 kcal./mole, respectively; while that for the lead compounds[1] is 99.1, 76.1, 61.5, and 51.4 kcal./mole, respectively.

DECOMPOSITION OF CRYSTALLINE NITRATES BY LIGHT IONS AT KILOVOLT ENERGIES[1]

By S. R. Logan and Walter J. Moore

Chemical Laboratory, Indiana University,[2] Bloomington, Indiana

Received October 24, 1962

Electromagnetically analyzed ionic beams of about 10 microamp. cm.$^{-2}$ from a radiofrequency source were allowed to impinge on targets of polycrystalline alkali metal nitrates. The ions used were D^+, He^+, and D_3^+, at energies from 2 to 16 kev. At these energies the incident particles and primary knock-ons give reactions typical of "hot atoms" rather than those associated with extensive electronic excitation. The reaction $NO_3 \rightarrow NO_2^- + {}^1/_2O_2$ proceeded cleanly and was followed by spectrophotometric analyses of the bombarded targets. At constant energy and beam intensity, the yield with respect to dose was approximately first order in undecomposed nitrate. A typical initial $G(NO_2^-)$ value was 1.54 for 10 kev. He^+ ions on KNO_3. Relative to K = 1.00, the yields were Li = 0.26, Na = 0.61, Rb = 0.58, Cs = 0.67. The yield from KNO_3 decreased with rise in T from 100 to 273°K. and then rose from 273 to 420°K. The initial yields were analyzed by a Monte Carlo computation in terms of a model based on hard sphere collisions of the fast incoming ion with atoms in the nitrate, and similar collisions of knock-out oxygen atoms in spurs along the track of the incoming particle. This model provided fairly good agreement with experiments on energy dependence of initial yield. An explanation of relative yields of the different nitrates would require an extension of the model to include structure specific energy losses to vibrational modes of the crystals.

Most fast particles obtained from nuclear reactors or from accelerators have energies far in excess of those required to displace atoms or to break chemical bonds by direct collisions. They lose most of their energy by processes resulting in electronic excitation and ionization, and much attention has been devoted to the chemical effects of such processes. Bombardment with slower particles has been used mainly for the study of physical processes such as the sputtering of metals.[3] We therefore know little about the chemical effects in solids caused by ionic and atomic beams in the energy range from 1 to 100 kev., in which energy is lost by nuclear collisions. These collisions are of the Rutherford, shielded-Coulomb, or hard-sphere type, depending on the nuclear charges and the speeds of the particles involved. As an introductory investigation of this field, the present work is concerned with the decomposition of the crystalline nitrates of Li, Na, K, Rb, and Cs, under bombardment with light ions such as D^+, D_3^+, and He^+ at kilovolt energies.

The decomposition of a given alkali metal nitrate induced by radiation yields comparable amounts of nitrite per 100 e.v. of energy [$G(NO_2^-)$] with ultraviolet light,[4] X-rays,[5] γ-rays,[6] or electrons,[7] but fission fragments, which have a much higher L.E.T., produce considerably higher yields.[8]

With KNO_3, G-values lie in the range 1.4 to 2.0 for the initial reaction with a sharp decrease at about 1.5% decomposition which appears to be related to distortions of the crystal structure by the oxygen formed in the reaction. There is paramagnetic evidence[9] that oxygen is trapped within the crystals as O_2 molecules, which can escape at a phase transition or on melting or dissolving. Radiation effects in lead nitrate can be annealed out by prolonged heating.[10]

The correlation between the "free space" within the unit cell and the G-values for radiolytic decomposition of the nitrates of the alkali metals[5,6b,9] or of the alkaline earths[5,11] illustrates the restrictive effect of the crystal structure. The decomposition of potassium nitrate by fission fragments,[8] with a G-value now estimated at 6.0, suggested the occurrence of a molten "thermal spike" due to the high L.E.T., about 730 e.v./Å. compared to about 0.06 e.v./Å. for the ^{60}Co γ-rays. Thermal effects in the tracks were also discussed by Hochanadel[12] with regard to his results using Po^{210} α-particles of L.E.T. $\sim$ 34 e.v./Å. Although the KNO_3 again gave the largest yield of nitrite, the increase in its G-value over that obtained by γ-radiolysis was much less than was observed in the case of $NaNO_3$ or $LiNO_3$.

In most of these studies only a few per cent of the nitrate was decomposed, but Cunningham and Heal[5] followed the X-radiolysis to about 30% reaction and showed that the results were in fair agreement with a first-order decomposition. A study of the thermal decomposition of sodium nitrate[13] indicated that this

(1) Presented at 141st National Meeting, American Chemical Society, Washington, D. C., March 21, 1962.

(2) Work assisted by U. S. Atomic Energy Commission and American Chemical Society (Petroleum Research Fund).

(3) The Proceedings of the "Colloque International sur le Bombardement Ionique," C.N.R.S., Bellevue, France, December, 1961, provide a contemporary survey of this field.

(4) P. Doigan and T. W. Davis, *J. Phys. Chem.*, **56**, 764 (1952).

(5) J. Cunningham and H. G. Heal, *Trans. Faraday Soc.*, **54**, 1355 (1958).

(6) (a) C. J. Hochanadel and T. W. Davis, *J. Chem. Phys.*, **27**, 333 (1957); (b) J. Cunningham, *J. Phys. Chem.*, **65**, 628 (1961); (c) J. Forten and E. R. Johnson, *J. Phys. Chem. Solids*, **15**, 218 (1960); E. R. Johnson and J. Forten, *Discussions Faraday Soc.*, **31**, 238 (1961).

(7) E. R. Johnson, *J. Phys. Chem.*, **66**, 755 (1962).

(8) D. Hall and G. N. Walton, *J. Inorg. Nucl. Chem.*, **6**, 288 (1958); **10**, 215 (1959).

(9) G. Hennig, R. Lees, and M. S. Matheson, *J. Chem. Phys.*, **21**, 664 (1953).

(10) A. G. Maddock and S. R. Mohanty, *Discussions Faraday Soc.*, **31**, 193 (1961).

(11) A. S. Baberkin, *Russ. J. Phys. Chem.*, **35**, 179 (1961).

(12) C. J. Hochanadel, *Radiation Res.*, **16**, 286 (1962).

reaction follows first-order reversible kinetics with respect to sodium nitrate and sodium nitrite, the reverse reaction being also first order with respect to oxygen pressure. Thus it might be expected that the radiolytic decomposition would not go to completion, especially since the formation of nitrate ions was detected on irradiation of nitrite ions in a potassium bromide matrix.[14]

Basic Collision Theory

The general theory of the collisions of atomic particles in solids was discussed by Bohr[15] and important applications to experimental encounters in the range of kilovolt energies were made by Kinchin and Pease,[16] and by Nielsen.[17]

As the energy is lowered, the effect of the electrons in screening the nuclear charges becomes more pronounced. This screening is usually taken into account by replacing the Coulombic potential (Rutherford scattering potential) by the screened Coulombic potential

$$V = \frac{Z_1 Z_2 e^2}{R} \exp(-R/a) \qquad (1)$$

The subscripts 1 and 2 refer to incoming and target particles, respectively. The screening constant is given from the theory of Thomas and Fermi as

$$a = a_0/(Z_1^{2/3} + Z_2^{2/3})^{1/2} \qquad (2)$$

where $a_0 = 5.29 \times 10^{-9}$ cm., the Bohr radius. The minimum distance of approach of two particles in a head-on collision with the Coulomb field is

$$b = \frac{Z_1 Z_2 e^2}{E_1}\left(\frac{M_1 + M_2}{M_2}\right) \qquad (3)$$

where E_1 is the kinetic energy of the incoming ion and M denotes mass. Only when $b/a << 1$ will it be possible to neglect screening. As an example, for a He^+ ion at 10 kev. incident on a stationary K^+ ion, $a = 1.79 \times 10^{-9}$ cm. and $b = 6.02 \times 10^{-10}$ cm., $b/a = 0.336$, and screening will clearly be appreciable. The qualitative effect of the screen is to reduce the importance of collisions at low angles θ [Rutherford cross section being $\sigma(\theta) = (b^2/16) \csc^4(\theta/2)$]. Lane and Everhart[18] have computed the cross sections for classical scattering by the screened Coulomb potential.

When the kinetic energy of the incoming ion falls below the interaction potential of the two nuclei separated by a distance equal to the radius of the screening electron cloud, the screen produces hard-sphere collisions. The upper energy limit for this approximation is given by Kinchin and Pease as

$$L_A = 2E_R Z_1 Z_2 (Z_1^{2/3} + Z_2^{2/3})^{1/2} \frac{M_1 + M_2}{M_2} \qquad (4)$$

where E_R is the Rydberg energy (13.60 e.v.). For He^+ on K, $L_A = 1260$ e.v. It would appear that screened-Coulomb cross sections would be most suitable for use in the systems under consideration, but hard-sphere cross sections should be a good approximation, provided they are made energy dependent. We thus take $\sigma = \pi R^2$ with R the solution of

$$E_1 = \frac{Z_1 Z_2 e^2}{R} \exp(-R/a) \qquad (5)$$

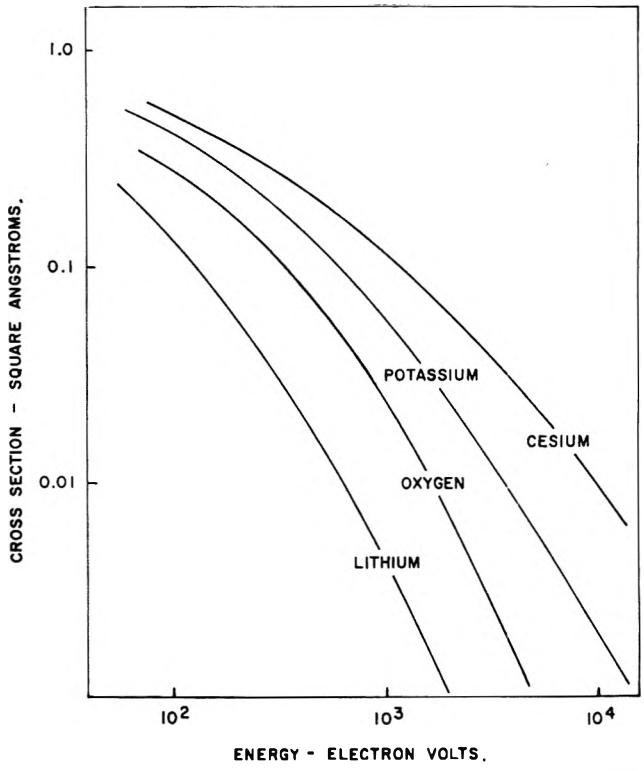

Fig. 1.—Collision cross sections for D^+ with several atoms according to the hard-sphere model.

Some of these computed cross sections are shown in Fig. 1.

In the range of energy below 10 kev., the incoming ion can readily capture an electron. The critical energy for electron capture is approximately that for which the velocity of the incoming ion $v < 1/2\ v_0$, where v_0 is the velocity of an electron in the hydrogen atom, $2\pi^2/h = 2.2 \times 10^8$ cm. sec.$^{-1}$. For a 10 kev. He^+ ion, $v = 9.6 \times 10^7$ cm. sec.$^{-1}$. Thus, during most of its encounters, the incoming ion will be neutralized and its behavior will be that of an extremely hot atom.

The question of energy loss due to collisions with electrons in the target material is difficult to treat quantitatively. According to Seitz,[19] the minimum energy for electronic excitation in an insulator is

$$L_c = (M_1/8m)I_t \qquad (6)$$

where I_t is the edge of the first main optical band and m is the electronic mass. (There is evidence, however, for some electronic excitation even at lower energies). For the alkali nitrates, $I_t = 4$ e.v., so that for a He^+ ion, $L_c = 4000$ e.v. Thus some energy loss by electronic excitation may be expected in these experiments, especially during the initial collisions of the faster ions. This conclusion seems to be verified by the secondary electron emission observed from the bombarded targets. Nevertheless, we can expect nuclear collisions to provide the dominant mode of energy loss over most of the track of the primary incident particle, and almost the exclusive mode for secondary displaced atoms.

(13) E. S. Freeman, *J. Phys. Chem.*, **60**, 1487 (1956).
(14) A. R. Jones and R. L. Durfee, *Radiation Res.*, **15**, 546 (1961).
(15) N. Bohr, "The Penetration of Atomic Particles Through Matter," Copenhagen, Munksgaard, 1953.
(16) G. H. Kinchin and R. S. Pease, *Rept. Progr. Phys.*, 18 (1955).
(17) K. O. Nielsen, in "Electromagnetically Enriched Isotopes and Mass Spectrometry," Butterworth, London, 1956.
(18) G. H. Lane and E. Everhart, *Phys. Rev.*, **117**, 920 (1960).
(19) F. Seitz, *Discussions Faraday Soc.*, **5**, 271 (1949).

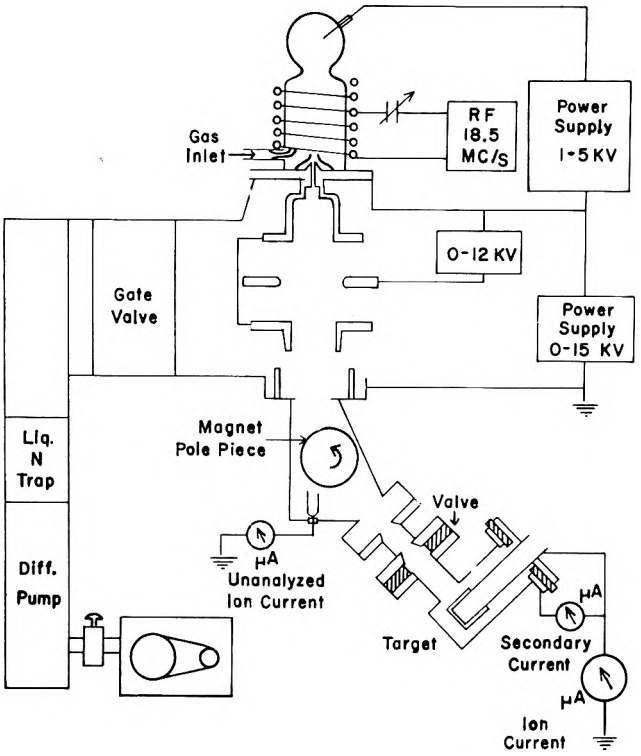

Fig. 2.—Experimental apparatus for bombardment of solid targets with ionic beams.

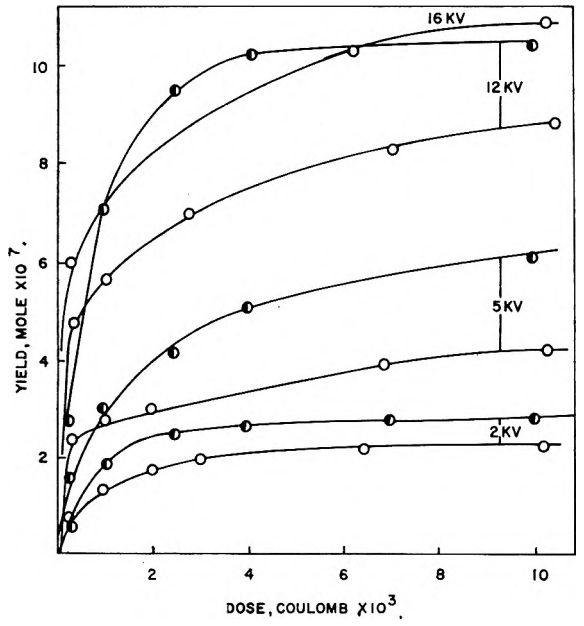

Fig. 3.—Total yield as a function of total dose for D^+ ions [◐] and He^+ ions [○] on KNO_3.

Experimental Procedures

A diagram of the apparatus is shown in Fig. 2. The ion source was a radiofrequency type[20] operating from a 18.5 Mc. oscillator by inductive coupling through a spiral of copper tubing. The glass section was cooled by air jets from holes in the inside of this spiral. Hydrogen or deuterium was admitted to the source through a palladium thimble, and helium, through an Alpert valve. The source was operated at a pressure of 20 to 30 μ. A potential of 1 kv. across the source tube extracted a beam of ions from the discharge. The ions were further accelerated to the desired energy, focused by an electrostatic einzel lens, and analyzed electromagnetically before they impinged on the target.

The pressure around the target was about 5×10^{-5} torr during a run. The vacuum system was constructed of brass with Teflon or rubber o-rings. The 15-cm. oil diffusion pump was equipped with a baffle cooled by liquid nitrogen. The system could be pumped to 10^{-7} torr.

In the first experiments, the beam was defined by two rings of 2.5 cm. diameter, with the second about 7.5 cm. from the surface of the target. In later experiments, the beam diameter was reduced to 1.25 cm. in order to make the intensity profile more uniform, and the usable beam current was then from 5 to 20 μa. depending on the ion used.

The samples to be bombarded were in the form of microcrystalline coatings of the salts, spread over a polished stainless-steel block, which could be internally heated or cooled. Teflon gaskets insulated the target block and the adjacent tube containing the defining diaframs from the surrounding case, so that it was possible to measure both the ion current to the target and the secondary current from the target to the case. About 100 mg. of nitrate was spread from a saturated solution onto the warmed metal block, electrolytically cleaned[21] just before use. In the case of lithium nitrate, which crystallizes as a hydrate below about 60°, the block was preheated close to 100° and inserted into the vacuum system immediately after coating. Two opposite sides of the block were coated together and bombarded successively, except for runs at elevated temperatures, where an unbombarded side was retained as a control on thermal decomposition. Under the microscope, the extent of coverage of the target surface was estimated as 98 ± 2% for KNO_3 and 95 ± 5% for the other nitrates. The total amount of nitrate deposited, about 100 mg. over about 5 cm.^{2}, would produce an average thickness several orders of magnitude greater than the maximum penetration depth of the fastest ions employed.

After bombardment, the target was dissolved in water and analysis for nitrite was made by the spectrophotometric method of Shinn.[22]

Experimental Results

Effects of Dose and Dose Rate.—The relation between yield of nitrite and dose is shown in Fig. 3 for the bombardment of KNO_3 by D^+ ions and by He^+ ions. The rapid initial decomposition caused by ions incident on pure nitrate is followed by a decline in rate, leading to a plateau as maximum yield is attained. There is good agreement between the experimental points and a theoretical expression for the yield y after a bombarding dose x given by

$$y = y_s(1 - e^{-bx}) \qquad (7)$$

where y_s represents the "saturation yield" for a selected value of the "rate constant" b in suitable units. This is the relation expected if a reaction first order with respect to dose is occurring in the layer of nitrate which is undergoing the ion bombardment. The saturation yield is temperature dependent and probably represents a steady state between decomposition of NO_3^- and its re-formation from NO_2^-. The extent of conversion in the layer of nitrate penetrated by the ions, however, is high. For example, the limiting yield with 10 kev. D^+ ions on KNO_3 with a target diameter of 1.25 cm. was 6×10^{-7} mole. This would be equivalent to the total conversion of all the KNO_3 in a layer 2340 Å. deep.

The results in Fig. 3 were obtained using the beams of smaller diameter, 1.25 cm. The yield–dose curves for the 2.5 cm.-diameter beam departed considerably from eq. 7. Such a difference might be expected since the beam is more intense in the central region than near its periphery. An extension of the model to include regions of differing initial rate proportional to beam intensity gave results in fair agreement with experiments for the broader beams, but this approach was not pursued in detail, since experimental improvement

(20) H. P. Eubank, R. A. Peck, and R. Truell, *Rev. Sci. Instr.*, **25**, 989 (1954).

(21) R. E. Kirk and D. F. Othmer, *Encyclopedia Chem. Tech.*, **5**, 619 (1950).

(22) M. B. Shinn, *Ind. Eng. Chem., Anal. Ed.*, **13**, 33 (1941).

of the beam uniformity gave good agreement with eq. 7.

It would appear that the only significant reaction is

$$NO_3^- \longrightarrow NO_2^- + {}^1/_2O_2 \qquad (8)$$

In the initial stages of reaction, further decomposition of nitrite and re-formation of nitrate are probably both negligible. If further disruption of nitrite occurred, the product might be NO^- or an oxide of the metal. In either case we might expect OH^- to be formed when water was added. A sample of KNO_3 was bombarded with a dose of 155 mcoulombs of 10 kev. D^+ ions and dissolved in 50 ml. of deionized water. The pH was compared to that from an unbombarded blank. The pH of the final solution was 7.00, compared to 5.90 for the blank and 5.85 for the water. The corresponding yield of OH^- would be 0.6×10^{-7} mole. The saturation yield of NO_2^- under these conditions would be 30×10^{-7} mole. The yield of OH^- was thus found to be only about 2% that of NO_2^-, although this dosage was about ten times that required to produce the maximum yield of NO_2^-. This experiment confirms the resistance of NO_2^- to further decomposition and indicates that a limiting yield of NO_2^- may be caused by the reversibility of the reaction, $NO_3^- \leftrightarrows NO_2^- + {}^1/_2O_2$.

Figure 4 shows some data obtained with 5 kev. D^+ ions on KNO_3 with two different beam apertures. The results at first suggested a true effect of dose rate on the yield. Closer analysis, however, indicated that most of the effect was due to space-charge spreading of the ion beam, so that its effective area increased with the ion current. It can indeed be shown, if we assume the beam cross section to be gaussian, that the variations in diameter of the intense central portion of the beam required to explain the apparent dose-rate effect in Fig. 4 agree closely with those predicted from the nomographic chart of beam spread given by Thonemann.[23] A simple calculation shows that true dose-rate effects are probably not to be expected at the current densities used. At the highest current density, the number of ions striking on a target area 10×10 Å. is about 1.2 per second, whereas Seitz[24] estimates the duration of a thermal spike as 10^{-11} sec.

Effect of Ion Energy.—The two parameters of the yield-dose curve, y_s and b, can be found quite simply from the initial yield and the saturation yield. We examined these two parts of the curve in detail for the bombardment of KNO_3 by several ions at different energies. The initial yields are shown in Fig. 5 for D^+ and He^+. Since a complete yield *vs.* dose curve was not always available, the yield for 0.25 millicoulomb has been taken as the value for "initial yield." The initial slopes give somewhat higher values. For example, for 2 kev. D^+ ions on the various nitrates the ratio of these two "initial yields" was 1.30 ± 0.06 (see Table II).

The yield *vs.* energy curves do not pass through the origin, but have a positive intercept at zero energy. The intercept corresponds to 12 molecules of NO_2^-/ion for He^+, 8 molecules of NO_2^-/ion for D^+ on KNO_3, for initial yields. This result might suggest that finite amounts of decomposition are effected by ions of thermal energy. Such a possibility cannot be ruled out on energetic grounds: for example, ΔH for $KNO_3 \rightarrow KNO_2 + {}^1/_2O_2$ is only about 1.3 e.v., whereas the first ionization potential of He is 24.6 e.v. In the case of H^+, we also have the possibility of chemical reduction of nitrate by the H atom. Theoretical calculations indicate, however, that the curves depart appreciably from

(23) P. C. Thonemann, *Progr. in Nuclear Phys.*, **3**, 219 (1955).
(24) F. Seitz and J. S. Koehler, *Solid State Phys.*, **2**, 305 (1956).

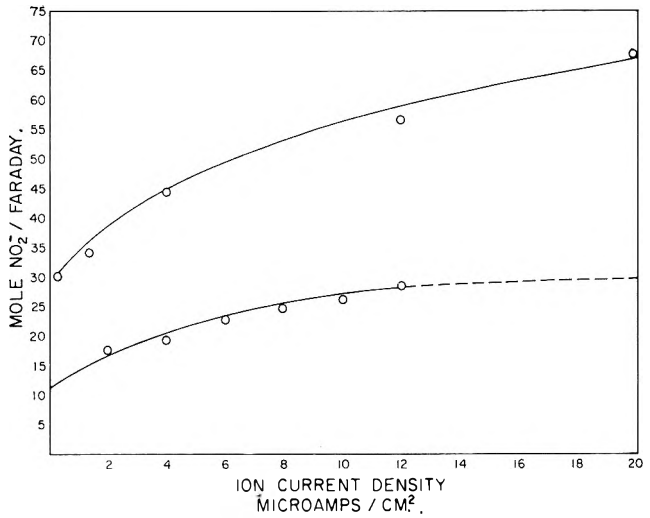

Fig. 4.—Yield per faraday as a function of ion current density with 5 kev. D^+ ions on KNO_3. Upper curve, 5.0 cm. diameter target; lower curve, 2.5 cm. Dose, 0.9 mcoulomb.

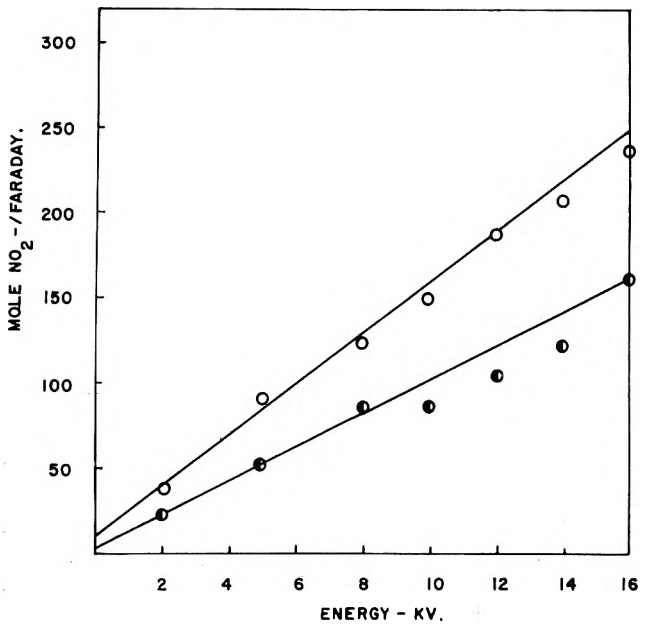

Fig. 5.—Initial yield per faraday as a function of ion energy for D^+ ions [◐] and He^+ ions [○] on KNO_3.

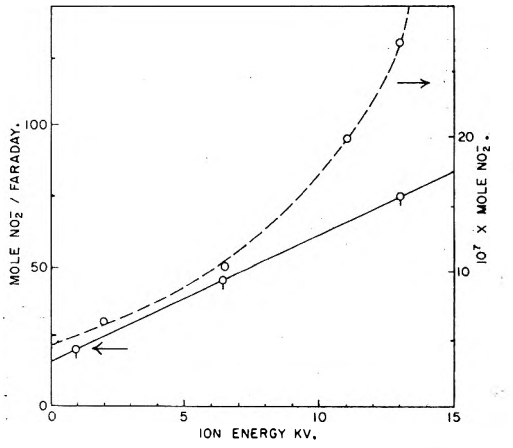

Fig. 6.—Initial yields (left) and saturation yields (right) for D_3^+ ions on KNO_3.

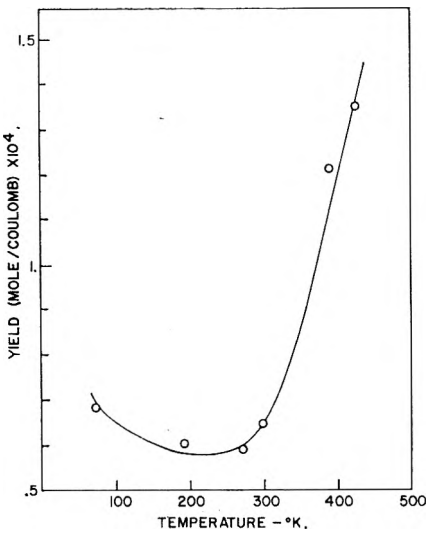

Fig. 7.—Variation with temperature of the yield with 2 kev. D^+ on KNO_3; dose 2.9 mcoulombs/cm.[2]

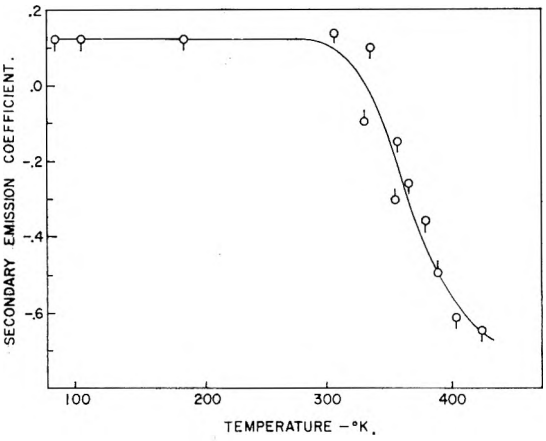

Fig. 8.—Variation with temperature of the secondary emission coefficient for 2 kev. D^+ ions on KNO_3.

linearity in the region < 1000 volts, so that the apparent intercept may be simply an indication of this fact.

Figure 6 shows both the initial yields and the saturation yields for bombardments with the ion D_3^+. Note that, unlike the atomic ions, the D_3^+ gave a non-linear curve for initial yield. Although the saturation yields with D^+ and He^+ are not shown, they also gave linear graphs. At these energies, we can expect the D_3^+ unit to disintegrate on the first hard collision, so that the special behavior of this ion may be related to the overlap between the tracks of the three D atoms generated from one D_3^+ ion. If disintegration produced three D atoms of equal energy, we might expect that the slope of the curve for saturation yield *vs.* dose for D_3^+ would be $^1/_3$ that for D^+ under identical conditions. The experimental value is $^1/_{2.5}$. We may note that the experimental ranges of H^+ and H_2^+ ions in aluminum[25] also suggested that fragments of unequal energy were formed in the first hard collision of the molecular ion.

Effects of Varying Target Cation.—Measurements were also made with targets of nitrates of Li, Na, Rb, Cs, with D^+ and He^+ ions. The yield from MNO_3 can be represented by a constant, f, times the yield from KNO_3 under the same conditions. Mean values of f for initial yields are given in Table I. Also included in the table are values of $\theta = V(MNO_3)/V(KNO_3)$, the ratios of the volumes per nitrate unit in the crystals.

(25) J. R. Young, *J. Appl. Phys.*, **27**, 1 (1956).

This figure gives an inverse measure of the density of target NO_3^- groups presented to the incoming beam. It is also related to the "free volume" in the crystal, which has been suggested as a factor measuring the ease of removal of an oxygen atom from a nitrate group.[8]

TABLE I

COMPARISON OF INITIAL YIELDS OF NITRITE FROM DIFFERENT ALKALI NITRATES

	D^+ (2 kev.)	He^+ (10 kev.)	θ
$LiNO_3$	0.30	0.26	0.599
$NaNO_3$	0.88	0.61	0.784
KNO_3	1.00	1.00	1.000
$RbNO_3$	0.80	0.58	0.981
$CsNO_3$	0.68	0.67	1.060

Based on a limited number of comparisons, it appeared that the values of f were approximately constant with dose. Thus under bombardment by a uniform beam, the yield–dose relation is given approximately by

$$y = y_s f(1 - e^{-bx})$$

The G-values for the different nitrates are in the same proportions as the f values in Table I. For the 2 kev. D^+ ions on KNO_3 the initial-yield [0.25 mc.] value is $G = 1.50$; for the 10 kev. He^+, $G = 1.54$.

The initial G-values[26] obtained with 2 kev. D^+ ions are shown in Table II along with those for several other types of radiation. It may be noted that for $LiNO_3$ and $NaNO_3$ the yields from D^+ ions and α-particles are much greater than those from X-rays or γ-rays.

TABLE II

COMPARISON OF $G(NO_2^-)$ OBTAINED BY VARIOUS TYPES OF IRRADIATION

	2 kev. D^+ ions	3.4 Mev. α-particles	1.5 Mev. electrons	45 kvp. X-rays	Co^{60} γ-rays	V_f, Å.[3]
$LiNO_3$	0.50 (0.60)	0.7	..	0.02	0.02*	17.1
$NaNO_3$	1.32 (1.80)	1.3	0.22	0.37	0.20	29.4
KNO_3	1.50 (2.00)	2.2	1.48	1.96	1.46	40.5
$RbNO_3$	1.20 (1.50)	..	..	0.64	0.60	35.2
$CsNO_3$	1.02 (1.40)	1.4	1.53	1.37	1.72	35.3
Ref.	(this work)	14	7	3	*4, 5	

Effect of Temperature.—The effect on initial yield of varying the temperature of the KNO_3 target is shown in Fig. 7. At low doses, the yield of nitrite passes through a distinct minimum at about room temperature. In separate experiments it was found that the effect persisted at high dosages (saturation yields) but the low temperature enhancement was decreased whereas the high-temperature enhancement was increased.

The secondary electrical emission from a target of KNO_3 bombarded with 1.9 kev. D^+ ions at about 8.5 μa. cm.$^{-2}$ was also measured over a range of temperatures, as shown in Fig. 8. At or below room temperature, the emission is positive, as might result from reflection of positive ions from the surface. Above 60° it becomes negative; this result suggests that emission of secondary electrons is favored by increasing temperature. With the target at room temperature, application of a negative potential of up to 100 v. to the surrounding case caused little increase in the current of

(26) The values in parentheses are the initial slopes of the complete yield–dose curves which were available in this case.

positive secondaries; on the other hand, a positive potential of 20 v. caused the secondary emission to change in sign, and to become increasingly more negative up to 100 v. We interpret this effect as a repression of ion reflection and an enhanced extraction of secondary electrons.

The increase in yield at higher temperatures can be related to the increased vibrational energy in the NO_3^- group. Since thermal decomposition sets in above 180° (case of KNO_3), we should expect such an increase in radiolysis with temperature. Also, the secondary electrons (δ-rays) will be projected in all directions and can produce reactions in regions of the target not accessible to the heavy primary ions and secondary hot atoms.

The increased yield at low temperature is difficult to explain without including a reverse reaction, which requires an activation energy itself (perhaps through a diffusive step). This explanation does not accord with the fact that the low temperature enhancement is greatest at lowest dosages. Thus, further study of the phenomenon will be required before we can adduce a satisfactory interpretation. Cunningham[5] has given a detailed discussion of diffusion models for the temperature effects, including effects of isotopic substitution.

Discussion of Mechanisms

Application of Collision Theory.—Although the entire yield *vs.* dose curve can only be understood on the basis of gradual depletion of the reactant layer by competing reactions of nitrate decomposition and reformation, the initial slopes may be analyzed on the basis of a much simplified model. We consider each bombarding ion to act independently of any other as it traverses a section of target. We assume that the ion is confronted with two cross sections, σ_1 characteristic of the metal atom, and σ_2 characteristic of the NO_3^- group. The latter is taken simply to be the sum $\sigma_N + 3\sigma_O$, where σ_N and σ_O are the nitrogen and oxygen cross sections. The reaction is formulated as a Monte Carlo process. The incoming ion strikes either a metal ion or a nitrate group, with probabilities determined by the fraction of cross sections, $\sigma_1/(\sigma_1 + \sigma_2)$. A parameter D, the displacement energy, determines whether the collision with NO_3^- breaks a bond and produces a rapidly moving oxygen atom. If an oxygen atom is produced, we follow its subsequent career until its energy has become less than D. For the encounters of the hot oxygen atom we also use cross sections calculated from eq. 5. In this model we have not considered secondary reactions produced by rapidly moving displaced alkali metal ions. This limitation is equivalent to the assumption that energy transmitted to the positive ions is all dissipated as heat. This assumption would be impossible to justify, but it seems reasonable that the positive charge of the metal ion will facilitate transfer of energy into vibrational modes of the crystal. The assumption therefore represents a consistent, but not physically valid, model to provide energy transfer to the lattice vibrations.

Hsiung and Gordus[27] have given a detailed classical calculation for the minimum net recoil energy required to effect bond rupture following a collision with momentum transfer to a polyatomic molecule. We have applied this theory to the case of the planar NO_3^- ion assuming that the momentum is transferred to an O atom. If the dissociation energy of the N–O bond is taken as 3.7 e.v.,[6c] we calculate that 6.9 e.v. must be transferred to the NO_3^- ion to effect bond rupture. We have used in the calculation of displacement cross section the parameter $D = 10$ e.v., in order to compensate somewhat for the surrounding structure. The calculated yield is quite sensitive to changes in the parameter D, but we have neglected the effect of crystal structure and density on D.

All collisions are averaged over all angles and the energy transfer per collision is always taken to have its average value. The total cross section for producing a displacement is

$$\sigma_D = \int_{\theta_D}^{\pi} d\sigma(\theta)$$

Since

$$D = T_m \sin^2 (\theta_D/2)$$

and for a hard-sphere collision, $d\sigma = (\pi d_{12}^2/2)\, d\omega$, this becomes

$$\sigma_D = \pi d_{12}^2 \left(1 - \frac{D}{T_m}\right) \qquad (9)$$

where

$$T_m = 4M_1M_2E/(M_1 + M_2)^2 \equiv 2ME \qquad (10)$$

is the maximum energy transfer. The fact that the targets are microcrystalline helps to make angular averaging more reasonable. The crystal is thus treated as a gas. The approximations involved are similar to those in simple mean-free-path calculations[28] of sputtering, which have given surprisingly good agreement with experiment. These calculations were carried out on the I.B.M. 709 computer of the Indiana University Research Computing Center.

The energy dependences of the computed initial yields with KNO_3 are in fair agreement with the experimental results, as shown in Table III. We do not have data on all the nitrates at all energies. No attempt has been made to adjust the cross sections and the calculation contains no adjusted parameters. Consequently we believe the results provide some support for the underlying hard-sphere collision model.

TABLE III

RATIO OF G(EXPERIMENTAL) TO G(THEORETICAL) [INITIAL YIELDS]

	kev.			
	10	7	4	1
He^+ on KNO_3	1.06	1.06	0.98	1.17
D^+ on KNO_3	0.71	0.62	0.62	0.50

The calculated G-values for He^+ on KNO_3 appear to be correct, but for D^+ on KNO_3 the calculated yields appear consistently too high. We should recall, however, that the true initial rates are somewhat higher than the 0.25 mc. rates. At the higher energies we would expect more electronic excitation in the case of D^+ (*cf.* eq. 16), and this effect may be evident in the experimental yields.

The crude momentum transfer model is not successful in explaining the relative yields from the different alkali nitrates, in particular the low yields from $LiNO_3$.

(27) C. H. Hsiung and A. A. Gordus, *J. Chem. Phys.*, **36**, 947 (1962).

(28) R. S. Pease, *Rend. Scuola Intern. Fis.*, **13**, 158 (1960).

The calculated (D = 10 e.v.) and observed yields Y with 10 kev. He^+ ions relative to the KNO_3 yields are shown in Table IV.

TABLE IV

RELATIVE YIELDS WITH 10 KEV. He^+ IONS

	Nitrate				
	Li	Na	K	Rb	Cs
Y Calcd.	1.72	1.05	1.00	0.87	0.95
Y Obsd.	0.26	0.61	1.00	.58	0.67
$Y\theta$ Calcd.	1.03	0.82	1.00	.85	1.00

We have also included $Y\theta$ where θ is the volume ratio given in Table I. It has been suggested that the yields from the different nitrates may be associated with the "free volumes" of the nitrate groups in these crystals. The free volume V_f can be defined as the volume of the unit cell per nitrate unit minus the volume $(4/3)\pi a^3$ (where a is the Pauling ionic radius of the cation) minus 30 Å.^{3} as a conventional "volume" of the NO_3^- group. These values of V_f were included in Table II, which gave the relative yields of the various nitrates with different kinds of radiation. It has been suggested that the lower the "free volume" the higher would be the activation energy required to remove an oxygen from a NO_3^- group, as the consequence of some kind of a "cage effect."

It is clear that the yields are correlated in some way with the volumes of the crystals and with the masses of the cations. We do not believe, however, that a cage effect of the type suggested can be entirely responsible. We have calculated from the collision theory the effect of changing the activation energy D from 10 to 20 e.v. The yield with 10 kev. He^+ ions on $LiNO_3$ is thereby lowered from G = 2.58 to G = 1.31. An unreasonable value of D (> 50 e.v.) would be required to explain the observed low yield of G = 0.40. Nevertheless the product $Y\theta$ may be considered to provide a rough correction of the computed yields for variation in D.

We may suggest that an important factor in lowering the yield with $LiNO_3$ is the greater ease of transferring energy into vibrational modes of the crystal structure as a whole (*cf.* ref. 12). The tightness of packing of the groups in $LiNO_3$ will raise the force constants and hence the vibration frequencies in $LiNO_3$. The low mass of the Li^+ ions will have a similar effect. Thus the density of vibrational states as well as their higher average energies will facilitate the dissipation of energy into the lattice vibrations. This model also helps to explain why the yield ratios, $G(KNO_3)/G(LiNO_3)$, for example, are so much higher for the X-rays than for the ionic beams. The X-radiation effects decomposition through a prior electronic excitation, and these electronic excited states (excitons) can readily undergo de-excitation through phonon processes that do not lead to breaking of the N-O bond.

Saturation Yield.—The collision-theory model can also provide a means of computing the range of the incident ion, and hence the depth of the reaction zone. Some of the incoming ions (following electron capture, atoms) must experience large-angle collisions and even a reversal of momentum, the phenomenon that causes sputtering. We can expect a forward-peaked gaussian distribution of effective ranges. We can apply neutron-age theory to calculate the slowing-down length $S^{1/2}$ of the incident particles, with

$$S = \frac{1}{3N^2q}\int_E^D \frac{d \ln E}{\sigma^2(E)} \qquad (11)$$

$$q = 1 + \frac{1 - M}{M} \ln (1 - M)$$

If we take a total cross section for the target and an average q factor we find the following results for D^+ on KNO_3:

E, kev.	2	5	10
$S^{1/2}$, Å.	1500	5200	17000
y_s, Å.	1120	2350	3860
$S^{1/2}/y_s$	1.34	2.21	4.40

This simplified treatment thus does not explain the energy dependence of the saturation yield. In this case also, there is probably some loss in energy by electronic excitation at $E > 4$ kev. Such losses would reduce the computed yields. Also, of course, the cross sections can only be approximate. In any case it is clear that we cannot explain the saturation yield simply as the conversion of almost all the nitrate to a depth equal to the computed slowing-down length.

The "Thermal Spike" Model.—As the primary recoil energy is spread over the spur of displaced atoms, there will be a region of local heating. Such regions were discussed by Seitz and Koehler,[8] who called them "thermal spikes." Hochanadel[12] found evidence for thermal spikes in nitrates in the dependence of initial yield on L.E.T. for various radiations. He compared yields with densely ionizing α-particles (L.E.T. $\sim$ 34 e.v./Å.) and cobalt γ-rays (L.E.T. $\sim$ 0.06 e.v./Å.). We may estimate the L.E.T. of our 10 kev. He^+ ions in KNO_3 as about 1.0 e.v./Å. The lower value is a consequence of the much reduced electronic excitation in this range of energy. The L.E.T. of the primary displaced atoms would be higher, however, about 10 e.v./Å. for a 1 kev. oxygen atom. It is not clear whether one is justified in treating a volume as small as the track of a displaced atom as a "thermal spike." In any case, there will be a region of excess energy in which reactions of the primary fragments may take place. In particular we cannot exclude the possibility that some re-formation of NO_3^- from NO_2^- occurs within such regions. Such diffusional recombination may therefore be a factor even in the initial rates. In such a case we should expect the rates as computed from the collision theory to be too high. Experiments on mixtures of $N^{16}O_3^-$ and $N^{18}O_3^-$ might resolve this question, but the analytical difficulties are considerable.

Acknowledgments.—We wish to thank Sylvester Brown for his patient and skillful assistance with part of the experimental work, and Ralph Christoffersen for his help and advice with the computer program.

HEATS OF FORMATION AND COÖRDINATE BOND ENERGIES OF SOME NICKEL(II) CHELATES

BY JAMES L. WOOD AND MARK M. JONES

Department of Chemistry, Vanderbilt University, Nashville 5, Tennessee

Received October 29, 1962

Heats of formation of eight inner complex salts of nickel(II) have been determined using measurements of their heats of combustion in an oxygen bomb calorimeter. Heats of vaporization of these complexes and their constituent ligands have been determined from static vapor pressure measurements with an isoteniscope. From these, coördinate bond energies for the Ni–O and Ni–N bonds have been determined by the use of a thermochemical cycle. These bond energies are not strictly constant, but show a definite dependence upon the coordination environment.

Earlier work in this Laboratory[1] showed how coördinate bond energies in inner complex salts could be obtained from heats of combustion and heats of vaporization of these materials. The present study extends these measurements to eight nickel(II) complexes, most of which contain nickel(II) in a square planar coördination environment. The complexes reported upon here contain only Ni–O or Ni–N coördinate bonds. Some work with sulfur-containing ligands was carried out but was found to be attended with special difficulties (*e.g.*, the corrosion of the calorimeter and poorlyd efined combustion products). Concentration of effort on complexes containing only two kinds of coördinate bonds has the advantage that a reasonable estimate of the constancy of the bond energy can be made. Every effort was also exerted to utilize the structural information on these complexes so that the bond energy calculations are in accord with such data as are available.

Experimental

A Parr adiabatic calorimeter was used to determine the heats of combustion. The general procedure and the calibrations were carried out as described previously.[1]

The bis-(acetylacetonato)-nickel(II) used in this work was obtained from the MacKenzie Chemical Works, Central Islip, Long Island, N. Y. It was recrystallized from chloroform prior to use. *Anal.* Calcd. for $Ni(C_5H_7O_2)_2$: Ni, 22.85. Found: Ni, 22.69.

Bis-(dimethylglyoximato)-nickel(II) was prepared by the scaling up of a standard procedure.[2] The product was dried in an oven at 105° for 2.5 hours prior to use. The complex was analyzed for its nickel content by first destroying it with boiling sulfuric acid, then evaporating the resulting solution to dryness. The residue was taken up with water, the solution was rendered ammoniacal and the nickel was then electrolytically deposited on a platinum cathode. This method was used for all the remaining complexes except the complex with 8-hydroxyquinoline, which was analyzed by ignition to NiO.

Calcd. for $NiC_8H_4O_4N_4$: Ni, 20.32. Found: Ni, 20.30.

Bis-(glyoximato)-nickel(II) was prepared by a direct precipitation. Reagent grade nickel chloride hexahydrate (40.8 g., 0.172 mole) was dissolved in water (100 ml.). A solution of glyoxime (32 g., 0.326 mole) in alcohol was slowly added to the nickel chloride solution. Powdered sodium bicarbonate was then added in small portions and the dark red complex precipitated as the solution became basic. The precipitate was filtered, washed with alcohol, and air dried; yield 36 g. (0.137 mole). Calcd. for $NiC_4H_6N_4O_4$: Ni, 25.22. Found: Ni, 25.10.

Bis-(salicylaldehydato)-nickel(II).—Reagent grade nickel chloride hexahydrate (23.7 g., 0.0997 mole) was dissolved in water, and redistilled salicylaldehyde (23.7 g., 0.194 mole) was added slowly and with constant stirring. Aqueous ammonia (30 ml. of 6 *M*) was then added and a greenish yellow precipitate was formed. After digesting the reaction mixture at 60° for one-half hour, the solution was filtered, the precipitate was washed with alcohol, and then dried in a vacuum oven at 110° for three hours; yield 24.7 g. (0.0821 mole). Calcd. for $NiC_{14}H_{10}O_4$: Ni, 19.51. Found: Ni, 19.69.

Bis-(salicylaldiminato)-nickel(II).—Redistilled reagent grade salicylaldehyde (23.7 g., 0.194 mole) was dissolved in alcohol (100 ml.). This solution was added to a solution of nickel chloride hexahydrate (23.7 g., 0.0997 mole) in water (100 ml.) to which concentrated aqueous ammonia (39.6 ml.) had been added. A reddish orange precipitate formed immediately and was collected on a filter, washed with alcohol and air-dried; yield 28.2 g. (0.0943 mole). Calcd. for $NiC_{14}H_{12}N_2O_2$: Ni, 19.64. Found: Ni, 19.30.

Bis-(8-quinolinato)-diaquonickel(II).—Nickel chloride hexahydrate (24.8 g., 0.104 mole) was dissolved in water (100 ml.) and concentrated aqueous ammonia solution (41.4 ml., 1.87 moles) was added. To this solution was added a solution of 8-quinolinol (30.3 g., 0.209 mole) in alcohol (100 ml.). The yellow precipitate which formed was collected on a filter, washed with alcohol, and dried in a vacuum oven at 110° for two hours. Calcd. for $NiC_{18}H_{16}N_2O_4$: Ni, 15.33, Found: Ni, 15.51.

Bis-(picolinato)-nickel(II).—A mixture of water (75 ml.) and aqueous ammonia (40 ml., 1.81 moles) was used to dissolve nickel chloride hexahydrate (32.9 g., 0.120 mole). Resublimed picolinic acid hydrochloride (44.4 g., 0.276 mole) dissolved in water (100 ml.) was added to this solution. The resulting blue solution was allowed to stir for one hour at 60° and was then filtered. Acetone (500 ml.) was added to the filtrate and a dark blue precipitate formed immediately. This precipitate was collected on a filter, washed with acetone, and then dried in a vacuum oven at 110° for eight hours. The final product was light blue; yield 29 g. (0.0957 mole). Calcd. for $NiC_{12}H_8N_2O_4$: Ni, 19.37. Found: Ni, 19.18.

TABLE I

ANALYSES OF SOLID COMBUSTION RESIDUES

Compound	% Ni found	Ni/NiO ratio
Bis-(acetylacetonato)-nickel(II)	77.62	All NiO
Bis-(dimethylglyoximato)-nickel(II)	Estimated[a]	All NiO
Bis-(glyoximato)-nickel(II)	Estimated[b]	All Ni
Bis-(salicylaldehydato)-nickel(II)	78.21	All NiO
Bis-(salicyliminato)-nickel(II)	96.99	6:1
Bis-(8-quinolinato)-diaquonickel(II)	82.38	1:5
Bis-(picolinato)-nickel(II)	99.12	All Ni
Bis-(glycinato)-nickel(II)	Estimated[b]	All Ni

[a] Estimated from the color and particle size of the residue. [b] Estimated from the solid Ni present.

Bis-(glycinato)-nickel(II).—A slurry of reagent grade nickel(II) carbonate (11.87 g., 0.10 mole) in water (100 ml.) was prepared. A slight excess of ammonia-free reagent grade glycine (15.76 g., 0.21 mole) was added slowly while the solution was stirred and heated to 60°. The slurry disappeared and a dark blue solution was obtained. The solution was first filtered to remove any insoluble impurities and then treated with acetone (500 ml.). A light blue precipitate formed immediately and was collected on a filter, washed with acetone, and then dried in a vacuum oven at 110° for eight hours. The result was a light green anhydrous salt. Both of these solids are extremely soluble in water; yield of anhydrous compound, 20.0 g. (0.0966 mole). Calcd. for $NiC_4H_8N_2O_2$: Ni, 28.50. Found: Ni, 28.25.

The values of the heats of combustion for these compounds are the averages of a minimum of four separate determinations. The reproducibility varied somewhat from compound to com-

(1) M. M. Jones, B. J. Yow, and W. R. May, *Inorg. Chem.*, **1**, 166 (1962).

(2) F. J. Welcher, "Organic Analytical Reagents," Vol. III, D. Van Nostrand Co., Inc., New York, N. Y., 1947, p. 176.

TABLE II

HEATS OF COMBUSTION

Compound	Formula wt.	ΔE combustion, cal./g.	ΔE combustion, kcal./mole	Δn, moles	ΔH combustion, kcal./mole
Bis-(acetylacetonato)-nickel(II)	256.93	−4133.2	−1061.9	−2	−1063.1
Bis-(dimethylglyoximato)-nickel(II)	288.94	−3973.4	−1148.1	0	−1148.1
Bix-(glyoximato)-nickel(II)	232.83	−2372.0	− 552.27	2.5	− 550.78
Bis-(salicylaldehydato)-nickel(II)	300.94	−5041.5	−1517.2	−1	−1517.8
Bis-(salicyliminato)-nickel(II)	298.98	−5332.0	−1594.2	−1.07	−1594.8
Bis-(8-quinolinato)-diaquonickel(II)	383.07	−5950.7	−2279.5	−1.9	−2280.6
Bis-(picolinato)-nickel(II)	302.92	−4086.4	−1237.9	1	−1237.3
Bis-(glycinato)-nickel(II)	206.83	−2018.9	− 417.57	1	− 413.97
8-Quinolinol	145.17	−7351.6	−1067.2	−1	−1067.8
Dimethylglyoxime	116.12	−5255.0	− 610.21	−1	− 610.81
Picolinic acid	107.12	−5297.4	− 567.46	−1	− 568.06

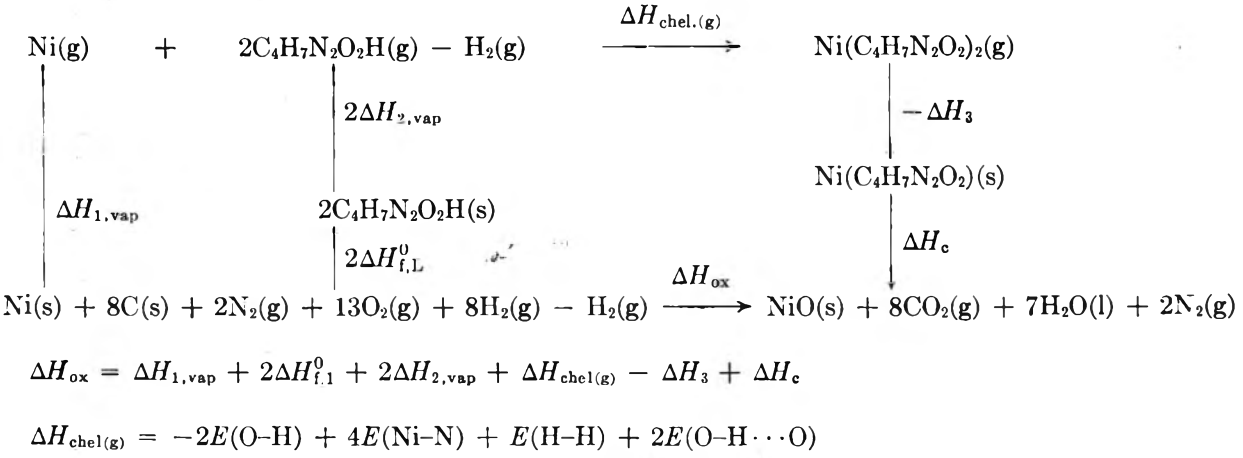

$$\Delta H_{ox} = \Delta H_{1,vap} + 2\Delta H^0_{f,1} + 2\Delta H_{2,vap} + \Delta H_{chel(g)} - \Delta H_3 + \Delta H_c$$

$$\Delta H_{chel(g)} = -2E(\text{O–H}) + 4E(\text{Ni–N}) + E(\text{H–H}) + 2E(\text{O–H}\cdots\text{O})$$

Fig. 1.—Thermochemical cycle for the empirical evaluation of coördinate bond energies in bis-(dimethylglyoximato)-nickel(II).

pound but was always within ±0.5%, with an average of ±0.33%. The Washburn corrections were omitted since they were smaller than the experimental uncertainty. The combustion products were taken as CO_2, N_2, H_2O, and either Ni or NiO. The solid residues from the combustion experiments were analyzed for their total nickel content by the standard gravimetric procedure.[2] The analyses are presented in Table I.

It was necessary to obtain the heats of combustion of three of the ligands in order to calculate their heats of formation. The picolinic acid and 8-hydroxyquinoline used were reagent grade materials. The dimethylglyoxime was prepared by the acidification of a solution of the reagent-grade sodium salt. Calcd. for $C_4H_8O_2N_2$: C, 41.37; H, 6.94. Found: C, 41.40; H, 6.76.

The vapor pressures of the nickel chelates and the parent ligands were determined over a range of temperatures by the isoteniscope method as modified by Burg and Truemper.[3] Each compound was made into a pellet using a pressure of 5000 p.s.i. From these pellets, small portions were taken and introduced into the isoteniscope. Due to the nature of these compounds, the reproducibility of the vapor pressure measurements was rather poor. As a result the heats of vaporization obtained are the best estimates that could be made. A calibration run with benzoic acid gave vapor pressures of 1.1 mm. at 94.8°, 1.9 mm. at 107.0°, and 2.7 mm. at 112.3°. The literature vaules for these temperatures are 0.94, 1.85, and 2.44 mm., respectiveiy.[4]

Results and Discussion

The measured heats of combustion for both the nickel complexes and the ligands are presented in Table II. The heats of sublimation are presented in Table III.

The bond energies were calculated using thermochemical cycles of the sort described earlier.[1] The cycle used for the nickel(II) complex with dimethylglyoxime is given in Fig. 1. The results of these calculations are summarized in Table IV.

(3) (a) E. W. Burg and J. W. Truemper, *J. Phys. Chem.*, **64**, 487 (1960); (b) J. W. Truemper, Ph.D. Thesis, Louisiana State University, Baton Rouge, 1959, MiC59-5529, University Microfilms, Ann Arbor, Michigan.

(4) "International Critical Tables," Vol. III, McGraw-Hill Book Co., New York, N. Y., 1928, p. 208.

TABLE III

HEATS OF SUBLIMATION (KCAL./MOLE)

Compound	ΔH_1 vap.	Compound	ΔH_1 vap.
Bis-(acetylacetonato)-nickel(II)	16.5[a]	Acetylacetone	11.5[a]
Bis-(dimethylglyoximato)-nickel(II)	7.7	Dimethylglyoxime	6.9
Bis-(glyoximato)-nickel(II)	13.4	Glyoxime	41.0
Bis-(salicylaldehydato)-nickel(II)	20.4	Salicylaldehyde	11.4[b]
Bis-(salicyliminato)-nickel(II)	37.8	Salicylimine	12.0[c]
Bis-(8-quinolinato)-diaquonickel(II)	16.8	8-Quinolinol	40.3[d]
Bis-(picolinato)-nickel(II)	18.3	Picolinic acid	21.0
Bis-(glycinato)-nickel(II)	8.1	Glycine	9.9

[a] J. W. Truemper, Thesis, Louisiana State University, Baton Rouge, 1959, mic. 59-5529, University Microfilm, Ann Arbor, Mich. [b] D. R. Stull, *Ind. Eng. Chem.*, **39**, 517 (1947). [c] Estimated on basis of value for salicylaldehyde. [d] Calculated from an estimated value of 30 kcal. for the heat of fusion. This value is close to that for similar compounds ("Handbook of Chemistry and Physics," Cleveland, Ohio, 41st Ed., 1959, pp. 2315–2317). The heat of vaporization of the liquid was found to be 10.44 kcal./mole.

The bond energies for the Ni–O bonds fall in the range 56.8 to 71.8 kcal, that of the Ni–N bond is close to 57 kcal. The average value for the Ni–O bond in the acetylacetonate complex was calculated on the basis of the structure given by Bullen, *et al.*[5] Solid "nickel(II)acetylacetonate" is a trimeric structure with each nickel octahedrally surrounded by six oxygen atoms. The value for the salicylaldehyde complex was calculated for two structures. The first of these is based upon a square planar structure for the complex in the vapor phase. The second is calculated on the assumption that the nickel is octahedrally coördinated in the vapor phase as is known to be the case in the solid.[6] The first assumption seems preferable.

(5) G. J. Bullen, R. Mason, and P. Pauling, *Nature*, **189**, 291 (1961).

(6) F. K. C. Lyle, B. Morosin, and E. C. Lingafelter, *Acta Cryst.*, **12**, 938 (1959).

TABLE IV

Compound	$\Delta H_{f,L}$	ΔH_{chel} (g)	ΔH_f, complex	ΔH_{ox}	Bond energy	σ^i
Bis-(acetylacetonato)-nickel(II)	−100.95[a]	−314.0	−413.18	−1476.3	(Ni–O) = 71.8	0.7
Bis-(dimethylglyoximato)-nickel(II)	− 38.92	−159.6	−140.03	−1288.4	(Ni–N) = 56.2[f]	1.5
Bis-(glyoximato)-nickel(II)	− 21.1[b]	−165.65	−108.44	− 600.8	(Ni–N) = 57.8[f]	2.9
Bis-(salicylaldehydato)-nickel(II)	− 66.73[c]	−157.7	−197.8	−1715.6	(Ni–O) = 68.7(45.8)[h]	1.3
Bis-(salicylaldiminato)-nickel(II)	− 50.0[d]	−120.5	−190.3	−1733.8	(Ni–O) = 60.3[g]	2.2
Bis-(8-quinolinato)-diaquonickel(II)	− 51.73	−125.7	− 84.09	−2218.3	(Ni–O) = 64.4[g]	1.7
Bis-(picolinato)-nickel(II)	− 82.45	−112.4	−221.0	−1400.9	(Ni–O) = 57.8[g]	4.5
Bis-(glycinato)-nickel(II)	−124.73[e]	−110.4	−290.57	− 649.1	(Ni–O) = 56.8[g]	3.5

[a] G. R. Nicholson, *J. Chem. Soc.*, 2431 (1957). [b] N.B.S. Circular 500, Table 23-47, p. 144. [c] Calculated from the value of the heat of combustion: "Handbook of Chem. and Phys.," 29th Ed., p. 1462. [d] Estimated on the basis of the value for salicylaldehyde. [e] "International Critical Tables," Vol. V, McGraw–Hill Book Co., New York, N. Y., 1928, p. 167. [f] Calculated using 26 kcal. for (O–H· · ·O) bond in the compound. [g] Calculated using average value of (Ni–N) bond. [h] Calculated value based on an octahedral complex. [i] Calculated as described in the text.

The complexes with glyoxime and dimethylglyoxime present a special problem because of the occurrence of very strong hydrogen bonds in both the solid and gaseous complexes. Since the hydrogen bond is formed when the complex is formed, its energy enters into the term designated $\Delta H_{chel(g)}$ in Fig. 1. An estimate of the bond strength of this hydrogen bond was made on the basis of the bond distance and bond strengths in other hydrogen bonds. Using values for several –O–H. . .O bonds as well as one F–H. . .N bond given by Ketelaar,[7] a graph of the bond energy *vs.* log of O–H. . .O bond length was prepared. Using the O–H. . .O distance for the dimethylglyoxime complex given by Godycki and Rundle[8] a bond energy of 26 kcal. was estimated for this hydrogen bond from the graph. An average of the two Ni–N bond energies was then used to calculate the Ni–O bond energies in the remainder of these compounds where the two types of bonds were present simultaneously. In the case of salicylaldimine, the heats of formation and sublimation of the ligand where estimated. This ligand is extremely unstable unless coördinated and does not lend itself to the direct calorimetric studies.

The values reported for the heats of sublimation are not as accurate as those given for the heats of combustion. This arises primarily from the concurrent thermal decomposition which occurred in some cases, as well as the experimental (manipulative) difficulties. These values are useable in this application since the error they introduce constitutes only a small fraction of the final bond energy.

In the calculation of the bond energies, the O–H bond energy was taken as 110 kcal./mole and the H–H bond energy as 103 kcal./mole. The heat of vaporization of solid nickel was taken as 91 kcal./mole,[9] and the energy of transition from the keto to the enol form of acetylacetone was taken as 2.61 kcal./mole.[10] The heats of formation of these chelates and some of the ligands were also calculated and these values are also presented in Table IV.

The values of the bond energies collected in Table IV show an encouraging consistency. The variation in the bond energies for the different complexes shows that structural features have a definite effect, but certainly not a greater effect than is found in organic compounds.

The values for the standard deviations given for the bond energy terms in Table IV were calculated from the standard deviations of the terms used in the thermochemical cycle by a standard method.[11] As an illustration, the values for the standard deviations of the terms found in Fig. 1 are

$$\Delta H_{1,vap.}, \text{ taken as a known quantity, } \sigma = 0 \quad (1)$$

$$\Delta H_{2,vap.}, \sigma = 1.3 \quad (2)$$

$$\Delta H^0_{f,L}, \sigma = 1.5 \quad (3)$$

$$\Delta H_{ox}, \sigma = 0 \quad (4)$$

$$\Delta H_3, \sigma = 0.4 \quad (5)$$

$$\Delta H_c, \sigma = 3.5 \quad (6)$$

$$\Delta H_{chel(g)}, \sigma = 5.3 \quad (7)$$

$$E(\text{O–H}\ldots\text{O}), \sigma = 5.0 \text{ (estimated)} \quad (8)$$

The values of E(O–H) and E(H–H) are taken as known quantities, $\sigma = 0$ (all in kcal./mole).

Acknowledgment.—This work was supported by a grant from the U. S. Atomic Energy Commission, for which we wish to express our thanks.

(7) J. A. A. Ketelaar, "Chemical Constitution," Elsevier Publishing Co., Amsterdam, 1958, p. 416.

(8) L. E. Godycki and R. E. Rundle, *Acta Cryst.*, **6**, 487 (1953).

(9) National Bureau of Standards Circular 500, Table 45-1, p. 245.

(10) B. Jakuszewski and M. Lazniewski, *Bull. Acad. Polon. Sci., Ser. Sci., Chim., Geol., et Geograph.*, **7**, 177 (1959); *Chem. Abstr.*, **54**, 16161 (1960).

(11) F. D. Rossini, Ed., "Experimental Thermochemistry," Interscience Publishers, Inc., New York, N. Y., 1956. Chapt. 14, p. 309.

DILUTE SOLUTION VISCOSITIES OF POLYMERS NEAR THE CRITICAL TEMPERATURE; CORRESPONDING STATE RELATIONS

BY L. UTRACKI[1] AND ROBERT SIMHA

Department of Chemistry, University of Southern California, Los Angeles 7, California

Received October 29, 1962

The viscosities of ten polystyrene fractions covering a molecular weight range from approximately 7×10^3 to 7×10^5 have been measured in cyclohexane over a range of temperatures from above $T = \theta$ to about $T = T_c$, the critical solution temperature. In the first paper we discuss the observed molecular weight dependence of two quantities, namely the intrinsic viscosity at T_c and k_1 at and below $T = \theta$. The results for the former show T_c to represent a corresponding temperature for the intrinsic viscosity and moreover at $T = T_c$, $[\eta]$ is inversely proportional to v_{2c}, the critical volume fraction for phase separation. By means of the $[\eta]$ values we estimate the average segment density within the encompassed coil volume at $T = T_c$ and find it to be equal to v_{2c} over the appropriate range of molecular weights. The results for k_1 lend further support to the corresponding states principle for solution viscosities previously developed.

I. Introduction

Solution viscosities in the dilute and moderately concentrated range have been studied by several authors. These investigations included good as well as poor solvents but never extended to temperatures lower than θ. The purpose of this and the following paper is to explore experimentally this region for the polystyrene–cyclohexane system and to examine the results in the light of current quantitative or semi-quantitative concepts, both regarding the limiting values and those at finite concentrations. Certain predicted effects should become more pronounced for $T < \theta$ and thus can be afforded a more sensitive test. Earlier[2] we established the existence of corresponding state relations in good and in θ-solvents and shall now extend these considerations.

II. Materials and Procedure

Seven polystyrene samples were obtained through the courtesy of Dr. H. W. McCormick of the Dow Chemical Company. These fractions are identical with those used by McCormick[3] and by Debye and his collaborators.[4,5] Three others were furnished through the courtesy of Dr. R. Milkovich of the Shell Chemical Company. These latter samples are reported to have M_w/M_n ratios ranging from 1.16 to 1.8.

The polymers were precipitated from toluene solutions by a large excess of methanol and dried in a vacuum oven for two to three days at 80°. Doubly rectified cyclohexane was kept and prior to each use freshly distilled over sodium wire. The physical properties of our solvent are: ν (34°) = 1.006 centistokes; d(34°) = 0.7649 g./ml.; $n^{20}D$ 1.4263; t_m = 5.6°.

The viscosities were determined in a specially devised closed system using viscometers of the Ubbelohde type (Fig. 1). The advantages of this system are a dust-free atmosphere, avoidance of vaporization of the solvent, and the use of solvent vapor instead of air to transport the solution of the upper bulb.

The viscometers were calibrated by means of National Bureau of Standards oils. Kinetic energy corrections were applied throughout. The temperature of the water bath was kept constant to within ±0.001° and flow times established by means of stop-watches with an accuracy of ±0.05 sec.

The measurements were carried out in the following manner. About 20 ml. of a filtrated solution (about 1 g./dl.) were introduced through the joint A directly to the bottom of the lower bulb which has a volume of *ca.* 150 ml. This joint is then closed by a Teflon cap, the viscometer is submerged into the bath, and the stopcocks are adjusted. By means of the pressure of the saturated solvent vapor through the entrance B the solution is transported to the upper bulb (volume *ca.* 4 ml.). Through the three-way stopcock, the pressure in the apparatus is reduced to atmospheric and the measurements are started. For dilution the appropriate amount of solvent is added through joint C. The requisite concentrations were made up by using a Friedman–La Mer weight buret. The characteristics of the viscometers are exhibited in Table I. The velocity gradients do not vary much but within this limitation no variations in our results could be observed.

TABLE I

CHARACTERISTICS OF VISCOMETERS

Viscometer	Capillary Length, cm.	Capillary Diameter, mm.	Upper bulb volume, ml.	Viscometer Constants[a] A	Viscometer Constants[a] B
A	10.0	0.6124	5.20	0.00883	0.978
B	10.0	.6124	5.15	.00824	1.120
C	10.1	.4634	5.25	.02763	0.371

[a] A and B are the constants in the equation $\nu = At - B/t$ where ν = kinematic viscosity in centistokes and t = time in sec.

III. Experimental Results

The solution viscosities of ten polystyrene samples were measured in cyclohexane at 36° and lower temperatures extending in most instances below the critical solution temperatures T_c. The characteristics and critical data of the polymers in cyclohexane are shown in Table II.

TABLE II

CHARACTERISTICS OF POLYSTYRENE SAMPLES

No.	$M_n \times 10^{-3}$	M_w/M_n	t_c, °C.	v_{2c}, %	$[\eta]_{tc}$
1	6.4	1.64	7.8	22.3	0.071
2	22.6	1.80	13.6	12.2	.118
3	78.1	1.05	19.8	6.88	.226
4	120	1.05	22.6	5.6	.256
5	147	1.04	22.9	5.0	.299
6	221	1.08	25.4	4.6	.347
7	310	1.16	25.9	3.6	.399
8	523	1.09	27.9	2.8	.562
9	526	1.68	27.9	2.7	.565
10	694	1.18	28.7	2.5	.651

[a] Samples 2, 7, 9 from Shell; others from Dow. [b] t_c and v_{2c} of samples 4, 5, 6, and 8 are taken directly from ref. 4. For the remaining samples inter- or extrapolation was used.

Typical data are presented in Fig. 2, where the linear portions of the reduced specific viscosity–concentration curves are exhibited for the highest and lowest molecular weight over a range of temperatures. Our measurements extended beyond this range, but will not be used here. Figure 3 shows the intrinsic viscosities as a function of temperature. For the three lowest molecular weights a twofold extrapolation

(1) Polish Academy of Sciences, Polytechnic Institute, Lodz, Poland.
(2) L. Utracki and R. Simha, *J. Polymer Sci.*, in press.
(3) H. W. McCormick, *J. Colloid Sci.*, **16**, 635 (1961).
(4) P. Debye, P. H. Coll, and D. Woermann, *J. Chem. Phys.*, **33**, 1746 (1960).
(5) P. Debye, B. Chu, and D. Woermann, *ibid.*, **36**, 1803 (1962).

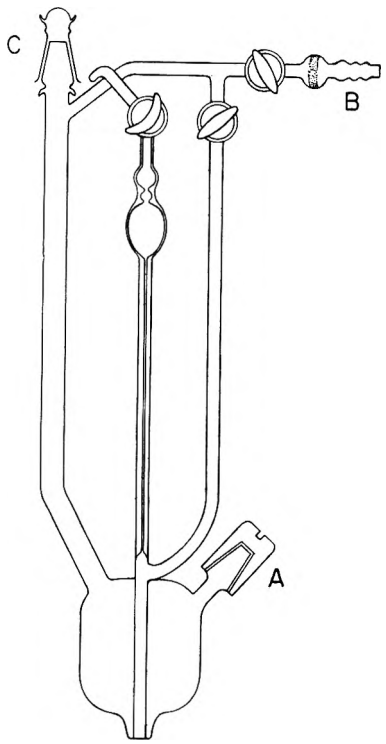

Fig. 1.—Sketch of viscometer. Description in the text.

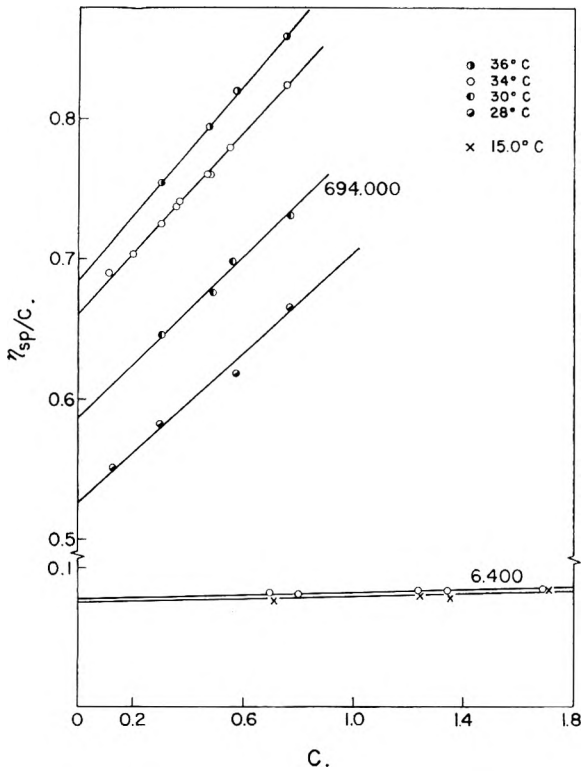

Fig. 2.—Representative viscosity–concentration curves for various temperatures. Upper family of lines for $\bar{M}_n$ = 694,000; lower for M_n = 6400.

is involved, namely in respect to the numerical values of T_c and the intrinsic viscosities at T_c. Finally Fig. 4 shows the k_1 parameters, defined by the equation

$$\eta_{sp}/(c[\eta]) = 1 + k_1[\eta]c \qquad (1)$$

at 34 and 28° as a function of M_n.

IV. Discussion

We want to consider here two quantities, namely k_1 and $[\eta]$ at $T = T_c$. In accord with the observations of

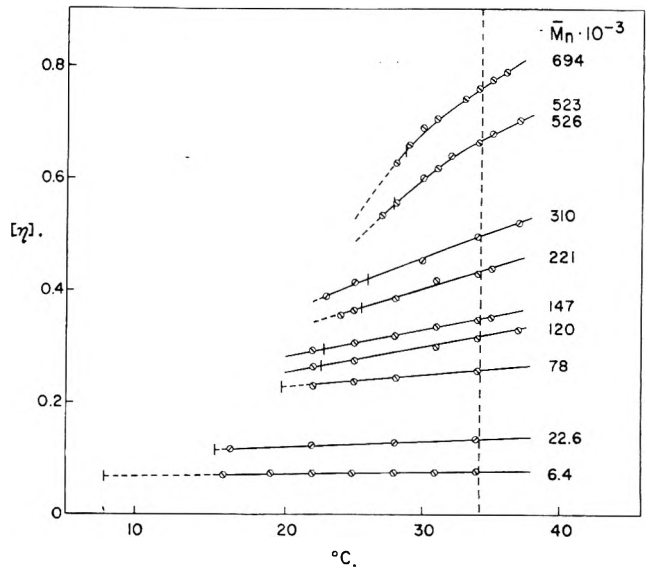

Fig. 3.—Intrinsic viscosity–temperature curves in cyclohexane for different molecular weights. Short vertical lines indicate t_c for each molecular weight, vertical dashed line indicates θ-temperature. Dashed portions, extrapolation of experimental data.

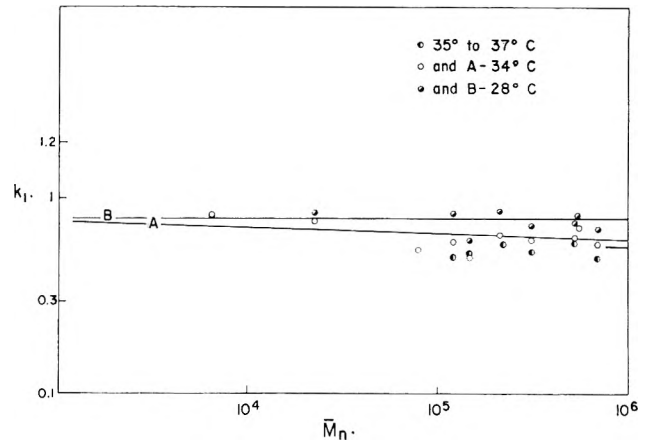

Fig. 4.—Dependence of parameter k_1, eq. 1, on molecular weight in cyclohexane at 34 and 28°. Third set of points, data between 35 and 37°. The short line on the right-hand side indicates eq. 1 for 36°.

earlier authors, we note generally, in very poor solvents, large values of k_1 which approach those characteristic of spherical suspensions.[6] Moreover there is a noticeable temperature effect beyond the considerable scatter for the higher molecular weights.

The concentration range available below $T = \theta$ is limited and we cannot establish the validity of corresponding state relations directly as we have done earlier.[2] However, we can compare the observed molecular weight dependence of k_1 with that predicted by the superposition principle and thus indirectly examine the validity of the earlier general relations for $T < \theta$. According to the superposition principle we have[2]

$$k_1 = a_1(\gamma[\eta])^{-1} \qquad (2)$$

where a_1 is a constant arising from the expansion of the master curve in a power series in the reduced concentration and γ the shift factor in the concentration scale. If we assume that γ is a function of molecular weight only, then it is proportional to v_{2c}, the

(6) R. Simha, *J. Appl. Phys.*, **23**, 1020 (1952).

critical volume fraction.[2] Now from Fig. 3 one derives by least square computations

$$[\eta]\ (T = \theta) = 9.02 \times 10^{-4}\ M_n^{0.503} \qquad (3)$$

$$[\eta]\ (t = 28^0) = 10.80 \times 10^{-4}\ M_n^{0.479}$$

Moreover[2]

$$v_{2c}(\%) = 13.82 \times 10^2\ M_n^{-0.471}$$

From eq. 2 and 3, therefore

$$k_1\ (T = \theta) = \text{const.}_1\ M_n^{-0.032}$$

$$k_1\ (t = 28^0) = \text{const.}_2\ M_n^{-0.008} \approx \text{const.}_2 \qquad (4)$$

The present result for $T = \theta$ differs slightly from that reported earlier[2] due to the difference between the $[\eta]$–M_n relation, eq. 3, and that obtained previously.[7] Equation 4 appears as the solid lines in Fig. 4. In the light of Fig. 2, the scatter of the experimental points in Fig. 4 was to be expected. Nevertheless, we feel that a satisfactory comparison with the predictions of eq. 3 can be made. Here, the constant for the θ-solvent has been obtained by fitting the equation to a particular molecular weight, namely 2.21×10^5. For 28°, the constant has been defined as the average of all experimental values, *viz.*, $k_1 = 0.80$.

Next, it is of interest to compare the results just obtained with those derived from our analytical expression for the master curve,[2] which reads

$$\log\ (\eta_{sp}/c[\eta]) = Ax + Bx_0\{1 - [(x/x_0 - 1)^2 + C]^{1/2}\}$$

where A, B, C, and x_0 are constants. Expansion in $x = c/\gamma$ leads to eq. 2 with

$$a_1 = 2.303[A + B(1 + C)^{-1/2}] \qquad (5)$$

The bracket represents the initial slopes in Fig. 6 of ref. 2. If we assume on the basis of this figure that the initial slopes are in good approximation equal for toluene and cyclohexane at $T = \theta$ and now by assumption include other temperatures as well, we calculate k_1 from (4) and (1)

$$k_1[\eta] \approx (2.303/\gamma)(A + B) \qquad (2a)$$

or

$$k_1 = \text{const.}\ M_n^{-(a-0.471)}$$

where $C/2$ has been neglected compared with unity. The logarithmic expression above does not rigorously, but only in good approximation yield the correct limit for $C \to 0$. The difference, however, is insignificant for our purposes. Substitution of the numerical values[2] for γ, A, and B then gives with eq. 3

$$k_1\ (T = \theta) \approx 0.94 M_n^{-0.032} \qquad (4a)$$

$$k_1\ (t = 28^0) \approx 0.79$$

The second value may be compared with the average 0.80, line B, Fig. 4. The first equation 4a shifts the line A as drawn in Fig. 4 downward by four units in the second place for $M_n = 10^4$ and correspondingly less for the higher molecular weights. This extent of agreement is all that can be expected and may be considered satisfactory. Thus we conclude that the experimental results for $T < \theta$ are also in accord with the predictions to be made from the superposition principle.

In Fig. 4 are also shown the experimental k_1 values for $T > \theta$, covering temperatures between 35 and 37° and lying generally below those at θ. If we use the intrinsic viscosities at 36° and eq. 2a, a line slightly below that for 34° is calculated as indicated on the right-hand side of Fig. 4.

Very recently, Stern[8] proposed an empirical relation for k_1 which can be cast in the form

$$k_1 = D + E[\eta]^{-2} \qquad (6)$$

with D and E independent of molecular weight. This equation is qualitatively similar to our relations inasmuch as it predicts an increase of k_1 with decreasing molecular weight. However, a fit of the experimental data of McCormick[3] and Simha–Zakin[7] can be obtained only over a limited range of molecular weights.

Next, we consider the dependence of the intrinsic viscosity $[\eta]$ $(T = T_c)$, obtained through Fig. 3, as a function of molecular weight. In Fig. 5 the reciprocal quantity is plotted and we note that a unique relationship exists regardless of the variations in the absolute magnitude of the temperature between about 8 and 29°. Such an interval produces appreciable changes in the intrinsic viscosity of a given fraction, particularly in the higher range of molecular weights (see Fig. 3). We conclude that the critical temperature represents a corresponding state with respect to the intrinsic viscosity. The line connecting the lower series of points in Fig. 5 has been drawn parallel to the least square line representing v_{2c} as a function of M_n, according to the equation established earlier.[2]

The correspondence between the two lines permits us to write the equations

$$[\eta]\ (T = T_c) = 1.091 \times 10^{-3}\ M_n^{0.471} \qquad (7)$$

$$[\eta]\ (T = T_c)v_{2c} = 1.51$$

It is not surprising to find that the exponent in the Mark–Houwink relation becomes less than 0.5 as the temperature is reduced below θ. However, no explicit results seem to have been reported. It follows from eq. 7 and previous work[2] that the product $[\eta]$ $(T = T_c) \times c$ may alternatively be regarded as a reduced concentration variable for the system polystyrene–cyclohexane. Moreover, we note from eq. 7 the following relation between $c_0 \approx 1.08/[\eta]$,[7,9] the concentration of incipient overlap of the average coils (as existing at infinite dilution) at $T = T_c$ and c_{crit}

$$c_{crit} \approx 1.51 c_0$$

assuming a density of 1.08 g./ml. for polystyrene. If it were permissible to assume that the coil dimensions are independent of concentration at $T = T_c$, this result would imply that the average distance between molecule centers is reduced by 13% between incipient overlap and precipitation.

We recall that the shift factor γ, see eq. 2, for toluene at 30 and 48° varies as the (-0.64) power of the molecular weight.[2] If the inverse relationship between $[\eta]$ $(T = T_c)$ and v_{2c}, eq. 7, and the proportionality

(7) R. Simha and J. L. Zakin, *J. Colloid Sci.*, **17**, 270 (1962).

(8) M. D. Stern, Paper presented at the 142nd National Meeting of the American Chemical Society, Atlantic City, N. J., September, 1962.

(9) R. Simha and J. L. Zakin, *J. Chem. Phys.*, **33**, 1791 (1960).

between v_{2c} and γ which was shown for cyclohexane,[2] are to be valid for toluene also, this would imply that $[\eta]$ $(T = T_c)$ should vary as the 0.64 power of M_n. If this should turn out to be true, and there exists currently no experimental evidence, it would imply a stiff chain at $T = T_c$. This is not impossible, provided T_c for toluene is sufficiently low and the effective internal rotation barrier high.

We may use these results to obtain an insight into the state of the solution at infinite dilution as compared with that prevailing at the critical point. Specifically, we shall compare the volume fraction v_{2coil} of polymer in the average volume encompassed by an isolated polymer coil at $T = T_c$ with v_{2c}. The former will be estimated by means of the intrinsic viscosity, disregarding the problem of hydrodynamic shielding effects. For a spherical coil we write

$$v_{2coil}\ (\%) = 3 \times 100\ M_n/[\rho N_A\ 4\pi(\bar{s^2})^{3/2}]$$

where ρ is the density and $\bar{s^2}$ the mean square radius of gyration. Writing the intrinsic viscosity in terms of the parameter Φ as

$$[\eta] = 6^{3/2}\ \Phi(\bar{s^2})^{3/2}/M_n$$

we have for polystyrene

$$v_{2coil}[\eta] = 5.396 \times 10^{-22}\ \Phi \qquad (8)$$

From (7) and (8) one obtains

$$(v_{2c}/v_{2coil})_{T=T_c} = 2.798 \times 10^{21}\ \Phi^{-1}\ (_{T=T_c}) \qquad (9)$$

Thus it is immediately evident that the ratio of volume fractions will be near unity. The actual value depends on the value to be assigned to Φ. If we take Φ to be a constant independent of solvent and molecular weight and approximately equal to 2.5×10^{21}, the critical ratio is simply 1.1. As an alternative we can use the result[10]

$$\Phi = 2.87 \times 10^{21}\ \alpha^{-0.74} \qquad (10)$$

which makes Φ a function of solvent and temperature through the expansion factor α, where $\alpha = 1$, by definition, for $T = \theta$. From eq. 3, 7, and 10, we derive therefore

$$\Phi\ (T = T_c) \approx 2.697 \times 10^{21} \times M_n^{0.0105}$$

$$(v_{2c}/v_{2coil})_{T=T_c} = 1.038 \times M_n^{-0.0105} \qquad (11)$$

Between $M_n = 10^4$ and 10^6, the critical ratio varies from 0.94 to 0.90, or in other words, is constant. For low molecular weights, however, it is not legitimate to continue employing these equations.

We have thus found that at $T = T_c$ the average density of segments inside a coil at infinite dilution equals the critical density in the solution, within the uncertainties of the calculations. The actual density in the coil, of course, decreases with increasing distance from the central core. It is not possible, however, to characterize the onset of precipitation by the condition of equal segmental volume fractions outside and inside the volume pervaded by the chain, since this volume is a function of concentration.[5,9] Under the solvent conditions in question, an expansion should take place.

(10) L. Utracki and R. Simha, *J. Phys. Chem.*, **67**, 1056 (1963).

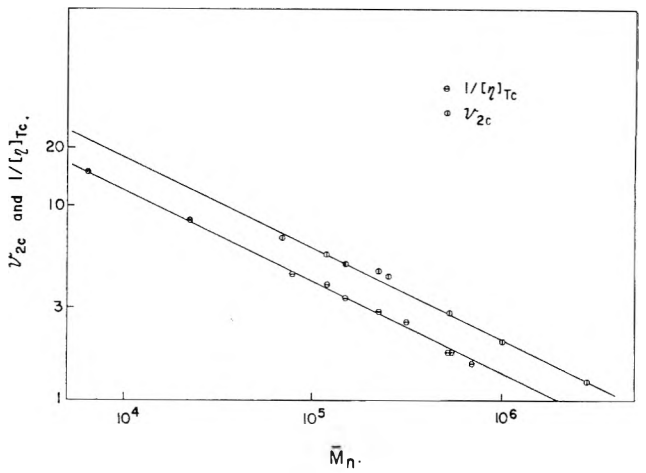

Fig. 5.—Molecular weight dependence of intrinsic viscosity at the critical temperature and of critical volume fraction. Upper line, least squares from data of ref. 4; lower line, drawn parallel.

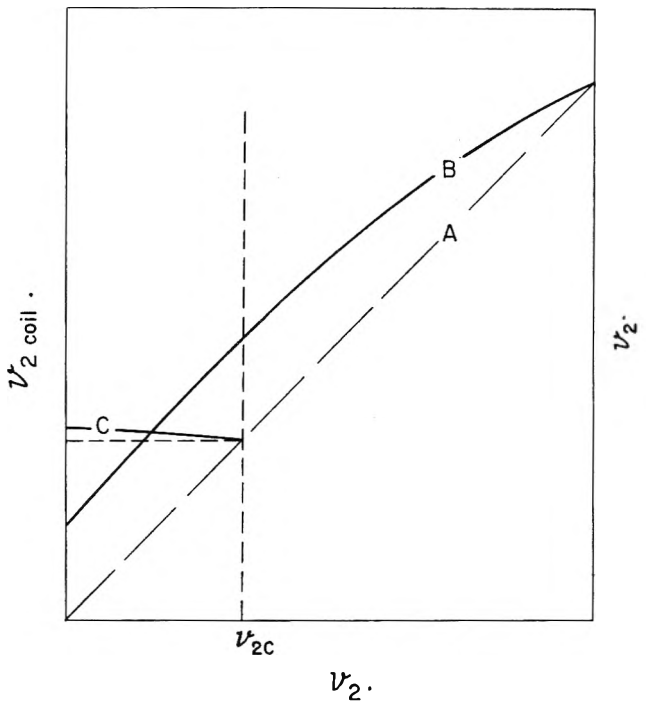

Fig. 6.—Relation between volume fraction in solution, v_2, and in coil, v_{2coil}; schematically. A, v_2; B, v_{2coil}, very good solvent; C, v_{2coil}, at critical temperature.

We should like to suggest the tentative and qualitative picture for good and poor solvents described in Fig. 6. In the good solvent, v_{2coil} is assumed to increase continuously with polymer concentration due to osmotic compression. In the precipitating solvent on the other hand, the initially high volume fraction in the coil is reduced or remains constant, until at some concentration v_{2coil} and v_2 become nearly equal and precipitation sets in. As the solution concentration increases, the distinction between the individual encompassed volumes is lost and what is being compared here are average and mean local concentrations around a given molecular center.

Acknowledgment.—The support of this work by grants from the California Research Corporation and the Socony Mobil Oil Company, Inc., is gratefully acknowledged.

MOLECULAR WEIGHT AND TEMPERATURE DEPENDENCE OF INTRINSIC VISCOSITIES IN VERY POOR SOLVENTS

BY L. UTRACKI[1] AND ROBERT SIMHA

Department of Chemistry, University of Southern California, Los Angeles 7, California

Received October 29, 1962

Measurements of intrinsic viscosities of polystyrene between the θ and the critical temperatures in cyclohexane for molecular weights varying between 6×10^3 and 6×10^6 are compared with theories of dilute solutions. The predicted relation between intrinsic viscosity and expansion factor α is obeyed for molecular weights M_n above 10^5. For smaller M_n, however, the ratio b_0/a_0, with b_0 a characteristic dimension of a bead and a_0 the length of a link, decreases with decreasing M_n. This cannot be quantitatively interpreted in terms of reduced hydrodynamic interaction. Moreover, b_0/a_0 is temperature and solvent dependent. The temperature coefficients of intrinsic viscosity at and below θ as a function of molecular weight can be interpreted in terms of the solvent effect alone, without allowing for the additional contribution of an internal rotation barrier. On the other hand, the dimensions, as calculated from the intrinsic viscosity at θ, indicate the existence of an appreciable barrier. Both results can be brought into accord by the picture of freely jointed segments, each containing five monomer units, or of a restricted angle of $\pm 42°$ for free rotation around C–C bonds. The exponent a in the Mark–Houwink relation decreases with increasing molecular weight for temperatures sufficiently below θ, in accord with theoretical predictions. Although the expressions used throughout are valid for α near unity, they also appear to describe the intrinsic viscosity of toluene solutions, possibly by a compensation of hydrodynamic and thermodynamic factors.

I. Introduction

The average molecular size and the intrinsic viscosity of polymers has been investigated by many authors and existing statistical and hydrodynamic theories have been compared with experimental results. However, these investigations were restricted to good solvents or to θ-temperatures. In the present paper the experimental results reported in the preceding paper[2] as well as some data pertaining to polystyrene solutions in good solvents are compared with recent theoretical work.[3,4]

II. Discussion

We require two quantities for our purposes, namely the extension factor α and the intrinsic viscosity $[\eta]$. The statistical mechanical theory for the former is most adequately developed for poor solvents where α is close to unity. For this case the expression[3,4]

$$(\alpha^3 - \alpha)(1 + 1/3\alpha^2) = (4/3)^{5/2} z$$

with

$$z = (6/\pi)^{1/2}(b_0/a_0)^3(1 - \theta/T)M^{1/2} \qquad (1)$$

where b_0^3 is proportional to the volume of a bead and a_0 the length of a link, may be expanded to

$$\alpha^3 = 1 + 2z + 1/3z^2 + 0(z^3) \qquad (1a)$$

Actually, for $|z| \leqq 0.2$, the range of most interest here, one can replace eq. 1a by a linear term

$$\alpha^3 = 1 + 2.053z \qquad (1b)$$

with an error smaller than 0.2%. The validity of eq. 1 has been shown[5] for $0 < z \leqq 0.2$.

The intrinsic viscosity is represented by the equation[3,4]

$$[\eta] = [\eta]_\theta[1 + 1.55\, z + 0(z^2)] \qquad (2)$$

with

$$[\eta]_\theta = 2.87 \times 10^{21} \times (\overline{r_\theta^2})^{3/2}/M$$

Here $\overline{r_\theta^2}$ is the mean square separation of chain ends in the θ-solvent and it is assumed that the hydrodynamic interaction between the beads is large. For small molecular weights, therefore, this equation has to be revised (see below). From eq. 1 and 2, the ratio $[\eta]/[\eta]_\theta$ should be a linear function of $M^{1/2}$ at a given temperature. This is confirmed in Fig. 1 for three temperatures below θ. The three lines are drawn by using the limiting values of b_0/a_0 derived below.

By means of eq. 1b and 2 one can write

$$[\eta] = [\eta]_\theta \alpha^{2.26} \qquad (3)$$

We shall make use of eq. 3 to calculate α-factors by means of measured intrinsic viscosities. From eq. 2 and 3 we obtain an expression for the factor defined by the Fox–Flory equation

$$[\eta] = \Phi[(\overline{r_\theta^2})^{3/2}/M]\alpha^3$$

viz.

$$\Phi = 2.87 \times 10^{21}\alpha^{-0.74} \qquad (2')$$

Finally we derive for the temperature coefficient

$$\mathrm{d} \ln [\eta]/\mathrm{d}T = 2.14(b_0/a_0)^3(\theta/T^2)M^{1/2}\alpha^{-3} + \mathrm{d} \ln (\overline{r_\theta^2})^{3/2}/\mathrm{d}T \qquad (4)$$

assuming b_0/a_0 to be a constant.

In order to obtain numerical values and apply a sensitive test to the behavior of the quantity b_0/a_0, we plot in Fig. 2 the ratio

$$(\alpha^3 - 1)/[(1 - \theta/T)M_n^{1/2}] = 2.053(6/\pi)^{1/2}(b_0/a_0)^3 \qquad (5)$$

as a function of M_n for the polystyrene–cyclohexane system at 25, 28, and 30°. Analogous plots for benzene solutions at 25°[6,7] and toluene solutions at 25°[8] and 30°[9] are also shown. It is assumed that θ(toluene) = 160°K. and θ(benzene) = 100°K. The horizontal portions of the lines are simply drawn as averages for a given temperature through all points corresponding to molecular weights larger than 10^5. No meaningful

(1) Polish Academy of Sciences, Polytechnic Institute, Lodz, Poland.
(2) L. Utracki and R. Simha, *J. Phys. Chem.*, **67**, 1052 (1963).
(3) M. Kurata, H. Yamakawa, and H. Utiyama, *Makromol. Chem.*, **34**, 139 (1959).
(4) M. Kurata, W. H. Stockmayer, and A. Roig, *J. Chem. Phys.*, **33**, 151 (1960).
(5) Y. Ohyanagi and M. Matsumoto, *J. Polymer Sci.*, **54**, S3 (1951).
(6) T. G Fox, Jr., and P. J. Flory, *J. Am. Chem. Soc.*, **73**, 1915 (1951).
(7) W. R. Krigbaum and P. J. Flory, *J. Polymer Sci.*, **11**, 37 (1953).
(8) H. W. McCormick, *J. Colloid Sci.*, **16**, 635 (1961).
(9) R. Simha and J. L. Zakin, *ibid.*, **17**, 270 (1962).

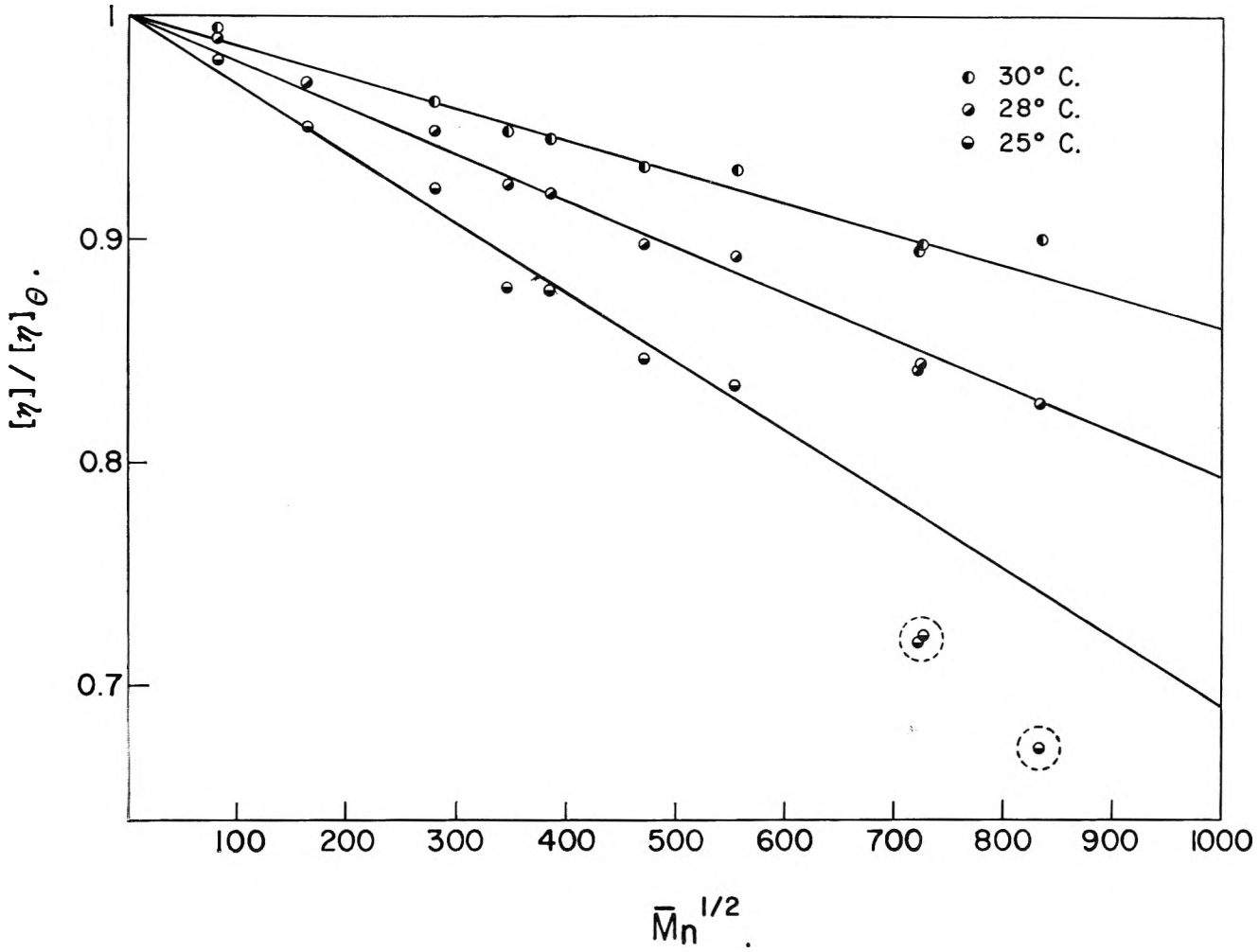

Fig. 1.—Application of eq. 2 at three temperatures. Dashed circles indicate extrapolation below T_c.

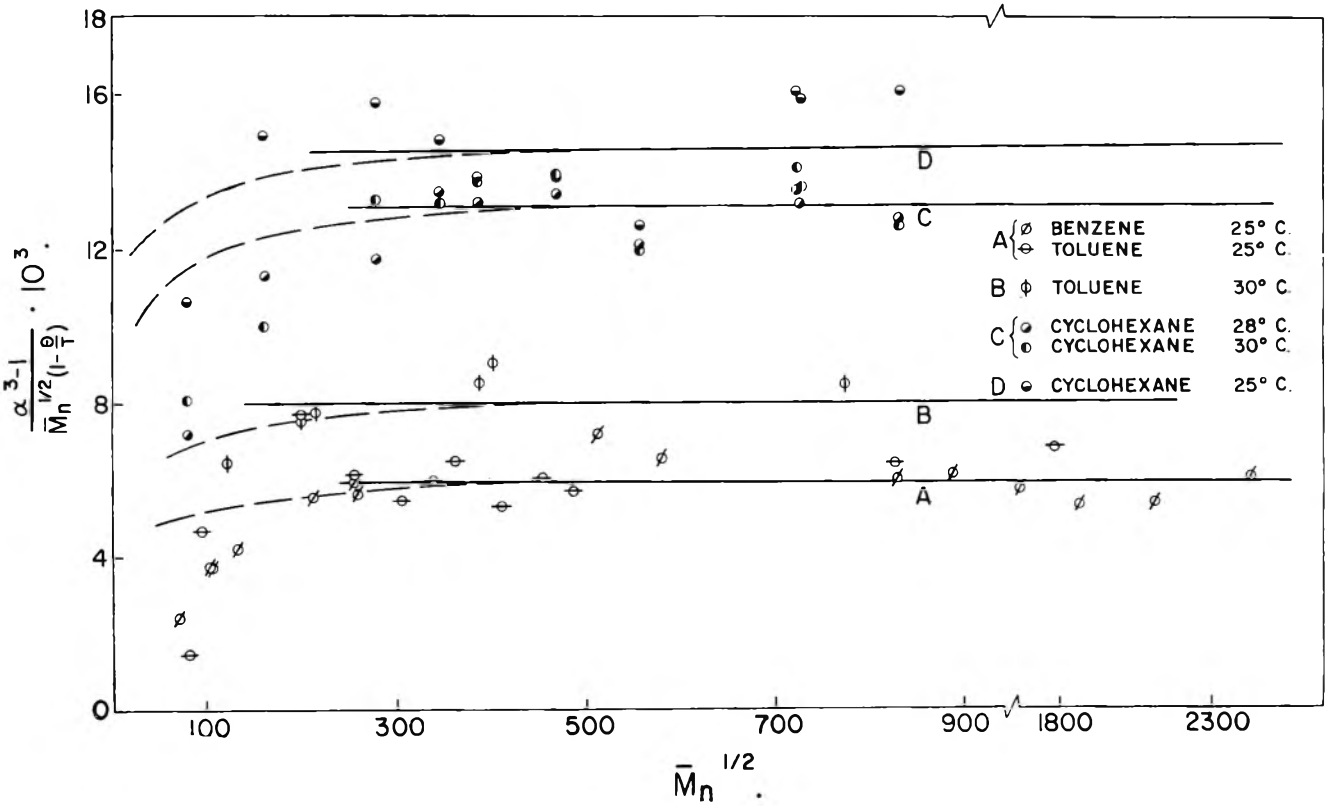

Fig. 2.—Expansion factors as function of molecular weight and temperature. Full lines, according to eq. 5. Dotted portions, hydrodynamic correction.

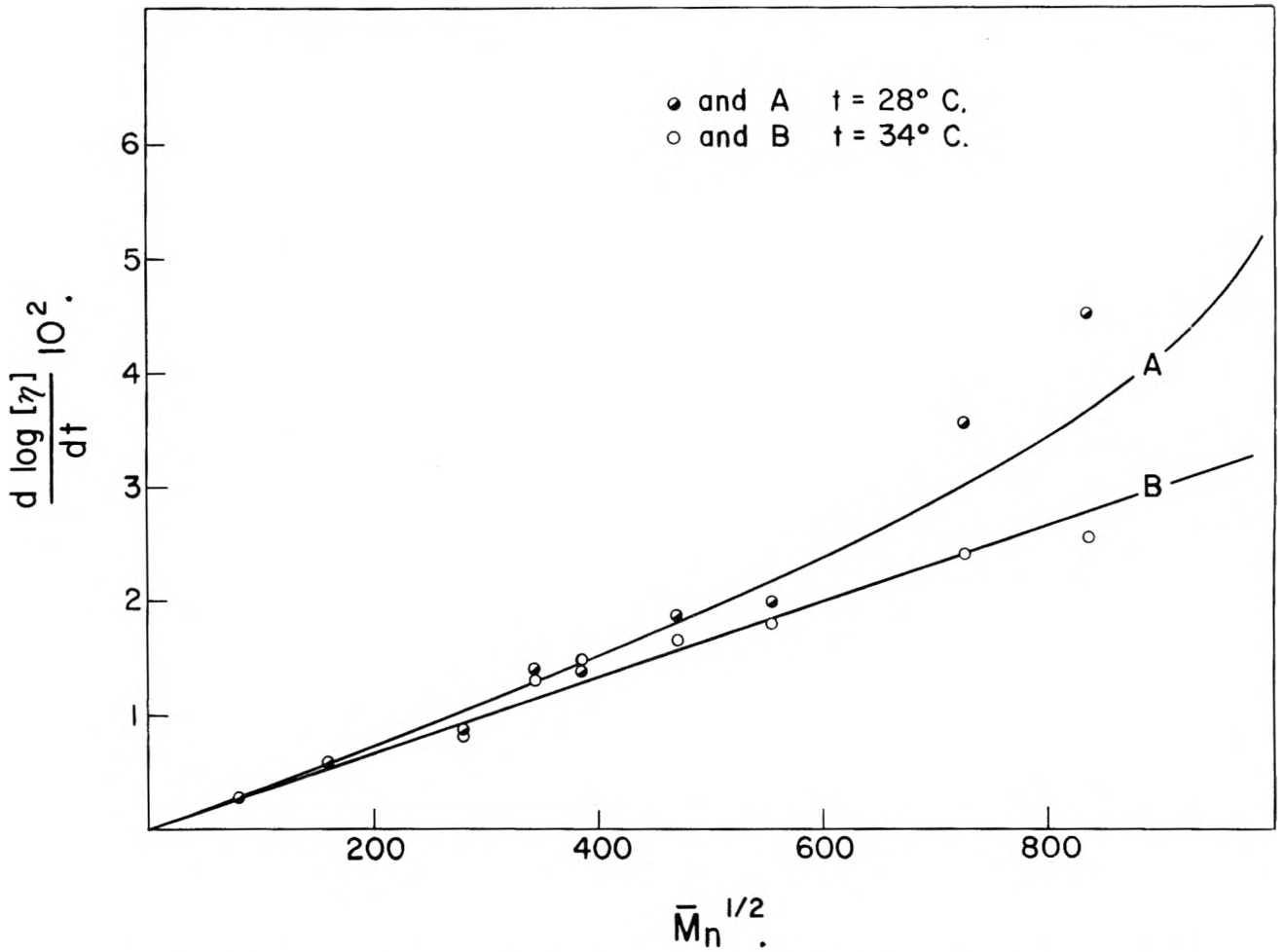

Fig. 3.—Temperature coefficients of intrinsic viscosities. Full lines calculated from the first term of eq. 4.

distinction can be made between 28 and 30° and the single line C encompasses both sets of data.

The following observations may be noted: First, there is a temperature effect, the ratio b_0/a_0 increasing with decreasing solvent power. The basis for this conclusion is restricted by the narrow temperature range in cyclohexane. Moreover, eq. 5 should not apply to toluene and benzene, except at very low molecular weights, because z is not sufficiently small. It is noteworthy that it is obeyed, nevertheless, even for large molecular weights, where z is close to 2. In toluene, the ratio b_0/a_0 actually increases with increasing temperature. There is nothing surprising, of course, in finding both the effective volume of a bead and the segment length to vary with temperature and solvent. Secondly, eq. 5 breaks down for small M. Here the assumption of complete hydrodynamic shielding is no longer valid and eq. 2 is modified to read[3]

$$[\eta] = [\eta]_\theta S(X, T, \theta)[1 + p(X)z + 0(z^2)] \quad (2'')$$

X is the hydrodynamic shielding parameter proportional to $M^{1/2}$ and S represents the ratio of the shielding functions for a specified value of X at T and θ, respectively. Thus, for $T < \theta$, we expect $S > 1$, due to the increased compactness of the coil. The function $p(X)$ has been tabulated.[3] In order to compare eq. 2'' with our experimental data, Fig. 2, we proceed as follows: For $X = 10$, $p(X) = 1.5$, *i.e.*, smaller by 3% than $p(\infty) = 1.55$. On the basis of Fig. 2 we assign this value to a molecular weight of 10^5 and thus fix the numerical value of the proportionality factor between X and $M_n^{1/2}$. From eq. 1b and 2'' we obtain the exponent of α which replaces the value of 2.26 in eq. 3. Assuming $S = 1$, the dotted lines in Fig. 2 are calculated. For benzene and toluene this procedure has no theoretical foundation but is purely empirical. In cyclohexane, the trend is qualitatively correct, but the calculated decrease is not sufficiently rapid. A choice of S-values larger than unity increases the discrepancy. For $S = 1$, the exponent in eq. 3 varies between 2.20 and 2.09 for $X = 10$ and 1.6, neglecting quadratic terms in z. The choice of a smaller "boundary" value for X would have improved the agreement somewhat.

The observed and calculated temperature coefficients at 28 and 34° are compared in Fig. 3 as a function of molecular weight. Equation 4 consists of two terms, the first describing the solvent effect and the second the influence of the internal rotation barriers. The former contains the quantity $(b_0/a_0)^3$ which we have just found to vary with temperature. This requires the addition of a term

$$(1.544z/\alpha^3)\mathrm{d} \ln (b_0/a_0)^3/\mathrm{d}T$$

to the right-hand side of eq. 4. It has the same $M^{1/2}$-dependence as the first one and vanishes at $T = \theta$. Assuming from Fig. 2 a temperature coefficient of (-3%) per degree, this expression becomes positive for $T < \theta$ and is less than 20% of the first term. However, on approaching θ, the temperature coefficient

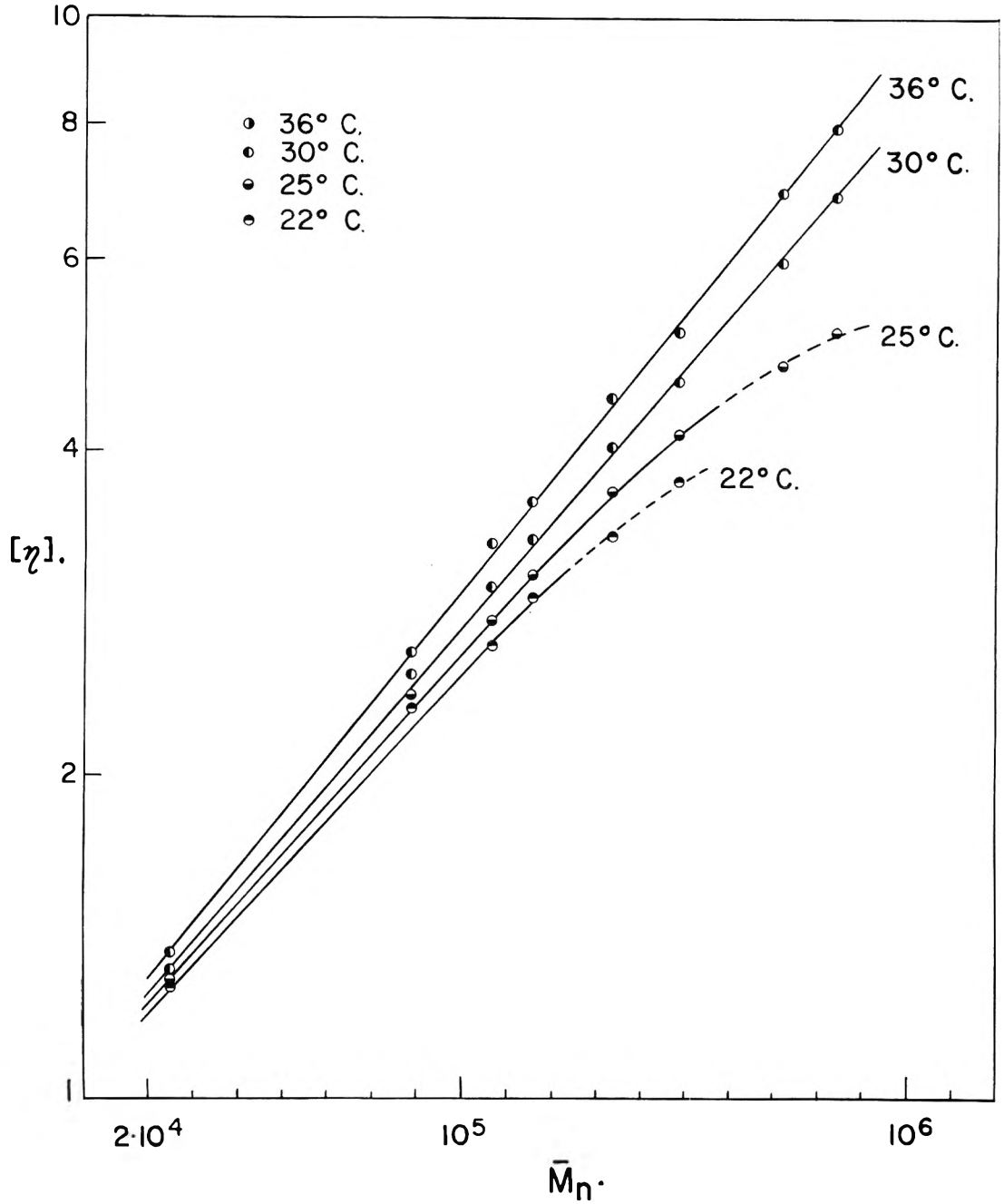

Fig. 4.—Molecular weight dependence of intrinsic viscosity above and below θ-temperature. Dashed lines indicate extrapolation below T_c.

could well be less than assumed above. The numerical factor of 2.14 in eq. 4 is based on the exponent 2.26 in eq. 3, but should decrease with decreasing molecular weight. This effect amounts to 10% for the lowest molecular weight and will be disregarded. Similarly, α^{-3} may be computed from eq. 3 with a constant exponent.

For the evaluation of the second term, several models may be investigated. A periodic potential of the polymethylene type with an energy difference $\epsilon > 0$ between the *gauche* and *trans* position yields[10]

$$\overline{r_\theta^2} = (2/3)Nl_0^2(1 + 2e^{\epsilon/RT}) \qquad (6)$$

where l_0 is the length and N the number of C–C bonds. This results in a negative and molecular weight independent contribution to the total temperature coefficient. The first term on the right-hand side of eq. 4 contains no disposable parameter and is represented by the solid lines in Fig. 3. At $t = 34°$ the experimental results are quite well described by this term and the barrier height ϵ must be assumed to be small, *i.e.*, less than 100 cal./mole. At 30°, the inclusion of the positive correction term would improve the agreement. Again, ϵ must be small.

On the other hand, eq. 6 may be used directly to evaluate ϵ. From eq. 2 and 6 and our data we find at $T = \theta$

$$\overline{r_\theta^2}/(2Nl_0)^2 = 5.07;\ \epsilon/(R\theta) \approx 1.96$$

which cannot be reconciled with the observed temperature coefficients and eq. 4. One can formally account for all observations by representing the molecule as a chain of freely jointed large segments. About 5 monomer units per such segment must then be postulated. Alternatively, a box potential with unrestricted

(10) A. V. Tobolsky, "Properties and Structure of Polymers," John Wiley and Sons, Inc., New York, N. Y., 1960, Append. D and H.

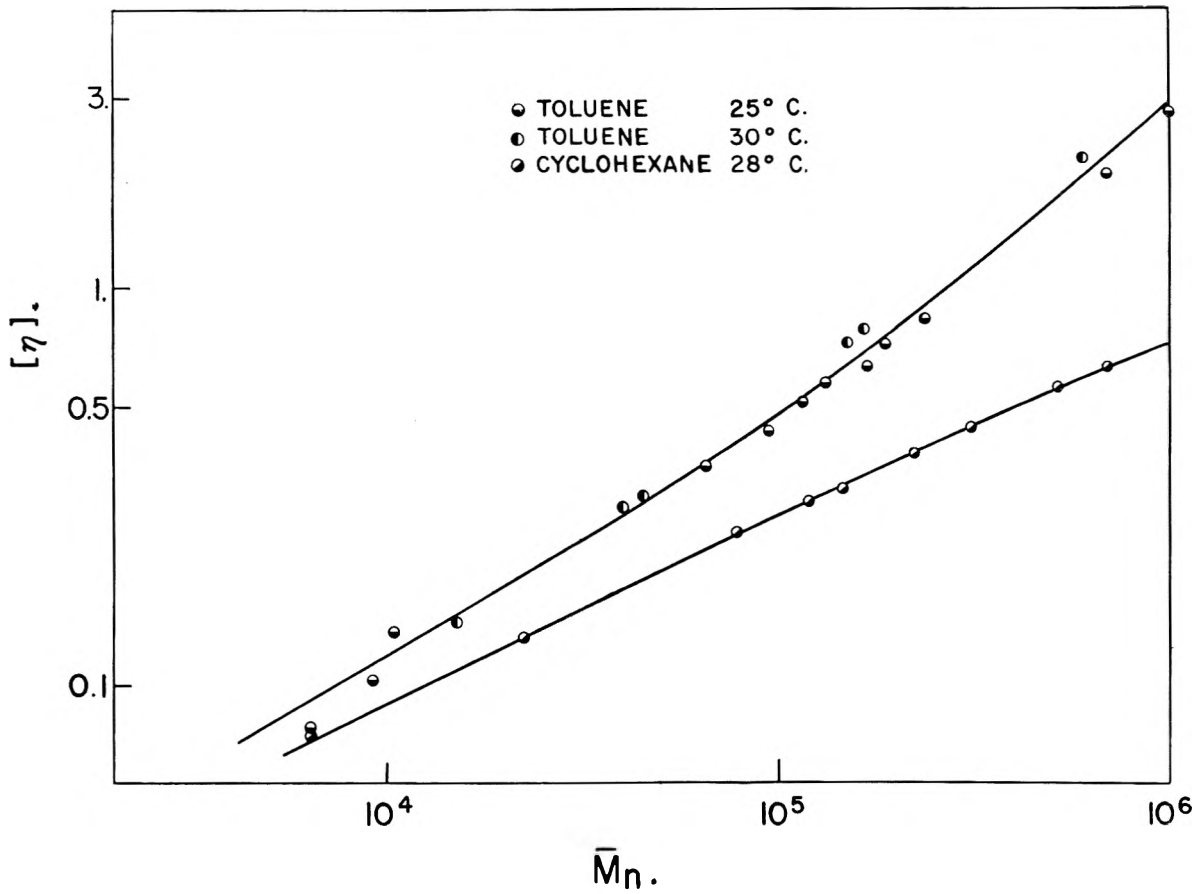

Fig. 5.—Comparison of theoretical, eq. 7, and experimental molecular weight dependence of intrinsic viscosity in good and poor solvents.

rotation around a C–C link within an angle δ may be used. This angle turns out to be about 84°.

The dependence of intrinsic viscosity on molecular weight is given from eq. 1b and 3 as

$$\ln [\eta] = A + (1/2) \ln M + 0.753 \ln [1 + B(1 - \theta/T) M^{1/2}]$$

with

$$A = \ln [2.87 \times 10^{21} (\overline{r_\theta^2})^{3/2}/M] \qquad (7)$$

$$B = 2.053(6/\pi)^{1/2}(b_0/a_0)^3$$

Here the logarithm should strictly be expanded to the first order term. However, we shall find it useful later on to use eq. 7 as shown. Moreover, B will be treated as independent of molecular weight. The error thus committed for low molecular weights amounts to about 15% in toluene where the effect is largest. We shall consider this as a second-order correction. By comparison with the Mark–Houwink relation

$$[\eta] = KM^a \qquad (8)$$

we obtain for the exponent a

$$a = 0.5 + 0.773\, z/(1 + 2.053z) \qquad (9)$$

For $z > 0$ $\qquad 0.5 \leqq a \leqq 0.877$

The infinity occurring for $z < 0$ has, of course, no physical reality, since from eq. 1b it occurs for $\alpha = 0$. The exponent a becomes zero and the intrinsic viscosity approaches that of a compact spherical particle when $z = -0.28$. This value cannot be taken literally, because the approximations are not valid for such z-values and a compact configuration is sterically impossible. Equation 9 indicates a decrease of the exponent a with decreasing z or T, which is more rapid below than above θ. Figure 4 exhibits the experimental molecular weight dependence of the intrinsic viscosity. Whereas for 36 and 30° the plots are linear, the curvature becomes increasingly pronounced as the temperature is lowered. Figure 5 illustrates the successful application of eq. 7 to data for polystyrene–toluene mixtures at 25°[8] and 30°[9] and cyclohexane solutions at 28°. The parameter A is assumed to have a universal value for all solvents and B is taken from Fig. 2.

Equation 1 suggests the introduction of a reduced temperature difference

$$\tau = z/z_{crit} = (1 - \theta/T)/(1 - \theta/T_c) \qquad (10)$$

neglecting the temperature dependence of b_0/a_0. From eq. 2 and 10 we have

$$[\eta]_\tau/[\eta]_\theta = 1 + K\tau \qquad (11)$$

where K is a constant for a given polymer–solvent system and the left-hand side is therefore constant for a specified value of τ. This is illustrated in Fig. 6. Here as in Fig. 2, systematic deviations appear for low molecular weights. This deviation is strongest at the lowest temperature $T = T_c$, $\tau = 1$, where $|z|$ is largest. The lower portion of Fig. 6 shows the relation of the parameter K to molecular weight. The average value is -0.141.

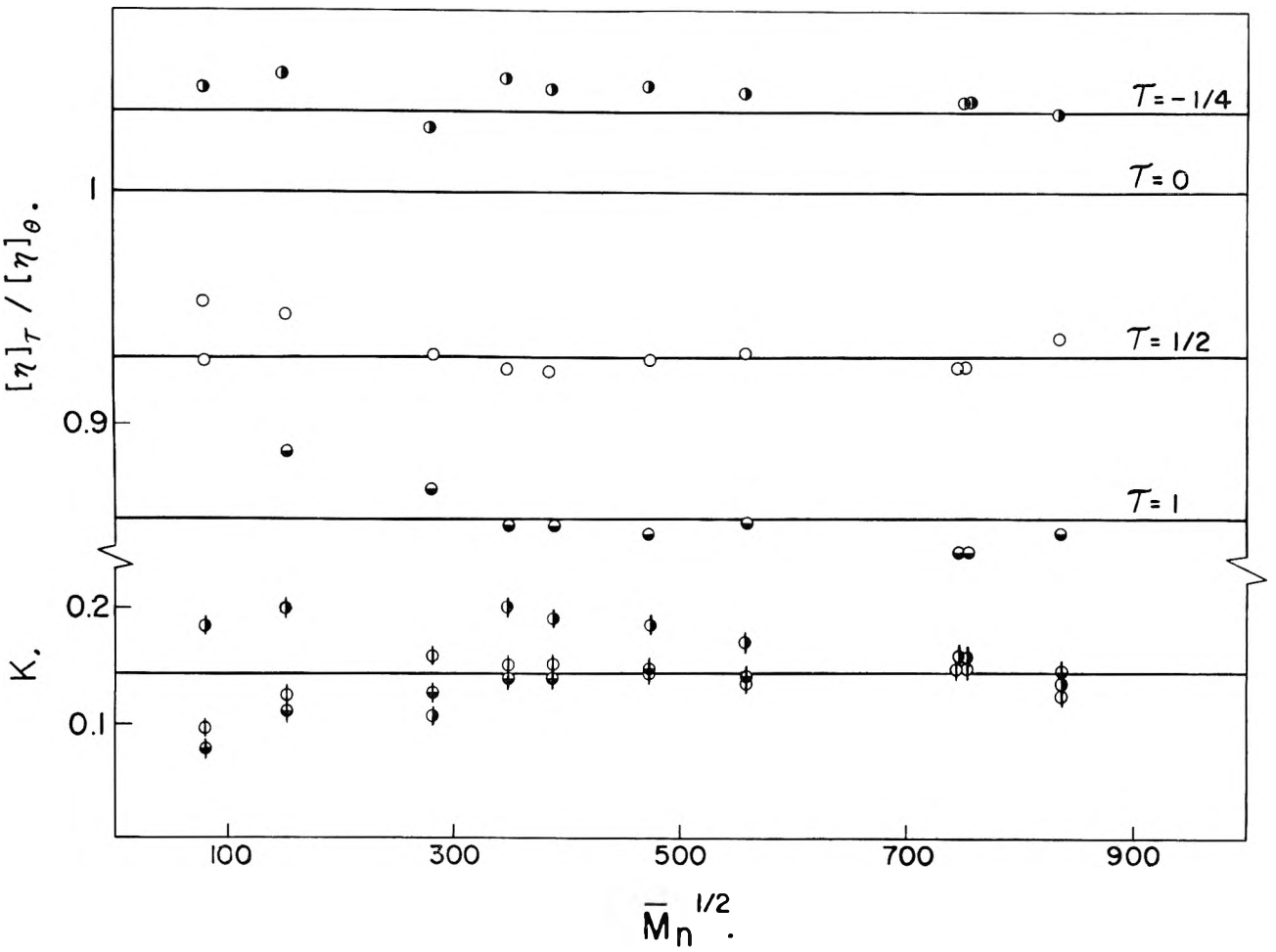

Fig. 6.—Reduced temperature representation of intrinsic viscosities, eq. 10 and 11. The lowest line (points with cross line) indicates the use of the above data for the evaluation of the parameter K.

We have thus examined the validity of eq. 2 and 1 in various ways. The representation in Fig. 6 covers the whole range of molecular weights and temperatures and provides a check on the observed molecular weight dependence of T_c as well as the temperature dependence of $[\eta]$.

We note finally from eq. 10 that $a = 0$ for a reduced temperature $\tau_0 \approx 2$ for both toluene and cyclohexane. Since $T_c/\theta \approx 1$, this would imply that the critical temperature T_c is the arithmetic mean of θ and the hypothetical temperature T_0 at which the intrinsic viscosity becomes molecular weight independent.

Acknowledgment.—The support of this work by grants from the California Research Corporation and the Socony Mobil Oil Company, Inc., is gratefully acknowledged.

THERMODYNAMIC PROPERTIES OF CALCIUM HYDRIDE[1]

By R. W. Curtis and Premo Chiotti

Institute for Atomic Research and Department of Metallurgy, Iowa State University, Ames, Iowa

Received October 31, 1962

The equilibrium hydrogen pressure over a system consisting of calcium and calcium hydride was measured in the temperature range 600–900°. The data below 780° can be represented by log P(atm.) = $-9610/T + 7.346$ and that above 780° by log P(atm.) = $-8890/T + 6.660$. The change in slope at 780° is to be expected on the basis of a solid state transformation existing in calcium hydride. The hydrogen dissociation pressures for the temperature range 600–780° were combined with known thermodynamic data for calcium along with known data on the calcium–hydrogen system to give the following thermodynamic relations: $\Delta F^0_{CaH_2} = -42{,}278 + 31.52T$ (440–780°) and $\Delta F^0_{CaH_2} = -41{,}410 + 24.78T + 1.93T \log T$ (25–440°).

Introduction

Previous work on the calcium–hydrogen system includes the measurement of equilibrium hydrogen pressures over the system consisting of calcium, calcium hydride, and hydrogen by Treadwell and Stecher[2a] and Johnson, *et al.*[2b] The results of their investigations were expressed as

(1) Contribution No. 1236. Work was performed in the Ames Laboratory of the United States Atomic Energy Commission.

(2) (a) W. D. Treadwell and J. Stecher, *Helv. Chem. Acta*, **36**, 1820 (1957); (b) W. C. Johnson, M. F. Stubbs, A. E. Sidwell, and A. Peahukas, *J. Am. Chem. Soc.*, **61**, 318 (1939).

$$\log P_{H_2}\,(\text{atm.}) = \frac{-9840}{T} + 7.32$$

and

$$\log P_{H_2}\,(\text{atm.}) = \frac{-10{,}820}{T} + 8.612$$

respectively, for the temperature range 778–900°. Brönsted[3] measured the dissociation pressure of calcium hydride in the temperature range 641–747°. He obtained from these data a value of −43,900 cal./mole for the room temperature heat of formation of calcium hydride. Brönsted also determined the heat of formation from calorimetric measurements on the heat of solution of calcium and the hydride. These measurements gave a room temperature value of −45,100 cal./mole as the enthalpy of formation. Lewis and Randall,[4] after re-evaluating the difference in heat capacity of the products and reactants for the calcium hydride decomposition, derived an expression for the free energy which was consistent with Brönsted's dissociation pressures and room temperature calorimetric enthalpy. Lewis and Randall point out, however, that the calculated entropy change for the dissociation, 34.6 cal./mole-deg., is probably about 4 entropy units too large.

A study of the allotropic modifications of calcium and the effect of various impurities on the transformations has been carried out by Smith and Bernstein[5] and by Smith, Carlson, and Vest.[6] The phase diagram for the calcium–calcium hydride system has been determined by Peterson and Fattore.[7] These new data and the availability of high purity calcium prompted a reinvestigation of the dissociation pressure of calcium hydride.

Materials and Experimental Procedure

Materials.—The calcium employed in this study was prepared at the Ames Laboratory.[6] The analysis of the metal is given in Table I.

TABLE I

Element	Content (p.p.m.)
Mg	250
C	200
O	~100
N	50
Fe	5
Others	<1

High purity hydrogen was obtained by the decomposition of UH_3.

The crucible material used to contain the calcium–calcium hydride mixture was made from commercial Armco iron containing 165 p.p.m. carbon. A 1-mil steel sheet, which was used to seal the crucible to prevent vaporization of the calcium, was decarburized by heating it with molten calcium in a tantalum crucible for 3 hr. at 875°. The carbon content was reduced from 1000 to 250 p.p.m. by this treatment. Low carbon iron was employed to avoid contamination of the calcium with carbon and as a precaution against the possible formation of methane. The reaction $Fe_3C + 2H_2 \rightarrow 3Fe + CH_4$ is thermodynamically favorable in the lower temperature range of the present investigation and could introduce an appreciable error in the measured equilibrium hydrogen pressure.

Apparatus.—The apparatus used was similar to the apparatus employed by Woerner.[8] In order to study the dissociation pressure of the hydride it was necessary to seal the sample inside an iron crucible fitted with a thin iron diaphram. The diaphram, made from one mil iron sheet, is impervious to calcium vapor but pervious to hydrogen. A similarly sealed crucible was employed by Johnson, *et al.*[2b] They point out that the reaction of calcium vapor with quartz caused erroneous results in the measured hydrogen pressure. The iron crucibles, 2 in. long by 0.5 in. inside diameter, were made from 0.75 in. Armco iron rod. The iron diaphram was held in place by a tapered sleeve of Armco iron. The sleeve with an outside taper of 6 mils/in. equal to the taper cut in the top of the iron crucible, was forced down in a hydraulic press to form a gas-tight seal against the iron foil diaphram. This operation was carried out with the crucible assembly under an atmosphere of hydrogen.

The apparatus used in measuring the equilibrium hydrogen pressures was constructed of Pyrex with the exception of a reaction tube and a tube containing uranium hydride which were both constructed of quartz. The stopcocks used in the apparatus were of the high vacuum, hollow plug, oblique bore type. The vacuum system consisted of a mechanical pump, a mercury diffusion pump, and a liquid nitrogen cold trap. A vacuum of 3×10^{-6} mm. was obtained with this system. The hydrogen pressure was measured with a McLeod gage. The gage reading R in centimeters was related to the pressure in atmospheres by the relation

$$P\,(\text{atm.}) = 3.425 \times 10^{-6} R^2$$

A McLeod gage reading of 1 cm. was the lowest pressure considered. At this pressure the leak rate of the system was negligible. No change in the McLeod gage reading could be detected after periods as long as 3 days.

Experimental Procedure.—The Armco iron crucible was outgassed at 900° for 12 hr. under a vacuum of 1×10^{-5} mm. The crucible was removed from the apparatus and a 2-g. sample of calcium was sealed inside the crucible under a hydrogen atmosphere.

The crucible and its contents were placed in the quartz reaction tube, the apparatus was evacuated and then isolated from the pumping system. The uranium hydride was heated until the amount of hydrogen admitted was just enough to convert about half of the calcium to CaH_2. The reaction tube was heated by means of a one inch split type resistance furnace to approximately 700° to permit the calcium to react with the hydrogen. The temperature of the furnace was controlled to ±0.5° by means of a proportional band temperature controller. After a constant pressure was attained, the system was evacuated and held at the same temperature until the pressure remained constant for 12 hr. In all cases the pressure returned to the same equilibrium value. The amount of hydrogen removed during the time the system was evacuated was small compared to the total amount of hydrogen originally admitted to the system. The time to attain equilibrium varied from 16 hr. at 888° to 2 days at 596°. After the pressure remained constant for a period of 8 to 12 hr. the system was assumed to be at equilibrium. It was found that the equilibrium pressures were not dependent on whether the equilibrium was approached from higher or lower pressures.

Results

The measured equilibrium hydrogen pressures are plotted as open circles in Fig. 1. Data from previous investigations are included for comparison only. It is apparent from these data that a change in slope exists at about 780°. This is to be expected on the basis of the solid state transformation shown on the calcium–calcium hydride phase diagram, Fig. 2. A least squares treatment of the data for the temperature range 578–780° gives the equation

$$\log P_{H_2}\,(\text{atm.}) = \frac{-9610}{T} + 7.346$$

The standard deviations are 134 and 0.146 for the slope

(3) J. N. Brönsted, *Z. Elektrochem.*, **20**, 81 (1914).
(4) G. N. Lewis and M. Randall, "Thermodynamics," McGraw-Hill Book Co., Inc., New York, N. Y., 1923, p. 473.
(5) J. F. Smith and B. T. Bernstein, *J. Electrochem. Soc.*, **106**, 448 (1959).
(6) J. F. Smith, O. N. Carlson, and R. W. Vest, *ibid.*, **103**, 409 (1956).
(7) D. T. Peterson and V. G. Fattore, *J. Phys. Chem.*, **65**, 2062 (1961).
(8) P. F. Woerner, Ph.D. thesis, Iowa State University of Science and Technology, 1960.

and intercept, respectively. The data for the temperature range 780–900° were fitted to the best straight line which intersects at 1053°K. (780°) the line represented by the above equation. The relation obtained is

$$\log P_{H_2}\,(\text{atm.}) = \frac{-8890}{T} + 6.66$$

The standard free energy change for the reaction

$$Ca(\beta) + H_2 \longrightarrow CaH_2(\alpha)$$

may be represented by the relation

$$\Delta F^0_{CaH_2} = RT \ln a_{Ca} - RT \ln a_{CaH_2} + RT \ln P_{H_2} \quad (1)$$

As indicated by this equation it is necessary to know the equilibrium activity of calcium and the activity of calcium hydride as well as the experimentally determined equilibrium hydrogen pressures to obtain the thermodynamic properties of CaH_2. The equilibrium activities may be estimated from the phase diagram. The phase diagram determined by Peterson and Fattore[7] yields the data given in Table II.

TABLE II

COMPOSITION OF CALCIUM-RICH PHASE IN EQUILIBRIUM WITH CALCIUM HYDRIDE

Temp., °C.	N_{Ca}	N_{H_2}
615	0.93	0.07
650	.92	.08
655	.91	.09
715	.89	.11
733	.87	.13
760	.86	.14
775	.83	.17

These data and the assumption that Sievert's law is valid permit the calculation of the activity of calcium, see Appendix 1. The calculated activities are given in Fig. 3. The average composition of the CaH_2-rich phase for the temperature range 200 to 780° was estimated from Fig. 2 and Treadwell and Stecher's data to be 95 mole % CaH_2. The corresponding activity for CaH_2 was taken to be 0.95. Calculated values of the equilibrium constant

$$K = \frac{a_{CaH_2}}{a_{Ca} P_{H_2}}$$

for the temperature range 578 to 780° are plotted in Fig. 4 as log K *vs.* $(10^4/T)$°K.$^{-1}$. A least squares treatment of these data yields the relation

$$\log K = \frac{9241}{T} - 6.890 \quad (2)$$

Consequently, for the reaction

$$Ca(\beta) + H_2 \longrightarrow CaH_2(\alpha)$$

$$\Delta F^0_{CaH_2} = -RT \ln K = -42{,}278 + 31.52T \quad (3)$$

The probable errors in the two constants were calculated to be 440 and 0.46, respectively. It was not possible to take ΔC_p for the reaction into account due to the lack of heat capacity data for calcium hydride. The difference in heat capacities in the temperature range of the measurements is probably very small. An additional error will be introduced by the assumption that ΔC_p is zero in calculating values for the thermodynamic

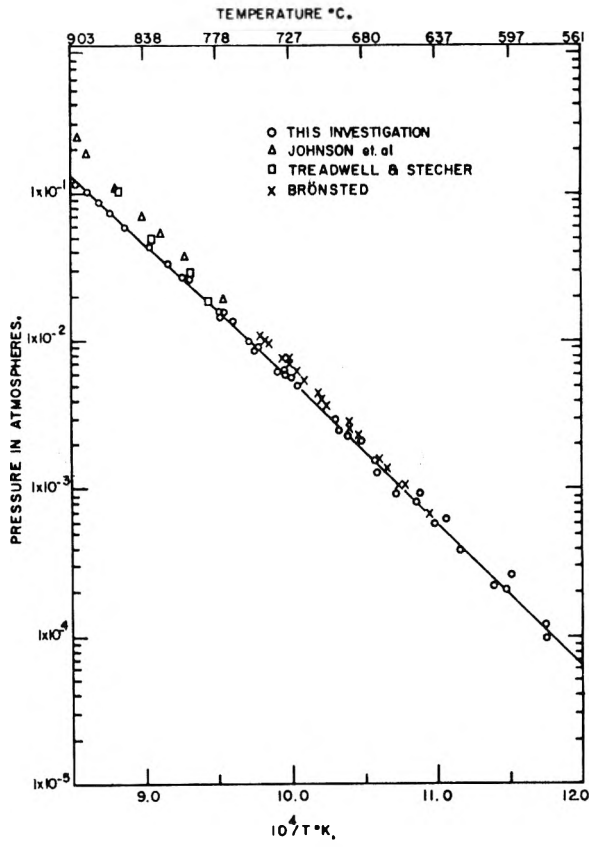

Fig. 1.—Equilibrium hydrogen pressure measured over calcium–calcium hydride as a function of temperature.

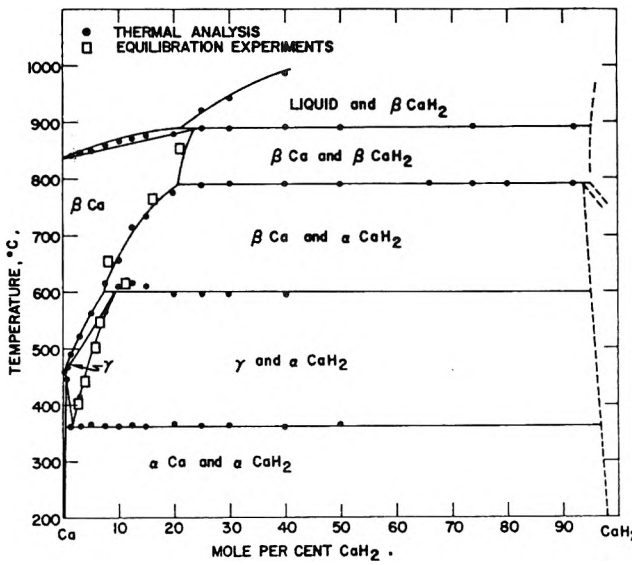

Fig. 2.—Calcium–calcium hydride phase diagram (after Peterson and Fattore[7]).

properties of CaH_2 for the temperature range 25 to 440° as outlined below. Because of this uncertainty only an average value for the difference in the heat capacity for the two forms of calcium was employed in the calculations.

Kelley[9] reports a value of 270 cal./mole for the 440° transformation $Ca(\alpha) \rightarrow Ca(\beta)$ and $5.25 + 3.44 \times 10^{-3}T$ and $2.68 + 6.80 \times 10^{-3}T$ for the heat capacity of α-calcium and β-calcium, respectively. From these data the average value of ΔC_p in the temperature range 298–713°K. was calculated to be −0.84 cal./deg. This average value of ΔC_p and the above enthalpy value

(9) K. K. Kelley, Bulletin 476, Bureau of Mines, U. S. Department of the Interior, Washington, D. C.

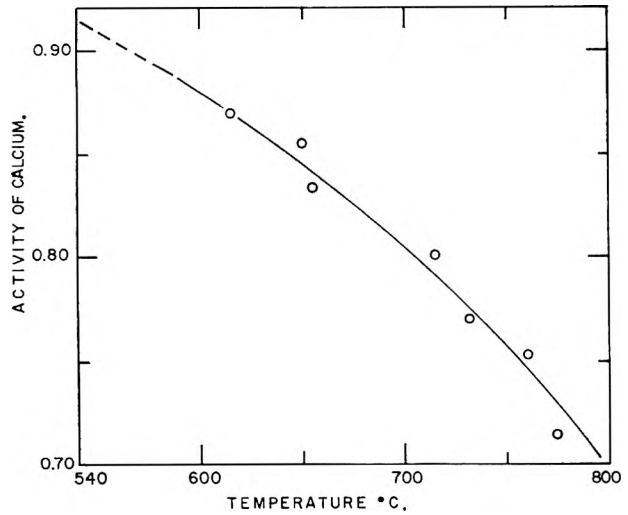

Fig. 3.—Activity of calcium, calculated from solubility data of Peterson and Fattore, as a function of temperature.

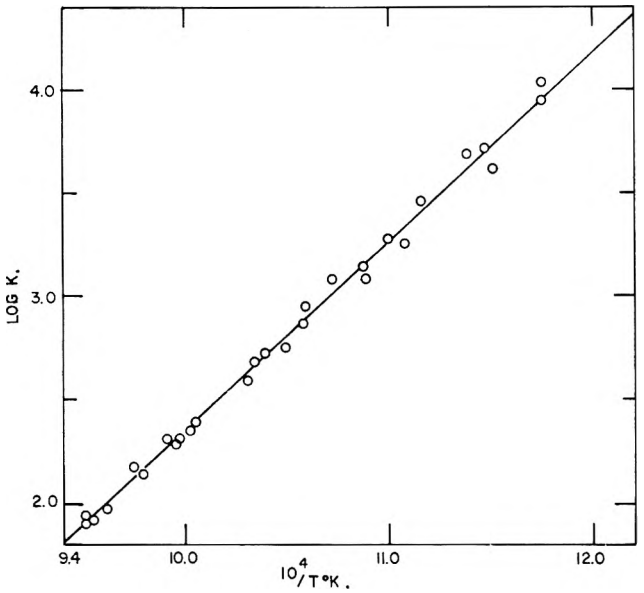

Fig. 4.—Logarithm of the equilibrium constant for the reaction $Ca(\beta) + H_2(P_{eq}) \rightarrow CaH_2(\alpha)$ as a function of temperature.

for the transformation were employed with eq. 3 to obtain

$$\Delta F^0_{CaH_2} = -41{,}410 + 24.78T + 1.93T \log T \quad (25\text{–}440°) \quad (4)$$

for the reaction

$$Ca(\alpha) + H_2(1 \text{ atm.}) \longrightarrow CaH_2(\alpha)$$

Values of ΔF^0, ΔH^0, and ΔS^0 of formation of CaH_2 at various temperatures are given in Table III.

TABLE III

FREE ENERGY, ENTHALPY, AND ENTROPY OF FORMATION OF CaH_2

Temp., °C.	$-\Delta F^0$, cal./mole	$-\Delta H^0$, cal./mole	$-\Delta S^0$, cal./deg. mole
25	32,610	41,650	30.4
400	21,060	41,970	31.1
500	17,910	42,280	31.5
600	14,760	42,280	31.5
700	11,610	42,280	31.5

The hydrogen pressure data obtained in the temperature range 780 to 890° permits an estimate to be made for the enthalpy or free energy change for the transformation of calcium hydride

$$CaH_2(\alpha) \longrightarrow CaH_2(\beta)$$

The phase diagram, Fig. 2, shows that the composition of the calcium hydride phase in the temperature range 780 to 890° is approximately constant at 95 mole % CaH_2, while a mean composition of the calcium-rich phase is approximately 22 mole % calcium. The activity of calcium was calculated to be 0.695 by the method described above, and the activity of CaH_2 was taken to be 0.95. The standard free energy of formation for $CaH_2(\beta)$ can be expressed as

$$\Delta F^0 = -RT \ln \frac{0.95}{0.695} + RT \ln P_{H_2} \quad (5)$$

The experimentally determined hydrogen pressure

$$\log P_{H_2} = \frac{-8890}{T} + 6.660$$

may be substituted in eq. 5 to give

$$\Delta F^0(CaH_2\beta) = -40{,}672 + 29.85T \quad (6)$$

This relation subtracted from eq. 3 gives

$$\Delta F^0 = 1606 - 1.67T \quad (7)$$

for the transformation of α-CaH_2 to β-CaH_2. The transformation temperature calculated from this equation is 961°K. or 688°. This temperature for the transformation of pure CaH_2 is only a rough approximation. The enthalpy change of 1600 cal./mole is probably fairly realistic.

Discussion

The value of 30.4 obtained for the standard entropy of formation of CaH_2 at 298°K. agrees well with the value predicted by Lewis and Randall.[4] It is very unlikely that this entropy value can be in error by more than ±1.5 entropy units. The uncertainty in the entropy determined from eq. 3 for the temperature range 578–780° is calculated from a least squares treatment of the data to be ±0.46 entropy unit. The probable error in the enthalpy for the same temperature range is similarly calculated to be ± 0.44 kcal. The standard free energy of formation values in Table III are estimated to be within 2% of the true values. The thermodynamic values were calculated on the basis of the data taken in the temperature range 578–780°; however, pressure measurements were also made in the temperature range 780–900°. These data along with data obtained by other investigators are shown in Fig. 1. The pressures in the higher temperature range were found to be lower than those reported by Treadwell and Stecher[2a] and Johnson, *et al.*[2b] Since calcium metal is often contaminated with magnesium, this discrepancy may be due to magnesium in the calcium used in their investigations. Johnson, *et al.*,[2b] report that their starting material was 97.12% calcium as determined by an oxylate precipitation. After a double distillation the analysis of their metal was 99.5% calcium. The method of analysis may not, however, give a true indication of the amount of magnesium present since magnesium may have been coprecipitated with the calcium. Treadwell and Stecher[2a] give no specific analysis of the

calcium employed but do state that the calcium was doubly distilled. Brönsted[3] measured the dissociation pressure of calcium hydride in the temperature range 641–745°. The pressures obtained by Brönsted agree quite well with those obtained in this investigation. However, the slope of the line obtained from a plot of log P_{H_2} (atm.) *vs.* $10^4/T$°K. from Brönsted's data is slightly different from that obtained in this investigation. The fact that the metal used in his investigation only analyzed 97.3% calcium could have caused this deviation.

Appendix 1

According to Sievert's law diatomic gases dissolve atomically in metals. In the case of the dissolution of hydrogen in calcium Treadwell and Stecher's data[2a] indicate that this is true. This being the case it is possible to relate the equilibrium hydrogen pressure, mole fraction of hydrogen, N_H, in the calcium-rich phase and the activity of hydrogen as

$$a_{H_2} = P_{H_2} = kN_H^2$$

Then according to the Gibbs–Duhem equation

$$N_{Ca}\, d \ln a_{Ca} = -N_{H_2}\, d \ln a_{H_2} = -N_{H_2}\, d \ln kN_H^2$$

At a given temperature k remains constant and N_H in terms of the variables N_{Ca} and N_{H_2} is given by the relation

$$N_H = \frac{2N_{H_2}}{N_{H_2} + 1}$$

The Gibbs–Duhem equation can therefore be written as

$$d \ln a_{Ca} = \frac{-2N_{H_2}}{1 - N_{H_2}}\, d \ln \frac{2N_{H_2}}{N_{H_2} + 1}$$

Integration of this relation with the condition that $a_{Ca} \to 1$ as $N_{Ca} \to 1$ yields the relation

$$a_{Ca} = \frac{N_{Ca}}{2 - N_{Ca}}$$

Utilizing the data in Table II the activity of calcium can be calculated.

THERMOCHEMICAL STUDIES. VII.[1] HEATS AND ENTROPIES OF STEPWISE NEUTRALIZATION OF PIPERAZINE AND TRIETHYLENETETRAMINE

BY PIERO PAOLETTI, MARIO CIAMPOLINI, AND ALBERTO VACCA

Istituto di Chimica Generale e Inorganica dell'Università di Firenze, Firenze, Italy

Received November 1, 1962

The results of a calorimetric investigation of the stepwise heat of neutralization for piperazine and triethylenetetramine in 0.1 *M* KCl at 25° are here reported and discussed. The pK values of the piperazine were also measured under the same experimental conditions. For some polyethylenepolyamines containing secondary and primary nitrogen atoms, a linear relationship is found between the heat or entropy of the first neutralization stage and the percentage of secondary nitrogen atoms.

Introduction

As a part of a calorimetric investigation on the heats of reaction of some polyethylenepolyamines with hydrogen ion[2] or with transition metal ions,[1] we have now measured the heats of stepwise neutralization of piperazine (pip) and triethylenetetramine (trien). For these two bases, values of the enthalpy changes derived from the variation of the basicity constants with the temperature are reported in the literature,[3,4] but it is recognized that this method can seldom give figures as accurate as those measured directly.

The calorimetric measurements were carried out in 0.1 *M* KCl at 25°.

Experimental

Materials.—Commercially available piperazine (Fluka) was twice recrystallized from light petroleum. Pure triethylenetetramine was obtained as previously described.[1] These bases were analyzed by potentiometric titrations against *ca.* 1.5 *N* hydrochloric acid and proved to be 99.9 and 99.8% pure, respectively. This same hydrochloric acid was standardized gravimetrically as silver chloride and used also in the measurements of the heats of neutralization. The solution of the amines in a carbon dioxide-free 0.1 *M* KCl were prepared according to the procedure previously described.[2]

Calorimetric Measurements.—The calorimeter and the experimental technique used has already been described.[2] At the end of the reaction the temperature was in the range 24.8–24.9° and no attempt was made to correct the heat value to 25°. The ionic medium used was the 0.1 *M* KCl solution.

Acid Dissociation Constants.—pH measurements were made using a Radiometer Model 4 pH meter equipped with saturated calomel and glass electrodes; 1.5 *N* hydrochloric acid was added to the solution of the base. The solution was stirred continuously and the temperature was kept constant at 25.0 ± 0.1°.

Results

The stepwise heats of neutralization were determined by measuring the heats evolved for different hydrochloric acid–amine ratios and by calculating the exact amount of the protonated forms of the polyamines before and after the reaction. The concentration equilibrium constants used with triethylenetetramine were those of Schwarzenbach[5] in 0.1 *M* KCl at 20° corrected to 25° using our ΔH values. For piperazine at 25° the values of pK_1 (9.72) and pK_2 (5.60) are in excellent agreement with those of Schwarzenbach, *et al.*,[6] (corrected to 25°) in 0.1 *M* $NaNO_3$, pK_1 = 9.69 and pK_2 = 5.59, as well as with the thermodynamic ones of Pagano, Goldberg, and Fernelius,[4] pK_1 = 9.79 and pK_2 = 5.59.

The experimental details of the calorimetric measurements are reported in Table I. The third column lists

(1) Part VI, L. Sacconi, P. Paoletti, and M. Ciampolini, *J. Chem. Soc.*, 5115 (1961).

(2) M. Ciampolini and P. Paoletti, *J. Phys. Chem.*, **65**, 1224 (1961).

(3) H. B. Jonassen, R. B. LeBlanc, A. W. Meibohm, and R. M. Rogan, *J. Am. Chem. Soc.*, **72**, 2430 (1950).

(4) J. M. Pagano, D. E. Goldberg, and W. C. Fernelius, *J. Phys. Chem.*, **65**, 1062 (1961).

(5) G. Schwarzenbach, *Helv. Chim. Acta*, **33**, 974 (1950).

(6) G. Schwarzenbach, B. Maissen, and H. Ackermann, *ibid.*, **35**, 2333 (1953).

the heat evolved in each run, corrected for the heat of dilution of hydrochloric acid. The last column reports the calculated correction for the heat effect due to the neutralization of hydroxyl ions which arise from the basic dissociation of the amines.

TABLE I

CALORIMETRIC DATA FOR THE SYSTEMS POLYAMINE + HCl

Base	Base, 10^{-5} mole	HCl, 10^{-5} mole	Q, cal.	$Q_{cor.}$[a] cal.
Piperazine	2696	2692	275.7	12.0
(vol., 946 ml.)	2723	2718	279.6	12.1
	2895	2892	296.9	12.5
	3031	1516	263.8	9.0
	2900	1469	254.2	8.8
	3262	1634	283.6	9.3
Triethylenetetramine	2917	2925	326.4	16.1
(vol., 928 ml.)	2952	2960	330.2	16.1
	2910	2905	324.3	16.1
	1475	2950	329.4	11.7
	1449	2905	324.6	11.6
	1458	2907	324.9	11.6
	967	2914	309.2	9.3
	988	2970	316.4	8.7
	986	2973	314.7	9.6
	749	3942	287.0	8.3
	716	3902	275.4	8.1
	709	3736	272.6	8.0

[a] This term is to be subtracted from the corresponding Q value.

Table II reports the values of the thermodynamic functions $-\Delta F$, $-\Delta H$, and ΔS relative to the successive reaction stages.

TABLE II

THERMODYNAMIC FUNCTIONS FOR THE SUCCESSIVE NEUTRALIZATION STAGES OF POLYAMINES AT 25°

	$-\Delta F$, kcal./mole	$-\Delta H$, kcal./mole	ΔS, e.u.
pip + $H^+ \rightarrow$ pipH^+	13.26	10.17	10.3
pipH^+ + $H^+ \rightarrow$ pipH_2^{2+}	7.64	7.12	1.8
trien + $H^+ \rightarrow$ trienH^+	13.34	11.01	7.8
trienH^+ + $H^+ \rightarrow$ trienH_2^{2+}	12.36	11.27	3.7
trienH_2^{2+} + $H^+ \rightarrow$ trienH_3^{3+}	8.93	9.53	− 2.0
trienH_3^{3+} + $H^+ \rightarrow$ trienH_4^{4+}	4.42	6.83	− 8.1

The values of ΔF have been calculated from the formula $\Delta F = -RT \ln K$, where K is the concentration equilibrium constant. This procedure involves the assumption that the ratios $[\gamma_{H^+} \cdot \gamma_{BH_{(n-1)}^{(n-1)+}} / \gamma_{BH_n^{n+}}]$ are taken as unity with respect to standard states in 0.1 M KCl. For piperazine this procedure is valid, as is shown by the extremely good agreement between the concentration equilibrium constants and the thermodynamic values. For triethylenetetramine this may not be the case especially for the last stages of protonation. Therefore ΔF and ΔS thus calculated may be affected by an error of uncertain size. Nevertheless it is likely that for the first stages of neutralization the uncertainities are negligible with respect to experimental error. The $-\Delta F_3$ and $-\Delta F_4$ values as well as the corresponding ΔS_3 and ΔS_4 values may therefore be too high. For example applying the Debye–Hückel theory to the results obtained for the systems ethylenediamine–H^+ and hexamethylenediamine–H^+ by Everett and Pinsent[7] a value of *ca.* 3 Å. for the mean distance of approach[8] was obtained. Using this value for triethylenetetramine the following values were obtained: $\Delta F_3 = -8.26$; $\Delta F_4 = -3.40$ kcal./mole and $\Delta S_3 = -4.3$; $\Delta S_4 = -11.5$ e.u.

The accuracy of the over-all heat of neutralization is of the same order of magnitude as the reproducibility of the calorimetric measurements, *i.e.*, better than ± 0.2%. On the contrary the values of the stepwise neutralization are less accurate as they depend on the values of the basicity constants used.

Discussion

The heat evolved in the first neutralization stage of piperazine (10.17 kcal./mole) is lower than that of ethylenediamine (11.92 kcal./mole),[9] while the entropy change (10.3 e.u.) is higher than that of ethylenediamine (5.7 e.u.).[9] This fact falls in line with what has already found for the aliphatic monobasic amines, *i.e.*, a primary amine exhibits a lower heat of neutralization but a higher entropy change than a secondary amine.[10]

For triethylenetetramine and diethylenetriamine which contain both secondary and primary nitrogen atoms the thermodynamic quantities of first neutralization $-\Delta H_1$ and ΔS_1 appear to be a linear function of the percentage of secondary nitrogen atoms. To illustrate this we have plotted in Fig. 1 the values of $-\Delta H_1$ and ΔS_1 for ethylenediamine,[9] diethylenetriamine,[2] triethylenetetramine and piperazine against the ratio of the number of secondary nitrogen atoms to the total number of nitrogen atoms; the points lie on two straight lines. Such a linear relationship leads to the conclusion that both the monoprotonated ions denH^+ and trienH^+ exist in two tautomeric forms, one salted in the primary and the other in the secondary nitrogen atoms, in almost statistical ratio. It may be stated, therefore, that the basicities of the primary and secondary amine-groups in these neutral polyethylenepolyamines are nearly the same, as happens with the aliphatic monoamines.[10]

For piperazine the $-\Delta H_2$ value is 3.07 kcal./mole lower than the $-\Delta H_1$ value, whereas for ethylenediamine the difference is only 1.7 kcal./mole.[9] This fact may be regarded as due to the weaker electrostatic repulsion between the positive poles which in the pipH_2^{2+} ion (predominantly in the chair form) are closer than in the enH_2^{2+} ion (predominantly in the *trans* form).

For triethylenetetramine $-\Delta H_2$ is greater than $-\Delta H_1$ in analogy with what was found for diethylenetriamine. This may mean that in the second stage of neutralization the fraction of primary amino groups that are being protonated is greater than in the first stage with the consequent greater evolution of heat. The structures of the diammonium ions would be

$^+H_3N \cdot CH_2 \cdot CH_2 \cdot NH \cdot CH_2 \cdot CH_2 \cdot NH \cdot CH_2 \cdot CH_2 \cdot NH_3^+$ (I)

$^+H_3N \cdot CH_2 \cdot CH_2 \cdot NH \cdot CH_2 \cdot CH_2 \cdot NH_2^+ \cdot CH_2 \cdot CH_2 \cdot NH_2$ (II)

(7) D. H. Everett and B. R. W. Pinsent, *Proc. Roy. Soc.* (London), **A215**, 416 (1952).

(8) H. S. Harned and B. B. Owen, "The Physical Chemistry of Electrolytic Solutions," 3rd Ed., Reinhold Publ. Corp., New York, N. Y., 1958, Chapter 2.

(9) T. Davies, S. S. Singer, and L. A. K. Staveley, *J. Chem. Soc.*, 2304 (1954).

(10) *Cf.*, D. H. Everett and W. F. K. Wynne-Jones, *Trans. Faraday Soc.*, **35**, 1380 (1939).

The structures with two adjacent charges would be much less probable due to electrostatic repulsion. Confirmation of the form (II) is supplied by the lower $-\Delta H_{1-2}$ value for the trien (22.30 kcal./mole) as compared to that of diethylenetriamine (23.15 kcal./mole). In fact if only form (I) did exist one would expect a greater heat of formation for trienH_2^{2+} than for denH_2^{2+}, due to the lower electrostatic repulsion.

The low $-\Delta H_3$ value (9.50 kcal./mole) may be attributed to the preferential protonation of the secondary nitrogen and a greater electrostatic repulsion of the positive charges. These two factors may also account easily for the sequence $-\Delta H_3$ (trien) > $-\Delta H_3$ (den) > $-\Delta H_4$ (trien).

The entropy changes for the first neutralization stage are positive whereas those for the successive steps decrease till they become negative. Such a trend has already been found for the neutralization of ethylenediamine and diethylenetriamine[2] and for other stepwise reactions as the formation of metal complexes with neutral[1,11] or anionic ligands.[12]

(11) M. Ciampolini, P. Paoletti, and L. Sacconi, *J. Chem. Soc.*, 4553 (1960).

(12) J. K. Kury, A. D. Paul, L. C. Hepler, and R. E. Comick, *J. Am. Chem. Soc.*, **81**, 4185 (1959); P. K. Gallagher and E. L. King, *ibid.*, **82**, 3510 (1960).

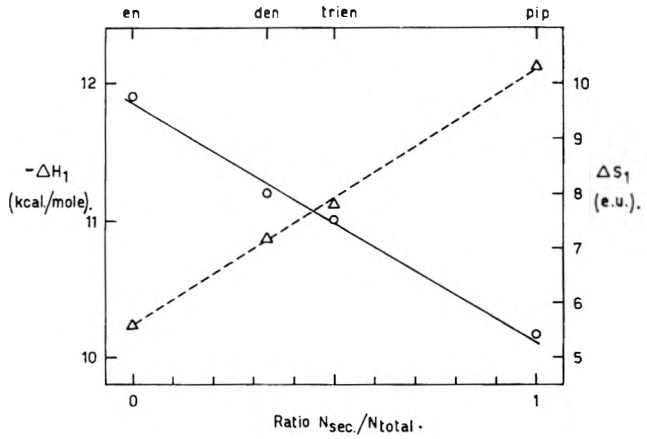

Fig. 1.—Plot of $-\Delta H_1$ (○) and ΔS_1 (△) against the ratio of the number of secondary nitrogen atoms to the total number of nitrogen atoms.

Acknowledgments.—The authors are indebted to Prof. L. Sacconi for helpful suggestions and criticism. Acknowledgment is made to the Italian "Consiglio Nazionale delle Ricerche" for the support of this research.

CHARGE TRANSFER INTERACTION BETWEEN IODINE AND AZINES: IONIZATION POTENTIALS OF AZINES[1]

BY V. G. KRISHNA[2] AND MIHIR CHOWDHURY

Whitmore Chemical Laboratory, The Pennsylvania State University, University Park, Pennsylvania

Received November 1, 1962

Charge transfer data on four azine–iodine complexes are reported. Azines are shown to be *n*-donors toward iodine. The trend of the charge transfer maxima indicates that the experimentally observed ionization potentials of the azines correspond to π-electron ionization.

Introduction

The following note will be concerned with the complexes formed between iodine and monocyclic azines: pyridine, pyrimidine, pyrazine and *s*-triazine. The aspects considered are (1) the perturbation of the visible band of iodine and the ultraviolet and infrared spectra of donor, (2) the equilibrium constants of the molecular complexes formed, and (3) the energy and extinction coefficient of the charge transfer (CT) bands.

Previous studies[3-5] have indicated that the N-heterocyclics are *n*-donors toward iodine. In the first two[3,4] a thorough investigation of the pyridine–iodine complex and in the third[5] the electron donating properties of substituted monoazines have been reported. The *n*-donor properties of monoazines are indirectly perturbed by the π-electronic structure.[6] In the present case of polyazines, in addition to the variation of the π-electronic structure,[7,8] the interaction of the *n*-orbitals also changes markedly[9] and the *n*-donor properties of these molecules should reflect both these changes.

An important aspect of this investigation is its relation to the ionization potentials of azines. The experimentally observed[10-11] ionization potentials of azines have received a varied interpretation by different authors as due to *n*-[10-13] and π-electron[7,14] ionizations. A more unambiguous interpretation is needed before the ionization potential data could be used as an experimental criterion for various theoretical models proposed for N-heterocyclics. In the following investigation an attempt will be made to resolve this ambiguity through the use of charge transfer data.

A linear relation between the charge transfer maxima and the ionization potentials of the donors in a series of molecular complexes with a common acceptor has been established.[15,16] Since the azines are *n*-donors toward

(1) This investigation was supported by a grant from the Air Force Office of Scientific Research to the University.

(2) Institute of Molecular Biophysics, The Florida State University, Tallahassee, Florida; from whom reprints can be obtained.

(3) C. Reid and R. S. Mulliken, *J. Am. Chem. Soc.*, **76**, 3869 (1954).

(4) E. K. Plyler and R. S. Mulliken, *ibid.*, **81**, 823 (1959).

(5) J. Nag-Chaudhuri and S. Basu, *Trans. Faraday Soc.*, **55**, 898 (1959).

(6) H. C. Longuet-Higgins, *J. Chem. Phys.*, **18**, 275 (1950).

(7) N. Mataga and K. Nishimoto, *Z. physik. Chem.* (Frankfurt), **13**, 140 (1957).

(8) R. McWeeny and T. E. Peacock, *Proc. Phys. Soc.* (London), **A70**, 41 (1957).

(9) L. Goodman, *J. Mol. Spectry.*, **6**, 109 (1961).

(10) I. Omura, H. Baba, K. Higasi, and Y. Kanaoka, *Bull. Chem. Soc. Japan*, **30**, 633 (1957).

(11) K. Higasi, I. Omura, and H. Baba, *J. Chem. Phys.*, **24**, 623 (1956).

(12) T. Nakajima and A. Pullman, *J. chim. phys.*, **55**, 793 (1958).

(13) K. Watanabe, T. Nakayama, and J. Mottl, quoted in ref. 14.

(14) M. A. El-Sayed, M. Kasha, and Y. Tanaka, *J. Chem. Phys.*, **34**, 334 (1961).

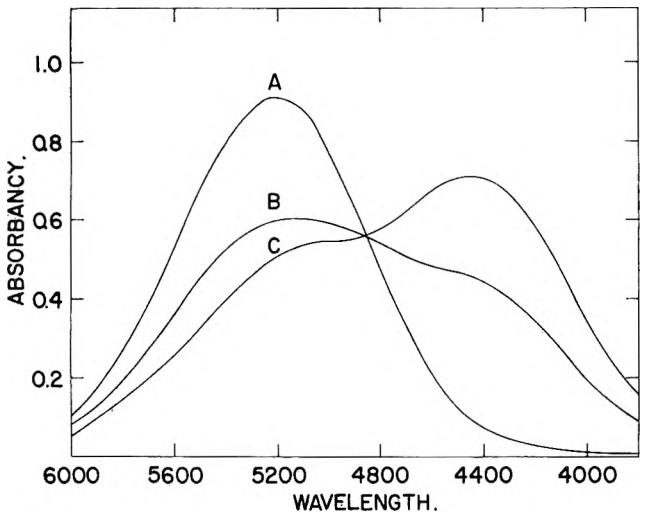

Fig. 1.—Perturbation of the 520 mμ iodine band by pyrazine. Concentration of iodine, $5.06 \times 10^{-4} M$; concentration of pyrazine: (A) 0; (B) $4.11 \times 10^{-2} M$; (C) $9.50 \times 10^{-2} M$. Cyclohexane is used as solvent.

iodine, the trend in CT maxima of the azine–iodine complexes should indicate the trend of *n*-ionization potentials of azines.

Experimental

A. Materials.—Absorption spectra were recorded on Warren Electronics, Inc., Spectrocord with fused silica cells of optical path 2.0 and 0.1 cm. The latter cells were used to investigate the CT bands and the perturbation of the donor bands with excess iodine. The rest of the absorption measurements were carried out with 2.0-cm. cells. All measurements were performed at room temperature. Infrared spectra were measured with Perkin–Elmer Model 21 spectrophotometer.

Matheson, Coleman and Bell Spectroquality cyclohexane was used as solvent without further purification. The azines used were pyridine (Eastman Kodak, Spectrograde), pyrazine (Aldrich Chemicals), pyrimidine (Nutritional Biochemicals), and *s*-triazine. The sample of *s*-triazine was previously obtained as a gift from Dr. R. C. Hirt of American Cyanamid Company. Pyridazine was found unsuitable for investigation: pyridazine–iodine solutions developed turbidity rapidly.

B. Procedures. 1. Shifted Iodine Band and *K* Values.—Visible spectra of cyclohexane solutions with fixed concentration of iodine but different amounts of donor were recorded with cyclohexane as blank. The equilibrium constants listed in Table I were calculated–assuming a 1:1 complex—from the decrease in optical density at 520 mμ. Any absorption due to the shifted iodine band at 520 mμ could be corrected because of its Gaussian shape.[17] Each *K* in Table 1 is an average of values on fifteen different solutions, except in the case of *s*-triazine, where it is an average of only two values.

The ϵ_{max} of shifted iodine bands were obtained from the optical density at the band maximum and the concentration of the complex.

2. CT Bands.—The CT bands of azine–iodine complexes were found in the spectral region where both donor and acceptor have considerable absorption (Fig. 2). For obtaining the wave lengths and extinction coefficients of CT bands a procedure similar to that of Reid and Mulliken[3] was used. Spectra of cyclohexane solutions with excess of donor and small amounts of iodine were recorded; cyclohexane solutions with an equal amount of donor were used as blanks. The absorption due to uncomplexed iodine was subtracted to get the absorption of azine–iodine complex. Since the light intensities reaching the phototube were low due to the donor absorption, high gain settings were used.

CT band maxima could be located with the same accuracy as in the ordinary ultraviolet spectral measurements. However the extinction coefficients measured by this procedure could not be accurate. An error of 25% was estimated.

CT spectra of three different solutions were recorded for each azine. The CT bands of *s*-triazine could not be detected.

3. Perturbation of Donor Bands.—The perturbation of the $n \rightarrow \pi^*$ bands and the first $\pi \rightarrow \pi^*$ bands of the donor was studied by measuring the absorption of the donors in a concentrated iodine solution against an iodine blank of an equal concentration. Donor to iodine ratio was 1:60 for $n \rightarrow \pi^*$ absorption at 330 mμ and 1:10 for $\pi \rightarrow \pi^*$ absorption at 260 mμ. Absorption of iodine at shorter wave lengths permitted only ten times excess of iodine in the region of $\pi \rightarrow \pi^*$ spectra.

Discussion

The Shifted Iodine Band.—Iodine in non-polar solvents shows a visible band with the maximum at 520 mμ. In presence of the donors this band undergoes a blue shift. A few spectra of the pyrazine–iodine system are presented in Fig. 1. Since the rest of the spectra are similar they will not be reproduced.

Table I shows that the blue shift of the visible band of iodine on complexation follows the order of the *K* values of the complexes and the pK_a values of the donors. However neither the $n \rightarrow \pi^*$ nor the $\pi \rightarrow \pi^*$ absorption of the donors showed any perturbation with excess of iodine concentration.[18] The infrared spectra of pyrazine ($\backsim 0.2 M$) in carbon tetrachloride between 3 and 15 μ showed very little perturbation with iodine concentrations up to 0.2 *M*. These facts indicate that the blue shift of the iodine band is mainly due to a repulsive interaction in the excited state of iodine. This is consistent with Mulliken's[19] explanation of the blue shift of the 520 mμ band of iodine.

TABLE I

PERTURBATION OF THE VISIBLE BAND OF IODINE

Donor	pK_a[a]	*K*	Shifted iodine band	
			Δλ	ϵ_{max}
Pyridine	5.2	96[b]	100	2150
Pyrimidine	1.3	17	90	1170
Pyrazine	0.6	12	80	1250
s-Triazine	0.0	2	50	..

[a] Taken from: S. F. Mason, *J. Chem. Soc.*, 1240 (1959).
[b] Previously reported values for the *K* of pyridine–iodine complex at room temperature are: 160 (ref. 1), 45 (ref. 3), 107 (A. G. Maki and E. K. Plyler, *J. Phys. Chem.*, **66**, 766 (1962), and 101 (A. I. Popov and R. H. Rygg, *J. Am. Chem. Soc.*, **79**, 4622 (1957)). The *K* increases with pyridine concentration beyond a pyridine to iodine ratio of 100.

From Table I it can be seen that the ϵ_{max} of the shifted iodine band increases with the stability of the complex. The explanation for this phenomenon is lacking at present. Borrowing of intensity from CT transition has been suggested as a possibility.[20]

Ionization Potentials.—Table I shows that *K* values of the azine–iodine complexes follow the trend of pK_a values of the donors. Thus the electrons that enter into hydrogen bond and CT interaction should be of the same type. The azines, then, should be *n*-donors and not π-donors. A similar conclusion has been drawn in two previous investigations.[3,5]

The CT maxima of azine–iodine complexes are: pyridine-235 mμ, pyrazine—242 mμ and pyrimidine—237 and 246 mμ.

(15) H. McConnell, J. S. Ham, and J. R. Platt, *J. Chem. Phys.*, **21**, 66 (1953).

(16) S. H. Hastings, J. L. Franklin, J. C. Schiller, and F. A. Matsen, *J. Am. Chem. Soc.*, **75**, 2900 (1953). See ref. 23 for further examples.

(17) This procedure cannot give accurate *K* for *s*-triazine where the shift is small and the complexation is poor. In spite of this inaccuracy, it can be compared with other *K* values in Table I.

(18) R. P. Lang, *J. Am. Chem. Soc.*, **84**, 1185 (1962). In this paper a blue shift of the thioacetamide band at 269 mμ by 3250 cm.$^{-1}$ on complexation with iodine has been reported. The thioacetamide–iodine complex is much stronger than azine–iodine complexes studied here. A greater interaction between donor and acceptor in the ground states is possible in the former case.

(19) R. S. Mulliken, *Rec. trav. chim.*, **75**, 845 (1956).

(20) H. Tsubomura and R. P. Lang, *J. Am. Chem. Soc.*, **83**, 2085 (1961).

The two maxima for pyrimidine–iodine complex indicate two CT transitions. The width of pyrimidine–iodine CT bands, which is about twice that of pyridine–iodine band support the view of two CT transitions. We interpret them, tentatively, as the two CT transitions corresponding to two non-bonding MO's. The energy difference of 1600 cm.$^{-1}$ between the two bands is higher than what is expected of n orbital interaction alone. The fact that the center of gravity of the two CT bands of pyrimidine–iodine system does not coincide with the CT maximum of pyridine–iodine complex shows that this split of 1600 cm.$^{-1}$ involves more than n orbital interaction.

In pyrazine–iodine system only a single absorption band is observed. This does not necessarily indicate the lack of two CT transitions. The energy difference of two CT bands in pyrazine–iodine systems corresponding to the two non-bonding MO's should be lower than in pyrimidine–iodine system. The resolution of two broad CT bands with small energy difference would not be possible at the high slits used. The broadness of the pyrazine–iodine CT band, which is comparable to that of pyrimidine–iodine CT bands, strongly indicate two CT transitions. The observed CT band maximum, then, is the average of the two CT maxima.

Two different (n, π^*) states in pyrazine with an energy difference of about 500 cm.$^{-1}$ have been observed experimentally.[21,22] Using this value for energy difference of the two non-bonding MO's, we infer that the maxima of two CT transitions in pyrazine–iodine complex should be at 244 and 241 mπ. However, the conclusions to be drawn in the following paragraph are independent of the value chosen for the energy difference of the two non-bonding MO's of pyrazine as long as it is less than the energy difference of the two non-bonding MO's in pyrimidine.

Now, it can be seen that for the CT bands involving the higher of the two non-bonding MO's the CT maxima of azine–iodine complexes follow the donor order: pyridine > pyrazine > pyrimidine; with the CT bands involving the lower of the non-bonding MO's the order is the pyridine = pyrimidine > pyrazine. The same order is expected for the n-ionization potentials of these compounds from the theoretical relation between CT maxima and ionization potentials.[15,16]

The ionization potentials observed by electron impact method follow the order: pyridine < pyrimidine < pyrazine. The trend of experimentally observed ionization potentials differs from that of the n-ionization potentials inferred from the CT spectra. These considerations indicate that the observed ionization potentials in azines[10,11] correspond to π-electron ionization but not to n-electron ionization. More experimental work on ionization potentials and CT maxima of different azines and their derivatives will serve to make this conclusion more trustworthy.

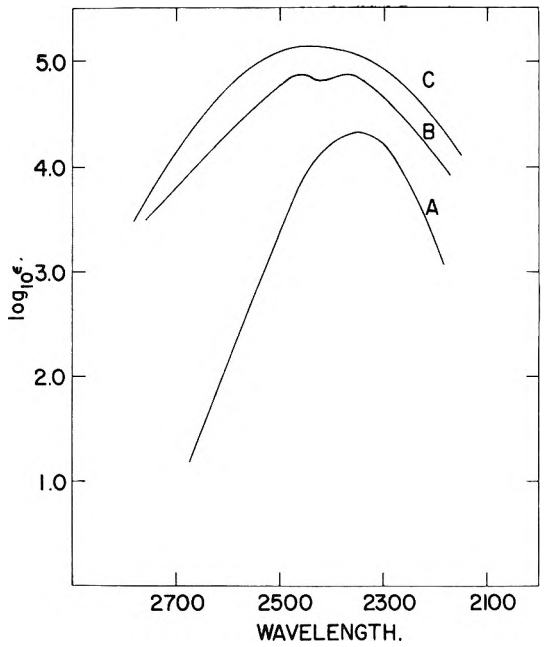

Fig. 2.—Charge transfer bands of (A) pyridine–iodine, (B) pyrimidine–iodine, and (C) pyrazine–iodine systems. See text for the details of the experimental procedure.

Figure 2 shows that the ϵ_{max} of the CT band decreases with the stability of the complex. This anomalous relation has been noted before in several cases.[23] A detailed explanation is lacking at present even though two mechanisms were proposed.[24,25]

Acknowledgments.—We wish to express our indebtedness to Professor Lionel Goodman for constant encouragement and for his helpful criticism of the manuscript. Our thanks are also due to Miss Beverly Jamattona for translating the article by Nakajima and Pullman.

(21) M. Ito, R. Shimada, T. Kuraishi, and M. Mizushima, *J. Chem. Phys.*, **26**, 1508 (1957).
(22) M. A. El-Sayed and G. W. Robinson, *Mol. Phys.*, **4**, 273 (1961).
(23) S. P. McGlynn, *Chem. Rev.*, **58**, 1113 (1958).
(24) L. E. Orgel and R. S. Mulliken, *J. Am. Chem. Soc.*, **79**, 4839 (1957).
(25) J. N. Murrell, *ibid.*, **81**, 5037 (1959).

A SIMPLE COMPUTATION OF EQUILIBRIUM CONSTANTS

By A. J. Poe[1]

Chemistry Department, Northwestern University, Evanston, Illinois

Received November 1, 1962

In many cases a simple arithmetical procedure can be used to derive stability constants quickly from $\bar{n}$:[L] data without recourse to a digital computer. Temporary values of the constants are necessary but these can be easily obtained by use of the Scatchard function or *Pseudo-constant*. Successive approximation may be necessary but can be performed rapidly. The values obtained agree well with those obtained by the computer method and standard deviations can be estimated by straightforward procedures.

Much work has been done on the computation of successive equilibrium constants, from various types of experimental data, either by graphical or by computational methods. This work has been thoroughly reviewed by several authors.[2] The computational methods originated with Bjerrum's successive approximation procedure[3] but recently much more emphasis has been placed on the use of digital computers[4] to overcome the difficulties in solving several simultaneous equations which are usually "ill-conditioned".[5] The purpose of this paper is to emphasize that the solution of the simultaneous equations is frequently very quick by a quite straightforward arithmetic procedure which occasionally involves a small number of successive approximations. This procedure has several advantages over Bjerrum's method.

As with Bjerrum's method it is necessary to derive initial approximate, or temporary, constants and this can best be done by a development of a method, derived independently by several authors,[6] which has received less attention than it deserves. (A similar method has been used by the author to represent kinetic data in successive substitution reactions.[7]) The treatment has so far been restricted to data relating the concentration, [L], of free ligand to the average number, $\bar{n}$, of ligands attached to each metal ion in a mononuclear complex.

The basic equation relating these quantities is

$$\bar{n} + (\bar{n} - 1)[\mathrm{L}]\beta_1 + (\bar{n} - 2)[\mathrm{L}]^2\beta_2 + \ldots + (\bar{n} - n)[\mathrm{L}]^n\beta_n + \ldots + (\bar{n} - N)[\mathrm{L}]^N\beta_N = 0 \ldots \quad (1)$$

where

$$\beta_n = \frac{[\mathrm{ML}_n]}{[\mathrm{M}][\mathrm{L}]^n} = \frac{\bar{n}}{(n - \bar{n})} \times \frac{1}{[\mathrm{L}]^n} \left\{ 1 + \sum_{p=1}^{n-1} (\bar{n} - p)[\mathrm{L}]^p\beta_p/\bar{n} + \sum_{q=n+1}^{N} (\bar{n} - q)[\mathrm{L}]^q\beta_q/\bar{n} \right\} \ldots \quad (2)$$

and N is the maximum number of ligands which can be bound to any one metal ion. β_n can therefore be calculated provided temporary values of the other constants are available and it is clearly desirable that the summation terms in equation 2 which involve the approximate values should be as small as possible. The first summation will contain only positive terms if $\bar{n} > n - 1$ and the second will contain only negative terms if $\bar{n} < n + 1$ and in the range $n - 1 < \bar{n} < n + 1$ the two sums will tend to cancel. At $\bar{n} = n$ the term involving β_n in equation 1 is zero and as $\bar{n}$ approaches n so β_n becomes more indeterminate. The best values of $\bar{n}$ for calculating β_n are, therefore, either $\bar{n} - 1 < \bar{n} \lesssim n - {}^1/_2$ or $n + {}^1/_2 \lesssim \bar{n} < n + 1$. At the integral values $n - 1$ or $n + 1$ the term involving β_{n-1} or β_{n+1}, respectively, is zero and the number of unknowns is reduced by one. In practice it is better to eliminate the term in β_{n-1} since this is larger than that in β_{n+1}.

One procedure is therefore to take temporary values β_3', β_4',... β_N' and to calculate β_2'' in terms of these from data at $\bar{n} = 1$. (The terms β_n' represent the initial values of β_n, and β_n'', β_n''', etc. represent improved values obtained by successive approximations.) β_1'' is then calculated from data in the range $0 < \bar{n} \lesssim 0.5$ in terms of β_2'', β_3', β_4'... β_N'. β_4'' is then obtained in terms of β_1'', β_2'', β_5', β_6'... β_N' from data at $\bar{n} = 3$ followed by β_3'' in terms of β_1'', β_4'', β_5'... β_N' from data at $\bar{n} = 2$. This alternation ensures that as many improved values of the constants as possible are used in the correction terms. In order to eliminate completely the term in β_{n-1} by making use of values of [L] at $\bar{n} = n - 1$ a process of graphical interpolation must be used similar to that used by Bjerrum[3] but which involves data at integral rather than half-integral values of $\bar{n}$. The procedure outlined here is somewhat quicker than Bjerrum's since the correction terms are in a more convenient form for calculation.

It is better, however, to use $\bar{n}$ and [L] values which are actually obtained directly from the experimental data rather than by interpolation. Although the advantage of eliminating one of the approximate constants is then lost, this is offset by a much clearer connection between the experimental errors in [L] and the resulting errors in the β_n values obtained. In this case the alternation procedure is not necessarily best although it may occasionally be useful. In both the interpolation and the point-by-point methods the first correction term in equation 2 involves constants which have already been improved whereas the second term involves less accurately known constants. The range of suitable data should therefore be extended to lower values of $\bar{n}$ than given by $n - 1 < n \lesssim n - {}^1/_2$, since the less accurate summation term becomes relatively smaller.

(1) On leave of absence from Imperial College, London, England (1961–1962).

(2) F. J. C. Rossotti and H. Rossotti, "The Determination of Stability Constants," McGraw-Hill Book Co., New York, N. Y., 1961, Chap. 5 and references therein.

(3) J. Bjerrum, "Metal Ammine Formation in Aqueous Solution," P. Haase and Son, Copenhagen, 1957, p. 35.

(4) (a) J. C. Sullivan, J. Rydberg, and W. F. Miller, *Acta Chem. Scand.*, **13**, 2023 (1959); (b) S. W. Rabideau and R. H. Moore, *J. Phys. Chem.*, **65**, 371 (1961); (c) W. J. Randall, D. F. Martin, and T. Moeller, *Proc. Chem. Soc.*, 340 (1961).

(5) A. M. Turing, *Quart. J. Mech. and Applied Math.*, **1**, 287 (1948).

(6) G. Scatchard, unpublished work quoted by J. T. Edsall, C. Felsenfeld, D. S. Goodman, and F. R. N. Gurd, *J. Am. Chem. Soc.*, **76**, 3054 (1954); V. Peticolas, Thesis, Northwestern University, 1954; A. J. Poë, unpublished work.

(7) A. J. Poë and M. S. Vaidya, *Proc. Chem. Soc.*, 118 (1960); *J. Chem. Soc.*, 2981 (1961).

The derivation of the temporary values of the constants can conveniently be done by using the Scatchard function[6] for which we have coined the name "Pseudo-constant." This name arises out of the basic concept of the method which is that any metal ion, M, can be regarded as having N sites which are potential positions for ligand attachment. (N is not necessarily the same as the number of coördinated solvent molecules.) When $\bar{n}$ of these sites have been filled the concentration of occupied sites is $\bar{n}$[M], and of unoccupied sites is $(N - \bar{n})$[M]. We may therefore write

$$K_{ps} = \frac{\bar{n}[M]}{(N - \bar{n})[M]} \times \frac{1}{[L]} = \frac{\bar{n}}{(N - \bar{n})[L]} = \text{the Scatchard function} \quad (3)$$

where K_{ps} is the "equilibrium constant" for the chemical equilibrium

$$\text{unoccupied site} + [L] \rightleftharpoons \text{occupied site}$$

K_{ps} is not expected to be constant with variation of $\bar{n}$ and [L] since the ease with which a site can be occupied will be expected to depend on the number of neighboring sites which are already occupied. This is one of the great advantages of the function in that a plot of K_{ps} *vs.* $\bar{n}$ immediately gives information of a chemical nature about the effect of already attached ligands on the ease of attachment of further ligands. This is because the statistical effect is implicitly allowed for in this treatment. An increase of K_{ps} with $\bar{n}$ indicates increasing ease of attachment and *vice versa*. This advantage is not shown by the more usual formation curves unless the effects are very large.

Extrapolation of the K_{ps} curve to $\bar{n} = 0$ gives K_1/N, and to $\bar{n} = N$ gives NK_N. The latter extrapolation is less accurate than the former since as $\bar{n}$ approaches N the uncertainty in $N - \bar{n}$ becomes large. In principle, values of K_2 and K_{N-1} can be calculated[6] from the slope of the log K_{ps} *vs.* $\bar{n}$ curve at $\bar{n} = 0$ and N, respectively, but these slopes are not usually well enough defined for this to be of much practical use. However, a further relationship is that $K_{ps}(\bar{n} = 0)/K_{ps}(\bar{n} = N) = x^{2(N-1)}$, where x is the spreading factor defined by Bjerrum.[8] This method of deriving x is much quicker than that involving the formation curve where the mid-point slope is related to x by a rather complicated expression.[9] The value of K_{ps} at $\bar{n} = N/2$ is equal to $\beta_N^{1/N}$, the average constant, provided that the log K_{ps} curve is symmetrical about $\bar{n} = N/2$. Once K_1, K_N, and x are known temporary values of the other constants can quickly be found.

If $N \leqslant 4$ it is better to calculate the intermediate constants from data at intermediate integral values of $\bar{n}$ rather than by using K_1 and x. Some examples, showing the advantages of these methods, will now be given.

The Cu^{2+}–NH_3 System.—The experimental data were those obtained by Bjerrum[10] and are given in Table I.

Table I

The Cu^{2+}–NH_3 System in 2 *M* NH_4NO_3 at 30°

$\bar{n}$	0.244	0.486	0.959	1.877	2.784	3.437	3.743	4.002
p[NH_3]	4.692	4.335	3.901	3.272	2.641	2.064	1.645	0.606
log K_{ps}	3.505	3.476	3.400	3.219	3.001	2.850	2.808	...

The values of log K_{ps} show immediately that complexing of Cu^{2+} and NH_3 becomes less easy the larger $\bar{n}$. Temporary values of the constants were obtained from the log K_{ps} curve by extrapolation (K_1 and K_4,), and by calculation from K_{ps} values at $\bar{n} = 2$ and 3 (β_3 and β_2). The use of the spreading function is not necessary here. The values, shown in Table II, were then applied in successive approximation methods using (a) interpolated K_{ps} values at $\bar{n} = 0.5$, 1, 2 and 3, and (b) the individual points taken in order as:

β_n	β_2	β_1	β_3	β_4
$\bar{n}$	0.959	0.244, 0.486	1.877	2.484, 3.437, 3.743

The values of β_1 and β_4 obtained from each of the experimental points were averaged after each cycle and the average used in the next cycle. The constants obtained after the second and third cycles agreed within ±0.2% and the equations for the last cycle are

$$\bar{n} = 0.959: \beta_2 = 5.839 \times 10^7 (1 - 5.370 \times 10^{-6} \beta_1 - 4.217 \times 10^{-12} \beta_3 - 7.893 \times 10^{-16} \beta_4)$$
$$= 5.839 \times 10^7 (1 - 0.0741 - 0.1455 - 0.0004) = 4.45 \times 10^7$$

$$\bar{n} = 0.244: \beta_1 = 1.586 \times 10^4 (1 - 2.981 \times 10^{-9} \beta_2 - 9.523 \times 10^{-14} \beta_3 - 2.640 \times 10^{-18} \beta_4)$$
$$= 1.586 \times 10^4 (1 - 0.1358 - 0.0033 - 0.0000) = 1.366 \times 10^4$$

$$\bar{n} = 0.486: \beta_1 = 2.045 \times 10^4 (1 - 6.661 \times 10^{-9} \beta_2 - 5.114 \times 10^{-13} \beta_3 - 3.306 \times 10^{-17} \beta_4)$$
$$= 2.045 \times 10^4 (1 - 0.3035 - 0.0176 - 0.0002) = 1.388 \times 10^4$$

$$\bar{n} = 1.877: \beta_3 = 1.094 \times 10^{10} (1 + 2.498 \times 10^{-4} \beta_1 - 1.837 \times 10^{-8} \beta_2 - 9.237 \times 10^{-14} \beta_4)$$
$$= 1.094 \times 10^{10} (1 + 3.441 - 0.8147 - 0.4387) = 3.488 \times 10^{10}$$

$$\bar{n} = 2.784: \beta_4 = 8.381 \times 10^{10} (1 + 1.466 \times 10^{-3} \beta_1 + 1.472 \times 10^{-6} \beta_2 - 9.272 \times 10^{-10} \beta_3)$$
$$= 8.381 \times 10^{10} (1 + 20.19 + 67.05 - 32.33) = 4.686 \times 10^{12}$$

$$\bar{n} = 3.437: \beta_4 = 1.100 \times 10^9 (1 + 6.117 \times 10^{-3} \beta_1 + 3.113 \times 10^{-5} \beta_2 + 8.172 \times 10^{-8} \beta_3)$$
$$= 1.100 \times 10^9 (1 + 84.24 + 1418 + 2850) = 4.788 \times 10^{12}$$

$$\bar{n} = 3.743: \beta_4 = 5.533 \times 10^7 (1 + 1.661 \times 10^{-2} \beta_1 + 2.389 \times 10^{-4} \beta_2 + 2.308 \times 10^{-6} \beta_2)$$
$$= 5.533 \times 10^7 (1 + 223 + 10{,}880 + 80{,}500) = 5.067 \times 10^{12}$$

Provided the values of β_1 and β_4 are averaged without weighting no further improvement in the constants can be obtained. The errors in the constants can be esti-

(8) Reference 2, p. 29.
(9) Reference 2, p. 31.
(10) Reference 2, p. 126.

mated relative to the error in measuring $[NH_3]$. Following Sullivan, *et al.*,[4a] a standard deviation of ± 0.7% has been assumed in these measurements. The standard deviations in the constants are then obtained by examining the dependence of β_n on $[NH_3]$ and on the other constants. The standard deviations of the other constants must be guessed initially but, since they only apply to relatively small terms, quite large errors in the guesses have little effect. Having estimated the standard deviations of each of the terms contributing to β_n the resultant can be calculated by using the usual rules for the standard deviations of sums, differences and products. The K_n values are not necessarily best obtained directly from $\beta_n:\beta_{n-1}$ ratios. It is evident from equation 2 and the equations for $\bar{n} = 3.743$ that

$$\bar{n} = 0.318: \beta_1 = 4.717 \times 10^7 (1 - 5.411 \times 10^{-16} \beta_2 - 8.145 \times 10^{-24} \beta_3)$$
$$= 4.717 \times 10^7 (1 - 0.0650 - 0.0000) = 4.410 \times 10^7$$

$$\bar{n} = 0.544: \beta_1 = 5.328 \times 10^7 (1 - 1.342 \times 10^{-15} \beta_2 - 5.066 \times 10^{-23} \beta_3)$$
$$= 5.328 \times 10^7 (1 - 0.1613 - 0.0002) = 4.468 \times 10^7$$

$$\bar{n} = 0.927: \beta_2 = 1.558 \times 10^7 (1 - 5.864 \times 10^{-9} \beta_1 - 9.237 \times 10^{-22} \beta_3)$$
$$= 1.558 \times 10^7 (1 - 0.2603 - 0.0036) = 1.147 \times 10^{14}$$

$$\bar{n} = 1.405: \beta_2 = 2.340 \times 10^{13} (1 + 9.160 \times 10^{-8} \beta_1 - 3.641 \times 10^{-20} \beta_3)$$
$$= 2.340 \times 10^{13} (1 + 4.066 - 0.145) = 1.152 \times 10^{14}$$

$$\bar{n} = 2.264: \beta_3 = 1.963 \times 10^{13} (1 + 6.485 \times 10^{-6} \beta_1 + 1.573 \times 10^{-11} \beta_2)$$
$$= 1.963 \times 10^{13} (1 + 287.8 + 1809) = 4.118 \times 10^{18}$$

$$\bar{n} = 2.643: \beta_3 = 5.839 \times 10^{13} (1 + 3.123 \times 10^{-5} \beta_1 + 6.139 \times 10^{-10} \beta_2)$$
$$= 5.839 \times 10^{13} (1 + 1387 + 70{,}600) = 4.204 \times 10^{18}$$

division by β_3 gives K_4 in terms of one large term (which varies inversely as $[NH_3]$) and relatively much smaller terms which depend on higher powers of $[NH_3]$ and on the other constants. The same applies, to a somewhat lesser extent, to equations for $\bar{n} = 3.437$ but it does not apply to those for $\bar{n} = 2.784$. K_4 should therefore be obtained with least error from data at $\bar{n} = 3.437$ and 3.743. However, the average value obtained from these two points ($\log K_4 = 2.150$) does not differ significantly from that obtained from the ratio of the β_4 and β_3 values obtained separately ($\log \beta_4/\beta_3 = 2.142$) and it is probably too ambitious to attempt to reduce the confidence limits much below the ± 0.02 estimated for the latter value. The former value, however, is accepted since its derivation is better, in principle, than the latter. The calculated values are given in Table II together with those obtained by other workers. The errors quoted are 96% confidence limits.

TABLE II

LOG K_n VALUES FOR THE Cu^{2+}–NH_3 SYSTEM

	Bjerrum's method	Temporary consts. (from K_{ps} curve)	Successive approx. using K_{ps} at $\bar{n} = 0.5, 1, 2, 3$	Point by point calc.	Computer method[4a]
$\log K_1$	4.15	4.127	4.143	4.139 ± 0.008	4.134 ± 0.008
$\log K_2$	3.50	3.527	3.511	3.520 ± 0.014	3.528 ± 0.016
$\log K_3$	2.89	2.871	2.893	2.884 ± 0.02	2.87 ± 0.02
$\log K_4$	2.13	2.177	2.137	2.150 ± 0.02	2.15 ± 0.04
$\log \beta_4$	12.67	12.702	12.684	12.690 ± 0.01	

The Ni^{2+}–en System.—Data for this system were also obtained by Bjerrum[11] and, following his example, glass electrode data were used where possible.

TABLE III

DATA FOR THE Ni^{2+}–en SYSTEM IN 1 *M* KCl AT 30°

$\bar{n}$	0.318	0.544	0.927	1.405	2.264	2.643	2.926
p[en]	8.005	7.650	7.128	6.498	4.935	4.299	3.683
$\log K_{ps}$	7.079	6.995	6.779	6.443	5.423	5.168	5.28

It is evident again that complexing becomes more difficult as more ligands become attached. The log K_{ps} *vs.* $\bar{n}$ curve shows that the point at $\bar{n} = 2.926$ is unreliable. The point-by-point procedure was followed as before by making use of temporary constants obtained from the K_{ps} curve (Table IV). The first set of calculations is

Averaging the values obtained and using these values in the next cycle increases β_1 by about 1% and increases β_2 and β_3 by only 0.2%. No further improvement is possible. The values of K_n and their 96% confidence limits were obtained as before, a standard deviation of 1% being assumed for [en]. The results are given in Table IV and compared with results calculated elsewhere. The confidence limits for $\log K_3$ are based on the almost complete dependence of K_3, obtained from $\bar{n} = 2.264$ and 2.643, on [en].

TABLE IV

LOG K_n VALUES FOR THE Ni^{2+}–en SYSTEM

			This work	
	Bjerrum	Block and McIntyre[12]	Temporary values	Point by point calc.
$\log K_1$	7.66	7.68 ± 0.08	7.62	7.651 ± 0.01
$\log K_2$	6.40	6.39 ± .10	6.46	6.414 ± .01[a]
				6.410 ± .02[b]
$\log K_3$	4.55	4.56 ± .01	4.52	4.558 ± .01
$\log \beta_3$	18.61	18.63	18.60	18.623 ± .02

[a] From $\bar{n} = 1.405$ only. [b] From $\bar{n} = 0.927$ and 1.405.

The method has also been applied to the Ni^{2+}–NH_3 system where $N = 6$. In principle the method is again straightforward but in this particular system convergent values of the constants are not obtained with successive cycles. Some experimental points are evidently unreliable and, in a recent computor treatment of the data, Rydberg[13] was forced to reject some points.

(11) Reference 2, p. 214.

(12) D. P. Block and C. H. McIntyre, *J. Am. Chem. Soc.*, **75**, 5887 (1953).

Discussion.—The graphical method of representing the data in terms of the Scatchard function or Pseudo-constant, K_{ps}, has definite advantages both in giving immediate information of chemical significance and in providing a rapid way of obtaining good temporary constants. The temporary constants listed in Table II are significantly better than those found[14] by Bjerrum's method and when $N \leq 4$ it is not necessary to assume a constant spreading factor, x, to obtain them. The point-by-point calculation shows clearly which points are appropriate for calculating a particular β_n constant and errors can be estimated quite rigorously in terms of experimental uncertainties. It is evident from Table II that this method is capable of just as good an accuracy as the computer method. The reason why the computer method seems to give a slightly less accurate value for K_4 in the Cu^{2+}–NH_3 system may lie in the different way in which the effect of errors in the data was treated.[4a] The method is both quicker than Bjerrum's method when interpolated K_{ps} values are used, and more accurate when the point-by-point method is used. Not needing a computer it is more readily available and cheaper than the computer method. It has the disadvantage that the estimation of errors involves an assumption of the error in the experimental data which cannot easily be checked by the method of external consistency[15] used in the computer technique. It has an advantage over graphical methods which are subject to systematic, subjective errors, which do not allow for objective estimates of standard deviations, and which tend to give equal weight to points irrespective of how sensitive the points are to changes in the constants. That the graphical method can lead to systematic errors is shown in the figure where the data[16] for the Ag^+–*para*-$Ph_2P{\cdot}C_6H_4SO_3^-$ system are represented by a K_{ps} *vs.* $\bar{n}$ plot. The continuous line was calculated by using the constants $\beta_1 = (1.35 \pm 0.03) \times 10^8$, $\beta_2 = (1.22 \pm 0.13) \times 10^{14}$, and $\beta_3 = (3.46 \pm 0.16) \times 10^{19}$ obtained by the point-by-point method. The limits are 96% confidence limits for calculation of the constants from the $\bar{n}$ and [L] values derived by Ahrland, *et al.*, from their potentiometric measurements.[16] The points calculated using their constants deviate systematically from the experimental points in contrast with the smooth curve. The value of $\Sigma\{(\bar{n}_{exp} - \bar{n}_{calc})\ 100/\bar{n}_{calc}\}^2$ obtained by using Ahrland's constants is nearly three times as large as that found by using the above values.

(13) J. Rydberg, *Acta Chem. Scand.*, **15**, 1723 (1961).
(14) Reference 2, p. 128.
(15) W. E. Deming, "Statistical Adjustment of Data," John Wiley and Sons, Inc., New York, N. Y., 1945.
(16) S. Ahrland, J. Chatt, N. R. Davies, and A. A. Williams, *J. Chem. Soc.*, 276 (1958).

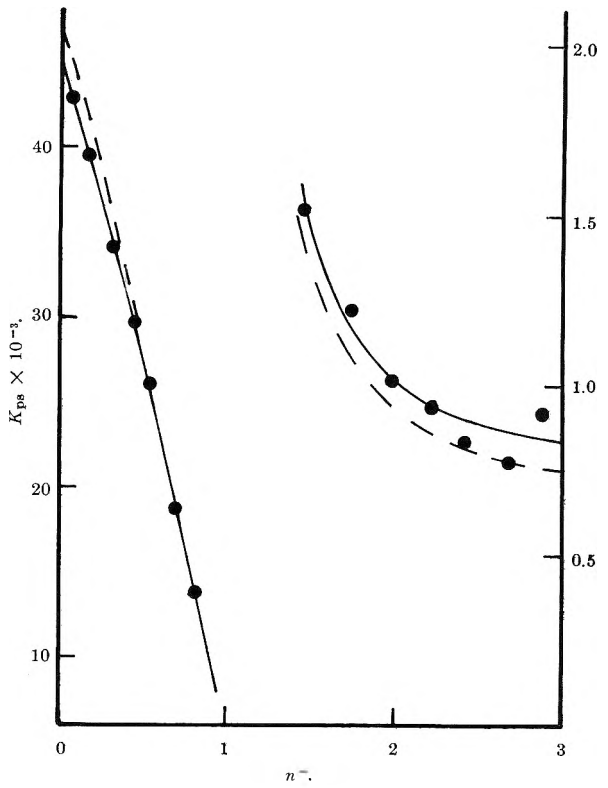

Fig. 1.—The pseudo-constant curve for the system: silver ion–diphenylphosphinobenzene-*p*-sulfonate ion. (Data from ref. 16). ●, exptl. points; ———, curve calculated with constants from this work; – – – –, curve calculated with constants from ref. 16.

The effort involved in rearranging the equations so that K_n values are obtained directly[3,12,17] instead of *via* β_n values does not appear to be justified. This is shown by the constants obtained by Block and McIntrye[12] for the Ni^{2+}–en system by a method which makes use of far more combinations of data than does ours and yet leads to less precise constants (Table IV). Our method was also found to show clearly the difficulties involved in computing constants when $x << 1$. The correction terms involving approximate constants are then relatively much larger, and much more accurate data are necessary in order to obtain reliable values.

Acknowledgment.—The author is grateful to the Atomic Energy Commission for a fellowship (under contract AT(11-1)-89-Proj. No. 2.) during the tenure of which this paper was written and to the Imperial College for a leave of absence.

(17) E. L. King and P. K. Gallagher, *J. Phys. Chem.*, **63**, 1073 (1959).

THE MASS SPECTRA OF THREE DEUTERATED PROPENES

BY W. H. McFADDEN

Western Regional Research Laboratory,[1] Albany, California

Received November 8, 1962

The mass spectra of 2-D_1-propene, 1,1-D_2-propene, and 3,3,3-D_3-propene are presented for 70 volt electrons. The data show considerable rearrangement of hydrogen and deuterium from all positions. The formation of $C_3H_5^+$ is due primarily to loss of hydrogen from positions 1 or 3. The rate of loss of CH_3 or CH_4 to form two carbon ions is sufficiently fast to allow only a few exchanges of hydrogen and deuterium prior to this breakdown.

I. Introduction

In an attempt to understand simple features of the mass spectra of $C_{10}H_{16}$ terpenes it has been found necessary to study the mass spectra of smaller unsaturated hydrocarbons. This is prompted principally because attempts to correlate the spectral features of terpenes with structure[2] are not sufficiently complete to be generally applicable and many important exceptions are encountered. The mass spectrum of camphene-8-C^{13} has shown that for this compound the methylene does not seem to be lost in forming C_8 or C_9 ions but that a general rearrangement and approximate equilibration of the C^{13} does occur in the formation of C_7 or smaller fragment ions.[3] The data are not sufficient for further clarification, however.

The reasons for exceptions to simple rules and for our lack of understanding of the mass spectra of these terpenes are partly revealed in the sparse literature on the mass spectra of lower molecular weight labeled olefins and cycloalkanes. Such data indicate the existence of more complex cracking patterns than would be expected. For example, the mass spectra of methylcyclopentane and methylcyclohexane show predominant ions due to loss of CH_3. However, the mass spectrum of methyl-C^{13}-cyclopentane shows that only about one-half of the events involve the original methyl group but the mass spectrum of α-deuterated methylcyclohexane shows that the original methyl is lost quantitatively.[4,5] From the mass spectrum of $CD_3CH_2CHCH_2$, in addition to other rearrangements, it appears that at low ionizing voltages the loss of CH_3 is more probable than loss of CD_3.[6] However, Natallis has shown that monodeuterocyclopentane gives statistical amounts of CH_3^+ and CH_2D^+ with electron voltages above 40 e.v. but strongly favors the formation of CH_3^+ at lower voltages.[7] This is not consistent with the conclusions drawn from the data of CD_3CH_2-$CHCH_2$. Obviously, rearrangements and exchanges occur which are not clearly understood or interpreted with the paucity of existing data and for this reason the mass spectra of the three deuterated propenes are presented.

II. Experimental

The three deuterated propenes were 2-D_1-propene, 1,1-D_2-propene and 3,3,3-D_3-propene. They were obtained from Merck, Sharp and Dohme of Canada, Limited, and were sold as 96% isotopically pure but low voltage analysis indicated that isotopic contaminants are considerably in excess of this amount. From the mass spectral data and high resolution n.m.r. analysis the isotopic compositions were determined and are presented in Table I.

TABLE I

ISOTOPIC COMPOSITION OF DEUTERATED PROPENES

Compound	% Present in CH_3-$CD{=}CH_2$	% Present in CH_3-$CH{=}CD_2$	% Present in CD_3-$CH{=}CH_2$
C_3H_6	8		
$CH_3{-}CD{=}CH_2$	72		
$CH_3{-}CH{=}CDH$	17	12	
$CH_2D{-}CH{=}CH_2$	3		
$C_3H_4D_2$		67	5
$C_3H_3D_3$		17	90
$C_3H_2D_4$		4	4.4
C_3HD_5			0.3

The spectra of the impure mixtures were used to calculate an approximate spectrum for each of the contaminants and make corrections to the original patterns. As thus presented, the data most likely contain small errors but these are not expected to cause serious changes in the general conclusions. For example, the corrections for the rather large amount of impurities present in $CH_3{-}CH{=}CD_2$ alter the larger peaks by 1–3% of the total ionization and the smaller peaks by only 0.2–0.5%. Maximum weighting of the possible errors in these approximate corrections would not alter the conclusions with respect to the cracking mechanism. The same arguments are valid for the corrections applied to the other two isotopic propenes.

The mass spectra were obtained from a CEC21-620 mass spectrometer modified to give increased resolution and control of the electron ionizing voltage. The samples were introduced through a stainless steel inlet system at 80° and a pressure of 40–50 μ. The temperature of the ionization chamber was 195 ± 5°. The sensitivity for the base peak of propene-D_0 was 41 div./μ.

III. Results and Discussion

The data obtained with 70-volt ionizing electrons are presented in Table II for propene-D_0 and the three deuterated propenes. The results are expressed as a percentage of the total ionization which was obtained from m/e 13 to the parent mass. Corrections have been made for the isotopic impurities but the data have not been corrected for the natural C^{13} content.

C_3 Ions.—The most abundant ion in the mass spectrum of propene is that due to loss of hydrogen from the parent ion. In the spectrum of CH_2CDCH_2 the intensity of the ion due to loss of one hydrogen contributes the same percentage (27.7%) to the total ionization as is observed from undeuterated propene. Statistically, one expects about 24%. Even though the isotope effect would enhance the abundance due to loss of hydrogen, one would not expect the contributions from the undeuterated and centrally deuterated propene to be equal and it thus appears that the central deuterium is not important in the formation of the propenyl ion.

The data for both the terminally labeled propenes show a significant reduction in the ion due to loss of one hydrogen. This suggests, as would be expected

(1) A laboratory of the Western Utilization Research and Development Division, Agricultural Research Service, U. S. Department of Agriculture.
(2) T. Gilchrist and R. I. Reed, *Experimentia*, **16**, 134 (1960).
(3) L. Friedman and A. P. Wolf, *J. Am. Chem. Soc.*, **80**, 2424 (1958).
(4) D. P. Stevenson, *ibid.*, **80**, 1571 (1958).
(5) Seymour Meyerson, private communication.
(6) W. A. Bryce and P. Kebarle, *Can. J. Chem.*, **34**, 1249 (1956).
(7) P. Natalis, *Bull. soc. roy. sci. Liège*, **27**, 201(1958).

TABLE II

THE MASS SPECTRA OF DEUTERATED PROPENES

m/e	CH_3CHCH_2	CH_3CDCH_2	CH_3CHCD_2	CD_3CHCH_2
13	0.4	0.3	0.2	0.3
14	1.0	.6	.6	.6
15	1.3	.9	.7	.2
16	0.1	.4	1.0	.7
17			.3	.5
18				.6
19	0.7	.4	.2	.1
19.5	.4	.5	.4	.4
20	.5	.4	.3	.3
20.5	.1	.4	.3	.2
21		.1	.3	.2
21.5			.1	.2
24	0.1	.1	.1	.1
25	0.5	.2	.4	.4
26	2.7	.9	1.5	1.6
27	10.0	4.4	4.2	4.2
28	0.1	7.2	3.9	3.9
29	0.3	0.3	4.8	4.0
30			1.1	1.1
31			0.8	0.3
32				.1
36	0.6	.4	.4	.4
37	3.4	1.6	1.3	1.3
38	4.9	2.7	2.7	2.4
39	18.9	7.6	4.1	3.3
40	7.2	13.4	11.6	7.5
41	27.7	7.9	8.4	9.6
42	18.5	27.7	8.5	5.1
43	0.5	20.8	22.8	12.3
44	0.1	0.8	18.2	18.2
45			0.5	19.3
46			0.2	.6

from previous work,[6] that exchanges or rearrangements occur to make the hydrogens on positions 1 and 3 approximately equivalent. The ion formed by loss of one deuterium is rather abundant in both cases. The isotope effect is sufficient to make the loss of hydrogen about 30% greater than the value expected by statistical rearrangement of H and D on all sites. This is inconsistent with the fact that bonds alpha to the double bond are preferentially broken, unless an exchange equilibrium of the type $CH_3\text{-}\dot{C}H\text{-}CH_2^+ \longleftrightarrow CH_2\text{-}\dot{C}H\text{-}CH_3^+$ occurs at a rate greater than the rate of loss of hydrogen.

The different behavior of the hydrogen on the central atom is also indicated in Fig. 1 which shows Γ as a function of per cent deuterium. Γ is defined by the equation

$$\Gamma = \frac{(P - H)_D}{n_H} \Big/ \frac{(P - H)_H}{n_D}$$

where (P − H) is the ionization due to loss of hydrogen from the deuterated or undeuterated molecule, respectively, and n is the number of hydrogens in the molecule. Since the data are reported here as per cent of total ionization this is slightly different from the usual Γ calculated from relative abundances. However, the difference is not important unless the distribution of deuterated ions affects the base peak in which case meaningful values of Γ can only be obtained from data expressed as per cent of total ionization.

In Fig. 1 it is seen that the two points for the terminally labeled propenes at 33.3 and 50% can be regarded as falling on a straight line from the origin

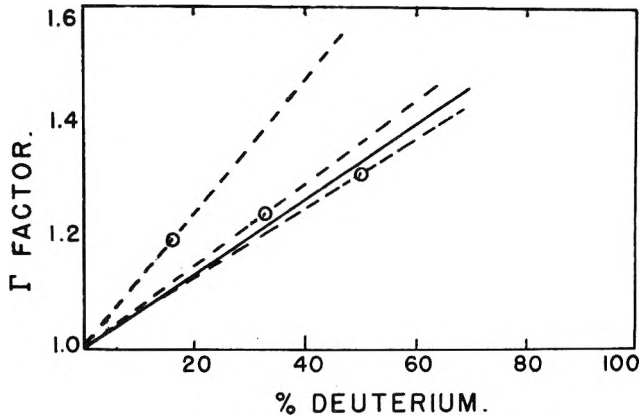

Fig. 1.—The Γ factor calculated from the mass spectra of three deuterated propenes.

which indicates that the C–H bonds of carbon 1 and carbon 3 dissociate at equivalent rates.[8] The point for the centrally labeled propene is notably higher which indicates that the hydrogen on this position is less labile.

An alternative interpretation of the data in Fig. 1 is suggested by the dotted lines. The deviation of the points for carbons one and three from the solid line may indicate that the hydrogens of all three positions are different in their lability hinting that a small fraction of the hydrogen is lost from position three before exchanges can occur. However, the data are not accurate enough for a firm conclusion and more points must be obtained.

C_2 Ions.—The two-carbon region of the propene mass spectrum is due chiefly to the ion $C_2H_3^+$ (10%) and $C_2H_2^+$ (2.7%). The data for the three deuterated propenes indicate rearrangements and exchanges but show that the loss of the CH_3 to form the vinyl ion occurs fast enough to prevent a statistical distribution of the H and D. Thus, from CH_3CDCH_2, loss of CH_3 without rearrangement would give a mass 28 intensity of about 9.5% or with complete randomization the intensity would be about 4.8%. The observed value is 7.1%. Similarly, from CH_3CHCD_2 or CD_3CHCH_2 the ions $CHCD_2^+$ or $CHCH_2^+$ are also intermediate between the values expected for no rearrangement and for random arrangement. This indicates that the reaction $CH_3\text{-}CHCH_2^+ \rightarrow \cdot CH_3 + CHCH_2^+$ must occur at a rate which is of the same order of magnitude as the exchange reactions between hydrogen and deuterium. A similar conclusion may be deducted from the deuterated butene data of Bryce[6] for the reaction $CH_3\text{-}CH_2CHCH_2^+ \rightarrow \cdot CH_3 + CH_2CHCH_2^+$.

From an estimation of the contribution of the ions $C_2H_2^+$ and C_2HD^+ to the mass spectrum of $CH_3\text{-}CDCH_2$ one may conclude that only about 20% of the events involve exchange of deuterium to the lost carbon fragment. This percentage is observed for loss of CH_3 to give the $C_2H_3^+$ ion (or deuterated equivalent) and for loss of CH_4 to give the $C_2H_2^+$ ion.

The estimated ionization for the various deuterated vinyl ions is compared with the statistical values in Table III. For each of the labeled compounds the amount of unrearranged vinyl ion is in excess of the statistical value. This indicates that loss of the CH_3 must occur considerably faster than equilibration of

(8) J. G. Burr, J. M. Scarborough, and R. H. Shudde, *J. Phys. Chem.*, **64**, 1359 (1960).

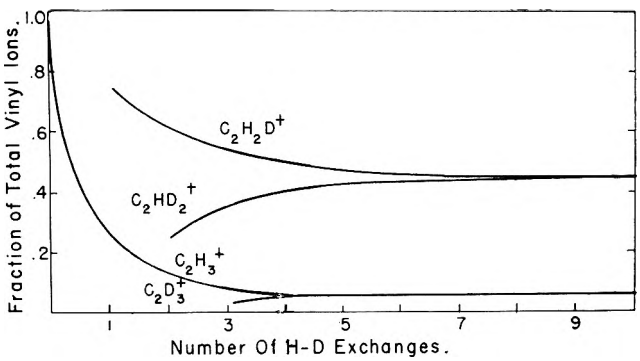

Fig. 2.—Rate of equilibration of hydrogen and deuterium in CD_3CHCH_2.

the hydrogen and deuterium. One notes further that if one assumes a hydrogen (or deuterium) from carbon 3 to be transferred to carbon 1, the vinyl ion expected occurs in an amount comparable to the statistical value ($C_2H_3^+$ from CH_3CHCD_2 and $C_2HD_2^+$ from CD_3CHCH_2) even though only a first step towards equilibrium has been achieved.

Table III

Estimated Fractions of Various Vinyl Ions

	CH_3CHCH_2	CH_3CDCH_2		CH_3CHCD_2		CD_3CHCH_2	
		Obsd.	Stat.	Obsd.	Stat.	Obsd.	Stat.
C_2H_3	1.00	0.26	0.5	0.22	0.20	0.29	0.05
C_2H_2D		0.74	0.5	.34	.60	.26	.45
C_2HD_2				.44	.20	.36	.45
C_2D_3						.09	.05

It is seen from the data of 2-D_1-propene that the fraction 0.74 of the vinyl ions involve the deuterium of carbon 2. It is therefore interesting to compare this value with the sum of the vinyl ion formed without rearrangement and the vinyl ion formed by transfer of one hydrogen (or deuterium) from carbon 3 to carbon 1 as suggested above. The values are 0.66 for 1,1-D_2-propene and 0.65 for 3,3,3-D_3-propene. The difference (0.10) may be regarded as a measure of the fraction of the ions that undergo further exchanges prior to breakdown.

Rate of H–D Exchange.—Because of the loss of CH_3 and the H–D exchange occur at a comparable rate, it is desirable to attempt to estimate the number of exchanges that correspond to the observed ratios of various deuterated vinyl ions. The actual molecular processes giving rise to these exchanges may involve such structures as $CH_3CHCH_2^+$, $CH_3CCH_3^+$, $H(CH_3)CHCH^+$, and others, but it is not possible to apply a weighting factor to account for the importance of each, nor is it practical to estimate the influence of the hydrogen–deuterium isotope effect. Furthermore, all ions will not experience the same number of exchanges, and the observed results will be averages of the various deuterated structures that can occur. Nevertheless, a useful estimation of the probable number of exchanges occurring can be obtained from a simplified model. An exchange mechanism is considered in which a hydrogen (or deuterium) from position three is transferred to positions one or two, and a statistically selected hydrogen (or deuterium) from those positions returned back to position three. Thus, for CD_3CHCH_2, the exchanges may be represented by $CD_3(C_2H_3)^+ \leftrightarrow CD_2(C_2H_3D)^+ \leftrightarrow CD_2H(C_2H_2D)^+ \leftrightarrow$ etc. and the rearranged ion $CD_2H(C_2H_2C)^+$ would lead to $CDH_2(C_2HD_2)^+$ and $CH_3(C_2D_3)^+$ in subsequent exchanges.

The results of applying this model to CD_3CHCH_2 without consideration for the isotope effect and simply giving a statistical weight to the removal of hydrogen or deuterium are presented in Fig. 2. It should be recognized that if the isotope effect were considered, then the approach to equilibrium would be faster than is illustrated. This results, of course, from the fact that the deuterium is originally on one carbon only. In the first transfer, deuterium must be exchanged but in subsequent transfers the lighter isotope will be favored. In addition, the model proposed actually involves two rearrangement reactions for each exchange process. This is done to take account of such structures as $CD_2CDHCH_2^+$ but in actuality the most probably first intermediate would be $CD_2CHCH_2D^+$ which could be readily expected to lose CH_2D without the necessity for subsequent rearrangements.

The most interesting feature of this model, as illustrated by Fig. 2, is the rapid approach to equilibrium. Thus, for all practical considerations, equilibrium values could be expected in three or four exchanges. The second feature to be noted is that if it were possible for one or two exchanges of this type to predominate, then $C_2H_2D^+$ would be the most abundant vinyl species contrary to observations. As expected, the model is overly simplified but the estimation of the number of exchanges required to reach equilibrium is valid and similar estimations are obtained for the other two deuterated propenes from the same model. It is concluded that most vinyl ions are formed with only a small number (0–5) of hydrogen–deuterium exchanges.

These conclusions place a considerable emphasis on the equilibrium $CH_3–\overset{+}{C}H–CH_2 \leftrightarrow CH_2–\overset{+}{C}H–CH_3$ and imply that it is the important mechanism controlling the distribution of hydrogen and deuterium. Such a suggestion is in accordance with the observed values for loss of H or D as discussed in the section on D_3 ions and in accordance with data obtained in 3-C^{13}-propene by Stevenson and Wagner.[9] The data they obtained for that isotopic compound indicated only about a 5% preference to form $C_2H_3^+$ over $C^{13}CH_3^+$. This is consistent with the present observations because equalization of carbons one and three can occur with very few exchanges; for such an observation, it is only necessary that the number of molecules that lose a methyl group after an even number of rearrangements be balanced by the number that have undergone an odd number of rearrangements. In addition their data suggests that a cyclopropane intermediate is not an important contributor to the many structures that may exist.

The data presented here also indicate, as would be expected, that other structures which require exchange of the hydrogen on carbon 2 must also be involved. An estimation of the importance of each would require additional data from other labeled olefins and in addition, a much more refined knowledge of the isotope effect than is currently possessed.

C_1 and Doubly Charged Ions.—The ionization due to doubly charged C_3 fragment and due to C_1 fragments

(9) D. P. Stevenson and C. Wagner, private communication.

does not constitute an important part of the total. There is obviously considerable scrambling of the hydrogens and deuteriums and for the most part they appear to be statistically arranged. However, the observed values and the statistical values are small so that a close comparison is not warranted.

Acknowledgment.—Miss Mary Sawyer ran the mass spectra and tabulated the data. Dr. R. E. Lundin performed the n.m.r. analyses which were so necessary in correcting the spectra for the isotopic impurities. Dr. C. Wagner very kindly made available the unpublished data on 3-C^{13}-propene. Reference to a company or product name does not imply approval or recommendation of the product by the U. S. Department of Agriculture to the exclusion of others that may be suitable.

DISSOCIATION PRESSURE OF AMMONIUM PERCHLORATE[1]

By S. Henry Inami, Willis A. Rosser, and Henry Wise

Stanford Research Institute, Menlo Park, California

Received November 8, 1962

The dissociation pressure of ammonium perchlorate has been measured in the temperature range of 520–620° K. by the transpiration method. The data indicate that ammonium perchlorate sublimes by the dissociation process $NH_4ClO_4(s) = NH_3(g) + HClO_4(g)$. The heat of dissociation has been found to be 58 ± 2 kcal./mole in the cited temperature range.

Introduction

During the past several years some efforts have been directed to elucidating the mechanism of the decomposition[2–7] and combustion[8,9] of ammonium perchlorate (AP). Bircumshaw and Newman[2] found that the decomposition of AP below 513°K. *in vacuo* left a residue after 20–30% of the salt had decomposed. This residue had a different crystalline appearance from the original material. However, it was confirmed to be AP by analytical and X-ray methods. Friedman and Levy[10] in their preliminary study of the reaction between NH_3 and $HClO_4$ reported that solid formation was observed in the mixing chamber under certain experimental conditions which gave a crude measure of the dissociation pressure of AP. This observation suggests that a dissociative process is involved in the sublimation of AP. It is apparent that the dissociation pressure of AP represents an important parameter in the analysis of the combustion mechanism of solid propellants based on this oxidizer.

Apparatus and Procedure.—The reagent grade AP from Matheson, Coleman and Bell Company was fractionated mechanically into two particle size ranges, 43–61 μ and > 61 μ. In a typical experiment a weighed sample of fractionated AP was placed in a glass-fritted cell (Fig. 1) and brought to the desired temperature by immersing the cell in a bath of molten salt.[11] The temperature of the molten bath was carefully regulated and measured with a glass-sheathed iron–constantan thermocouple. The decomposition and dissociation products of AP were carried away in a helium gas stream passing in an upward direction through the glass frit and the powdered sample. The volumetric flow rate of helium was determined by suitable calibrated flowmeters. All experimental measurements were carried out on that portion of AP which remains after decomposition of 20 to 30% of the original sample.[2] Before the dissociation pressure measurement, the sample was heated for approximately an hour. During the initial stage of decomposition a rapid exothermic reaction occurs which may elevate the temperature of the powder bed as much as 100°K. above the bath temperature with the evolution of brownish-yellow vapors. The residual material was a porous, amorphous solid, which crumbled easily. At this time a water-cooled cold finger was quickly placed in position in the transpiration cell (Fig. 1). The distance between the cold finger and the sample was about 2 cm. in most experiments; in some cases it was increased to 4 cm. The temperature of the water in the cold finger was maintained at approximately 340 ± 10°K. to prevent the condensation of H_2O. After a suitable reaction time, the finger was removed carefully and the white sublimate washed into a flask with about 50 ml. of distilled water. The solution was analyzed primarily for NH_4^+, ClO_4^-, and Cl^- in some cases.[12–14] The dissociation pressure of AP may be readily deduced from the flow rate of helium and the quantity of AP deposited on the finger.

Results and Discussions

In a number of runs the following major parameters were varied: (1) flow rate of helium gas, (2) reaction temperature, (3) initial mass of AP, (4) initial particle size, and (5) partial pressure of NH_3 added to carrier gas. As shown in Table I the sublimates analyzed were found to contain equimolar quantities of NH_4^+ and ClO_4^-; therefore, the results may be interpreted in terms of an equilibrium dissociation of NH_4ClO_4

$$NH_4ClO_4(s) = NH_3(g) + HClO_4(g) \qquad (1)$$

Since equivalent amounts of NH_3 and $HClO_4$ are produced, the dissociation pressure P_d is equal to the sum of P_{NH_3} and P_{HClO_4} provided there is no excess of either gas initially. The calculated dissociation pressures based on the analyses of NH_4^+ and ClO_4^- are in satisfactory agreement. The small variations observed are within the precision of the analytical techniques estimated to be ±10% for NH_4^+ and ClO_4^-. Based on

(1) This work was supported by the Office of Naval Research, Department of the Navy.

(2) L. L. Bircumshaw and B. H. Newman, *Proc. Roy. Soc.* (London), **A227**, 115 (1954); **A227**, 228 (1955).

(3) L. L. Bircumshaw and T. R. Phillips, *J. Chem. Soc.*, 4741 (1957).

(4) A. K. Galwey and P. W. M. Jacobs, *ibid.*, 837 (1959); 5031 (1960).

(5) A. K. Galwey and P. W. M. Jacobs, *Trans. Faraday Soc.*, **55**, 1165 (1959); **56**, 581 (1960).

(6) A. K. Galwey and P. W. M. Jacobs, *Proc. Roy. Soc.* (London), **A254**, 455 (1960).

(7) P. W. M. Jacobs and A. R. Tariq Kureishy, "Eighth Symposium (International) on Combustion," The Williams and Wilkins Company, Baltimore, Maryland, 1962, p. 672.

(8) R. Friedman, R. G. Nugent, K. E. Rumbel, and A. S. Scurlock, "Sixth Symposium (International) on Combustion," Reinhold Publ. Corp. New York, N. Y., 1957, p. 612.

(9) J. B. Levy and R. Friedman, "Eighth Symposium (International) on Combustion," The Williams and Wilkins Company, Baltimore, Maryland, 1962, p. 663.

(10) R. Friedman and J. B. Levy, Final Technical Report AFOSR 2005, Atlantic Research Corporation, Alexandria, Virginia (1961).

(11) J. A. Beattie, *Rev. Sci. Instr.*, **2**, 458 (1931).

(12) F. D. Snell and C. T. Snell, "Colorimetric Methods of Analysis," 3rd. Ed., Vol. II, D. van Nostrand Co., Inc., New York, N. Y., 1949, p. 815.

(13) E. A. Burns and R. F. Muraca, *Anal. Chem.*, **32**, 1316 (1960).

(14) D. M. Coulson and L. A. Cavanagh, *ibid.*, **32**, 1245 (1960).

Table I

Experimental Conditions and Data on Dissociation Vapor Pressure Measurements

Runs	Bath temp. (°K.)	Initial mass of AP (g.)	Flow rate, cc./min.	Collection time, min.	Total moles in sublimate, mole × 10^3			Vapor pressure, mm., based on		Remarks[a]
					NH_4^+	ClO_4^-	Cl^-	NH_4^+	ClO_4^-	
1	523	1.00	152	90	0.012	..	..	0.032	..	43–61 μ
2	523	2.00	152	135	.016	..	..	.028	..	43–61 μ
3	525	2.00	152	105	.014	..	..	.032	..	
4	525	6.00	152	90	.013	..	0.0017	.035	..	
5	528	2.00	152	105	.021	0.024	.0010	.049	0.057	AP sample heated for more than 4 hr. before collection
6	537	2.00	152	85	.024	..	..	.070	..	
7	538	2.00	152	70	.029	..	..	.079	..	
8	547	6.00	152	120	.047	..	..	.098	..	
9	548	2.00	152	60	.034	.035	..	.14	.14	
10	551	1.00	293	100	.113	..	..	.14	..	43–61 μ
11	551	1.00	152	90	.053	..	..	.14	..	43–61 μ
12	551	2.00	152	60	.038	..	..	.15	..	
13	561	2.00	152	60	.047	..	..	.20	..	
14	561	2.00	152	60	.057	..	..	.23	..	Distance between powder bed and cold finger is 4 cm.
15	561	2.00	293	63	.097	..	..	.19	..	
16	561	6.00	152	60	.051	..	..	.21	..	
17	562	2.00	293	60	.0045	..	.0025	..	..	20 cc./min. NH_3 added
18	577	2.00	152	60	.098	..	..	.40	..	
19	575	2.00	293	60	.19	.19	pos	.41	.40	
20	573	2.00	152	60	.090	.085	..	.37	.32	AP sample heated for more than 4 hr. before collection
21	588	2.00	152	63	.19	.16	pos	.74	.64	
22	588	2.00	152	60	.20	.17	pos	.81	.70	
23	600	2.00	152	60	.027	nil	.027	..	..	20 cc./min. NH_3 added
24	600	2.00	152	30	.15	.15	..	1.26	1.23	Distance between powder bed and cold finger is 4 cm.
25	602	2.00	152	30	.15	.13	.0087	1.19	1.09	
26	615	2.00	152	30	.28	..	..	2.29	..	
27	616	2.00	152	30	.27	.28	.0018	2.24	2.26	

[a] Initial particle size >61μ, and, distance between powder bed and cold finger 2 cm., except where noted.

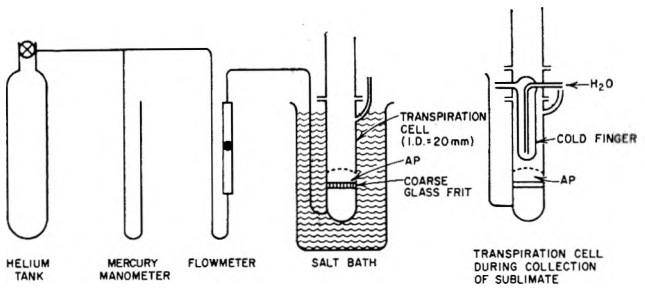

Fig. 1.—Schematic diagram of apparatus.

these data the dissociation pressures are plotted against the reciprocal of the absolute temperature as shown in Fig. 2. The resulting line may be expressed by the equation

$$\log P \text{ (mm.)} = -\frac{6283.7}{T} + 10.56 \qquad (2)$$

In our experiments the flow rate of the carrier gas was selected sufficiently high so that the mass transfer from the powder to the cold finger was not diffusion-limited. Yet the flow velocity was kept low enough to eliminate mechanical carry-over of particulate matter. The absence of mechanical transport of powdered AP particles onto the cold finger could be demonstrated by: (1) the agreement observed in experimental measurements of dissociation pressures in which the flow velocity was increased by a factor of two, and (2) the non-appearance of a deposit at temperatures at which dissociative sublimation is negligibly small. Under these experimental conditions there is no evidence of any serious cooling of the powder, since the results obtained are comparable within the experimental precision when the finger is placed 2 or 4 cm. from the bed (Table I, runs 14 and 24). In addition, it can be shown that the decomposition of $HClO_4$ is negligibly small in the temperature range studied from the rate constant for the decomposition of gaseous perchloric acid reported by Levy.[15]

To test the saturation of the carrier gas by the dissociation products, the flow rate of helium gas was varied by a factor of two and the initial mass of the sample by a factor of six. A decrease in the flow rate of helium and an increase in the initial mass of the sample will tend to favor saturation of carrier gas since the residence time of the products is increased. Under most favorable conditions (helium flow of 152 cc./min. and a 6-g. sample) the results obtained were comparable to runs made under most unfavorable conditions (low mass + high flow).

Experimentally the dissociation pressure measurements were limited to a temperature range from 510 to 620°K. At lower temperatures the quantity of sublimate collected within a reasonable length of time was too small for analysis; at temperatures above 620°K. the decomposition of the perchloric acid can no longer be neglected.

(15) J. B. Levy, AFOSR TN 1555, Atlantic Research Corporation, Alexandria, Virginia (1961).

During the determination of the dissociation pressure of AP, it has been observed that dissociation (reaction 1) and thermal decomposition occur simultaneously. After the sample was heated for an hour at 513°K. the pressure of the decomposition products calculated from the composition of the gas mixture as determined by thermal conductivity measurements was found to be roughly three times greater than the dissociation pressure. Experiments at 498°K. and at 573°K. in which the sample was heated for more than four hours before starting collection of disociation products gave pressure data in good agreement with those runs in which the sample was heated for a much shorter time (Table I, runs 5 and 20). On the basis of these results it may be assumed that the thermal decomposition reaction does not affect the dissociative sublimation.

As indicated in Table I, the sublimates were found to contain, besides NH_4^+ and ClO_4^-, small amounts of Cl^- (2–3 mole %). In the sublimates collected from experiments in which 20 cc./min. of NH_3 were introduced to the carrier gas, equimolar amounts of NH_4^+ and Cl^- were found to be present; however, only traces of ClO_4^- were detected (see runs 17 and 23). A simple calculation shows that when NH_3 is added the pressure of $HClO_4$ is suppressed to nearly zero. From these results it is reasonable to assume (1) that the chloride ion is most likely present as NH_4Cl arising from the interaction of Cl_2 (thermal decomposition product) with NH_3

$$8NH_3 + 3Cl_2 = 6NH_4Cl + N_2 \qquad (3)$$

and (2) that the AP sublimes by the dissociation process (reaction 1). As indicated by reaction 3, for each mole of NH_3 that reacts with Cl_2, $^3/_4$ of a mole is recovered as NH_4^+.

Since the chloride analyses were made in only a few runs and the precision of the analysis of Cl^- was probably ±10%, no attempts were made to compensate for this small loss of NH_4^+. Due to this small loss the error in the calculated dissociation pressure based on the NH_4^+ is estimated to be smaller than the analytical errors. On the other hand, the loss of NH_3 by reaction 3 reduces the amount of $HClO_4$ on the cold finger. Consequently, the error in the calculated dissociation pressure based on the ClO_4^- analysis is somewhat larger.

The entropies of sublimation with dissociation at pressure of 10 mm. were calculated for NH_4Cl,[16] NH_4NO_3,[17] and NH_4ClO_4 and are listed in Table II. The entropy of AP is consistent with the other ammonium compounds which further suggests the equilibrium dissociation of AP (reaction 1) rather than sublimation of a NH_4ClO_4 molecule as an entity. The latter fact is further substantiated by the pronounced suppression of sublimation by ammonia gas in the carrier stream as observed in our experiments.

A comparison of the experimental heat of dissociation with a theoretical value based on the heat of reaction 1 is made difficult because of lack of information concerning the heat of formation of gaseous $HClO_4$. An estimate of the heat of reaction at 298°K. may be

(16) W. H. Rodebush and J. C. Michalek, *J. Am. Chem. Soc.*, **51**, 748 (1929).

(17) G. Feick, *ibid.*, **76**, 5858 (1954).

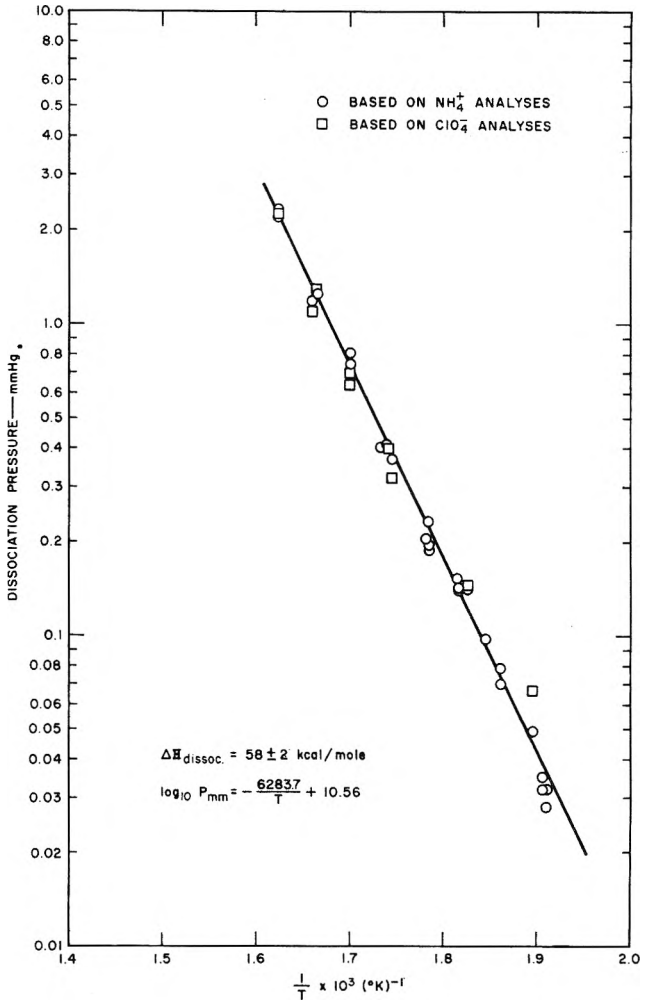

Fig. 2.—Dissociation pressure of ammonium perchlorate.

TABLE II

ENTROPY OF DISSOCIATION

Compounds	ΔH dissoc. (kcal./mole)	Temp. at which dissoc. press. = 10 mm. (°K.)	ΔS at cited temp. (cal./deg. mole)
NH_4NO_3(l)	39.8	485	~82
NH_4Cl(s)	39.4	483	~83
NH_4ClO_4(s)	58	657[a]	~88

[a] Based on extrapolation to 10 mm.

obtained by using the following values NH_4ClO_4(s),[18] $(\Delta H_f^0)_{298} = -70.7$ kcal./mole; NH_3(g),[19] $(\Delta H_f^0)_{298} = -11.0$ kcal./mole; $HClO_4$(l),[19] $(\Delta H_f^0)_{298} = -9.8$ kcal./mole. The value of $(\Delta H_f^0)_{298}$ for $HClO_4$(g) of −0.4 kcal./mole is based on the assumption that the heat of evaporation of $HClO_4$(l) is the same as that of HNO_3(l), *i.e.*, 9.4 kcal./mole. From these thermodynamic data, the heat of dissociation of NH_4ClO_4(s) is calculated to be 59.3 kcal./mole, a value only slightly different from that obtained experimentally at higher temperatures.

Acknowledgment.—The authors are indebted to Mr. Oliver Smith and Miss Elizabeth McCarthy for the chemical analyses.

(18) A. A. Gilliland and W. H. Johnson, *J. Research Natl. Bur. Standards*, **65A**, 67 (1961).

(19) National Bureau of Standards Report No. 7437, "Preliminary Report on the Thermodynamic Properties of Selected Light-Elements and Some Related Compounds," Jan., 1962.

CALCULATION OF COMPLEX CHEMICAL EQUILIBRIA BY SEARCH TECHNIQUES

BY R. G. ANTHONY AND D. M. HIMMELBLAU

Department of Chemical Engineering, The University of Texas, Austin 12, Texas

Received November 12, 1962

A new technique for solving problems involving complex equilibria is proposed, one which is substantially different from the iterative techniques of Brinkley, Huff, and White. The new procedure employs the method of "direct search" and must be carried out on a large size computer. The search procedure has the potential to handle more difficult classes of problems than the classical techniques. Application of the procedure to a simple problem gave the same results as the classical methods; application to a more complex problem previously reported by Brinkley brings out some of the paradoxes involved in solving sets of non-linear equations.

Introduction

The application of thermodynamics to complex equilibria calculations has been the subject of a number of articles[1-18] in the last twenty years. Excluding graphical methods, the basic three approaches to the calculation of complex compositions at equilibrium are those of Brinkley, Huff, and White. These are all iterative methods and of about the same degree of effectiveness from the viewpoint of convergence and time required. In order to compare the methods, they should all start with the same initial guesses for parameters. However, the technique used by Brinkley requires the guesses to satisfy the equilibrium conditions while White's technique requires them to satisfy the mass balances. Zeleznik and Gordon[16] have modified the two methods to avoid these restrictions, and shown that all three in essence are equivalent computationally.

We propose another iterative method of solution of the problem, but one which is quite different in procedure from those mentioned above, namely the use of the search technique.

Search Technique

Hooke and Jeeves[19] have proposed a procedure called "Direct Search" for use in optimization which seems to be well suited for use in equilibrium computations. Consider the following completely determined set of non-linear equations

$$f_\nu(x_1, x_2, \ldots, x_m) = 0 \qquad (1)$$

These can be solved for $x_1, x_2, \ldots, x_m$ by solving the following problem: Determine the values of x_i which minimize Φ, where

$$\Phi = \sum_{\nu=1}^{p} f_\nu(x_1, x_2, \ldots, x_m)^2 \qquad (2)$$

Direct search calls for assuming some initial values of the parameters x_i, finding the value of Φ, changing each of the values of x_i in rotation by a small amount Δx_i in a so-called "exploratory move," and checking the value of Φ each time to ascertain whether the change Δx_i has improved Φ (made it lower). On each trial, if Φ is lower, then a new value of x_i is adopted; if not, the sign of Δx_i is changed and the trial repeated. After one or more exploratory moves, a "pattern move" is made in which the distance moved in each coördinate x_i is proportional to the total number of successful exploratory moves previously made.

In this way large steps in one or more coördinate directions can be taken to reduce the time of computation. After taking repeated pattern moves, one finds a value of Φ which is a minimum. One can then (or earlier) cut down the step size of Δx_i so as to further refine the values of x_i, and repeat the whole procedure. The step sizes can be reduced until finally the change in Φ or x_i is small enough to warrant stopping.

In essence, the search technique proposed by Hooke and Jeeves is a clever logical scheme of search which can be modified in the details to suit one's personal fancies as to the best way to proceed.

Requirements for Complex Equilibria Calculations

To avoid confusion, let us define the following notation (all terms are presumed to be on the same basis, *i.e.*, per unit mass or mole of initial mixture)

a_{ij} = Stoichiometric coefficient giving the gram atoms of the ith element in the jth compound or species

b_i^0 = Initial gram atoms of the ith element of the mixture

b_i = Gram atoms of the ith element of the mixture at any intermediate composition; $b_i = \sum_{j=1}^{n} a_{ij}n_j$, $i \leq 1 \leq l$

G = Gibbs free energy for the jth compound or species, or for the ith element as indicated by the appropriate subscript. The superscript zero means standard state.

n_j = Moles of the jth species in the mixture, $1 \leq j \leq n$

Four essential physical statements are needed to completely define the calculation of the composition at equilibrium. These are:

(a) First, the mass balances for the individual elements

$$b_i - b_i^0 = 0 \qquad 1 \leq i \leq l \qquad (3)$$

For each element present one obtains a linear algebraic equation. In addition, a balance on the total number of moles of gas often is convenient to use.

(1) H. Kühl, *Forschungsheft*, **6**, 373 (1935).
(2) G. Damköhler, and R. Edse, *Z. Elektrochem.*, **49**, 178 (1943).
(3) S. Traustel, *Z. Ver. deut. Ing.*, **88**, 688 (1944).
(4) S. R. Brinkley, Jr., *J. Chem. Phys.*, **14**, 563 (1946).
(5) S. R. Brinkley, Jr., *ibid.*, **15**, 107 (1947).
(6) F. J. Krieger and W. B. White, *ibid.*, **16**, 358 (1948).
(7) H. J. Kandiner and S. R. Brinkley, Jr., *Ind. Eng. Chem.*, **42**, 850 (1950).
(8) V. N. Huff, S. Gordon, and V. E. Morrell, NACA Report 1037, 1951.
(9) W. B. White, S. M. Johnson, and G. B. Dantzig, *J. Chem. Phys.*, **28**, 751 (1958).
(10) S. Gordon, F. J. Zeleznik, and V. N. Huff, NASA TN D-132, 1959.
(11) D. S. Villars, *J. Phys. Chem.*, **63**, 521 (1959).
(12) S. R. Goldwasser, *Ind. Eng. Chem.*, **51**, 595 (1959).
(13) R. L. Potter and W. Vanderkulk, *J. Chem. Phys.*, **32**, 1304 (1960).
(14) B. R. Kubert and S. E. Stephanou in "Kinetics, Equilibria and Performance of High Temperature Systems," ed. by G. S. Bahn and E. F. Zukoski, Butterworths, London, 1960.
(15) F. P. Boynton, *J. Chem. Phys.*, **32**, 1880 (1960).
(16) F. J. Zeleznik and S. Gordon, NASA TN D-473, 1960.
(17) R. H. Boll, *J. Chem. Phys.*, **34**, 1108 (1961).
(18) R. C. Oliver, S. E. Stephanou, and R. W. Baier, *Chem. Eng.*, 121 (February 19, 1962).
(19) R. Hooke and T. A. Jeeves, *J. Assn. Comp. Mach.*, **8**, 212 (1961).

$$n_T = \sum_{j=1}^{n} n_j \qquad (4)$$

(b) The second set of statements are all inequalities, namely that the mole values cannot be negative.

$$n_j \geq 0 \qquad (5)$$

In a computer program for search it is easy to reject negative values of n_j by merely reverting to the old base value, or by applying a penalty function as indicated by Hooke and Jeeves.

(c) The third set of statements has to do with the criteria for equilibrium, and involves the free energy or its equivalent, the equilibrium constant. Two alternative ways of stating the physical situation exist, depending upon whether one wants to solve a completely determined set of nonlinear equations subject to equation 5, or whether one wants to carry out the solution by use of non-linear programming techniques. Both methods of specification can be solved by the search technique.

(1) As a first selection, one might state that the criterion for equilibrium is that the free energy change across a reaction is zero.

$$G_j - \sum_{i=1}^{l} a_{ij} G_i = 0 \qquad (6)$$

By selecting a suitable number of independent reactions, it is possible to obtain a set of completely determined equations of which part (equations 3 and 4) are linear, and part (equations 6) are non-linear.

If one introduces the definition of the equilibrium constant, $G_j^0 = -RT \ln K_{aj}$, where K_a is the equilibrium constant based on activities, then equation 6 can be converted into an equivalent set of non-linear equations involving the equilibrium constant.

(2) An alternative specification of the criterion of equilibrium is to state that the free energy of the system must be a minimum.

$$\text{minimize } \theta = \sum_{j=1}^{n} G_j n_j \qquad (7)$$

This is a non-linear objective function since $G_j = G_j^0 + RT \ln a_j$, and a_j is equal to a function of n_j (equal to n_j/n_T for unit activity coefficients and pressure). In applying a mathematical programming technique for solution, equations 3 and 4 are the constraints of the system and equations 5 are the non-negativity conditions.

(d) The fourth statement gives the value of G_j^0 by specifying P and T or P and H or P and S. By suitable substitution of alternate specifications, one might solve for other variables in addition to, or other than, the equilibrium composition.

Complex Equilibria Calculations by Search

If specification (c-1) is to be used, then one can solve the resulting set of completely determined non-linear equations using the search technique as previously indicated, *i.e.*, by solving equation 2 and thus in effect, equation 1.

As a simple example, we calculated the equilibrium concentration of an ideal producer gas at 1 atmosphere and 700° with the initial air composition: O_2, 17.335%; N_2, 65.214; H_2O, 17.451%. This example is taken from Gumz.[20] On the basis of one mole of initial mixture, with y designated as the mole fraction and n as the moles, we have

Equilibrium relations

$$K_1 = 1.07266 = \frac{(y_{CO})^2 P}{y_{CO_2}} = \frac{(n_{CO})^2 P}{(n_{CO_2})(n_T)}$$

$$K_2 = 1.66179 = \frac{(y_{CO})(y_{H_2})P}{y_{H_2O}} = \frac{(n_{CO})(n_{H_2})P}{(n_{H_2O})(n_T)}$$

$$K_3 = 0.031769 = \frac{y_{CH_4}}{(y_{H_2})^2 P} = \frac{(n_{CH_4})(n_T)}{(n_{H_2})^2 P}$$

Conservation equations

$$O_2: \ {}^1/_2(0.17451) + 0.17335 = n_{CO_2} + {}^1/_2 n_{CO} + {}^1/_2 n_{H_2O}$$

$$H_2: \ 0.17451 = n_{H_2} + 2n_{CH_4} + n_{H_2O}$$

$$N_2: \ 0.65214 = n_{N_2}$$

Gas phase balance

$$n_T = n_{CO} + n_{H_2} + n_{CO_2} + n_{H_2O} + n_{CH_4} + n_{N_2}$$

P is identical with 1, and the nitrogen balance eliminates n_{N_2}, leaving 3 non-linear and 3 linear equations involving 6 unknowns. Table I shows the excellent agreement between the final compositions obtained by search, and those reported by Gumz. The time required for each run was 40 seconds, and all trials converged to the same set of final values of n_i. The final values of Φ were all less than 1×10^{-15}.

If the ratio of the highest to lowest equilibrium concentrations becomes very large, say of the order 10^4 to 10^5, certain difficulties arise with the search (or any other) procedure. These are the loss of significant numbers on addition or subtraction either in equation 2 or in equations 3, 4, and 6. Fortunately, the search procedures forces these issues out into the open whereas most iterative or gradient techniques obscure and/or ignore the loss of significant decimals. The topic is analogous to the solution of linear sets of equations involving ill-condition matrices, both in its nature and in that little attention is usually paid to the possible loss of meaning in the numerical output.

In search, the dilemma can be ameliorated to some extent by suitable selection of the form of equations 3 for processing, and/or the scaling of the terms in equation 2. For example, consider the problem reported by Brinkley[7] detailed in Table II (using the correct values of K) which involved five linear material balance equations and six non-linear equilibrium relations, and in which the ratio of the largest to the smallest equilibrium concentration was 7×10^4. In solving the set of eleven equations by the search technique using equation 2, the search process ordinarily weights each one of the functions of f_ν equally, if one looks at equation 2 in a statistical (least square) sense. The final compositions so obtained do not agree with Brinkley's because he did not "weight" his equations equally but in fact unavoidably placed more emphasis on fitting certain of the equations (see Table III). The difficulty, of course, is that the terms in the non-linear

(20) W. Gumz, "Gas Producers and Blast Furnaces," John Wiley and Sons, New York, N. Y., 1950, pp. 50–58.

TABLE I

RESULTS OF SEARCH PROCEDURE FOR AN EQUILIBRIUM PRODUCER GAS COMPOSITION

Trial No.	CO	CO_2	H_2O	CH_4	H_2	N_2	Total
			Initially assumed values of n_i				
1	0.2	0.05	0.4	0.08	0.3	0.65	1.0
3	0.1	0.1	0.2	0.3	0.2	0.65	0.9
6	5.0	25.0	35.0	45.0	5.0	0.65	25.0
			Final values of n_i for all trials				
	0.33176	0.08271	0.02403	0.00057	0.14933	0.65214	1.2405
			Final values on a percentage basis				
Search	26.74	6.67	1.94	0.05	12.04	52.56	100.00
Gumz[20]	26.74	6.67	1.94	0.05	12.04	52.56	100.00

TABLE II

EQUATIONS FOR THE PROBLEM OF BRINKLEY[7] [a]

Linear Equations:

$$f_1 = 3 + n_5 + {}^1/_2 n_6 - {}^1/_2 n_7 - n_8 - n_9 - 2n_{10} - n_1 = 0$$
$$f_2 = 4 - n_5 - {}^1/_2 n_6 - {}^1/_2 n_7 - n_2 = 0$$
$$f_3 = 20 - {}^1/_2 n_9 - n_3 = 0$$
$$f_4 = -n_5 - {}^1/_2 n_6 + {}^1/_2 n_7 + n_8 + n_9 + 2n_{10} - n_4 = 0$$
$$f_{11} = n_1 + n_2 + n_3 + n_4 + n_5 + n_6 + n_7 + n_8 + n_9 + n_{10} - n_T = 0$$

Non-linear Equations:

$$f_5 = \frac{n_1 n_5}{n_2 n_4} - (1.93 \times 10^{-1}) = 0$$
$$f_6 = \frac{n_6 (n_1)^{1/2} (n_T)^{1/2}}{(n_2)^{1/2} (n_4)^{1/2}} - (2.597 \times 10^{-3}) = 0$$
$$f_7 = \frac{n_7 (n_T)^{1/2} (n_4)^{1/2}}{(n_1)^{1/2} (n_2)^{1/2}} - (3.448 \times 10^{-3}) = 0$$
$$f_8 = \frac{n_8 n_T n_4}{n_1} - (1.799 \times 10^{-5}) = 0$$
$$f_9 = \frac{n_9 n_T n_4}{n_1 (n_3)^{1/2}} - (2.155 \times 10^{-4}) = 0$$
$$f_{10} = \frac{n_{10} n_T (n_4)^2}{(n_1)^2} - (3.846 \times 10^{-5}) = 0$$

[a] All symbols are in Brinkley's notation; 1 = CO_2, 2 = H_2O, 3 = N_2, 4 = CO, 5 = H_2, 6 = H, 7 = OH, 8 = O, 9 = NO, 10 = O_2, T = 11 = Total.

TABLE III

ANALYSIS OF THE PROBLEM OF BRINKLEY[7] BY SEARCH TECHNIQUES

Tria		1	2	3	4	5	6	7	8	9	10	11	Φ
1	Initial n_i selections[a]	2.9158	3.9609	19.9863	0.0842	0.02215	0.00072	0.0332	0.00042	0.02741	0.03114	27.0722	1.1×10^{-4}
	Final n_i values	2.9342	3.9225	19.9867	0.0657	0.01696	0.00398	0.11674	1.63×10^{-6}	0.02635	2.7×10^{-5}	27.073	3.2×10^{-6}
	Weights	1	1	1	1	1	1	1	1	1	1	1	
	$(f_i - 0)$:	1.7×10^{-10}	-1×10^{-5}	-5×10^{-5}	0	6.5×10^{-4}	-2.2×10^{-3}	-2.9×10^{-3}	-1.8×10^{-5}	-1.8×10^{-4}	3.8×10^{-5}	1.3×10^{-5}	
2[b]	Initial selections	1.0	3.0	2.0	3.0	4.0	0.5	0.7	3.0	6.0	7.0	40.0	8×10^4
	Final values	2.9556	3.9867	19.9715	0.0444	0.0115	0.0033	0.00024	0.00051	0.0569	2.7×10^{-5}	27.03	1.2×10^{-6}
3[c]	Final values	2.735	3.8667	19.9741	0.2637	0.07194	0.00826	0.1139	0.00508	0.05211	0.1126	27.205	2×10^{-4}
	Weights used	1	1	1	1	10	10^4	10^4	10^6	10^5	10^5	1	1
4[d]	Initial selections	0.1	0.2	0.3	0.4	0.05	0.06	0.07	0.09	0.10	0.30	30	2.5×10^{12}
	Final values	2.7371	3.8669	19.9974	0.2641	0.0720	0.00827	0.1138	0.00507	0.05206	0.1124	27.205	2.4×10^{-4}
	$(f_i - 0)$:	2.3×10^{-5}	3.3×10^{-6}	-9.3×10^{-5}	-2.3×10^{-6}	-2.3×10^{-6}	0.8×10^{-6}	3.5×10^{-6}	5.4×10^{-6}	0.6×10^{-6}	1.3 10^5	1.3 10^{-5}	

[a] This row is identical with Brinkley's final answers. [b] Same weights as in Trial no. 1. [c] Same initial guesses as in Trial no. 2. [d] Same weights as in Trial no. 3.

equations can be very small relative to the set of linear material balance equations so that the objective function 2 practically ignores the former. By judicious weighting (scaling) of the equations 1 so that the terms in equation 2 are all roughly of the same magnitude, an entirely different set of results can be obtained. These still do not agree with Brinkley's results as can also be seen in Table III. The weights employed in preparing Table II were not chosen arbitrarily but developed by scaling of the equilibrium relations. For example, for the reaction

$$CO_2 \rightleftarrows CO + O$$

multiplying the quantity

$$\left[\frac{n_8 n_{11} n_4}{n_1} - 1.799 \times 10^{-5}\right]^2 \qquad (8)$$

by

$$\alpha = \left[\frac{n_1}{n_{11} n_4}\right]^2 \qquad (9)$$

is equivalent to processing the function

$$\left[1.799 \times 10^{-5} \frac{n_1}{n_{11} n_4} - n_8\right]^2 \qquad (10)$$

The magnitude of the two terms in the brackets in equation 10 can be seen to be more nearly comparable to that of the material balance equations than the magnitude of the terms in equation 8 which are two to three orders of magnitudes smaller.

This weighting procedure implies that if one knows the free energy data for certain reactions with more precision than others, one can give more weight to

these reactions than the others in the search procedure by assigning selected weights to the functions comprising equation 2, selected in the sense that the weights might be proportional to the precision of the data. If one is particularly concerned with a given component(s) in a reaction, it seems feasible to bias the weighting arbitrarily to fit best the functions (in equation 2) which involves that component.

Our experience shows that in large dimensional problems, by suitable arrangement and combination of the linear material balance equations, the time of search can be substantially reduced. While no general rules can be offered, the schematic arrangement of Brinkley seems to be as suitable a method as any.

We now need to make a few remarks about the alternate specification (c-2). If specifications (c-2) is to be used, one has to solve a typical non-linear programming problem. In other words we have given a set of m linear equations with more unknowns (p unknowns) than equations (equations 3 and 4), the non-negativity conditions, and a non-linear objective function (equation 7). The direct search program proceeds as follows.

Select $(p - m)$ initial variables in equations 3 and 4. Calculate the remaining m unknowns by using equation 2, or by some alternate method. Next, calculate the value of the objective function. Now one begins to carry out the usual search routine. The first variable is changed by the selected amount, the other variables remaining the same except for the reserved group of m, which have to be redetermined each time. One now calculates the objective function to see if it has improved, and then goes back and changes the next successive variable. Only $(p - m)$ variables will ever be used in the search since the same m variables are always then completely determined. To control the operation of a computer program for this type of solution one needs some accessory logic in addition to the regular search routine, but the general scheme is essentially the same. Work is continuing on the non-linear programming problem to ascertain its scope and limitations.

COÖRDINATION COMPOUNDS. V. DETERMINATION OF THE DISSOCIATION CONSTANTS OF ACETYLACETONE IN MIXED SOLVENTS

BY PHILIP S. GENTILE, MICHAEL CEFOLA,

Department of Chemistry, Fordham University, Bronx 58, N. Y.

AND ALFRED V. CELIANO

Department of Chemistry, Seton Hall University, South Orange, N. J.

Received November 12, 1962

Dissociation constants of acetylacetone have been determined in methanol–, ethanol–, 1-propanol–, 2-propanol–, dioxane– and water mixtures, and various methanol–ethanol–water solutions at 25°. A linear relationship resulted when the pK_D's were plotted *vs.* the reciprocal of the dielectric of the media. A scheme was developed for approximating pK_D's from the molecular weight or "apparent" molecular weight of the organic solvent or solvents used in preparing the solvent systems.

Introduction

Stability constants of chelate compounds and dissociation constants of chelating agents have often been measured in mixed solvents because of the insolubility of one or more of the reactants in water. However, since these constants vary with solvent composition, the comparison and correlation of these constants is very difficult owing to the wide range of experimental conditions. In addition, the thermodynamic quantities for these reactions calculated from these data are limited to specific solvent systems. Consequently, studies have been made to determine the effect of the solvent on the dissociation constants.

The search for a correlating factor goes back to the work of Thomson[1] and Nernst[2] who suggested a connection between the dielectric constant of a solvent and its dissociating power. Wynne-Jones[3] showed that the ratio of the ionization constants of two weak electrolytes was a function of the dielectric constant of the medium, and varied linearly with $1/D$. Elliott and Kilpatrick[4] and Harned[5] find that the relationship fails in dioxane–water mixtures of high dioxane concentration. This failure of the Wynne-Jones relationship has also been observed in the data of James and Knox,[6] where deviations occur in the region of a dielectric of 35. However, the theory seems to be valid, at least in the dielectric range from 80 to 30, for the dissociation of formic and acetic acids in ethanol–water mixtures,[7] tetrabutylammonium iodide and sodium bromate in dioxane–water mixtures,[8] and the complexation of some metal ions with inorganic ligands in various solvents.[9]

A more theoretical approach to using the dielectric constant as a parameter in describing any solvent system may be found in the Bjerrum–Fuoss ion-pair model.[10,11] Denison and Ramsey[12] have constructed a model by assuming that two oppositely charged ions exist either in contact as an associated ion-pair, or at such a large distance apart that the coulombic force between them is negligible (*viz.*, in the state of free ions).

(1) J. J. Thomson, *Phil. Mag.*, **36**, 313 (1893).
(2) W. Nernst, *Z. physik. Chem.*, **13**, 535 (1894).
(3) W. F. K. Wynne-Jones, *Proc. Roy. Soc.* (London), **A140**, 440 (1933).
(4) J. H. Elliott and M. Kilpatrick, *J. Phys. Chem.*, **45**, 485 (1941).
(5) H. S. Harned, *ibid.*, **43**, 275 (1939).
(6) J. C. James and J. G. Knox, *Trans. Faraday Soc.*, **46**, 254 (1950).
(7) E. Grunwald and B. J. Berkowitz, *J. Am. Chem. Soc.*, **73**, 4939 (1951).
(8) R. M. Fuoss and C. A. Kraus, *ibid.*, **79**, 3304 (1957).
(9) J. Bjerrum, "Stability Constants," Part II, The Chemical Society, London, 1958, pp. 66 and 74.
(10) J. Bjerrum, *Kgl. Danske Videnskab Selskab.*, **7**, No. 9 (1926).
(11) R. M. Fuoss and C. A. Kraus, *J. Am. Chem. Soc.*, **55**, 1019 (1933).
(12) J. T. Denison and J. B. Ramsey, *ibid.*, **77**, 2615 (1955).

Despite the fact that an equation utilizing the dielectric constant offers a theoretical correlating factor, most authors have discarded it in favor of the mole fraction of organic solvent because the constants exhibit linearity with the latter over a wider range.

Van Uitert, *et al.*,[13] showed that the negative logarithm of the dissociation constant (pK_D) of some β-diketones is a linear function of the mole fraction of dioxane (0.1 to 0.4). in dioxane–water mixtures of low dioxane concentration. The same relationship has been established for a number of organic compounds in dioxane–water[14-19] and methanol–water mixtures.[20]

The relationship utilizing the mole fraction parameter is certainly valid for the individual solvent systems studied. It will be shown, however, that this parameter cannot be used to correlate data for dissociation constants in *various* solvent systems in as simple a manner as when the dielectric constant is employed as the correlating factor. However, the mole fraction relationship will be shown to be more useful than presently thought by the study of the dissociation constant of one chelating agent in a variety of solvent systems, an approach which has not been used up to now.

Experimental

Reagents.—The acetylacetone, 1-propanol and 2-propanol (Fisher Scientific Co.) were purified by fractional distillation. Ten per cent tetramethylammonium hydroxide (Eastman Kodak Co.) was used after potentiometric standardization with 0.1 *N* HCl. The methanol and dioxane were commercial grade, purified by standard methods. The reagent grade absolute ethanol was purified by fractional distillation and stored over activated alumina.

Procedure. The Dissociation Constants of Acetylacetone.—The dissociation constant of acetylacetone was determined potentiometrically according to the method of Van Uitert.[21] All measurements were made at 0, 25 and 40 ± 0.1° with a Beckman Model G pH meter equipped with a glass (Beckman type E)–saturated calomel electrode system. The temperatures were checked with a thermometer calibrated by the National Bureau of Standards.

pK_D Determination in Two-Component Solvent Systems.—Since the reading given by the pH meter is the true hydrogen ion activity only when the solvent is water, it is necessary to calibrate the glass electrode when solvents other than water are used. To accomplish this, 8.6 ml. of 0.0500 *M* HCl in 1.41 ml. of 0.0307 *M* NaCl were added to 40, 30, 20, 15, 10, 5, and 0 ml. of distilled water in each of seven 50-ml. volumetric flasks. Enough of a recorded amount of organic solvent was added to each of the flasks to make the total volume 50 ml. Each flask then contained 0.0086 *M* hydrochloric acid and sodium chloride. This procedure was followed for each of the five organic solvents used in these determinations.

To measure the dissociation constants of acetylacetone, a stock solution of 3.441 g. of acetylacetone made up to 100 ml. with distilled water was prepared; 5 ml. of this stock solution then contained 0.00172 mole of acetylacetone. Twenty ml. of the tetramethylammonium hydroxide diluted to 100 ml. with water was equivalent to a 0.2186 *N* solution, 3.93 ml. of which will neutralize 0.00086 mole of the diketone. Individual solutions were prepared from these stock solutions by adding 5 ml. of acetylacetone stock solutions, 3.93 ml. of the tetramethylammonium hydroxide and 1.07 ml. of water to the same quantities of water and organic solvent used in the preparation of the calibration solutions. These solutions were freshly prepared before use because they were not stable over long periods of time.

pK_D Determination in Three-Component Solvent System.—To calibrate the glass electrode, 8.6 ml. of 0.500 *M* HCl and 1.41 ml. of 0.0307 *M* NaCl were added to each of ten 50-ml. volumetric flasks. These solutions were then diluted to 50 ml. with solvent.

To measure the dissociation constants, 5 ml. of acetylacetone and 3.93 ml. of tetramethylammonium hydroxide stock solutions (prepared as described above) and 1.07 ml. of water were added to the same quantities of water, ethanol and methanol used in the preparation of the calibration solutions.

Calibration of the Glass Electrode.—Retaining the terminology of Van Uitert[21] all pH readings taken in mixed solvents will hereafter be called "*B*" values since the term "pH" refers only to aqueous solutions. The *B* values obtained from the calibration solutions were converted to a quantity U_H, which is defined by

$$U_H = \text{antilog } (-B)/[H^+] \qquad (1)$$

where $[H^+]$ is the known stoichiometric hydrogen ion concentration of the solutions, assuming 100% dissociation of the acid not only in aqueous solutions, but also in partially aqueous solutions. U_H is then a conversion factor for obtaining the hydrogen ion concentration from the meter reading *B* according to the equation

$$-\log [H^+] = B + \log U_H \qquad (2)$$

and it is a function of ionic concentration and solvent composition. Van Uitert has also shown that by correcting the hydrogen ion concentration values to hydrogen ion activities by interpolating the mean activity coefficients, $\gamma_\pm$, for HCl from data given by Harned and Owen,[22] one can obtain an absolute calibration factor, log U_H^0, defined by

$$U_H^0 = U_{H/\gamma_\pm} \qquad (3)$$

which is a factor independent of ionic concentration and, therefore, corresponds to the correction at zero ionic strength in the solvent under consideration. The dielectric constants were obtained from the data of Åkerlöf.[23,24]

The glass electrode was calibrated in essentially the same way for the three-component solvent systems, but with a slight modification. Methanol and ethanol were added in definite weight ratios, 1:1, 3:1, and 1:3. The relative amounts of organic solvents and water were varied to give a representative sampling of the system ethanol–methanol–water. The dielectric constants for these solutions were obtained from the data of Gentile, *et al.*[25]

The Dissociation Constants of Acetylacetone.—When a weak acid dissociates, the expression for the dissociation constant, K_D, is

$$K_D = \frac{a_{H^+}a_{A^-}}{a_{HA}} = \frac{[H^+][A^-]}{[HA]} \times \frac{\gamma_{H^+}\gamma_{A^-}}{\gamma_{HA}} \qquad (4)$$

where "*a*" denotes the activity of each species and [ ] denotes concentrations. When $[A^-] = [HA]$, by taking logarithms and substituting equation 2 into 4, pK_D may be calculated by the use of the following approximations: (1) Set γ_{HA} equal to unity. This is an approximation neglecting salt effects on the neutral molecule; (2) For $\gamma_{H^+}\gamma_{A^-}$ use $\gamma_\pm^2$ obtained for HCl in the same medium and at the same total ionic concentration. Thus, the expression for obtaining the thermodynamic dissociation, pK_D, of a weak acid in mixed solvents becomes

$$pK_D = B + \log U_H + \log 1/\gamma_\pm^2 \qquad (5)$$

and the expression for obtaining the concentration constant, pK_D', is merely

$$pK_D' = B + \log U_H \qquad (6)$$

The acid dissociation constants of acetylacetone at 25° ob-

(13) L. G. Van Uitert, C. G. Haas, W. C. Fernelius, and B. E. Douglas, *J. Am. Chem. Soc.*, **75**, 455 (1953).
(14) H. Irving and H. Rossotti, *Analyst*, **80**, 245 (1955).
(15) H. Irving and H. Rossotti, *Acta Chem. Scand.*, **10**, 72 (1956).
(16) M. E. Maley and D. P. Mellor, *Australian J. Sci. Res.*, **A2**, 92 (1949).
(17) B. Saxton and H. F. Maier, *J. Am. Chem. Soc.*, **56**, 1918 (1934).
(18) H. S. Dunsmore and J. C. Speakman, *Trans. Faraday Soc.*, **50**, 236 (1954).
(19) J. C. James and J. G. Knox, *ibid.*, **46**, 254 (1950).
(20) W. F. K. Wynne-Jones and G. Salomon, *ibid.*, **34**, 1321 (1938).
(21) L. G. Van Uitert and C. G. Haas, *J. Am. Chem. Soc.*, **75**, 451 (1953).
(22) H. S. Harned and B. B. Owen, "The Physical Chemistry of Electrolytic Solutions," Reinhold Publ. Corp., New York, N. Y., 1958, p. 716 ff.
(23) G. Åkerlöf, *J. Am. Chem. Soc.*, **54**, 4125 (1932).
(24) G. Åkerlöf and O. A. Short, *ibid.*, **58**, 1241 (1936).
(25) P. S. Gentile, M. Cefola and A. Celiano, "Dielectric Constants of the Ternary System Ethanol–Methanol–Water," unpublished data.

tained by this procedure are reported in Table I. The activity data of Gentile, et al.,[26] was used for the 1-propanol system. The average deviation of these values was found to be ±0.02 log units, and the value in water agrees within the limits of experimental error with the values of Eidinoff[27] and Cartledge.[28]

TABLE I

THE DISSOCIATION CONSTANTS OF ACETYLACETONE IN TWO-COMPONENT SOLVENT SYSTEMS AT 25°

Solvent system	Mole fraction of organic solvent	$1/D$	pK_D'	pK_D
Ethanol–Water	0.0000	0.0127	8.86	8.97
	.0771	.0146	8.98	9.12
	.1822	.0174	9.14	9.32
	.2480	.0196	9.28	9.49
	.3286	.0217	9.45	9.69
	.4299	.0251	9.67	9.96
	.5601	.0292	9.93	10.28
Methanol–Water	0.1059	0.0142	8.96	9.09
	.2402	.0162	9.06	9.22
	.3210	.0176	9.20	9.38
	.3992	.0190	9.27	9.47
	.5200	.0212	9.39	9.63
	.6474	.0237	9.50	9.77
Dioxane–Water	0.0526	0.0167	9.08	9.25
	.1285	.0238	9.57	9.85
	.1800	.0302	9.93	10.31
	.2467	.0408	10.38	10.92
2-Propanol–Water	0.0603	0.0152	9.06	9.21
	.1442	.0190	9.25	9.46
	.2002	.0221	9.45	9.71
	.2712	.0264	9.68	10.01
1-Propanol–Water	0.0619	0.0151	9.04	9.19
	.1453	.0188	9.29	9.50
	.2011	.0219	9.46	9.72
	.2732	.0255	9.66	10.07
	.3676	.0306	9.95	10.44

Results

The expected linear relationship between pK_D' and the mole fraction of the organic solvent[13,29] is observed for each of the five two-component solvent systems as shown in Fig. 1. It is noted such a plot yields curves of different slope for each solvent system. A plot of pK_D' *vs.* $1/D$ on the other hand, resolves all the data to a single linear relationship for values of D between 80 and 30. A plot of pK_D, the thermodynamic constant, *vs.* $1/D$, likewise gives rise to a linear relationship. The equations for these curves in the linear region, as determined by the least squares are

$$pK_D = 77.02(1/D) + 7.99 \qquad (7)$$

and

$$pK_D' = 66.33(1/D) + 7.96 \qquad (8)$$

This shows that the relationship advanced by Wynne-Jones[3] is also valid for a single ligand in various mixed solvents throughout a dielectric constant range of 80 to 30.

Below a dielectric range of 30, the pK_D as a function of $1/D$ deviates from linearity as expected. Glasstone, Laidler and Eyring[30] have attributed this deviation to the fact that organic solvent–water mixtures are generally treated as homogeneous media of uniform dielectric constant. However, it is possible that in such solutions, there will be preferential orientation of the water molecules around the ions, thus placing them in an environment of higher dielectric constant. Since the measured

(26) P. S. Gentile, L. Eberle, M. Cefola, and A. V. Celiano, *J. Chem. Eng. Data*, in press.

(27) M. L. Eidinoff, *J. Am. Chem. Soc.*, **67**, 2072 (1945).

(28) G. H. Cartledge, *ibid.*, **73**, 4416 (1951).

(29) H. S. Harned and L. D. Fallon, *ibid.*, **61**, 2377 (1939).

(30) S. Glasstone, L. K. Laidler, and H. Eyring, "The Theory of Rate Processes," McGraw-Hill Book Co., New York, N. Y., 1941, p. 432.

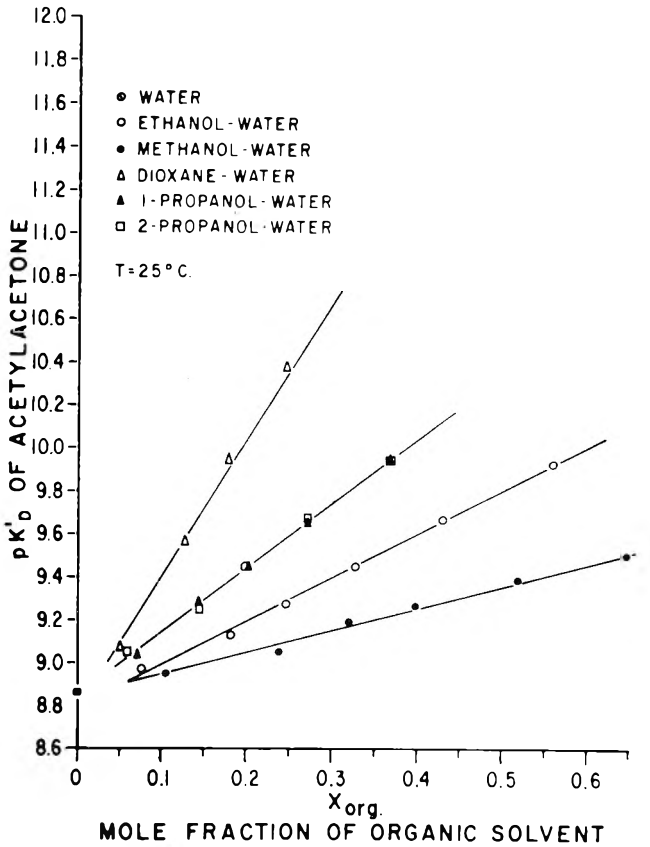

Fig. 1.—The pK_D' of acetylacetone as a function of the mole fraction of the organic solvent.

dielectric constant is that of the bulk of the medium, a lower pK_D is expected and observed. An examination of Fig. 1, in which pK_D' is found to be a linear function of mole fraction, leads to an interesting observation. The slopes of these lines (dpK_D'/dX_{org}), determined by the method of least squares, are found to be a linear function of the molecular weight of the organic solvent. This relationship is valid for the two-component solvent systems studied, when the solvents are within the same class, *i.e.*, for the alcohol–water mixtures, but not for the dioxane–water system. The equation for the line is

$$\frac{dpK_D'}{dX_{org}} = 0.0703(\text{m.w.}) - 1.247 \qquad (9)$$

If this relationship is valid for all alcohol–water systems it follows that the pK_D' of a given ligand can be approximately predicted by employing equation 9 in conjunction with the value of pK_D' for that same ligand in pure water. For example, if one wishes to calculate the pK_D' of acetylacetone in a system where the molecular weight of the alcohol is 50, one would first determine the value of dpK_D'/dX_{org} from equation 9, and then draw a line with this slope through the value of pK_D' for acetylacetone in water, where $X_{org} = 0$. This latter value is not the experimental value determined in H_2O but is the average value of intercepts determined in Fig. 1. This curve would be similar to those of Fig. 1. pK_D' can then be determined for any mole fraction of organic solvent. A similar procedure could be followed for a prediction of pK_D.

If one wishes to study and correlate dissociation constants of chelating agents and stability constants of chelate compounds in the dielectric region of 80–30, it appears that the choice of alcohol–water systems might be more advisable than the dioxane–water systems.

A good test of the validity of the approach spoken of above is not a mere application of equation 9 to encompass other alcohols, but rather its applicability to a three-component system.

pK_D' of Acetylacetone in the Solvent System Methanol–Ethanol–Water.—Table II presents data for pK_D' of acetylacetone determined in a variety of methanol–ethanol–water mixtures. pK_D values could not be calculated since activity coefficient data is not available. A plot of pK_D' *vs.* $1/D$ yields a

Table II

The Dissociation Constants of Acetylacetone in the Ternary System Ethanol–Methanol–Water at 25°

Weight % water	Weight % ethanol	Weight % methanol	$1/D$	pK_D'
85.2	7.4	7.4	0.0141	9.00
69.0	15.5	15.5	.0160	9.05
51.4	24.3	24.3	.0187	9.25
83.5	4.1	12.4	.0142	8.92
65.6	8.6	25.8	.0163	9.08
45.8	13.6	40.6	.0196	9.31
83.5	12.4	4.1	.0144	8.91
45.8	40.6	13.6	.0207	9.36
24.0	57.0	19.0	.0267	9.79

Table III

Comparison of Calculated and Observed pK_D' Values of Acetylacetone in Ethanol–Methanol–Water Solvent Systems

"Apparent" mol. wt.	Total organic mole fraction	$(pK_D')_{calcd}$	$(pK_D')_{obsd}$
37.8	0.077	8.92	9.00
37.8	.180	9.07	9.05
37.8	.311	9.26	9.25
34.7	.094	8.93	8.92
34.7	.216	9.07	9.08
34.7	.380	9.30	9.31
41.5	.079	8.95	8.91
41.5	.340	9.39	9.36
41.5	.580	9.79	9.79

straight line, as in the two-component systems, the equation for which is

$$pK_D' = 69.99\left(\frac{1}{D}\right) + 7.94 \qquad (10)$$

and compares favorably with equation 8. The composite equation for all values determined in both two- and three-component systems over the dielectric constant range 80–30 is

$$pK_D' = 67.18\left(\frac{1}{D}\right) + 7.96 \qquad (11)$$

In order to calculate the approximate values of pK_D' in the three-component solvent system as described above, it is necessary to assign an "apparent" molecular weight to the mixture of organic solvents. The apparent molecular weight was determined from the following equation

$$(\text{m.w.})_{app.} = [(MW)X]_{MeOH} + [(MW)X]_{EtOH} \qquad (12)$$

where

$$X_{MeOH} = \frac{\text{moles MeOH}}{\text{moles MeOH} + \text{moles EtOH}}$$

and $X_{EtOH} = 1 - X_{MeOH}$. On this basis the data in Table II can be resolved into 3 separate solvent systems where the apparent molecular weights of the organic solvents are 34.7, 37.8 and 41.5, for 3:1, 1:1, 1:3 methanol–ethanol weight ratios, respectively. Employing the graphical technique described previously, the predicted pK_D' values are compared to the experimental values in Table III. The mole fractions listed are for total organic solvent present in the three-component mixture. Agreement between the two values is good.

In the discussion of the effect of solvents on the dissociation of acetylacetone it is clear that the reciprocal of the dielectric constant of the solvent is related in a simple manner to the dissociation constant and in solvents of similar basic strength it may be employed, without regard to the nature or number of organic solvents. It seems reasonable to presume that the dissociation constant may be predicted from a knowledge of the dielectric constant of the solvent alone.

In the case of alcohol–water mixtures, however, it has also been shown that the dissociation constant may be predicted without knowing the dielectric constant of the solvent, but merely from a knowledge of the molecular weight and mole fraction of the alcohol.

Acknowledgment.—We are grateful to Miss M. V. Orna for helping us obtain this data. This research was supported by the Atomic Energy Commission under contract AT(30-1)-906.

INFRARED SPECTRA OF GASEOUS AlF_3, $LiAlF_4$, AND $NaAlF_4$[1]

By Lawrence D. McCory, Robert C. Paule, and John L. Margrave

Department of Chemistry, University of Wisconsin, Madison, Wisconsin

Received November 14, 1962

Gaseous AlF_3 has been studied at 1340–1424°K. and found to have a strong infrared absorption at 945 cm.$^{-1}$ (10.6 μ). The vapors over $3LiF \cdot AlF_3$ and Na_3AlF_6 at 1200–1600°K. show absorptions at 775–783 cm.$^{-1}$ (12.8–12.9 μ) and 853–880 cm.$^{-1}$ (11.4–11.7 μ) which are presumably characteristic of the $LiAlF_4$ and $NaAlF_4$ gaseous molecules.

Introduction

Within the last few years, an increased interest has been exhibited in the species that exist in the vapor over various alkali fluoride–aluminum fluoride mixtures. Although several investigators[2] were able to prepare $MAlF_4$ solid phases, there was no indication of such species in the vapor phase until 1954 when Howard[3] performed experiments with cryolite (Na_3AlF_6) which he interpreted as indicating the presence of a new gaseous compound, $NaAlF_4$. Dewing[4] has shown the existence of an analogous gaseous compound, $NaAlCl_4$, for the NaCl–$AlCl_3$ system. Thus, one might expect to form solid $MAlX_4$ by condensation. Solid "$NaAlF_4$," however, decomposes into chiolite and AlF_3 according to the reaction

$$5(NaF \cdot AlF_3) \xrightarrow{470\text{–}480^\circ} 5NaF \cdot 3AlF_3 + 2AlF_3$$

Vapor pressure studies on the NaF–AlF_3 system by Ginsberg and Bohm,[5] by Vajna and Bacchiega,[6] and by Vetyukov, Bliustein and Poddymov[7] support the idea of a gaseous $NaAlF_4$ species. Frank[8] has shown

(1) Abstracted in part from the Ph.D. Thesis of R. C. Paule and the M.S. Thesis of L. D. McCory, submitted to the University of Wisconsin in 1962 and 1961, respectively.

(2) (a) P. P. Fedotieff and K. Timofeeff, *Z. anorg. allgem. Chem.*, **206**, 263 (1932); (b) Z. C. Brosset, *ibid.*, **235**, 139 (1937); **239**, 301 (1938).

(3) E. N. Howard, *J. Am. Chem. Soc.*, **76**, 2041 (1954).

(4) E. W. Dewing, *ibid.*, **77**, 2639 (1955).

(5) H. Ginsberg and A. Bohm, *Z. Elektrochem.*, **61**, 2, 315 (1957).

(6) A. Vajna and R. Bacchiega, *Met. ital.*, **52**, 481 (1960).

(7) M. Vetyukov, M. Bliustein, and V. Poddymov, *Zav. Tsvet. Met.*, **2**, 126 (1959).

the probable importance of the $NaAlF_4$ species in the electrolysis of fused cryolite–Al_2O_3 mixtures. Porter and Zeller[9] have shown $LiAlF_4$ to be the major vapor species over certain mixtures of LiF and AlF_3 from mass spectrometer studies.

The present study reports the infrared spectra of pure AlF_3 and of the complex vapors that exist over the solid mixture $3LiF \cdot AlF_3$ and over the compound Na_3AlF_6 over the range 2–15 μ.

Experimental Techniques

The spectra were obtained by using a modified Beckman IR-2 model recording spectrophotometer. The source beam of light was chopped before passing through the sample to eliminate the problem of radiation emission and reflection by the graphite container tube. Sodium chloride optics were used.

The furnace, which was placed between the monochromator and the source, was a Kanthal wire-wound tube furnace. A 24-in. long graphite tube served as the container tube for the sample. Water-cooled brass heads were attached to the ends of the graphite tube extending from the furnace, and KBr windows were then attached to these metal heads. Nitrogen gas was passed over the outside of the graphite tube to reduce the rate of oxidation of the tube, and argon gas was slowly flushed past the windows at each end.

With the graphite absorption cell empty, the furnace was heated and several background spectra were taken. The procedure was then repeated with either AlF_3, Na_3AlF_6, or the $LiF–AlF_3$ mixture in the graphite tube. Difficulty was encountered with the Na_3AlF_6 melting at about 1000° and running out of the hot zone of the graphite tube. Consequently, a graphite boat, which partially blocked the light path, had to be used to contain the Na_3AlF_6. The spectra of the gaseous compounds were reproduced at least twice in separate runs. Several grams of fluoride were vaporized in each run. The temperature was measured with an optical pyrometer. The effective spectral emissivity for the KBr window and mirror was about 0.46 ± 0.10.

In a normal run, the NaCl monochromator was used and the spectra were observed in the 2–15 μ region. However, due to strong absorption bands caused by CO_2 and H_2O vapor in the air, it was possible to detect only strong sample absorption bands in the 2–8.3 μ region.

Samples of AlF_3 and Na_3AlF_6 were furnished by the Aluminum Company of America and were used as received. The LiF was a Baker Reagent Grade Chemical.

Results

For gaseous AlF_3, only one band above that of the background was observed. This band was very strong and appeared at 10.6 μ (945 cm.$^{-1}$). The AlF_3 band first appeared at a temperature of about 950° and was observed over the temperature range 950–1250°.

Since AlF_3 is a planar molecula with a threefold axis, one can show that the observed experimental absorption peak must be characteristic of the doubly-degenerate fundamental vibrational frequency, ν_3. The observed absorption frequency, 945 cm.$^{-1}$, is fairly close to the 900 cm.$^{-1}$ estimated for ν_3 in the JANAF Tables.[10]

Klemperer[11] has observed a single absorption frequency for monomeric gaseous $AlCl_3$ in the 1200–325 cm.$^{-1}$ region, and his value of 610 cm.$^{-1}$ correlates well with the frequency observed here when corrected for the mass effect.

A crude measurement of the variation of intensity with temperature for the 10.6 μ AlF_3 band gave ΔH^{sub}_{298} = 59 ± 10 kcal./mole with the biggest uncertainty arising from the poorly defined length of the absorption path and the non-isothermal nature of the absorption cell, which had windows at room temperature.

The infrared absorption peaks for the vapor above $3LiF \cdot AlF_3$, above Na_3AlF_6 and for the background of a hot empty graphite tube have been observed over the temperature range 900–1200°. Two weak bands at 13.3 and 13.1 μ were sometimes observed over Na_3AlF_6. These bands could not be reproduced consistently and were apparently due to impurities.

A strong absorption at 13.5–13.6 μ was temperature independent and was found to be due to a thin condensed film on the KBr windows. Solid Na_3AlF_6 in a KBr pellet was run to obtain an infrared spectrum for comparison but the resultant spectrum was so broad and non-distinctive that no comparison could be made. The observed peak did not correspond to any features in the spectrum of solid NaF and neither solid $NaAlF_4$ nor its infrared spectrum are available. McCory[12] found that the SiF_6^{-2} ion in a variety of hexafluorosilicates has a strong band in the 13.4–14.0 μ region. Heslop, Ketelaar, and Buchler[13] recently have identified an absorption at 13.75 μ as characteristic of Na_2SiF_6 and named it as a frequent contaminant on the windows of high temperature cells in which fluorides were being studied. Thus, the 13.5–13.6μ absorption seems likely to be from a fluorosilicate window deposit.

The two remaining broad absorption peaks at 11.4–11.7 μ and at 12.8–12.9 μ which were not due to the background, were reproducible and dependent on the temperature, or more correctly, on the vapor pressures of $NaAlF_4$ and $LiAlF_4$. There were no characteristic absorption peaks from gaseous AlF_3 at 10.6 μ, or from gaseous LiF or NaF which would absorb at 10.2–10.4 and ~17.3 μ, respectively.[10,14,15]

The observed vibrational frequencies are likely due to Al-F vibrations and appear to be nearly independent of the alkali metal ion. The possibility of a common C–Al–F compound or C–F compound in these experiments cannot be absolutely excluded, but the formation of such compounds does not seem likely. The observed spectra do not correspond to the spectrum of CF_4.[10]

The JANAF Tables[10] list the frequencies 750 (1), 276 (2), 325 (3), 750 (3), and 800 (3) for $LiAlF_4$(g) based on the model of Porter and Zeller[9] which has C_{3v} symmetry and on analogies with KBF_4, SiF_4, and LiF. These agree reasonably well with the observed absorptions at 783–775 and 853–880 cm.$^{-1}$. Among the alternative, plausible structures for gaseous $MAlF_4$ are a square pyramid with a planar AlF_4 group and the alkali metal ion at the apex or a structure with tetrahedral coördination about the Al and fluorine bridges between the Al and Li. Further detailed infrared and electron diffraction studies will be necessary to establish the molecular configuration conclusively.

Acknowledgments.—The authors are pleased to acknowledge the financial support of this work by the Army Research Office (Durham) and by the Wisconsin Alumni Research Foundation.

(8) W. B. Frank, *J. Phys. Chem.*, **65**, 2081 (1961).
(9) R. F. Porter and E. A. Zeller, *J. Chem. Phys.*, **33**, 858 (1960).
(10) JANAF Tables of Thermochemical Data, Dow Chemical Company, Midland, Michigan, edited by D. R. Stull.
(11) W. Klemperer, *J. Chem. Phys.*, **24**, 353 (1956).
(12) L. D. McCory, M. S. Thesis, University of Wisconsin, 1961.
(13) W. R. Heslop, J. A. Ketelaar, and A. Buchler, *Spectrochem. Acta*, **16**, 513 (1960).
(14) E. S. Rittner, *J. Chem. Phys.*, **19**, 1030 (1951).
(15) (a) G. L. Vidale, *J. Phys. Chem.*, **64**, 314 (1960); (b) W. Klemperer, private communication.

STANDARD POTENTIAL OF THE SILVER–SILVER CHLORIDE ELECTRODE AND ACTIVITY COEFFICIENTS OF HYDROCHLORIC ACID IN AQUEOUS METHANOL (33.4 WT. %) WITH AND WITHOUT ADDED SODIUM CHLORIDE AT 25°

BY ROGER G. BATES AND DONALD ROSENTHAL

Solution Chemistry Section, National Bureau of Standards, Washington, D. C.

Received November 15, 1962

From measurements of the e.m.f. of hydrogen–silver chloride cells at 25°, the standard potential of the silver–silver chloride electrode has been found to be 0.2010 v. in aqueous methanol (33.4 wt. %). The activity coefficient of hydrochloric acid has been determined for molalities from 0.016 to 1.3 in 33.4% methanol and has been found to fit the extended Debye–Hückel equation with an ion size of 4.3 Å. The variation of the activity coefficient of hydrochloric acid (γ_1) in HCl–NaCl mixtures of constant total ionic strengths 0.16 to 1.3 in 33.4% methanol was found to be linear with the molality of salt, m_2. The coefficient α_{12} in the equation $\log \gamma_1 = \log \gamma_{1(0)} - \alpha_{12} m_2$ (where $\gamma_{1(0)}$ is the activity coefficient of hydrochloric acid in a salt-free solution of the same total ionic strength) has the values 0.040 and 0.034 at ionic strengths of 0.16 and 1.3, respectively.

Introduction

Electromotive force measurements of the cell

$$\text{Pt; } H_2 \text{ (g., 1 atm.), HCl}(m) \text{ in } CH_3OH \ (X \text{ wt. \%}), H_2O, \text{AgCl, Ag}$$

with pure methanol as the solvent have been made by Nonhebel and Hartley[1] and by Austin, Hunt, Johnson, and Parton.[2] Aqueous methanol solvents were studied by Harned and Thomas[3] (X = 10 and 20), by Parton, *et al.*,[2] (X = 43.3, 64.0, 84.2, and 94.2) and by Oiwa[4] (X = 20, 40, 60, 80, and 90).

It appears that the molality (m) of hydrochloric acid did not exceed 0.1 in any of the media with methanol content greater than 20%. The behavior of the activity coefficient of hydrochloric acid in mixtures of the acid and sodium chloride of constant total molality of unity in aqueous methanolic solvents (X = 10, 20, 30, 40, 50, and 60) has been investigated, however, by Akerlof, Teare, and Turck.[5]

For a study of salt effects and medium effects on indicator equilibria, the activity coefficient of hydrochloric acid at molalities between 0.01 and 1.0 in aqueous methanol (X = 33.4) was needed, as well as the influence of added sodium chloride on the activity coefficient in this range of total ionic strengths. An interpolation of the standard potential for the cell did not seem to be feasible, inasmuch as the results of Harned and Thomas[3] and of Oiwa[4] differ by 0.6 mv. at X = 20.

Measurements of the e.m.f. at 25° of the cell were therefore made in the medium X = 33.4 for solutions in which m varied from 0.016 to 1.3 and for selected mixtures of hydrochloric acid and sodium chloride of constant total ionic strength. The mixtures were studied at five ionic strengths between 0.16 and 1.3. The standard electromotive force of the cell at 25° was determined, activity coefficients were calculated, and the "Harned rule" coefficient α_{12} was determined for the acid–salt mixtures in aqueous methanol (X = 33.4).

(1) G. Nonhebel and H. Hartley, *Phil. Mag.* [6], **50**, 729 (1925).

(2) J. M. Austin, A. H. Hunt, F. A. Johnson, and H. N. Parton, unpublished work cited by R. A. Robinson and R. H. Stokes, "Electrolyte Solutions," 2nd Ed., Academic Press, Inc., New York, N. Y., 1959, Appendix 8.2.

(3) H. S. Harned and H. C. Thomas, *J. Am. Chem. Soc.*, **57**, 1666 (1935); **58**, 761 (1936).

(4) I. T. Oiwa, *Sci. Rpts. Tohoku Univ.*, **I**, **41**, 47 (1957).

(5) G. Akerlof, J. W. Teare, and H. Turck, *J. Am. Chem. Soc.*, **59**, 1916 (1937).

Experimental

The cells used were of the same general design as those long in use in this laboratory,[6] modified in the following ways to enhance their suitability for measurements with non-aqueous and mixed solvents: The size of the cell was considerably reduced, and the top portion of each electrode compartment was constructed entirely of glass. The compartments were joined at the bottom by a short length of capillary tubing, and each accommodated only one electrode, instead of a pair of identical electrodes as in the larger cells. A dual saturator for the entering hydrogen gas was a part of each cell. The saturator contained about 12 ml. of solution, whereas the electrode compartments themselves required about 20 ml. The electrodes were prepared by methods already described elsewhere.[7]

The solutions were prepared in 100-ml. amounts from 40 ml. of Spectro Grade methanol and aqueous solutions of hydrochloric acid and sodium chloride of known concentration. Polarographic examination of the methanol[8] showed that the concentration of formaldehyde was less than 3×10^{-5} M. The weight of methanol and the total weight of solution were determined, making possible the calculation of the molalities of the solutes and the weight composition of the solvent. The latter varied from 33.4 wt. % for the most dilute solution to 34.3 wt. % for the most concentrated. All of the observed e.m.f. data were adjusted to correspond to a solvent composition of 33.4 wt. %. For the most concentrated solutions studied, this adjustment added 0.57 mv. to the measured e.m.f. Corrections to 1 atm. partial pressure of hydrogen were made with the use of known vapor pressure data for methanol–water mixtures.[9]

Results

Standard Potentials.—The corrected values of the e.m.f. (E) for solutions of hydrochloric acid are summarized in Table I. In order to determine the standard electromotive force ${}_sE^0$ of the cell[10] (by definition[11] also the standard electrode potential of the silver–silver chloride electrode) the mean ionic activity coefficient of hydrochloric acid in 33.4 wt. % methanol was expressed by the extended Debye–Hückel equation, modified as necessary for concentrations on the molal scale. The density of the solvent was taken as 0.944 at 25°, the dielectric constant 64.0,[12] and the mean molecular weight 21.1.

By trial it was found that a value of 4.3 Å. for the ion-size parameter a^* gave a good fit of the experi-

(6) R. G. Bates and S. F. Acree, *J. Res. Natl. Bur. Std.*, **30**, 129 (1943).

(7) R. G. Bates, "Electrometric pH Determinations," John Wiley and Sons, Inc., New York, N. Y., 1954, pp. 166 and 205.

(8) The authors are indebted to J. K. Taylor and G. Marinenko for the polarographic examination of the methanol.

(9) J. A. V. Butler, D. W. Thomson, and W. H. Maclennan, *J. Chem. Soc.*, 674 (1933).

(10) The subscript s signifies that the standard state is aqueous methanolic solvent rather than pure water.

(11) J. A. Christiansen, *J. Am. Chem. Soc.*, **82**, 5517 (1960).

(12) P. S. Albright and L. J. Gosting, *ibid.*, **68**, 1061 (1946); T. Shedlovsky and R. L. Kay, *J. Phys. Chem.*, **60**, 151 (1956).

TABLE I

ELECTROMOTIVE FORCE (E) OF THE CELL Pt; H_2(g., 1 ATM.), HCl(m) [SOLVENT: 33.4 WT. % CH_3OH, 66.6 WT. % H_2O], AgCl; Ag AT 25° (IN V.)

Standard Electromotive Force ($_sE^0$) at 25°		
m	E	$_sE^0$
0.01590	0.42240	0.20127
.02113	.40855	.20104
.03178	.38911	.20126
.06356	.35622	.20080
.09560	.33717	.20093
.1276	.32374	.20108
.1595	.31323	.20113
.3198	.27955	.20096
.6436	.24365	.20085
.9741	.22070	.20105
1.307	.20284	.20101

Mean: 0.20103 ± 0.00011

Std. dev. of the mean: 0.00005 v.

mental data. This is the same value found for hydrochloric acid in water,[13,14] suggesting that ion association is negligible in 33.4 wt. % methanol.

The complete formula for $_sE^0$ thus becomes

$$_sE^0 = E + \frac{4.6052RT}{F}(\log m + \log {}_s\gamma_\pm) \quad (1)$$

where

$$\log {}_s\gamma_\pm = -\frac{0.6725\sqrt{m}}{1 + 1.521\sqrt{m}} + 0.132\,m + [\text{Ext.}] - \log(1 + 0.0422\,m) \quad (2)$$

The slope $4.6052RT/F$ has the value 0.11831 v. at 25°. The extended terms [Ext.] were obtained with the aid of the tables given by Gronwall, La Mer, and Sandved.[15] The coefficient (0.132) of the m term in equation 2 was determined graphically by plotting, as a function of m, the apparent $_sE^0$ values (computed without the second term on the right of eq. 2).

The values of $_sE^0$ derived from each e.m.f. measurement are listed in the last column of Table I. The average value is 0.20103 v., the mean departure from the average value is 0.00011 v., and the standard deviation of the mean is 0.00005 v. By application of the standard formulas interrelating the concentration scales, the standard potential on the molar scale, $_sE_c^0$, is found to be 0.1980 v., whereas that on the mole fraction scale, $_sE_N^0$, is 0.0027 v. These values appear to agree with the (interpolated) results of Oiwa[4] within 0.1 mv.

Activity Coefficients.—The activity coefficient of hydrochloric acid, $_s\gamma_\pm$, related to unity at infinite dilution in 33.4 wt. % methanol, was calculated by equation 2 at round molalities from 0.005 to 1.2 and is given in Table II. The corresponding values of [Ext.] (eq. 2) are listed in the second column.

The primary medium effect is a measure of the change of free energy which accompanies the transfer of one mole of HCl from infinite dilution in water to infinite dilution in 33.4% methanol

$$\text{HCl(in } H_2O) = \text{HCl(in 33.4\% MeOH)}$$

(13) H. S. Harned and B. B. Owen, "The Physical Chemistry of Electrolytic Solutions," 3rd Ed., Reinhold Publ. Corp., New York, N. Y., 1958, Chapters 11 and 14.

(14) R. G. Bates and V. E. Bower, *J. Res. Natl. Bur. Std.*, **53**, 283 (1954).

(15) T. H. Gronwall, V. K. La Mer, and K. Sandved, *Physik. Z.*, **29**, 358 (1928).

TABLE II

MEAN IONIC ACTIVITY COEFFICIENT, $_s\gamma_\pm$, OF HYDROCHLORIC ACID IN THE SOLVENT CH_3OH (33.4 WT. %), H_2O (66.6 WT. %) AT 25°

m	[Ext.]	$_s\gamma_\pm$
0.005	−0.0006	0.906
.01	.0009	875
.02	.0012	837
.05	.0014	.780
.07	.0015	.758
.1	.0015	.735
.2	.0013	.696
.5	.0009	.671
.7	.0007	.678
1.0	.0005	.703
1.2	.0003	.725

It is customarily expressed as an activity coefficient, $_m\gamma_\pm$. From the standard potentials of the cell in the two solvents, $\log {}_m\gamma_\pm = (0.22234 - 0.20103)/0.11831 = 0.1801$ at 25° and $_m\gamma_\pm = 1.514$. This expresses the well known fact that the escaping tendency of hydrochloric acid is greater in methanol–water solvents than in the pure aqueous solutions.

Mixtures of Hydrochloric Acid and Sodium Chloride.—The linear variation (with composition) of log $\gamma_\pm$ for hydrochloric acid and alkali chlorides in their mixtures of constant total ionic strength has been established not only for aqueous solutions[13] but also for methanol–water solvents up to $X = 60$.[5] This relationship is often called the "Harned rule." In the notation of Harned

$$\log \gamma_1 = \log \gamma_{1(0)} - \alpha_{12}m_2 \quad (3)$$

where γ_1 is the activity coefficient of hydrochloric acid in the mixture of HCl(m_1) and NaCl(m_2) and $\gamma_{1(0)}$ is the activity coefficient of the acid in a salt-free solution of the same ionic strength as the mixture.

Electromotive force data were obtained at 25° for nine mixtures of hydrochloric acid(m_1)–sodium chloride(m_2) at five different ionic strengths (I) in 33.4 wt. % methanol. The values of log $_s\gamma_\pm$ for hydrochloric acid in each solution were computed by the equation

$$-\log {}_s\gamma_\pm = \frac{(E - {}_sE^0)}{0.11831} + 1/2 \log m_1(m_1 + m_2) \quad (4)$$

whereas those for the salt-free solutions were calculated by eq. 2. These two quantities are, respectively, the log γ_1 and log $\gamma_{1(0)}$ of eq. 3.

The slope α_{12} was computed from the measurements

TABLE III

ACTIVITY COEFFICIENTS IN MIXTURES OF HYDROCHLORIC ACID AND SODIUM CHLORIDE, SOLVENT: 33.4 WT. % METHANOL, AT CONSTANT TOTAL IONIC STRENGTH (I); VALUES OF α_{12}

	Molality of			$-\log {}_s\gamma_\pm$		
I	HCl	NaCl	E_{25} (v.)	Obsd.	Calcd.[a]	Mean α_{12}
0.1595	0.1595	...		0.1502	...	
	.1277	0.03191	0.31904	.1520	0.1513	
	.06366	.09575	.33701	.1525	.1536	0.040 ± 0.016
0.3200	0.3200	...		0.1691	...	
	.1280	0.1920	0.30411	.1774	0.1758	
	.06385	.2560	.32204	.1779	0.1781	0.039 ± 0.005
0.6435	0.6435	...		0.1706	...	
	.3217	0.3217	0.26300	.1817	0.1819	
	.1287	.5150	.28753	.1903	.1886	0.036 ± 0.002
0.9712	0.9712	...		0.1550	...	
	.3238	0.6473	0.25180	.1779	0.1777	
	.1295	.8418	.27620	.1852	.1845	0.036 ± 0.001
1.306	1.306	...		0.1318	...	
	0.3261	0.9799	0.24252	.1653	0.1661	0.034

[a] For $\alpha_{12} = 0.035$ at each ionic strength.

on each mixture, and the mean value is given in the last column of Table III. The result at $I = 1$ is in good agreement with 0.034 interpolated for $X = 33.4$ and $t = 25°$ in the values found by Akerlof, Teare, and Turck[5] for a total ionic strength of unity.

It has already been noted[5,13] that addition of methanol to the aqueous solvent is almost without effect on the value of α_{12} (the value is 0.033 for aqueous mixtures of hydrochloric acid and sodium chloride of $I = 1$[5]). The results given in Table III suggest that α_{12} decreases slightly with increasing I, but the reduced accuracy with which α_{12} can be determined at ionic strengths below 1 probably makes such a conclusion unwarranted. Thus, the values of $-\log {}_s\gamma\pm$ in the sixth column of Table III (calculated with a constant value of $\alpha_{12} = 0.035$ at each ionic strength) differ from the "observed" values on the average by hardly more than the experimental error.

THE KINETICS OF THE REACTION BETWEEN VANADIUM(V) AND IRON(II)[1]

BY N. A. DAUGHERTY[2] AND T. W. NEWTON

University of California, Los Alamos Scientific Laboratory, Los Alamos, New Mexico

Received November 16, 1962

The kinetics of the reaction V(V) + Fe(II) = V(IV) + Fe(III) have been studied in acid perchlorate solutions from 0.047 to 1.0 *M* in $HClO_4$ over a temperature range from 0 to 55.6° at $\mu = 1.0$. The rate law found is $-d[V(V)]/dt = k'[V(V)][Fe(II)]$, where k' may be given by: $k' = a[H^+]^{-1} + b + c[H^+]$. The $c[H^+]$ term strongly predominates the others; values of ΔH^* and ΔS^* for this path were found to be 1.52 ± 0.16 kcal./mole and −37.3 ± 0.6 e.u.

Introduction

It has been found that the rapid reaction between V(V) and Fe(II) can be studied by an extension of ordinary spectrophotometric techniques. This reaction is of interest to us for two reasons. First, V(V) in acid solution is probably VO_2^+ and is structurally similar to the +5 actinide ions,[3] and a comparison of the kinetics of its reduction reactions with the analogous ones of the actinide ions should help elucidate some of the factors which determine such rates. One of these factors is the formal ionic entropy of the activated complex which for reactions involving actinide ions appears to be predominantly determined by the charge on the complex.[4] The second reason for interest is to see whether this correlation extends to reactions between transition metal ions.

Previous kinetic work on the reduction of V(V) by inorganic ions in non-complexing solutions is that of Ramsey, *et al.*, who studied the reduction by iodide ions.[5]

Experimental

Reagents.—Two stock solutions of V(V) perchlorate were prepared. For the first, Fisher Scientific Co. "purified" ammonium meta vanadate was recrystallized from hot water and heated to about 900° in an electric muffle to convert the ammonium salt to the oxide. This was dissolved in 3.34 *M* $HClO_4$ and treated with ozone to oxidize traces of V(IV) to V(V). Excess ozone was removed by passing oxygen through the solution for 16 hr. The second solution was prepared by dissolving vanadium metal in 5 *M* HNO_3 and fuming with $HClO_4$ to remove nitrate and to oxidize the vanadium to V(V). The V(V) content of these solutions was determined by titration of aliquots with standard $FeSO_4$ solution, according to the method of Hammett.[6] The titrations were done in 6 *M* H_2SO_4 to the ferrous phenanthroline end point. The two stock solutions were found to be 0.16 and 0.02 *M* in V(V). The free acid in the first stock solution was estimated to be 3.2 *M* based on the initial acid concentration and the final V(V) concentration. The second stock solution contained far less vanadium and the acid was found to be 4.2 *M* by titration with NaOH to the brom phenol blue end point. For the kinetic runs, only a small fraction of the total acid came from that present in the vanadium stock solutions; so errors in the estimation of the acid concentration in these stock solutions were completely negligible.

Most of the kinetic runs were made using the first stock solution but several were made with the second. Within the experimental error the same concentrations of the two solutions gave the same results; so it is unlikely that significant concentrations of catalytic impurities were present in either stock solution.

A stock solution of Fe(II) was prepared by dissolving a weighed amount of Mallinckrodt analytical grade iron wire in 0.5 *M* $HClO_4$ and then adding sufficient 3 *M* $HClO_4$ to give a solution 0.10 *M* in Fe and 0.50 *M* in $HClO_4$ upon dilution to the final volume. The solution was found to contain about 10^{-4} *M* Cl^-.

Solutions of $HClO_4$ were prepared by diluting analytical reagent grade concentrated acid. The concentrations of the solutions were determined from density measurements.[7] The concentrated acid had been freed of reducing impurities by boiling at atmospheric pressure and cooling in a stream of scrubbed argon.

Solutions of $LiClO_4$ were prepared by neutralizing analytical reagent grade Li_2CO_3 with $HClO_4$, boiling out the CO_2, and crystallizing from water at least three times. The salt solutions were analyzed by density determinations; the concentration *vs.* density functions were determined from previously analyzed solutions.[8]

The water used in the preparation of all solutions was doubly distilled; the second distillation was from alkaline $KMnO_4$ in an all Pyrex still.

Apparatus.—Rate runs were made in specially shaped Pyrex cells which were positioned in a small water-filled thermostat in the light beam of a Cary recording spectrophotometer, Model 14. The cells were similar to small erlenmeyer flasks to which two 25 mm o.d. tubes were sealed coaxially to provide a light path of about 10 cm. The ends of these tubes were left rounded since the water in the small thermostat eliminated most of the focussing effect which otherwise would have been present. The contents of the cells were stirred from below by means of Teflon covered magnetic stirring bars. The spectrophotometer was operated in the ultraviolet range using the hydrogen lamp. Since the cover of the sample-containing cell compartment was removed during kinetic runs, measurements were made with the room darkened. The reaction was started by injec-

(1) Work done under the auspices of the U. S. Atomic Energy Commission.

(2) Los Alamos Scientific Laboratory, Summer Staff Member.

(3) M. J. LaSalle and J. W. Cobble, *J. Phys. Chem.*, **59**, 519 (1955).

(4) T. W. Newton and S. W. Rabideau, *ibid.*, **63**, 365 (1959).

(5) J. B. Ramsey, E. L. Colichman, and L. C. Pack, *J. Am. Chem. Soc.*, **68**, 1695 (1946).

(6) C. H. Walden and L. P. Hammett, *ibid.*, **56**, 57 (1934).

(7) L. H. Brickwedde, *J. Res. Natl. Bur. Std.*, **42**, 309 (1949).

(8) T. W. Newton, *J. Phys. Chem.*, **62**, 943 (1958).

ing one of the reagents into a stirred solution of the other already in the cell. The injection was made by means of a 5-ml. hypodermic syringe with a large stainless steel needle. With this apparatus 5 ml. from the syringe could be mixed into 60 ml. in the cell in about 2 seconds.

In spite of the curvature of the cell windows, adherence to Beer's law was found to be satisfactory. Tests with $CoSO_4$ and $Pr(ClO_4)_3$ solutions showed that the total spread in apparent extinction coefficients up to an absorbance of 1.7 was 0.4 and 0.9%, respectively.

Procedure.—The reaction was followed spectrophotometrically by measuring the absorbance of the reaction mixture as a function of time. The wave lengths used were in the range of 3050 to 3500 Å. The general procedure for the kinetic measurements was as follows: Dilute stock solutions of V(V) and Fe(II) were made from the concentrated ones previously described. The concentration of Fe(II) was determined by pipetting aliquots into a measured excess of standard Ce(IV) and titration of the excess with standard $FeSO_4$ to the ferrous phenanthroline end point.

A 10-ml. aliquot of the dilute pervanadyl stock and 50 ml. of $HClO_4$–$LiClO_4$, to adjust acidity and ionic strength to the desired level, were pipetted into the reaction cell and the cell was placed in the small thermostat in the cell compartment. The analyzed Fe(II) stock was kept in a separate vessel at approximately the same temperature. After temperature equilibrium had been established, 5 ml. of the Fe(II) solution was injected into the stirred V(V) solution at the same time that the spectrophotometer recorder strip chart was started. The course of the reaction was recorded as absorbance at the desired wave length *vs.* time; chart speeds of 8 in./min. were used. The temperature of the reaction mixture was taken with a small thermometer about one minute after injection.

Calculations.—The initial reactant concentrations were calculated from those of the analyzed stock solutions. The extent of reaction was determined from the initial absorbance, the final absorbance and the absorbance *vs.* time. At the wave lengths used, the absorbance is due primarily to the V(V) in the solution. Apparent second-order rate constants were calculated from the data of each run using a nonlinear least-squares program for the IBM 7090 computer. This program minimizes the sum of the squares of the differences between the observed and calculated absorbance values.[9]

Stoichiometry.—The reaction

$$VO_2^+ + Fe^{+2} + 2H^+ = VO^{+2} + Fe^{+3} + H_2O \quad (1)$$

is known to be quantitative in acid solutions. The oxidation potentials[10] lead to an equilibrium constant of 7.9×10^3. A value of 6.2×10^4 has been reported for 25° and unit ionic strength.[11] Further, the reaction is used successfully in the determination of V(V).[6]

Results

V(V) and Fe(II) Dependences.—All of the rate runs were consistent with the assumption that the reaction is first order with respect to both V(V) and Fe(II), that is: $-d[V(V)]/dt = -d[Fe(II)]/dt = k'[V(V)]\cdot[Fe(II)]$. The least squares calculations described above give absorbance values in agreement with experimental ones and the deviations show no systematic trends. Additional evidence is provided by the agreement of a series of runs in which the initial concentrations of V(V) and Fe(II) were varied over a wide concentration range. These data are shown in Table I. The fit of the data for the individual rate runs is indicated by the standard deviations of the k' values and the root mean square deviations between the observed and calculated absorbance values. These quantities are listed in the forth and fifth columns of Table I.

(9) We are indebted to R. H. Moore for writing this program. It is based on R. H. Moore and R. K. Zeigler, Los Alamos Scientific Laboratory Report, LA-2367, October 15, 1959. Available from the Office of Technical Services, U. S. Department of Commerce, Washington, D. C.; $2.25.

(10) W. M. Latimer, "Oxidation Potentials," Second Edition, Prentice-Hall, Inc., New York, N. Y., 1952.

(11) J. Kenttamaa, *Suomen Kem. B.*, **31B** 273 (1958), quoted by Higginson, *et al.*, *Discussions Faraday Soc.*, **29**, 49 (1960).

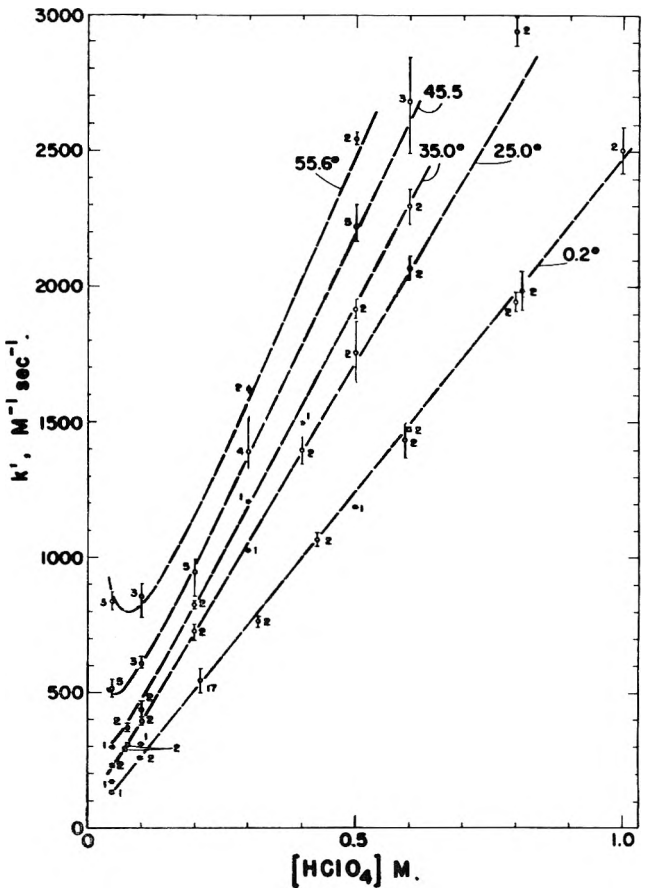

Fig. 1.—Average apparent second-order rate constant, k', *vs.* $HClO_4$ concentration at $\mu = 1.0$. Vertical lines represent the range; the numeral is the number of determinations.

TABLE I

APPARENT SECOND-ORDER RATE CONSTANT, k', AT DIFFERENT INITIAL CONCENTRATIONS OF V(V) AND Fe(II)

Conditions: 0.2°, 0.21 *M* $HClO_4$, and $\mu = 1.0$ ($LiClO_4$)

Initial V(V), $M \times 10^5$	Initial Fe(II), $M \times 10^5$	k' M^{-1} sec.$^{-1}$	Standard dev.	R.m.s. deviation (Absorbance)
4.97	41.6	521	6	0.0010
4.97	20.8	525	8	.0012
4.97	10.4	551	4	.0010
4.97	2.6	535	9	.0010
4.97	41.6	529	7	.0008
49.6	6.08	559	22	.0010
30.8	6.08	571	13	.0012
24.8	6.08	593	8	.0007
6.2	6.08	570	6	.0012

Hydrogen Ion and Temperature Dependence.—Rate runs were made at 0.2, 25.0, 34.0, 35.0, 45.4, and 55.6° in $LiClO_4$ solutions of unit ionic strength. The $HClO_4$ concentrations ranged from 0.045 to 1.00 *M*. The results of these runs are summarized in Fig. 1 where the average k' value is plotted against $[H^+]$. The range of values and the number of determinations are also indicated. The data taken at 34° have been omitted from the plot for clarity. The plots at the three lower temperatures are essentially linear, but a decided up-turning is noticed at the low acid ends of the two upper lines.

Ionic Strength Dependence.—The effect of ionic strength on the reaction was found to be quite large. Determinations were made in 0.067 *M* acid at 0.2° and in 0.07 *M* acid at 25.0°. The ionic strength of the solutions was varied up to about 2.5 *M* by the addition

of $LiClO_4$. The results of these experiments are given in Table II.

TABLE II

EFFECT OF IONIC STRENGTH ON THE APPARENT SECOND-ORDER RATE CONSTANT

Results at 0.2°, 0.067 M $HClO_4$

μ, M	0.067	0.229	0.516	1.04	2.46
k', M^{-1} sec.$^{-1}$	35, 44	65	102	190	516, 525

Results at 25.0°, 0.070 M $HClO_4$

μ, M	0.070	0.200	0.500	1.00	2.50
k', M^{-1} sec.$^{-1}$	63, 67	108, 109	181, 181	291, 291	793, 801

Interpretation and Discussion

The Rate Law.—The plots of the data (Fig. 1) show that the reaction rate is predominantly first power in the hydrogen ion concentration. One or more additional terms in the rate law is required, however, to account for the non-zero intercepts and for the curvature at the ends of the two upper plots. An empirical rate law which is in accord with the data is

$$-\mathrm{d}[\mathrm{V(V)}]/\mathrm{d}t = (a[\mathrm{H^+}]^{-1} + b + c[\mathrm{H^+}])[\mathrm{VO_2^+}][\mathrm{Fe^{+2}}] \quad (2)$$

The concentrations of the principal species, $[VO_2^+]$ and $[Fe^{+2}]$, have been used instead of the stoichiometric ones, [V(V)] and [Fe(II)], since neither substance is appreciably hydrolyzed in the experimental solutions.[12] Approximate values for the parameters in (2) were estimated as follows, c and b from the slopes and intercepts of the linear portions of the curves and a by difference. These values are listed in Table III.

TABLE III

APPARENT RATE CONSTANTS FOR THE REACTION BETWEEN V(V) AND Fe(II)

Temp., °C.	a, sec.$^{-1}$	b, M^{-1} sec.$^{-1}$	c, M^{-2} sec.$^{-1}$	c, calcd.[a] M^{-2} sec.$^{-1}$
0.2	0	20	2450	2450
25.0	0	60	3400	3370
35.0	0	90	3680	3780
45.4	8	120	4270	4240
55.6	17	240	4610	4710

[a] Calculated using $\Delta H^* = 1.52$ kcal./mole and $\Delta S^* = -37.3$ e.u.

The form of the rate law suggests three paths for the reaction described by the following net activation processes

$$\mathrm{VO_2^+ + Fe^{+2} + H_2O = (VO_2 \cdot Fe \cdot OH^{+2})^*} \quad (3)$$

$$\mathrm{VO_2^{+2} + Fe^{+2} = (VO_2 \cdot Fe^{+3})^*} \quad (4)$$

$$\mathrm{VO_2^+ + Fe^{+2} + H^+ = (H \cdot VO_2 \cdot Fe^{+4})^*} \quad (5)$$

However, Table III shows that a and b are far smaller than c, and therefore a decision cannot be made as to whether a and b are due to medium effects or to the operation of minor paths such as (3) and (4). Changing the hydrogen ion concentration at constant ionic strength probably makes small changes in the rate constants for the various paths. These changes for the predominant path are absorbed in the terms for the minor paths in the empirical rate law. Thus, although c is a good measure of the rate constant for (5), a and b are probably poor estimates of the rate constants for (3) and (4).

The over-all reaction, equation 1, requires two hydrogen ions; so it is not surprising that one hydrogen ion is required in the most important net activation process. Other reductions of ions of the MO_2^+ type which show the same hydrogen ion dependence are the reduction of NpO_2^+ by Fe^{+2} [13] and by Np^{+3},[14] and the reduction of PuO_2^+ by PuO_2^{+} [15] and the reduction of UO_2^+ by UO_2^+.[16]

The Thermodynamic Quantities of Activation.—The thermodynamic quantities of activation for process (5) have been calculated under several assumptions with respect to the minor paths.

In the first two calculations a was assumed to be zero and the data giving rise to the curvature in the plots were omitted. It was also assumed that the temperature dependence of b, as well as c, is given by the expression from absolute reaction rate theory[17]

$$k_i = k_b/h \exp(\Delta S_i^*/R) \exp(-\Delta H_i^*/RT) \quad (6)$$

In the third and fourth calculations a was not assumed to be zero, its temperature dependence was assumed to be given by (6) and no data were omitted. It should be noted that even though a and b may be partially determined by medium effects, the assumption of (6) is justified on the basis of the relative sizes of a and b with respect to c and because the exponential function is very similar to other two-parameter functions over short ranges in T. For the fourth calculation, ΔH_b^* was arbitrarily fixed at 5 kcal./mole, a value which might be expected if b is the rate constant of process (4). The dashed curves in Fig. 1 are given by this calculation.

In the fifth calculation b was assumed to be zero, (6) was assumed for the temperature dependences of a and c, and no data were omitted.

For all of the calculations a least-squares procedure was used which minimizes the sum of the squares of the per cent deviations between the observed and calculated k' values.[9] The results of these calculations are summarized in Table V; the apparent values of the activation parameters (ΔS^* and ΔH^*) are given together with a measure of the fit of the data to the assumed function. For this we have used the root mean square per cent deviation, defined by

$$\text{r.m.s. \% dev.} = 100[(1/n) \sum (k'_{obs} - k'_{calc})^2/(k'_{obs})]^{1/2}$$

The results in Table IV show that a variety of assumptions with respect to the minor paths lead to nearly the same values for the thermodynamic quantities of activation for the predominant path. Thus, we believe that although no conclusions can be reached with respect to possible minor paths, for net activation process (5) $\Delta H^* = 1.52 \pm 0.16$ kcal./mole and $\Delta S^* = -37.3 \pm 0.6$ e.u. These values have been used to calculate the values of c or k_1 the rate constant for the

(12) J. Bjerrum, G. Schwarzenbach, and L. G. Sillén, "Stability Constants, Part II, Inorganic Ligands," The Chemical Society, London, 1958, Special Publication No. 7, also, F. Rossotti and H. Rossotti, *Acta Chem. Scand.*, **10**, 957 (1956); and D. Dryssen and T. Sikine, *ibid.*, **15**, 1399 (1962).

(13) J. R. Huizenga and L. B. Magnusson, *J. Am. Chem. Soc.*, **73**, 3202 (1951).

(14) J. C. Hindman, J. C. Sullivan, and D. Cohen, *ibid.*, **80**, 1812 (1958).

(15) S. W. Rabideau, *ibid.*, **79**, 6350 (1957).

(16) H. Imai, *Bull. Chem. Soc. Japan*, **30**, 873 (1957).

(17) S. Glasstone, K. Laidler, and H. Eyring, "The Theory of Rate Processes," McGraw-Hill Book Co., Inc., New York, N. Y., 1941, p. 196.

TABLE IV

APPARENT THERMODYNAMIC QUANTITIES OF ACTIVATION

	I Data at $[H^+] \leq 0.1M$ omitted	II Data at $t \geq 45^c$ omitted	III No data omitted	IV ΔH_b^* fixed[a]	V b term omitted
ΔS_c^*, e.u.	-37.1 ± 0.4[b]	-37.9 ± 0.4	-36.7 ± 0.3	-37.5	-37.2 ± 0.2
ΔH_c^*, kcal./mole	1.57 ± 0.12	1.36 ± 0.12	1.68 ± 0.08	1.46	1.54 ± 0.06
ΔS_b^*, e.u.	-35.0 ± 7.5	-30.6 ± 3.3	-57.9 ± 11.4	-34.3	...
ΔH_b^*, kcal./mole	4.6 ± 2.3	5.8 ± 1.0	-1.7 ± 3.1	5.0 (fixed)	...
ΔS_a^*, e.u.	...	...	-3.6 ± 4.0	+2.54	-10.7 ± 1.9
ΔH_a^*, kcal./mole	...	...	15.9 ± 1.3	18.0	13.6 ± 0.6
r.m.s. % deviation	4.76	5.69	5.29	5.45	5.94
No. of data points	77	78	113	113	113

[a] ΔH_b^* fixed at 5.0 kcal./mole and the other quantities computed by least squares. [b] The uncertainties listed in this table are the standard deviations computed by the least-squares program.

TABLE V

THERMODYNAMIC QUANTITIES OF ACTIVATION, 25°

Net activation process	ΔH^*, kcal./mole	ΔS^*, e.u.	S^* complex[a]	From data in ref.
1. $VO_2^+ + Fe^{+2} + H^+ = (H \cdot VO_2 \cdot Fe^{+4})^*$	1.52	-37.3 ± 0.6	-70 ± 1	This work
2. $NpO_2^+ + Fe^{+2} + H^+ = (H \cdot NpO_2 \cdot Fe^{+4})^*$	8.6	-38	-69	13
3. $Fe^{+2} + Fe^{+3} + H_2O = (Fe \cdot OH \cdot Fe^{+4})^* + H^+$	19.4	$+9.9 \pm 1.4$	-70 ± 1	20
4. $Cr^{+2} + Cr^{+3} + H_2O = (Cr \cdot OH \cdot Cr^{+4})^* + H^+$	22	-2 ± 5	-79 ± 5	21
5. $Fe^{+2} + Co^{+3} + H_2O = (Fe \cdot OH \cdot Co^{+4})^* + H^+$	18.8	$+16 \pm 4$	-66 ± 4	22
6. $V^{+3} + VO^{+2} + H_2O = (V \cdot OH \cdot VO^{+4})^* + H^+$	20.1	-3 ± 5	-77 ± 5	23
7. $V^{+3} + VO_2^+ = (VO_2 \cdot V^{+4})^*$	16.6	$+5 \pm 6$	-65 ± 6	24

[a] Formal ionic entropy of the activated complex, $S^*_{complex} = \Delta S^* + \Sigma S^0_{reactants}$. Values used for $S^0_{reactants}$: H^+, 0.00; VO_2^+, -5.4[3]; NpO_2^+, -4[25]; Cr^{+2}, (-24 ± 3); Fe^{+2}, -27[10]; VO^{+2}, -26 ± 3[3]; V^{+3}, (-65 ± 3); Cr^{+3}, (-67 ± 3); Fe^{+3}; -70[10]; Co^{+3}, (-72 ± 3); H_2O, $+16.7$.[10] Estimates are given in parentheses.

predominant path given in the last column of Table III.

The most striking feature of the V(V)–Fe(II) reaction appears to be its low heat of activation, lower than those for other reactions in which metal–oxygen bonds are broken such as the analogous reduction of Np(V) by Fe(II),[13] lower than that for the $Fe(CN)_6^{-4}$–$Fe(CN)_6^{-3}$ electron exchange,[18] and almost as low as for the oxidation of Fe(II) by $Ir(Cl)_6^{-2}$ or by $Fe(phen)_3^{+3}$.[19]

In contrast to ΔH^*, ΔS^* for the V(V)–Fe(II) reaction is essentially what was to be expected. This is shown in Table V where the thermodynamic quantities of activation are given for a series of reactions for which the charge on the activated complex is +4. It is seen that although the ΔS^* values range from -38 to $+12$ e.u., the formal ionic entropies of the activated complexes range from -65 to -79 e.u. Just as in the case of actinide ion reactions,[4] the charge on the activated complex seems to be the predominant factor in determining its entropy. Since the values are similar to those for activated complexes formed from two actinide ions, the size of the complex does not seem to be an important factor.

The activated complexes in Table V are shown as if only a single atom or group lies between two metal ions. This was done for convenience only; as yet there is no evidence for or against the inner-sphere structures shown.

Acknowledgement.—The authors thank Dr. F. B. Baker for help and advice in the experimental part of this work.

(18) C. F. Deck, *Microfilm Dissert. Abstr.*, **16**, 1578 (1956).
(19) N. Sutin and B. Gordon, *J. Am. Chem. Soc.*, **83**, 70 (1961); B. Gordon, L. Williams, and N. Sutin, *ibid.*, **83**, 2061 (1961).
(20) J. Silverman and R. W. Dodson, *J. Phys. Chem.*, **56**, 846 (1952).
(21) A. Anderson and N. A. Bonner, *J. Am. Chem. Soc.*, **76**, 3826 (1954).
(22) L. E. Bennett and J. C. Sheppard, *J. Phys. Chem.*, **66**, 1275 (1962). We thank these authors for making available the data plotted in their Fig. 2.
(23) S. C. Furman and C. S. Garner, *J. Am. Chem. Soc.*, **74**, 2333 (1952).
(24) W. C. E. Higginson, *et al.*, *Discussions Faraday Soc.*, **29**, 49 (1960).
(25) D. Cohen and J. C. Hindman, *J. Am. Chem. Soc.*, **74**, 4682 (1952).

RATE OF ADSORPTION OF CALCIUM DINONYLNAPHTHALENE SULFONATE AT THE OIL–WATER INTERFACE[1]

BY FREDERICK M. FOWKES[2]

Shell Development Company, Emeryville, California

Received November 17, 1962

The rate of adsorption of calcium dinonylnaphthalene sulfonate (CaDNNS) from dilute solutions in *n*-decane at the interface with 1 *M* aqueous $Ca(NO_3)_2$ was determined at 25° by the drop-volume method for interfacial tension. It is found in this system that during the initial 35 dynes/cm. decrease of interfacial tension (taking about 70 seconds with 10^{-5} molar solutions) every molecule diffusing to the interface immediately enters the interfacial monolayer. In this region the area per molecule (*A*) of adsorbed CaDNNS can be calculated from the age of the interface by diffusion theory. In this way, a π–*A* relation was obtained which shows that in this system the interfacial monolayer of CaDNNS is solvated by both water and *n*-decane to form an ideal two-dimensional solution.

Rates of adsorption of small surface-active molecules at aqueous surfaces have been investigated mainly by the decrease of surface tension with time as measured by the vibrating jet technique[3–5] and the results have often been subjected to a more rigorous kinetic treatment than the accuracy justified.[6–10] Other dynamic methods have proven even less accurate.[11,12]

The above methods treat the decrease of surface tension of solutions with surface ages on the order of a second or less and despite the fact that considerable liquid motion occurs during the measurements it has always been tacitly assumed that negligible stirring occurs in the layer of solution in which diffusion takes place. To avoid such stirring it appears desirable to measure rates of adsorption in quiet systems where negligible motion is involved in the measurements. Static methods of surface tension measurement used in time periods of 10 seconds to 10 minutes appear most suitable. This requires very dilute solutions ($\sim 10^{-5}$ *M*) of highly surface-active substances. Adsorption of calcium dinonylnaphthalene sulfonate (CaDNNS) at the oil–water interface from dilute solutions in *n*-decane[13] appears ideal in this respect. The equilibrium value of interfacial tension (γ_{ow}) is 0.9 dyne/cm. for all concentrations in excess of 10^{-6} mole/liter (or perhaps 10^{-7} mole/liter) so that very slow rates of diffusion may be observed in very dilute solutions without the usual limitation of a considerable rise in the equilibrium value of interfacial tension. The diffusing species is a 12-molecule micelle, and the diffusion coefficient is 1.43×10^{-6} cm.²/sec. at 25° and known to be concentration-independent in the range used for this paper.[13]

Theory

The diffusion equations of Fick, when applied to diffusion at a plane interface, are

$$\frac{dm}{dt} = D \times \frac{dc}{dx} \tag{1}$$

and

$$\frac{dc}{dt} = D \times \frac{d^2c}{dx^2} \tag{2}$$

which lead to

$$\frac{dm}{dt} = \sqrt{\frac{D}{\pi t}}\,(c_0 - c)e^{-x^2/4Dt} \tag{3}$$

where m is grams of solute per cm.², t is time in seconds, D is the diffusion coefficient in cm.²/sec., c is concentration of solute in g./cm.³ at x cm. from the boundary, and c_0 is the original concentration of the bulk of the solution. In diffusion toward an interface x is zero at the interface and consequently the rate of arrival of solute at an interface is given by [6,14]

$$\left(\frac{dm}{dt}\right)_{x=0} = \sqrt{\frac{D}{\pi t}}\,(c_0 - c) \tag{4}$$

These equations should apply where the activity coefficient is constant over the concentration range c to c_0, but not otherwise. It is quite possible that previously demonstrated deviations from equation 4 with solution concentrations approaching saturation may be explainable by this factor.[6] In the system under discussion a nearly constant activity coefficient has been demonstrated over the range of 10^{-6} to 10^{-3} mole/l.[13]

In the early stages of adsorption it is customary to assume that equilibrium exists between the adsorbed solute and the solute in the layer of solution immediately adjacent to the surface. This point will be proved later with respect to the system under discussion. The diffusion boundary (where $x = 0$) is located in this layer, and the c of equation 4 applies to this layer. Since newly-formed interfaces have very dilute adsorbed monolayers, the chemical activity of the adsorbed solute is extremely low initially and therefore c is so small that the $(c_0 - c)$ term of equation 4 is negligibly different from c_0 during the early part of the adsorption. Under these conditions a simple integral form of equation 4 may be used[14–16]

$$m = 2c_0\sqrt{\frac{Dt}{\pi}} \tag{5}$$

(1) Presented at the 142nd National Meeting of the American Chemical Society at Atlantic City, N. J., Sept., 1962.
(2) Sprague Electric Company, North Adams, Mass.
(3) C. C. Addison, *Phil. Mag.*, **36**, 73 (1945).
(4) R. Defay and J. R. Hommelen, *J. Colloid Sci.*, **13**, 553 (1958).
(5) R. S. Hansen, *et al.*, *J. Phys. Chem.*, **62**, 210 (1958).
(6) A. F. H. Ward and L. Tordai, *J. Chem. Phys.*, **14**, 453 (1946).
(7) A. F. H. Ward in "Surface Chemistry," Bordeaux, 1947, Interscience, New York, N. Y., 1949, p. 55.
(8) C. M. Blair, *J. Chem. Phys.*, **16**, 113 (1948).
(9) S. Fordham, *Trans. Faraday Soc.*, **50**, 593 (1954).
(10) R. S. Hansen, *J. Phys. Chem.*, **64**, 637 (1960); *J. Colloid Sci.*, **16**, 549 (1961).
(11) H. Lange, *Kolloid Z.*, **121**, 130 (1951).
(12) K. Schäfer, *Z. Elektrochem.*, **59**, 273 (1955).
(13) F. M. Fowkes, *J. Phys. Chem.*, **66**, 1843 (1962).
(14) I. Langmiur and V. Schaefer, *J. Am. Chem. Soc.*, **59**, 2400 (1937).
(15) R. Defay and J. R. Hommelen, *J. Colloid Sci.*, **14**, 411 (1959).
(16) L. Ter Minassian-Saraga, *ibid.*, **11**, 398 (1956).

Diffusion at a spherical interface (such as the drops used in this work) can be represented by the above equations when the diffusion layer is very small compared with the radius of the sphere (a). As demonstrated by Crank,[17] the variation of spherical diffusion (in terms of $\sqrt{t}$ values) from the predictions of equations 4 or 5 is less than -1% at $\sqrt{Dt}/a = 0.05$, is -3% at $\sqrt{Dt}/a = 0.1$, and -20% at $\sqrt{Dt}/a = 0.2$. These predictions are for diffusion from a drop of solution (CaDNNS in n-decane in this case) into an unsaturated monolayer at the interface. In the case where the CaDNNS solution surrounds a drop of aqueous solution and diffusion occurs *toward* the drop, the corrections should be positive and of slightly smaller values. Experimental results were obtained mainly with $\sqrt{Dt}/a = 0.05$, but some were also obtained with values of 0.1 and 0.2. The experimental findings confirm the above calculations quantitatively, as will be shown.

As adsorption proceeds the above regime is terminated as either the subsurface concentration c becomes significantly larger, or the activation energy required for entry of molecules into the monolayer becomes significant. In the studies with aqueous solutions of short-chain alcohols and acids the increase of c assumes importance first.[3-10] However, in this study the system chosen is one in which the equilibrium concentration in the subsurface is extremely small compared with c_0 until the interfacial tension falls to less than 1 or 2 dynes/cm. Consequently the "back-diffusion" concept of Ward and Tordai[6] is not applicable in this study.

The conversion of rates of adsorption (dm/dt) in g./cm.^{2}/sec. to lowering of surface and interfacial tension in dynes/cm./sec. has never been treated very satisfactorily, mainly because of the lack of suitable equations of state for adsorbed monolayers of soluble surface-active compounds. However, now that a thermodynamically-derived equation can be substituted for the formerly-used "gas" equation approximations,[18] the shape of the surface tension *vs.* time relation such as that presented by Defay and Hommelen[19] and discussed by Hansen[10] is easily predicted. In a monolayer of component 1 adsorbed from solvent 2 the mole fraction of solvent (x_2) is related to the decrease of surface tension π by[18]

$$\pi = \frac{-kT \ln x_2 \varphi_2}{\bar{\sigma}_2} \tag{6}$$

where $\bar{\sigma}_2$ is the average partial molecular area of the solvent over the range of film pressure from 0 to π, and σ_2 is the activity coefficient of the solvent in the monolayer which is usually unity for soluble monolayers. In the case of water $\bar{\sigma}_2$ is 9.7 to 10.0 Å.^{2} The area per molecule of solute A_1 is given by[18]

$$A_1 = \sigma_1 + \frac{x_2}{1 - x_2}\sigma_2 \tag{7}$$

and

$$m_1 = \frac{M}{NA_1} \tag{8}$$

so by combining equations 5, 6, 7, and 8 one can calculate the time-dependence of film pressure

$$m = 2c_0\sqrt{\frac{Dt}{\pi}} = \frac{M}{N}\,\frac{1 - e^{-\pi\bar{\sigma}_2/kT}}{\sigma_1 + (\sigma_2 - \sigma_1)e^{-\pi\bar{\sigma}_2/kT}} \tag{9}$$

Equation 9 is a bit cumbersome for everyday use, so in practice a series of x_2 *vs.* π values are calculated from equation 6 with $\varphi_2 = 1$, and then A_1 *vs.* π values from equation 7, and finally π *vs.* $c_0\sqrt{t}$ values from equations 8 and 5 combined.

In some systems, such as aqueous solutions of n-alkyl sulfates, σ_1 is pressure-independent (26.5 Å.^{2}).[18] However, in the system under discussion σ_1 *vs.* π relations obtained with insoluble films on a film-balance were required.

If an interfacial monolayer is solvated by *both* liquid phases, equation 6 has an additional term.[20] Let σ_2 and σ_3 refer to the partial molecular areas of water and oil, respectively; then

$$\pi = \frac{-kT \ln x_2\varphi_2}{\bar{\sigma}_2} - \frac{kT \ln x_3\varphi_3}{\bar{\sigma}_3} \tag{10}$$

In this system

$$\frac{n_2}{n_1} = \frac{A_1 - \sigma_1}{\sigma_2} \text{ and } \frac{n_3}{n_1} = \frac{A_1 - \sigma_1}{\sigma_3}$$

With these equations a π *vs.* A_1 relation and a π *vs.* $\sqrt{t}$ relation are easily calculable.

The initial slope of interfacial tension γ *vs.* $\sqrt{t}$ has been discussed in some detail by Hansen[5] and illustrated experimentally by Defay and Hommelen.[19] This can be derived from equation 5

$$\frac{d\gamma}{d\sqrt{t}} = -2c_0\sqrt{D/\pi} \times \frac{d\pi}{dm} \tag{11}$$

If the above equation is implemented for an interfacial monolayer as represented by equation 10 and where both sides of the monolayer are ideally solvated (φ_2 and φ_3 both equal unity)

$$\frac{d\pi}{dm} = -\frac{zkT}{\sigma_2}\frac{d \ln x_2}{dm} - \frac{kT}{\sigma_3}\frac{d \ln x_3}{dm} \tag{12}$$

where z is the coefficient of dissociation of the adsorbed material ($z = 1$ for CaDNNS on the 1 M $Ca(NO_3)_2$ substrate used in this study). Since both interfacial solutions are binary systems

$$x_2 = 1 - x_1 = n_2/(n_1 + n_2)$$

$$x_3 = 1 - x_1 = n_3/(n_1 + n_3)$$

With dilute monolayers ($x_1 << 1$), $\ln(1 - x_1)$ may be approximated by $-x_1$. Further, x_1 for the aqueous side of the monolayer may be approximated by n_1/n_2 and n_2/cm.^{2} by $1/\sigma_2$. Similarly x_1 for the decane side of the monolayer may be approximated by n_1/n_3 and n_3/cm.^{2} by $1/\sigma_3$. Thus we obtain

$$\ln x_2 \doteq -mN\sigma_2/M$$

$$\ln x_3 \doteq -mN\sigma_3/M$$

(17) J. Crank, "The Mathematics of Diffusion," Clarendon Press, Oxford, 1956, pp. 85–90, Figure 6.4.

(18) F. M. Fowkes, *J. Phys. Chem.*, **66**, 385 (1962).

(19) R. Defay and J. R. Hommelen, *J. Colloid Sci.*, **14**, (1958359).

(20) F. M. Fowkes, *J. Phys. Chem.*, **66**, 1863 (1962).

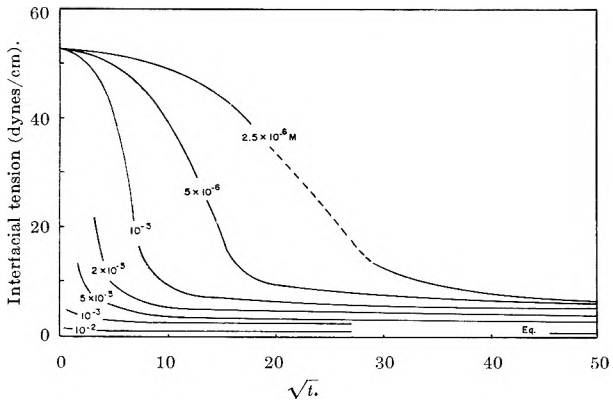

Fig. 1.—Time-dependence of the interfacial tensions at 25° between 1 M aqueous $Ca(NO_3)_2$ and n-decane solutions of CaDNNS of various concentrations.

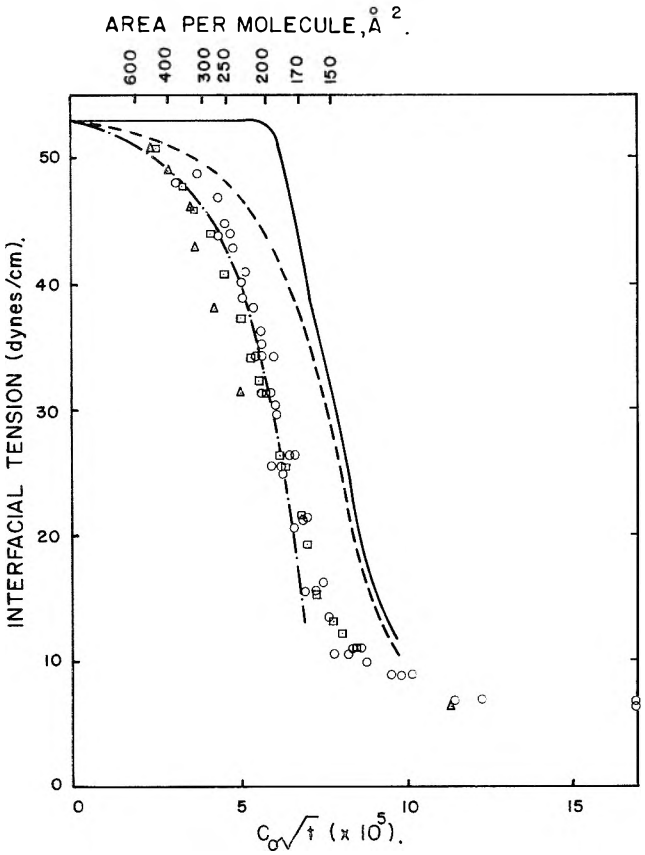

Fig. 2.—Time-dependence of interfacial tension used to determine pressure–area isotherms. Lines are theoretical relations for water- and decane-solvated monolayers (left), decane-solvated monolayers (middle), and non-solvated monolayers (right). Circles are data for 10^{-5} M CaDNNS, squares for 5×10^{-6} M, and triangles for 2.5×10^{-6} M.

which when combined with equations 11 and 12 leads to

$$\frac{d\gamma}{d\sqrt{t}} \doteq \frac{-2(z+1)c_0RT}{M}\sqrt{D/\pi} \qquad (13)$$

The value $(z + 1)$ holds for the doubly solvated film; if it were a surface film on an aqueous substrate this term would be z and if it were an interfacial film solvated by oil and not by the aqueous phase this term would be unity.[18] For the system illustrated in Fig. 2 the limiting slope calculated from equation 13 is -0.67 dyne/cm./$\sqrt{\text{sec.}}$, which fits the lower curve very well.

Experimental

The n-decane was Phillips 99 mole % grade dried over molecular sieves, and the CaDNNS was specially synthesized and purified and analyzed at each step of the synthesis as previously described.[13] The aqueous phase was 1 M $Ca(NO_3)_2$ of reagent grade in redistilled water. The interfacial tension between n-decane and this solution was 53.0 dynes/cm.

Interfacial tensions were obtained by use of the drop-volume technique, using micrometer-driven syringes with special tips of stainless steel tapered by G. S. Ronay so that the bottom of the tip was a sharp edge, yet cut off flat and perpendicular to the tubing. This sharp edge eliminated errors resulting from uneven wetting of the tip. The corrections of Harkins and Brown[21] were applied.

The technique used to obtain time-dependence was to form the drop of chosen size in 2–5 seconds and then let it hang undisturbed on the tip until the interface had aged sufficiently that the drop fell off. In this way γ_{ow} $vs.$ $\sqrt{t}$ relations were easily determined.

Much effort was required to eliminate convectional stirring resulting from temperature differences. The work was done in a constant temperature room (25 ± 0.5°), and inside an air-bath in this room. Furthermore, aluminum foil was necessary as a radiation shield. All these precautions were taken stepwise and with each the precision and reproducibility of the data increased.

Drops of aqueous solution were formed in the n-decane solution. Between drops the more dilute solutions were stirred with a stream of nitrogen bubbles to eliminate pockets of reduced concentration. Vessel walls were saturated with adsorbed CaDNNS and experiments progressed from higher to lower concentrations; in all cases the vessel and syringe were rinsed thoroughly with the solution next to be measured. In this way concentrations as low as 10^{-7} mole per liter were measurable.

A pressure–area isotherm was obtained at 25° with CaDNNS spread from hexane onto 1 M $Ca(NO_3)_2$ using a previously-described recording film balance.[22]

Discussion of Results

The amount of surface-active substance present in a freshly-formed interface (m) is proportional to the concentration (c_0) and the square root of the interfacial age ($\sqrt{t}$) as previously demonstrated in equation 5, provided no energy barrier limits the rate of entry into the adsorbed monolayer. The interfacial tension (γ_{ow}), obtained as CaDNNS adsorbs from decane onto droplets of aqueous $Ca(NO_3)_2$, is shown as a function of $\sqrt{t}$ in Fig. 1 for a wide range of concentrations.

At all concentrations γ_{ow} falls very slowly at first while the monolayer is in a very dilute and compressible state. As the interfacial tension decreases (and the film pressure of the adsorbed film increases) the monolayer becomes less compressible and the slope $d\gamma/d\sqrt{t}$ becomes steeper. However, below 15 dynes/cm. the slope begins to level off asymptotically to interfacial tensions well above the equilibrium value (indicated in the lower right corner of the graph). Even at fairly high concentrations the equilibrium interfacial tension is approached very slowly. Presumably the energy barrier for entry of CaDNNS molecules into the monolayer becomes appreciable at film pressures of about 40 dynes/cm. and greater.

The superposition of γ_{ow} $vs.$ $\sqrt{t}$ curves obtained at different concentrations is accomplished by plotting γ_{ow} as a function of $c_0\sqrt{t}$, as predicted by equation 5 for diffusion at plane interfaces. The results shown in Fig. 2, illustrate the deviations of experimental results obtained with inward spherical diffusion from the predictions for planar diffusion. The calculations of Crank[17] may be used to predict these deviations (from the value of $\sqrt{Dt}/a$, where a is the radius of the

(21) W. D. Harkins and F. E. Brown, *J. Am. Chem. Soc.*, **41**, 499 (1919).
(22) M. J. Schick, *J. Polymer Sci.*, **25**, 465 (1957).

sphere). For these experiments, a was 0.18 cm. at 30 dynes/cm. Thus at 30 dynes/cm·$\sqrt{Dt}/a$ was 0.05, 0.1, and 0.2 for the 10^{-5}, 5×10^{-6}, and 2.5×10^{-6} molar solutions, respectively. These values lead to the prediction that in Fig. 2 the curves should be about 1% (circles), 3% (squares), and 20% (triangles), respectively, to the left of the diffusion curve for planar diffusion. The close correspondence of experiment with theory gives strong support to using the 10^{-5} molar data (without correction for spherical diffusion) to determine the area per molecule of CaDNNS (A_1) using the values shown across the top of Fig. 2 which were calculated from equations 5 and 8. At a film pressure of 3 dynes/cm. (γ_{ow} = 50 dynes/cm.) A_1 is about 500 Å.^{2}, but at 33 dynes/cm. A_1 is only 170 Å.^{2}; this shows the film to be highly compressible.

The known π–A relations can also be plotted against this scale. Shown in the figure are three π–A relations for CaDNNS; the solid line is for a nonsolvated film as measured with a film balance using an insoluble film of CaDNNS on a $Ca(NO_3)_2$ solution where

$$A_1 = \sigma_1$$

the dashed line is for the film solvated by oil molecules, where

$$A_1 = \sigma_1 + \frac{x_3\sigma_3}{1 - x_3}, \text{ and}$$

$$\pi = \frac{-kT \ln x_3}{\bar{\sigma}_3}$$

and the dashed and dotted line is for the film solvated by both oil and water, where

$$A_1 = \sigma_1 + \frac{x_3\sigma_3}{1 - x_3} + \frac{x_2\sigma_2}{1 - x_2}, \text{ and}$$

$$\pi = \frac{-kT \ln x_3}{\bar{\sigma}_3} - \frac{kT \ln x_2}{\bar{\sigma}_2}$$

It can be seen that the latter fits the experimental data very well and is strong evidence that there is no appreciable energy barrier to the movement of arriving CaDNNS molecules into the adsorbed film at film pressures less than 35–40 dynes/cm.

Conclusions

In this system the rate of adsorption is limited only by diffusion until the adsorbed monolayer has reached about 85% of its equilibrium population (and a film pressure of 35–40 dynes/cm.). The entry of additional molecules into the film requires increasingly greater activation energies, and in this region the entry into the monolayer becomes the rate-determining step.

Measurements of surface or interfacial tensions of freshly-formed surfaces can be used to provide pressure–area isotherms. The isotherm produced in this work shows that the interfacial monolayer of CaDNNS acts as an ideal two-dimensional solution with solvation of the hydrocarbon groups by oil and of the polar groups by water.

The ideal two-dimensional solution isotherm for soluble surface-active agents is a useful relation for calculating the change of film pressure during adsorption.

Acknowledgment.—The author wishes to thank Dr. R. C. Nelson for the pressure–area isotherm of CaDNNS, and Mr. S. C. Beckley for his painstaking care in the measurements of interfacial tension.

CORRELATION OF TURBIDITY AND ACTIVITY DATA. II. TUNGSTOPHOSPHORIC AND TUNGSTOSILICIC ACIDS[1]

BY M. KERKER, J. P. KRATOHVIL, R. H. OTTEWILL,[2] AND E. MATIJEVIĆ

Department of Chemistry, Clarkson College of Technology, Potsdam, N. Y.

Received November 19, 1962

Turbidity and differential refractive index data up to concentrations of about 1 g. per ml. are given for 9-tungstophosphoric acid at 546 mμ and for 12-tungstosilicic acid at 436 and 546 mμ. Also, densities of 12-tungstosilicic acid are reported. Solvent activities calculated from the turbidity are compared with those obtained from isopiestic vapor pressure data and good agreement was found. Similarly, turbidities determined by these two techniques agree. The difference among the turbidity results for 12-tungstosilicic acid reported by various workers is discussed. An error in our earlier work[4] on the turbidity of the tungstophosphoric acids is corrected.

Introduction

The recent interest in light scattering by heteropoly compounds is due to their fortuitous combination, for an inorganic compound, of a remarkably high solubility and a relatively high molecular weight. Intermediate between simple electrolytes and polyelectrolytes, they provide a model system for studying such phenomena as light scattering,[3–7] viscosity,[8] ultracentrifugation,[7,8] electrolytic coagulation,[9–11] electrophoresis,[12] acidimetry,[10,13] etc.

For ideal solutions, light scattering can be used to calculate the molecular weight and molecular configuration. Otherwise, activities are obtained, in much the

(1) Supported by the U. S. Atomic Energy Commission Contract No. AT(30-1)-1801.

(2) On leave from Department of Colloid Science, University of Cambridge, Cambridge, England.

(3) M. Kerker, D. Lee, and A. Chou, *J. Am. Chem. Soc.*, **80**, 1539 (1958).

(4) E. Matijević and M. Kerker, *ibid.*, **81**, 1307 (1959).

(5) J. B. Goehring, M. Kerker, E. Matijević, and S. Y. Tyree, Jr., *ibid.*, **81**, 5280 (1959).

(6) M. J. Kronman and S. N. Timasheff, *J. Phys. Chem.*, **63**, 629 (1959).

(7) J. S. Johnson, K. A. Kraus, and G. Scatchard, *ibid.*, **64**, 1967 (1960).

(8) M. C. Baker, P. A. Lyons, and S. J. Singer, *J. Am. Chem. Soc.*, **77**, 2011 (1955).

(9) E. Matijević and M. Kerker, *J. Phys. Chem.*, **62**, 1271 (1958).

(10) E. Matijević and M. Kerker, *J. Am. Chem. Soc.*, **81**, 5560 (1959).

(11) E. Matijević, D. Broadhurst, and M. Kerker, *J. Phys. Chem.*, **63**, 1552 (1959).

(12) M. Kerker, J. R. Keller, J. Siau, and E. Matijević, *Trans. Faraday Soc.*, **57**, 780 (1961).

(13) J. R. Keller, E. Matijević, and M. Kerker, *J. Phys. Chem.*, **65**, 56 (1961).

same fashion as from any colligative property. Thus, Johnson, Kraus, and Scatchard[7] have compared activities of 12-tungstosilicic acid obtained from equilibrium ultracentrifugation measurements with those from turbidities. In the first paper of this series[5] we have compared turbidity and isopiestic vapor pressure measurements for 9- and 12-tungstophosphoric acids.

The results of such measurements are useful in several ways. Obviously, they may provide a confirmation of the validity of the fluctuation treatment of turbidity, especially for electrolyte systems. Secondly, it has been suggested that these solutions might provide a series of turbidity standards covering an extensive range of turbidities.[7] Finally, as will appear from the work to be reported here, turbidity measurements may offer an alternate means for the determination of the activity of such electrolyte systems, and, therefore, a tool for studying the influence of added salts and mixed solvents upon these activities.

In this paper we report turbidity, density, and refractive index data for 12-tungstosilicic acid (12-TSA). In addition, turbidity data for 9-tungstophosphoric acid (9-TPA) at higher concentrations than previously reported are given (up to 1.05 g./ml.). In the earlier work with 9-TPA the light scattering data did not overlap with the isopiestic measurements which were at higher concentrations. All results are now discussed along the lines of the above comments.

In a forthcoming paper, we will consider the influence of added salt.

Experimental

Material.—The 9-tungstophosphoric acid (9-TPA) was synthesized as described earlier.[4] Several commercial samples of 12-tungstosilicic acid (12-TSA) were used (Baker's Analyzed Reagent, Fisher's Certified Reagent, Baker and Adamson Reagent) and they were purified as described earlier,[10] except that the extraction was repeated several times. Some measurements were also carried out with unpurified commercial samples as well as with a sample synthesized in another laboratory.[11] The moisture content was determined by drying to constant weight at 230°. There was no further change in weight upon continued drying of 12-TSA at 300°. One sample of purified 12-TSA was stored in a stoppered container for a period of one year. This gave identical results for moisture content (determined 3 times), turbidity, density, and refractive index increment during this period. Doubly-distilled water from all-Pyrex stills was used. We found that a Fisher Catalog No. 9-107 still gave particularly good-quality water for light scattering work.

Preparation of Solutions.—All glassware used for light scattering measurements was cleaned with chromic acid, thoroughly washed and then subjected to condensing acetone vapors. Stock solutions for light scattering were prepared by weighing the solid acid in a volumetric flask and filling to the mark with doubly distilled water. Light scattering readings were obtained for these stock solutions, and dilutions were then made from them in the light scattering cell. As the cell became filled solution was withdrawn and solvent was added for continued dilution. This addition was carried out so that there was an overlap of concentrations. In several runs covering the range of very low concentrations of 12-TSA the technique described by Kronman and Timasheff[6] was applied. In this case small increments of concentrated clarified solution of the acid were added to the water in the cell. Solutions and solvents were passed either through ultra-fine sintered glass filters or Millipore filters (0.45 μ porosity) several times under slight helium or nitrogen pressure. In a number of cases, we checked for differences in the concentration after the clarification procedure and none were found. Also, the use of Millipore filters of 0.1 μ porosity did not influence either the turbidities or dissymmetries. Only solutions showing dissymmetries close to unity were used. No time effects were noticed for any of the light scattering measurements.

Light Scattering Measurements.—Two essentially different techniques, were used for the determination of the turbidity of the heteropoly acids.

A. Some of the light scattering measurements with 12-TSA (but covering the same range of concentration as under part B below) were determined by means of a Brice–Phoenix Dual Photomultiplier Photometer, Model 1000-D calibrated with standard diffusors. The instrument was actually operated as the standard single photomultiplier model. The working-standard method of Brice, Halwer, and Speiser[15] was used. The instrument was calibrated by means of two opal glass standard diffusors that differed in their values of the corrected diffuse transmittance, TD. The agreement in calibration performed by means of these two diffusors was within 1%. The transmittances of neutral filters were checked and found in agreement with the values supplied by the manufacturer. In view of discrepancies reported recently[16-18] we preferred to determine the residual refraction correction, R_w/R_c, experimentally for several liquids of different refractive indices, rather than to accept the values listed in the manual. In agreement with the findings of others,[16,17] the values we found for a 40 × 40 mm. cell (*e.g.*, for toluene, $n = 1.51$, $R_w/R_c = 1.04$; for water, $n = 1.34$, $R_w/R_c = 1.02$) were considerably lower than those given originally by Brice, *et al.*,[15] and recommended by the manufacturer.

As shown by Brice, Nutting, and Halwer,[19] by applying the working standard method, the correction for absorption becomes small even for relatively highly absorbing solutions. In this work, the highest correction amounted to 3% for a sample of unpurified commercial 12-TSA at 436 mμ at a concentration of 0.525 g./ml.

For solutions containing less than 0.4 g./ml. of 12-TSA, where the turbidities are smaller than the apparent turbidity of, *e.g.*, benzene, we observed a gradual increase of dissymmetry with decreasing concentration, reaching finally for pure water the values of 5 and 8 for wave lengths 436 and 546 mμ, respectively. This arose from strong reflections in the 45° direction. Since such reflections could also be present in the 90° direction, this problem was studied very carefully. Several cells of different size and shape were tested in connection with four different slit combinations. Cells were rinsed several times with redistilled water collected directly from the still prior to the final collecting and filling. Because of the extremely low scattering intensity of the water, these tests for stray reflections were quite rigorous. We found for the standard large semioctagonal cell (Phoenix Catalog No. D-101) in combination with the standard (12 × 15 mm.) slits that when the outside of the back face of the cell as well as the entrance and exit faces (except for the windows) were painted black, dissymmetries close to unity were obtained. In addition the apparent Rayleigh ratio of water, R_{90}, (true R_{90} plus small residual contribution of reflections) was in excellent agreement with values reported in the literature.[20] According to Tomimatsu and Palmer,[21] light scattering readings at 90° as measured in a blackened cell will be too low by about 4% because of the loss of the contribution of the scattered light reflected from the back face of the cell. We have found that blackening the cell in the manner described above reduced our readings at 90° by about 3 to 5%. This reduction, which corresponds to the above effect, indicates the absence of stray light at 90°. In practice, all measurements were taken in the blackened cell in order to be able to check the dissymmetry. The readings at 90° were then increased by 4%.

B. For 9-TPA and some of the 12-TSA solutions, a Brice–Phoenix light scattering photometer, 1000 series, was employed and benzene, contained in a cell of square cross-section (24 × 24 mm.) was used as a secondary standard. A cylindrical cell

(14) We are indebted to Professor S. Y. Tyree, Jr., of the University of North Carolina for a sample of 12-tungstosilicic acid synthesized in his laboratory.

(15) B. A. Brice, M. Halwer, and R. Speiser, *J. Opt. Soc. Am.*, **40**, 768 (1950).

(16) Y. Tomimatsu and K. J. Palmer, *J. Polymer Sci.*, **35**, 549 (1959).

(17) A. F. Sirianni, D. J. Warsfold, and S. Bywater, *Trans. Faraday Soc.*, **55**, 2124 (1959).

(18) J. P. Kratohvil, Gj. Deželić, M. Kerker, and E. Matijević, *J. Polymer Sci.*, **57**, 59 (1962).

(19) B. A. Brice, G. C. Nutting, and M. Halwer, *J. Am. Chem. Soc.*, **75**, 824 (1953).

(20) D. A. I. Goring and P. G. Napier, *J. Chem. Phys.*, **22**, 147 (1954); R. W. Fessenden and R. S. Stein, *ibid.*, **22**, 1778 (1954); J. Kraut and W. B. Dandliker, *ibid.*, **23**, 1544 (1955); K. J. Mysels and L. H. Princen, *J. Phys. Chem.*, **63**, 1696 (1959).

(21) Y. Tomimatsu and K. J. Palmer, *J. Polymer Sci.*, **54**, S21 (1961).

(26 mm. i.d.) with a planar window for the incident beam was used for the solutions. In front of the standard receiving nosepiece (12 mm. away from it) a smaller stop of 2 mm. cross-section was inserted. Such a combination of light stops reduced stray reflections. Values of 46×10^{-6} and 15.5×10^{-6} cm.$^{-1}$ for 436 and 546 mμ were used for the Rayleigh ratio, R_{90}, of benzene. The arguments in favor of these values have been analyzed in a previous paper.[18] Appropriate corrections for the refraction of the emerging rays at the face of the cell (C_D), for the volume effect (C_V), and for absorption were made.

Since the 9-TPA is colored yellow and absorbs strongly at 436 mμ, light scattering could not be used at this wave length. Even at 546 mμ a correction has to be applied for absorption[3] when the technique described under B was used. Solutions of 9-TPA tended to develop a green coloration upon prolonged standing (reduction of W^{+6} to blue W^{+5}) especially in strong light. Therefore, measurements were carried out as quickly as possible after preparation and optical density determinations for the absorption correction were made on the filtered solutions immediately after measurement of the scattered intensity. A drop of bromine water added to the solution prior to filtration obviated the development of the green coloration. It was only necessary to correct for absorption by solutions of 12-TSA at the higher concentrations. In this case, the coloration was stable at both wave lengths. A Beckman Model DU spectrophotometer was used for determining optical densities for evaluation of the correction for absorption.

A Brice–Phoenix differential refractometer was used for determining refractive index increments. In the early phase of this work, the cell with open top and flat glass cover regularly supplied with the instrument (Phoenix Catalog No. R-100) was employed. Later it was replaced by the sealed type cell No. R-101-4, in which the cover plate is permanently fused to the cell and the two compartments are closed by means of ground glass stoppers. The instrument was calibrated against sucrose solutions using the refractive index data given by Gosting and Morris[22] and by Maron and Lou,[23] as well as against NaCl and KCl solutions using the data given by Kruis.[24] In our earlier work,[3-5] the Brice–Phoenix differential refractometer was calibrated by using the refractive index data for sucrose at 589 mμ given by Browne and Zerban[25] and the conversion factors for the other two wave lengths as supplied in the manufacturers instructions. Our present results have led to a new calibration constant for our instrument which necessitates correcting all earlier values of dn/dc and H by the factors 0.985 and 0.970, respectively. The constancy of the dn/dc of heteropoly acids was confirmed for the concentrations up to 0.3 g./ml. by stepwise observation in the differential refractometer at both 436 and 546 mμ. Solutions were compared at 0.05 g./ml. intervals. For higher concentrations (up to 1 g./ml.), refractive indices were measured by means of an Abbé refractometer at 589 mμ, and Δn values and dn/dc values calculated. dn/dc was again constant, but slightly lower due to the use of light of longer wave length.

Since dn/dc was constant throughout the whole concentration range, refractive indices of the solutions at a given concentration necessary for the calculation of the optical constant H were calculated from corresponding dn/dc values.

Results

The light scattering results are presented as Hc/τ *vs.* c for 9-TPA in Fig. 1 and for 12-TSA in Fig. 2. The excess turbidity is denoted by τ, the concentration in g./ml. by c and the parameter H is defined by

$$H = \frac{32\pi^3 n^2}{3N\lambda_0^4}\left(\frac{dn}{dc}\right)^2 \qquad (1)$$

where n is the refractive index of the solution, N is Avogadro's number, and λ_0 is the wave length *in vacuo*. Although n^2 is often approximated by n_0^2 (n_0 is the refractive index of the solvent), this is not possible here

(22) J. Gosting and M. S. Morris, *J. Am. Chem. Soc.*, **71**, 1998 (1949).
(23) S. Maron and R. L. H. Lou, *J. Phys. Chem.*, **59**, 231 (1955).
(24) A. Kruis, *Z. physik. Chem.*, **34B**, 13 (1936).
(25) C. A. Browne and F. W. Zerban, "Physical and Chemical Methods of Sugar Analysis," 3rd Ed., New York, N. Y., 1941.

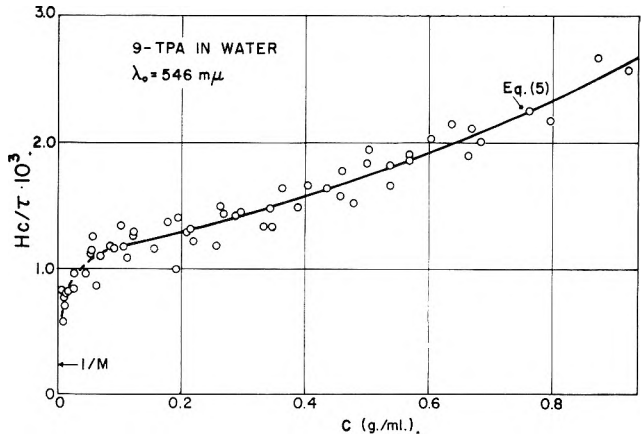

Fig. 1.—Hc/τ *vs.* c for aqueous solutions of 9-tungstophosphoric acid at 546 mμ. The arrow indicates the reciprocal of the molecular weight (M = 4369).

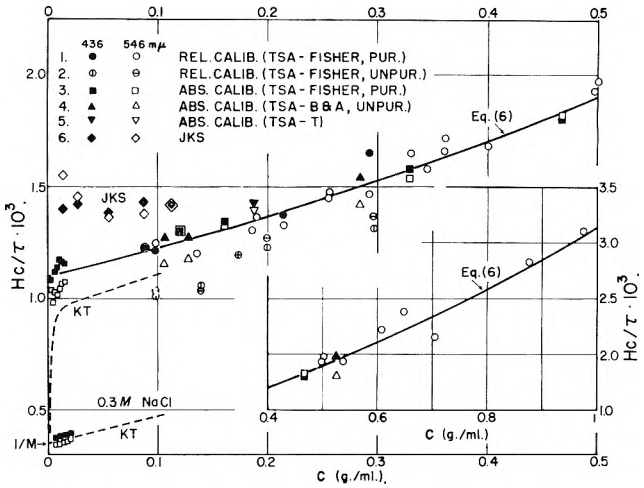

Fig. 2.—Hc/τ *vs.* c for solutions of 12-tungstosilicic acid in water and 0.3 M NaCl at 436 mμ and 546 mμ: (1) purified Fisher acid, relative calibration; (2) unpurified Fisher acid, relative calibration; (3) purified Fisher acid, absolute calibration; (4) unpurified Baker and Adamson acid, absolute calibration; (5) Tyree's sample, absolute calibration; (6) The results of Johnson, Kraus, and Scatchard[7] (JKS); - - -, the results of Kronman and Timasheff[6] (KT). The arrow indicates the reciprocal of the molecular weight (M = 2875).

where $n >> n_0$. Accordingly, H is not constant but can be represented by the following expressions:

For 9-TPA at 546 mμ

$$H \times 10^6 = 1.386 + 0.234c + 0.008c^2 \qquad (2)$$

For 12-TSA at 546 mμ

$$H \times 10^6 = 1.110 + 0.170c - \frac{0.0006}{c} \qquad (3)$$

For 12-TSA at 436 mμ

$$H \times 10^6 = 3.095 + 0.560c - 0.035c^2 \qquad (4)$$

The refractive index increment, dn/dc, of 9-TPA at 546 mμ and 25° was 0.1123 ml./g. Our values of dn/dc for 12-TSA agree precisely with those reported both by Kronman and Timasheff[6] (KT) and by Johnson, Kraus, and Scatchard[7] (JKS) as shown in Table I. Furthermore, we have determined dn/dc both for 12-TSA purified by the procedure described above and for two samples (Fisher's Certified and Baker and Adamson Reagent) that were not purified. Values were independent of purification. They were also independent

of the presence of 0.3 M NaCl in the solutions, in agreement with the observations of KT.

TABLE I

COMPARISON OF VARIOUS DETERMINATIONS OF dn/dc FOR 12-TUNGSTOSILICIC ACID

Authors	dn/dc (ml./g.) 436 mμ	546 mμ
Kronman and Timasheff[6]	0.1065	..
Johnson, Kraus, and Scatchard[7]	.1063	0.1001
This paper	.1066	.1005

For 9-TPA the data can be represented for $c > 0.1$ g./ml. by the least squares expression

$$(Hc/\tau) \times 10^3 = 1.08 + 0.89c + 0.87c^2 \quad (5)$$

At lower concentrations the data indicate a downward trend as was found by KT for 12-TSA.

The results for all samples of 12-TSA, with the exception of Fisher's unpurified acid, agree within the expected experimental error, as illustrated in Fig. 2, and can be represented by the least squares expression

$$(Hc/\tau) \times 10^3 = 1.10 + 1.16c + 0.88c^2 \quad (6)$$

Again, this expression is not applicable at the lowest concentrations ($c < 0.01$ g./ml.), where the limited number of experiments we have carried out seems to indicate a downward trend in Hc/τ values, in agreement with KT's results.

Additional values of Hc/τ were obtained for low concentrations ($c < 0.02$ g./ml.) of 12-TSA in the presence of 0.3 M NaCl and these were extrapolated to zero concentration to yield the precise value of the molecular weight (2.88×10^3). These results are also presented in Fig. 2 together with the best line through KT's points for 436 mμ.

It should be pointed out that in the low concentration range ($c < 0.02$ g./ml.) both for aqueous solutions and solutions containing 0.3 M NaCl, there is a systematic difference in Hc/τ values between 436 and 546 mμ. The turbidities for the latter wave length are somewhat higher. Since the reflections we discussed in the Experimental part were always stronger at 546 mμ (see also Kraut and Dandliker[26]), one can assume that small residual reflections at this wave length are still present in the 90° direction. However, the differences are sufficiently small (at the most 10%) so that they do not invalidate the trend of the curves.

As already mentioned above, the results for unpurified Fisher's 12-TSA did not agree with other data. Hc/τ values are somewhat lower. They are also plotted in Fig. 2 and for comparison there is also an extrapolation of KT's curve ($c > 0.1$ g./ml.). Furthermore, the data of JKS ($c < 0.12$ g./ml.) are plotted on the same diagram.

In Table II are presented values of turbidity at 546 mμ of 9-TPA at rounded concentrations calculated from smoothed Hc/τ (equation 6) (L.S.) and activity of the water, a_1, obtained from isopiestic vapor pressure measurements (V.P.).[5] In Table III the corresponding data for 12-TSA are given.[27] The relation between activity of the solvent a_1 and turbidity due to solute is given by

$$\tau = \frac{Hc\bar{V}_1}{-\mathrm{d} \ln a_1/\mathrm{d}c} \quad (7)$$

and

$$\log a_1 = -\frac{1}{2.303}\int_0^c \frac{Hc\bar{V}_1}{\tau}\,\mathrm{d}c \quad (8)$$

where $\bar{V}_1$ is the partial molal volume of the solvent.

The density of aqueous solutions of 12-TSA is given in Table IV. From these data, the partial molal volume of water $\bar{V}_1$, which appears in the above equations, is 18.0 ± 0.1 ml./mole over the entire range of concentration. The same result was found earlier for 9-TPA.[5] The lowest concentration for which we obtained the density of 12-TSA (c = 0.0574 g./ml.) overlaps with the highest value obtained by Johnson, Kraus, and Scatchard[7] (c = 0.0925 g./ml.) and agrees with their expression for low concentrations to within about 0.2%. Differences of this magnitude can have no appreciable effect upon the calculated partial molal volume of water.

In Tables II and III, the turbidity calculated from the vapor pressure data (V.P.) is obtained from equation 7 while the activities calculated from turbidities (L.S.) are obtained from equation 8.

TABLE II

TURBIDITY (AT 546 Mμ) AND ACTIVITY OF 9-TPA SOLUTIONS

c (g./ml.)	(Hc/τ) $\times 10^3$	$\tau \times 10^4$ (cm.$^{-1}$) L.S.	V.P.	a_1 L.S.	V.P.
0.0				1.0000	1.0000
.2	1.29	2.21	2.28	0.9957	0.9954
.4	1.58	3.76	3.76	.9906	.9902
.6	1.93	4.76	4.70	.9844	.9842
.8	2.35	5.38	5.20	.9769	.9767
1.0	2.84	5.74	5.39	.9679	.9668

TABLE III

TURBIDITY (AT 546 Mμ) AND ACTIVITY OF 12-TSA SOLUTIONS

c (g./ml.)	$(Hc/)\tau$ $\times 10^3$	$\tau \times 10^4$ (cm.$^{-1}$) L.S.	V.P.	a_1 L.S.	V.P.[27]
0.0				1.0000	1.0000
.2	1.37	1.67	1.53	0.9956	0.9956
.4	1.71	2.75	2.50	.9901	.9897
.6	2.11	3.44	3.12	.9833	.9817
.8	2.59	3.84	3.59	.9750	.9726
1.0	3.14	4.07	3.78	.9650	.9621

TABLE IV

DENSITY OF AQUEOUS 12-TUNGSTOSILICIC ACID AT 25°

c (g./ml.)	Density
0.0574	1.0491
.1702	1.1455
.2775	1.2368
.406	1.3455
.532	1.4531
.771	1.6562
.987	1.8424
1.156	1.9860
1.351	2.152
1.521	2.295

Discussion

The correlation between the light scattering and the vapor pressure methods for obtaining either the turbidity or the solvent activity, a_1, of 9-TPA and 12-TSA is well within the experimental error. Although the separate comparisons of τ and of a_1 shown in Tables II and III are actually equivalent, we have chosen to

(26) J. Kraut and W. B. Dandliker, *J. Chem. Phys.*, **23**, 1544 (1955).

(27) We are most indebted to Professor S. Y. Tyree, Jr., of the University of North Carolina for making these activities, obtained by the isopiestic vapor pressure method, available to us in advance of publication of his more complete results.

list each of them, in order to illustrate the precision in each case. Because the calculation of a_1 from light scattering data involves evaluation of the anti-logarithm of a small number, a precise value is obtained even when the light scattering data themselves are not very precise. On the other hand the vapor pressure data do not yield turbidity values of such high precision.

In this work we were primarily interested in the range of concentrations of 12-TSA solutions higher than that covered by KT and JKS. Our results overlap with theirs only in the vicinity of $c = 0.1$ g./ml., and then again at concentrations lower than 0.02 g./ml. Our results fall between those of these other two groups (Fig. 2). JKS have tried to account for the discrepancy that amounted up to 25% between their data and those of KT but have concluded that the "reasons for the discrepancy are not clear."

We are also unable to offer a clearcut explanation. If these workers used the value of the residual refraction correction, R_w/R_c, supplied by the manufacturer (see Experimental part of this paper) their reported turbidities are actually too high and their Hc/τ values correspondingly too low. JKS used the dissymmetry cell standard with the Brice–Phoenix instrument for which the magnitude of this error in R_w/R_c is about 4 to 5% for dilute aqueous solutions. Correcting for this error would make Hc/τ correspondingly higher. Because KT used a cell of only 1 cm.^{2} cross-section, the comparable error would be even greater. Also, as already pointed out by JKS, it appears that KT used the dn/dc for the free acid rather than for the sodium salt, although they titrated the acid with NaOH to pH 4.5 to 5.0. JKS found that although the activity coefficients for the acid and the sodium salt appear to be the same, the dn/dc of the sodium salt is about 2% higher leading to a 4% increase in KT's Hc/τ values and bringing their values closer to ours. Indeed, if KT used the manufacturers value for R_w/R_c, their finally corrected values of Hc/τ would be approximately within 10% of ours.

Both JKS and KT used commercial acids without further purification for their experiments. It is not clear just how this could influence their results. We found that acids of different origin behaved differently (see Fig. 2). When we carried out several measurements with Fisher's certified reagent 12-TSA without further purification, we obtained values of Hc/τ that were significantly lower than our other results. The solutions of the unpurified Fisher acid exhibited a dissymmetry of about 1.10 and higher which could not be reduced by repeated filtration, and also showed appreciable optical absorption at 436 mμ. The dissymmetries for the purified Fisher acid, on the other hand, as well as for other samples, purified or not, were less than 1.05.

The values of Hc/τ reported by JKS are higher than ours, especially at the lowest concentrations. They used Baker and Adamson 12-TSA without further purification.[28] We have also carried out some measurements with this reagent as supplied by the manufacturer and obtained values in agreement with our other results.

The Hc/τ data of JKS as presented in Fig. 2 appear to go through a minimum and at the lowest concentrations exhibit a negative slope. This agrees with their finding that log $\gamma_\pm$ obtained from equilibrium ultracentrifugation goes through a minimum at an ionic strength of about 0.2 m. Indeed, JKS found general agreement between their experimental turbidities and those computed from ultracentrifugation (see Table II, ref. 7). In addition to our work and that of KT, other workers have invariably obtained positive slopes for solutions of similar systems such as polymolybdates,[29] simple electrolytes,[30,31] silicic acid and sodium silicates,[32,33] colloidal silica,[34] complex ionic species[35] and for many detergents in water.

Obviously, it is not possible, on the basis of existing information, to resolve definitely the differences among these three sets of data. However, we submit our light scattering results in view of (a) the variety of samples we have used, (b) the care we have taken in purification of the acids, in clarification of the solutions, in elimination of stray light, and in calibration of the instrument, (c) the determination of the correct molecular weight of the 12-TSA in 0.3 M NaCl, (d) the fact that measurements were taken independently by two of us at quite different times and with different instruments, cells, and experimental procedures, (e) the consistency of our results at the two wave lengths, (f) the correlation of our results with those based on vapor pressure data both for 12-TSA and 9-TPA over a wide range of concentrations.

Error in Earlier Work.—Two of us would like to point out an error in earlier work[4] which has recently come to our attention. Turbidities of 9- and 12-tungstophosphoric acids in aqueous solutions were not corrected for the volume effect and the refraction of the emergent ray. When this correction is made, the turbidities and the apparent molecular weights reported[4] must be decreased by 20%.

In Fig. 4 of this earlier work,[4] the apparent molecular weights, obtained by extrapolation of Hc/τ to zero concentration, were shown to be strongly dependent upon the added salt concentration. For 9-tungstophosphoric acid a limiting value of 5200 in 0.5 M KCl was obtained and for 12-tungstophosphoric acid the limiting value was 3800 in 0.3 M HNO_3. When the above corrections are applied, these upper limits for the apparent molecular weight become 4160 and 3040, which compare quite well with the formula molecular weights of 4369 and 2916 for 9-tungstophosphoric and 12-tungstophosphoric acids.

This result, that in the presence of "swamping electrolyte" correct molecular weights are obtained, is in agreement with the experience of Kronman and Timasheff with 12-TSA[6] and also with our results reported in this paper.

Acknowledgment.—We wish to acknowledge the assistance of Mr. R. Stein, a National Science Foundation Summer Research Participant, in obtaining the density data.

(28) G. Scatchard, private communication, December 8, 1961.

(29) M. Kestigian, P. Colodny, and R. S. Stein, *J. Chem. Phys.*, **21**, 952 (1953).

(30) R. Lochet, *Ann. phys.*, **8**, 14 (1953).

(31) R. W. Fessenden and R. S. Stein, *J. Chem. Phys.*, **22**, 1778 (1954).

(32) M. F. Bechtold, *J. Phys. Chem.*, **59**, 532 (1955).

(33) R. V. Nauman and P. Debye, *ibid.*, **55**, 1 (1951).

(34) Gj. Deželić and J. P. Kratohvil, *Kolloid-Z.*, **173**, 38 (1960); *J. Phys. Chem.*, **66**, 1377 (1962).

(35) J. K. Ruff and S. Y. Tyree, Jr., *J. Am. Chem. Soc.*, **80**, 1523, 5654 (1958).

POLARIZABILITY AND APPARENT RADIUS OF GLYCINE FROM REFRACTIVE INDEX DATA

BY WILLIAM H. ORTTUNG

Department of Chemistry, Stanford University, Stanford, California

Received November 19, 1962

The refractive indices of glycine solutions have been measured at 436, 546, and 578 mμ in the concentration range 0.05 to 0.7 molal at 25° using a Brice–Phoenix differential refractometer. Application of Böttcher's method gave a radius of 2.8 Å. and a satisfactory prediction of the concentration dependence of the molar polarization. The dispersion data were in agreement with similar data for crystalline glycine, and could be explained by a single absorption maximum at 91 mμ with an oscillator strength of 10.4.

Introduction

During the past few decades, the study of biological polymers has been significantly advanced by the measurement and interpretation of various dielectric properties, such as dielectric constant, refractive index, Kerr effect, optical rotation, etc. However, it is clear that increasingly detailed interpretations can be made only after the properties of the basic units of these systems are well understood. The study of the refractive index of glycine solutions was undertaken as a step in this direction.

Glycine solutions are also of interest in relation to dielectric theory. The equations of electrostatics are a good approximation at optical frequencies if the dielectric constant is replaced by the square of the refractive index. The basic equation of electrostatics (obtained from Coulomb's law) is then

$$(n^2 - 1)\mathbf{E} = 4\pi\mathbf{P} \qquad (1)$$

where $\mathbf{E}$ is the average electric field in the medium, and $\mathbf{P}$ is the polarization, or dipole moment per unit volume. $\mathbf{P}$ may be given a molecular interpretation if it is assumed that there is an average local field $\mathbf{F}_i$ at a molecule, i, such that

$$\mathbf{P} = \sum_i N_i\alpha_i\mathbf{F}_i \qquad (2)$$

where N_i is the number of molecules of species i per ml. and α_i is the average polarizability of such a molecule. Using the Lorentz internal or local field,[1] one obtains the Lorenz–Lorentz equation for a binary solution

$$\frac{n^2 - 1}{n^2 + 2}\frac{M}{d} = \frac{4\pi}{3}N_A(x_1\alpha_1 + x_2\alpha_2) \qquad (3)$$

where $M = x_1M_1 + x_2M_2$, x_1 and x_2 being mole fractions and M_1 and M_1 molecular weights of solvent and solute, respectively; d is the density of the solution; and N_A is Avogadro's number. The quantity on the left in eq. 3 is known as the molar refraction of the solution. If $(4\pi/3)N_A\alpha_1$ is replaced by the molar refraction of the pure solvent, then eq. 3 may be solved for α_2

$$\alpha_2' = \frac{1}{x_2}\frac{3}{4\pi}\frac{1}{N_A}\left(\frac{n^2 - 1}{n^2 + 2}\frac{M}{d} - x_1\frac{n_1^2 - 1}{n_1^2 + 2}\frac{M_1}{d_1}\right) \qquad (4)$$

The prime has been added to α_2 in eq. 4 to avoid confusion with the value of α_2 obtained by Böttcher's method,[1] which incorporates the internal field of a model proposed by Onsager.[2] When this internal field is used, the analog of eq. 3 is

$$\frac{(n^2 - 1)(2n^2 + 1)}{12\pi n^2} = \frac{N_1\alpha_1}{1 - \frac{\alpha_1}{a_1^3}\frac{2n^2 - 2}{2n^2 + 1}} + \frac{N_2\alpha_2}{1 - \frac{\alpha_2}{a_2^3}\frac{2n^2 - 2}{2n^2 + 1}} \qquad (5)$$

where a_1 is defined as the radius of a spherical cavity in a uniform dielectric of dielectric constant n^2 about a solvent molecule. a_2 has a similar definition for a solute molecule. Equation 5 may be rearranged to

$$\frac{1}{\alpha_2^*} = N_2\left[\frac{(n^2 - 1)(2n^2 + 1)}{12\pi n^2} - \frac{N_1\alpha_1}{1 - \frac{\alpha_1}{a_1^3}\frac{2n^2 - 2}{2n^2 + 1}}\right]^{-1} \qquad (6)$$

where

$$\frac{1}{\alpha_2^*} = \frac{1}{\alpha_2} - \frac{1}{a_2^3}\frac{2n^2 - 2}{2n^2 + 1} \qquad (7)$$

By plotting $1/\alpha_2^*$ against $(2n^2 - 2)/(2n^2 + 1)$, it is possible to obtain both α_2 and a_2 if α_1 and a_1 are already known.

Although Böttcher's internal field is more realistic for liquids than the Lorentz internal field, it has not been accepted by all workers in the field. Satoh and Hayashi[3] chose to ignore Böttcher's suggestion, while Fajans[4] rejected it because values of α_2 obtained from glycol–water and glycerol–water mixtures did not agree with α_2' values calculated from data on pure liquid glycerol and glycol.[5] However, Brown[6] has shown by a numerical analysis that Böttcher's result is superior to the Lorenz–Lorentz equation, although the use of a spherical cavity about the molecule is an obvious limitation. Both the Lorenz–Lorentz equation and Böttcher's result are considered in interpreting the new data on glycine solutions.

Available data on the refractive indices of amino acid solutions are not numerous. Some measurements were made by Frankel,[7] and by Wallace and Austin.[8]

(1) C. J. F. Böttcher, "Theory of Electric Polarization," Elsevier Publishing Co., Amsterdam, 1952.

(2) L. Onsager, *J. Am. Chem. Soc.*, **58**, 1486 (1936).

(3) T. Satoh and K. Hayashi, *J. Phys. Soc. Japan*, **15**, 1658 (1960).

(4) K. Fajans, in "Physical Methods of Organic Chemistry," Vol. I, Part II, 3rd Edition, Interscience Publishers, Inc., New York, N. Y., 1960, pp. 1194–1195.

(5) C. J. F. Böttcher and Th. G. Scholte, *Rec. trav. chim.*, **70**, 209 (1951).

(6) W. F. Brown, Jr., "Handbuch der Physik," Vol. 17, Springer-Verlag Berlin, 1956, pp. 1–154.

(7) M. Frankel, *Biochem. Z.*, **217**, 378 (1930).

(8) W. J. L. Wallace and T. Austin, *Chemist Analyst*, **32**, 76 (1943).

A few accurate measurements have been made on glycine solutions by Lyons and Thomas[9] in connection with diffusion studies. Recently, McMeekin, *et al.*,[10] reported the molar polarization of a wide range of amino acids, but did not include the concentration and wave length dependence.

Experimental

Apparatus.—A Brice–Phoenix differential refractometer[11,12] equipped with 436, 546, and 578 mμ glass filters was used for the refractive index measurements. Its operation is based on the image displacement method, and its limiting precision is about $\pm 3 \times 10^{-6}$ with a range of 0.01 in Δn. Densities were measured in JB-2250 Robertson specific gravity bottles[13,14] with volumes of about 20 ml. All weighings were made on a Sartorius Selecta Rapid balance.

Materials and Solutions.—Mallinckrodt Analytical Reagent KCl was used for the bulk of the calibrations. Checks were made with Baker Analyzed KCl (assay 99.9%), Baker and Adamson Reagent NaCl (assay 99.5% min.), and Baker and Adamson Reagent NH_4NO_3. The KCl and NaCl were dried at 120° and the NH_4NO_3 was dried in a vacuum oven for 12 hours at 105°. N.R.C. Grade A glycine was obtained from the California Corporation for Biochemical Research. It was recrystallized three times from hot water and alcohol, dried at about 80°, and stored under vacuum. The water was distilled from alkaline permanganate a second time and stored (never more than a few days) in a polyethylene bottle. Solutions were used within a few hours of preparation. All weighings were corrected to vacuum.

Procedures.—Water was pumped through the cell jacket from a bath whose temperature was 24.92 ± 0.05°, according to an NBS-calibrated thermometer, and was constant to ±0.05°. The room temperature was held to 24 ± 1° by an air conditioner. The first measurement of a series was always taken with water in both sides of the divided cell. Subsequent measurements were made after replacing the water on one side with solution. The quantity, Δd, representing the raw data, is given by

$$\Delta d = (d_1 - d_2)_{\text{soln.}} - (d_1 - d_2)_{\text{solvent}} \qquad (8)$$

where d_1 is the reading of the micrometer eyepiece (in tenths of a scale division) with the cell handle toward the light source, and d_2 is the reading after rotating the cell by 180°. Each reading was repeated four times, or until a definite value was obtained (±0.1 scale division). A slit width of about 6 scale divisions on the micrometer eyepiece was found to give the greatest precision for the present observer. KCl and glycine solutions were measured at random during the time that data were being taken.

The procedure for obtaining densities will be described in connection with another investigation. A bath regulated to 25.12 ± 0.03° and constant to ±0.004° was used, and a precision of better than $\pm 2 \times 10^{-5}$ in the resulting densities was obtained.

Calibration.—The data of Kruis[15] (from interferometric measurements, corrected to vacuum) for KCl (436, 546 mμ), NaCl (436, 546, 578 mμ), and NH_4NO_3 (436, 546 mμ) were interpolated with respect to concentration. Values for KCl interpolated to 578 mμ were also available.[11] The precise wave lengths (in air) for the lines of the low pressure mercury arc are 435.8, 546.1, and 577.0–579.1 mμ. Since the latter two are of about equal intensity, it is reasonable to use 578 mμ as an average. The General Electric AH-3 lamp used in the present experiments operates at 28 atm.[16] A survey of available literature on the effect of pressure on the mercury lines indicates that any shifts are well below 1 mμ.

The calibration data on KCl were fitted to expressions of the form

$$\Delta n \times 10^6 = k\Delta d - f(\Delta d)^5 + \Delta \qquad (9)$$

The values of the constants for the three wave lengths are shown in Table I.

(9) M. S. Lyons and J. V. Thomas, *J. Am. Chem. Soc.*, **72**, 4500 (1950).
(10) T. L. McMeekin, M. Wilensky, and M. L. Groves, *Biochem. Biophys. Res. Commun.*, **7**, 151 (1962).
(11) Phoenix Precision Instrument Co., Philadelphia 40, Pa.
(12) B. A. Brice and M. A. Halwer, *J. Opt. Soc. Am.*, **41**, 1033 (1951).
(13) Scientific Glass Apparatus Co., Bloomfield, N. J.
(14) G. R. Robertson, *Ind. Eng. Chem., Anal. Ed.*, **11**, 464 (1939).
(15) A. Kruis *Z. physik. Chem.* (Leipzig), **B34**, 13 (1936).
(16) B. T. Barnes and W. E. Forsythe, *J. Opt. Soc. Am.*, **27**, 83 (1937).

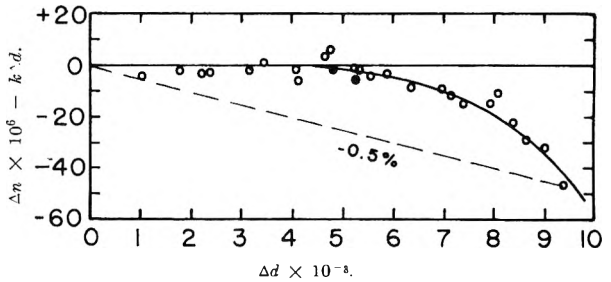

Fig. 1.—Deviation plot of KCl calibration data for 436 mμ: ○, Mallinckrodt; ●, Baker Analyzed; ———, $-f(\Delta d)^5$.

TABLE I
CALIBRATION PARAMETERS

λ(mμ)	k	$f \times 10^{20}$
436	0.9733	58
546	.9707	64
578	.9705	68

A deviation plot for the 436 mμ data is shown in Fig. 1. The non-linear term provided a satisfactory representation for all three wave lengths. Brice and Halwer[12] claimed only that the linearity was within 0.5% for the prototype of the present instrument. Calibration data on NaCl and NH_4NO_3 fell about 0.3% below the KCl line on Fig. 1 at mid-range, but were not used because of the greater uncertainty in purity, and also because of the good agreement between KCl samples from different sources.

Results

Refractive Indices.—Measurements were taken between 0.05 and 0.7 molal. The values of Δn (referred to vacuum) given in Table II were calculated from eq. 8 and 9, assuming $\Delta = 0$ in eq. 9. Both molality, m, and molarity, c, are given, $M_2 = 75.0677$ (C^{12} scale) being used in the calculation. The data were fitted to quadratic equations in both m and c of the form

$$\Delta n' = am + bm^2 \qquad (10a)$$

$$\Delta n'' = a'c + b'c^2 \qquad (10b)$$

the coefficients of which are given in Table III.

TABLE II
REFRACTIVE INDEX INCREMENTS

		$\Delta n \times 10^6$		
m	c	436 mμ	546 mμ	578 mμ
0.05064	0.05039	699	680	679
.09931	.09859	1370	1339	1332
.14642	.14508	2015	1968	1956
.19776	.19551	2708	2648	2629
.23374	.23072	3192	3125	3106
.30254	.29776	4112	4027	4002
.35664	.35018	4830	4729	4705
.40300	.39492	5446	5322	5294
.45162	.44164	6075	5943	5920
.48819	.47665	6556	6403	6381
.54098	.52699	7237	7076	7044
.61188	.59424	8144	7969	7939
.65420	.63419	8687	8487	8458
.70415	.68116	9327	9105	9088

TABLE III
PARAMETERS FOR GLYCINE DATA

λ(mμ)	a	$-b$	a'	$-b'$
436	13882	930	13923	372
546	13571	906	13611	346
578	13509	888	13549	334

The average deviation of all points from eq. 10a was 3.2×10^{-6}, while the standard deviation was 4.6×10^{-6},

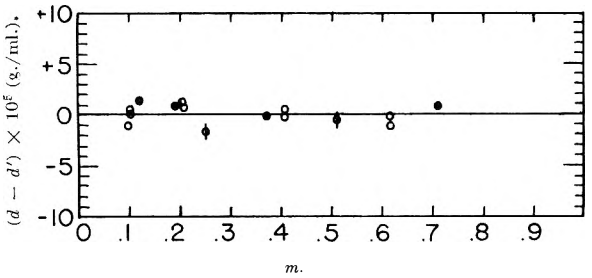

Fig. 2.—Deviation of density data from eq. 11 for $m < 0.7$: ϕ, ref. 19; ○, ref. 20; ●, present work. Points from ref. 18 and 20 which deviate more than 10×10^{-5} are not shown.

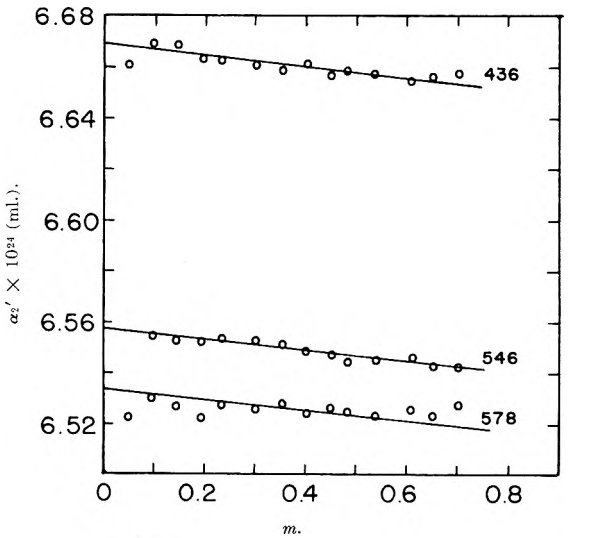

Fig. 3.—α_2' *vs.* m for the three wave lengths studied.

in satisfactory agreement with the limiting precision of the apparatus (3×10^{-6}). Lyons and Thomas[9] obtained $\Delta n \times 10^6 = 13613c - 321c^2$ for the 546 mμ line for $c < 0.7$. The agreement is satisfactory below c = 0.4, but the present data are 10×10^{-6} lower at c = 0.6.

Values of n, the absolute refractive indices of the solutions, were obtained by adding the values of n for water at 25°[17] to the Δn's of Table II. The appropriate values for water at each wave length are

436 mμ	546 mμ	578 mμ
1.340073	1.334335	1.333218

Densities.—The densities of glycine solutions have been measured by Dalton and Schmidt,[18] Daniel and Cohn,[19] and Gucker, *et al.*,[20] and some new values have been taken. The data were fitted to a function, d', valid for $m < 0.8$

$$d' = d_1 + 0.03190m - 0.00216m^2 \qquad (11)$$

where $d_1 = 0.997074$ g./ml. Deviations are shown in Fig. 2. Values of d' were used in the calculations, and it can be seen that the uncertainty in density is 1–2 $\times 10^{-5}$ in the concentration range of interest.

Calculations

Molar Refraction.—Using the value of M_2 mentioned above, with $M_1 = 18.01534$ and $N_A = 6.02261 \times 10^{23}$,[17] values of α_2' were calculated from eq. 4, and are shown in Fig. 3 for the three wave lengths. The curves through the points were predicted by Böttcher's method, as discussed below.

Böttcher Plot.—$1/\alpha_2^*$ was plotted against $(2n^2 - 2)/(2n^2 + 1)$ according to eq. 7, and the result is shown in Fig. 4. For water, the value $a_1 = 1.44$ Å. was used, along with the values of α_1 reported elsewhere[17]

436 mμ	546 mμ	578 mμ
1.363018	1.345611	1.342197

The straight lines through the 436 and 546 mμ points were given by a least squares fit, neglecting the points at the lowest (m = 0.05) and highest (m = 0.7) concentrations. A least squares fit was not attempted for the 578 mμ data, the slope predicted by the other two wave lengths being drawn through the point, $\bar{x},\bar{y}$. The results are summarized in the first two rows of Table IV. The uncertainties given were obtained from the standard deviations of the slopes and intercepts of Fig. 4,[21] and are therefore a measure of precision rather than accuracy.[22] More significant figures are shown

TABLE IV

PARAMETERS FROM BÖTTCHER PLOT

	436 mμ	546 mμ	578 mμ
a_2 (Å.)	2.8 ± 0.1	2.8 ± 0.1	(2.8)
$\alpha_2 \times 10^{24}$ (ml.)	6.419 ± 0.1	6.318 ± 0.1	6.297
$\alpha_2' \times 10^{24}$ (ml.) (m = 0)	6.669	6.558	6.534

for α_2 than seem warranted by the uncertainty. These are useful for analysis of the dispersion, where the absolute uncertainty in a_2 is less important.

Equation 5 may be written in the form

$$\frac{n^2 - 1}{n^2 + 2}\frac{M}{d} = \frac{4\pi}{3} N_A \frac{9n^2}{(2n^2 + 1)(n^2 + 2)} \times \left[\frac{x_1\alpha_1}{1 - \frac{\alpha_1}{a_1^3}\frac{2n^2 - 2}{2n^2 + 1}} + \frac{x_2\alpha_2}{1 - \frac{\alpha_2}{a_2^3}\frac{2n^2 - 2}{2n^2 + 1}}\right] \qquad (12)$$

which, if substituted for the corresponding quantity in eq. 4, gives Böttcher's prediction of the Lorenz-Lorentz polarizability as a function of concentration

$$\alpha_2' = \frac{x_1}{x_2}\left[\frac{9n^2}{(2n^2 + 1)(n^2 + 2)}\frac{\alpha_1}{1 - \frac{\alpha_1}{a_1^3}\frac{2n^2 - 1}{2n^2 + 2}} - \alpha_1'\right] + \frac{9n^2}{(2n^2 + 1)(n^2 + 2)}\frac{\alpha_2}{1 - \frac{\alpha_2}{a_2^3}\frac{2n^2 - 2}{2n^2 + 1}} \qquad (13)$$

Values calculated from eq. 13 have been plotted in Fig. 3 to show that Böttcher's refinement is sufficient to account for the concentration dependence of α_2'. The values of α_2' at m = 0 from eq. 13 are also shown in Table IV.

Dispersion.—In many cases, the wave length dependence of the polarizability in the visible region may be related to a single ultraviolet peak in the absorption spectrum. If $\omega_0 = 2\pi c/\lambda_0$ is the frequency and f the "oscillator strength" of the ultraviolet absorption, then

(17) W. H. Orttung, *J. Phys. Chem.*, **67**, 503 (1963).
(18) J. B. Dalton and C. L. A. Schmidt, *J. Biol. Chem.*, **103**, 549 (1933).
(19) J. Daniel and E. J. Cohn, *J. Am. Chem. Soc.*, **58**, 415 (1936).
(20) F. T. Gucker, W. L. Ford, and C. E. Moser, *J. Phys. Chem.*, **43**, 153 (1939).
(21) W. J. Youden, "Statistical Methods for Chemists," John Wiley and Sons, Inc., New York, N. Y., 1951.
(22) C. J. F. Böttcher, *Rec. trav. chim.*, **65**, 19 (1946).

$$\alpha = \frac{f e^2/m}{w_0^2 - w^2} \qquad (14)$$

which may be written

$$\frac{1}{\alpha} = \frac{A}{f}\frac{1}{\lambda_0^2} - \frac{A}{f}\frac{1}{\lambda^2} \qquad (15)$$

where $A = 4\pi^2 mc^2/e^2$. In Fig. 5, $1/\alpha_2$ and $1/\alpha_2'$ are plotted *vs.* $1/\lambda^2$ for the glycine data. The resulting straight line indicates that eq. 14 is consistent with the data. The slope, $-A/f$, gives a value of f, and the intercept then gives λ_0^2. The values obtained for the Lorenz–Lorentz and Böttcher approximations are shown in Table V.

TABLE V
DISPERSION PARAMETERS

	λ_0 (mμ)	f
Lorenz–Lorentz	94	10.0
Böttcher	91	10.4

Using the above parameters, the molar refraction, $4\pi N_A \alpha_2'/3$, for the sodium-D line, 589.3 mμ, at $m = 0$, is found to be 16.47 ml., in satisfactory agreement with the value of 16.54 ± 0.1 reported by McMeekin, *et al.*[10] Lebedev[23] reported the principal refractive indices of crystalline glycine at 686.7 and 486 mμ. A polarizability, α_2'', was obtained from each principal index by using eq. 3 with $x_1 = 0$ and $d = 1.607$ g./ml.[24] The reciprocal of the average at each wave length was then plotted on Fig. 5. It is apparent that the dispersion of the solid data is consistent with that of the solution data. Parameters similar to those given in Table V have been found for other organic molecules.[25]

Discussion

The value obtained for the radius of the cavity surrounding a glycine molecule, 2.8 Å., is in good agreement with the value of 2.7 Å. estimated by Kirkwood[26] in connection with solubility data in water–alcohol mixtures. It should be pointed out, however, that glycine is not strictly spherical,[27] so that the above radius is an average value. The percentage difference between the polarizabilities predicted by the Lorenz–Lorentz and Böttcher equations is appreciably less for glycine (3%) than for water (10%).[17] This trend is to be expected because the radius of glycine (2.8 Å.) is appreciably larger than that of water (1.44 Å.), It appears that there is little to be gained by application of Böttcher's approach to solutes that are much larger than glycine. In addition, it is clear from Fig. 4 that much greater precision would be required for larger molecules.

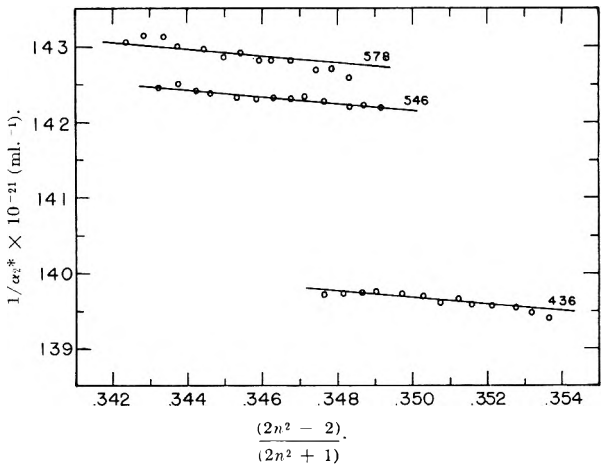

Fig. 4. Application of Böttcher's method.

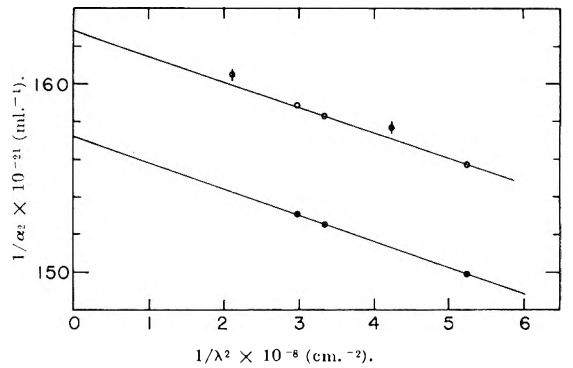

Fig. 5.—Analysis of dispersion data: ○, from Böttcher plot; ●, from Lorenz–Lorentz equation; ϕ, from data on crystal.[23]

Acknowledgments.—The author is indebted to Professor H. S. Loring for use of the refractometer. Support of the National Science Foundation under Grant No. G 15555 is also acknowledged.

(23) See A. N. Winchell, "The Optical Properties of Organic Compounds," Academic Press, Inc., New York, N. Y., 1954, p. 66.
(24) R. E. Marsh, *Acta Cryst.*, **11**, 654 (1958).
(25) W. Kauzmann, "Quantum Chemistry," Academic Press, Inc., New York, N. Y., 1957, pp. 688–693.
(26) J. G. Kirkwood, *J. Chem. Phys.*, **2**, 351 (1934).
(27) A. D. Buckingham, *Australian J. Chem.*, **6**, 323 (1953).

HYDROGEN BONDING EFFECT ON THE ELECTRONIC ABSORPTION OF SOME SECONDARY AMINES

BY ABANI BHUSAN SANNIGRAHI AND ASISH KUMAR CHANDRA

Department of Chemistry, University College of Science and Technology, Calcutta-9, India

Received November 26, 1962

The effect of hydrogen bonding on the near ultraviolet absorption spectra of pyrrole, 2-methylindole, carbazole, and diphenylamine was studied with diethyl ether, tetrahydrofuran, and 1,4-dioxane. The results show that the $\pi \rightarrow \pi^*$ bands of the proton donor shift toward longer wave lengths and using this change of absorption spectrum, the equilibrium constant between proton donor and acceptor was evaluated. From the result it was concluded that proton accepting power decreases in the order 1,4-dioxane > tetrahydrofuran > diethyl ether and the proton donating power increases in the order diphenylamine < pyrrole < 2-methylindole < carbazole. Some discussions also were made on the mechanism of hydrogen bonding.

It was recognized by various workers that the electronic absorption spectra of organic molecules, in the visible and ultraviolet region, are not independent of the environment. This phenomenon may briefly be classified into two types. One of them is the ordinary solvent effect. Another is the effect of specific interaction between solute and solvent molecules. The effect of hydrogen bonding on the electronic spectra belongs to the latter. The fact that the $\pi \rightarrow \pi^*$ bands of phenols shift to longer wave length as the result of hydrogen bonding was pointed out by Coggeshall and Lang[1] and by Nagakura and Baba.[2] Brealey and Kasha[3] observed that the absorption bands of ketones, aldehydes, pyridazine, pyridine N-oxide, etc., arising from the singlet–singlet $n \rightarrow \pi^*$ transitions undergo blue shift as the result of hydrogen bonding. Furthermore it was shown by some authors[4,5] that these phenomena are applicable to the determination of the free energy change for the equilibrium between various proton acceptors and proton donors and therefore are very useful for the study on the mechanism of hydrogen bonding itself.

Systematic investigations[4,6] of the hydrogen bonding effect on the electronic spectra of various phenols were made but the similar study on the absorption bands of pyrrole, indole, and carbazole is still lacking. Moreover, no definite information in regard to the relative order of acidity or basicity in these three molecules is so far known. The purpose of the present investigation is to find a definite answer to this question. In the present paper, pyrrole, 2-methylindole, carbazole, and, for comparison, diphenylamine, whose basic dissociation constant is known, were taken as proton donors and the effect of hydrogen bonding on their absorption bands appearing in the 250–350 mμ region was studied in the presence of ether, tetrahydrofuran, and 1,4-dioxane as proton acceptors. The latter were chosen because they have no absorption bands superposed on that of proton donors. On the basis of the results obtained in the present experiment, some discussions will be made on the mechanism of hydrogen bonding.

Experimental

The B.H.D. reagent pyrrole was distilled before use. The 2-methylindole was purified by repeated sublimation. The carbazole and diphenylamine were E. Merck reagents and were recrystallized before use.

Commercial tetrahydrofuran, 1,4-dioxane, and diethyl ether were made peroxide-free by treatment with ferrous sulfate. They then were refluxed over solid caustic potash for several hours and finally distilled from metallic sodium.

Solvent used was B.D.H. reagent cyclohexane which was purified by chromatographic absorption on Al_2O_3. The purified solvent showed cut off at 230 mμ. Spectral measurements were made with Beckman Model DU spectrophotometer using 1-cm. silica cells at 27°.

Method of Calculation

The physico-chemical basis of the method of calculating the stability constant of the hydrogen bonded complexes was described in detail in a previous communication by Chandra and Basu.[5]

If the equilibrium between a proton donor B and a proton acceptor A be represented by

$$A + B \rightleftarrows AB \qquad K = \frac{[AB]}{[A][B]} \qquad (1)$$

where [B] represents the equilibrium concentration of B and [A] that of A and [AB] that of hydrogen bonded complex. It follows that

$$\frac{[A]}{\bar{\epsilon} - \epsilon_0} = \frac{1}{(\epsilon_1 - \epsilon_0)K} + \frac{[A]}{\epsilon_1 - \epsilon_0} \qquad (2)$$

In relation (2) $\bar{\epsilon}$ is the formal extinction coefficient, ϵ_0 and ϵ_1 are the extinction coefficient of the proton donors and the complex, respectively. From the slope and intercept of the linear plot of $[A]/(\bar{\epsilon} - \epsilon_0)$ *vs.* [A], the equilibrium constant K can be evaluated. Above, equation 2 was derived under two assumptions. The first is that the concentration of hydrogen bonded proton donor is negligibly small compared with that of proton acceptor. The second is that the proton donor and proton acceptor interact one for one. These two assumptions seem to be satisfied for the solutions used in the present investigations, because concentration of proton acceptor in these solutions is several hundred or thousand times larger than that of proton donor.

Results

When increasing amount of proton acceptor was added to a solution containing proton donor we observed that the absorption bands characteristic of the free proton donor molecule became progressively less prominent and at the same time a new band appearing on the longer wave length side of the original band became stronger. From these results it is concluded that the new band should be due to the hydrogen bonded proton donor molecule or more exactly the original absorption band of the proton donor shifts toward longer wave

(1) N. D. Coggeshall and G. M. Lang, *J. Am. Chem. Soc.*, **70**, 3283 (1948).
(2) S. Nagakura and H. Baba, *ibid.*, **74**, 5693 (1952).
(3) G. J. Brealey and M. Kasha, *ibid.*, **77**, 4462 (1955).
(4) S. Nagakura, *ibid.*, **76**, 3070 (1954).
(5) A. K. Chandra and S. Basu, *Trans. Faraday Soc.*, **56**, 632 (1960).
(6) S. Nagakura and M. Gouterman, *J. Chem. Phys.*, **26**, 881 (1957).

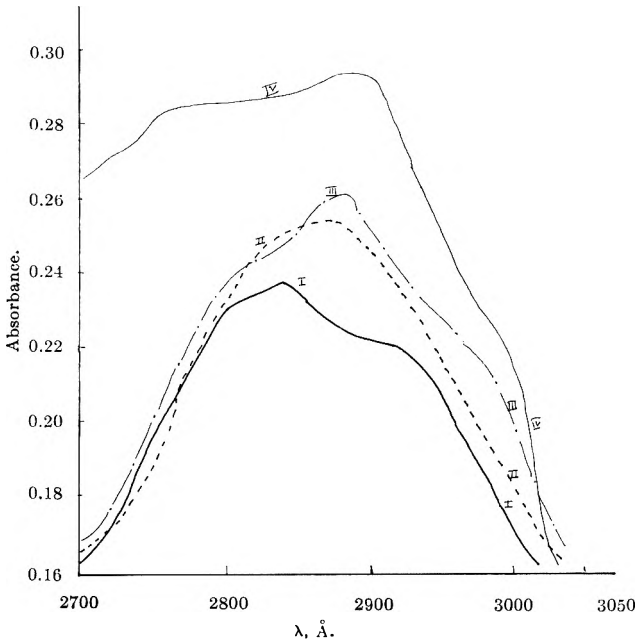

Fig. 1.—Absorption spectra of diphenylamine (I) in cyclohexane and of the hydrogen bonded diphenylamine with ether (II), tetrahydrofuran (III), and 1,4-dioxane (IV). The concentration of diphenylamine is 1.108×10^{-5} mole/l. for all absorption curves.

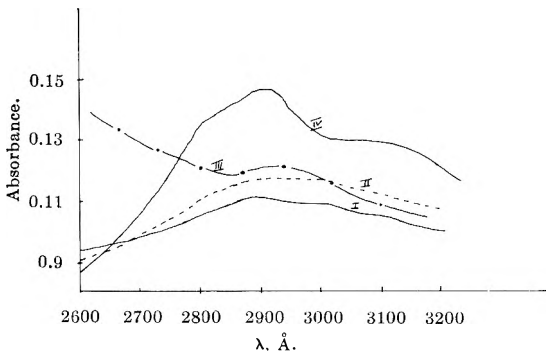

Fig. 2.—Absorption spectra of pyrrole (I) in cyclohexane and of the hydrogen bonded pyrrole with ether (II), 1,4-dioxane (III), and tetrahydrofuran (IV). The concentration of pyrrole is 1.003×10^{-3} mole/l. for all absorption curves.

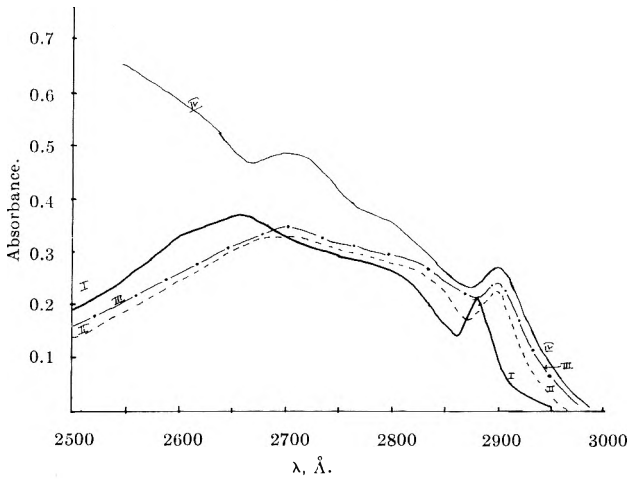

Fig. 3.—Absorption spectra of 2-methylindole (I) in cyclohexane and of the hydrogen bonded 2-methylindole with ether (II), tetrahydrofuran (III), and 1,4-dioxane (IV). The concentration of 2-methylindole is 4.854×10^{-5} mole/l. for all absorption curves.

length as the result of hydrogen bonding. So when the concentration of the proton acceptor was several times larger than that of the proton donor, the proton donor

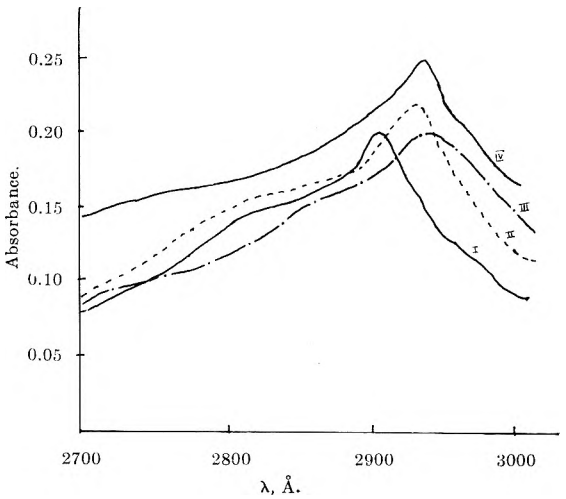

Fig. 4.—Absorption spectra of carbazole (I) in cyclohexane and of the hydrogen bonded carbazole with ether (II), tetrahydrofuran (III), and 1,4-dioxane (IV). The concentration of carbazole is 6.348×10^{-6} mole/l. for all absorption curves.

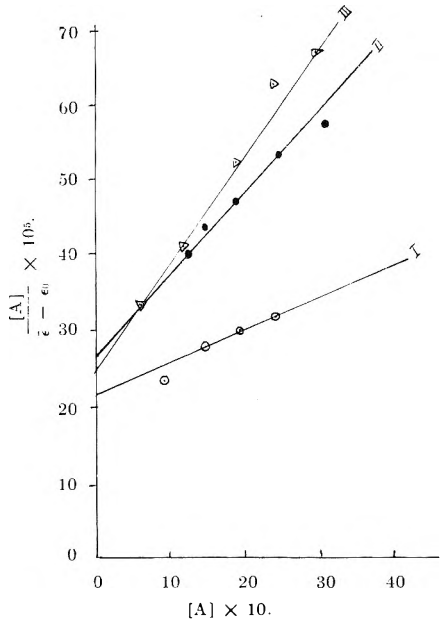

Fig. 5.—I, diphenylamine and ether; II, diphenylamine and tetrahydrofuran; III, diphenylamine and 1,4-dioxane. All the spectral measurements in this figure were made at 290 mμ.

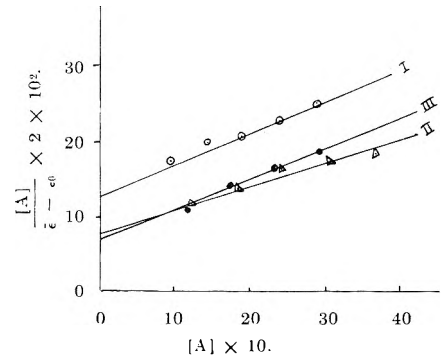

Fig. 6.—I, pyrrole + ether; II, pyrrole + tetrahydrofuran; III, pyrrole + 1,4-dioxane. All the spectral measurements in this figure were made at 292 mμ.

might be assumed to exist completely in the hydrogen bonded state and the peak of the band should be associated with that of the hydrogen bonded complex while the peak in cyclohexane solution was associated with the characteristic $\pi \rightarrow \pi^*$ band of the proton donor.

TABLE I

EQUILIBRIUM CONSTANTS FOR HYDROGEN BONDED COMPLEXES

Proton donors	Concn. of proton donor, moles/l.	Proton acceptors	Range of acceptor concn. (moles/l.)	Equilibrium constant K
		Ether	0.965–2.4120	0.18
Diphenylamine	1.108×10^{-5}	Tetrahydrofuran	.617–3.0810	.40
		1,4-Dioxane	.5875–2.9375	.58
		Ether	.965–2.8950	.28
Pyrrole	1.003×10^{-3}	Tetrahydrofuran	1.233–3.6990	.38
		1,4-Dioxane	1.175–2.938	.78
		Ether	0.965–2.8950	.48
2-Methylindole	4.854×10^{-5}	Tetrahydrofuran	1.233–3.6990	.56
		1,4-Dioxane	1.175–3.5251	1.87
		Ether	0.965–2.8950	0.70
Carbazole	6.348×10^{-6}	Tetrahydrofuran	.617–4.3160	1.50
		1,4-Dioxane	.5875–2.9375	2.49

TABLE II

WAVE NUMBER SHIFTS IN THE ABSORPTION BANDS OF PROTON DONOR AND LONE PAIR DIPOLES AND IONIZATION POTENTIALS OF THE PROTON ACCEPTORS

Proton acceptors	$\Delta\nu$, cm.$^{-1}$				Lone pair dipole moment, D.	Lone pair ionization potential
	Diphenylamine	Pyrrole	2-Methylindole	Carbazole		
Ether	380	350	440,240	300	2.841	9.72[a]
Tetrahydrofuran	500	170	560,240	370	2.736	..
1,4-dioxane	570	410	580,250	470	2.701	9.52[a]

[a] J. D. Morrison and A. J. C. Nicholson, *J. Chem. Phys.*, 20, 1021 (1952).

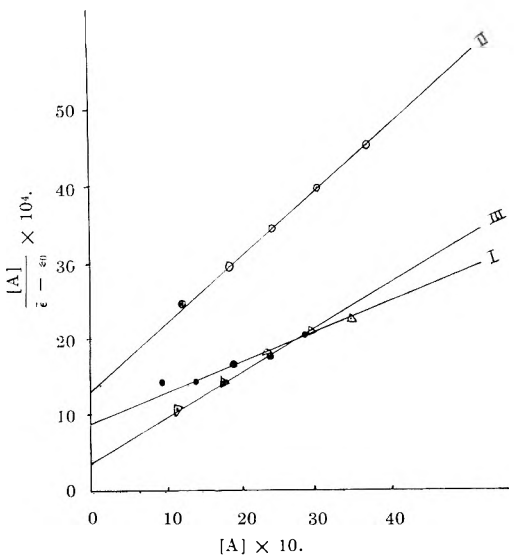

Fig. 7.—I, 2-methylindole + ether; II, 2-methylindole + tetrahydrofuran; III, 2-methylindole + 1,4-dioxane. All the spectral measurements in this figure were made at 294 mμ.

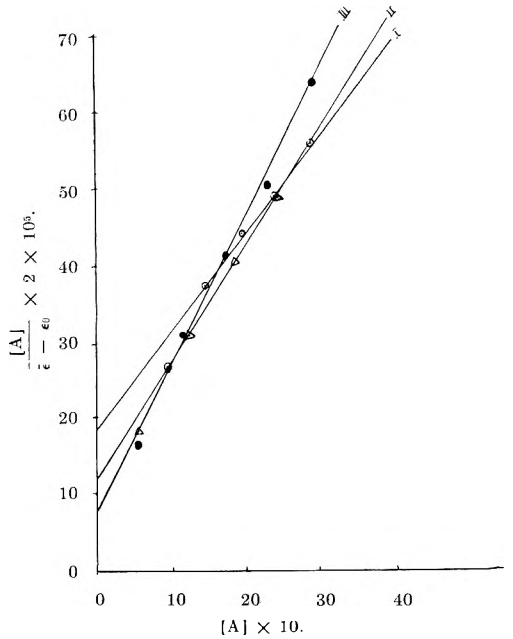

Fig. 8.—I, carbazole + ether; II, carbazole + tetrahydrofuran; III, carbazole + 1,4 dioxane. All the spectral measurements in this figure were made at 295 mμ.

In Fig. 1 to 4 are shown the absorption bands of the free proton donors and the hydrogen bonded proton donors with ether, tetrahydrofuran, and 1,4-dioxane. In all cases it was shown that the characteristic $\pi \rightarrow \pi^*$ bands of the free proton donors shifted to longer wave lengths. Next we tried to determine the equilibrium constant between proton donor and acceptor. For this purpose, the absorbance measurements were made on mixtures of a proton donor with different proton acceptors at several wave lengths near the peak of the complex species. The plot of $[A]/(\bar{\epsilon}-\epsilon_0)$ against $[A]$ was found to be linear in all cases. From the slope and intercept of these curves the equilibrium constant for the hydrogen bonded complexes was calculated using relation 2. The values of equilibrium constant for a given system were almost constant within 10%. In Fig. 5–8 are shown the plots at one such wave length and results are summarized in Table I, where the average values of the equilibrium constants measured at several wave lengths are given. In Table II are given the wave number shift ($\Delta\nu$ cm.$^{-1}$) of the longest wave length bands due to hydrogen bonding.

Discussion

It is seen that the frequency shift caused by the hydrogen bonding increases in the order of 1,4-dioxane > tetrahydrofuran > ether for a series of the same proton donor. The position of tetrahydrofuran with pyrrole is however anomalous. This anomaly may be due to the very approximate nature in determining the position of the center of the bands of pyrrole. The

above order of frequency shift is in complete accordance with that of equilibrium constant given in Table I. This is consistent with the fact that the proton acceptor which forms the strongest hydrogen bond exertsthe largest perturbation on the absorption spectrum of the proton donor. However, for a series with the same proton acceptor the frequency shift of the $\pi \rightarrow \pi^*$ bands of the proton donors due to hydrogen bonding is not systematic. But on the basis of equilibrium constant measurements it can be concluded that the proton donating power has the order carbazole > methylindole > pyrrole > diphenylamine. Dodd and Stephenson[7] measured the relative shifts in the N–H stretching vibration frequencies of some amines in the infrared region in acetone and pyridine in which there is strong hydrogen bonding interaction. They concluded from the results of these measurements that proton donating power has the order indole > pyrrole > diphenylamine. This result is in support of our conclusion and furthermore we can conclude that carbazole has the strongest proton donating power of the four amines. Our results which are coincident with that derived from the measurements in the infrared region support the electrostatic theory of hydrogen bonding.

The hydrogen bond also may be regarded as a special case of electron donor–acceptor interaction. For the formation of a stable hydrogen bond, which may be written as X–H . . . Y, the only requirement of the acceptor is that the charge distribution of the X–H bond orbital be such as to leave the proton sufficiently unscreened. For a series of electron donors with the same electron acceptor the magnitude of electrostatic interaction will depend not on the dipole moment of the donor molecules, as was wrongly supposed by Nagakura and Gouterman,[6] but on the lone pair dipole moment.[8] The magnitude of the lone pair dipole moments in ether, tetrahydrofuran, and 1,4-dioxane has been calculated from the hybridization parameters, which in turn are obtained from the reported COC bond angles,[9,10] in these three molecules. The observed bond angles increase from 108 to 112° in the order dioxane > tetrahydrofuran > ether and lone pair dipole moments decrease in the order 1,4 dioxane < tetrahydrofuran < ether as shown in Table II. Hence the equilibrium constants of a proton donor with these proton acceptors should follow the reverse order rather than what was obtained in the present work.

Using accurate molecular wave functions (s.c.f.l.c.a.o.) of water and ammonia calculated by Ellison and Shull[11] and by Higuchi,[12] and then by unitary transformations to equivalent orbitals, Burnelle and Coulson[13] calculated the lone pair dipole moment at different valence angles. They have shown that the $d\mu_2/d\alpha$, where μ_2 is the lone pair dipole moment and α the valence angle in water and ammonia, is always positive in the range of α from 105–120°. So unless accurate molecular wave functions are used in calculating lone pair dipoles, it would be dangerous to use the lone pair dipoles as a rough measure of donor strength. From the results of accurate calculations on the water molecule, we may conclude that the lone pair dipoles of the electron donors of our interest increase in the order 1,4-dioxane > tetrahydrofuran > ether, which is the order of equilibrium constants with a given proton donor. It therefore may be suggested that the lowering of equilibrium constant in the above order is due to lowering of electrostatic energy in the same order.

Besides the electrostatic force, the charge transfer force may have some contribution to the stabilization of hydrogen bonding. The charge transfer force or delocalization force means the stabilization due to electron migration from a non-bonding orbital of the proton acceptor to the N–H antibonding orbital of the proton donor. The contribution of this force has been discussed by several authors.[14–16] According to this, the proton accepting power depends on the ionization potential of the non-bonding electron of the proton acceptor and the lower it is, the stronger the hydrogen bonding is. The ionization potential of tetrahydrofuran is not known but the ionization potential of 1,4-dioxane is less than that of ether (Table II). It seems, therefore, that in the present systems both the charge transfer force and electrostatic force have contributions to the stabilization of hydrogen bonding and that they act in the same direction.

Acknowledgments.—The authors thank Professor B. N. Ghosh for his kindness in providing laboratory facilities and to the University of Calcutta for awarding a research fellowship to A. B. S.

(7) R. E. Dodd and G. W. Stephenson, in "Hydrogen Bonding," D. Hadzi, Ed., Pergamon Press, 1959.
(8) W. G. Schneider, *J. Chem. Phys.*, **23**, 26 (1955).
(9) J. Y. Beach, *ibid.*, **9**, 54 (1954).
(10) P. W. Allen and L. E. Sutton, *Acta Cryst.*, **3**, 46 (1950).
(11) F. O. Ellison and H. Shull, *J. Chem. Phys.*, **23**, 2348 (1955).
(12) J. Higuchi, *ibid.*, **24**, 535 (1956).
(13) L. Burnelle and C. A. Coulson, *Trans. Faraday Soc.*, **53**, 463 (1957).
(14) I. Fischer, *Arkiv Fysik*, **1**, 495 (1949).
(15) H. Tsubomura, *Bull. Chem. Soc. Japan*, **27**, 445 (1954).
(16) C. A. Coulson and I. Danielsson, *Arkiv Fysik*, **8**, 239, 245 (1955).

MOLAL ACTIVITY COEFFICIENTS OF METHANE- AND ETHANESULFONIC ACIDS AND THEIR SALTS

BY HARRY P. GREGOR, MICHAEL ROTHENBERG, AND NORMAN FINE[1]

Department of Chemistry of the Polytechnic Institute of Brooklyn, Brooklyn, N. Y.

Received November 28, 1962

The molal activity coefficients of methane- and ethanesulfonic acids and their lithium, sodium, potassium, ammonium, tetramethyl-, tetraethyl-, and tetrabutylammonium salts were measured at molalities ranging from 0.1 to about 8. The acids and alkali metal salts had activity coefficients quite similar to those of the corresponding chlorides. The quaternary ammonium salts showed behavior similar to that of the acids or lithium salts, with their activity coefficients rising sharply with increasing concentration. The behavior of the organic ions was explained in terms of the "ice-like" structure of water. The tetrabutylammonium salts showed micelle formation at relatively low concentrations, in agreement with a fall in their activity coefficients.

This contribution describes the preparation of a number of alkali metal and quaternary ammonium sulfonates and the isopiestic measurement of their molal activity coefficients. The compounds studied were methane- and ethanesulfonic acids and their lithium, sodium, potassium, ammonium, tetramethyl-, tetraethyl-, and tetrabutylammonium salts. Determinations were made for molalities from approximately 0.1 to 4 at 25°, and for higher concentrations at 30°. Most of these electrolytes are miscible with water in almost all proportions.

Experimental

In this contribution use is made of the isopiestic measurement described by Sinclair,[2] Robinson and Sinclair,[3] and Wishaw and Stokes.[4] A number of electrolytic solutions are allowed to come to isopiestic equilibrium, one being a salt whose activity coefficient is known. Activity coefficients of the other salts are calculated using the Gibbs–Duhem equation.[5]

Isopiestic measurements were made at 25° using potassium chloride as reference electrolyte for concentrations up to 4 *m*. Then weighed samples were placed in humidistats[6] over standard sulfuric acid solutions and their molalities measured. Mean molal activity coefficients for these latter systems were calculated by assuming that their activity coefficients did not vary significantly in the 5° interval and again employing the Gibbs–Duhem relationship, with the reference state being the highest solute activity values obtained previously. That this procedure was valid and led to negligible errors was ascertained by plotting the molality of a given solute against the activity of the solvent of isopiestic solutions of both the potassium chloride and sulfuric acid standards; the two curves overlapped within experimental error.

Commercially available methane- and ethanesulfonic acids (Indoil Chem. Co.) were obtained at the following purity: at least 95% the sulfonic acid; 1% sulfuric acid; 0.05% ash; the remainder largely water. Each alkanesulfonic acid was purified by adding water and barium hydroxide followed by heating to boiling, standing at room temperature for two days and filtering off precipitated barium sulfate. The barium sulfonate salts are rather soluble. When this filtrate gave a negative test for both sulfate (with barium hydroxide) and barium (with sulfuric acid), the acid was considered to be sufficiently pure. Alkali metal and quaternary ammonium salts were prepared by adding the base to a known weight of purified and standardized acid to a pH meter end-point and evaporating to dryness. The dry weight of all salts was within ±0.5% of the calculated weight. Certain of these were further purified by crystallization from hot ethanol. The purity of the ammonium salts was established further by titrating with standard alkali in ethanol; the per cent NH_4 found in ammonium methanesulfonate was 15.96 compared with the calculated value of 15.90; for ammonium ethanesulfonate the per cent found was 14.20 compared to a calculated value of 14.16. Tetramethylammonium salts were also further purified by crystallization, but the tetraethylammonium and higher homologs could not be purified by recrystallization because of their high solubility in a number of solvents; these were dried at 110° and used as such. The tetrabutylammonium salts decomposed upon drying and were used in solution as prepared. While the purity of these salts was probably only 99%, it is expected that their activity coefficients are almost identical with values for reagent grade materials because the impurities present were undoubtedly quite similar to the compounds themselves.

Isopiestic measurements against potassium chloride used stainless steel dishes 1.4 cm. in diameter and 2 cm. high, weighing 16 grams. Otherwise, the apparatus was conventional. Care was taken to ensure the attainment of isopiestic equilibrium; for details, the thesis should be consulted.[1] Molal activity coefficients were calculated by graphical integration, making use of those given in Harned and Owen.[7] Tables I and II give numerical values, which also are shown in Fig. 1 and 2. The Debye–Hückel expression

$$-\log \gamma = 0.509I^{1/2}/(1 + 0.329\mathring{a}I^{1/2})$$

where $\mathring{a}$ is the distance of closest approach in Ångstrom units and I the ionic strength, was found to give a constant value of $\mathring{a}$ = 3.96 in the concentration range 0–1 *m* potassium methanesulfonate (a value identical with that for potassium chloride). The same plot gave $\mathring{a}$ values for potassium ethanesulfonate which increased with $I^{1/2}$ and for potassium toluenesulfonate which decreased with $I^{1/2}$, both compounds appearing to give $\mathring{a}$ = 4 at $I^{1/2} < 0.1$. Figures 3 and 4 show value of γ in the concentration range 4 to 12 *m*.

The critical micelle concentration of tetrabutylammonium ethanesulfonate was determined by measuring the solubilization point of a dilute (0.001%) solution of Eosin OJ. The non-solubilized dye formed a yellow-orange-green turbid solution

TABLE I

MEAN MOLAL ACTIVITY COEFFICIENTS OF METHANESULFONATES AT 25°

Molality	H	Li	Na	K	NH_4	Me_4N	Et_4N	Bu_4N
0.1	0.813	0.793	0.780	0.770	0.770	0.790	0.761	0.796
.2	.792	.757	.734	.718	.719	.753	.724	.765
.3	.789	.743	.713	.688	.691	.734	.726	.755
.4	.794	.733	.690	.666	.670	.724	.715	.751
.5	.804	.729	.686	.650	.657	.718	.710	.754
.7	.816	.732	.669	.625	.635	.717	.706	.753
1.0	.849	.743	.659	.604	.617	.729	.717	.799
1.5	.913	.748	.654	.582	.602	.760	.759	.868
2.0	1.000	.834	.661	.573	.599	.826	.825	.905
2.5	1.123	.891	.673	.569	.598	.896	.91	.918
3.0	1.234	.951	.692	.563	.599	.975	.993	.898
3.5	1.380	1.035	.713	.561	.603	1.051	1.103	.897
4.0	1.58	1.11	.730	.560	.610	1.15	1.21	.890
6.0[a]	6.60	3.91	1.73	1.07	1.20	3.31	5.37	1.26
8.0[a]	16.2	7.4	3.09	1.62	1.86	6.92	13.5	1.74

[a] Values at 30°.

(1) Abstracted in part from the thesis of Norman Fine, submitted in partial fulfillment of the requirements for the degree of Master of Science in Chemistry at the Polytechnic Institute of Brooklyn, May, 1954.

(2) D. A. Sinclair, *J. Phys. Chem.*, **37**, 495 (1933).

(3) R. A. Robinson and D. A. Sinclair, *J. Am. Chem. Soc.*, **56**, 1830 (1934).

(4) B. F. Wishaw and R. H. Stokes, *Trans. Faraday Soc.*, **49**, 27 (1953).

(5) R. A. Robinson and D. A. Sinclair, *J. Am. Chem. Soc.*, **56**, 1830 (1934).

(6) H. P. Gregor, B. R. Sundheim, K. M. Held, and M. H. Waxman, *J. Colloid Sci.*, **7**, 511 (1952).

(7) H. S. Harned and B. B. Owen, "The Physical Chemistry of Electrolytic Solutions," Reinhold Publ. Corp., New York, N. Y., 1950.

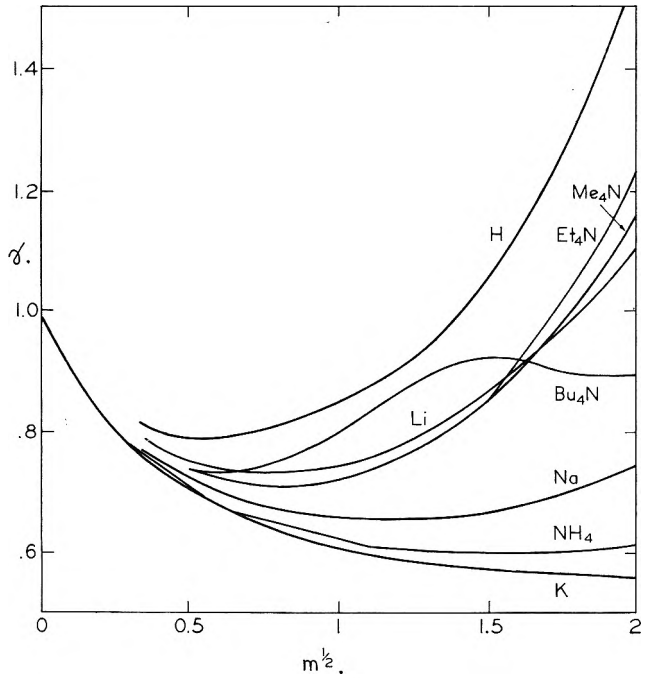

Fig. 1.—Mean molal activity coefficient of methanesulfonic acid and its salts at 25°.

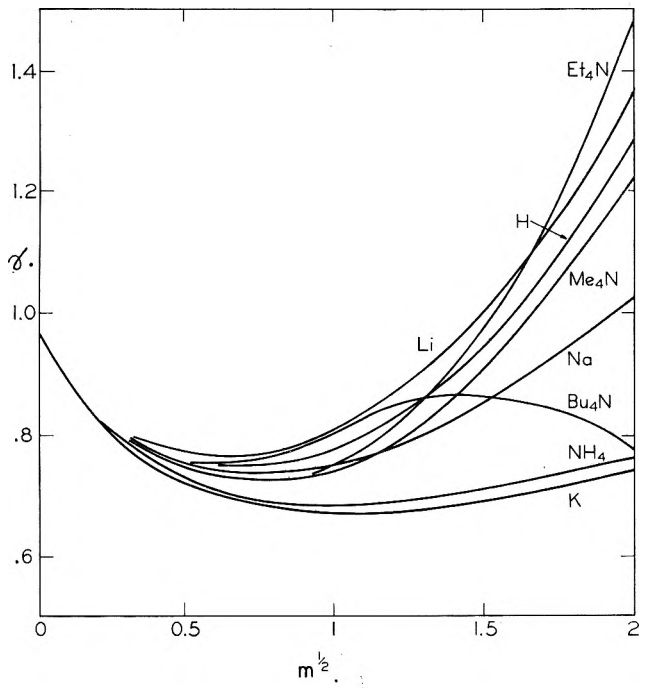

Fig. 2.—Mean molal activity coefficient of ethanesulfonic acid and its salts at 25°.

while the solubilized dye was pink-green in color. The critical micelle concentration was 0.030 ± 0.005 *m*.

Discussion

Certain physical properties of sulfonic acids and their salts have been studied. McBain, Dye, and Johnson[8] and McBain and Bolduan[9] measured the conductivity, viscosity, density, and refractive index of solutions of linear C_1 to C_{14} aliphatic sulfonic acids and concluded that there was a transition from fully dissociated electrolytes for the lower homologs (C_1–C_7) to micelle-forming colloidal electrolytes for the higher members (C_9–C_{14}). McBain and Betz[10] measured activity coefficients of the C_{11},C_{12}, and C_{14} aliphatic sulfonic acids by the freezing point method; plots of γ *vs.* $m^{1/2}$ showed characteristic dips in the vicinity of 0.1 *m*, indicating micellization.

(8) E. L. McBain, W. B. Dye, and S. A. Johnson, *J. Am. Chem. Soc.*, **61**, 3210 (1939).

(9) J. W. McBain and O. E. A. Bolduan, *J. Phys. Chem.*, **47**, 94 (1943).

(10) J. W. McBain and M. D. Betz, *J. Am. Chem. Soc.*, **57**, 1905 (1935).

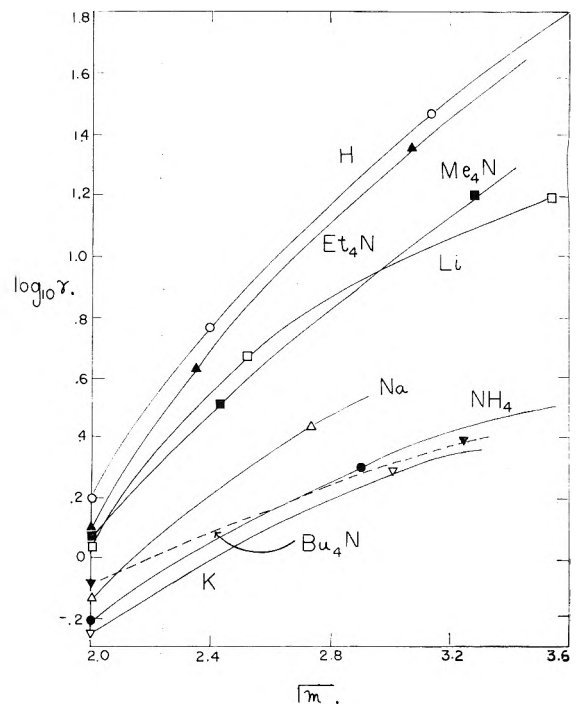

Fig. 3.—Mean molal activity coefficient of methanesulfonic acid and its salts at 30°.

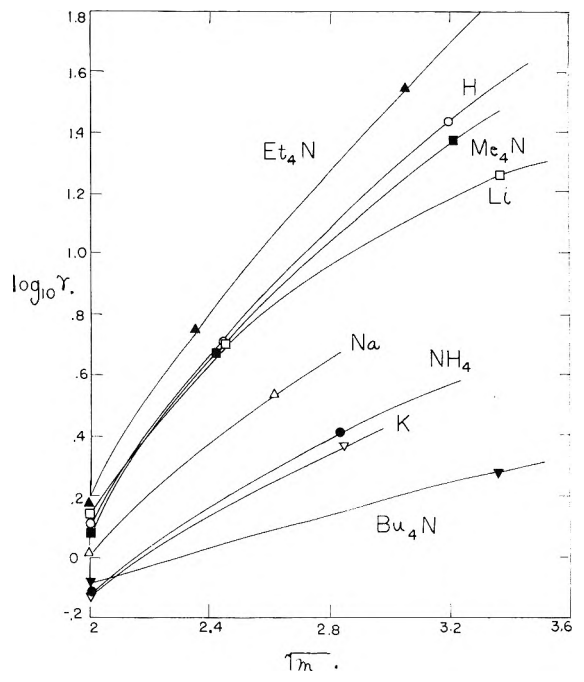

Fig. 4.—Mean molal activity coefficient of ethanesulfonic acid and its salts at 30°.

Activity coefficients of the toluenesulfonates were measured by Robinson[11] using vapor pressure measurements. The sodium and potassium salts of *p*-toluenesulfonic acid showed a slight but definite concavity toward the concentration axis at 0.7 *m*. The lithium salt, however, showed a smooth curve, but somewhat flatter than for other comparable lithium salts. The dispersion of the curves was also appreciably less than for other alkali metal salts, although the potassium

(11) R. A. Robinson, *ibid.*, **57**, 1165 (1935).

TABLE II

MEAN MOLAL ACTIVITY COEFFICIENTS OF ETHANESULFONATES AT 25°

Molality	H	Li	Na	K	NH_4	Me_4N	Et_4N	Bu_4N
0.1	0.797	0.801	0.796	0.774	0.781	0.795	0.798	0.795
.2	.774	.776	.764	.731	.740	.756	.752	.760
.3	.756	.766	.754	.709	.719	.740	.737	.751
.4	.751	.760	.747	.693	.702	.732	.728	.751
.5	.752	.770	.744	.684	.692	.728	.728	.756
.7	.766	.779	.742	.673	.680	.731	.728	.770
1.0	.781	.811	.754	.664	.675	.748	.756	.803
1.5	.839	.882	.790	.666	.680	.799	.825	.857
2.0	.910	.961	.834	.676	.695	.871	.916	.861
2.5	.988	1.053	.875	.690	.713	.962	1.034	.853
3.0	1.073	1.156	.928	.706	.730	1.040	1.119	.834
3.5	1.176	1.231	.971	.721	.747	1.130	1.321	.804
4.0	1.280	1.356	1.028	.734	.750	1.220	1.465	.780
6.0[a]	5.25	5.02	2.54	1.41	1.55	5.13	7.25	1.10
8.0[a]	12.3	9.6	4.57	2.24	2.51	11.5	20.4	1.38

[a] Values at 30°.

values were approximately the same. Robinson noted further[12] that the activity coefficients of lithium, sodium and potassium halides decreased in the order I > Br > Cl, at a given concentration. With the larger cations Rb and Cs, however, the order was reversed, Cl > Br > I.

The thermodynamic properties of tetraalkylammonium salts were studied by Ebert and Lange,[13] who measured osmotic coefficients of their halide salts and found pronounced individual differences as contrasted with the properties of the alkali metal halides. Freezing point measurements by Lange[14,15] on dilute solutions of these salts showed both positive and negative deviations from the Debye–Hückel slope, even in dilute solutions. Other studies have shown the same, marked variations in the thermodynamic properties of the quaternary ammonium salts. Kraus[16] concluded from his studies on the alkyltrimethylammonium salts that when more than sixteen carbon atoms were present micelles were formed; salts of lower members of the series appeared to be normal 1–1 electrolytes.

The behavior of methane- and ethanesulfonic acids and their alkali metal salts bears a striking resemblance to that of the corresponding halides. The curves for potassium chloride and potassium methanesulfonate coincide over a wide range of concentrations. Similarly, the curve for methanesulfonic acid is but slightly lower than that for hydrochloric acid, even in concentrated solutions. For example, in 4 *m* solutions $\gamma_\pm = 1.73$ for hydrochloric acid and 1.58 for methanesulfonic acid. Further, the familiar halide sequence of activity coefficients is followed: $H^+ > Na^+ > K^+ = NH_4^+$.

The behavior of the quaternary ammonium salts is of particular interest. The curve for tetramethylammonium methanesulfonate is quite similar to that for the corresponding lithium salt and also for lithium chloride. At even higher concentrations (see Fig. 3) the tetramethyl- and tetraethylammonium salts of methanesulfonic acid show ever-increasing activity coefficients, resembling lithium chloride in this respect. The tetrabutylammonium salt starts to rise much more sharply, but then falls off as micelles start to form. Micelle formation is usually associated with long-chain compounds, but in this case we have a spherical ion of the requisite number of carbon atoms. The behavior of these quaternary ammonium salts (with the exception of tetrabutyl-) is of particular interest. Robinson and Stokes have explained a rise in the activity coefficient at high concentrations in terms of a hydration model, but there is no corroborative evidence for strong hydration of these organic cations. Indeed, the applicability of Walden's rule and of Stokes' hydrodynamics[17] is good evidence to the contrary.

The behavior of these salts can be explained, in large measure, by the model of electrolytic solutions proposed by Frank,[18] who views water as being in a state of equilibrium between ice-like and non-ice-like forms. Organic ions, particularly those having a low dielectric constant, are classified as "structure-making" in that they favor ice-like structures[19]; the presence of the latter makes for a lowered water activity, as is observed here. This favoring of ice-like forms increases with increasing molecular weight of the solute, and is observed in this study for both the homologous series of quaternary ammonium ions and in comparing methane- and ethanesulfonic acids. Of special interest is the fact that activity coefficients for methanesulfonic acid are substantially higher than for its salts, but this is not at all the case with ethanesulfonic acid.

A comparison between the activity coefficients of methane-, ethane-, and toluenesulfonic acids and their salts deserves mention. All show the "regular" sequence $\gamma_K < \gamma_{Na} < \gamma_{Li}$, but the mean activity coefficients of the potassium salts (as an example) in 1 *m* solutions are 0.604, 0.664 and 0.509 for the methanesulfonate, ethanesulfonate and toluenesulfonates, respectively. The low activity coefficient of the aromatic salt is undoubtedly due to anionic association. Attempts have been made to explain changes in the selectivity coefficients of cross-linked polystyrenesulfonic acid ion-exchange resins with their degree of cross-linking (see, *e.g.*, the data of Gregor and Bregman[20]) by making comparisons based on the activity coefficients of corresponding salts of toluenesulfonic acid. This concept has been extended[21] to comparisons based upon the salts of *p*-toluenesulfonic acid and 2,5-dimethylbenzenesulfonic acid. Our results indicate that interactions between ions of opposite sign, which must be the basis for predicting the selective behavior of ion-exchange resins based upon ion-pairing, are very much the same with the methane- and ethanesulfonates as with the halides, and presumably very much the same for all sulfonates.

Acknowledgment.—The authors wish to thank L. Osipow of Foster D. Snell, Inc., New York, for performing the solubilization studies. Part of this study was supported by a grant from the National Science Foundation.

(12) R. A. Robinson, *J. Am. Chem. Soc.*, **57**, 1161 (1935).
(13) L. Ebert and J. Lange, *Z. physik. Chem.*, **A139**, 584 (1928).
(14) J. Lange, *Z. Elektrochem.*, **39**, 545 (1933).
(15) J. Lange, *Z. physik. Chem.*, **A168**, 147 (1934).
(16) C. A. Kraus, *Trans. N. Y. Acad. Sci.*, **12**, 215 (1950).
(17) See, *e.g.*, R. A. Robinson and R. H. Stokes, "Electrolyte Solutions," Butterworths Scientific Publications, London, 1955.
(18) H. S. Frank and W.-Y. Wen, *Discussions Faraday Soc.*, **24**, 133 (1957).
(19) H. S. Frank and M. W. Evans, *J. Chem. Phys.*, **13**, 507 (1945).
(20) H. P. Gregor and J. I. Bregman, *J. Colloid Sci.*, **6**, 323 (1951).
(21) O. D. Bonner, V. F. Holland, and L. L. Smith, *J. Phys. Chem.*, **60**, 1102 (1956).

AMMONIA EQUILIBRIUM BETWEEN VAPOR AND LIQUID AQUEOUS PHASES AT ELEVATED TEMPERATURES

BY MERLE E. JONES

Knolls Atomic Power Laboratory,[1] Schenectady, N. Y.

Received December 1, 1962

The equilibrium concentrations of ammonia in the vapor and liquid phases were measured over a temperature range of 147 to 326° for aqueous solutions containing approximately 2, 20, and 200 p.p.m. of ammonia. The relative volatility was found to be a function of both concentration and temperature. The variation with concentration was shown to be due to the ionization of ammonia in the liquid phase. After correction for ionization, the relative volatility decreases from a value of 9.8 at 150° to 2.8 at 325°.

Introduction

The partial pressure of ammonia over aqueous solutions of ammonia has been reported for high concentrations of ammonia at temperatures up to 121°.[2] There was a need for values at much lower concentrations and at higher temperatures. A series of measurements was made of the distribution of ammonia between liquid and vapor phases over the temperature range of 147 to 326° for aqueous solutions containing approximately 2, 20, and 200 p.p.m. of ammonia.

Experimental

A large (25-l. capacity) stainless steel autoclave was used as a container in these tests. It was provided with two dip legs so that samples of both the liquid and the vapor phases could be removed at operating temperature. Each dip leg was connected through a valve to a water-cooled condenser. A glass capillary tube on each condenser introduced the sample into a 15-ml. centrifuge tube containing 6 ml. of 0.005 *M* H_2SO_4. The autoclave temperature was measured with a chromel–alumel thermocouple using a Leeds and Northrup potentiometer.

In actual operation, 15.0 liters of deionized, deoxygenated water was placed in the autoclave. The required amount (few milliliters) of a dilute ammonium hydroxide solution was added and the solution was sparged with argon. The autoclave head was installed and the autoclave was evacuated to a pressure of 0.5 to 1.0 p.s.i. The autoclave was then heated to temperature and the temperature was maintained for 24 hr. before sampling and readjusting to another temperature.

Evacuating the autoclave prior to heating reduced the amount of inert gas removed in sampling the vapor phase. Preliminary tests made without evacuating the autoclave before heating indicated that some loss of ammonia occurred when a vapor phase sample was taken in a tube containing only water. Collecting the sample in dilute acid and evacuating the autoclave prior to heating prevented this loss. Subsequent vapor phase samples collected in a tube containing dilute acid had the same ammonia content as those collected in an evacuated bulb.

The centrifuge tube was weighed before and after sampling to obtain the weight of the sample. Two samples of the vapor phase and two samples of the liquid phase were removed at each temperature. Aliquots of the solutions were analyzed for ammonia using a colorimetric method employing Nessler's reagent. At least duplicate analyses were made of each sample. A Beckman DU spectrophotometer was used to measure the intensity of the color. The analytical procedure ended with a final solution volume of 10 ml. Absorption cells were used which had a 10 cm. path length. This favorable path length to volume ratio, in addition to the high sensitivity of the Nessler's reagent, made it possible to obtain multiple analyses of samples containing only a few micrograms of ammonia. The use of a large autoclave and removal of small samples was desirable to minimize the deviation from equilibrium conditions within the autoclave during sampling. Less than 4% of the vapor phase was removed in any one set of samples.

Results

The averaged values of the ammonia concentration in the vapor and liquid phases at each temperature are listed in Table I. The units of concentration are parts per million, that is, micrograms ammonia per gram of condensed sample. Relative (to water) volatility values calculated from these data are also included. The relative volatility is equal to the concentration of ammonia in the vapor phase sample divided by the concentration of ammonia in the liquid phase sample. The data for each run are listed in the order of increasing temperature. This was not the order in which the samples were taken.

TABLE I

Temp., °C.	Ammonia concn., p.p.m. Vapor	Liquid	Relative volatility
147	16.9	2.01	8.43
172	15.7	2.17	7.21
201	12.1	2.04	5.93
245	8.38	1.80	4.66
254	8.08	1.88	4.31
292	5.75	1.77	3.24
326	4.52	1.73	2.61
149	171	19.0	8.95
175	141	17.7	7.93
203	112	16.7	6.71
245	79.9	16.3	4.89
266	66.4	15.3	4.33
289	53.7	14.5	3.69
318	41.5	13.7	3.04
147	1750	180	9.71
206	963	147	6.56
260	632	144	4.40
317	423	139	3.04

Discussion

The distribution of ammonia between liquid and vapor phases is a function of the ammonia concentration. This is shown in Fig. 1. It is due to the ionization of ammonia in the liquid (aqueous) phase. Thus, in addition to the reaction for the equilibrium between liquid and vapor phase, $NH_3(l) \rightleftarrows NH_3(v)$, there is also a competing reaction in the liquid phase $NH_3(l) + H_2O(l) \rightleftarrows NH_4^+(l) + OH^-(l)$. (l) refers to the liquid (aqueous) phase and (v) refers to the vapor phase. The hydration of the various species has been ignored for purposes of writing these reactions. The second reaction is concentration dependent.

The equilibrium constant for this reaction over the temperature range used in our tests has been reported by Noyes.[3] Using equations for the ionization of ammonia and water, it is possible to derive the equation

$$K_{NH_3} m_{NH_3} \alpha^3 + (K^2_{NH_3} - K_{H_2O} - K_{NH_3} M_{NH_3})\alpha^2 - 2K^2_{NH_3}\alpha + K^2_{NH_3} = 0$$

(1) The Knolls Atomic Power Laboratory is operated for the United States Atomic Energy Commission by the General Electric Company.

(2) T. A. Wilson, University of Illinois, Eng. Exp. Sta. Bull. 146.

(3) A. A. Noyes, *J. Am. Chem. Soc.*, **30**, 335 (1908).

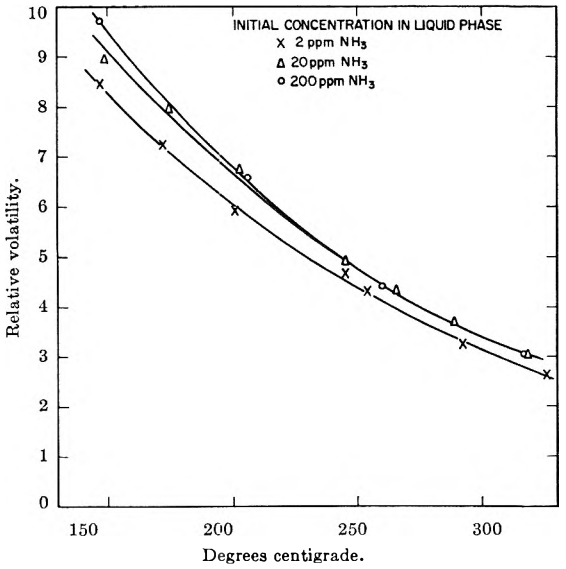

Fig. 1.—Relative volatility of ammonia solutions.

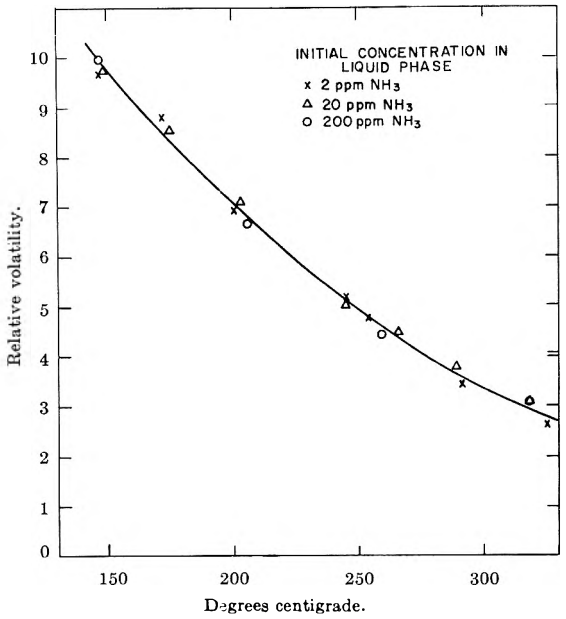

Fig. 2.—Relative volatility of ammonia solutions when the ammonia concentration in the liquid phase is corrected for ionization.

where

K_{NH_3} is the ionization constant for ammonia in aqueous sol.
K_{H_2O} is the ion product of water
m_{NH_3} is the molal concn. of total ammonia (ionized plus un-ionized)
α is the fraction of the total ammonia that is ionized

When known values of the ionization constant for ammonia and the ion product of water[4] are inserted into the above equation, it is possible to calculate the fraction ionized for a given concentration of total ammonia in solution. This has been done for three total ammonia concentrations at four temperatures. The fraction of ammonia that is not ionized is given in Table II, since it is the un-ionized part that is important in the distribution between the liquid and vapor phases.

The ammonia in solution becomes less ionized as the temperature increases and as its concentration increases.

When the concentrations of ammonia in the liquid phase found in the distribution measurements are corrected for the fraction ionized, the relative volatility values listed in Table III are obtained. The values are plotted in Fig. 2. The points corresponding to the various concentrations of ammonia fall on a single line, indicating that ionization in solution is the cause of the concentration dependence of the distribution coefficient.

TABLE II

Temp., °C.	$K_{NH_3} \times 10^6$	$K_{H_2O} \times 10^{12}$	% Un-ionized 2 p.p.m. NH_3	20 p.p.m. NH_3	200 p.p.m. NH_3
149	7.87	2.10	77.3	92.1	97.5
204	2.75	5.00	86.0	95.3	98.5
260	1.00	6.60	91.4	97.2	99.1
316	0.05	5.30	98.5	99.4	99.8

TABLE III

Temp., °C.	P.p.m. ammonia in liquid	% Un-ionized	P.p.m. un-ionized ammonia	Cor. relative volatility
147	2.01	77.2	1.75	9.67
172	2.17	82.0	1.78	8.80
201	2.04	85.5	1.75	6.94
245	1.80	89.7	1.62	5.19
254	1.88	90.5	1.70	4.76
292	1.77	95.1	1.68	3.42
326	1.73	99.5	1.72	2.63
149	19.0	91.9	17.5	9.75
175	17.7	93.3	16.6	8.51
203	16.7	94.8	15.9	7.07
245	16.3	96.3	15.7	5.08
266	15.3	96.8	14.8	4.47
289	14.5	98.2	14.3	3.77
318	13.7	99.4	13.6	3.05
147	180	97.3	175	9.98
206	147	98.3	144	6.67
260	144	99.0	142	4.44
317	139	99.8	138	3.05

The distribution of ammonia between liquid and vapor phases varies with temperature. For a given concentration of ammonia in the liquid phase, the concentration of ammonia in the vapor phase increases as the temperature increases. This is not obvious from the concentration of ammonia in the condensed steam since the concentration of ammonia in the vapor phase does not increase as rapidly as the concentration of water in that phase as the temperature is raised. This results in both the concentration of ammonia in the condensed steam and the relative volatility being lower at the higher temperatures. The data from the 20 p.p.m. ammonia test have been used together with the density of saturated steam[5] to calculate the concentration of ammonia in the vapor phase.

$$\text{relative volatility} \times \text{density of steam} \times 10^{-3} = \frac{\text{p.p.m. } NH_3(v)}{\text{p.p.m. } NH_3(l)} \times \frac{\text{g.}}{\text{cc.}} \times 10^{-3} = \frac{\text{g. } NH_3(v) \text{ per l.}(v)}{\text{p.p.m. } NH_3(l)}$$

The values are listed in Table IV.

These values are somewhat similar to Henry's law constants but the concentration of ammonia in the vapor phase is used rather than the partial pressure.

(4) Average of the values of Bjerrum, Heydiveiller, and Lewis and Randall as reported in N. E. Dorsey, "Properties of Ordinary Water Substance," Reinhold Publ. Corp., New York, N. Y., 1940, p. 378.

(5) Computed from the data of J. H. Keenan and F. G. Keyes, "Thermodynamic Properties of Steam," 1st Ed., J. Wiley and Sons, New York, N. Y., 1936, pp. 28–31.

TABLE IV

Temp., °C.	Relative volatility	Density, g./cc.	g. NH_3(v) per l.(v) per p.p.m. NH_3(l)
149	8.95	0.00248	2.2×10^{-5}
175	7.93	.00462	3.7×10^{-5}
203	6.71	.00833	5.6×10^{-5}
245	4.89	.0183	9.0×10^{-5}
266	4.33	.0265	11×10^{-5}
289	3.69	.0389	14×10^{-5}
318	3.04	.0632	19×10^{-5}

Since the concentration of ammonia in the condensed steam was the quantity actually measured, it was preferable to calculate a value that did not involve a pressure (which would have required a gas law assumption). In calculating these values, it has been assumed that the density of the water vapor over the ammonia solution was equal to the saturation pressure over pure water. This should be a good approximation since the liquid phase contained only 13 to 19 p.p.m. ammonia. It should also be pointed out that the values in Table IV only apply to a liquid phase concentration in this range since it has been shown in the previous paragraphs that the ammonia distribution is concentration dependent.

The increase in concentration of ammonia in the vapor phase as the temperature increases (for a given liquid phase concentration) is very different behavior from that of gases such as helium, nitrogen, oxygen, and xenon. All of the latter have less tendency to be in the vapor phase as the temperature is raised in the range of 100 to 315°.[6]

(6) J. M. Smith and D. L. Katz, "Physical Behavior of the $H-O_2-H_2O$ System Under Pressure," ORNL-1069.

ELECTRICAL CONDUCTIVITY OF POTASSIUM THIOCYANATE

BY JUAN M. LOMELIN[1] AND THEODORE J. NEUBERT

Department of Chemistry, Illinois Institute of Technology, Chicago 16, Illinois

Received December 3, 1962

The electrical conductivity of polycrystalline KSCN was studied as a function of temperature from room temperature to the melting point (175°) using zone refined, analytical reagent grade, and impurity doped samples. Unless all traces of H_2O were removed, conductivities at low temperature were anomalously high. Log conductivity *vs.* reciprocal temperature curves for carefully dehydrated samples showed two straight line portions with a sharp bend at *ca.* 120°. The activation energy for the conduction process in the high temperature (intrinsic) region is 2.13 e.v.; that for the low temperature (extrinsic) region is 1.30 e.v. Addition of 10^{-2}% $BaCl_2$ enhances the conductivity in the low temperature region, indicating that positive ion vacancies play a role in the conduction process; addition of 10^{-2}% Na_2S caused no change in conductivity. The implications of these observations are discussed and the conductivity behavior of KSCN is shown in relation to that of KCl and CsBr.

Some time ago we became curious to know whether KSCN by virtue of its low melting point (175°) exhibited any unusual behavior with regard to its electrical conductivity. The work to be reported extends some previous conductivity measurements by Plester, *et al.*[2]

X-ray diffraction studies by Klug[3a] have shown KSCN to have an orthorhombic unit cell containing 4 KSCN with lattice parameters: $a = 6.66$ Å., $b = 6.635$ Å., $c = 7.58$ Å. Analysis of the infrared spectrum of solid KSCN by Jones[3] indicates that the SCN^- ion is linear and that the N–C and S–C distances are approximately 1.17 and 1.61 Å., respectively. The arrangement of K^+ and SCN^- ions in crystalline KSCN resembles the arrangement of ions in CsCl and CsBr. The SCN^- ion lie in parallel planes, alternating with planes of K^+ ions. In the anion planes, each SCN^- ion is perpendicular to its neighboring SCN^- ions. A drawing depicting the crystal structure is given in Jones' paper.[3b]

Experimental

Conductivity Measuring Apparatus.—Preliminary tests indicated that conductivities in the range 10^{-13} to 10^{-5} mho would be encountered and that measuring currents would have to be kept smaller than *ca.* 10^{-7} amp.

(a) Low conductivities (10^{-13} to 10^{-7} mho) were measured by observation of the current which flowed through the sample upon application of a known e.m.f. (1.5–7.5 v.). The current sensing instrument was a Keithley Model 210 electrometer with a Keithley Model 2008 decade shunt. The working batteries and the necessary switches were housed in a shielded junction box which was provided with Teflon-insulated connectors and internal desiccant in order that the "no sample" conductivity be less than 10^{-13} mho. In shielding leads to the conductivity cell, care was taken to keep lead capacitances low so that the time constant of the circuit would not be disagreeably long. Measurements were made with current flow of each sign, and were averaged.

(b) High conductivities (10^{-7} to 10^{-5} mho) were determined by matching the current through the sample with that through a standard variable resistance using a galvanometer to indicate equivalence (4.3×10^{-9} amp./mm.; period, 3 sec). The operating potential (0.01–0.75 v.) was applied by means of a set of motor driven switches in a cycle of four pulses: two pulses alternating in sign applied to the sample and two pulses alternating in sign applied to the variable resistance per cycle. The kind of switches and the switching circuit used were of the sort in which all thermal e.m.f.'s were opposed by presumably equal but opposite thermal e.m.f.'s.

Conductivity Cells.—The typical conductivity cell envelope consisted of a (vertical) Pyrex glass tube (44 cm. long × 25 mm. o.d.) having, approximately half way along its length, an inclined side arm for introduction of sample. The upper end of the cell fitted into a standard taper cap which was connected to a vacuum line and into which were waxed three long glass tubes; two for platinum electrodes, one for a copper–constant thermocouple. The electrode surfaces (6 mm. diam. × 0.25 mm. thick) were oriented vertically with a spacing of *ca.* 7 mm. and were positioned *ca.* 3.5 cm. from the bottom of the cell envelope, which was normally filled to a depth of *ca.* 9 cm.

Sample Materials.—The principal sample material was J. T. Baker Chemical Co. Reagent Grade potassium thiocyanate, Lot 1125. Some measurements, however, were made with zone refined KSCN. Typical conditions of refinement were: (a) horizontal glass tube (45 cm. long × 25 mm. o.d.) half filled with

(1) Instituto Mexicano de Investigaciones Technologicas, Calzada Legaria 694, Mexico 10, D. F. Mexico.

(2) D. W. Plester, S. E. Rogers, and A. R. Ubbelohde, *Proc. Roy. Soc.* (London), **235**, 469 (1956).

(3) (a) H. P. Klug, *Z. Krist.*, **85**, 214 (1938); (b) L. N. Jones, *J. Chem. Phys.*, **25**, 1069 (1956).

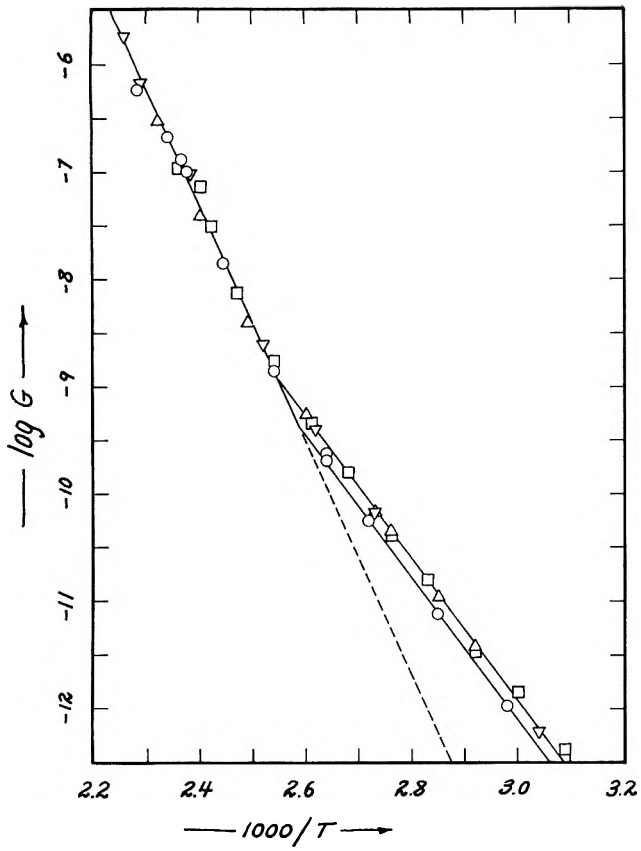

Fig. 1.—Electrical conductivity (G in ohm^{1-} cm.$^{-1}$) of dry polycrystalline KSCN as a function of temperature: (a) run 27 (round points) on zone refined KSCN; (b) run 12 (triangular points) on stock bottle KSCN; (c) run 8 (square points) on material of stock bottle quality to which 10^{-4} mole fraction of Na_2S had been added.

salt; (b) heater speed, 4 cm./hr.; (c) width of melted zone, 20 mm.; (d) vacuum atmosphere, (3) 32 zone passes.

Routine of Measurement.—In beginning a set of measurements, after the electrodes had been cleaned with HNO_3 and their alignment checked, sample was placed in the inclined sidearm of the cell and the system closed and evacuated. After a while the KSCN was melted by gently warming with a flame and permitted to run down into the electrode region where it was held as a liquid *in vacuo* at *ca.* 180° for *ca.* 15 hr., *i.e.*, until all traces of water had been removed. Following the dehydration operation, in order to have homogeneity in grain size and composition, the molten salt was quenched by means of a water bath at room temperature. Only four-fifths of the salt was permitted to freeze rapidly; enough liquid phase was left in order to provide by slower cooling sufficient material for filling the depressed central core which formed. Finally a heater furnace was put in place and the system was heated at *ca.* 165° for an hour or so. Conductivities were then measured, in most cases with decreasing temperatures.

Calculation of Conductivity Values.—Specific conductivities G_s ought to be computed from measured conductivities G_m using the relation $G_s = G_m(L/A)/(F)$, which in addition to the term describing the ratio of electrode separation to electrode area includes a further term (F) to take account of the "fringing field." The (L/A) term for the electrode geometry used is *ca.* 2.5 cm.$^{-1}$; the (F) term calculated by relations due to Kirchhoff[4] is of the order of 2.5–3.7 cm.$^{-1}$. Since these two terms so nearly compensate one another, and in view of uncertainties arising from polycrystallinity of samples, it was decided to use the measured conductivities in lieu of specific conductivities. At low temperatures, measured conductivities were corrected by subtracting the "no sample" conductivity of the apparatus. This correction was trivial for conductivities above 10^{-12} ohm^{-1} cm.$^{-1}$.

Experimental Results

Figure 1 shows three sets of data: (a) run 27 (round points) on zone refined KSCN, (b) run 12 (triangular points) on stock bottle KSCN, and (c) run 8 (square points) on material of stock bottle quality to which 10^{-4} mole fraction Na_2S had been added. In preparing the figure the data for the zone refined sample were taken as standard and the other curves superimposed by matching the high temperature linear portions. This was achieved by lowering the data for S^{-2} doped KSCN by 0.1 log unit and raising those for stock bottle material by 0.4 log unit. Such manipulation is presumed to be justified by the vagaries of polycrystalline samples.

It is evident from Fig. 1 that the log G *vs.* $1000/T$ data for each of the three samples may be represented by two straight line segments. For zone refined material the high temperature line obeys the relation $G = 3.1 \times 10^{18} \exp(-24{,}700/T)$; the low temperature line obeys the relation $G = 4.4 \times 10^{7} \exp(-15{,}000/T)$.

Conductivities in the high temperature region are expected to be intrinsic and independent of impurities, whereas conductivities in the low temperature region are expected to be impurity sensitive.[5] Such is the case in alkali halide systems, where conductivities in the low remperature regions are enhanced roughly in proportion to the concentration of divalent cationic impurities. The fact that the zone refined data are lower than the other data in the low temperature region by 0.2 log unit suggested that the concentration of divalent cationic impurities has been decreased relative to stock bottle material. The data for S^{-2} doped KSCN indicate no change in conductivity as a result of adding Na_2S to the system. This may be explained in three ways: (a) The S^{-2} failed to be incorporated substitutionally either because of lack of solubility in KSCN or because of chemical reaction with some impurity. (b) The substitutionally incorporated S^{-2} was bound in an immobile complex with the negative ion vacancy which accompanies its introduction into the crystal or with a divalent cationic impurity.[6] (c) Free negative ion vacancies in KSCN are not very mobile.

In order to be certain of the influence of divalent cation impurities the conductivity of Ba^{+2} doped KSCN was investigated. Doping was done in two ways: (1) by adding the requisite amount of $BaCl_2$ in aqueous solution to solidified stock bottle KSCN in the conductivity cell and then heating, melting, and dehydrating in the manner already described, and (2) by adding to molten KSCN the requisite amount of a previously fused concentrated mixture of anhydrous KSCN and anhydrous $BaCl_2$ which will be referred to as a "solid solution." Figure 2 shows three sets of data relating to doped stock bottle KSCN: (a) run 13 (triangular points) containing 2×10^{-5} mole fraction $BaCl_2$ added as "solid solution," (b) run 14 (square points) containing 10^{-4} mole fraction $BaCl_2$ added as "solid solution" and (c) run 18 (circular points) containing 10^{-4} mole fraction $BaCl_2$ added *via* aqueous solution. Conductivities were measured with decreasing temperatures, except for run 13 in which measurements were made in both directions. The dotted portions of Fig. 2 reproduce the data for zone refined KSCN from Fig. 1, and in preparing Fig. 2 the plotted points were shifted (run 13 by +0.2 unit, run 14 by

(4) "American Institute of Physics Handbook," McGraw-Hill Book Co., New York, N. Y., 1957, pp. 5-14.

(5) A. B. Lidiard, "Encyclopedia of Physics," Vol. XX, Springer Verlag, 1957, pp. 246–349.

(6) H. W. Morgan and P. A. Staats, *J. Appl. Phys.*, **33**, 364 (1962).

+0.4 log unit, and run 18 by −0.05 log unit) to give agreement with the zone refined sample in the high temperature region.

It is clear from Fig. 2 that doping with Ba^{+2} enhances the conductivity of KSCN in the low temperature impurity sensitive region. Further, the method of doping causes no discernable differences in behavior provided the drying is effective. As is the case with purer material (Fig. 1) the data are satisfactorily represented by two straight lines. The low temperature lines in Fig. 2 for 2×10^{-5} and 10^{-4} mole fraction Ba^{+2}, however, are separated from one another by 0.3 log unit instead of the expected 0.7 long unit. Experiments were done at other doping levels but the results are confusing. At lower Ba^{+2} ion concentrations the changes were difficult to discern because of scattering of experimental points. At higher concentrations the enhancements of conductivity observed in the low temperature region were larger, but, although the samples had been dried as previously described, the general shape of the curves was such as to suggest that the drying operation had been ineffective.

Traces of water have a strong influence on the electrical conductivity of polycrystalline KSCN. For example, upon completion of run 18 (circular points of Fig. 2) a few drops of water were added to the cell, the sample was melted, held *in vacuo* for only 1 hr. instead of the usual 15 hr., frozen, and quickly remeasured. As a result of the small amount of water residual in the sample the entire conductivity curve was raised above that shown in Fig. 2. The slope in the high temperature region was approximately the same as before; the slope at low temperature was smaller by more than a factor of two and the transition between regions was very gradual making a resolution into two straight line segment difficult. These effects depend upon the amount of water present and are not limited to doped KSCN. Similar observations were made in other samples, both doped and pure.

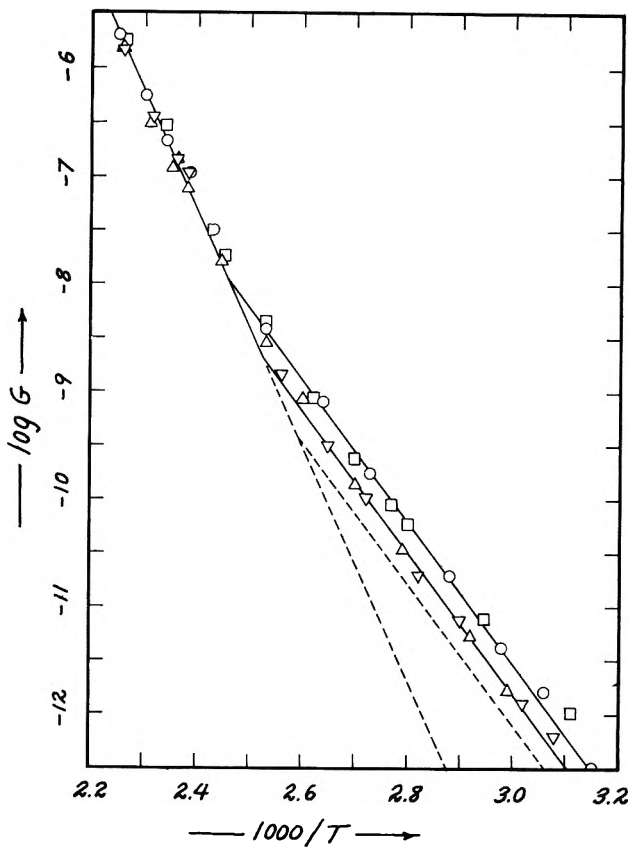

Fig. 2.—Electrical conductivity (G in ohm^{-1} $cm.^{-1}$ of Ba^{+2} doped dry polycrystalline KSCN as a function of temperature: (a) run 13 (triangular points) containing 2×10^{-5} mole fraction $BaCl_2$ added as "solid solution"; (b) run 14 (square points) containing 10^{-4} mole fraction $BaCl_2$ added as "solid solution"; (c) run 18 (circular points) containing 10^{-4} mole fraction $BaCl_2$ added *via* aqueous solution.

Discussion

A comparison of the electrical conductivity of KSCN with that of KCl and of CsBr is shown in Fig. 3. The KSCN data are for zone refined material; the KCl data are for a sample of Harshaw Chemical Co. single crystal measured in this Laboratory in an experiment preliminary to other work; the CsBr curve has been taken from a recent paper by Lynch.[7] Although conductivities of polycrystalline and single crystalline material are compared, early work by Phipps, *et al.*,[8] showed that polycrystalline and single crystalline results were reasonably concordant.

The gross aspects of the three sets of data in Fig. 3 are seen to be qualitatively similar. Apart from the displacement of the KSCN curve to lower temperature, there are three notable differences. (a) At the melting points, the conductivity of polycrystalline KSCN is about two orders of magnitude lower than that of KCl single crystal and three orders of magnitude lower than that of CsBr single crystal. (b) The activation energy for the conduction process in the high temperature region is 2.13 e.v. for KSCN, *ca.* 2.0 e.v. for KCl, and 1.29–1.44 e.v. for CsBr. (c) The activation energy for

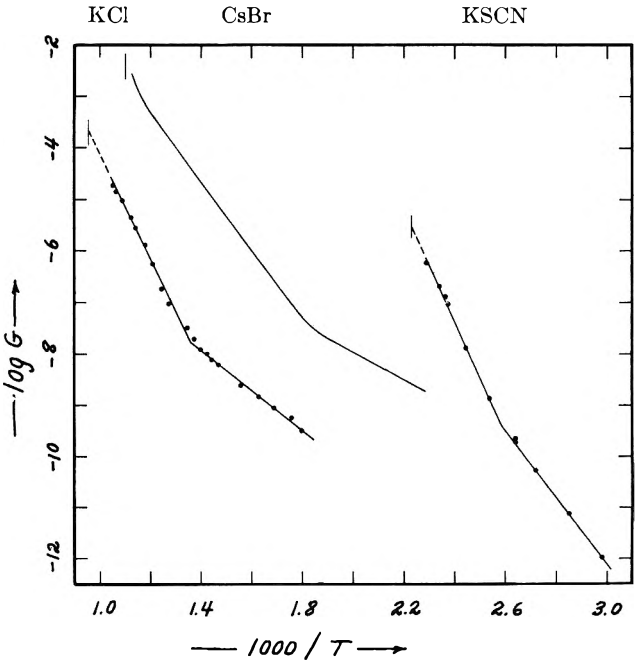

Fig. 3.—Comparison of the electrical conductivities (G in ohm^{-1} $cm.^{-1}$) of dry polycrystalline KSCN, single crystalline CsBr (curve taken from ref. 7), and single crystalline (Harshaw) KCl.

the conduction process in the low temperature region is 1.30 e.v. for KSCN, 0.77 e.v. for KCl, and 0.53 e.v. for CsBr. Plester, *et al.*, report the activation energies to be 2.05 e.v. at high temperature and *ca.* 0.3 e.v. at low

(7) D. W. Lynch, *Phys. Rev.*, **118**, 468 (1960).

(8) T. E. Phipps, *et al.*, *J. Am. Chem. Soc.*, **48**, 112 (1926); **50**, 2412 (1928); **51**, 1331 (1929).

temperature. Although the agreement at high temperatures is satisfactory, the shape of their log G *vs.* $1/T$ curve and the very low value of 0.3 e.v. for the slope in the low temperature region indicate that their samples were not entirely free of water contamination.

In the case of CsBr, which has a crystal structure similar to that of KSCN, Lynch[7] was able to conclude, on the basis of electrical conductivity and diffusion coefficient measurements, that electrical conductivity is ionic and probably proceeds *via* a vacancy mechanism. The diffusion coefficient measurements, however, indicated that both positive and negative ion vacancies were mobile.

In the case of KSCN, since the crystal structure resembles that of CsBr, it is perhaps possible that electrical conduction proceeds *via* a vacancy mechanism and that both positive and negative ion vacancies may have comparable transport numbers. The mobility of positive ion vacancies is demonstrated by the fact that the low temperature conductivity is enhanced by doping with Ba^{+2}. At the moment, however, not enough is known about the KSCN system to come to any definite conclusion with regard to the details of the conduction process or the meaning to be ascribed to the energies, 2.13 and 1.30 e.v., calculated from the slopes of the straight line portions of the KSCN log G *vs.* $1/T$ curves. Diffusion coefficient and transport number measurement would be required in addition to further electrical conductivity measurements, and these would have to be carried out on a single crystalline zone refined material in an atmosphere completely devoid of water.

Acknowledgment.—We are grateful to the Atomic Energy Commission, Division of Research, Chemistry Branch, Contract No. AT(11-1)-1044, which provided the apparatus and materials required in this investigation. J. M. L. also wishes to acknowledge a Bank of Mexico Fellowship which with a leave of absence from the Insituto Mexicano de Investigaciones Technologicas enabled him to undertake the investigation.

INFRARED SPECTRA OF, AND HYDROGEN BONDING IN, SOME ADDUCTS OF PHENOLS WITH THEIR PHENOXIDES AND OTHER OXYGEN BASES

BY D. HADŽI, A. NOVAK, AND J. E. GORDON

The Chemical Institute Boris Kidrič, Ljubljana, Yugoslavia, and Mellon Institute, Pittsburgh 13, Pa.

Received December 5, 1962

Adducts of phenols with the corresponding phenoxides, some carboxylates, and with trimethylamine oxide have been prepared and their infrared spectra examined. Very strong hydrogen bonds occur in these adducts and may be classified into three different types: asymmetrical intermolecular, symmetrical intermolecular, and symmetrical intramolecular. Behavior of the hydroxylic bands of the bonded OH. . O groups as a function of the type of hydrogen bond is discussed.

It has been shown that acid salts of carboxylic acids of the general formula (RCOOH, $RCOO^-Me^+$) contain very strong hydrogen bonds of various types joining the carboxylic and carboxylate groups.[1-4] We were interested in compounds where similar hydrogen bonds, *i.e.*, between a hydroxylic group and a negatively charged oxygen atom, are expected. Some adducts of phenols with their phenoxides and with neutral salts of carboxylic acids have been reported in the earlier literature and their stoichiometric formulas have been given,[5-14] but no systematic investigation of their infrared spectra or hydrogen bonding has been published. We have therefore prepared several adducts of phenols with their phenoxides of the general formula (ROH, RO^-Me^+), with potassium acetate and oxalate (ROH, $R'COO^-Me^+$), and with trimethylamine oxide (ROH, $(CH_3)_3NO$) and recorded their spectra in the solid state and in solution in dimethyl sulfoxide (DMSO). The spectral features make it possible to divide the adducts into two groups. The spectra of the first group are characterized by the appearance of two distinct bands near 2500 and 1800 cm.$^{-1}$, respectively, one of which is clearly attributable to the OH stretching vibration. The second group has no such bands; in fact the only candidate for an OH stretching mode is the absorption observed for some of them near 1600 cm.$^{-1}$. This and some other evidence leads us to the conclusion that symmetrical hydrogen bonds connect the phenoxide groups in these cases. From changes on dissolution it can be shown that some of these hydrogen bonds are intramolecular and others intermolecular, the symmetry of the latter being destroyed on dissolving the adduct. Assignments of the hydroxylic bands of the bonded OH. . O group have been made in most cases, and it is shown that the γ-OH band increases in frequency with the strength of the hydrogen bond as estimated from the position of the ν-OH band, but that no such trend is observed for δ-OH bands.

The adducts may be divided according to their composition into phenol–phenoxide, phenol–carboxylate, and phenol–trimethylamine oxide groups. However, we shall follow the division according to the type of hydrogen bonding as demonstrated by the spectral features and the changes in state.

Adducts with Asymmetrical Intermolecular Hydrogen Bonds.—This group comprises phenol–phenoxide adducts (potassium hydrogen di-(4-cyanophenoxide) and

(1) J. C. Speakman, *et al.*, *J. Chem. Soc.*, 3357 (1949); 185 (1951); 180 1954); 1151, 1164 (1961).
(2) D. Hadži and A. Novak, "Infrared Spectra of, and Hydrogen Bonding in, Some Acid Salts of Carboxylic Acids," University of Ljubljana, 1960.
(3) R. Blinc and D. Hadži, *Spectrochim. Acta*, **16**, 853 (1960).
(4) R. Blinc, D. Hadži, and A. Novak, *Z. Elektrochem.*, **64**, 567 (1960).
(5) J. Fritzsche, *J. prakt. Chem.*, **1**, 75, 268 (1858); *Ann.*, **110**, 150 (1859).
(6) E. von Gorup-Besanez, *Ann.*, **143**, 129 (1867).
(7) J. C. W. Frazer, *Am. Chem. J.*, **30**, 309 (1903).
(8) C. Gentsch, D.R.P. 156761, *Chem. Zentr.*, **I**, 313 (1905).
(9) J. Potratz, D.R.P. 237019, *ibid.*, **II**, 405 (1911).
(10) R. F. Weinland and W. Denzel, *Ber.*, **47**, 737, 2244, 2990 (1914).
(11) R. F. Weinland and G. Bärlocher, *ibid.*, **52**, 148 (1919).
(12) D. Goddard and A. E. Goddard, *J. Chem. Soc.*, 54 (1922).
(13) H. Meyer. *Z. anal. Chem.*, **64**, 72 (1924).
(14) P. Pfeiffer, "Organische Molekülverbindungen," Verlag von F. Enke, Stuttgart, 1927, p. 50.

TABLE I

ABSORPTION BANDS OF THE ASYMMETRICALLY HYDROGEN-BONDED OH. . O GROUP OF PHENOLS AND THEIR ADDUCTS IN THE SOLID STATE

4-Cyanophenol	4-Cyanophenol-*d*	Potassium hydrogen di-(4-cyano-phenoxide)	Potassium deuterium di-(4-cyano-phenoxide)	Potassium hydrogen pyrocatechoxide hemihydrate	Assignment
3280 vs,b	...	2570 m,b	...	2530 s,b	ν-OH
		1820 m,b	?	1870 s,b	Combination or ν-OH
...	2455 vs,b	...	1880 m,b		ν-OD
1455 s	1425 m	1450 s,b		1370 s,b	
1370 s	1306 m	1400 s,b			δ-OH + R
1220 vs	...	1255 s,b	...	1240 s,b	
	1014 s	1030 w	1030 m,b	...	
960 w	996 s		990 m,b		δ-OD + R
945 w	975 s				
669 s	...	912 m,b	...	1070 m,b	γ-OH
...	n.i.	...	690 m,b		γ-OD

Potassium trihydrogen pyrocatechoxide hemihydrate	Potassium trideuterium pyrocatechoxide hemideuterate	Potassium trihydrogen guaiacoxide	Adduct of pyrocatechol with potassium oxalate	Assignment
2560 s,b	...	2550 s,b	2580 s,b	ν-OH
1890 s,b	?	1870 s,b	...	Combination or ν-OH
...	1890 s,b	...	...	ν-OD
1355 s,b	...	1408 s,b		
1175 s	...	1225 vs	1227 s	δ-OH + R
...	1008 s,b			
	980 s,b			δ-OD + R
	958 s,b			
1035 m,b	...	870 m,b	890 m,b	γ-OH

Adduct of 4-nitrophenol with potassium acetate	Adduct of 4-nitrophenol-*d* with potassium acetate	Adduct of 4-nitrophenol with trimethyl-amine oxide	Adduct of 4-nitrophenol-*d* with trimethyl-amine oxide	Assignment
2420 m,b	...	2300 w,b	...	ν-OH
1920 m,b	?	1900 w,b	?	Combination or ν-OH
...	1900 m,b	...	1900 ?	ν-OD
1250 s,b	...	1180 s,b	...	δ-OH + R
...	1020 m,b	1290 s,b	?	δ-OD + R
	1000 m,b			
995 m,b	...	800 m,b	...	γ-OH

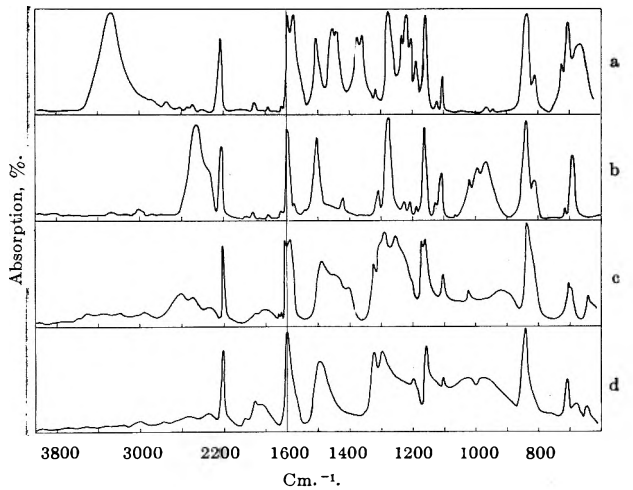

Fig. 1.—Infrared spectra of 4-cyanophenol (a), 4-cyanophenol-*d* (b), potassium hydrogen di-(4-cyanophenoxide) (c), same, but deuterated (d). Spectra combined from mulls in Nujol and hexachlorobutadiene.

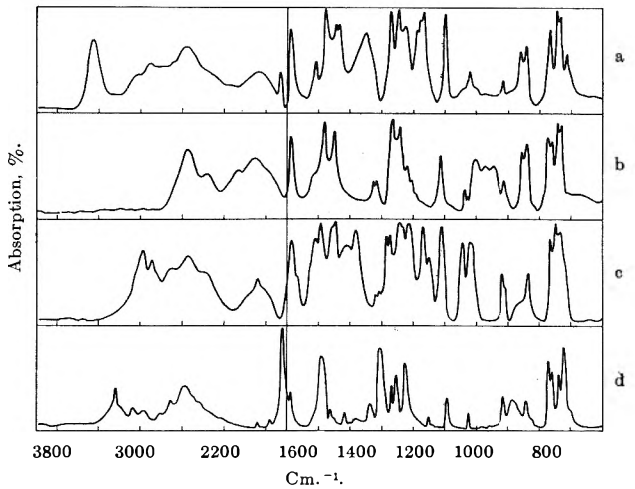

Fig. 2.—Infrared spectra of potassium trihydrogen pyrocatechoxide hemihydrate (a), same, but deuterated (b), potassium trihydrogen guaiacoxide (c), adduct of pyrocatechol with potassium oxalate (d). Spectra combined from mulls in Nujol and hexachlorobutadiene.

potassium acid phenoxides of pyrocatechol and guaiacol) as well as adducts of phenols with carboxylates (4-nitrophenol–potassium acetate and pyrocatechol–potassium oxalate) and trimethylamine oxide. Their infrared spectra are shown in Fig. 1–3 together with those of some deuterated derivatives; the hydroxylic bands are listed in Table I and their assignment is given. The main spectral characteristics are the bands in the 2600–1700 cm.$^{-1}$ region. The band at about 2500 cm.$^{-1}$ clearly disappears on deuteration and is accordingly assigned to an OH stretching vibration. The origin of the second band is much less clear. Bands in the 1900–1650 cm.$^{-1}$ region have often been observed in the spectra of substances with strong hydrogen bonds[2-4,15] and attributed either to a δ-OH

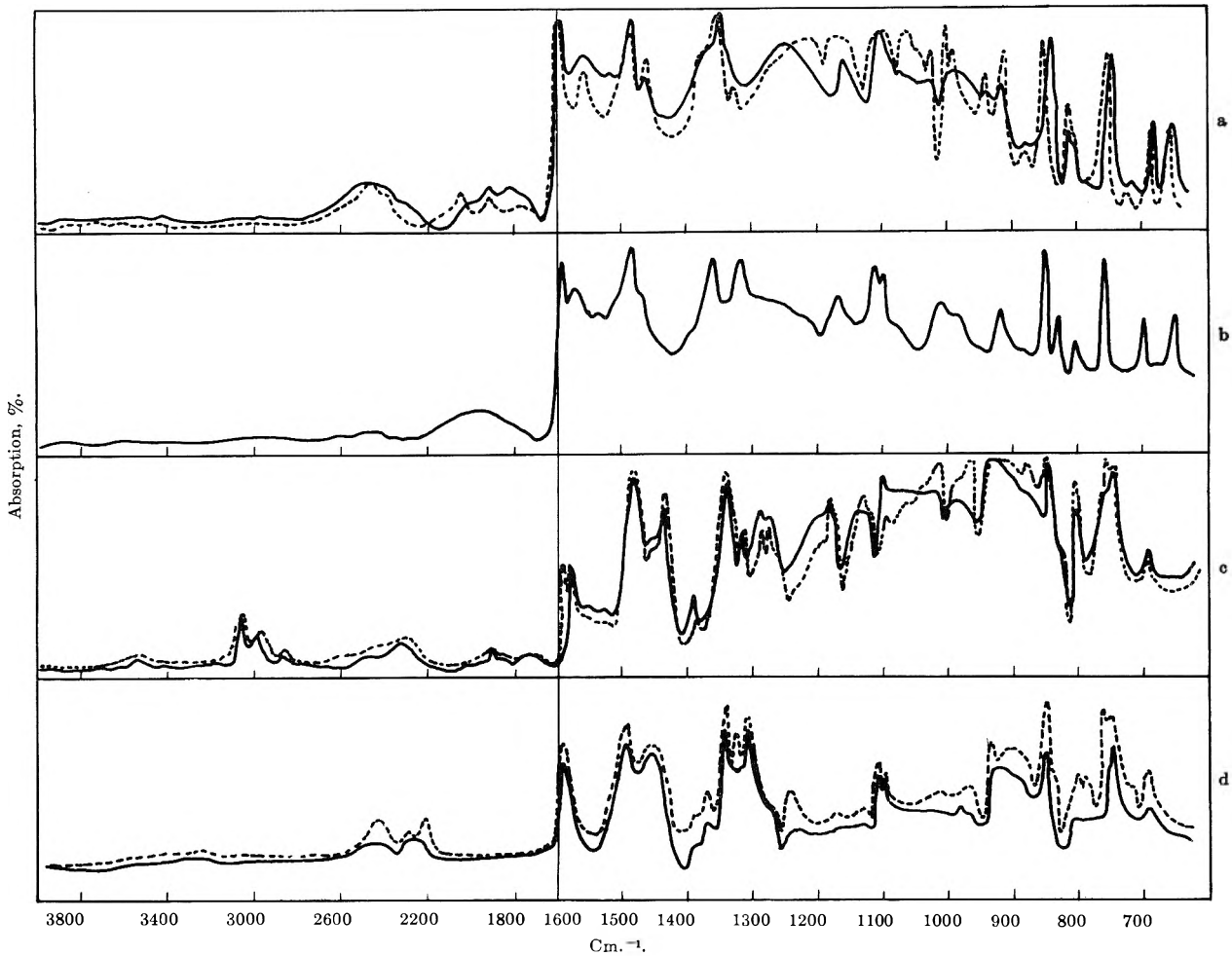

Fig. 3.—Infrared spectra of adducts of 4-nitrophenol with potassium acetate (a), same, but deuterated (b), 4-nitrophenol with trimethylamine N-oxide (c), same, but deuterated (d). Spectra combined from mulls in Nujol and hexachlorobutadiene; full line, room temperature; dotted line, cooled with liquid nitrogen.

band or to another ν-OH fundamental which results from the splitting of the vibrational levels because of the proton tunnelling between two potential energy minima.[16] The first possibility may be eliminated because the δ-OH band is assigned in the spectra of these adducts at much lower frequencies as shown below. The second possibility cannot be confirmed on the ground of infrared spectra alone since this band may alternatively be a combination band, and the results of deuteration do not help because the first band usually shifts into the region of the second and no deuterated analog has been observed for the second band.

The comparison of the spectra of the adducts with those of their deuterated analogs and original phenols made it possible to assign the δ-OH and γ-OH bands. As a starting point the spectra of 4-cyanophenol and potassium hydrogen di-(4-cyanophenoxide) are discussed in detail.

Comparison of the spectra of 4-cyanophenol and 4-cyanophenol-*d* (Fig. 1) makes the assignment of the ν-OH (3280 cm.$^{-1}$) and γ-OH (669 cm.$^{-1}$) bands straightforward; they are also similar to the corresponding bands in the spectra of phenol and phenol-*d*.[17] The identification of the δ-OH band, however, appears to be more difficult; there are strong bands at 1455 and 1370 cm.$^{-1}$ (in fact each of them is split into two bands about 12 cm.$^{-1}$ apart which is probably due to the effect of the crystal) and a very strong band at 1220 cm.$^{-1}$. These three bands disappear on deuteration and new strong bands are observed at 1014, 996, and 975 cm.$^{-1}$. It is known that the OH bending mode of phenol is strongly coupled with a ring stretching mode[17,18] and it is thus possible that the OH bending mode of 4-cyanophenol couples with two skeletal modes. It is significant that after deuteration medium bands at 1306 and 1425 cm.$^{-1}$ appear and they may be related to the strong 1370 and 1445 cm.$^{-1}$ bands after uncoupling. Similarly, there are weak bands near 960 and 945 cm.$^{-1}$ in the 4-cyanophenol spectrum; the corresponding vibration may interact with the OD bending mode giving rise to intense bands at 1014, 996, and 975 cm.$^{-1}$ in the spectrum of 4-cyanophenol-*d*. The 1220 cm.$^{-1}$ band is thus regarded as a mainly δ-OH band.

In the spectrum of potassium hydrogen di-(4-cyanophenoxide) the 2570 cm.$^{-1}$ band is identified as the ν-OH band because it shifts to 1880 cm.$^{-1}$ on deuteration, and the broad 912 cm.$^{-1}$ band must be the γ-OH band (γ-OD is at 690 cm.$^{-1}$) on similar grounds. The δ-OH mode appears to behave similarly as in the corresponding phenol; there are strong broad bands near 1450, 1400, and 1255 cm.$^{-1}$ which disappear on deuteration and new bands appear near 1030 and 990 cm.$^{-1}$. The "mainly" δ-OH band is then that at 1255 cm.$^{-1}$.

(15) J. T. Braunholtz, G. E. Hall, F. G. Mann, and N. Sheppard, *J. Chem. Soc.*, 868 (1959).

(16) R. Blinc and D. Hadži, *Mol. Phys.*, **1**, 391 (1958).

(17) J. C. Evans, *Spectrochim. Acta*, **16**, 1382 (1960).

(18) R. Mecke and G. C. Rossmy, *Z. Elektrochem.*, **59**, 866 (1955).

Comparison of the hydroxylic bands of 4-cyano-phenol and its acid phenoxide (Table I) shows that the ν-OH frequency of the acid phenoxide is strongly decreased ($\Delta\nu \cong 700$ cm.$^{-1}$), that of the γ-OH strongly increased ($\Delta\nu \cong 250$ cm.$^{-1}$) and that of the δ-OH band but slightly increased ($\Delta\nu = 35$ cm.$^{-1}$). All hydroxylic bands as well as those due to coupled vibrations involving the OH bending mode are much broader in the spectrum of the acid phenoxide than in the phenol spectrum because of the stronger hydrogen bonding. Similar behavior has been observed for some acid salts of carboxylic acids[2] and some inorganic compounds with strong hydrogen bonds.[19]

Essentially similar conclusions for the assignments of the hydroxylic bands can be reached for the remaining phenol–phenoxide, phenol–carboxylate, and phenol–trimethylamine oxide adducts, all of which contain one strong hydrogen bond of this type (Table I). Some adducts, however, contain additional, weaker hydrogen bonds and/or water of crystallization. The corresponding ν-OH bands can be distinguished on the basis of comparison of the solid state and solution spectra of adducts and phenols (Fig. 4). The spectra of solutions of phenol in DMSO show a very strong band in the 3200–3100 cm.$^{-1}$ region which indicate hydrogen bonded adducts of phenol with DMSO. The solution spectra of the adducts which contain only one hydrogen bond per formula unit have broad bands near 2500 and 1800 cm.$^{-1}$, similar to those in the corresponding solid state spectra, which show that hydrogen-bonded phenol–phenoxide adducts persist in solution. The adducts which contain additional, weaker hydrogen bonds show in the solution spectra bands near 3200–3100, 2500, and 1800 cm.$^{-1}$; this indicates that weaker hydrogen bonds in the solid state are broken and the corresponding hydroxylic groups associate subsequently with the solvent molecules, but that strong hydrogen bonds between phenol and phenoxide persist in solution.

The hydroxylic bands in the solid state spectra of the adducts of this group appear with variable breadth. In the spectrum of the 4-nitrophenol–trimethylamine oxide adduct it is difficult to recognize individual contributions of δ-OH and γ-OH bands, and the 1600–600 cm.$^{-1}$ region looks like a very extended absorption on which other bands are superimposed. The spectrum of pyrocatechol–potassium oxalate adduct on the other hand shows comparatively sharp bands; this is the only adduct of this group which has no second 1800 cm.$^{-1}$ band in its spectrum. We have prepared several other adducts of phenols with neutral salts of carboxylic acids using Weinland's methods[10]; their infrared spectra show strong ν-OH bands in the 3200–2600 cm.$^{-1}$ region and indicate weaker hydrogen bonds: potassium acetate–pyrocatechol (2950, 2750 cm.$^{-1}$); potassium succinate–3-pyrocatechols (3150 cm.$^{-1}$); potassium succinate–5-pyrocatechols (3120, 2730, 2640 cm.$^{-1}$); potassium acetate–pyrogallol (2920, 2650 cm.$^{-1}$).[20]

Adducts with Symmetrical Intermolecular Hydrogen Bonds.—This group comprises phenol–phenoxide adducts (abbreviations are given in brackets): cesium hydrogen di-(pentachlorophenoxide), (CsH(PeCP)$_2$); cesium hydrogen di-(3-nitrophenoxide), (CsH(MNP)$_2$); sodium hydrogen di-(4-nitrophenoxide) dihydrate, (NaH(PNP)$_2$); potassium hydrogen di-(4-nitrophenoxide) dihydrate, (KH(PNP)$_2$). The most characteristic features in the spectra of these compounds (Fig. 5 and Table II) are an extremely broad absorption between, roughly, 1600 and 600 cm.$^{-1}$ and the fact that there is no band above 1600 cm.$^{-1}$ which could be assigned to an OH stretching vibration. This is shown quite

(19) P. Tarte in "Hydrogen Bonding," Pergamon Press, London, 1959, p. 115.

(20) Unpublished results from this Laboratory.

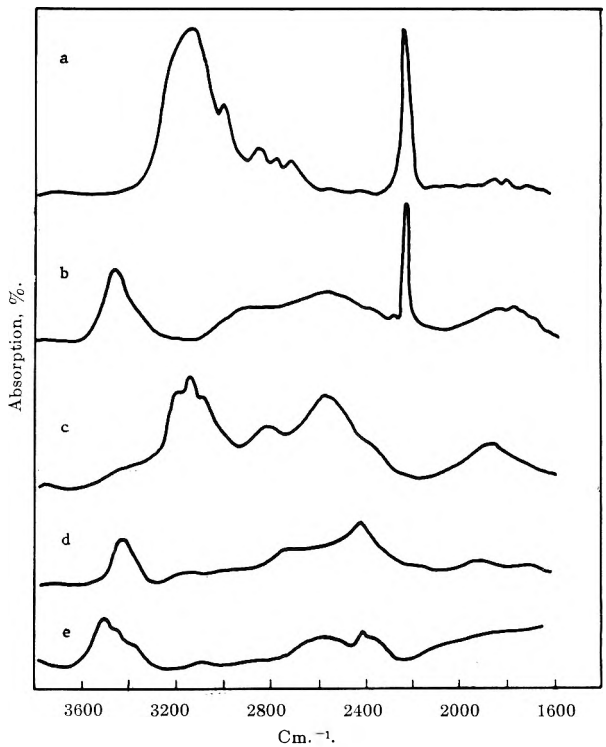

Fig. 4.—Infrared spectra of 4-cyanophenol (a), potassium hydrogen di-(4-cyanophenoxide) (b), potassium trihydrogen pyrocatechoxide hemihydrate (c), cesium hydrogen di-pentachlorophenoxide) (d), cesium hydrogen di-(3-nitrophenoxide) (e). Solutions in dimethyl sulfoxide, compensated with the solvent.

TABLE II

ABSORPTION BANDS OF THE SYMMETRICALLY HYDROGEN-BONDED OHO GROUP OF ACID PHENOXIDES IN THE SOLID STATE

Cesium hydrogen di-(pentachlorophenoxide)	Cesium hydrogen di-(3-nitrophenoxide)	Potassium and sodium hydrogen di-(4-nitrophenoxide) dihydrate	Assignment
	Solid state		
Broad single absorption between 1600 and 600 cm.$^{-1}$ with maximum at about 800 cm.$^{-1}$			Individual contributions in terms of ν-OH, δ-OH, and γ-OH bands unidentifiable
	Solution		
2450 m,b	2500 m,b 1800 w,b	2300 m,b	ν-OH Combination or ν-OH

Sodium acid salt of 2,2′-dihydroxybiphenyl	The same but deuterated	Sodium acid salt of 2,2′-methylene bis-(4-chlorophenol)	The same but deuterated	Assignment
1630 m,b	.....	1630 m,b	.....	ν-OH
1360 s,b	.....	1390 sh	.....	δ-OH + R
1200 s,b	.....	1215 s	.....	
.....	1045 m,b			δ-OD
?		1018 m,b	.....	γ-OH

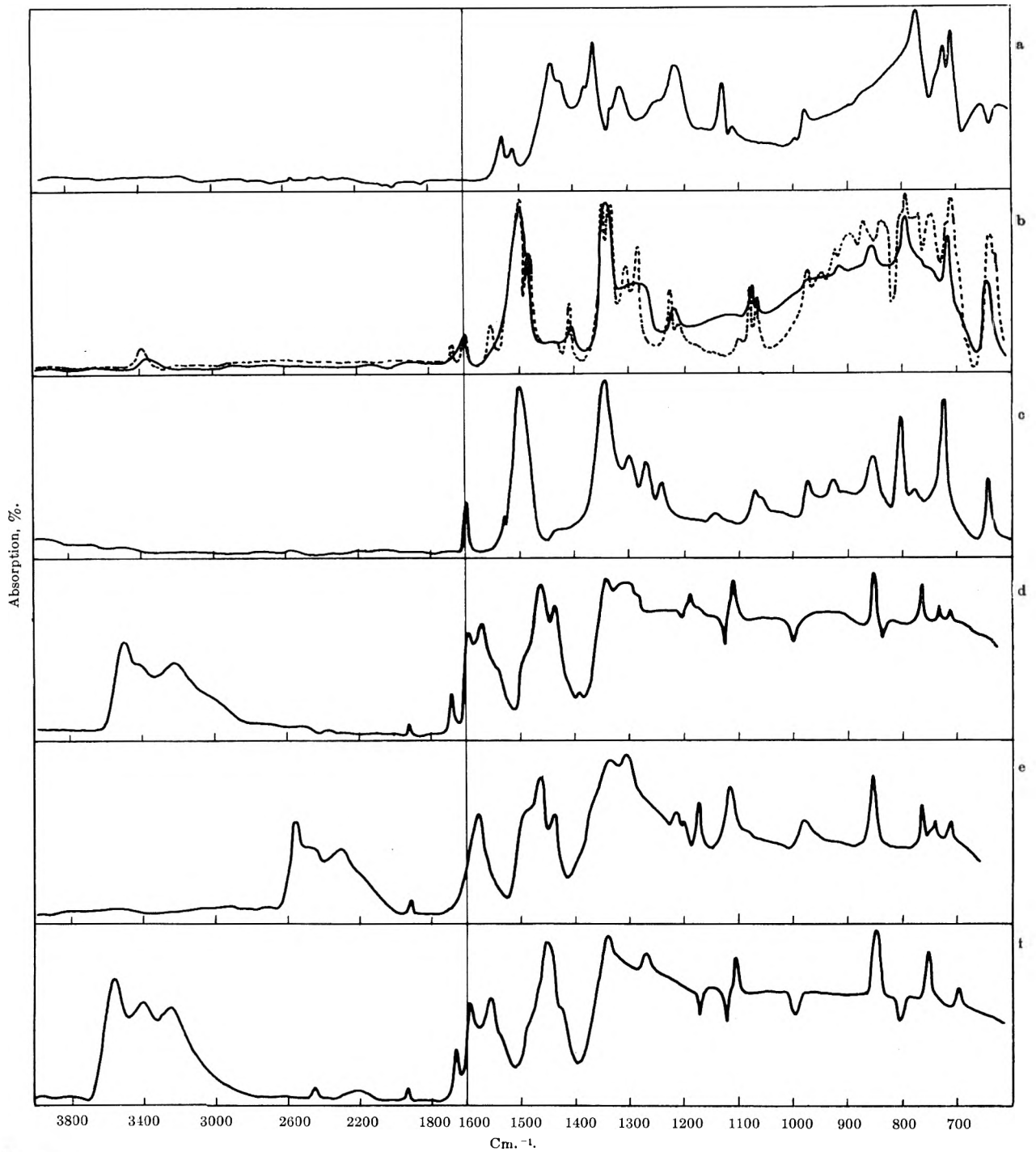

Fig. 5.—Infrared spectra of cesium hydrogen di-(pentachlorophenoxide) (a), cesium hydrogen di-(3-nitrophenoxide) (b), same, but deuterated (c), sodium hydrogen di-(4-nitrophenoxide)·$2H_2O$ (d), same, but deuterated (e), potassium hydrogen di-(4-nitrophenoxide)·$2H_2O$ (f). Spectra combined from mulls in Nujol and hexachlorobutadiene; full line, room temperature; dotted line, cooled with liquid nitrogen.

clearly in the spectra of $CsH(PeCP)_2$ and $CsH(MNP)_2$ which do not contain water or crystallization; practically no bands, except a very weak ν-CH band in the spectrum of the latter, are observed in the 4000–1600 cm.$^{-1}$ region. In the spectra of $NaH(PNP)_2$ and $KH(PNP)_2$, which contain two water molecules per formula unit, three medium-to-strong bands are observed in the 3600–3100 cm.$^{-1}$ region. They can be assigned to the stretching vibrations of the hydrogen-bonded water molecules in the crystal. It seems highly unlikely that one of these bands could be due to the phenolic hydroxyl group because no acid phenoxide investigated shows a ν-OH band above 2700 cm.$^{-1}$. Two bands between 1700 and 1660 cm.$^{-1}$ are due to the H_2O bending modes.

The limits of the broad absorption extending over the middle region of the spectrum are poorly defined. The maximum appears to be at about 800 cm.$^{-1}$. Narrower bands are superimposed on this broad absorption and they can be correlated with the R bands of the $(ROHOR)^-$ ion; several of them appear much broader and less well defined than their analogs in the spectra of the corresponding phenol or phenoxide. Narrow transmission regions are also observed.[21] This broad absorption is somehow connected with the

(21) J. C. Evans, *Spectrochim. Acta*, **18**, 507 (1962).

vibrations of the hydrogen-bonded OHO group of the acid phenoxides because it is not observed in the spectra of the phenoxides and phenols, and because it is affected by deuteration and is temperature sensitive. For instance, the spectrum of $CsD(MNP)_2$ shows a considerable flattening of the broad absorption band and in the spectrum of $CsH(MNP)_2$ cooled to liquid nitrogen temperature an appreciable contraction of this band is observed. Very similar phenomena, *i.e.*, absence of any OH band above 1800 cm.$^{-1}$ and broad absorption at lower frequencies, have been observed for a number of substances, such as some acid salts of carboxylic acids, trona,[2] dichlorodiphenyl hydrogen phosphate,[22] and acetamide hemihydrochloride,[23] which contain symmetrical hydrogen bonds confirmed by various methods.[1-4] This similarity indicates that the hydrogen bonds ROHOR in the above acid phenoxides are of the symmetrical type or very close to it. The spectra of $CsH(PeCP)_2$ and $CsH(MNP)_2$ solutions in DMSO (Fig. 4) give further support: a broad band near 2500–2400 cm.$^{-1}$ appears in these spectra. Comparison with the spectra of the solutions of pure phenols shows that this band is due to the hydrogen bonded OH group ROH. .OR, because the solutions of phenols in DMSO show the ν-OH bands in the 3200–3100 cm.$^{-1}$ region. The hydrogen bond of the acid phenoxide which is symmetrical in the crystal becomes asymmetrical in the DMSO solution. Similar behavior has been observed for potassium hydrogen bisphenylacetate and potassium hydrogen di-(4-chlorobenzoate).[24]

Adducts with Symmetrical Intramolecular Hydrogen Bonds.—Two acid phenoxides of dihydric phenols belong to this group: sodium acid phenoxide of 2,2′-dihydroxybiphenyl (NaHBP) and sodium acid phenoxide of 2,2′-methylenebis-(4-chlorophenol) (NaHMBCP). The steric conditions in these dihydric phenols are favorable for the formation of strong intramolecular hydrogen bonds and in fact evidence for such a hydrogen bond in 2,2′-dihydroxybiphenyl was obtained.[25,26]

The infrared spectra of NaHBP and NaHMBCP are rather similar (Fig. 6); the most conspicuous feature is a broad band of medium intensity at about 1630 cm.$^{-1}$. This band disappears on deuteration and it has no analogs in the spectra of the respective phenols and phenoxides. It may thus be assigned to an OH stretching vibration of the OH. .O group because there are no other bands at higher wave numbers which could be attributed to this motion. Although the frequency appears to be very low it matches well with other ν-OH bands in the spectra of compounds with symmetrical hydrogen bonds.[2,4] There is also the broad absorption with maximum near 1100–1200 cm.$^{-1}$, though it appears much less intense than in the spectra of adducts with symmetrical intermolecular hydrogen bonds. These characteristics indicate a symmetrical hydrogen bonding in NaHBP and NaHMBCP. It should, however, be emphasized that the broad absorption is not connected with symmetrical hydrogen bonds only but appears also with some other very strongly hydrogen-bonded compounds, such as the adduct of 4-nitrophenol with trimethylamine oxide (Fig. 3) and nickel dimethylglyoxime.[27]

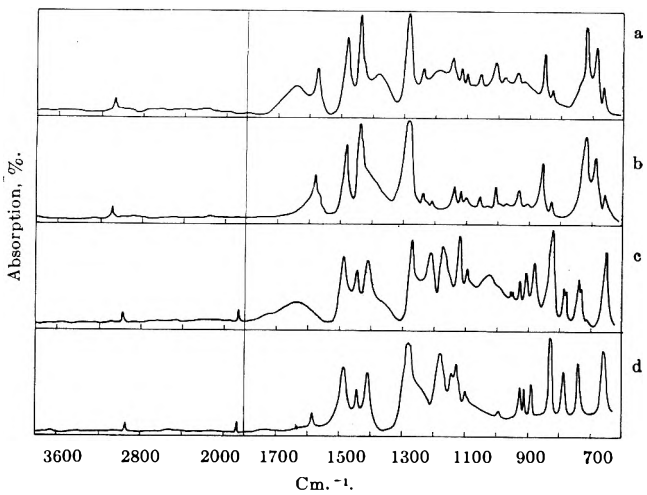

Fig. 6.—Infrared spectra of sodium acid salt of 2,2′-dihydroxybiphenyl (a), same, but deuterated (b), sodium acid salt of 2,2′-methylene bis-(4-chlorophenol) (c), same, but deuterated (d). Spectra combined from mulls in Nujol and hexachlorobutadiene.

In order to establish whether the hydrogen bond is intermolecular or intramolecular the infrared spectra of the under-cooled melt and of a solution of NaHBP in DMSO have been investigated. They are very similar to the crystal spectrum and, in particular, the 1630 cm.$^{-1}$ band is observed unchanged. This behavior differs from that of acid phenoxides with intermolecular symmetrical hydrogen bonding and it supports the assumption of an intramolecular hydrogen bond in NaHBP. The same applies to NaHMBCP because of the great similarity of the spectra.

Intramolecular symmetrical hydrogen bonding has been so far confirmed for potassium hydrogen maleate[28]; a comparison of its infrared spectrum[24] to those of NaHBP and NaHMBCP shows a few essential similarities: the ν-OH band at 1640 cm.$^{-1}$,[2,24] broadened absorption bands, and the fact that dissolution in DMSO does not bring about any strong changes.[24]

There is another difference between the spectra of acid phenoxides with symmetrical inter- and intramolecular hydrogen bonding; individual contributions of the OH modes in the spectra of the former are not identifiable in view of a broad single 1600–600 cm.$^{-1}$ absorption. This is no longer so in the spectra of the latter. For instance, in the spectrum of NaHMBCP strong bands near 1390, 1200, and 1018 cm.$^{-1}$ are observed, apart from the ν-OH band at 1630 cm.$^{-1}$, but not in the spectrum of its deuterated derivative; they can thus be attributed to the OH in-plane (and those coupled with it) and out-of-plane bending modes (Table II).

Experimental[29]

Cesium Hydrogen Di-(pentachlorophenoxide), $CsH(C_6Cl_5O)_2$.—A solution of 1 mmole of CsOH in 3 ml. of boiling ethanol was added to a solution containing 2 mmoles of pentachlorophenol in 15 ml. of benzene and the resulting solution was concentrated to about half of the original volume. Transparent prisms were deposited during 3 days.

(22) D. Hadži and A. Novak, *Proc. Chem. Soc.*, 241 (1960).
(23) W. Takei, Ph.D. Thesis, California Institute of Technology, 1957.
(24) D. Hadži and A. Novak, *Spectrochim. Acta*, **16**, 853 (1962).
(25) J. E. Gordon and S. L. Johnson, *J. Phys. Chem.*, **66**, 534 (1962).
(26) H. Musso and H. G. Matthies, *Ber.*, **94**, 356 (1961).
(27) R. Blinc and D. Hadži, *J. Chem. Soc.*, 4536 (1958).
(28) S. W. Peterson and H. A. Levy, *J. Chem. Phys.*, **29**, 948 (1958).
(29) Adducts were dried at room temperature and 10^{-4} mm. unless otherwise stated. Phenols used were commercial products and were not further purified unless otherwise stated.

Anal. Calcd. for $C_{12}HCl_{10}O_2Cs$: C, 21.69; H, 0.15; Cl, 53.35. Found: C, 21.89; H, 0.17; Cl, 53.16.

Cesium Hydrogen Di-(3-nitrophenoxide), $CsH(NO_2C_6H_4O)_2$.—This compound was obtained as large transparent ruby rhombohedra[7] using the above procedure, or by using ether in place of benzene.

Anal. Calcd. for $C_{12}H_9N_2O_6Cs$: C, 35.14; H, 2.21; N, 6.83. Found: C, 35.32; H, 2.48; N, 6.97.

Sodium Hydrogen Di-(4-nitrophenoxide) Dihydrate, $NaH(NO_2C_6H_4O)_2 \cdot 2H_2O$.—A solution containing 10 mmoles of 4-nitrophenol in 3 ml. of methanol was treated with 5 ml. of 1 *N* NaOH. The resulting orange needles[5] were twice recrystallized from water.

Anal. Calcd. for $C_{12}H_{13}N_2O_8Na$: C, 42.86; H, 3.90; N, 8.33; Na, 6.84. Found: C, 42.93; H, 4.25; N, 8.38; Na, 6.41.

Potassium hydrogen di(4-nitrophenoxide) dihydrate, $KH(NO_2C_6H_4O)_2 \cdot 2H_2O$, was prepared as above using KOH instead of NaOH.

Anal. Calcd.: neut. equiv., 352.3. Found: neut. equiv., 350.8.

Potassium Hydrogen Di-(4-cyanophenoxide), $KH(CNC_6H_4O)_2$.—To a solution of 2 mmoles of 4-cyanophenol (Aldrich Chemical Co.; three times crystallized from chloroform–carbon tetrachloride and once from water; m.p. 112° (lit.[30] m.p. 113°)) in 12 ml. of anhydrous ether was added 1 ml. of 1 *N* methanolic potassium hydroxide. White crystals of acid phenoxide precipitated. This substance was a monomethanolate as found by analysis; drying of the compound for 10 hr. at 75° and 10^{-4} mm. gave unsolvated acid phenoxide.

Anal. Calcd. for $C_{14}H_9N_2O_2K$: C, 59.07; H, 3.43; N, 10.60; K, 14.79. Found: C, 59.29; H, 3.57; N (Kjeldahl), 10.29; K, 14.62.

Potassium Hydrogen Pyrocatechoxide Hemihydrate, $KO(OH)C_6H_4 \cdot {}^1/_2H_2O$.—This compound was prepared from pyrocatechol (Eastman Kodak White Label) and a 15% solution of potassium hydroxide in ethanol using Weinland's method.[10]

Anal. Calcd.: neut. equiv., 157.2. Found: neut. equiv., 158.0.

Potassium trihydrogen pyrocatechoxide hemihydrate, $KO(OH)C_6H_4 \cdot C_6H_4(OH)_2 \cdot {}^1/_2H_2O$, was prepared similarly as above using 1 *N* KOH.[10]

Anal. Calcd.: neut. equiv., 267.3. Found: neut. equiv., 266.5.

Potassium Trihydrogen Guaiacoxide, $KOC_6H_3OCH_3 \cdot 3HOC_6H_4OCH_3$.—To a 10% ethanolic solution of guaiacol (Matheson Coleman & Bell Co.), 1 *N* KOH was slowly added. White crystals deposited and were recrystallized from water.

Anal. Calcd.: neut. equiv., 534.5. Found: neut. equiv., 530.1.

(30) O. L. Brady and F. P. Dunn, *J. Chem. Soc.*, 871 (1914).

Sodium acid salt of 2,2′-dihydroxybiphenyl, $NaOC_6H_4C_3H_4OH$, was prepared by careful half-neutralization of phenol solution in ethanol with 1 *N* NaOH. White crystals deposited from the solution which was concentrated by evaporation. Aldrich Chemical Co. 2,2′-dihydroxybiphenyl was crystallized 5 times from toluene, m.p. 108–109.5° (lit.[31] m.p. 108°), neut. equiv.: calcd. 186.2; found 186.6.

Sodium acid salt of 2,2′-methylenebis-(4-chlorophenol), $NaOC_6H_3(Cl)\text{-}CH_2\text{-}(Cl)C_6H_3OH$, was prepared as above. 2,2′-Methylenebis-(4-chlorophenol) (British Drug House) was crystallized four times from ethylene chloride, m.p. 167–169° after sintering at 162°; neut. equiv. calcd. 268; found 270.

Adduct of 4-Nitrophenol with Potassium Acetate, $NO_2C_6H_4OH \cdot KOOCCH_3$.—A solution containing 20 mmoles of 4-nitrophenol in 50 ml. of ethanol was treated with 20 mmoles of potassium acetate dissolved in water. Yellow crystals (m.p. 327°) deposited after a few hours and were recrystallized from ethanol.

Anal. Calcd.: neut. equiv., 237.2. Found: neut. equiv., 240.1.

Adduct of 4-Nitrophenol with Trimethylamine Oxide, $NO_2C_6H_4OH \cdot NO(CH_3)_3$.—This adduct was prepared by adding a solution of 4-nitrophenol in ethanol to a solution of trimethylamine oxide in equimolar ratio. Yellow crystals (m.p. 115°) deposited and were recrystallized from ethanol. Trimethylamine oxide dihydrate was synthesized according to reference 32.

Adduct of Pyrocatechol with Potassium Oxalate, $2C_6H_4(OH)_2 \cdot K_2C_2O_4$.—This adduct was prepared by adding an aqueous solution of pyrocatechol (Eastman Kodak White Label) to potassium oxalate solution (molar ratio 2:1). White crystals deposited and were recrystallized from water.

Deuterated Compounds.—Substances were deuterated on the vacuum line by exchange with methanol-*d* or deuterium oxide.

Dimethyl sulfoxide (Light and Co.) was distilled under reduced pressure from molecular sieves (type 4-A, Linde Air Products).

Infrared Spectra.—Substances were prepared for spectroscopical work as mulls in Nujol and hexachlorobutadiene. Some adducts were investigated at liquid nitrogen temperature as mulls in Nujol; a low temperature cell of a conventional design was used for this work. About 20% solutions of adducts and of phenols in dimethyl sulfoxide (DMSO) were studied as thin films between NaCl plates using the compensation method. The spectra were recorded on Perkin–Elmer Model 21 and Beckman IR-4 spectrophotometers equipped with sodium chloride prisms.

Acknowledgment.—D. H. and A. N. are grateful to the Boris Kidrič Fund for a substantial contribution toward the expenses of experimental work.

(31) W. R. Spencer and F. R. Duke, *Anal. Chem.*, **26**, 919 (1954).

(32) J. Meisenheimer and K. Bratring, *Ann.*, **397**, 286 (1913).

DISSOCIATION CONSTANT OF PYRROLIDINIUM ION AND RELATED THERMODYNAMIC QUANTITIES FROM 0 TO 50°

BY HANNAH B. HETZER, ROGER G. BATES, AND R. A. ROBINSON

Solution Chemistry Section, National Bureau of Standards, Washington, D. C.

Received December 6, 1962

The thermodynamic dissociation constant of pyrrolidinium ion (BH^+) at 11 temperatures from 0 to 50° has been determined from e.m.f. measurements of hydrogen–silver bromide cells without liquid junction. The dissociation constant (K_{bh}) for the process $BH^+ + H_2O \rightleftarrows B + H_3O^+$ is given as a function of T (°K.) by the equation $-\log K_{bh} = 2318.85/T + 5.2942 - 0.005923T$. At 25°, $-\log K_{bh}$ is 11.305, ΔH^0 is 54,470 j. mole^{-1}, ΔS^0 is −33.7 j. deg.$^{-1}$ mole^{-1}, and ΔC_p^0 is 68 j. deg.$^{-1}$ mole^{-1}.

Introduction

In an earlier contribution from this Laboratory,[1] the acidic dissociation constant of piperidinium ion from 0 to 50° was reported. This paper describes a continuation of work on the dissociation constants of nitrogenous bases by extending measurements to the next lower member of the series, pyrrolidine (tetramethyleneimine $(CH_2)_4NH$). Apart from the interest in a comparison of the thermodynamic properties of these two closely related bases, pyrrolidine is important in being the parent of the amino acids proline and hydroxyproline, whose dissociation constants have already been measured.[2] Moreover, the ring structure of four

(1) R. G. Bates and V. E. Bower, *J. Res. Natl. Bur. Std.*, **57**, 153 (1956).

(2) P. K. Smith, A. T. Gorham, and E. R. B. Smith, *J. Biol. Chem.*, **144**, 735 (1942).

TABLE I

ELECTROMOTIVE FORCE OF THE CELL Pt; H_2(g, 1 ATM.), $(CH_2)_4NH_2Br(m_1)$, $(CH_2)_4NH(m_2)$, AgBr; Ag FROM 0 TO 50° (IN V.)

m_1	m_2	0°	5°	10°	15°	20°	25°	30°	35°	40°	45°	50°
0.09946	0.05042	0.79210	0.79330	0.79423	0.79495	0.79542	0.79580	0.79584	0.79573	0.79555	0.79509	0.79454
.09520	.04954	.79333	.79455	.79556	.79633	.79688	.79721	.79738	.79731	.79708	.79658	.79581
.08348	.03799	...	...	...	...	...	.79626	.79644	.79638	.79616	.79573	.79517
.08296	.04024	.79411	.79532	.79635	.79711	.79763	.79802	...	...	...	...	...
.07904	.04006	.79587	.79717	.79822	.79898	.79958	.79990	.80002	.80001	.79983	.79961	.79913
.07409	.03372	...	...	...	...	...	.79843	.79863	.79862	.79842	.79809	.79748
.07239	.03511	.79644	.79771	.79875	.79956	.80015	.80057	...	...	...	...	...
.06928	.03605	.79883	.80013	.80123	.80208	.80271	.80313	.80338	.80344	.80335	.80301	.80300
.06741	.03068	...	...	...	...	...	.80022	.80048	.80050	.80034	.79996	.79943
.06482	.03144	.79824	.79947	.80062	.80151	.80214	.80254	...	...	...	...	...
.06169	.03127	.80035	.80169	.80276	.80359	.80419	.80468	.80495	.80505	.80509	.80478	.80434
.05568	.02897	.80259	.80403	.80522	.80620	.80690	.80729	.80772	.80780	.80786	.80763	.80720
.05062	.02303	...	...	...	...	...	.80573	.80609	.80625	.80623	.80600	.80561
.04797	.02326	.80365	.80507	.80624	.80720	.80793	.80847	...	...	...	...	...
.04395	.02287	.80684	.80831	.80954	.81057	.81133	.81187	.81229	.81251	.81264	.81254	.81226
.03865	.01959	...	.81032	.81156	.81253	.81327	.81385	.81426	.81458	.81468	.81458	.81433
.03080	.01561	.81273	.81430	.81560	.81669	.81756	.81814	.81857	.81894	.81911	.81905	.81891
.02918	.01328	...	...	...	...	...	.81632	.81681	.81711	.81727	.81722	.81698
.02624	.01273	.81443	.81599	.81732	.81843	.81933	.82004	...	...	...	...	...
.01922	.01000	.82152	.82306	.82459	.82580	.82684	.82759	.82830	.82877	.82917	.82936	.82939

carbon atoms and one basic nitrogen atom occurs in many natural products, such as the alkaloids hygrine and nicotine, chlorophyll, and hemoglobin.

Method and Procedure

The electromotive force method employed was essentially that used in previous studies of bases in this Laboratory.[1,3-5] As in the study of *t*-butylamine,[5] the silver–silver bromide electrode, because of its lower solubility in amine solutions, was used in place of the silver–silver chloride electrode. The cell used may be represented as

$$\text{Pt; } H_2\text{(g, 1 atm.)},(CH_2)_4NH_2Br(m_1),\ (CH_2)_4NH(m_2),\text{AgBr; Ag}$$

where m is molality. The preparation of the electrodes and of the hydrobromic acid solution have been described elsewhere, and the values used for the standard potential of the cell have already been reported.[6]

Two separate lots of pyrrolidine, commercial grade, were distilled through a Podbielniak column with platinum Heligrid packing, under an atmosphere of nitrogen. The middle fractions were analyzed chromatographically, and the fractions used were those for which the chromatogram showed only the pyrrolidine peak. Analysis of a sample from the first distillation with the mass spectrograph revealed only one component.[7] Although the purified amine was protected from moisture and carbon dioxide during storage, evidence of decomposition (slight initial instability of the electrodes and lower e.m.f. values) was observed in buffer solutions prepared from purified pyrrolidine several weeks after the distillation had been carried out.[8] There was no evidence, however, of decomposition of the base used to prepare the buffer solutions for the determination of the dissociation constant.

Since pyrrolidine is rather volatile (b.p. 86.5° at 760 mm.), the ratio of salt to free base (m_1/m_2) in the buffer solutions was kept at approximately 2. The molality of free pyrrolidine (m_2) in the stock solutions was determined by weight titration with the standard solution of hydrobromic acid to the calculated equivalence point (pH 6.1 in 0.1 *M* solution), the end point being determined with a glass electrode. Insofar as possible, all of the solutions containing pyrrolidine were prepared and handled under an atmosphere of nitrogen.

The vapor pressure of pyrrolidine from the most concentrated buffer solution, $m_1 = \sim 0.1$; $m_2 = \sim 0.05$, was measured at 50° by a gas transpiration method and found to be approximately 0.5 mm. The pressure corrections to one atmosphere of dry hydrogen, calculated with and without inclusion of the partial pressure of the amine, agreed to within 0.01 mv. The partial pressure of the amine was therefore neglected.

Although the cells were equipped with the extra triple saturators used in this Laboratory for solutions with volatile components,[3] the e.m.f. values at 25° measured in the middle of the series and at the end were lower than the original values. This decrease was found to be approximately 0.1 mv. after the measurements from 0 to 20° and approximately 0.4 mv. after those from 30 to 50°. The e.m.f. at temperatures other than 25° was therefore adjusted by amounts roughly proportional to time and concentration, determined from the changes in the successive readings at 25°. The largest adjustment made (that for the solution with $m_1 = 0.03080$ at 50°) amounted to 0.008 pK unit.

No data on the stability of the pyrrolidine complex with silver ion were found. Even if the stability constant were considerably higher than that for the ammonia and piperidine complexes, however, the low solubility of silver bromide would keep the concentration of complex very low. Consequently, no correction to the stoichiometric concentration of bromide was necessary. Hydrolysis corrections to the buffer ratio were made in the usual way.

Results

The e.m.f. data are listed in Table I. Each value represents the mean of two electrode combinations in the same cell, corrected as described in the previous section for removal of the volatile base by the bubbling hydrogen. The usual correction to a hydrogen partial pressure of 1 atm. has also been made.

The calculation of K_{bh}, the thermodynamic dissociation constant of the pyrrolidinium ion (BH^+) on the molal scale, was made in the manner already described.[9] Once again, a value of 0 for the ion-size parameter gave a straight-line plot of the "apparent" log K'_{bh}, namely log K'_{bh}, as a function of ionic strength, I. The equation for the calculation of $-\log K'_{bh}$ was therefore

$$-\log K_{bh}' = \frac{E - E^0}{2.3026RT/F} + \log \frac{m_1(m_1 + m_{OH})}{m_2 - m_{OH}} - 2A\sqrt{m_1 + m_{OH}} \quad (1)$$

(3) R. G. Bates and G. D. Pinching, *J. Res. Natl. Bur. Std.*, **42**, 419 (1949).
(4) H. B. Hetzer and R. G. Bates, *J. Phys. Chem.*, **66**, 308 (1962).
(5) H. B. Hetzer, R. A. Robinson, and R. G. Bates, *ibid.*, **66**, 2696 (1962).
(6) H. B. Hetzer, R. A. Robinson, and R. G. Bates, *ibid.*, **66**, 1423 (1962).
(7) The authors are indebted to Dr. R. T. Leslie for the distillation, to Dr. Leslie and E. L. Weise for the vapor-liquid chromatographic analyses, and to E. E. Hughes for the mass spectrographic examination.
(8) Decomposition of pyrrolidine has been observed by R. V. Helm, W. J. Lanum, G. L. Cook, and J. S. Ball, *J. Phys. Chem.*, **62**, 858 (1958), and R. H. Linnell, M. Aldo, and F. Raab, *J. Chem. Phys.*, **36**, 1401 (1962).
(9) R. G. Bates and H. B. Hetzer, *J. Phys. Chem.*, **65**, 667 (1961).

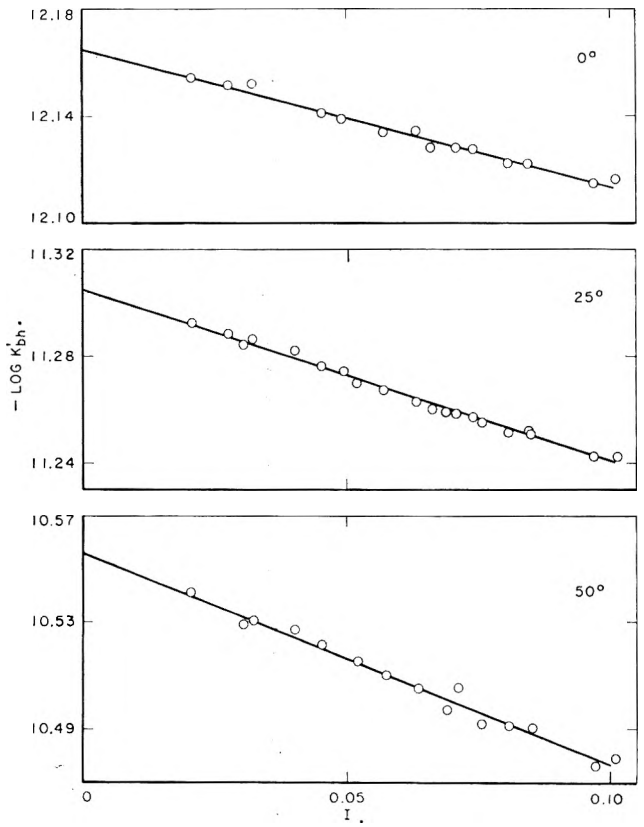

Fig. 1.—Plot of $-\log K'_{bh}$ as a function of ionic strength ($I = m_{Cl} + m_{OH}$) at 0, 25, and 50°.

where A is the Debye–Hückel slope. The concentration of hydroxide ion was estimated from the values of $p(a_H\gamma_{Cl})$ and pK_w in the manner suggested by Bates, Siegel, and Acree.[10]

The values of $-\log K'_{bh}$ at 0, 25, and 50° are plotted as a function of ionic strength in Fig. 1. The intercepts ($-\log K_{bh}$), summarized in Table II, were determined by the method of least squares, and the standard deviation of the intercept (σ_i) is given in the third column of the table. Values of $-\log K_b$, the negative logarithm of the basic dissociation constant, are given in the last column.

The constant K_{bh} is the equilibrium constant for the reaction

$$BH^+ + H_2O \rightleftarrows B + H_3O^+ \qquad (2)$$

that is, the acidic dissociation of pyrrolidinium ion, whereas K_b is the equilibrium constant for the reaction

$$B + H_2O \rightleftarrows BH^+ + OH^- \qquad (3)$$

The product of these two constants is K_w, the autoprotolysis constant for water, values for which were taken from the paper of Harned and Robinson.[11]

Thermodynamic Quantities.—The following equations, the constants of which were determined by the method of least squares, represent the values of $-\log K_{bh}$ and $-\log K_b$ with a mean deviation less than 0.001 unit

$$-\log K_{bh} = \frac{2318.85}{T} + 5.2942 - 0.005923T \qquad (4)$$

(10) R. G. Bates, G. L. Siegel, and S. F. Acree, *J. Res. Natl. Bur. Std.*, **31**, 205 (1943).

(11) H. S. Harned and R. A. Robinson, *Trans. Faraday Soc.*, **36**, 973 (1940).

TABLE II

VALUES OF $-\log K_{bh}$ AND $-\log K_b$ FROM 0 TO 50°

t, °C.	$-\log K_{bh}$	σ_i	$-\log K_b$
0	12.165	0.001	2.779
5	11.984	.002	2.750
10	11.807	.001	2.728
15	11.636	.001	2.711
20	11.469	.001	2.698
25	11.305	.001	2.692
30	11.147	.001	2.686
35	10.994	.001	2.686
40	10.845	.001	2.690
45	10.698	.001	2.698
50	10.556	.002	2.706

and

$$-\log K_b = \frac{2195.67}{T} - 11.6690 + 0.023461T \qquad (5)$$

where T is the temperature in degrees Kelvin (t°C. + 273.15).

By application of the usual thermodynamic equations to the expression given in eq. 4, the standard thermodynamic quantities for the dissociation of pyrrolidinium ion (eq. 2) given in Table III have been calculated. The corresponding quantities for the basic dissociation (eq. 3) at 25° are

$$\Delta G^0 = 15{,}350 \text{ j. mole}^{-1}$$

$$\Delta H^0 = 2{,}110 \text{ j. mole}^{-1}$$

$$\Delta S^0 = -44.4 \text{ j. deg.}^{-1} \text{ mole}^{-1}$$

$$\Delta C_p^0 = -270 \text{ j. deg.}^{-1} \text{ mole}^{-1}$$

TABLE III

THERMODYNAMIC QUANTITIES FOR THE ACIDIC DISSOCIATION OF PYRROLIDINIUM ION (BH^+) FROM 0 TO 50°

t, °C.	ΔG^0, j. mole^{-1}	ΔH^0, j. mole^{-1}	ΔS^0, j. deg.$^{-1}$ mole^{-1}
0	63,620	52,850	−39.4
5	63,810	53,170	−38.3
10	64,000	53,480	−37.1
15	64,180	53,810	−36.0
20	64,360	54,140	−34.9
25	64,530	54,470	−33.7
30	64,700	54,810	−32.6
35	64,860	55,160	−31.5
40	65,010	55,510	−30.3
45	65,160	55,870	−29.2
50	65,310	56,230	−28.1
25°:	$\Delta C'_p{}^0 = 68$ j. deg.$^{-1}$ mole^{-1}		

Discussion

Earlier determinations of the dissociation constant of pyrrolidinium ion all seem to have been based on the e.m.f. of cells with liquid junction (l.j.).[12–15] These values are summarized in Table IV.

The values of ΔH^0 and ΔS^0 at 30° calculated by Searles, Tamres, Block, and Quarterman[14] from their dissociation constants at 25 and 35° are greatly at variance with those found in this investigation. These values are 33,500 j. mole^{-1} and −104 j. deg.$^{-1}$ mole^{-1},

(12) L. C. Craig and R. M. Hixon, *J. Am. Chem. Soc.*, **53**, 4367 (1931).

(13) A. Albert, "Heterocyclic Chemistry," Athlone Press, London, 1959, p. 6.

(14) S. Searles, M. Tamres, F. Block, and L. A. Quarterman, *J. Am. Chem. Soc.*, **78**, 4917 (1956).

(15) J. A. Broomhead, H. A. McKenzie, and D. P. Mellor, *Australian J. Chem.*, **14**, 649 (1961).

respectively. On the other hand, the heat of neutralization of pyrrolidine with hydrochloric acid in aqueous solution at 25° determined by Sacconi, Paoletti, and Ciampolini[16] leads to a value of 51,750 j. mole^{-1} for ΔH^0, in reasonably good agreement with 54,570 j. mole^{-1} calculated from the change of K_{bh} with temperature. These authors have given a value of 38.9 j. deg.$^{-1}$ mole^{-1} for ΔS^0,[17] but, combined with our values for ΔG^0 at 25°, their calorimetric data lead to $\Delta S^0 = -42.9$ j. deg.$^{-1}$ mole^{-1}. This figure is to be compared with -33.7 j. deg.$^{-1}$ mole^{-1} listed in Table III.

TABLE IV

COMPARISON OF VALUES FOR $-\log K_{bh}$ (PYRROLIDINIUM ION)

t, °C.	Ionic strength	$-\log K_{bh}$	Method	Ref.
..	...	11.11[a]	H_2, l.j.	12
20	...	11.3	....	13
25	0	11.27	Glass, l.j.	14
	0	11.305	H_2, AgBr	This investigation
	0.2	11.4	Glass, l.j.	15
35	0	11.08	Glass, l.j.	14
	0	10.994	H_2, AgBr	This investigation

[a] If temperature is taken to be 25°.

Pyrrolidinium ion is a slightly weaker acid than piperidinium ion,[1] with which it is closely related structurally. The enthalpy and entropy changes on dissociation of the two acids are strikingly similar; the changes of heat capacity are rather large and positive for both acids.

Acid	$-\log K_{bh}$	ΔH^0, j. mole^{-1}	ΔS^0, j. deg.$^{-1}$ mole^{-1}	ΔC_p^0, j. deg.$^{-1}$ mole^{-1}
Piperidinium	11.123	53,390	−33.9	88
Pyrrolidinium	11.305	54,470	−33.7	68

The data are for a temperature of 25°.

The presence of a carboxyl group adjacent to the NH in the proline molecule, $(CH_2)_3(CHCOOH)NH$, lowers the basicity of the nitrogen. Thus, pK_2 for proline is 10.640 at 25°[2] as compared with 11.305 for pyrrolidine. It is well known that a hydroxyl group, by virtue of its electron-attracting nature, also lowers the basicity of nearby nitrogen atoms. The value of pK_2 for hydroxyproline is 9.662 at 25°.[2]

The elucidation of the effect of structure of acids and bases upon the change of ΔS^0 and ΔC_p^0 for dissociation processes is complicated by the profound effect of electrostatic terms arising from differences in charge type. Whereas the dissociation of pyrrolidinium ion is an isoelectric process, $BH^+ = B + H^+$, both of the dissociation steps of proline and hydroxyproline involve hybrid ions or zwitterions (designated by the superscript $\mp$). The process usually designated as the "first dissociation" is the dissociation of the carboxyl group, which can be represented $BHH^+ = BH^\mp + H^+$. At high pH values, a proton is removed from the nitrogen ("second dissociation"), and the charge effects are as follows: $BH^\mp = B^- + H^+$.

Neither of these is an isoelectric process. Although the behavior of the activity coefficient of a hybrid ion in solution has sometimes been found to approximate that of an uncharged molecule, it seems likely that the extent of solvation (upon which the magnitudes of ΔS^0 and ΔC_p^0 appear to depend) will often be quite different. If the two charge centers in the molecule $B^\mp$ interact with solvent dipoles independently,[18] it may be imagined that the second dissociation step matches more closely, from the electrostatic viewpoint, the dissociation of pyrrolidinium ion than does the first. If, on the contrary, "overlapping" of the charges in the hybrid ion creates virtually an uncharged species, the first dissociation may be expected to approximate an isoelectric process.

The changes of entropy and heat capacity for the two steps in the dissociation of proline and hydroxyproline have been recalculated from the data of Smith, Gorham, and Smith.[2] The values at 25° are as follows:

	ΔS^0, j. deg.$^{-1}$ mole^{-1}	ΔC_p^0, j. deg.$^{-1}$ mole^{-1}
First dissociation		
Proline	−32.1	−184
Hydroxyproline	−22.0	−123
Second dissociation		
Proline	−60.6	0
Hydroxyproline	−53.8	− 51

From a comparison of the entropies, it would appear that the first dissociation of proline parallels more closely the dissociation of pyrrolidinium ion than does the second. The large negative change in heat capacity is, however, not a usual accompaniment of truly isoelectric dissociation processes[19] most of which, like that for pyrrolidinium ion, have positive values of ΔC_p^0.

As molecular models show, pyrrolidine can be formed from diethylamine with little distortion of the bonds, and a comparison of the thermodynamic properties of these two bases is therefore pertinent. Fyfe[20] found pK 10.98 for diethylamine at 25°, in fair agreement with the value of 10.92 interpolated from the data of Evans and Hamann.[21] For ΔH^0, Fyfe found 43.1 kj. mole^{-1} whereas Evans and Hamann give 53.4 kj. mole^{-1}. The corresponding entropy values are −66 and −30 j. deg.$^{-1}$ mole^{-1}, respectively. In view of these differences, it is difficult to pursue the comparison with pyrrolidine. On the assumption that the thermodynamic properties of diethylamine and pyrrolidine should not differ greatly, however, the data of Evans and Hamann might perhaps be preferred.

(16) L. Sacconi, P. Paoletti, and M. Ciampolini, *J. Am. Chem. Soc.*, **82**, 3831 (1960).

(17) The negative sign ascribed to ΔS for the neutralization reaction appears to be in error.

(18) See, for example, N. Bjerrum, *Z. physik. Chem.*, **104**, 147 (1923); I. M. Kolthoff and L. S. Guss, *J. Am. Chem. Soc.*, **60**, 2516 (1938).

(19) See Table III of ref. 9.

(20) W. S. Fyfe, *J. Chem. Soc.*, 1347 (1955).

(21) A. G. Evans and S. D. Hamann, *Trans. Faraday Soc.*, **47**, 34 (1951).

HEAT CAPACITIES FROM 11 TO 305°K., ENTROPIES, AND FREE ENERGIES OF FORMATION OF L-VALINE, L-ISOLEUCINE, AND L-LEUCINE[1]

BY JOHN O. HUTCHENS, ARTHUR G. COLE, AND J. W. STOUT

Departments of Physiology and Chemistry and the Institute for the Study of Metals, University of Chicago, Chicago, Illinois

Received December 8, 1962

The heat capacities of L-valine, L-isoleucine and L-leucine have been measured from 11 to 305°K. The entropies in cal. mole^{-1} degree^{-1} at 298.15°K. were found to be 42.75 for L-valine, 49.71 for L-isoleucine, and 50.62 for L-leucine. Heat capacities, entropies, $(H^\circ - H_0^\circ)/T$, and $-(F^\circ - H_0^\circ)/T$ are tabulated as a function of temperature for the three substances from 10 to 310°K. Standard free energies of formation are calculated for glycine, L-alanine, L-valine, L-isoleucine, and L-leucine.

We have previously reported the heat capacities of glycine and L-alanine from 11 to 305°K.[2] To complete the series of naturally occurring monoaminomonocarboxylic aliphatic amino acids, we present here our data concerning L-valine, L-isoleucine, and L-leucine. These data have been used in conjunction with reported values for heats of combustion[3,4] to calculate free energies of formation for the five amino acids.

Experimental

Amino Acids.—The amino acids used in these studies were provided by the late Jesse P. Greenstein of the National Institutes of Health. Unidirectional paper chromatography using five different solvent systems (formix, MeOH–pyridine, ketone mix, phenol, and butanol–acetic acid) indicated that all three substances were free of other amino acids. They were 99.9% free of the D-isomer according to the criteria of Meister, *et al.*[5] Each amino acid was crystalline as indicated by microscopic examination in polarized light. None of the materials lost a detectable amount of weight when pumped overnight at 10^{-6} mm. in a system trapped with liquid nitrogen, nor did the heat capacity measurements disclose any significantly high values in the neighborhood of the ice point. Flame photometric tests for Na and K and ash analyses on 5–10-g. samples of the amino acids indicated negligible salt content.

Methods and Calculations.—The apparatus, methods for measuring heat capacities, and treatment of experimental data have been previously described.[6] We used the calorimeter with six radial fins and the thermometer bearing the laboratory designation "H." Sample weights, *in vacuo*, were 44.380 g. for L-valine, 46.405 g. for L-isoleucine, and 45.858 g. for L-leucine. The heat capacity of the empty calorimeter represented 40–50% of the total heat capacity for each of the three substances over most of the temperature range. The ice point was taken as 273.15°K., and 1 cal. = 4.1840 abs. joules. Symbols employed by us in Tables I–VII conform to the usage of the Circular of the National Bureau of Standards 500.[7] For definitions of terms connected with heats of combustion employed by previous authors, the original papers should be consulted.

Results

The experimentally measured quantities ($\Delta H/\Delta T$) are given in Table I for L-valine, in Table II for L-isoleucine, and in Table III for L-leucine. The individual values are listed in the chronological order in which they were obtained. Where ΔT cannot be deduced from the tables, the limits stated in a previous

TABLE I

HEAT CAPACITY OF L-VALINE IN CAL. DEG.$^{-1}$ MOLE^{-1}

0°C. = 273.15°K., mol. wt. $(CH_3)_2CHCH(NH_2)COOH$ = 117.15

T, °K.	$\Delta H/\Delta T$	T, °K.	$\Delta H/\Delta T$	T, °K.	$\Delta H/\Delta T$
54.06	8.854	161.32	25.22	283.25	38.76
58.90	9.838	166.89	25.90	289.25	39.29
63.81	10.81	172.44	26.57	294.91	39.89
68.91	11.74	177.93	27.29	301.02	40.68
74.10	12.66	183.59	27.80	11.07	0.353
78.77	13.53	188.92	28.41	11.95	0.425
82.88	14.28	194.23	28.97	13.08	0.539
87.79	15.12	199.80	29.55	14.31	0.682
92.82	15.94	205.47	30.18	15.66	0.862
97.70	16.68	211.22	30.76	17.06	1.075
101.81	17.30	217.07	31.49	18.90	1.386
107.07	18.11	219.68	31.67	21.04	1.776
112.50	18.90	225.94	32.51	23.53	2.254
118.04	19.68	231.67	32.98	25.90	2.746
123.43	20.42	237.37	33.61	28.39	3.268
128.70	21.12	243.00	34.29	31.19	3.897
132.67	21.66	248.79	34.81	34.32	4.596
137.97	22.40	254.01	35.42	37.76	5.343
143.11	23.03	259.96	36.13	41.53	6.194
150.22	23.84	265.80	36.76	45.67	7.088
155.68	24.55	271.61	37.46	50.09	8.054
		277.45	38.02		

TABLE II

HEAT CAPACITY OF L-ISOLEUCINE IN CAL. DEG.$^{-1}$ MOLE^{-1}

0°C. = 273.15°K., mol. wt. $CH_3CH_2CH(CH_3)CH(NH_2)COOH$ = 131.17

T, °K.	$\Delta H/\Delta T$	T, °K.	$\Delta H/\Delta T$	T, °K.	$\Delta H/\Delta T$
301.01	45.86	162.49	28.35	299.98	44.97
		168.10	29.04	306.30	46.09
51.52	10.17	173.60	29.74		
56.28	11.23	179.22	30.43	10.71	0.806
61.79	12.42	184.90	31.10	11.65	0.931
66.87	13.49	190.29	31.75	12.73	1.093
72.12	14.51	195.90	32.40	13.94	1.313
77.45	15.54	201.58	33.08	15.33	1.579
82.38	16.52	207.34	33.70	16.85	1.890
87.25	17.45	213.05	34.43	18.65	2.282
91.25	18.11	219.10	35.16	20.88	2.788
96.61	18.99	225.16	35.88	23.26	3.352
102.18	19.88	231.11	36.75	26.03	4.034
107.90	20.80	237.30	37.37	29.09	4.774
113.39	21.65	243.63	38.18	32.24	5.560
118.78	22.46	249.74	38.97	35.54	6.392
124.06	23.18	255.77	39.66	39.19	7.268
129.43	23.94	261.72	40.39	43.20	8.231
134.82	24.72	run lost		47.67	9.283
140.23	25.46	274.43	42.22	51.52	10.167
145.69	26.15	280.82	42.79		
151.07	26.88	287.14	43.57	267.00	41.03
156.75	27.61	293.61	44.46	272.69	41.72

(1) The heat capacity studies reported here were entirely supported by the U. S. Atomic Energy Commission. Ancillary studies were supported by a grant from the National Institutes of Health and by the Wallace A. and Clara M. Abbott Memorial Fund of the University of Chicago. Support of the cryogenic facilities by the National Science Foundation is gratefully acknowledged.

(2) J. O. Hutchens, A. G. Cole, and J. W. Stout, *J. Am. Chem. Soc.*, **82**, 4813 (1960).

(3) T. Tsuzuki, D. O. Harper, and H. Hunt, *J. Phys. Chem.*, **62**, 1594 (1958).

(4) T. Tsuzuki and H. Hunt, *ibid.*, **61**, 1668 (1957).

(5) A. Meister, L. Leventow, R. B. Kingsley, and J. P. Greenstein, *J. Biol. Chem.*, **192**, 535 (1951).

(6) A. G. Cole, J. O. Hutchens, R. A. Robie, and J. W. Stout, *J. Am. Chem. Soc.*, **82**, 4807 (1960).

(7) National Bureau of Standards Circular 500, "Selected Values of Chemical Thermodynamic Properties," U. S. Govt. Printing Office, Washington, D. C., February 1, 1952.

TABLE III

HEAT CAPACITY OF L-LEUCINE IN CAL. DEG.$^{-1}$ MOLE^{-1}

0°C. = 273.15°K., mol. wt. $(CH_3)_2CHCH_2CH(NH_2)COOH$ = 131.17

T, °K.	$\Delta H/\Delta T$	T, °K.	$\Delta H/\Delta T$	T, °K.	$\Delta H/\Delta T$
303.29	49.16	155.81	27.70	279.73	44.57
		161.57	28.16	286.41	45.85
53.09	11.00	167.29	28.91	291.45	46.65
58.06	12.06	168.87	29.09	298.28	48.09
63.54	13.21	174.50	29.86	305.23	49.49
68.85	14.23	180.41	30.60	11.34	0.820
73.91	15.15	186.43	31.34	12.17	0.956
78.82	16.06	192.54	32.06	13.39	1.201
83.50	16.96	198.67	32.86	14.73	1.485
88.36	17.76	201.89	33.22	16.25	1.839
93.60	18.65	208.21	34.04	18.01	2.257
96.68	19.14	214.31	34.92	19.99	2.743
101.90	19.93	220.18	35.61	22.25	3.318
107.15	20.74	226.02	36.41	24.84	4.008
111.99	21.46	228.80	36.80	27.59	4.738
117.07	22.21	234.94	37.62	30.56	5.539
122.32	22.93	241.17	38.63	33.75	6.391
127.74	23.72	247.53	39.52	37.18	7.274
133.25	24.45	253.74	40.40	41.05	8.220
139.61	25.30	259.61	41.24	45.38	9.265
144.96	26.02	266.14	42.35	50.12	10.372
150.34	26.72	272.95	43.51	55.24	11.479

TABLE IV

THERMODYNAMIC PROPERTIES OF L-VALINE, CAL. DEG.$^{-1}$ MOLE^{-1}

T, °K.	$C_p°$	$S°$	$\frac{H° - H_0°}{T}$	$-\frac{(F° - H_0°)}{T}$
10	0.263	0.095	0.070	0.025
15	.763	.288	.211	.077
20	1.581	.615	.447	.168
25	2.554	1.070	.769	.301
30	3.627	1.629	1.155	.474
35	4.746	2.273	1.588	.685
40	5.847	2.978	2.052	.927
45	6.941	3.731	2.535	1.196
50	8.006	4.517	3.029	1.488
55	9.052	5.330	3.529	1.801
60	10.06	6.161	4.032	2.129
70	11.96	7.857	5.031	2.826
80	13.77	9.573	6.011	3.562
90	15.47	11.29	6.969	4.326
100	17.05	13.01	7.899	5.108
110	18.54	14.70	8.799	5.904
120	19.97	16.38	9.671	6.707
130	21.31	18.03	10.52	7.514
140	22.60	19.66	11.33	8.324
150	23.86	21.26	12.13	9.132
160	25.09	22.84	12.90	9.940
170	26.27	24.39	13.65	10.74
180	27.42	25.93	14.38	11.55
190	28.53	27.44	15.10	12.34
200	29.61	28.93	15.80	13.13
210	30.69	30.40	16.48	13.92
220	31.79	31.86	17.15	14.70
230	32.88	33.29	17.81	15.48
240	33.95	34.71	18.46	16.25
250	35.04	36.12	19.10	17.02
260	36.13	37.52	19.74	17.78
270	37.25	38.90	20.36	18.54
280	38.36	40.28	20.99	19.29
290	39.45	41.64	21.61	20.04
300	40.56	43.00	22.22	20.78
310	41.66	44.35	22.83	21.52
273.15	37.59	39.34	20.56	18.77
298.15	40.35	42.75	22.11	20.64
310.15	41.68	44.37	22.84	21.53

TABLE V

THERMODYNAMIC PROPERTIES OF L-ISOLEUCINE, CAL. DEG.$^{-1}$ MOLE^{-1}

T, °K.	$C_p°$	$S°$	$\frac{H° - H_0°}{T}$	$-\frac{(F° - H_0°)}{T}$
10	0.655	0.283	0.200	0.083
15	1.516	.702	.488	.215
20	2.582	1.281	.875	.406
25	3.781	1.984	1.334	.649
30	5.003	2.781	1.844	.937
35	6.243	3.646	2.384	1.262
40	7.462	4.559	2.943	1.616
45	8.657	5.508	3.512	1.996
50	9.818	6.480	4.085	2.396
55	10.95	7.469	4.658	2.812
60	12.04	8.469	5.228	3.241
70	14.09	10.48	6.349	4.132
80	16.05	12.49	7.440	5.051
90	17.90	14.49	8.501	5.989
100	19.55	16.46	9.524	6.938
110	21.13	18.40	10.51	7.892
120	22.63	20.30	11.46	8.847
130	24.05	22.17	12.37	9.800
140	25.42	24.00	13.25	10.75
150	26.74	25.80	14.11	11.69
160	28.02	27.57	14.94	12.63
170	29.29	29.31	15.75	13.56
180	30.52	31.02	16.53	14.48
190	31.72	32.70	17.30	15.40
200	32.90	34.35	18.05	16.30
210	34.08	35.99	18.79	17.20
220	35.26	37.60	19.51	18.09
230	36.47	39.19	20.22	18.98
240	37.70	40.77	20.92	19.85
250	38.95	42.34	21.62	20.72
260	40.19	43.89	22.31	21.58
270	41.41	45.43	22.99	22.44
280	42.67	46.96	23.67	23.28
290	43.92	48.48	24.35	24.13
300	45.24	49.99	25.02	24.96
310	46.58	51.49	25.70	25.79
273.15	41.81	45.91	23.21	22.70
298.15	45.00	49.71	24.90	24.81
310.15	46.60	51.51	25.71	25.81

paper apply.[2] Analyses of the individual experiments indicated that curvature corrections were unnecessary within the limits of accuracy claimed.[6] The values given for $\Delta H/\Delta T$ are therefore equal to C_p at the specified temperatures. The thermodynamic properties of L-valine, derived from the data of Table I, are given in Table IV. Similar data for L-isoleucine and L-leucine are given in Tables V and VI, respectively.

Discussion

Using the entropy data reported here and in an earlier paper,[2] we have calculated the values of the standard entropies of formation from the elements at 298.15°K., $\Delta S_f°$, given in Table VII. Values for the entropies of the elements were taken from National Bureau of Standards Circular 500.[7] To obtain the values of the standard enthalpies of formation, $\Delta H_f°$, in Table VII, we proceeded as follows. Heats of combustion, ΔE_B, given by Tsuzuki, *et al.*,[3,4] were corrected to the standard internal energy change $\Delta E_c°$ by Prosen's method.[8] Professor Herschel Hunt kindly supplied the necessary ancillary data. Then $\Delta H_c° = \Delta E_c° + \Delta(PV)°$. In calculating $\Delta H_f°$, the values taken

(8) E. J. Prosen, in "Experimental Thermochemistry," F. D. Rossini, Ed., Interscience Publishers, Inc., New York, N. Y., 1956, Chapter 6.

TABLE VI

THERMODYNAMIC PROPERTIES OF L-LEUCINE, CAL. DEG.$^{-1}$ MOLE^{-1}

T, °K.	C_p°	S°	$\frac{H° - H_0°}{T}$	$\frac{-(F° - H_0°)}{T}$
10	0.586	0.207	0.154	0.053
15	1.546	.613	.447	.166
20	2.749	1.220	.870	.350
25	4.047	1.971	1.374	.597
30	5.385	2.827	1.931	.897
35	6.710	3.758	2.520	1.238
40	7.963	4.736	3.122	1.614
45	9.178	5.745	3.728	2.017
50	10.34	6.773	4.332	2.441
55	11.43	7.810	4.928	2.882
60	12.47	8.849	5.513	3.336
70	14.44	10.92	6.649	4.272
80	16.30	12.97	7.741	5.231
90	18.03	14.99	8.790	6.204
100	19.65	16.98	9.796	7.182
110	21.16	18.92	10.76	8.162
120	22.62	20.83	11.69	9.138
130	24.02	22.69	12.59	10.11
140	25.37	24.52	13.45	11.07
150	26.68	26.32	14.29	12.03
160	27.97	28.08	15.10	12.98
170	29.25	29.82	15.90	13.92
180	30.52	31.52	16.67	14.85
190	31.77	33.21	17.44	15.77
200	33.01	34.87	18.18	16.68
210	34.28	36.51	18.92	17.59
220	35.59	38.13	19.65	18.49
230	36.95	39.75	20.37	19.38
240	38.35	41.35	21.09	20.26
250	39.80	42.94	21.81	21.13
260	41.33	44.53	22.53	22.00
270	42.95	46.12	23.26	22.87
280	44.64	47.71	23.99	23.73
290	46.44	49.31	24.73	24.58
300	48.40	50.92	25.49	25.43
310	50.52	52.54	26.26	26.28
273.15	43.47	46.62	23.49	23.14
298.15	48.03	50.62	25.35	25.27
310.15	50.55	52.56	26.27	26.29

for $\Delta H_f°$ of CO_2 and H_2O were, respectively, -94.0518 and -68.3174 kcal. mole^{-1}.

TABLE VII

THERMODYNAMIC PROPERTIES OF SOME AMINO ACIDS AT 298.15°K.

Substance	$-\Delta S_f°$, cal. mole^{-1} deg.$^{-1}$	$-\Delta H_f°$, kcal. mole^{-1}	$-\Delta F_f°$, kcal. mole^{-1}
Glycine(s)	127.96	128.4	90.3
L-Alanine(s)	154.33	134.5	88.5
L-Valine(s)	207.60	147.7	85.8
L-Isoleucine(s)	233.21	152.5	83.0
L-Leucine(s)	232.30	154.6	85.4

The values given in Table VII for glycine and L-leucine require comment regarding their reliability. As stated, we have used the recent combustion data of Tsuzuki, *et al.*,[3,4] without regard for older values of the heats of combustion of glycine and L-leucine. We have done this (a) because the new values were obtained by burning samples of the materials removed from our calorimeter following the heat capacity measurements reported here, and (b) because we wished to make clear the full magnitude of any discrepancies resulting from the new *vs.* old values.

Huffman, Fox, and Ellis[9] give values of $-\Delta E_B$ as 3103.0 ± 0.3 cal. g.$^{-1}$ for glycine and 6520.7 ± 0.7 cal. g.$^{-1}$ for L-leucine. Huffman, Ellis, and Fox[10] give 4346.5 ± 0.7 cal. g.$^{-1}$ for D-alanine. We have recalculated their data using the molecular weights currently accepted and modern values for the heats of formation of CO_2 and H_2O. The chief difference between their calculations and ours arises from their use of $\Delta H_f° = 94.24$ kcal. mole^{-1} for CO_2. The Washburn corrections applied by them are very near (10–40 cal.) the corrections calculated by us for Hunt's data using Prosen's method. Therefore, we have employed the original corrections.[9,10] We find the value of $\Delta H_f°_{298.15}$ in kcal. mole^{-1} to be -126.32 for glycine, -134.11 for D-alanine, and -152.34 for L-leucine, which should be compared with the values given in Table VII. There are no previously reported values for any form of isoleucine or valine.

The differences in heats of combustion of glycine and L-leucine described above are so large that we can only attribute them to the burning of different compounds or to methodological errors which we are unable to identify. Older preparations of leucine were frequently impure.[11] On the other hand, impurities in glycine seem an unlikely explanation. Because of the small heat of combustion per gram of this substance, however, only a small percentage of impurity in the form of another amino acid could produce a marked elevation in the heat of combustion. Obviously, additional and independent studies of these heats of combustion are desirable.

In view of the above discussion, minor differences in entropies of these substances seem unimportant. The only comparison to be made here is between our measurements on L-leucine and those reported by Huffman and Ellis.[12] They give $S°_{298.1} - S°_{90}$ a value of 35.61 cal. mole^{-1} deg.$^{-1}$, whereas we find $S°_{298.15} - S°_{90}$ to be 35.63 cal. mole^{-1} deg.$^{-1}$. Our experimental value for $S°_{90}$ is 14.99 cal. mole^{-1} deg.$^{-1}$, which is 1.09 cal. mole^{-1} deg.$^{-1}$ higher than the one they obtained by extrapolation. In contrast, extrapolation procedures yielded a higher figure than the experimental one for L-alanine and glycine.[2] It therefore seems impossible to apply any consistent rule in the correction of these older entropy values. There are no previously reported entropies for any form of isoleucine or valine.

(9) H. M. Huffman, S. W. Fox, and E. L. Ellis, *J. Am. Chem. Soc.*, **59**, 2144 (1937).

(10) H. M. Huffman, E. L. Ellis, and S. W. Fox, *ibid.*, **58**, 1728 (1936).

(11) J. P. Greenstein and M. Wenitz, "Chemistry of the Amino Acids," Vol. 2, John Wiley and Sons, New York, N. Y., 1961.

(12) H. M. Huffman and E. L. Ellis, *J. Am. Chem. Soc.*, **59**, 2150 (1937).

THE BASICITY IN WATER OF α,β,γ,δ-TETRA-(4-PYRIDYL)-PORPHINE[1]

BY EVERLY B. FLEISCHER AND L. E. WEBB[2]

George Herbert Jones Laboratory, University of Chicago, Chicago 37, Illinois

Received December 1, 1962

The equilibrium constant for the addition of two protons to the free base form of a water-soluble porphyrin, α,β,γ,δ-tetra-(4-pyridyl)-porphine, was determined by spectrophotometric titration. Spectral data show that the intermediate monocation of this porphyrin is either in low concentration or does not exist in solution. Alkali metal and alkaline earth ions enter into equilibria with the free base form of the porphyrin. Since these ions and hydrogen ions change the porphyrin spectrum in a similar manner, buffer solutions containing alkali metal or alkaline earth ions should not be used for the spectrophotometric determination of porphyrin basicity.

The interpretation of data from previous work on the basicities of porphyrin compounds is complicated by the fact that most studies have been carried out in non-aqueous or phase-partioned systems because of the low solubility of porphyrins in water. Studies in aqueous systems have included buffer solutions whose effect on porphyrins was not understood. In his review of porphyrin ionization behavior, Phillips discusses these investigations and some of the difficulties in their interpretation.[3]

The species involved in the present work are the free base, monocation, and dication as shown in Fig. 1. The terms monocation and dication do not refer to the charge of the entire molecule but only to the positive charge associated with the pyrrole ring nitrogens. The concentration quotients for the dissociation of protons from the pyrrole nitrogen atoms are here defined as

$$k_1 = c_1 a/c_2 \qquad k_2 = c_0 a/c_1$$

and the thermodynamic equilibrium constants are

$$K_1 = k_1 \frac{\gamma_1}{\gamma_2} \qquad K_2 = k_2 \frac{\gamma_0}{\gamma_1}$$

where c_0, c_1, and c_2 refer to the concentrations of the free base, monocation, and dication, respectively, γ_0, γ_1, and γ_2 are the activity coefficients of these species, and "a" is the hydrogen ion activity. Molar extinction coefficients will be designated by ϵ, where ϵ_0, ϵ_1, and ϵ_2 refer to the extinctions of the free base, monocation and dication, respectively.

Almost all of the direct measurements of porphyrin basicities in aqueous solution have been done by Neuberger and Scott, who obtained values for k_1 and k_2 from spectra which, they said, established the existence of monocations of certain porphyrins in aqueous solution.[4] However, they used buffer solutions which contained sodium and potassium ions. Since we have found that these ions change the spectrum of the free base form, as shown below, we believe Neuberger and Scott's results to be somewhat questionable. They used porphyrins with carboxylic and sulfonic acid groups attached to the conjugated ring to maintain a desirable water solubility. However, these groups may interact with the ring electronically and cause spectral changes, especially since these groups would be expected to ionize in the pH range used by Neuberger and Scott in their spectrophotometric titrations.

α,β,γ,δ-Tetra-(4-pyridyl)-porphine (hereafter denoted as TPyP) was employed in our investigation of porphyrin acid–base equilibria. Aqueous, unbuffered HCl solutions of TPyP were used in spectrophotometric titrations. The pyridyl groups make this porphyrin soluble in aqueous solutions having a pH lower than about 2.5, and the free base form has the structure shown in Fig. 1d, in solutions of this acidity. The hydrogen ions bonded to the pyridine nitrogen atoms would not be expected to dissociate in the pH range of 0 to 2 used in this study. Steric models show that the pyridyl groups cannot be in the plane of the conjugated ring. Therefore, spectra taken at various concentrations of HCl should not be complicated by changes resulting from interactions of the pyridyl group with the porphyrin ring.

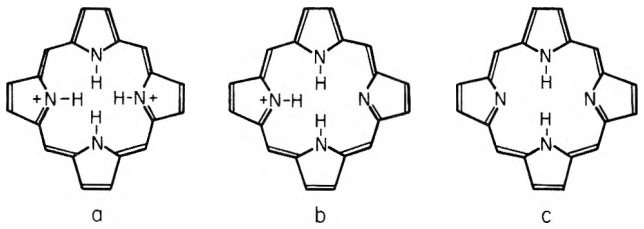

Fig. 1.—(a) Porphyrin dication; (b) monocation; (c) free base. Side chains are omitted for clarity.

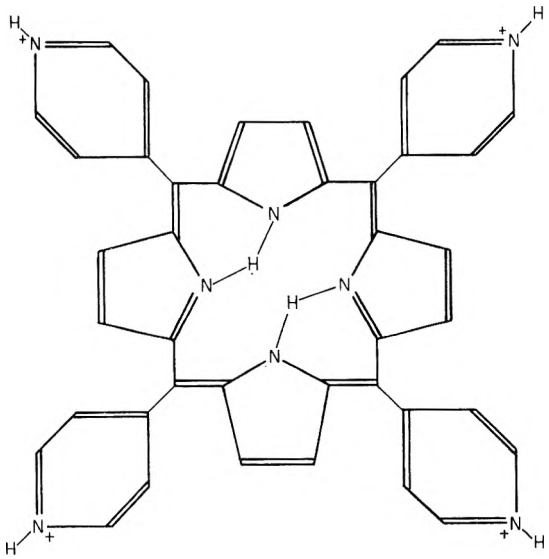

Fig. 1d.—Free base form of α,β,γ,δ-tetra-(4-pyridyl)-porphine in solutions having a pH lower than about 2.5.

Data on the TPyP spectra in various solvents have been reported.[5] The spectrum of an aqueous HCl solution of TPyP at a pH of 2.3 is similar to the spec-

(1) This work was supported by a Public Health Service Grant and a Block Fund Grant.

(2) National Science Foundation Summer Predoctoral Fellow.

(3) J. N. Phillips, *Rev. Pure. Appl. Chem.* (Australia), **10**, 35 (1960).

(4) A. Neuberger and J. J. Scott, *Proc. Roy. Soc.* (London), **A213**, 307 (1952).

(5) E. B. Fleischer, *Inorg. Chem.*, **1**, 493 (1962).

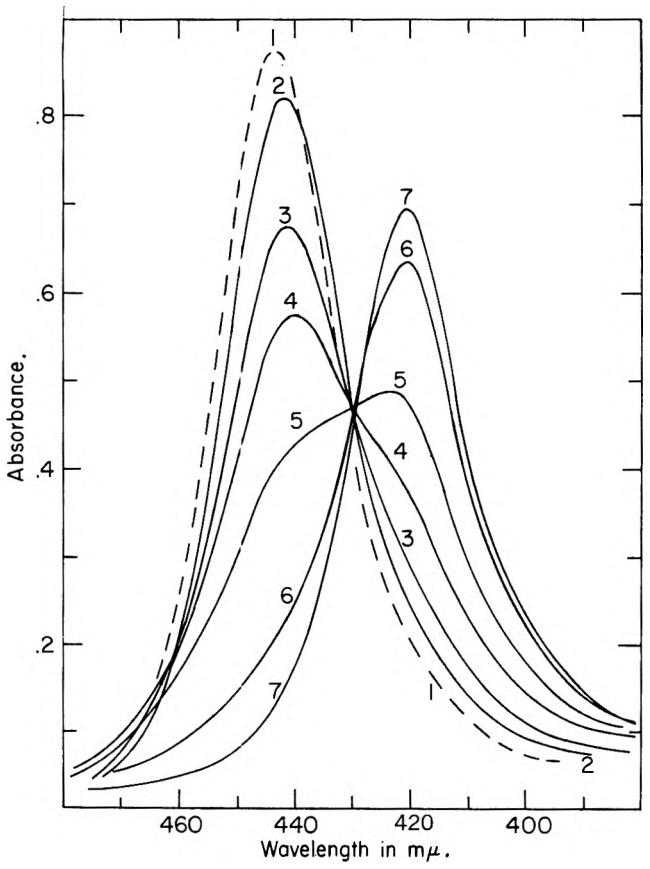

Fig. 2.—Soret band spectra of aqueous solutions of $\alpha,\beta,\gamma,\delta$-tetra-(4-pyridyl)-porphine.

Solution	pH value[a]
1	0.00 ± 0.05
2	.57
3	.85
4	1.03
5	1.22
6	1.62
7	2.30

Spectrum number one is shown as a dotted line because it is believed to be shifted from the isobestic point by the high ionic strength.

[a] The experimental values agreed to within 0.03 pH unit with values calculated assuming the pH in the hydrochloric acid to be given by pH = $-\log a_{HCl}$.

trum in organic solvents. This indicates that TPyP exists at this pH in the free base form shown in Fig. 1c.

Experimental Procedures.—The TPyP was synthesized and purified as described previously.[5] Aqueous HCl solutions of the porphyrin were prepared by adding measured volumes of standard HCl to TPyP. Measurements of pH were taken on a Coleman Companion pH meter using standardizing buffer solutions. The spectra were taken in 10.0 mm. matched cells in a Cary Model 14 spectrophotometer. All salts added to the TPyP solutions were Reagent Grade.

Results

It was found that aqueous TPyP solutions at a pH of 1.0 followed Beer's law for porphyrin concentrations ranging from 4.5×10^{-6} to 9.0×10^{-5} M in the visible region and from 2.0×10^{-7} to 4.0×10^{-6} M in the Soret region. The Soret band spectra for aqueous HCl solutions of 2.89×10^{-6} M TPyP are shown in Fig. 2. The pH of the solutions ranged from 2.3 to 0.0.

Since the absorbance at 442 mμ reaches a maximum at a pH of zero, the TPyP is assumed to be all in the acid form, either monocation or dication, at this pH.

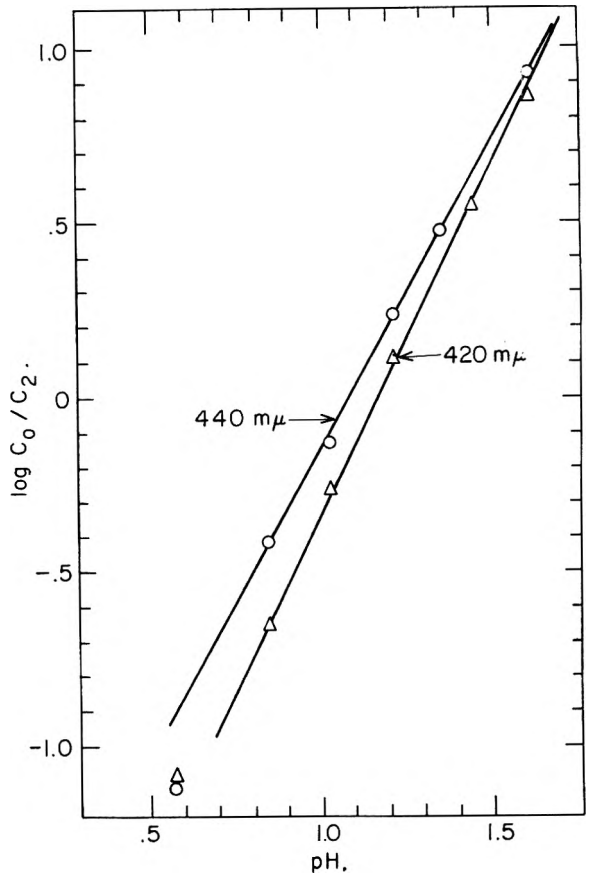

Fig. 3.—Log $(D_A - D)/(D - D_B)$ *vs.* pH at two wave lengths for aqueous HCl solutions of $\alpha,\beta,\gamma,\delta$-tetra-(4-pyridyl)-porphine. The slopes are 2.00 at 442 mμ and 1.75 at 420 mμ.

Several interpretations of the isobestic point are possible. First, the acidity may not be high enough for the dication to be formed. In this case $(D_A - D)/(D - D_B) = c_0/c_1$ where D_A is the absorbance at a pH of 0.0, D_B is the absorbance at a pH of 2.3, and D is the absorbance at an intermediate pH. But, since $(H^+)(D_A - D)/(D - D_B)$ varies by at least a factor of five as the acidity is changed, whereas $(H^+)^2(D_A - D)/(D - D_B)$ is relatively constant, c_2 must not be equal to zero, and the two protons are adding to the free base with the formation of the porphyrin dication.

The only other possible conditions which could result in an isobestic point are: (1) $c_1 = 0$ and $\epsilon_0 = \epsilon_2$ at the isobestic point and (2) $c_1 \neq 0$ and $\epsilon_0 = \epsilon_1 = \epsilon_2$ at the isobestic point. If c_1 is equal to zero, $(D_A - D)/(D - D_B) = c_0/c_2$. Since it was found in preliminary calculations that $(H^+)^2(D_A - D)/(D - D_B)$ was relatively constant, the hypothesis that $c_1 = 0$ and therefore that the quantity $[(D_A - D)/(D - D_B)]a^2\ \gamma_0/\gamma_2$ represented the over-all equilibrium constant $K = K_1K_2$ was tested with the results shown in Fig. 3 and Table I.

TABLE I

CALCULATED pK AND k VALUES FOR TPyP

Wave length, mμ	pK	k[a]
420	1.18	4.4×10^{-3}
442	1.09	6.5×10^{-3}
Av.	1.14	5.4×10^{-3}

[a] $k = k_1k_2$.

The linear plot of Fig. 3 can be explained by the equation $\log (c_0/c_2) = 2\text{pH} + \log K - \log \gamma_0/\gamma_2 =$

2pH + log k. If the activity coefficient ratio is constant and $c_1 = 0$, a graph of log $[(D_A - D)/(D - D_B)]$ *vs.* pH should be linear with a slope of 2. The pK is given by the zero intercept on the pH axis. The linear form of the plot obtained with our data, the fact that the slope is nearly 2.0, and the agreement of the pK values at two different wave lengths all support the hypothesis that c_1 is zero or very small.

The second possibility for the explanation of the isobestic point, that of equal extinction coefficients of all three species at the isobestic point can be eliminated because a plot of log $[(D_A - D)/(D - D_B)]$ *vs.* pH would not be linear. Thus, the assumption in accordance with experiment is that the concentration of the intermediate monocation is zero or negligibly small.

The hitherto unrecognized effect of buffer solutions and salts added to maintain constant ionic strength, which are commonly used in spectroscopic study of porphyrins, has contributed to much of the confusion of past work. As shown in Fig. 4, lithium, sodium, and potassium ions change the spectra of the free base form of TPyP at a pH of 2 in water to spectra similar to that of the dication acid form. Apparently the alkali metal ions are associating with the porphyrin in the same way as hydrogen ions. Addition of $CdCl_2$, $MgCl_2$, $SrCl_2$, or $CaCl_2$ also changed the spectrum. The results are summarized in Table II.

TABLE II

MAXIMUM MOLAR EXTINCTION COEFFICIENTS OF TPyP SOLUTIONS 1.8 *M* IN VARIOUS SALTS

A HCl solution at a pH of 0.0 with no added salt is included for comparison

Added compound	Absorption max. (mμ)	($\epsilon \times 10^{-4}$) (l. mole^{-1} cm.$^{-1}$)
HCl	442	2.9
LiCl	443	2.0
NaCl	442	1.8
KCl	442	1.7
$CdCl_2$	443	2.3
$MgCl_2$	445	2.4
$SrCl_2$	445	2.4
$CaCl_2$	445	2.5

Discussion

The absence of an intermediate monocation might imply a trimolecular reaction with simultaneous addition of two protons. This has been considered unlikely because of electrostatic repulsion.[4] A small or zero value of c_1 implies that k_2 is much greater than k_1. In other words, the addition of the first proton creates an unstable species which is immediately protonated to the dication form. Lack of evidence for a monocation in spectrophotometric titrations has been reported for other porphyrins.[6,7]

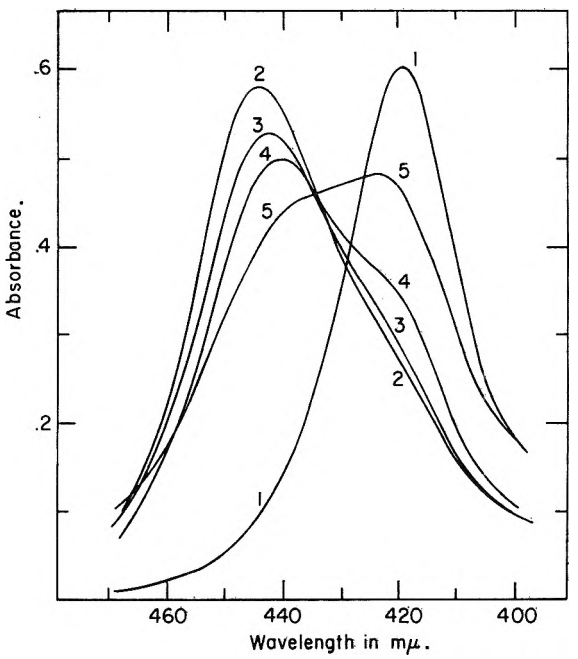

Fig. 4.—Effect on addition of alkali metal ions on the spectra of TPyP. Spectrum no. 1 is of the free base form at a pH of 2.0. The other spectra are of the same solution with salt concentrations as follows: (2) 1.8 *M* LiCl; (3) 1.8 *M* NaCl; (4) 1.8 *M* KCl; (5) 1.0 *M* KCl.

The present work leads to the following conclusions. First, the pK for the dissociation of two protons from the dication of TPyP is about 1.1. The low value of the pK is explained by the high positive charge on the molecule. More important than the absolute pK value is the conclusion that the concentration of the monocation of TPyP is either zero or very small, which implies that k_2 is much greater than k_1. Finally, attention is directed to the spectral changes of the TPyP caused by the alkali metal and alkaline earth metal ions. The free base porphyrin and these metal ions enter into an equilibrium which, interestingly, is similar to the hydrogen ion equilibrium with the free base. This phenomenon merits further investigation.

Acknowledgments.—We wish to thank Mr. Richard Palmer for his helpful assistance in this investigation.

(6) S. Aronoff, *J. Phys. Chem.*, **62**, 428 (1958).
(7) S. Aronoff and C. A. Weast, *J. Org. Chem.*, **6**, 550 (1941).

INTRAMOLECULAR ENERGY TRANSFER IN UNIMOLECULAR REACTIONS. II. A WEAKLY-COUPLED-OSCILLATORS MODEL[1]

BY JOSEPH W. BRAUNER AND DAVID J. WILSON

Department of Chemistry, University of Rochester, Rochester 20, New York

Received December 12, 1962

Intramolecular energy transfer in a reactant molecule during the time intervals between collisions is treated as a Markov process in which single quanta of vibrational energy are transferred randomly between the s weakly coupled, degenerate harmonic oscillators representing the reactant molecule. The resulting differential-difference equations are solved exactly for all the eigenvalues for the relaxation of a system in which no chemical reaction occurs. An approximation method is used for the case in which chemical reaction occurs, and a previously derived formalism[4] is used to calculate log–log plots of unimolecular rate constants *vs.* pressure. The effects of the magnitude of the oscillator–oscillator coupling parameter are investigated, and comparison is made with Kassel's theory.[2]

Introduction

In the distant past, Rice, Ramsperger, and Kassel (RRK) developed the theory of unimolecular rates which has been the workhorse theory for interpreting unimolecular rates ever since.[2] Conceptually, their approach is very simple. One takes the simplest sort of collision mechanism and combines it with the simplest sort of model for a molecule which permits one to take into account the number of degrees of freedom possessed by the molecule. The resulting theory permits ready computation of plots of unimolecular rate constants as functions of pressure,[3] in marked contrast to the more recent theories.[4]

Interestingly enough, the very simple model of RRK theory provides plots of rate constants *vs.* pressure which are generally in good agreement with experimental data, and which are amazingly similar to the plots computed from the more recent theories. In Kassel theory the salient assumptions are two. One assumes a strong collision mechanism, whereby any activated molecule is deactivated to a thermal equilibrium distribution on suffering a single collision. The reactant molecules are represented by sets of "weakly coupled" oscillators, and intramolecular energy transfer takes place by a random scrambling process whereby the distribution of energy among the oscillators at any instant is completely independent of the distribution immediately preceding it. Thus, the intramolecular energy transfer mechanism is represented by a coupling between the oscillators which is sufficiently weak that one may neglect the energy stored in the coupling mechanism, yet sufficiently strong to obliterate completely any correlation between consecutive distributions of energy in the set of oscillators representing a molecule.

We had previously investigated[4f] in some detail what happens when one replaces the strong collision assumption of RRK theory by a stepwise collision mechanism of the sort investigated by Shuler and his collaborators.[5] We were somewhat surprised to find that the major change in the nature of the collision mechanism made no significant difference in the appearance of plots of rate constant *vs.* pressure. At about the same time we briefly investigated some of the qualitative implications of passing from the RRK type of coupled oscillators model, in which the intramolecular energy transfer involves at least moderately strong coupling, to a truly weakly coupled oscillators model.[6] We concluded that, qualitatively, a truly weak intramolecular energy transfer process should lead to plots of log rate constant *vs.* log pressure which show a broader transition region between the low and high pressure limits than are shown by the corresponding RRK curves. The present paper describes the results obtained by numerical analysis of one such truly weakly coupled model for intramolecular energy transfer. Our justifications for treating such a naive model are (1) the success of RRK theory and its more recent modification at the hands of Marcus,[4d] (2) the probable inadequacy of the harmonic approximation of Slater's theory,[4b] and (3) the fact that employment of Slater's "new approach to rate theory"[4b,7] involves such great computational difficulties for even the simplest cases[4a,4c,8-11] as to make the analysis of such molecules as N_2O_5, cyclopropane, etc., utterly out of the question at present. In all probability, Slater's "new approach" and the machine computations for small molecules will have their chief application in the construction of reasonably tractable models, the parameters of which may be assigned more or less in terms of molecular parameters (number of degrees of freedom, the nature of the reaction coördinate, vibration frequencies and so on); these models should be consistent with Slater's new approach and with the machine computations. The RRK and Marcus approaches are of this type, and it is in this spirit that the calculations outlined below were done.

The Model

The model of a reactant molecule we used is very similar to that employed by Kassel in his simple quantum theory of unimolecular reaction rates. The mole-

(1) This work was supported by the National Science Foundation.

(2) See L. S. Kassel, "Kinetics of Homogeneous Gas Reactions," Chemical Catalog Company, New York, N. Y., 1932, for a discussion and references.

(3) (a) R. E. Powell, *J. Chem. Phys.*, **30**, 724 (1959); (b) E. W. Schlag, B. S. Rabinovitch, and F. W. Schneider, *ibid.*, **32**, 1599 (1960); (c) E. M. Willbanks, "The Evaluation of the Kassel Integral *via* IBM 704," Los Alamos Scientific Laboratory, Report LA-2178, 1958. Available from the Office of Technical Services, U. S. Dept. of Commerce, Washington 25, D. C.

(4) (a) D. L. Bunker, *J. Chem. Phys.*, **37**, 393 (1962); (b) N. B. Slater, "Theory of Unimolecular Gas Reactions," Cornell University Press, Ithaca, N. Y., 1959; (c) E. Thiele and D. J. Wilson, *J. Chem. Phys.*, **35**, 1256 (1961); (d) R. A. Marcus, *ibid.*, **20**, 352, 355, 359, 364 (1952). See also G. M. Wieder, Ph.D. Thesis, Polytechnic Institute of Brooklyn, 1961; (e) F. P. Buff and D. J. Wilson, *J. Am. Chem. Soc.*, **84**, 4063 (1962); (f) F. P. Buff and D. J. Wilson, *J. Chem. Phys.*, **32**, 677 (1960).

(5) The most recent in the series of papers by these workers is K. E. Shuler, G. H. Weiss, and K. Anderson, *J. Math. Phys.*, **3**, 550 (1962).

(6) D. J. Wilson, *J. Phys. Chem.*, **64**, 323 (1960).

(7) E. Thiele, *J. Chem. Phys.*, **36**, 1466 (1962).

(8) F. P. Buff and D. J. Wilson, *J. Am. Chem. Soc.*, **84**, 4063 (1962).

(9) E. Thiele, private communication. We are indebted to Dr. Thiele for informing us of his results prior to their publication.

(10) A. Kuppermann, private communication. We are similarly indebted to Professor Kuppermann.

(11) N. Chow Hung and D. J. Wilson, *J. Chem. Phys.*, **38**, 828 (1963).

cule is represented as a collection of s degenerate quantum harmonic oscillators, and reaction may occur whenever a particular oscillator, the reactive oscillator, acquires a critical number, n^*, of quanta. We do not assume (as Kassel does) a completely random redistribution of quanta among the oscillators roughly every $1/\nu$ seconds; we consider a Markov process in which each new distribution of energy depends strongly on the preceding distribution.

We postulate that the intramolecular energy transfer probabilities are of the same form as the concurrent collisional transition probabilities for simultaneous changes in vibrational excitation of two colliding harmonic oscillators employed by Shuler.[12] This is consistent with our assumption of a weakly-interacting-oscillators model, as discussed in Shuler's paper. Therefore for joint intramolecular transition between two oscillators in the hypothetical molecule we write

$$\begin{aligned} P_{n,n+1;m,m-1} &= \alpha(n+1)(m) \\ P_{n,n-1;m,m+1} &= \alpha(n)(m+1) \end{aligned} \qquad (1)$$

where $P_{n,n+1;m,m-1}$ is the probability per unit time for the joint transition $n \rightarrow n+1$, $m \rightarrow m-1$ for the two oscillators, and α is a proportionality constant.

If we let $A(i_1, i_2, \ldots i_s)$ be the concentration of reactant molecules having i_1 quanta in the first oscillator, etc., then we can write out the equations governing the time dependence of this concentration in the absence of collisions and chemical reaction. For even small values of s and n (the total number of quanta in each molecule; $n = \sum_{k=1}^{s} i_k$), these equations are quite unwieldy. However, in a given chemical reaction it is often one particular reaction coördinate of the reactant molecule which attains a critical value; we let the reaction coördinate's degree of freedom correspond to oscillator number 1. The remainder of the reactant molecule we represent as an $(s-1)$-fold degenerate oscillator containing $(n - i_1)$ quanta; the reactive oscillator then undergoes joint transitions with this $(s-1)$-degenerate oscillator. We generalize[11] the transition probabilities of equations 1 to describe the joint transitions of a 1-oscillator and an $(s-1)$-oscillator; the result is

$$\begin{aligned} P(i_1, n-i_1;\ i_1+1, n-i_1-1) &= \alpha(i_1+1)(n-i_1) \\ P(i_1, n-i_1;\ i_1-1, n-i_1+1) &= \alpha i_1(n+s-i_1-1) \end{aligned} \qquad (2)$$

where $P(i_1, n-i_1;\ i_1+1, n-i_1-1)$ is the probability per unit time that one quantum will be transferred to the reactive oscillator from the rest of the molecule, and n is the total number of quanta in the molecule.

Let A_{in} be the concentration of reactant molecules having a total of n quanta, i of which are in the reactive oscillator. Then, in the absence of external perturbations and terms corresponding to chemical reaction

$$\begin{aligned} \frac{dA_{in}}{dt} &= \alpha(i+1)(n+s-i-2)A_{i+1,n} + \\ &\quad \alpha i(n-i+1)A_{i-1,n} - \alpha[(i+1)(n-i) + \\ &\quad i(n+s-i-1)]A_{in},\ i = 0, 1, 2, \ldots n \end{aligned} \qquad (3)$$

(12) K. E. Shuler, *J. Chem. Phys.*, **32**, 1692 (1960); see also A. I. Osipov, *Doklady Akad. Nauk SSSR*, **130**, 523 (1960).

or, more compactly in matrix notation

$$\frac{d\mathbf{A}_n}{dt} = \mathbf{M}^{(n)}\mathbf{A}_n$$

In the usual manner, this set of linear, coupled differential equations can be converted into an eigenvalue problem by the substitution $A_{in} = B_{in}\, e^{\lambda t}$. We found empirically that the eigenvalues of the matrix $\mathbf{M}^{(n)}$ are given by

$$\begin{aligned} -\lambda_k &= (k-1)(k+s-2)\alpha \\ k &= 1, 2, \ldots n, n+1 \end{aligned} \qquad (4)$$

We are indebted to Mrs. P. J. Eberlein, of the Computing Center of the University of Rochester for a proof of this result: her proof will be published elsewhere.[13]

The effect of chemical reaction may be introduced into equations 3 by assuming that a molecule dissociates with a rate constant ν whenever the number of quanta in the reactive oscillator exceeds some critical value n^*. We introduce a term $-\nu$ into the $(n^*+1)^{th}$ and subsequent main diagonal elements of the matrix $\mathbf{M}^{(n)}$, $n \geqslant n^*$. We would more or less expect ν to be the order of molecular vibration frequencies, and, since this is the microscopic decomposition rate of a single oscillator, it is reasonable that it be approximated as constant.

Introduction of chemical reaction may be looked upon as a perturbation of the relaxing system; and the eigenvalues of the perturbed energy transfer matrix will be perturbed to new values less than or equal to the corresponding eigenvalues of the unperturbed matrix, since the perturbation is negative semidefinite.[14] In particular, λ_1, which is zero (according to equation 4) in the absence of chemical reaction, will be perturbed to a small negative value. The results of hand calculation on simple cases indicate that the only eigenvalue for which $\Delta\lambda_j$, the perturbation, is comparable to or larger than λ_j in magnitude, is λ_1. We shall accept the unperturbed values of the λ_j, $j \neq 1$, as adequate approximations and calculate improved values for the λ_1.

First, we employ a perturbation method which, as we shall see, yields Kassel's result for the rate of decomposition of activated molecules. The principle of detailed balance applied to an isolated molecule yields

$$M_{ji}^{(n)} g_{s-1}(i) = M_{ij}^{(n)} g_{s-1}(j) \qquad (5)$$

where $g_s(m) = (m+s-1)!/[m!(s-1)!]$

We perform a similar transformation on $\mathbf{M}^{(n)}$

$$\mu_{ji}^{(n)} = [g_{s-1}(j)]^{-1/2} M_{ji} [g_{s-1}(i)]^{-1/2} \qquad (6)$$

This converts $\mathbf{M}^{(n)}$ into a symmetric matrix $\boldsymbol{\mu}^{(n)}$ having the same eigenvalues. One can then readily show that

$$\tilde{\mathbf{X}}_1^{(n)} = [(g_{s-1}(n))^{1/2}, (g_{s-1}(n-1))^{1/2}, \ldots (g_{s-1}(0))^{1/2}] \qquad (7)$$

is the eigenvector of $\boldsymbol{\mu}^{(n)}$ corresponding to $\lambda_1 = 0$ by direct multiplication

(13) See also, J. Brauner, Ph.D. Thesis, The University of Rochester, 1962, p. 32.

(14) R. Courant and D. Hilbert, "Methods of Mathematical Physics," Interscience Publishers, New York, N. Y., 1953.

$$\mathbf{u}^{(n)}\mathbf{X}_2^{(n)} = \mathbf{0}$$

The perturbation is approximately given by

$$\Delta\lambda_1 = \tilde{\mathbf{X}}_1^{(n)} \begin{bmatrix} 0 & 0 & \cdot & \cdot & & 0 \\ 0 & 0 & & & & \\ \cdot & & & & & \\ \cdot & & 0 & & & \\ \cdot & & & -\nu^0 & & \\ & & & 0 & -\nu & \\ & & & & & \ddots \\ 0 & & & & & -\nu \end{bmatrix} \tilde{\mathbf{X}}_1^{(n)}/\tilde{\mathbf{X}}_1^{(n)}\mathbf{X}_1^{(n)} \quad (8)$$

where all the elements of the matrix vanish except those along the main diagonal which correspond to n^* or more quanta in the reactive oscillator. Doing the multiplication indicated and simplifying yields

$$\Delta\lambda_1 = \lambda_1 = -\nu\frac{n!(n - n^* + s - 1)!}{(n - n^*)!(n + s - 1)!} \quad (9)$$

Thus, if we assume an initial random distribution of quanta among the oscillators of the molecule, we find a single time constant, λ_1 for the exponentially decaying probability that the molecule has not reacted by a time t, and this time constant is exactly that calculated by Kassel theory. This is due to the fact that $\mathbf{X}_1^{(n)}$ exactly corresponds to an initial random distribution of quanta. Use of a simple modification[6] of Slater's "new approach to unimolecular rate theory" then yields Kassel's results for the unimolecular rate constant as a function of pressure.

This rederivation of Kassel's theory does not give us the further refinement in unimolecular rate theory that we desired. We therefore calculated the exact values of the perturbed λ_1's; two starting values taken were $\lambda_1 = 0$ and $\lambda_1 = \lambda_{\text{Kassel}}$ (equation 9), and then a modification of Newton's method was used through as many iterations as were necessary to obtain precisely the root of the secular equation which was nearest to zero. The computation was done on the IBM 7070 of the University of Rochester's Computing Center, and is described in detail in reference 13. The program also calculated the Kassel values of the microscopic decomposition rate (m.d.r.) from equation 9. The results are given in Tables I, II, and III. The parameter v is ν/α, and ν in equation 9 has been replaced by v. The numbers following the E's are exponents of 10. Table I shows that increasing the magnitude of the chemical sink perturbation ν increases the magnitude of λ_1, but not by as much as one would expect from Kassel's theory; a particular λ_1 is always less than the corresponding λ_{Kassel}. We also observe that the departures of λ_1 from λ_{Kassel} increase with the number of quanta in the molecule, for fixed n^*, s, and v. Table II shows that increasing n^* decreases the degree of departure of a particular λ_1 from the corresponding λ_{Kassel}. Table III shows that increasing s decreases both λ_1 and λ_{Kassel} and decreases the discrepancy between them. The last set of λ_1's in this table shows the effects of machine truncation error, but this does not affect the qualitative conclusions.

We now are in position to calculate the unimolecular rate constant as a function of pressure. We proceed as follows. The solution of equations 3 yields

$$A_{\text{in}}(t) = \sum_{k=1}^{n+1} h_k c_{\text{ink}} \exp(\lambda_k t) \quad (10)$$

where the c_{ink} are the elements of the kth right eigenvector of the matrix $\mathbf{M}^{(n)}$ (including the chemical sink terms) and the h_k are determined by the initial conditions $A_{\text{in}}(0)$. Note that this solution holds only in the absence of collisions. Then the fraction of reactant molecules in the nth energy state at time t is simply

$$P(n,t) = \sum_{i=0}^{n} A_{\text{in}}(t) / \sum_{i=0}^{n} A_{\text{in}}(0) = \sum_{k=1}^{n+1} d_{\text{nk}} \exp(\lambda_k t) \quad (11)$$

where

TABLE I

EFFECT OF CHANGING v

$s = 3$; $n^* = 16$; $v = 10$ (first set), 1 (second set)

No. of quanta in molecule	Kassel's m.d.r. $\lambda_{\text{Kassel}}(n)$	Our m.d.r. $\lambda_1(n)$	$\lambda_{\text{Kassel}}/\lambda_1$
16	6.536 E-02	4.105 E-02	1.592
17	1.754 E-01	9.263 E-02	1.893
18	3.158 E-01	1.477 E-01	2.138
19	4.762 E-01	2.038 E-01	2.336
20	6.493 E-01	2.601 E-01	2.496
21	8.300 E-01	3.162 E-01	2.625
16	6.536 E-03	6.161 E-03	1.061
17	1.754 E-02	1.609 E-02	1.090
18	3.158 E-02	2.834 E-02	1.114
19	4.762 E-02	4.201 E-02	1.134
20	6.494 E-02	5.652 E-02	1.149
21	8.300 E-02	7.152 E-02	1.161

TABLE II

EFFECT OF INCREASING THE ACTIVATION ENERGY

$s = 3$; $v = 10$; $n^* = 9$ (first set), 16 (second set)

No. of quanta in molecule	Kassel's m.d.r. $\lambda_{\text{Kassel}}(n)$	Our m.d.r. $\lambda_1(n)$	$\lambda_{\text{Kassel}}/\lambda_1$
9	1.818 E-01	9.216 E-02	1.972
10	4.545 E-01	1.928 E-01	2.357
11	7.692 E-01	2.937 E-01	2.619
12	1.099 E-00	3.931 E-01	2.795
13	1.429 E-00	4.905 E-01	2.912
14	1.750 E-00	5.860 E-01	2.986
16	6.536 E-02	4.105 E-02	1.592
17	1.754 E-01	9.263 E-02	1.893
18	3.158 E-01	1.477 E-01	2.138
19	4.762 E-01	2.038 E-01	2.336
20	6.494 E-01	2.601 E-01	2.496
21	8.300 E-01	3.162 E-01	2.625

TABLE III

EFFECT OF CHANGING s

$v = 1$; $n^* = 16$; $s = 3$ (first set), 7 (second set)

No. of quanta in molecule	Kassel's m.d.r. $\lambda_{\text{Kassel}}(n)$	Our m.d.r. $\lambda_1(n)$	$\lambda_{\text{Kassel}}/\lambda_1$
16	6.536 E-03	6.161 E-03	1.061
17	1.754 E-02	1.609 E-02	1.090
18	3.158 E-02	2.834 E-02	1.114
19	4.762 E-02	4.201 E-02	1.134
20	6.494 E-02	5.652 E-02	1.149
21	8.300 E-02	7.152 E-02	1.161
16	1.340 E-05	1.293 E-05	1.037
17	6.934 E-05	6.341 E-05	1.094
18	2.080 E-04	2.019 E-04	1.030
19	4.743 E-04	4.598 E-04	1.032
20	9.121 E-04	8.850 E-04	1.031
21	1.561 E-03	1.513 E-03	1.031

$$\sum_{k=1}^{n+1} d_{nk} = 1$$

By following Slater,[3b,15] as indicated in our earlier paper,[6] one finds that the probability that a molecule containing n vibrational quanta will react (in the absence of collisions) in the time interval t to $t + dt$ is

$$-\frac{\partial P(n,t)}{\partial t}\,dt = \sum_{k=1}^{n+1} -d_{nk}\lambda_k \exp(\lambda_k t)dt \quad (12)$$

The fraction of molecules which react before suffering a collision is then given by

$$-\int_0^\infty \sum_{k=1}^{n+1} d_{nk}\lambda_k \exp(\lambda_k t)\exp(-bMt)dt = \sum_{k=1}^{n+1} \frac{-d_{nk}\lambda_k}{\lambda_k + bM} \quad (13)$$

where b is the gas kinetic collision constant for A-M collisions, and A is assumed to be present in trace quantities in comparison to the inert gas M.

We now multiply this factor by the rate at which reactant molecules are being excited to the (degenerate) energy state having n quanta to obtain the rate of formation of products from this state. We here make the usual assumption of a strong collision mechanism,[4f] so that the rate of activation of molecules to the nth state is just $AbMP_n$ where P_n is given by $g_s(n)\exp(-nh\nu'/kT)/[1 - \exp(-h\nu'/kT)]$, ν' is the frequency of the degenerate oscillators, s and $g_s(n)$ have been previously defined, and the other symbols have their usual meanings. To obtain the total rate of reaction, we merely sum the rate of reaction from each activated state ($n \geq n^*$) over all activated states; the result is

$$-\frac{dA}{dt} = AbM \sum_{n=n^*}^{\infty} P_n \left[-\sum_{k=1}^{n+1} \frac{d_{nk}\lambda_{nk}}{\lambda_{nk} + bM}\right] = kA \quad (14)$$

If the sum over the index k in equation 14 includes only one term, we simply recover the general Lindemann expression. Properly at this point we should compute exactly all of the $n + 1$ eigenvalues and eigenvectors for the nth level, compute the d_{nk} by assuming initial random distributions of quanta among the oscillators, and do the indicated summation. This would have been ruinous financially, so we simplified and approximated as follows. We took the exact values of the λ_1's as calculated previously, approximated the λ_2's by αs, the value computed in the absence of the chemical perturbation from equation 4, and ignored the higher eigenvalues altogether. (We thereby lump together the effects of all of the higher eigenvalues and associate with them a single time constant αs.)

The approximation of λ_2 by αs was checked for some simple cases. For $n = 3$ quanta, $n^* = 3, s = 4, \nu/\alpha = 2$, the approximate value for λ_2/α is -4, the exact value (-4.55) is some 14% larger. This was the largest discrepancy we observed. The values of $k/k\alpha$ are very insensitive to this type of error, as indicated by some simple model calculations.

We must still calculate d_{n1} and d_{n2}. We know that $d_{n1} + d_{n2} = 1$ from equation 11. We assume that at the instant of excitation a molecule having a total of n quanta has a probability of decomposing per unit time given by Kassel; this yields

$$\frac{\nu g_s(n - n^*)}{g_s(n)} = -(d_{n1}\lambda_1 + d_{n2}\lambda_2) \quad (15)$$

in addition to $d_{n1} + d_{n2} = 1$. We solve these equations simultaneously for d_{n1} and d_{n2}.

(15) N. B. Slater, *J. Chem. Phys.*, **24**, 1256 (1956).

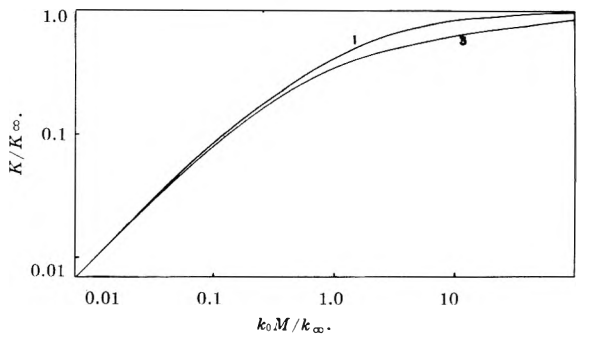

Fig. 1.—Comparison of Kassel theory (curve 1) to the new theory (curve 3): $n^* = 30$, $n_{max} = 50$, $s = 3$, $\nu = 10$, $\theta_{vib} = 300°$K., and $T = 298°$K.

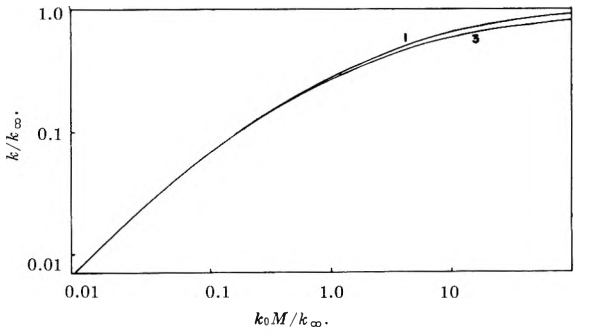

Fig. 2.—Comparison of Kassel theory (curve 1) to the new theory (curve 3): $n^* = 30$, $n_{max} = 50$, $s = 6$, $\nu = 10$, $\theta_{vib} = 300°$K., and $T = 298°$K.

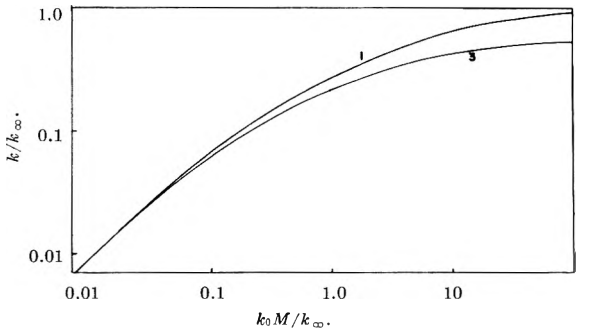

Fig. 3.—Comparison of Kassel theory (curve 1) to the new theory (curve 3): $n^* = 30$, $n_{max} = 50$, $s = 6$, $\nu = 50$, $\theta_{vib} = 300°$K., and $T = 298°$K.

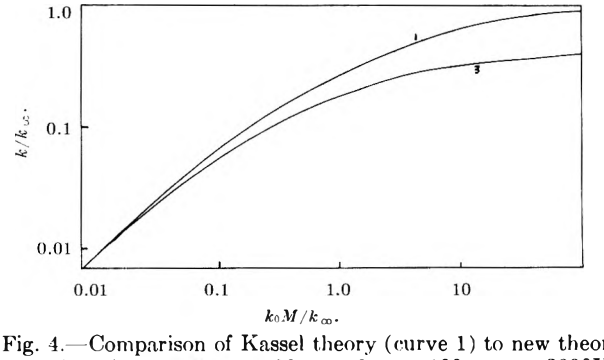

Fig. 4.—Comparison of Kassel theory (curve 1) to new theory (curve 3): $n^* = 30$, $n_{max} = 50$, $s = 6$, $\nu = 100$, $\theta_{vib} = 300°$K., and $T = 298°$K.

The expression for the unimolecular first-order rate constant is then given by

$$k = bM \sum_{n=n^*}^{\infty} - P_n \left(\frac{d_{n1}\lambda_1}{-\lambda_1 + bM} + \frac{d_{n2}\lambda_2}{-\lambda_2 + bM} \right) \tag{16}$$

where $\lambda_2 = \alpha s$ for all n, and the λ_1's are computed for the various values of n as indicated above.

Equation 16 was then evaluated by machine computation, and plots of log (k/k_∞) *vs.* log (k_0M/k_∞) were made. ($k_\infty = \lim_{M\to\infty} k$; $k_0 = \lim_{M\to 0} k/M$.) Equation 15 implies that k_∞ calculated by this theory is equal to k_∞ calculated by Kassel theory for a model having the same values of s, ν, $h\nu'/kT$ and n^*; the two theories also lead to the same value of k_0.

The salient features of the results are illustrated in Fig. 1 through 4. A comparison of Fig. 1 and 2 shows that increasing the number of degrees of freedom decreases the discrepancy between the Kassel theory curves and those obtained by our theory. Comparison of Fig. 2, 3, and 4, in which ν/α, the ratio of the chemical sink rate factor to the parameter governing intramolecular energy transfer, takes on the values 10, 50, and 100, respectively, indicates that decreasing the efficiency of intramolecular energy transfer causes a very marked broadening of the transition region between the low and high pressure limits. θ_{vib} in all cases is equal to $h\nu'/k$. As we had predicted earlier,[6] the weak intramolecular energy transfer theory always leads to curves having a broader transition region between the low and high pressure limits. Variation of θ_{vib} and n^* produced relatively minor effects; increasing n^* tends to make curves calculated by the two theories more similar.

Machine calculations on the vibration of highly energetic triatomic molecules[4a,4c,9-11] indicate that energy "scrambling" among the normal modes is extremely rapid; this casts doubt on the utility of the model discussed here. We would like to mention a suggestion made by Prof. Slater that the effects of anharmonicities may be substantially less extreme in more complex molecules; this possibility makes the model discussed here somewhat more reasonable. Nonetheless, as pointed out by one of our referees, the effects of anharmonicity will certainly be large just prior to the molecule's decomposition, no matter how large the molecule may be; the effects of anharmonicities in such highly distorted molecules may well be quite important. We are currently working on machine calculations to investigate Slater's rather reasonable conjecture.

Acknowledgment.—We are indebted to Prof. Frank Buff and Dr. Everett Thiele for helpful discussions.

THE THORIUM SULFATE COMPLEXES FROM DI-*n*-DECYLAMINE SULFATE EXTRACTION EQUILIBRIA

BY KENNETH A. ALLEN[1] AND W. J. McDOWELL

Oak Ridge National Laboratory, Oak Ridge, Tennessee[2]

Received December 14, 1962

A general method is described for obtaining aqueous complex formation constants from solvent extraction equilibria. The method involves experimentally controlled constancy of the chemical potentials in the aqueous phase, constant composition of the equilibrium organic phase being used as the criterion. A single-parameter Debye–Hückel equation with an arbitrarily fixed distance term is used as an analytic model for the ionic interactions of the aqueous species. At constant sulfuric acid activity, constant extractant concentration, and constant organic thorium molarity the distribution of thorium between di-*n*-decylamine sulfate in benzene and aqueous phases of varying sulfate ion concentrations is shown to lead to the following values of the hitherto-unreported formation constants of the thorium tri- and tetra-sulfate complexes, at zero ionic strength, $K_{23} = \frac{[Th(SO_4)_3^{-2}]}{[Th(SO_4)_2][SO_4^{-2}]} = 5.7 \pm 1.2$ and $K_{34} = \frac{[Th(SO_4)_4^{-4}]}{[Th(SO_4)_3^{-2}][SO_4^{-2}]} = 0.009 \pm 0.003$.

Introduction

Formation constants and energy data for the aqueous mono- and disulfate complexes of thorium have been reported.[3] A search of the literature has been unsuccessful in finding any published reference to species containing more than two sulfates per thorium. The existence of such negatively charged species has been inferred by Kraus and Nelson[4] from the negative slopes of plots of thorium distribution ratios between an anion-exchange resin and aqueous phases of varying sulfate ion concentration. Corresponding solvent extraction data, taken under experimental conditions ensuring constant composition of the organic phases, became available in the di-*n*-decylamine sulfate extraction system.[5] The present paper describes a general method, incorporating Debye–Hückel activity corrections, for obtaining complex formation constants from such data. The method is used in the computation of constants for the formation of the thorium tri- and tetrasulfate complexes.

Experimental

The materials and procedure used in making the thorium distribution measurements have been described previously.[5] Solutions (Na_2SO_4–H_2SO_4) of varying sulfate ion concentration and constant sulfuric acid activity (6.4×10^{-5} *M*) were prepared according to data compiled by Baes.[6] While these tests extended to higher ionic strengths than were covered in Baes' treatment, titration of the equilibrated organic phases for total acid confirmed the constancy of aqueous sulfuric acid activity to within the precision of the titration, ±0.5%. Other parameters were held as constant as practicable: total amine molarity 0.1 ± 0.0005, temperature

(1) Deceased.

(2) Operated for the U.S.A.E.C. by Union Carbide Nuclear Company.

(3) (a) E. L. Zebroski, H. W. Alter, and F. K. Heumann, *J. Am. Chem. Soc.*, **73**, 5646 (1951); (b) A. J. Zielen, *ibid.*, **81**, 5022 (1959).

(4) K. A. Kraus and F. Nelson, ORNL, private communication, 1959.

(5) W. J. McDowell and K. A. Allen, *J. Phys. Chem.*, **65**, 1358 (1961).

(6) C. F. Baes, Jr., *J. Am. Chem. Soc.*, **79**, 5611 (1957).

25 ± 0.05° and total thorium molarity 0.005 ± 0.000005. Constant total thorium concentration was used to establish constant organic thorium levels since extraction coefficients were high and nearly all the thorium was extracted.[7]

All the sulfate variation data were obtained from equilibrations done by the quiescent interface technique,[8] so that the data are internally consistent in this regard.

Method.—In interpreting experimental information reflecting the activity behavior of aqueous species from observation of their equilibrium distribution to an organic phase, it is necessary to have some knowledge of the chemical potentials in the organic phase. Since activity data in organic phases are almost entirely lacking, the remaining alternative is to keep the composition of the organic phase constant in regard to all distributing species. Under these conditions one may be sure that the equilibrium aqueous species activities are also constant, since their chemical potentials are the same as in the organic phase, if all solutions are homogeneous and organic phase concentrations are held well below their individual solubility limits.[9] Thus, the essential part of the method used here is that the organic extractant phases were kept at essentially identical composition throughout the entire series of experiments, during which the aqueous sulfate ion concentration varied. The aqueous-insoluble organic extractants are ideal for this arrangement since they allow an organic phase of known and reproducible composition which is easily analyzed for the distributing ions of interest.

In addition to the conditions described above it is also necessary to have an evaluation of the relative activity coefficients of the aqueous ionic species. For this purpose a Debye–Hückel expression was used, of the form

$$\log G = -0.509\Delta(Z_i^2)I^{1/2}/(1 + pI^{1/2})$$

In the calculations involving this equation the value of p was set at 2. This corresponds to a mean interionic distance of ~6 Å., a reasonable value not far from that chosen by others in similar systems.[10]

Thus, using an aqueous phase W, distribution experiments are run in such a way that a metal ion of charge i, M^{+i}, varies in concentration while an anion of charge j, A^{-j}, also changes concentration, the two changes compensating each other so as to maintain constancy of the activity of the species $MA_{i/j}$, as shown by its constant concentration in the organic phase and therefore constant chemical potential in both phases. One further convenient experimental condition is that $[M^{+i}] << [A^{-j}]$, to obviate the necessity of correcting $[\Sigma A]$ for the quantity of A complexed. Under the rule of Debye–Hückel ionic behavior, the neutral species $MA_{i/j} = MA_k$, out of the following series of possible complexes[11]

$$M^{+i}, MA^{i-j}, MA_2^{i-2j}, \ldots, MA_{t/j}, \ldots, MA_n^{i-nj}$$

is at constant concentration throughout. The neutral complex MA_k may be formed from each non-neutral species MA_t^{i-jt} *via* the reaction

$$MA_t^{i-jt} + (k - t)A^{-j} = MA_k \qquad (A)$$

for which an equilibrium constant may be written

$$K_{tk} = G_{tk}[MA_k][A^{-j}]^{(t-k)}/[MA_t^{i-jt}] \qquad (B)$$

where $K_{tk} = 1/K_{kt}$ is the reciprocal of the formation constant of MA_t^{i-jt} from MA_k, and G_{tk} is the appropriate activity coefficient ratio. From the ionic strength $I = {}^1/_2\Sigma c_n Z_n^2$, which may be computed from the data, and the net change in the squares of the ionic charges, $\Delta(Z_{tk}^2) = -(i - jt)^2 - (k - t)(j)^2$, numerical values for G_{tk} are obtained from the Debye–Hückel relation

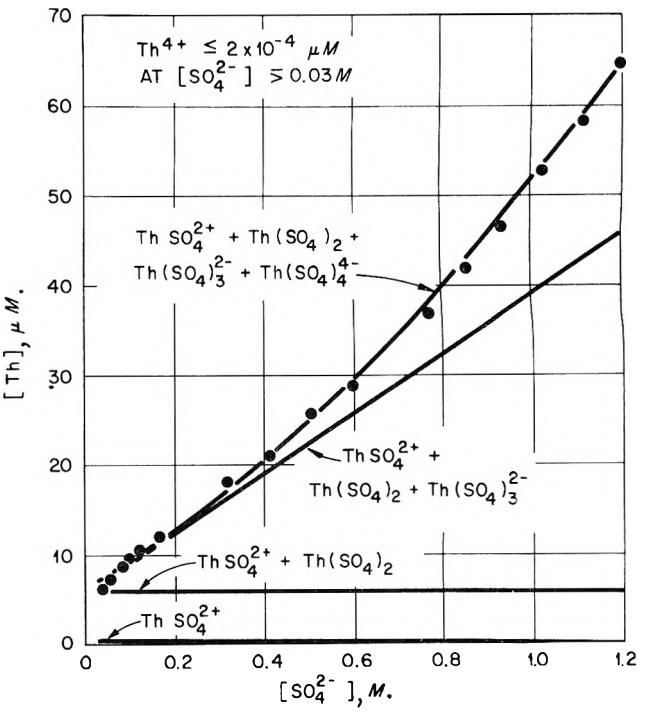

Fig. 1.—Total aqueous thorium concentration as a function of aqueous sulfate ion concentration at constant thorium sulfate activity, and constant sulfuric acid activity of $6.4 \times 10^{-5} M$. Points, experimental values. Curves, calculated from least squares evaluation of $Th(SO_4)_2 = 0.578 \pm 0.075\ \mu M$ and the fractional distribution of Fig. 2.

$$\log G_{tk} = -0.509\Delta(Z_{tk}^2)I^{1/2}/(1 + 2I^{1/2}) \qquad (C)$$

Solving (B) for the concentrations of the various species MA_t^{i-jt} and adding these to $[MA_k]$ results in a material balance relation for the total aqueous metal[12]

$$[\Sigma M] = [MA_k] + [MA_k]\Sigma G_{tk}[A^{-j}]^{t-k}K_{kt} \qquad (D)$$

The constant concentration $[MA_k]$ and the formation constants K_{kt} can be evaluated by simultaneous least-squares analysis of the extraction data.

Results and Conclusions

The pertinent data from the thorium sulfate distribution experiments,[5] conducted as outlined in the foregoing discussion, are summarized in Table I. The aqueous thorium species of interest are Th^{+4}, $ThSO_4^{+2}$, $Th(SO_4)_2$, $Th(SO_4)_3^{-2}$, etc.[13] The continuing decrease of total aqueous thorium as the sulfate concentration approached zero (experimental points, Fig. 1) suggested that the species Th^{+4} and $ThSO_4^{+2}$ were not present in important amounts and could be neglected in the calculation of formation constants of the higher complexes. Consequently, only the di-, tri-, and tetrasulfate complexes were considered in calculating K_{23} and K_{24}. (The low concentration of the monosulfate complex was estimated using preliminary values of K_{23} and K_{24} together with K_{01} and K_{02} from the literature, Table II, and was compensated for in the final evaluation.) Equation D thus became

$$[\Sigma Th] = [Th(SO_4)_2] + [Th(SO_4)_2]G_{32}[SO_4^{-2}]^{-1}K_{23} + [Th(SO_4)_2]G_{42}[SO_4^{-2}]^{-2}K_{24} \qquad (E)$$

(7) The initial aqueous thorium molarity was 0.005. Since the highest equilibrium aqueous thorium molarity was $<7 \times 10^{-5}$ (at the point corresponding to highest aqueous SO_4^{-2} level) then the largest error made in the organic phase composition was an assumed 0.00500 *vs.* an actual 0.00493, a deviation of −1.4% in the organic phase and hence also in the aqueous phase. This deviation, which could have been neglected, was readily compensated in the final evaluation of the formation constants.

(8) K. A. Allen and W. J. McDowell, *J. Phys. Chem.*, **64**, 887 (1960).

(9) This condition is usually easily met by operating on the steeply rising linear portion of the appropriate distribution curve.

(10) In some cases, where sufficient data are available, this term may be evaluated as a statistically adjustable parameter.

(11) Note that when limited to mononuclear complexes, as found in the thorium–sulfate–amine system,[5] $i/j = k$ must be an integer.

(12) This expression is formally identical with equation 16 of Kraus and Nelson, ref. 4.

(13) The data of K. A. Kraus and R. W. Holmberg, *J. Phys. Chem.*, **58**, 325 (1954), and S. Hietanen, *Rec. trav. chim.*, **75**, 711 (1956), indicate that hydrolytic species need not be considered at the acidity used here.

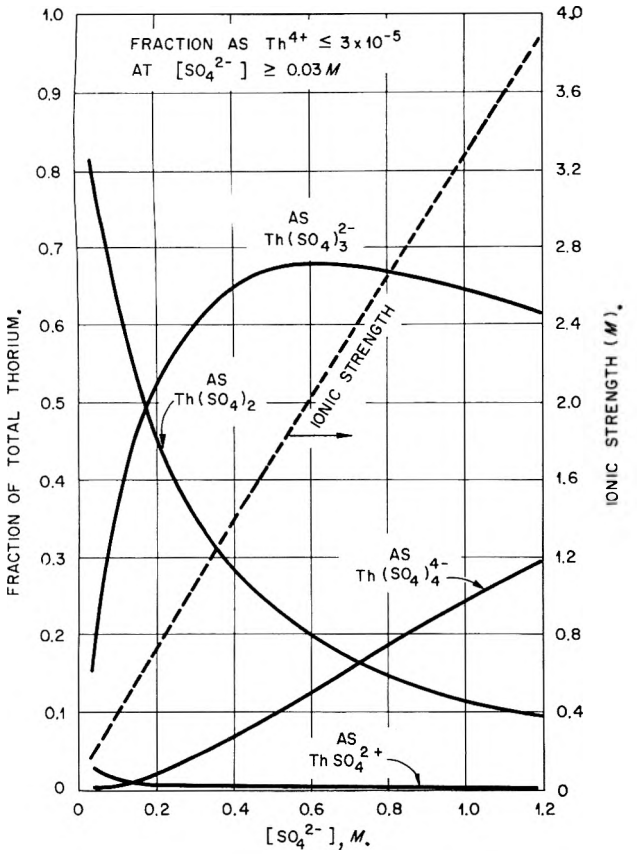

Fig. 2.—Fractions of total thorium existing as the various sulfate complexes, at constant sulfuric acid activity of 6.4×10^{-5} M and varying ionic strength as shown.

TABLE I

AQUEOUS PHASE COMPOSITIONS FOR THORIUM EXTRACTIONS AT CONSTANT AQUEOUS SULFURIC ACID ACTIVITY

$a_{H_2SO_4} = 6.4 \times 10^{-5}$ M

(Organic phase constant at 0.1 M amine, 0.07 M H_2SO_4, ~0.005 M Th)

$[H_2SO_4]_{aq}$, M	$[Na_2SO_4]_{aq}$, M	$[SO_4^{-2}]_{aq}$, M	$[Th]_{aq}$,[a] μM	I, M
0.094	0.006	0.033	6.00	0.166
.097	.018	.037	6.33	.189
.100	.040	.053	7.35	.246
.105	.085	.085	8.75	.360
.105	.095	.093	9.46	.386
.110	.130	.120	10.5	.480
.115	.185	.165	12.0	.630
.130	.360	.317	18.1	1.124
.136	.464	.414	21.3	1.43
.142	.558	.505	25.7	1.71
.149	.653	.597	28.7	2.00
.160	.840	.77	36.8	2.54
.166	.934	.86	41.9	2.82
.172	1.028	.94	46.5	3.08
.180	1.12	1.03	52.6	3.36
.185	1.21	1.12	58.2	3.63
.190	1.30	1.20	64.8	3.89

[a] μM = μmoles/l. = $M \times 10^6$.

Simultaneous least squares analysis (by computer) with the distribution data in Table I gave $K_{23} \approx 6$ and $K_{34} \approx 0.009$ (specifically, $[Th(SO_4)_2] = 5.78 \pm 0.75$ μM, $K_{23} = 5.7 \pm 1.2$, $K_{24} = 0.054 \pm 0.009$, and $K_{34} = K_{24}/K_{23} = 0.0095 \pm 0.0028$, at 95% confidence limit of error), evaluated at zero ionic strength. It is interesting to note that the constants for the formation of the dinegative species $UO_2(SO_4)_2^{-2}$ and $Th(SO_4)_3^{-2}$ appear to be the same (Table III).

TABLE II

FORMATION CONSTANTS FOR $ThSO_4^{+2}$ AND $Th(SO_4)_2$

	As Reported[a]	Converted[b]	
	$I = 2$	$I = 2$	$I = 0$
Zebroski, Alter, and Heumann, ref. 3a	$K_1 = 159$	$Q_{01} = 1.9 \times 10^3$	$K_{01} = 1.9 \times 10^6$
	$K_2 = 2850$	$Q_{02} = 4.0 \times 10^5$	$K_{02} = 1.3 \times 10^{10}$
		$Q_{12} = 2.1 \times 10^2$	$K_{12} = 6.8 \times 10^3$
Zielen, ref. 3b	$\beta_1 = 166$	$Q_{01} = 2.0 \times 10^3$	$K_{01} = 2.0 \times 10^6$
	$\beta_2 = 3610$	$Q_{02} = 5.1 \times 10^5$	$K_{02} = 1.6 \times 10^{10}$
		$Q_{12} = 2.6 \times 10^2$	$K_{12} = 8.2 \times 10^3$

[a] $K_1 = \beta_1 = [ThSO_4^{+2}][H^+]/[Th^{+4}][HSO_4^-]$; $K_2 = \beta_2 = [Th(SO_4)_2][H^+]/[Th^{+4}][HSO_4^-]$. [b] $Q_{01} = [ThSO_4^{+2}]/[Th^{+4}][SO_4^{-2}] = K_1/K_{(HSO_4)}$; $Q_{02} = [Th(SO_4)]/[Th^{+4}][SO_4^{-2}]^2 = K_2/K^2_{(HSO_4)}$; $\log K_{01} = \log Q_{01} - 0.509(-16)I^{1/2}/(1 + 2I^{1/2})$; $\log K_{02} = \log Q_{02} - 0.509(-24)I^{1/2}/(1 + 2I^{1/2})$; $K_{12} = K_{02}/K_{01}$.

TABLE III

COMPARISON: FORMATION OF DINEGATIVE SULFATE COMPLEX FROM NEUTRAL SPECIES UO_2SO_4 AND $Th(SO_4)_2$

Reaction	K	Source
$UO_2SO_4 + SO_4^{-2}$	7	Ahrland, 1951 (potentiometric)
$\rightleftarrows UO_2(SO_4)_2^{-2}$	8	Ahrland, 1951 (spectrophotometric)
	30	Kraus and Nelson, 1957 (anion exchange) (ref. 4)
	6	Allen, 1958 (TOA extraction)
$Th(SO_4)_2 + SO_4^{-2}$	6	Present paper
$\rightleftarrows Th(SO_4)_3^{-2}$		

NOTE: Neither of these reactions is subject to Debye–Hückel ionic interaction corrections, since $\Delta(Z_n^2) = 0$.

These constants were used together with those from the literature (Table II) to evaluate the fractional distribution of the thorium among its aqueous species as a function of sulfate ion concentration at constant sulfuric acid activity, Fig. 2. Note that this is not the "total" analytical sulfate, but the actual $[SO_4^{-2}]$ as shown in Table I.

The fractional distributions were further used with the least squares evaluation of $[Th(SO_4)_2] = 5.78$ μM to synthesize thorium concentration curves for comparison with the experimental points (Fig. 1). The agreement above $[SO_4^{-2}] \approx 0.1$ is good. The experimental points show slightly more curvature than does the calculated curve. This could be taken as suggesting perceptible contribution from a still higher sulfate complex, but the difference is not sufficient to warrant testing such a possibility with these data.

Acknowledgment.—It is a pleasure to give due credit to G. N. Case for technical assistance in the experimental work, to the ORNL Analytical Division for aqueous thorium determinations, to the ORNL Mathematics Panel for advice and computer service, and to C. F. Coleman for invaluable aid in editing the manuscript.

FLOW BIREFRINGENCE MEASUREMENTS ON SWOLLEN COLLAGEN FIBRILS

BY RUDY KOUHOUPT

Ethicon, Inc., Somerville, New Jersey

Received December 15, 1962

To determine certain optical and rheological properties of collagen, an instrument was devised and constructed for measuring the flow birefringence of very small volumes of material. The shear gradient of the apparatus is very low, making it useful for measuring flow birefringence in any liquid system where the particles are easily oriented by flow. Detailed studies have been carried out on dispersions of swollen beef tendon collagen fibrils. The effect of fibril length at constant concentration is given as a function of the flow birefringence of the dispersion. Interpretation of the results leads to the tentative conclusion that fibrils having a nominal length greater than approximately 12.5 μ behave the same as rod-shaped, optically positive particles, while those of nominal length less than approximately 12.5 μ behave like disk-shaped, optically negative particles. Using collagen dispersions in which the nominal fibril length exceeded 200 μ, the concentration dependence of flow birefringence was measured. A direct, linear relationship between collagen concentration and flow birefringence was found.

Introduction

Past work on flow birefringence has been carried out with several forms of cylinder apparatus. Signer[1] and others[2,3] have used an apparatus consisting of a stationary outer cylinder and a rotating inner cylinder operated by the revolving stage of a polarizing microscope. Other devices in which the outer cylinders rotated and the inner cylinders were stationary have been reported,[4-6] but none of these are completely suitable for work with collagen because of their long light path. The optical properties of swollen collagen fibrils are such that a short light path is necessary to prevent excessive scattering and absorption of the light. In the work reported here, a small flow birefringence chamber was especially constructed for measuring the flow birefringence of collagen dispersions with a microscope. The light path through this chamber is only 3 mm. in length, and the entire annulus is in the field of view when a 35X magnification is used on the associated microscope. The outer cylinder wall of the chamber is powered by the motor-driven, revolving microscope stage,[7] and the inner cylinder wall is stationary. The volume of the chamber is 0.01 ml. which makes it particularly useful when working with materials that are available only in limited quantities. The light source, polarizer, compensators, analyzer, and optics of the microscope make up the optical system for the birefringence measurements.

Most of the work on flow birefringence in the past has dealt with molecular species. Some work has been reported on aggregation of particles such as casein[3] and gelatin.[8] The purpose of the present study is to extend flow birefringence measurements to dispersions of swollen collagen fibrils from beef leg tendon. These fibrils are far above molecular dimensions, ranging from 5 to 2000 μ in length depending upon the length chosen when microtoming the tendon. Because of their large dimensions, the data obtained on fibrils cannot be interpreted fully in the light of existing theory which is based on molecular models.

Experimental

A. Flow Birefringence Chamber.—The physical arrangement of the parts of the flow birefringence chamber constructed for this work is shown in Fig. 1. It consists of a rotating outer cylinder and a stationary inner cylinder with a relatively broad intercylinder space. The light path is vertical. The outer cylinder wall is 1.25 mm. in radius and 3 mm. tall formed by boring through a solid piece of mild steel rod. This part is mounted in the exact center of a microscope slide to provide an optically flat bottom to the chamber. The inner cylinder wall is in the form of a mild steel piston 0.75 mm. in radius and 3 mm. long. A slight taper on the bottom end prevents entrainment of air bubbles as the piston is inserted into the sample in the chamber. This part is mounted on a cover slip which seals the top of the chamber and also provides the optically flat upper surface that is required for proper viewing. Insertion and positioning of the inner cylinder with its attached cover slip is accomplished with a micro-manipulator. When the sample is inserted and the chamber fully assembled, the resulting annulus is 0.5 mm. in width and 3 mm. long.

Generally, the flow birefringence chamber is operated at a speed of 3 r.p.m. for making measurements on swollen collagen fibrils. At this low speed, shear is sufficient to orient the fibrils, while thermal effects resulting from frictional forces are negligible. Temperature control of the sample is achieved by operating the device in a room where the temperature is maintained at 72° ±1° F. The velocity gradient, G, of this chamber was calculated by the method presented by Scheraga and Signer[9] in their excellent treatise on the subject of flow birefringence and is shown in Fig. 2 in which G is plotted as a function of the distance from the center of rotation.

B. Preparation of Collagen Fibrils.—The collagen fibrils used in these experiments, derived from beef leg tendon, are quite long, ranging up to 2000 μ. The fibrils are discussed in detail by Borysko,[10] particularly with reference to their swollen state. They are oriented parallel to the long axis of the tendon, enabling short fibril lengths to be obtained by cutting transverse sections on a Spencer Microtome. The nominal fibril lengths cut for the work reported here were 5, 10, 15, 20, 25, 50, 100, and 200 μ.

C. Preparation of Dispersions.—After cutting the fibrils to the desired length, a dispersion containing less than 0.9% by weight of collagen was made in a solution containing equal weights of methanol and water with a sufficient quantity of cyanoacetic acid to bring the final pH to approximately 2.8. In this solution, the collagen fibrils swelled to approximately a hundred times their original volume. This technique has also been described by Borysko.[11] Dispersion was accomplished in a Thomas Tissue Grinder after a preliminary period of swelling. It was found that in dispersions containing more than approxi-

(1) R. Signer and H. Gross, *Z. physik. Chem.*, **A165**, 161 (1933).

(2) H. Nitschmann, *Helv. Chim. Acta*, **21**, 315 (1938).

(3) H. Nitschmann and H. Guggisberg, *ibid.*, **24**, 434, 574 (1941).

(4) V. R. Gray and A. E. Alexander, *J. Phys. Colloid Chem.*, **53**, 9 (1949).

(5) A. S. C. Lawrence, J. Needham, and S. C. Shen, *J. Gen. Physiol.*, **27**, 201 (1944).

(6) J. T. Edsall, A. Rich, and M. Goldstein, *Rev. Sci. Instr.*, **23**, 695 (1952).

(7) A paper entitled "A Motor-Driven, Rotating Microscope Stage for Studying Rheological Properties, Elasticity and Birefringence of Fibrils Measuring 1-10 Microns in Diameter" was presented by the author at the Micro '62 Symposium in Chicago, Illinois on June 10, 1962, and is about to be published in "The Microscope."

(8) G. Scatchard, J. L. Oncley, J. W. Williams, and A. Brown, *J. Am. Chem. Soc.*, **66**, 1980 (1944).

(9) A. Weissberger, "Physical Methods of Organic Chemistry," 3rd Ed., Interscience Publishers, Inc., New York, N. Y., 1959, pp. 2387-2457.

(10) R. Borasky, "Ultrastructure of Protein Fibers," Academic Press, Inc., New York, N. Y., 1963.

(11) S. S. Breese, Jr., "Electron Microscopy," Vol. 2, Academic Press Inc., New York, N. Y., 1962, p. T-9.

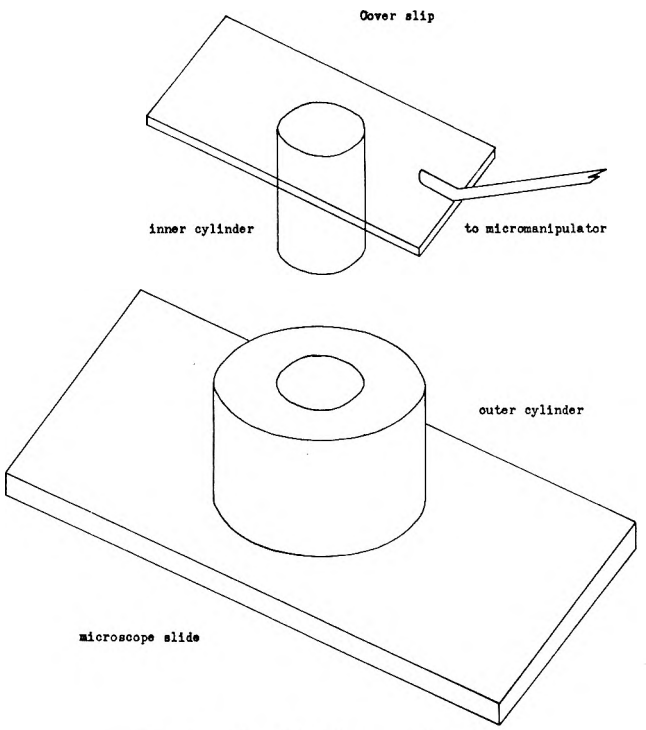

Fig. 1.—Flow birefringence chamber.

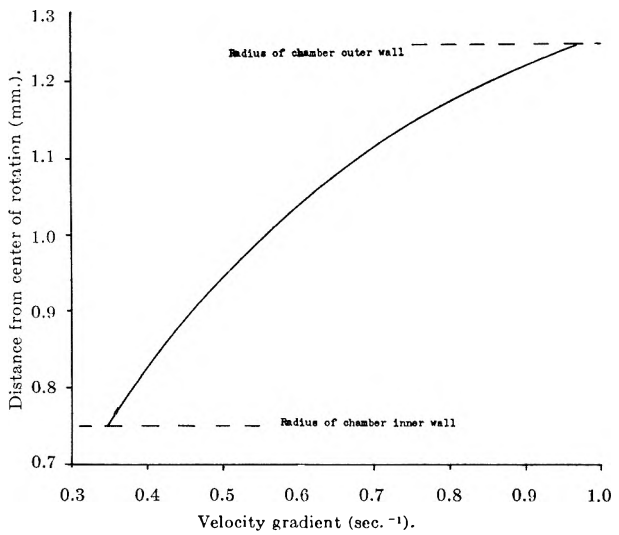

Fig. 2.—Velocity gradient developed across the annulus at a rotational speed of 3 r.p.m.

mately 0.9% collagen, there is not enough free fluid present to permit the fibrils to swell completely. In such a system, the fibrils are severely limited in motion by contact with one another. Free fluid is necessary in the dispersion to permit proper orientation of the fibrils under flow.

D. Experimental Measurements of Flow Birefringence.—Samples of the dispersions of swollen collagen fibrils were introduced into the flow birefringence chamber through a drawn-out dropper. The chamber was closed and sealed by introducing the inner cylinder and its supporting cover slip. Rotation of the stage was started and allowed to continue for a minimum of 60 seconds before any readings were taken. This was found to be sufficient time for the dispersions to attain their maximum birefringence indicating complete orientation of the fibrils. The compensation angle, Δ^9, was measured by rotation of the analyzer. Either a quartz or mica plate was used as the compensator, although the quartz plate was preferred, since it seemed to give a more reproducible end point. A total of ten readings was taken on each sample, the angle reported representing the average of ten readings.

E. Optical Properties of Tendon.—Beef leg tendon takes on a hard, horny consistency when allowed to air dry at room temperature. Transverse sections 50 μ in thickness were cut

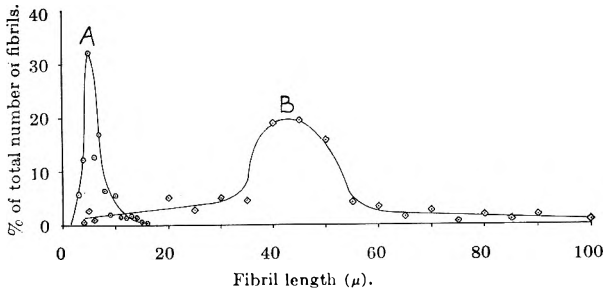

Fig. 3.—Fibril length distribution of microtomed samples: A, 5 μ nominal fibril length; B, 50 μ nominal fibril length.

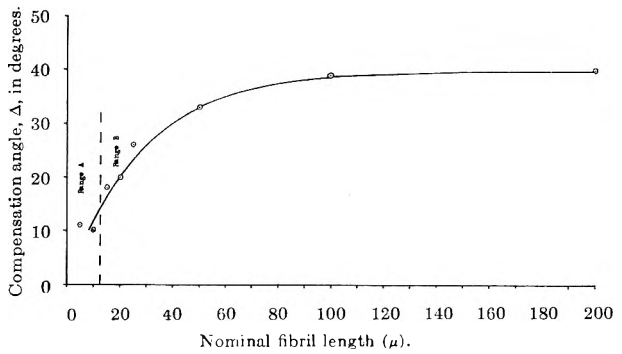

Fig. 4.—Effect of fibril length on flow birefringence: range A, optically negative; range B, optically positive.

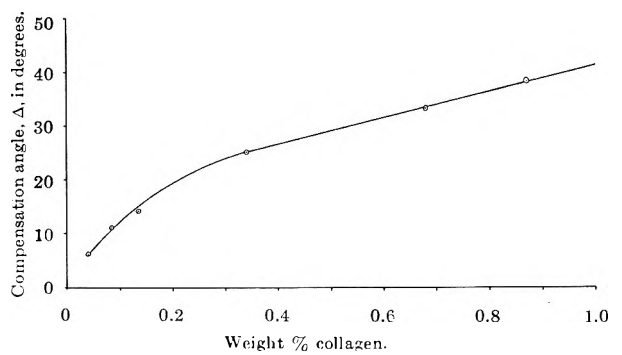

Fig. 5.—Concentration dependence of flow birefringence.

from air-dried tendon and examined in the polarizing microscope. This revealed that the tendon behaves optically as a uniaxial positive crystal. Using the Becke line method, the two values of refractive index for the tendon were found to be 1.5375 and 1.5402 at 23°.

Results and Discussion

Effect of Fibril Length on Flow Birefringence.—A dispersion of swollen collagen fibrils is necessarily a polydisperse system. Microscopic examination of swollen collagen fibrils from beef leg tendon reveals variations in diameter ranging from 0.5 to 10 μ. When the cross sections are cut to produce a certain nominal fibril length, a spectrum of lengths is produced by the normal variations in section thickness that occur because of knife chatter and other mechanical abberations of the microtome. In spite of this, most of the sections are close to the nominal fibril length, producing a distribution of lengths in any given sample with its peak at or near the nominal length. The narrowest distribution of fibrillar length is noted in the thinnest sections. Figure 3 shows experimentally derived fibril length distribution curves for the nominal fibril lengths of 5 and 50 μ. In the 5 μ nominal fibril length, the range of size is from 3 to 16 μ with 74% of the fibrils in the 4 to 7 μ category. A broad range of 4 to 100 μ was noted with the nominal fibril length of 50 μ. However, 63%

of the fibrils were in the 35 to 55 μ category. These two specific length distribution curves are presented to exemplify the variations in fibril length produced by the sectioning operation.

Since the birefringence measurements were made in tungsten light, the birefringence of the dispersions is best expressed as the compensation angle, Δ. The effect of fibril length on flow birefringence of the swollen collagen fibrils is shown graphically in Fig. 4 in which the compensation angle is plotted against the nominal fibril length. Each dispersion used in this determination contained 0.86% collagen by weight in the standard methanol–water–cyanoacetic acid solution. The only difference between dispersions in the series was in fibrillar length.

All preparations having a nominal fibril length of 15 μ or greater were found to be optically positive, while the 5 and 10 μ preparations were optically negative. In view of the fact that dry tendon sections were found to be uniaxial positive, it is apparent that the greater index of refraction of the fibril is along its major axis, since the fibrils are oriented longitudinally in the tendon. Consideration of these two observations together seems to indicate that the swollen collagen fibrils of 15 μ or greater nominal length behave as rod-shaped, optically positive bodies[9] which become oriented circumferentially in the annulus when subjected to the shear force. Further, it seems reasonable to conclude that the fibrils of 5 and 10 μ nominal length behave as disk-shaped, optically negative bodies[9] which become oriented radially in the annulus when subjected to the shear force.

The leveling off of the curve at the nominal fibril lengths of 100 to 200 μ seems to indicate that the flow birefringence measured above 100 μ is an intrinsic property of the collagen fibrils. The abrupt decrease in briefringence of preparations having nominal fibril length less than 50 μ is attributable to the influence of an increasing proportion of short, optically negative particles in each of the dispersions. As the shorter fibril length preparations are made, in the region from 50 μ down to 15 μ, more and more of the short negative particles are present in each sample, depressing the over-all birefringence of the dispersions. At some point between 10 and 15 μ, the effect of the disk-shaped bodies predominates over that of the rod-shaped bodies so that the optic sign becomes negative. An exact determination of the fibril length at which the change of optic sign occurs could not be made because of the technical impossibility of producing a dispersion of fibrils of uniform dimensions as demonstrated by the length distribution curves in Fig. 3.

From a consideration of the fibrillar diameters reported above, it would seem that the change of optic sign should occur at some length less than 10 μ. However, it must be kept in mind that the swollen fibrils imbibe considerable quantities of fluid making them quite deformable, so that they cannot behave as either rigid disks or rods. In view of the deformability of the fibrils and the polydispersity of the system, an exact interpretation of the hydrodynamic flow behavior based on birefringence data alone is impossible.

Concentration Dependence of Flow Birefringence.—Using dispersions in which nominal fibril length exceeded 200 μ, the effect of collagen concentration was measured. For this series of dispersions, all of the fibrils were from the same source and were mixed in the standard methanol–water–cyanoacetic acid solution. The only difference between dispersions in the series was in their actual collagen content.

The concentration dependence of flow birefringence is shown graphically in Fig. 5 in which the compensation angle is plotted against weight per cent collagen. The curve rises steeply from 0 to 0.34% collagen becoming linear in the region from 0.34 to 0.9% collagen. This probably indicates that below 0.34% collagen, there is a sufficient excess of free fluid so that the principal interaction is between the fibrils and the surrounding fluid. Above 0.34% collagen, the fibrils are becoming restricted in their movements by other fibrils. This results in a circumferential packing of the fibrils and a consequently higher degree of orientation than in dispersions containing less than 0.34% collagen. Above 1.0% collagen, there is no free fluid present, the fibrils are incompletely swollen, and measurement of flow birefringence becomes meaningless.

MOLAR ENTHALPIES OF MIXING IN THE MOLTEN LITHIUM FLUORIDE–POTASSIUM FLUORIDE SYSTEM

BY ROBERT A. GILBERT

Chemistry Division, Oak Ridge National Laboratory,[1] *Oak Ridge, Tennessee*

Received December 17, 1962

A new method for the determination of enthalpies of mixing of high melting fused salt systems is presented. The enthalpies of mixing in the molten LiF–KF system have been measured at 875° with an experimental error of approximately one per cent. The data may be represented by the following relationship between the molar integral enthalpy of mixing and the mole fraction of LiF(X)

$$\Delta H^{M} = X(1 - X)[-3878 - 1051X - 1521X(1 - X)]$$

Introduction

Recent theoretical interest in fused salts has led to the development of techniques for the measurement of thermodynamic properties of salt mixtures at elevated temperatures. One such study was made by Kleppa and Hersh[2] who determined, by a direct method, the heats of mixing of all possible combinations of the binary liquid alkali nitrate systems using a twin Calvet reaction calorimeter modified to operate up to 500°. The heats were exothermic in every case and the magnitude of the molar mixing enthalpy increased in a regular

(1) Operated by Union Carbide Corporation for the U. S. Atomic Energy Commission.

(2) O. J. Kleppa and L. S. Hersh, *J. Chem. Phys.*, **34**, 351 (1961).

TABLE I

HEAT OF MIXING DATA FOR THE MOLTEN LiF–KF SYSTEM AT 875°

Compn. mole fraction LiF	Total moles	Heat content measured, cal.	Heat content calcd.,[a] cal.	Heat of mixing of sample, cal.	ΔH^M, cal./mole	$\Delta H^M/X(1-X)$, cal./mole
0.1009	0.1833	3330.0	3331	3399	−68	−370	−4080
.1009	.1833	3332.4					
.1930	.1921	3422.0	3420	3551	−131	−680	−4370
.1930	.1921	3417.1					
.1930	.1921	3419.0					
.1930	.1921	3423.4					
.3014	.2077	3617.7	3616	3813	−197	−950	−4510
.3014	.2077	3614.4					
.3850	.2280	3935.4	3937	4187	−250	−1100	−4650
.3850	.2280	3938.4					
.5027	.2407	4083.8	4082	4374	−292	−1210	−4840
.5027	.2407	4080.5					
.5927	.2600	4402.0	4404	4705	−301	−1160	−4810
.5927	.2600	4405.1					
.5927	.2600	4405.2					
.7467	.3340	5681.9	5682	5993	−311	−930	−4920
.7467	.3340	5681.3					
.8997	.3441	5970.9	5970	6125	−155	−450	−4990
.8997	.3441	5969.1					

[a] From the following pure component heat contents for the 0.101, 0.301, 0.503, 0.900 mixtures ΔH_{LiF} = 17,707 cal./mole; ΔH_{KF} 18,639 cal./mole. For the 0.193, 0.385, 0.593, 0.747 mixtures, ΔH_{LiF} = 17,697 cal./mole; ΔH_{KF} = 18,679 cal./mole.

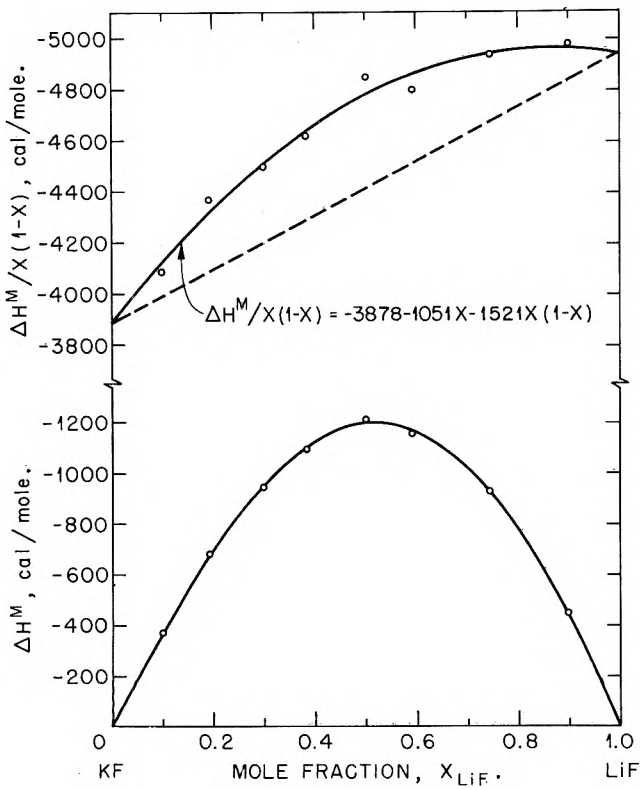

Fig. 1.—Molar integral heats of mixing (ΔH^M) in mixtures of LiF–KF at 875°.

fashion with increasing difference in size between the two cations.

Due to the temperature limitations of their calorimeter these authors were not able to make similar measurements on the theoretically more interesting alkali halide systems. Aukrust, *et al.*,[3] however, reported from an analysis of phase diagram studies that the maximum heat of mixing of the KF–LiF system should be about 1.2 kcal. In view of this observation, it was felt that heat of mixing data might be obtainable, as the difference between large numbers, by the use of a precision heat content calorimeter. Since the heat of mixing is exothermic, the heat contents of the mixtures will be lower than values calculated from the molar heat contents for the pure materials multiplied by the number of moles of each present.

Experimental

The measurements were made at 875° using a Bunsen ice calorimeter similar to that employed by Ginnings, Douglas, and Ball[4] of the NBS. Our calorimeter differs from theirs in the following minor details. The cylinders in the furnace core are nickel instead of silver and the central tube is platinum from a point midway in the lower cylinder to the top of the furnace. The remainder of the center tube is Inconel since the heat transfer of platinum is too great for it to be used for the entire length. These changes have no effect as far as the present system is concerned but will be important when systems involving NaF (melting point approx. 995°) are measured. Dry helium at 34 cc./min. is passed up the central calorimeter well to improve heat transfer and prevent condensation of moisture. In addition, a 50 cc./min. helium flow is maintained through the central tube in the furnace core in order to attain thermal equilibrium more rapidly and reduce oxidation of the capsule. The accuracy of this calorimetric system has been reported previously.[5] Temperatures were measured with a platinum *vs.* platinum 10% rhodium thermocouple compared at 875° with a similar NBS calibrated couple.

Eleven capsules were used in the measurements and were machined from a single bar of Nichrome V in order to avoid errors due to differences in alloy composition. They were sealed by heliarc welding after being filled and are inert to the reagents used. Eight contained the mixtures and two the pure components. The eleventh served as a blank whose heat content was subtracted from that of the filled capsules. The weight of each capsule was adjusted to 31.313 g. so that only a single blank determination was necessary.

The LiF was Harshaw Chemical Company single crystal material and was of high purity. The KF was reagent grade material which had been melted in a platinum crucible under

(3) E. Aukrust, B. Björge, H. Flood, and T. Förland, *Ann. N.Y. Acad. Sci.*, **79**, 830 (1960).

(4) D. C. Ginnings, T. B. Douglas, and A. F. Ball, *J. Am. Chem. Soc.*, **73**, 1236 (1951).

(5) R. A. Gilbert, *J. Chem. and Eng. Data*, **7**, 388 (1962).

helium and then slow cooled. From the resulting solid, clear crystals were hand picked for use.

The capsules were filled and weighed in an inert atmosphere box containing an analytical balance. In each case the weight of material was approximately 10 g. The capsules were then taken in a closed chamber to another inert atmosphere box equipped with welding electrodes and welded shut under one atmosphere of helium purified by passing it through a liquid N_2 cooled charcoal trap. The loss of weight during the sealing process was negligible. The capsules were then tested for leaks by checking the capsule weight at intervals. If constant weight was not reached within three hours, a leak was assumed and the capsule was resealed.

Since the values desired are the differences between heat contents, it is imperative that the measured heat contents for any set of mixtures be compared with those calculated from pure component heat contents which have been measured at the same temperature. The controls on the furnace are manual and were adjusted such that the equilibrium temperature with zero drift was slightly above the temperature desired. When the capsule was pulled into the center nickel cylinder, the latter was cooled below the desired temperature. The system was then allowed to re-equilibrate and at the moment the temperature drifted through a value preset on the potentiometer, the capsule was dropped into the calorimeter and the heat effect measured by the usual procedure.[4] At drop time the temperature drift never exceeded 0.03° per minute. At least two measurements were made on each capsule and additional drops were made if these heat contents differed by more than 0.1%.

With such an operating procedure only minor deviations from a fixed temperature should result unless a gross error in the temperature measurement occurred. In these experiments an error did indeed occur after the heat contents of the blank, pure components and mixtures at approximately 0.2, 0.4, 0.6, 0.75 mole fraction LiF had been measured. This was due to the inadvertent brushing of the hot couple against some rubber insulating material, contaminating the couple. After the contaminated section was removed, the couple was reinserted in new protection tubing and a standardization at 875° repeated. The heat contents of the blank, pure components, and the rest of the mixtures were then measured at a slightly different setting on the potentiometer. The two temperatures differed by less than 0.5° and it is evident from the consistency of the two sets of data that any error due to possible temperature dependency of the heat of mixing is well within the over-all experimental uncertainty.

Results

The experimental results are presented in Table I and the molar heat of mixing ΔH^M and the deviation function $\Delta H^M/X(1 - X)$ are plotted as a function of the mole fraction LiF in Fig. 1. The values of ΔH^M are, as indicated previously, obtained from the average of at least two measurements. The maximum deviation of a measured ΔH^M value from the average was 2.5% at $0.193X_{LiF}$. Most deviations, however, were 1% or below.

The maximum heat of mixing (−1210 cal.) confirms the value estimated by Aukrust.[3] The plot of $\Delta H^M/X(1 - X)$ clearly shows the energetic asymmetry of the system. Since it was obvious that the data could not be represented by a straight line, an expression of the form

$$\Delta H^M = X(1 - X)[a + bX + cX(1 - X)]$$

was used. The values of the constants were calculated by the method of least squares to give

$$\Delta H^M = X(1 - X)[-3878 - 1051X - 1521X(1 - X)]$$

From this, it is possible by standard methods to calculate the following equations for the relative partial molal heat contents of the two components

$$\bar{L}_{KF} = -X^2_{LiF}(1306 + 8186X_{LiF} - 4563X^2_{LiF})$$

$$\bar{L}_{LiF} = -X^2_{KF}(4459 + 3982X_{KF} - 4563X^2_{KF})$$

A more complete analysis of these data will be deferred until completion of measurements on additional alkali fluoride systems now under study.

Acknowledgments.—The author is grateful to Dr. Milton Blander of Atomics International for suggesting this approach to the determination of heats of mixing and for encouragement and discussions during the measurements.

THE ELECTRICAL CONDUCTIVITY OF SOLUTIONS OF METALS IN THEIR MOLTEN HALIDES. VI. LANTHANUM, CERIUM, PRASEODYMIUM, AND NEODYMIUM IN THEIR MOLTEN IODIDES[1]

BY A. S. DWORKIN,[2a] R. A. SALLACH,[2b] H. R. BRONSTEIN,[2a] M. A. BREDIG,[2a] AND J. D. CORBETT[2b]

Chemistry Division, Oak Ridge National Laboratory, Oak Ridge, Tennessee, and Department of Chemistry and Institute for Atomic Research, Iowa State University, Ames, Iowa

Received December 20, 1962

The electrical conductivities of solutions of the series La, Ce, Pr, and Nd in their molten triiodides are similar to those of the corresponding chloride systems, and thus likewise reflect the gradual increase in stability of the dipositive ion M^{2+}. For example, in solutions containing 15 mole % metal, the specific electronic contribution $\kappa_{soln} - \kappa_{salt}$ decreases from 22 and 25 ohm^{-1} $cm.^{-1}$ for La and Ce, respectively, to 4 for Pr and ~0 for Nd. The positive temperature dependence of the conductivity in the concentration range where electronic contribution is sizable indicates that there is thermal excitation of electrons from the solute. The phase equilibrium diagrams near the MI_3 and MI_2 compositions are discussed in terms of the solute species. The MI_3 liquidus data are compatible with the postulated M^{2+} solute or its dissociation into M^{3+} and anion-like electrons. The metallic character of the molten diiodides, which are metal-like ($M^{3+}(I^-)_2e^-$) in the solid state, appears to decrease in the melt in the order La > Ce > Pr.

Introduction

Rather systematic variations in the electrical conductivities of solutions of La, Ce, Pr, and Nd metals in their respective trichlorides[3,4] can be correlated with a regular trend observed in the phase diagrams of

(1) Work performed for the U. S. Atomic Energy Commission at the Oak Ridge National Laboratory, operated by the Union Carbide Corporation, Oak Ridge, Tennessee.

(2) (a) Oak Ridge, Tennessee; (b) Ames, Iowa.

(3) (a) H. R. Bronstein, A. S. Dworkin, and M. A. Bredig, *J. Phys. Chem.*, **66**, 44 (1962); (b) A. S. Dworkin, H. R. Bronstein, and M. A. Bredig, *Discussions Faraday Soc.*, **32**, 188 (1961).

(4) A. S. Dworkin, H. R. Bronstein, and M. A. Bredig, *J. Phys. Chem.*, **66**, 1201 (1962).

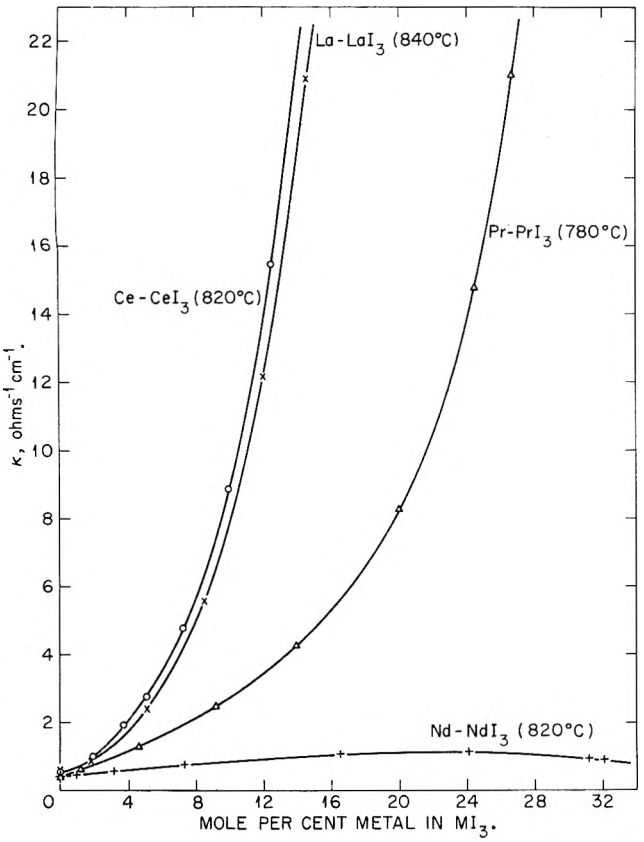

Fig. 1.—Specific conductivity of rare earth metal–rare earth metal triiodide systems.

these systems. Specifically, these differences have been interpreted as resulting from a gradual increase in the stability of the dipositive cation ($La^{2+} \sim Ce^{2+} < Pr^{2+} < Nd^{2+}$), as indicated by an increase in solubility of metal and ultimately formation of reduced chlorides of Pr and Nd.[5,6]

In contrast to the chlorides, the diiodides of all these metals are found to exist in the solid state. However, there is a striking dissimilarity between the neodymium dihalides and the diiodides of lanthanum, cerium, and praseodymium. The former compounds are typically salt-like in that they are electrical *insulators*, while all of the latter group are electrical *conductors*, *i.e.*, $M^{3+}(I^-)_2e^-$.[7] Magnetic measurements confirm that the neodymium ion is truly Nd^{2+}, but that the lanthanum ion, and presumably also cerium and praseodymium ions, are present as M^{3+} in their diiodides.[8] The corresponding chloride and bromide systems of lanthanum and cerium exhibit only dissolution of metal without the formation of intermediate solid phases, while praseodymium forms only $PrCl_{2.3}$ and $PrBr_{2.4}$.[5,8-10]

Because of the unusual behavior of these four iodide systems with regard to formation of solid phases and because a greater range of metal concentrations can be studied in the melts, the electrical conductivities of these MI_3 + M solutions have been measured. These results and some further discussion of the phase relationships are contained herein.

(5) L. F. Druding, J. D. Corbett, and B. N. Ramsey, to be published.
(6) L. F. Druding and J. D. Corbett, *J. Am. Chem. Soc.*, **83**, 2462 (1961).
(7) J. D. Corbett, L. F. Druding, W. J. Burkhard, and C. B. Lindahl, *Discussions Faraday Soc.*, **32**, 79 (1961).
(8) R. A. Sallach and J. D. Corbett, to be published.
(9) F. J. Keneshea and D. Cubicciotti, *J. Chem. Eng. Data*, **6**, 507 (1961).
(10) G. W. Mellors and S. Senderoff, *J. Phys. Chem.*, **63**, 1110 (1959).

Experimental

The molybdenum parallel electrode assembly used to measure the conductivity of the metal iodide solutions, the sapphire capillary cell used with the pure salts, and the experimental procedure have been described in detail previously.[3] Measurements were largely limited to conductivities up to 20 ohm^{-1} $cm.^{-1}$ because of the rapidly increasing contribution of the electrode resistance to the total resistance. A capillary cell of single crystal MgO was found to be noticeably attacked by the molten triiodides.

The triiodides were prepared from the elements by the method of Druding and Corbett[6] and were vacuum sublimed before use to remove traces of oxide contaminants.

Results and Discussion

Table I contains the results of the specific conductivity measurements of the pure triiodides. As was the case in the chloride systems, these values form a regular series of specific conductivity κ *vs.* t curves where κ decreases with increasing atomic number or decreasing size of the cation. The curve for NdI_3 lies somewhat lower than expected for a completely regular trend in the series, a fact that may be connected with the relatively high melting point of β-NdI_3. The temperature dependence in all four systems corresponds to an activation energy of approximately 5.5 kcal. $mole^{-1}$.

TABLE I
SPECIFIC CONDUCTIVITY, κ, OF RARE EARTH METAL TRIIODIDES

t, °C.	κ, ohm^{-1} $cm.^{-1}$	t, °C.	κ, ohm^{-1} $cm.^{-1}$
LaI_3 (m.p. 778–779°)[7]		PrI_3 (m.p. 738°)[7]	
796	0.456	763	0.399
822	.493	786	.426
847	.524	809	.452
871	.555		
CeI_3 (m.p. 760–761°)[7]		NdI_3 (m.p. 787°)[6]	
796	0.448	799	0.396
814	.470	818	.416
836	.499	842	.440
860	.523		

The results of the specific conductivity measurements for the metal-in-salt solutions are given in Table II and illustrated in Fig. 1. The conductivity behavior of these systems in general resembles that of the corresponding chloride systems[3,4] to a remarkable degree. The rapid increase in conductivity with metal concentration in the La and Ce solutions (an approximately exponential dependence) indicates considerable electronic contribution to the total conductance. The Nd solutions can be described as salt-like with little if any electronic conductance, while the Pr solutions are again intermediate as predicted.[7] The conductivity increases more rapidly on addition of metal to the iodides than to the chlorides, a phenomenon that was also found with solutions of the alkali metals in their halides where it was attributed to the influence of halide ion polarizability on electron transfer.[11] The maximum in the conductivity of the NdI_3 + Nd system at or near 50 mole % NdI_2 (16.7 mole % Nd metal) may be indicative of the possible electron exchange process between two adjacent oxidation states (Nd^{2+} and Nd^{3+}) postulated previously[3] for the chloride system; this aspect is under further investigation.

(11) H. R. Bronstein and M. A. Bredig, *ibid.*, **65**, 1220 (1961).

TABLE II

SPECIFIC CONDUCTIVITY, κ, OF MI_3–M SYSTEMS

LaI_3 + La at 840°		CeI_3 + Ce at 820°	
Mole % metal	κ, ohm^{-1} cm.$^{-1}$	Mole % metal	κ, ohm^{-1} cm.$^{-1}$
0	0.515	0	0.480
1.84	0.874	1.96	1.00
5.1	2.39	3.74	1.92
8.5	5.54	5.08	2.74
11.9	12.2	7.25	4.75
14.6	20.9	9.9	8.88
		12.5	15.5
		19.4	~60
PrI_3 + Pr at 780°		NdI_3 + Nd at 820°	
0	0.420	0	0.418
1.20	0.608	0.98	0.476
4.62	1.28	3.14	0.585
9.14	2.48	7.27	0.759
13.9	4.24	16.5	1.033
15.4	4.89	24.1	1.102
20.0	8.25	31.2	0.980
24.5	14.8	32.1	0.930
26.6	21.0		

The character of the conductivity data presented in Fig. 1 for La, Ce, and Pr, with an increasing contribution from the dissolved metal with increasing concentration, is the same as found not only with the corresponding chloride systems, but also in KX + K melts.[11,12] In the absence of unlikely density anomalies, it may be presumed that the equivalent metal contribution Λ_M will also show a positive dependence on metal concentration. Although this is plausible according to a number of possible models, any further detailed interpretation of this relationship in mechanistic terms without additional information seems somewhat speculative. It is clear, however, that in this concentration range, the observed conduction electrons must arise *via* excitation from some solute species, since the temperature coefficient is positive over a considerable range of metal concentration not only here but also in other salt-rich systems.[11,12] This in itself allows no distinction to be made between possible solute entities, although the different electronic contributions to the total conductivity in various rare earth metal systems may allow stability trends to be deduced.

A few preliminary measurements of the temperature dependence of conductivity in the iodide systems present some interesting comparisons. First, for the solution of 8.5 mole % La in LaI_3, the relative rate of change of conductivity with temperature $((1/\kappa)\cdot(d\kappa/dT))$ (and hence also the apparent activation energy for the process) was found to be substantially the same as that of the pure solvent. This is all the more striking since the electronic contribution at this point is roughly 91% of the total conductivity. This suggests that in dilute solutions there may be some similarity between the motion of electrons and of the iodide ions that are presumably the principal carriers in LaI_3. Of course, at higher metal concentrations, the temperature coefficient must decrease and ultimately become metallic (negative) in character. The more concentrated solution of 15.4 mole % Pr in PrI_3 shows a diminished though still positive temperature dependence, one-third of that of PrI_3, although κ_e/κ_{total} is about the same as above, 90%. The solution of 31.2 mole % Nd in NdI_3 ($NdI_{2.06}$) exhibits an apparent activation energy approximately equal to that of NdI_3, as would be expected from the magnitude of κ, which indicates ionic conductance, and from the stability of the Nd(II) state. The implications of the temperature dependence as a function of concentration and of the nature of the system are being investigated further.

Analysis of the published[7] freezing point depressions of the four triiodides by added metal using recently determined heats of fusion[13] gives results quite comparable with those obtained from the chloride systems.[3] The cryoscopic number n of approximately three so obtained is consistent with the formation of either $3M^{2+}$ or $3e^-$ per metal atom dissolved.[14] The observed n may be ascribed to solvated electrons or to an equilibrium between these and M^{2+}, if the electrons are taken to be trapped in anion-like "vacancies," although there is no direct evidence for such a species. The decrease in the conductivity contribution of the added metal in the series (La,Ce), Pr and Nd results from an increasing stability of the M^{2+} ion. If any other electron trap were to be considered, it would have to be devised so as to also increase in stability in the same manner. The former model is not only more conventional, but more plausible since there is good evidence for M^{2+} ions of Ce, Pr, and Nd in the solid chlorides.[5,6,8]

Although the above discussion pertains only to dilute to moderate concentrations of the metals, some thermodynamic evidence for continued, notable differences in concentrated solutions is evident from the liquidus curves of the solid diiodides. In this case, an extrapolation of these curves to the pure compound is necessary for the incongruently-melting PrI_2 and CeI_2, while the observed solid composition $NdI_{1.95}$ can best be taken as the pure phase in spite of the oxidation state complications due to the iodide deficiency. If, for the purposes of contrast, the liquid diiodides are all taken to be $M^{2+}(I^-)_2$, so that added MI_3 introduces one foreign cation, apparent heats of fusion of roughly 50, 20–25, 13–15, and 6–7 kcal. mole^{-1} are calculated for La, Ce, Pr, and Nd diiodides, respectively, from the limiting d ln N_{MI_2}/d$(1/T)$. The last is a reasonable value for a normal MI_2 salt or for a diiodide plus metallic electrons, since the latter, as in a metal, would not contribute appreciably to the enthalpy change. However, the particularly unlikely "ΔH_f" obtained for LaI_2 points out the fallacious character of the solution model selected. This, of course, is to be expected, as all information indicates that LaI_2 is most likely $La^{3+}(I^-)_2e^-$, with metal-like electrons, so that the addition of LaI_3 provides only common ions, and the

(12) H. R. Bronstein and M. A. Bredig, *J. Am. Chem. Soc.*, **80**, 2007 (1958).

(13) The calorimetrically measured heats of melting for CeI_3, PrI_3, and NdI_3 are 12.4, 12.7, and 9.7 kcal. mole^{-1}, respectively, the low value for NdI_3 being obviously connected with the α–β transformation at a little more than 200° below the melting point (ref. 6). A. S. Dworkin and M. A. Bredig, *J. Phys. Chem.*, **67**, 697 (1963).

(14) Cryoscopic numbers for La and Ce in their chlorides and iodides actually appear closer to 2.4–2.6 than 3 on the basis of the published phase diagrams. Even more striking is the observation of numbers of 1.6–1.7 and 2.0 with the bromides of La and Ce (ref. 8). Since it is not likely that all the phase diagrams would be in error this much, these differences can be better interpreted in terms of a more fundamental deficiency, the formation of significant solid solutions in LaX_3 and CeX_3. This seems slightly more reasonable than invoking admixtures with M^+, M^0, or intermediate solutes because of the unusual and irregular trend observed for n within the halides of either element.

depression of the activity and hence the melting point comes about effectively only through "dilution" of the electrons in the metallic conduction band. Unfortunately, the quantitative cryoscopic treatment in this case is not obvious. Consequently the intervening "ΔH_f" values obtained for CeI_2 and PrI_2 can merely be taken as indicative of the intermediate character of these melts, with a greater tendency toward localization of the electron in liquid PrI_2. The ability of competing electronic states to coexist in solutions, of course, allows more subtle trends to be observed than is possible in pure solids.

In comparison to the results in Fig. 1, the apparent heat obtained above for CeI_2 seems somewhat low, since the conductivity in the more dilute CeI_3 + Ce solutions is actually slightly greater than with lanthanum. This may be the result of only a different concentration dependence of the conductivity in the two cases in the intervening region. Alternatively, an apparent heat up to about 40 kcal. mole^{-1} could be obtained by a more subjective reconstruction of the liquidus curve through a greater than usual scatter of experimental points so as to give an initially smaller rate of freezing point depression. Conductivity data for more concentrated solutions as well as for the solids at higher temperatures will be useful here as well as in assessing more clearly the character of liquid PrI_2.

THE HEAT OF FORMATION OF HYDROGEN FLUORIDE

By H. M. Feder, W. N. Hubbard,

Chemical Engineering Division, Argonne National Laboratory, Argonne, Illinois

S. S. Wise, and J. L. Margrave

Department of Chemistry, University of Wisconsin, Madison, Wisconsin

Received January 4, 1963

The combination of high precision data from fluorine bomb calorimetry with other thermochemical data is proposed for the evaluation of the heat of formation of gaseous hydrogen fluoride. For example, the heat of the reaction $SiO_2 + 2F_2 = SiF_4 + O_2$ may be combined with the heat of the reaction $SiF_4 + 2H_2O = SiO_2 + 4HF$ to yield a value of $\Delta H^0f_{298}(HF) = -64.92 \pm 0.12$ kcal. mole^{-1}. This result agrees with some recent determinations by other methods, and favors a replacement of the previously recommended value, -64.2 kcal. mole^{-1}, by a more negative one.

Introduction

The heat of formation of hydrogen fluoride plays a role in fluorine bomb and flame calorimetry analogous to the role played by the heat of formation of water in oxygen bomb and flame calorimetry. As Armstrong[1] has stated, "In the value for the [heat of formation of HF(g)], combined with the heat of solution of gaseous hydrogen fluoride in water, lies the key to much of the existent literature of the thermochemistry of fluorine compounds, dependent as it has been upon the calorimetric study of reactions of aqueous solutions of hydrogen fluoride." It is essential for progress in fluorine thermochemistry that the standard heat of formation of hydrogen fluoride gas should be determined with good precision and by more than one method. That the goal has not yet been achieved is evident in Table I, which contains the modern determinations of the quantity.[2-10] As indicated by the last entry in the table, a considerable part of the variation of the reported results arises from the very uncertain correction for the imperfection of hydrogen fluoride gas at room temperature. In 1952 the compilers of Circular 500[11] selected a value of ΔHf^0_{298} (-64.2 kcal. mole^{-1}) which represented the best estimate available at that time. More recently Armstrong[1] cited evidence that the recommended value should be replaced by a more negative one.

It is not the purpose of this paper to discuss the relative merits of the results of previous experimental methods. Rather, the purpose is to point out that with the advent of high precision fluorine bomb calorimetry[12-17] it is now possible to reverse the usual procedure of computing the heat of formation of certain fluorides from that of hydrogen fluoride, and, instead, to obtain the heat of formation of hydrogen fluoride by combination of the measured heats of certain well-defined reactions. The following are examples of such schemes.

$$A + \frac{x}{2}F_2(g) = AF_x;\ \Delta H(1) \qquad (1)$$

$$AF_x + \frac{x}{2}H_2(g) = A + xHF(g);\ \Delta H(2) \qquad (2)$$

(1) G. T. Armstrong, in "Experimental Thermochemistry," Vol. II, H. A. Skinner, Editor, Interscience Publishers, Inc., New York, N. Y., 1962, p. 144.

(2) H. von Wartenberg and O. Fitzner, *Z. anorg. allgem. Chem.*, **151**, 313 (1926).

(3) O. Ruff and W. Menzel, *ibid.*, **198**, 375 (1931). This paper corrects a computational error which occurred in ref. 2 and 5.

(4) J. Simons and J. H. Hildebrand, *J. Am. Chem. Soc.*, **46**, 2183 (1924).

(5) O. Ruff and F. Laass, *Z. anorg. allgem. Chem.*, **183**, 217 (1929).

(6) H. von Wartenberg and H. Schütza, *ibid.*, **206**, 65 (1932).

(7) J. W. C. Johns and R. F. Barrow, *Proc. Roy. Soc.* (London), **A251**, 504 (1959).

(8) G. T. Armstrong and R. S. Jessup, *J. Res. Natl. Bur. Standards*, **64A**, 49 (1960).

(9) R. W. Long, J. H. Hildebrand, and W. E. Morrell, *J. Am. Chem. Soc.*, **65**, 182 (1943).

(10) W. Strohmeier and G. Briegleb, *Z. Elektrochem.*, **57**, 662 (1952).

(11) F. D. Rossini, D. D. Wagman, W. H. Evans, S. Levine, and I. Jaffe, "Selected Values of Chemical Thermodynamic Properties," Circular 500 of The National Bureau of Standards, Washington, D. C., 1952.

(12) W. N. Hubbard, in "Experimental Thermochemistry," Vol. II, H. A. Skinner, Editor, Interscience Publishers, Inc., New York, N. Y., 1962, Chap. 6.

(13) W. N. Hubbard, J. L. Settle, and H. M. Feder, *Pure and Applied Chem.*, **2**, 39 (1961).

(14) E. Greenberg, J. L. Settle, H. M. Feder, and W. N. Hubbard, *J. Phys. Chem.*, **65**, 1168 (1961).

(15) J. L. Settle, H. M. Feder, and W. N. Hubbard, *ibid.*, **65**, 1337 (1961).

(16) (a) S. S. Wise, J. L. Margrave, H. M. Feder, and W. N. Hubbard *ibid.*, **65**, 2157 (1961); (b) **66**, 381 (1962); (c) **67**, 815 (1963).

(17) E. Greenberg, J. L. Settle, and W. N. Hubbard, *ibid.*, **66**, 1345 (1962).

TABLE I

DETERMINATIONS OF $\Delta Hf^0_{298.15}$ (HF)

Year	Investigator	Method	$\Delta Hf^0_{298.15}$	Source of cor. for gas imperfection
1926	H. von Wartenberg and O. Fitzner[2]	$H_2 + F_2$ flame at ~35°	−63.8 ± 0.3[3]	Simons and Hildebrand[4]
		NaCl + $^1/_2F_2$ reaction	−65.0	Simons and Hildebrand[4]
1929	O. Ruff and F. Laass[5]	$H_2 + F_2$ flame at ~35°	−64.2 ± 0.3[3]	Simons and Hildebrand[4]
1932	H. von Wartenberg and H. Schütza[6]	$H_2 + F_2$ flame at 100°	−64.45 ± 0.1	
1959	J. W. C. Johns and R. F. Barrow[7]	U.V. dissociation limit of dilute HF	−65.1 ± 0.4[a]	
1960	G. T. Armstrong and R. S. Jessup[8]	$NH_3 + F_2$ flame at 32°	−64.22 ± 0.13	Long, Hildebrand, and Morrell[9]
			−64.63 ± 0.07	Strohmeier and Briegleb[10]

[a] Uncertainty due principally to the uncertainty in the dissociation energy of fluorine.

$$\Delta Hf(\mathrm{HF}) = \frac{1}{x}\{\Delta H(1) + \Delta H(2)\}$$

$$\mathrm{AO}_{x/2} + \frac{x}{2}\mathrm{F_2(g)} = \Delta F_x + \frac{x}{4}\mathrm{O_2\ (g)};\ \Delta H(3) \qquad (3)$$

$$\mathrm{AF}_x + \frac{x}{2}\mathrm{H_2O(g)} = \mathrm{AO}_{x/2} + x\mathrm{HF(g)};\ \Delta H(4) \qquad (4)$$

$$\frac{x}{2}\mathrm{H_2(g)} + \frac{x}{4}\mathrm{O_2(g)} = \frac{x}{2}\mathrm{H_2O(g)};\ \Delta H(5) \qquad (5)$$

$$\Delta Hf(\mathrm{HF}) = \frac{1}{x}\{\Delta H(3) + \Delta H(4) + \Delta H(5)\}$$

In seeking suitable data to use in these schemes we have been guided by two criteria: (a) the heats to be summed should be known with good accuracy; and (b) reactions involving hydrogen fluoride gas at room temperature should be avoided because of the uncertainty in the correction to the standard state.

Results

Of the experimental results in fluorine bomb calorimetry so far published only those involving silicon tetrafluoride are useful for our purpose. One set of reactions which meets the above mentioned criteria is shown below.

$$\mathrm{SiO_2}(\alpha\text{-quartz}) + 2\mathrm{F_2(g)} = \mathrm{SiF_4(g)} + \mathrm{O_2(g)};\ \Delta H(6) \qquad (6)$$

$$\mathrm{SiO_2(crystobalite)} = \mathrm{SiO_2}(\alpha\text{-quartz});\ \Delta H(7) \qquad (7)$$

$$2\mathrm{H_2(g)} + \mathrm{O_2[g]} = 2\mathrm{H_2O(g)};\ \Delta H(8) \qquad (8)$$

$$\mathrm{SiF_4(g)} + 2\mathrm{H_2O(g)} = \mathrm{SiO_2(cristobalite)} + 4\mathrm{HF(g)};\ \Delta H(9) \qquad (9)$$

$$\Delta Hf(\mathrm{HF}) = \frac{1}{4}\{\Delta H(6) + \Delta H(7) + \Delta H(8) + \Delta H(9)\} \qquad (10)$$

The relevant heats and their uncertainty intervals[18] (in kcal. mole^{-1}) have been determined as follows. The heat of reaction 6 has been measured by fluorine bomb calorimetry with the result[16b,c] ΔH^0_{298} (6) = −168.26 ±0.28. The heats of reactions 7 and 8 are known: $\Delta H_{298}(7)$ = −0.35 ± 0.05[19]; $\Delta H^0_{298}(8)$ = −115.596 ± 0.020.[11] The equilibrium in reaction 9 has been investigated by Lenfesty, Farr, and Brosheer[20] from 200 to 800°. At the latter temperature the equilibrium solid was definitely shown to be cristobalite. Because the temperature was sufficiently high the partial pressures of the gases at equilibrium may be taken to be equal to their fugacities. The equilibrium constant for reaction 9 at 1073°K., log (k_P, atm.) = log (p^4_{HF}/p_{SiF_4}-$p^2_{H_2O}$) = −0.405. We estimate the uncertainty interval in the logarithm of this equilibrium constant to be ±0.070 (*vide infra*). Hence, $\Delta G(9)_{1073}$ = +1.99 ± 0.35. The free energy functions $[(G^0_T - H_{298})/T]$ for HF(g), SiF_4(g) and H_2O(g) were interpolated from the JANAF tables[21] and the free energy function of cristobalite from tabular data given by Kelley.[22] The third-law calculation yielded ΔH^0_{298} (9) = +24.53 ± 0.36, and by substitution in equation 10, ΔHf^0_{298}(HF) = −64.92 ± 0.12.

As a check on this result one may also use the equilibrium data of Lenfesty, *et al.*,[20] for the lowest temperature (300°) at which they obtained consistent measurements. According to these authors the solid phase which established the equilibrium at this temperature was vitreous silica. The relevant new equations are then

$$\mathrm{SiO_2(vitreous)} = \mathrm{SiO_2}(\alpha\text{-quartz});\ \Delta H(11) \qquad (11)$$

$$\mathrm{SiF_4(g)} + 2\mathrm{H_2O(g)} = \mathrm{SiO_2(vitreous)} + 4\mathrm{HF(g)};\ \Delta H(12) \qquad (12)$$

$$\Delta Hf(\mathrm{HF}) = \frac{1}{4}\{\Delta H(6) + \Delta H(11) + \Delta H(12) + \Delta H(8)\} \qquad (13)$$

For $\Delta H_{298}(11)$ we have taken the average of two literature values,[23] −2.27 ± 0.10. The equilibrium constant for reaction 12 at 573°K., log (k_P, atm.) = −5.607 ± 0.190, hence $\Delta G_{573}(12)$ = 14.70 ± 0.50. This datum was reduced as in the previous example to yield ΔH_{298} (12) = +26.37 ± 0.51 and ΔHf^0_{298} (HF) = −64.93 ± 0.15.

Discussion

By combination of the fluorine bomb calorimetric results with those for the equilibria of HF with cristobalite and vitreous silica two values of ΔHf^0_{298} (HF), −64.92 ± 0.12 and −64.93 ± 0.15 kcal. mole^{-1}, respectively, have been derived. The former is to be preferred because cristobalite is a much better characterized variety of silica than the vitreous form. Because these results each require the combination of four reaction heats it is important to be certain that the rather small assigned uncertainties are realistic. The calorimetri-

(18) F. D. Rossini, Chapter 14, in "Experimental Thermochemistry," F. D. Rossini, Editor, Interscience Publishers Inc., New York, N. Y., 1956, p. 297.

(19) J. Coughlin, Bur. of Mines Bulletin 542, Washington, D. C., 1954.

(20) F. A. Lenfesty, T. D. Farr, and J. C. Brosheer, *Ind. Eng. Chem.*, **44**, 1448 (1952).

(21) JANAF Thermochemical Tables, The Dow Chemical Co., Midland, Mich., 1962.

(22) K. K. Kelley, U. S. Bureau of Mines Bull. 584 (1960).

(23) O. Mullert, *Z. anorg. Chem.*, **75**, 198 (1912); V. R. Wietzel, *ibid.*, **116**, 71 (1921).

cally determined reaction heats all appear to be known with sufficient reliability. The accuracy with which the free energy functions for H_2O, HF, SiF_4 and SiO_2 are known (<0.050 cal. deg.$^{-1}$ mole^{-1}) introduces virtually no uncertainty in the calculation of ΔH_{298} from the value of ΔG_T. The bulk of the uncertainty therefore resides in the value of ΔG_T for reactions 9 and 12. In estimating the latter uncertainties we have adopted the conservative practice of increasing the usual uncertainty intervals by an additional factor of two.

The present value for ΔHf^0(HF) does not differ significantly from those derived from the spectroscopic study,[7] the most recent flame calorimetric study[8] in combination with the preferred[1] P–V–T data for hydrogen fluoride,[10] and von Wartenberg's study[2] of the NaCl + F_2 reaction; it does not overlap the values derived from the earlier flame calorimetric studies.[2,5,6] Our conclusion, in agreement with Armstrong's,[1] is that the previously recommended value should be replaced by a more negative one. Other thermochemical combinations based on forthcoming fluorine bomb calorimetric results will be helpful in the re-evaluation of this important quantity.

Acknowledgment.—This research was supported in part by the U. S. Atomic Energy Commission. We wish to thank Professor T. F. Young and Dr. E. Rudzitis for useful discussions.

NOTES

NOTE ON THE RATE EQUATIONS GOVERNING CHARGE TRANSFER CONTROLLED SURFACE REACTIONS

By G. A. Somorjai and R. R. Haering

IBM Corporation, Thomas J. Watson Research Center, Yorktown Heights N. Y.

Received August 1, 1962

The rates of semiconductor surface reactions involving charge transfer have been generally found to depend exponentially on the charge concentration.[1,2] This has been explained by the boundary layer[3,4] theory which assumes that the reaction rate is limited by the rate of arrival of electrons (or holes) at the surface of the semiconductor. As the reaction proceeds, a space charge layer is built up at the surface which opposes subsequent electron (or hole) flow. The characteristically exponential rate equation follows since the number of electrons with sufficient energy to overcome the space charge barrier varies as $\exp(-W/kT)$. W is the instantaneous barrier height at time t, and depends on the number of electrons which have been transferred to the surface prior to time t.

In the present note we discuss an alternate mechanism whereby a charge transfer limited surface reaction may proceed; namely, quantum mechanical tunneling. We show that the rate equations for the two processes are similar, and we point out the conditions under which tunneling through the barrier, rather than diffusion over the barrier, determines the reaction rate. Furthermore, we discuss how the tunneling process may be experimentally recognized. For definiteness, we consider surface reactions of the above type for a non-degenerate n-type semiconductor. The relations we derive are equally valid for non-degenerate p-type materials and could also be modified to apply to degenerate materials.

Consider a typical charge transfer limited surface reaction in which an atom of type A is chemisorbed on the surface of some n-type material by combining with an electron supplied by bulk of the material.

$$A + e \longrightarrow A^-$$

As this reaction proceeds, a dipole layer is formed which consists of a negatively charged surface layer (due to the A^- present), and a positively charged space charge region near the surface (due to ionized donor atoms). This situation is depicted schematically in Fig. 1.

The arrival rate dn/dt of electrons at $x = 0$ due to tunneling through the barrier is given[5] by

$$\frac{dn}{dt} = \int_0^{\sqrt{2mW}} dp_x \int_{-\infty}^{\infty} dp_y \int_{-\infty}^{\infty} dp_z \frac{N}{(2\pi mkT)^{3/2}} \times e^{-\frac{[p_x^2 + p_y^2 + p_z^2]}{2mkT}} \times \frac{p_x}{m} \times T(p_x) \quad (1)$$

In equation 1, N denotes the bulk electron concentration, m is the effective electron mass, k is Boltzmann's constant, x denotes the normal to the surface, located at $x = 0$, and $T(p_x)$ is the transmission coefficient for an electron of momentum p_x. This coefficient is approximately[6] given by

$$T(p_x) = \exp\left\{-2\int_0^{x_0}\left[\frac{2m}{\hbar^2}\left\{V(x) - \frac{p_x^2}{2m}\right\}\right]^{1/2} dx\right\} \quad (2)$$

where x_0 is defined by $V(x) = p_x^2/2m$. $V(x)$ is the potential resulting from the dipole layer and is given by[7,8]

$$V(x) = \frac{2\pi e^2 N_D}{\kappa}[x - d]^2 \quad (3)$$

(1) M. Green, J. A. Kafalas, and P. H. Robinson, in "Semiconductor Surface Physics," Philadelphia, U. of Pa. Press, 1957, p. 349.

(2) D. A. Melnick, *J. Chem. Phys.*, **26**, 1136 (1957).

(3) P. B. Weisz, *ibid.*, **21**, 1531 (1953).

(4) K. Hauffe and H. J. Engell, *Z. Elektrochem.*, **56**, 366 (1952).

(5) D. Bohm, "Quantum Theory," Prentice-Hall, Inc., New York, N. Y., 1951, p. 277.

(6) This approximation is not valid for $T(p_x) \simeq 1$, *i.e.*, for electrons near the top of the barrier. However, the number of such electrons is negligible under conditions when tunneling is important.

(7) The presence of a uniform potential surface at the solid surface ($x = 0$) is assumed when the tunneling reaction begins.

(8) W. Shockley, *Bell Syst. Tech. J.*, **28**, 435 (1949).

In equation 3 N_D is the ionized donor concentration within the space charge region whose width is d, and κ is the dielectric constant. This width is related to the A^- surface density, n, through the relation $n = N_D d$. The height W of the space charge barrier is thus

$$W = \frac{2\pi e^2 n^2}{\kappa N_D} \tag{4}$$

The integrations over p_y and p_z in equation 1 are easily performed and yield

$$\frac{dn}{dt} = \frac{N/m}{(2\pi mkT)^{1/2}} \int_0^{\sqrt{2mW}} dp_x \, T(p_x) \times p_x \times e^{-p_x^2/2mkT} \tag{5}$$

Two limits of equation 5 are of particular interest and we shall discuss these separately.

$$\text{Case 1: } W/kT \gg \left[\frac{2mWd^2}{\bar{h}^2}\right]^{1/2}$$

Equation 5 may then be integrated approximately to yield

$$\frac{dn}{dt} \simeq 0.63N \left(\frac{kT}{2\pi m}\right)^{1/2} e^{-[2mWd^2/\bar{h}^2]^{1/2}} \tag{6}$$

This result should be compared with the corresponding result[4] for flow over the top of the barrier, which is

$$\frac{dn}{dt} = N\left(\frac{kT}{2\pi m}\right)^{1/2} e^{-W/kT} \tag{7}$$

Apart from a trivial numerical factor, the chief difference is the fact that the barrier transmission probability factor is $e^{-W/kT}$ for electrons flowing over the top of the barrier, whereas it is $e^{-[2mWd^2/\bar{h}^2]^{1/2}}$ for electrons tunneling through it. Since by assumption $W/kT \gg [2mWd^2/\bar{h}^2]^{1/2}$, we conclude that under these conditions the charge transfer reaction proceeds by tunneling and not by flow over the top of the barrier.

Using the expression for W and d in equation 6, we find the following rate equation for the tunneling process

$$\frac{dn}{dt} \simeq 0.63Ke^{-\alpha n^2} \tag{8}$$

where

$$K = N\left(\frac{kT}{2\pi m}\right)^{1/2}$$

and

$$\alpha = \left[\frac{2m}{\bar{h}^2}\,\frac{2\pi e^2}{\kappa N_D{}^3}\right]^{1/2}$$

This rate equation is of identical form to that obtained for the charge transfer[3] over the top of the barrier.

$$\text{Case 2: } W/kT \ll \left[\frac{2mWd^2}{\bar{h}^2}\right]^{1/2}$$

An approximate integration of equation 5 then yields

$$\frac{dn}{dt} = 0.45N \left(\frac{kT}{2\pi m}\right)^{1/2} \left[\frac{W/kT}{\left[\frac{2mWd^2}{\bar{h}^2}\right]^{1/3}}\right] e^{-W/kT} \tag{9}$$

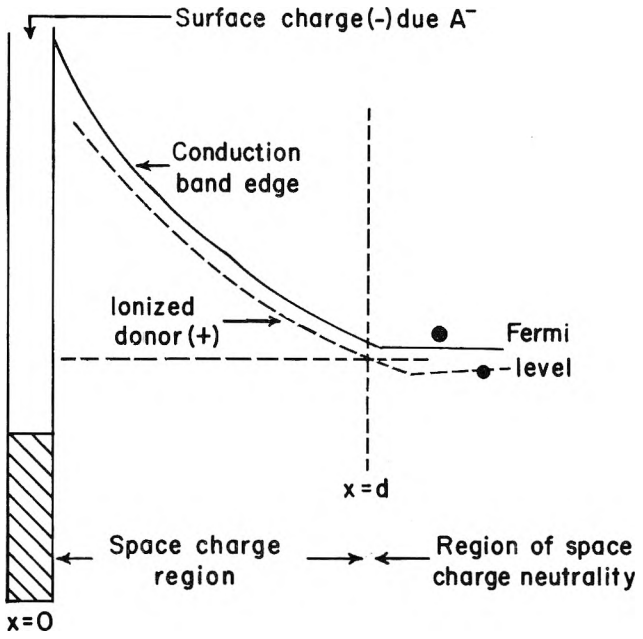

Fig. 1.—Potential energy distribution near the surface resulting from the dipole layer.

This rate equation is again similar to equation 7 but differs by a numerical factor

$$0.45 \left\{\frac{W/kT}{\left[\frac{2mWd^2}{\bar{h}^2}\right]^{1/3}}\right\}$$

which by assumption is small compared to one. Hence, we conclude that under these conditions, the charge transfer reaction proceeds by flow of electrons over the top of the barrier.

We have shown that space charge limited, charge transfer surface reactions may proceed either by flow of electrons over the top of the space charge barrier or by tunneling of electrons through the barrier. Which of the two processes is the important one depends on the relative magnitudes of the numerical parameters W/kT and $[2mWd^2/\bar{h}^2]^{1/2}$. If $W/kT \gg [2mWd^2/\bar{h}^2]^{1/2}$ the reaction proceeds primarily by tunneling, whereas the converse leads to a reaction which proceeds *via* flow over the top of the barrier. By substituting the expressions for W and d into the above inequality, it becomes apparent that the criterion does not depend on n, *i.e.*, on the degree to which the reaction has proceeded.

The criterion for a tunneling process may in fact be written as

$$kT \ll \left[\frac{\pi\bar{h}^2 e^2 N_D}{\kappa m}\right]^{1/2} \tag{11}$$

Assuming an effective mass equal to the true electronic mass and $\kappa \sim 3$, we obtain from equation 11

$$kT \ll 10^{-11} N_D{}^{1/2} \tag{12}$$

In equation 12, kT must be expressed in electron volts and N_D in cm.$^{-3}$. It can thus be seen that at room temperature, tunneling reactions are important only when $N_D \lesssim 10^{17}$ cc. At lower temperatures, tunneling may dominate even for larger carrier concentrations.

The reaction rates dn/dt for the two processes are identical in their dependence on the concentration n of the chemisorbed species, being of the form

$$\frac{dn}{dt} = Ce^{-\delta n^2} \qquad (13)$$

However, the coefficient δ in the exponent of (13) is temperature independent in the case of the tunneling process, whereas δ varies as T^{-1} in the case of flow over the barrier top. This difference makes it easy to recognize the tunneling process experimentally.

AN EXTRAPOLATION METHOD FOR ESTIMATING STEADY-FLOW VISCOSITY AND STEADY STATE COMPLIANCE FROM CREEP DATA

By Kazuhiko Ninomiya

Japan Synthetic Rubber Co., Yokkaichi, Japan, and Department of Chemistry University of Wisconsin, Madison, Wisconsin

Received October 24, 1962

The steady-flow viscosity, η, and the steady state compliance, J_e, of an amorphous polymer can be directly obtained by prolonging creep measurements into steady flow and/or by measuring the creep recovery thereafter. In practice, however, sometimes the direct method is not so desirable for several reasons, since the sample specimen may have to be kept at a rather high temperature for a considerable length of time. Therefore it would be convenient to introduce a conventional method to estimate the values of η and J_e from creep data taken somewhat before attainment of steady flow.

Creep compliance in shear at the steady state, denoted here by $J(t)_{ss}$, can be written in the form

$$J(t)_{ss} = J_e + (t/\eta) \qquad (1)$$

where t represents the time. Division of both sides in eq. 1 by t gives

$$J(t)_{ss}/t = (J_e/t) + (1/\eta) \qquad (2)$$

Therefore, when $J(t)/t$ is plotted against $1/t$, the intercept at the ordinate gives the value of $1/\eta$ and the initial tangent is equal to the value of J_e.

The following relationship may also be introduced.

$$\lim_{t \to \infty} [dJ(t)/dt] = \lim_{1/t \to 0} [mJ(t)/t] = 1/\eta \qquad (3)$$

$$m \equiv d \log J(t)/d \log t$$

The value of m appears to be less than unity and it approaches unity when steady state creep is reached. The plot of $mJ(t)/t$ *vs.* $1/t$ may be expected to converge to $1/\eta$ with much less curvature than that of $J(t)/t$ *vs.* $1/t$ so that extrapolation toward the ordinate axis would be easier for the former plot. Hence, it is suggested that $mJ(t)/t$ *vs.* $1/t$ may first be extrapolated toward the ordinate to give the intercept and then another plot may be properly smoothed to obtain the value of the initial tangent. The accuracy of J_e can never be expected to be as good as that of η, regardless of the method of its estimation.

In practice, creep data with the value of m from 0.7 to 0.9, which are fairly removed from the steady state, may be used successfully. In most cases plots of $mJ(t)/t$ *vs.* $1/t$ can be approximated by straight lines in the region of $0.7 < m < 1$ to give reasonable values for η.

To illustrate the reliability of the values of η and J_e thus estimated, a comparison is made using data of Leaderman and others[1] on the shear creep of polyisobutylene samples.[2] Figure 1 shows a typical example of the extrapolation method for these data. Table I compares the values of η and J_e for seven samples of polyisobutylene from direct measurements extending into the steady flow state, as reported by Leaderman,[1] with those estimated by the extrapolation method from data in advance of the steady state.

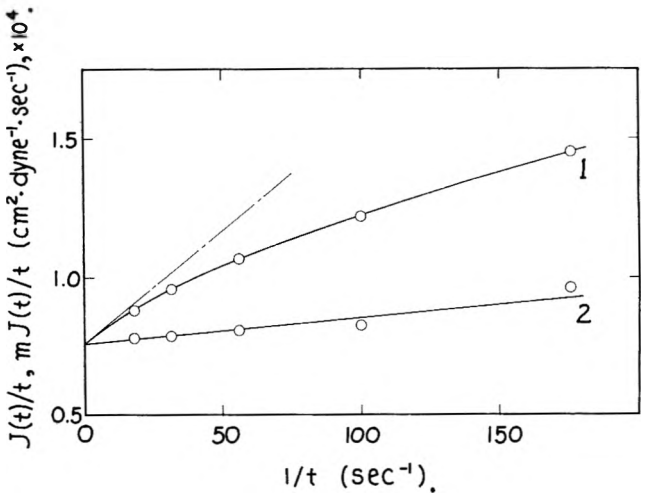

Fig. 1.—Example of extrapolation plots (polyisobutylene F5R at 30°): 1, $J(t)/t$; 2, $mJ(t)/t$.

Table I

Values of η and J_e for Polyisobutylene Samples at 30°

Sample	$\eta \times 10^{-6}$, poise S.S.[a]	$\eta \times 10^{-6}$, poise extrap.[b]	$J_e \times 10^6$, cm.²/dyne S.S.[a]	$J_e \times 10^6$, cm.²/dyne extrap.[b]
F5R	1.32	1.32	1.1	0.86
E	1.80	1.82	17.2	17
H	8.10	8.26	15.8	18
J	56.3	56.5	10.1	10
K	182	185	5.6	6.3
G	330	330	4.36	4.6
F2	642	641	3.35	3.5

[a] Obtained by Leaderman from steady-state measurements. [b] Extrapolated by eq. 2 and 3 from data of Leaderman before the steady state, *i.e.*, for $m = 0.7$ to 0.9.

The agreement between the corresponding values in Table I is very satisfactory.

Acknowledgment.—This work was supported in part by a grant from the National Science Foundation. The author is grateful for the interest and discussions of Professor J. D. Ferry of the University of Wisconsin, Professor H. Fujita of Osaka University, and Professor J. Furukawa of Kyoto University.

(1) H. Leaderman, R. G. Smith, and L. C. Williams, *J. Polymer Sci.*, **36**, 233 (1959).

(2) The numerical data of $J(t)$ as well as η and J_e for those samples were furnished through the kindness of Dr. H. Leaderman of the National Bureau of Standards.

THE "SHAKING EFFECT" IN PRECISION CONDUCTANCE MEASUREMENTS

By J. E. Prue[1]

Department of Physical and Inorganic Chemistry, University of New England, Armidale, New South Wales, Australia

Received November 5, 1962

Conductance measurements with a precision of 0.01% or better are of current interest in order to test[2] new theoretical equations for the dependence of molar con-

ductance on concentration in dilute solution, and to derive physically significant parameters from them.[3] In very dilute aqueous and non-aqueous solutions, a troublesome drift of conductance with time, reversed by shaking the solution in the conductance cell, has often[3] been commented upon, but never thoroughly examined or satisfactorily explained. As usually reported, an increase of conductance with time is wholly or partially reversed on shaking the solution. The most careful investigation of the effect so far reported is that of Deubner and Heise[4] who christened it a "Schütteleffekt" and ascribed it to carbon dioxide contamination of solutions.

Experimental

The main series of measurements reported were made with a Pyrex glass conductance cell in which two circular platinum electrodes of about 20 mm. diameter were set about 5 mm. apart in an electrode chamber of 20 ml. capacity joined to a mixing chamber of 70 ml. which makes possible the elimination of any error due to the Soret effect.[5] The cell constant was 0.1264 cm.$^{-1}$. Measurements were made with both bright and lightly platinized electrodes. The conductance bridge was a Leeds and Northrup Jones–Dike bridge used in conjunction with a variable frequency oscillator, tuned amplifier, and C.R.O. detector. The measurements were made at a frequency of 2100 c./sec. with a resistance of 20,000 ohms in parallel with the cell. The conductance water used was prepared by passing laboratory distilled water through a column of mixed ion-exchange resin and had a conductance of less than 1×10^{-7} ohm^{-1} cm.$^{-1}$. The water, monitored by conductance measurements, was passed directly into the conductance cell. Most of that in the mixing bulb was displaced by CO_2-free argon; small additions of electrolyte solutions were made as desired and the stoppers quickly inserted. The cell was thermostated at 25° in an oil-filled bath constant to within ±0.002°. The cell contents were mixed in the mixing bulb without removal from the thermostat after 20 minutes had elapsed from the time of insertion into the bath and readings taken thereafter. Any Soret effect was thereby eliminated.[5]

The typical behavior of CO_2-contaminated water is shown in curve 1 of the figure in which (specific) conductance κ is plotted against time. The conductance of the stagnant solution steadily increased, but after pouring the solution to and from the mixing chamber several times, the measured value of κ dropped sharply. Overnight, κ rose to 10.8×10^{-7} ohm^{-1} cm.$^{-1}$ and dropped to 8.5×10^{-7} ohm^{-1} cm.$^{-1}$ on mixing the solution. The magnitude of the decrease in κ on mixing the solution depends therefore on the length of time the solution has been left undisturbed. The general increase in the κ values measured immediately after mixing must be due to the solution of electrolyte from the glass. The detailed nature of this process is unknown; depending on the pH and composition of the solution there can be ion exchange in either direction occurring at the glass surface $\equiv Si{-}O^-Na^+ + H^+ \rightleftarrows \equiv Si{-}OH + Na^+$ as well as the breaking away of soluble polysilicic acid or polysilicate fragments by hydrolysis of $\equiv Si{-}O{-}Si \equiv$ links. With 2×10^{-5} *M* solutions of hydrochloric acid or sodium hydroxide the conductance decreased with time presumably due in the first case to the replacement of HCl by NaCl in solution, and in the second case to the disappearance of NaOH from solution.

Returning to dilute solutions with a pH near 7, both

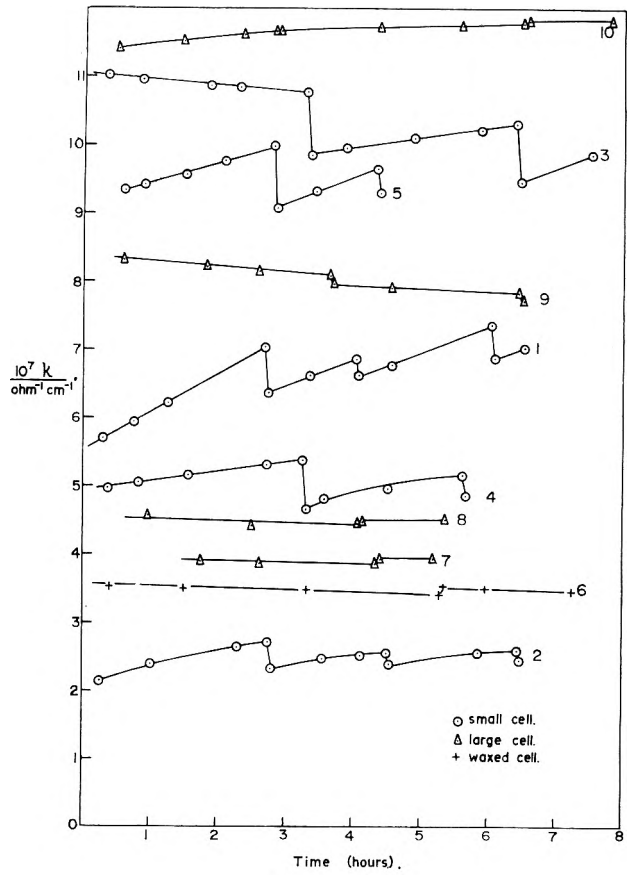

Figure 1.

the "shaking effect" and the rate of solution of glass are less when the carbon dioxide content of the water is lower as shown by curve 2. Overnight κ only rose to 3.0×10^{-7} ohm^{-1} cm.$^{-1}$ and fell to 2.6×10^{-7} ohm^{-1} cm.$^{-1}$ on mixing the solution. Deubner and Heise[4] likewise observed a correlation between the magnitude of the shaking effect and the carbon dioxide content of a solution. However, the effect is not specifically due to carbon dioxide, for very dilute solutions of hydrochloric acid (curves 3 and 4) also show similar behavior. One notes also, particularly in curve 3, that the values of κ immediately after mixing decrease with time; ion-exchange replacement of HCl by NaCl occurs. The shaking effect in fact seems to occur with any very dilute electrolyte solution, and has been observed in this work with solutions (κ values in the range 5–15 $\times 10^{-7}$ ohm^{-1} cm.$^{-1}$) of NaOH, NH_4OH, KCl, NH_4Cl, NaOAc, KH_2PO_4, Na_2HPO_4, and $LaCl_3$. Curve 5 shows some results for the last salt.

The effect of platinizing the electrodes was examined. If the electrodes are not thoroughly washed and soaked with conductance water after platinization, the apparent shaking effect is much larger. Electrolyte slowly diffusing out of the platinum black into the region between the electrodes increases κ and there is a large drop when the foreign ions are distributed by shaking the solution. However, in the cell used in this work, with adequately washed platinized electrodes the shaking effect was no greater than with bright electrodes. More pertinently, the shaking effect disappears if the interior of the conductance cell is waxed. Curve 6, which is displaced by —0.5 unit, shows some results for CO_2-contaminated water. The slight increase in κ on mixing must be due to traces of electrolyte from the sur-

(1) Chemistry Department, The University, Reading, Berkshire, England.
(2) R. H. Stokes, *J. Phys. Chem.*, **65**, 1242 (1961).
(3) J. E. Prue and P. J. Sherrington, *Trans. Faraday Soc.*, **57**, 1795 (1961).
(4) A. Deubner and R. Heise, *Ann. Physik* [6], **9**, 213 (1951).
(5) R. H. Stokes, *J. Phys. Chem.*, **65**, 1277 (1961).

face of the wax. The disadvantages of waxing the interior of a cell with a small electrode bulb are twofold; any wax deposited on the electrodes themselves results in a marked frequency dependence of κ, while if it flakes off changes of cell constant will result. Siliconing the interior of the cell only slightly reduced the shaking effect.

A second cell was made in which a pair of electrodes similar to those in the first cell at about the same distance apart were sited at the middle of an electrode chamber of 70-ml. capacity (the cell constant was 0.0918 cm.$^{-1}$). In this cell only slight displacement of κ occurred on shaking the solutions. Results are shown in the figure for CO_2 (7), HCl (8 and 9) and $LaCl_3$ (10). The curves are displaced by -2, -1, -1, and -4 units for economy of space and clarity. Slight drifts of κ with time remain. These can be prevented by waxing the interior of the cell; there is no objection to so doing with a cell in which the deposition of wax on the electrodes themselves can be avoided.

No explanation has yet been offered for the shaking effect. It seems to occur when the electrode edges are close to the internal glass surface of the electrode chamber, for in the small cell the electrode edges around their circumference were within about 2 mm. of the glass surface of the chamber. The same was true of the conductance cells used by Prue and Sherrington.[3] It is difficult to avoid the conclusion that the trouble is caused by the concentration of electrolyte at the polar glass surfaces (perhaps because of surface ion-exchange) which provides a ring of solution of lowered resistance between the edges of the electrodes. The effect would more properly be called a stagnation effect, for the low resistance ring of solution slowly forms in the undisturbed cell and is dispersed on shaking. It is also possible that there is a contribution from conduction over the glass surface between the points where the electrode leads are sealed in. That the removal of ions from the glass surface is involved is supported not only by the effect of waxing but also by the observation that thorough shaking is necessary to cause the maximum decrease of κ, and that the process is slower with a siliconed glass surface. To prevent the effect it is necessary for the diameter of the electrode chamber to be considerably larger than the diameter of the electrodes. The disadvantage of this is that the time taken to attain thermal equilibrium is longer. It is possible that quartz cells would not show the effect. An enhancement of the conductance of a solution near a glass surface is in fact well known to those concerned with electrokinetic phenomena.[6]

Acknowledgment.—The author is indebted to Professor R. H. Stokes for helpful discussions.

(6) J. W. McBain, C. R. Peaker, and A. M. King, *J. Am. Chem. Soc.*, **51**, 3294 (1929).

THE HEAT OF MIXING OF ISOPROPYL ALCOHOL IN BINARY SYSTEMS CONTAINING CARBON TETRACHLORIDE, DIISOPROPYL ETHER, AND POLY-(PROPYLENE OXIDE)

By R. F. Blanks and J. M. Prausnitz

Department of Chemical Engineering, University of California, Berkeley, Calif.

Received November 12, 1962

Heats of mixing at 25° were measured for the three systems isopropyl alcohol–carbon tetrachloride, isopropyl alcohol–isopropyl ether, and isopropyl alcohol–poly-(propylene oxide). The calorimeter used to obtain these measurements was a semimicro, liquid–liquid calorimeter which is described in detail elsewhere.[1] It is of the non-isothermal type, heat quantities being calculated by the temperature changes which are a result of the mixing process. The estimated experimental error was $\pm 1.0\%$ of the measured heat of mixing.

The solvents used in this investigation were obtained from Matheson, Coleman and Bell. Isopropyl alcohol and carbon tetrachloride were of spectroscopic grade. These materials were fractionated in a 10-plate Oldershaw-type column and stored with Linde Molecular Sieve pellets in a dry nitrogen atmosphere. The poly-(propylene oxide) had the structure

$$CH_3CH_2CH_2CH_2{-}O{-}\left(\begin{matrix}H & H\\ C{-}C{-}O\\ H & CH_3\end{matrix}\right)_n{-}CH_2CH_3$$

It was a liquid of average molecular weight 1600, supplied by Union Carbide Chemicals Co. The specific gravity of the polymer was 0.9850 at 20/20.

The results are given in Tables I, II, and III, and are shown in Fig. 1. The endothermic heat of mixing

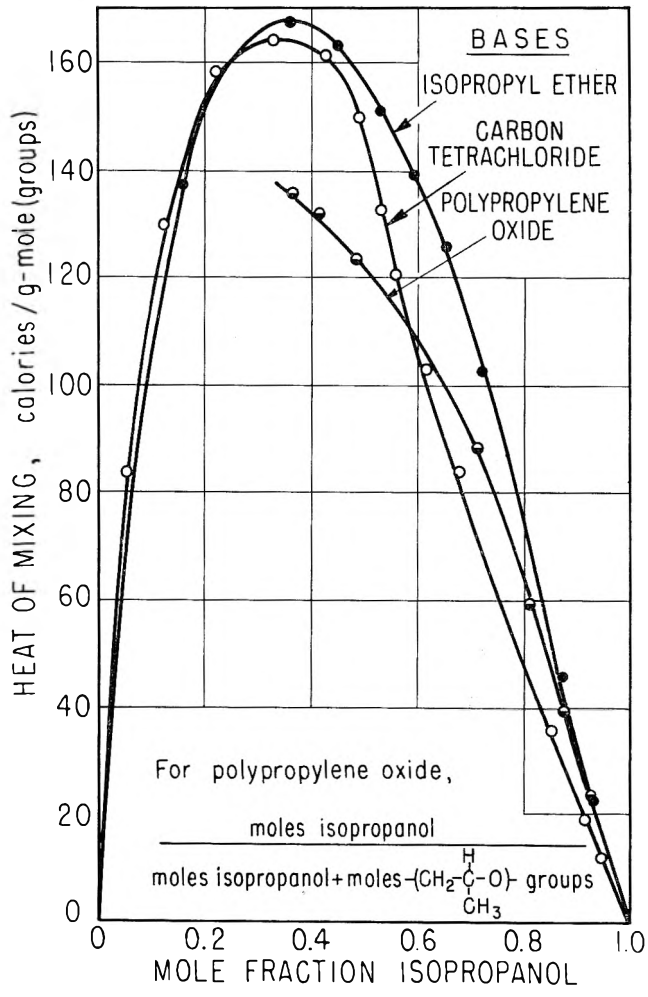

HEAT OF MIXING, ISOPROPANOL–BASE, 25°C

Figure 1.

curves for these systems are unsymmetrical with the maximum occurring at about 0.35 to 0.4 mole fraction isopropyl alcohol. The curves are similar to those ob-

(1) R. Anderson and J. M. Prausnitz, *Rev. Sci. Instr.*, **32**, 1224 (1961).

tained for alcohol–carbon tetrachloride systems[2–5] and for alcohol–ether systems.[3]

TABLE I

HEAT OF MIXING FOR THE CARBON TETRACHLORIDE (1)–ISOPROPYL ALCOHOL (2) SYSTEM AT 24.92 ± 0.01°

x_1	x_2	ΔH^m, cal./g. mole
0.057	0.943	11.5[a]
.090	.910	18.0[a]
.148	.852	35.1[a]
.317	.683	84.1
.384	.616	103
.463	.537	133
.664	.336	164[a]
.773	.227	158[a]
.877	.123	130[a]
.870	.121	132[a]
.945	.055	84.1[a]

[a] Calculated from heat of dilution.

TABLE II

HEAT OF MIXING FOR THE DIISOPROPYL ETHER (1)–ISOPROPYL ALCOHOL (2) SYSTEM AT 24.92 ± 0.01°

x_1	x_2	ΔH^m, cal./g. mole
0.063	0.937	22.5[a]
.125	.875	46.9[a]
.281	.719	102
.337	.663	126
.404	.596	139
.466	.534	151
.542	.458	163[a]
.633	.367	160[a]
.795	.205	150[a]

[a] Calculated from heats of dilution.

TABLE III

HEAT OF MIXING FOR THE POLY-(PROPYLENE OXIDE) (1)–ISOPROPYL ALCOHOL (2) SYSTEM AT 24.92 ± 0.01°

x_1[b]	x_2[b]	ΔH^m, cal./g. mole (group basis)
0.075	0.925	24.4[a]
.122	.878	40.0[a]
.189	.811	59.9[a]
.282	.718	88.5[a]
.448	.552	121
.519	.481	123
.586	.414	132
.634	.366	136
.639	.361	135

[a] Calculated from heat of dilution. [b] x_2 = moles isopropyl alc. / (moles isopropyl alc. + moles of $-\left[\begin{array}{c} H \\ | \\ CH_2-C-O \\ | \\ CH_3 \end{array}\right]-$ groups)

In these systems two types of hydrogen bonding are possible. The pure alcohol is highly associated and therefore as the pure alcohol is mixed with a second liquid, alcohol–alcohol hydrogen bonds are broken with an endothermic heat effect. The alcohol, however, is also capable of hydrogen bonding with the second liquid, causing an exothermic heat effect.[6] The positive heat-of-mixing results show that for these three systems the breaking of alcohol–alcohol association bonds is the dominant factor in determining the net observed heat of mixing. The similarity of the three curves shows the interesting result that these three proton acceptors are about equally capable of breaking the alcohol–alcohol bond and that the amount of solvation is apparently a secondary effect. The data also show that monomeric isopropyl ether and the polymeric ether, poly-(propylene oxide), mix with isopropyl alcohol to produce similar heat-of-mixing curves. It appears that polymer and monomeric ethers exhibit very similar energetic effects when mixed with isopropyl alcohol.

Acknowledgment.—The authors are grateful for financial support given by the Kettering Foundation in the form of a grant and by the Woodrow Wilson Foundation, in the form of a fellowship.

(2) R. F. Blanks and J. M. Prausnitz, to be published.

(3) H. Hirobe, as quoted by J. Timmermans, "Physico-Chemical Constants of Binary Systems in Concentrated Solutions," Interscience, New York, N. Y., 1959.

(4) J.-E. A. Otterstedt and R. W. Missen, *Trans. Faraday Soc.*, **58**, 869 (1962).

(5) G. Scatchard, S. E. Wood, and J. M. Mochel, *J. Am. Chem. Soc.*, **68**, 1963 (1946); **74**, 3724 (1952).

(6) Alcohol–carbon tetrachloride solvation is discussed by Otterstedt and Missen.[4] Isopropyl alcohol–isopropyl ether and isopropyl alcohol–poly-(propylene oxide) heats of solvation are reported elsewhere.[2]

THEORY OF RADIATION CHEMISTRY. VI. CYLINDRICAL DIFFUSION MODEL WITH A SCAVENGER[1]

BY ARYEH H. SAMUEL AND JAMES S. MILLS

Stanford Research Institute, Menlo Park, California

Received October 1, 1962

Previous papers of this series[2] have outlined a simplified mathematical model for the simultaneous diffusion and recombination of ions and radicals formed in the track of ionizing particles. This model (the Magee model) is useful to the degree that it is susceptible of analytic mathematical treatment while remaining reasonably similar to the actual events in irradiated materials.

The main characteristic of the Magee model is a discontinuity of the concentration of active species (ions or radicals) at the boundary of the expanding track (cylindrical) or spur (spherical). The concentration is assumed to be uniform in space, though varying in time, both outside (background concentration, y) and inside the boundary.

In this paper, the cylindrical model of ref. 2a is modified by the introduction of a homogeneously distributed scavenger (solute) which ultimately reacts with all active species which do not undergo pairwise recombination. The presence of such a scavenger is a feature of most real systems. The cylindrical model is appropriately used for irradiations with particles of high linear energy transfer (LET).

The scavenger is assumed to be present in constant concentration c_s. Depletion of the scavenger in the tracks is ignored; the inaccuracies introduced by this assumption have been discussed by Kuppermann and Belford[3] for the case of irradiated water and are found to be small. The bimolecular reaction rate of the scavenger with the active species is k_s. These two quantities always appear as the product $k_s c_s = A$. The species formed in the scavenger reaction is assumed stable by comparison with the active species.

It should be noted that this is a "one-radical" model

(1) Presented in part at the Second International Congress of Radiation Research, Harrogate, Yorkshire, England, August 5–11, 1962.

(2) (a) J. L. Magee, *J. Am. Chem. Soc.*, **73**, 3270 (1951); (b) A. H. Samuel, *J. Phys. Chem.*, **66**, 242 (1962).

(3) A. Kuppermann and G. G. Belford, *J. Chem. Phys.*, **36**, 1427 (1962).

and that it should not be used if the parameters are expected to be grossly different for the species formed. For example, it should not be used for ions unless it is believed that the electrons will attach to molecules to form negative ions.

Solution of the Mathematical Model.—This model leads to the following differential equation for the number of active particles (N) per unit length inside the track

$$dN/dt = -kN^2/v - AN + y\, dv/dt \qquad (1)$$

where k is the rate constant of recombination, and v is the track volume per unit track length

$$v = v_0 + Dt \ (D = \text{diffusion constant}) \qquad (2)$$

At zero time (the moment of passage of the primary particle), $v = v_0$, $N = N_0 = w_0 + v_0y_0$, where w_0 is the number of active species per unit track length formed by the primary ionizing particle (this is proportional to the LET).

Outside the track boundary, the change in the background concentration, y, is described by

$$dy/dt = -ky^2 - Ay \ (y = y_0 \text{ when } t = 0) \qquad (3)$$

a differential equation with separable variables having the solution

$$y = y_0 \exp(-At)\{1 + ky_0A^{-1}[1 - \exp(-At)]\}^{-1} \qquad (4)$$

On substituting (2) in (4) and the derivative of (2) in (1), the following differential equation is obtained

$$\frac{dN}{dv} = -\frac{kN^2}{Dv} - \frac{AN}{D} + \frac{y_0 \exp[-AD^{-1}(v - v_0)]}{1 + ky_0A^{-1}\{1 - \exp[-AD^{-1}(v - v_0)]\}} \qquad (5)$$

This is a Riccati equation and can be converted into a linear differential equation if a particular solution can be found. As the particular solution N' we take the case $w_0 = 0$. This corresponds to zero LET of the primary particle or an "empty track" so that (4) applies inside the track also

$$N' = vy = \frac{vy_0 \exp[-AD^{-1}(v - v_0)]}{1 + ky_0A^{-1}\{1 - \exp[-AD^{-1}(v - v_0)]\}} \qquad (6)$$

This is a solution of (5). The general solution is found by substituting

$$N = N' + 1/Z \qquad (7)$$

A linear differential equation in Z results, which is solved in the usual manner

$$Z = kD^{-1} e^{qx}\{1 + p[1 - e^{-q(x-1)}]\} \times \left\{p^{-2} \sum_{i=1}^{\infty} i[p/(1 + p)]^{i+1} e^{(i-1)q} Ei(-iqx) + C\right\} \qquad (8)$$

Here $p = ky_0/A$, $q = Av_0/D$, $x = v/v_0$, and Ei stands for the exponential integral. (It will be noted that $pq = \beta$ of ref. 2a.) The constant of integration C is found by substituting the initial condition $N = N_0$, hence $Z = 1/w_0$, when $x = 1$. This gives as the complete solution, after substitution in (7)

$$N = \frac{y_0v_0x \exp[-q(x - 1)]}{1 + p\{1 - \exp[-q(x - 1)]\}} + \frac{\exp[-q(x - 1)][1 + p\{1 - \exp[-q(x - 1)]\}]^{-2}}{w_0^{-1} + p^{-2}kD^{-1} \sum_{i=1}^{\infty} i[p/(1 + p)]^{i+1} e^{qi} \times [Ei(-iqx) - Ei(-iq)]} \qquad (9)$$

This is a general solution giving the number of active species in the track at any moment of its life.

Special Cases.—Magee[2a] has shown that when densely ionizing particles pass through liquids or solids, the background concentration, y, is very low for all normal dose rates. It is therefore useful to have a special form of (9) for the case of negligible y. Either by solving the Bernoulli equation produced by dropping the last term of (5), or by simple substitution of $y = y_0 = 0$, hence $p = 0$, in (9), one obtains

$$N = e^{-q(x-1)}\{w_0^{-1} + kD^{-1} e^q[Ei(-qx) - Ei(-q)]\}^{-1} \qquad (10)$$

Another approximation is needed for small A, when p becomes large and q small. The tabulation of $Ei(-x)$ does not extend to very small arguments, but one may then use the approximation

$$Ei(-iqx) - Ei(-iq) = \ln x - iq(x - 1) \qquad (11)$$

If $\ln x >> qi(x - 1)$, the summation can be obtained in closed form as

$$\sum_{i=1}^{\infty} i(p/1 + p)^{i+1} e^{qi} \ln x = p^2e^q(1 + p)^{-2} \times [1 - pe^q/(p + 1)]^{-2} \ln x \qquad (12)$$

This obviates the necessity of calculating many terms of the summation when $p >> 1$.

Use of the Formulas.—To use (9) for the study of real systems, it is necessary to relate it to an experimentally observable quantity. The most easily observed such quantity is the fraction of active species which react with the scavenger. We give here a five-step procedure for the calculation of this fraction as a function of the track parameters.

1. The necessary parameters for a calculation are k, $k_sc_s = A$, w_0, D, v_0, and y_0. All except y_0 must be known or assumed in advance. Instead of y_0, we shall use the dose rate as our sixth independent variable, as shown in steps 2 and 3. It is usually not too difficult to estimate w_0, D, and c_s. When not known experimentally, values of k and k_s can be obtained from estimates of the activation energy and steric factor for the recombination and the scavenger reaction, respectively. The value of v_0 in gases is available from cloud chamber experiments; in liquids there are conflicting views of its magnitude.

2. The next step is to fix the expansion ratio of the track. As in ref. 2a, we call the final track volume at the moment the track is traversed by another ionizing particle v_m. Then $x_m = v_m/v_0$. The value of x_m is obtained from

$$x_m(x_m - 1) = (W/2)w_0D/Iv_0^2 \qquad (13)$$

where W is the energy (in e.v.) necessary to form an ion or radical pair, and I is the dose rate (in e.v./cm.^{3}/sec.). This formula is essentially the same as eq. 15 of ref. 2a.

3. The value of y_0 is then calculated by trial and error. A value of y_0 is assumed and $N(x_m)$ is calculated by (9). When the correct value is found, $N(x_m) = v_0 y_0 x_m$. If the trial N is too high, raise y_0, and *vice versa*. We have found that about six trials are necessary; but it is sometimes observed that the second term of (9) is very insensitive to changes in y_0, so that the labor is much reduced.

4. Using the value of y_0 thus obtained, calculate N and y for $v_0 \leq v \leq v_m$, using (9) and (4), respectively.

5. The fraction of the active species reacting with the scavenger, F_s, is then found by numerical integration

$$F_s = \frac{Av_0}{Dw_0} \int_1^{x_m} [N + yv_0(x_m - x)]\mathrm{d}x \quad (14)$$

This formula is based on the fact that in this steady state model the total number of active species consumed per unit track length during the track lifetime is just w_0. The fraction F_s is therefore derived by calculating the number of reactions with the scavenger inside and outside the track boundary and dividing by w_0. Ultimately all active species either recombine or react with the scavenger, and the fraction recombining is simply $(1 - F_s)$.

A calculation of F_s for a set of parameters takes at most a few hours with a desk calculator. Small values of p and large values of q greatly reduce the required effort. It thus becomes possible to estimate the effect of variation of track parameters without using electronic computers.

Since the simplified equation 10 suffices for most liquid and solid irradiations, the procedure we have outlined is useful primarily for study of gases. The overlapping of spurs to form a cylindrical track is essentially independent of density, so that (9) applies to the same types of radiation (low-energy protons, α-rays, fission fragments) as the cylindrical model in liquids.[3] However, it has been shown (ref. 2a, Fig. 4) that, for the relatively low LET of alpha particles and protons, track effects will be observed only when dose rates are below a few rads/sec.

We have found that for all types of radiation it is possible to vary F_s by changing a number of parameters. It will be obvious that changes in c_s and I can change F_s. We have also found that F_s can be changed if only the pressure is varied. Among the basic parameters, k and k_s are independent of pressure, w_0 and c_s (hence A) are directly proportional to pressure, and D is inversely proportional, while v_0 is inversely proportional to the square of the pressure. The yield of a gas chemical reaction induced by heavy ionizing particles can thus be varied by changing the pressure only. Some preliminary calculations indicate that this effect may be important in the design of a fissiochemical reactor such as has been proposed for nitrogen fixation.[4] Indeed, the experiments of Harteck and Dondes[4] show a marked pressure dependence of gaseous reactions induced by fission fragments, which probably is due to these track effects.

(4) P. Harteck and S. Dondes, *Z. Elektrochem.*, **64**, 983 (1960); NYO-9967 (1961).

ION-EXCHANGE KINETICS. IV. DEMONSTRATION OF THE DEPENDENCE OF THE INTERDIFFUSION COEFFICIENT ON IONIC COMPOSITION

BY F. HELFFERICH

Shell Development Company, Emeryville, Cal.

Received October 17, 1962

In part I and part II of this series, a theoretical treatment of particle-diffusion controlled ion exchange has been given on the basis of the Nernst–Planck equations; in part III, experimental confirmation for the forward and reverse exchanges of H^+ and Na^+ has been presented.[1] The decisive point in which the new theory differs from the earlier ones is that the Nernst–Planck equations, which include the effect of electric potential gradients, lead to an interdiffusion coefficient which depends on ionic composition of the ion exchanger and thus changes locally and with time as ion exchange progresses, while the earlier theories assumed a constant interdiffusion coefficient. Although experimental evidence obtained with ion-exchanger beads[2] and membranes[3] supports the validity of the Nernst–Planck equations (or refinements thereof), the dependence of the interdiffusion coefficient on ionic composition is still questioned by some investigators. The experiments described below were designed to provide a simple, direct, and convincing demonstration of this dependence.

The following system was chosen. A cation-exchanger membrane is inserted between two dilute and well stirred solutions containing HCl and NaCl. A series of experiments is made with solution compositions as listed in the first four columns of Table II; the total concentration (HCl + NaCl) is kept constant in both solutions at 0.1 N and the concentration differences of H^+ and Na^+ between the two solutions are also kept constant at 0.02 N, while the H^+ concentration is systematically increased from one experiment to the next and the Na^+ concentration is correspondingly reduced. The process occurring is interdiffusion of H^+ and Na^+ across the membrane. Since the membrane material has practically no selectivity for either counterion in equilibrium with HCl–NaCl mixtures, the differences in the intramembrane concentrations of H^+ and Na^+ between the membrane boundaries are practically the same in all experiments, and all that is changed is the (average) concentration ratio of H^+ and Na^+ in the membrane. A variation of the interdiffusion flux of H^+ and Na^+ across the membrane from one experiment to the other thus demonstrates clearly the variation of the interdiffusion coefficient with this concentration ratio.[4]

The membrane used was a condensation polymer of

(1) Part I: F. Helfferich and M. S. Plesset, *J. Chem. Phys.*, **28**, 418 (1958); part II: M. S. Plesset, F. Helfferich, and J. N. Franklin, *ibid.*, **29**, 1064 (1958); part III: F. Helfferich, *J. Phys. Chem.*, **66**, 39 (1962).

(2) See part III.

(3) See, for example, F. Helfferich and H. D. Ocker, *Z. physik. Chem.* (Frankfurt), **10**, 213 (1957); D. Mackay and P. Meares, *Kolloid Z.*, **171**, 139 (1960); **176**, 23 (1961); M. A. Peterson and H. P. Gregor, *J. Electrochem. Soc.*, **106**, 1051 (1959).

(4) Similar experiments have been carried out as early as 1957 by E. R. Gilliland, R. F. Baddour, and D. J. Goldstein (*Can. J. Chem. Eng.*, **35**, 10 (1957)) with a porous diaphragm instead of an ion-exchanger membrane. Their results show the same trend as ours but, having been obtained with a membrane without ion-exchange properties, are only indirect evidence on ion-exchange kinetics.

phenolsulfonic acid and formaldehyde, prepared as described in part III. The relevant membrane properties are listed in Table I. The interdiffusion experiments were carried out in a standard two-compartment cell[5] under conditions which exclude effects of unstirred films.[6] After an initial two-hour period for attainment of the steady state in the membrane,[7] the interdiffusion flux was measured by determining both the H^+-concentration increase with time in one compartment and the decrease in the other by acidimetric titration of aliquots; increase and decrease equalled one another, showing that the steady state had indeed been attained. The flux J_H is calculated from

$$J_H = \frac{V\Delta C_H}{A\Delta t} \qquad (1)$$

where ΔC_H is the change in H^+ concentration in the time Δt, V is the solution volume in the compartment, and A is the membrane surface area exposed to the solutions. The changes ΔC_H were kept to a few per cent of the concentration differences between the two solutions. The experimental error is about $\pm 5\%$. Furthermore, it was ascertained by titration of Cl^- before and after the experiment that no detectable Cl^- transfer across the membrane had occurred. To rule out errors that might have arisen from a slow change in membrane properties, the experiments were reproduced after the whole series had been completed.

Table I

Membrane Properties in Equilibrium with 0.1 N Solutions of HCl and NaCl at 25°

Thickness	d	= 0.18 cm.
Exposed surface area	A	= 2.5 cm.²
Ion-exchange capacity (basis swollen resin)	$\bar{C}$	= 1.10 ± 0.03 meq./cm.³
Water content		62 ± 1% wt.
Cl^- content (basis swollen resin)		0.012 ± 0.001 meq./cm.³
Intraresin diffusion coefficients	$\bar{D}_H$	= 2.4×10^{-5} cm.²/sec. ± 5%
	$\bar{D}_{Na}$	= 3.5×10^{-6} cm.²/sec. ± 5%
Selectivity coefficient (varies linearly with $\bar{C}_H/\bar{C}$)	α_{Na}^{H}	= 1.06 + 0.1(1 − $\bar{C}_H/\bar{C}$)

The observed fluxes are listed in Table II (column 5). The fluxes increase markedly as the amount of H^+ in the system is reduced and that of Na^+ is increased. This variation is as predicted by the theory. As has been pointed out in part I and as is apparent from eq. 3, the counterion which is in the minority has the stronger effect on the interdiffusion coefficient; accordingly, this coefficient and thus the flux should increase as the concentration of the faster counterion, H^+, is reduced (see also Fig. 1 in part I).

In principle, membrane selectivity may obscure the results by affecting the flux through its effect on the intramembrane boundary concentrations. To show that such selectivity effects are minor in the systems studied here, integral interdiffusion coefficients $\bar{D}$ were calculated from

$$J_H = \bar{D}\frac{\bar{C}_H' - \bar{C}_H''}{d} \qquad (2)$$

where d is the membrane thickness, and $\bar{C}_H'$ and $\bar{C}_H''$ are the intramembrane boundary concentrations on the left and right membrane side, respectively, determined by independent equilibrium measurements. (Since the boundary concentrations change by a few per cent during the time Δt of the flux measurement, time averages were used for $\bar{C}_H'$ and $\bar{C}_H''$.) The coefficients $\bar{D}$ are integral averages over the whole membrane, but are unaffected by membrane selectivity which can only change the values of C_H' and C_H''. Table II (column 7) shows that $\bar{D}$ follows the same trend as the flux and is far from being constant.

Table II

Interdiffusion Fluxes and Integral Interdiffusion Coefficients at 25°

Solution compn. mmoles/cm.³ Left HCl	Left NaCl	Right HCl	Right NaCl	Interdiffusion flux, mmoles cm.⁻² sec.⁻¹ Obsd.	Theor.	Integral interdiffusion coefficient, cm.²/sec. Obsd.	Theor.
0.10	0	0.08	0.02	4.9×10^{-6}	4.2×10^{-6}	4.4×10^{-6}	3.8×10^{-6}
.08	0.02	.06	.04	5.2	5.3	4.6	4.7
.06	.04	.04	.06	7.6	6.9	6.6	6.0
.04	.06	.02	.08	9.9	10.2	8.2	8.4
.02	.08	0	.10	15.8	20.1	12.1	15.4

Beyond establishing qualitative agreement with the predictions, it is tempting to test how far the simple theory based on the Nernst–Planck equations can account quantitatively for the observed fluxes and integral interdiffusion coefficients. For this purpose, theoretical values of the fluxes and interdiffusion coefficients were calculated from the individual intramembrane diffusion coefficients $\bar{D}_H$ and $\bar{D}_{Na}$ determined by independent conductivity measurements as described in part III. As shown in part I, the Nernst–Planck equations for H^+ and Na^+, with the appropriate conditions and simplifying assumptions as discussed there, lead to the interdiffusion flux

$$J_H = -\left[\frac{\bar{D}_H\bar{D}_{Na}\bar{C}}{\bar{D}_H\bar{C}_H + \bar{D}_{Na}\bar{C}_{Na}}\right]\text{grad}\,\bar{C}_H \qquad (3)$$

where $\bar{C} = \bar{C}_H + \bar{C}_{Na}$ is the (constant) concentration of fixed membrane charges, and the expression in brackets is the (variable) interdiffusion coefficient. With the additional assumption that diffusion occurs normal to the membrane surfaces through the membrane area exposed to the solutions, integration of eq. 3 across the membrane in the steady state (div $J_H = 0$) gives

$$J_H = \frac{\bar{D}_H\bar{D}_{Na}\bar{C}}{(\bar{D}_H - \bar{D}_{Na})d}\ln\frac{\bar{D}_{Na} + (\bar{D}_H - \bar{D}_{Na})\bar{C}_H'/\bar{C}}{\bar{D}_{Na} + (\bar{D}_H - \bar{D}_{Na})\bar{C}_H''/\bar{C}} \qquad (4)$$

The theoretical fluxes obtained from eq. 4 and the integral interdiffusion coefficients obtained from these

(5) See, for example, F. Helfferich, *Z. Elektrochem.*, **56**, 947 (1952).

(6) See F. Helfferich, *Z. physik. Chem.* (Frankfurt), **4**, 386 (1955), for conditions that guarantee absence of film effects.

(7) See ref. 5 for time required to attain the steady state.

fluxes by use of eq. 2 are included in Table II (columns 6 and 8, respectively). The agreement with the experimental values is as good as one can expect in view of the simplifying assumptions of the theory and the limited accuracy of the experiments. The deviations between experiment and theory are small in comparison with the changes in the flux and the interdiffusion coefficient, which vary by about the factor three in the range studied.

One fact emerges clearly from this investigation: the dependence of the interdiffusion coefficient on ionic composition, as predicted by the Nernst–Planck equations, is real. While more elaborate theories which include further effects will undoubtedly be needed for more complicated systems,[8] no such theory can afford to ignore this dependence.

Acknowledgment.—The help of Mr. W. J. Parker and Mr. D. Dere in carrying out the experiments is gratefully acknowledged.

(8) For steady-state membrane systems, such theories have been developed; see ref. 3 and R. Schlögl, *Z. physik. Chem.* (Frankfurt), **1**, 305 (1954), **3**, 73 (1955).

THE EFFECT OF MOLECULAR COMPLEXING ON pK VALUES

BY G. CILENTO AND M. BERENHOLC

Departamento de Química, Faculdade de Filosofia, Ciências e Letras, Universidade de São Paulo, São Paulo, Brazil

Received October 8, 1962

When a compound having a titrable group forms a molecular complex, it is obvious that the pK of the group may be modified, especially if the group is involved in the association. Hence protons may be released or captured. This might be of considerable biological significance.

The change in pK for an acid AH can be calculated by applying the Henderson–Hasselbach equation to the dissociation of the complexed acid and by expressing in the latter equation the concentration of the complexed acid and of complexed conjugate base in function of their association constants, respectively, K_1 and K_2

$$pK = pH + \log \frac{[AH]K_1}{[A^-]K_2}$$

Therefore the pK of the complexed acid corresponds to that pH at which $[AH]/[A^-] = K_2/K_1$. This pH is calculated by applying the Henderson–Hasselbach equation to the ionization of AH, whereby

$$\Delta pK = \log \frac{K_1}{K_2}$$

Results

Due to experimental difficulties it is not always possible to determine both K_1 and K_2 by current spectrophotometric methods. In some instances this can be partly overcome by substituting the insoluble component by a strictly related compound having a solubilizing group removed from the zone of association.

The Effect of the Binegative Anion from 3,5-Diiodo-4-hydroxybenzoic Acid on the pK_a (10.2)[1] of Riboflavin.—In bicarbonate solution, pH 8.40, where free riboflavin should exist almost wholly in the neutral form, the association constant was found to be 42.8 l. mole^{-1}. In sodium hydroxide solution 0.66–0.80 N, where riboflavin exists essentially in the anionic form, the equilibrium constant is smaller, 10.5 ± 0.6 l. mole^{-1}, probably because the electron acceptor ability of riboflavin is markedly reduced. Thus complexing with the binegative anion raises the pK_a of riboflavin by 0.6 pH unit.

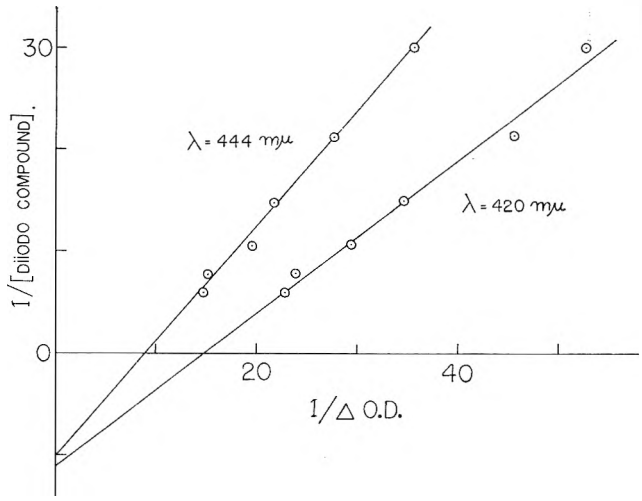

Fig. 1.—Spectrophotometric determination of the equilibrium constant for the complex of anionic riboflavin with the binegative anion from 3,5-diiodo-4-hydroxybenzoic acid. The riboflavin concentration, 3.5×10^{-4} M, was kept constant. Ordinates, the inverse of the molar concentration of the iodinated compound. Abscissas, the inverse of the variation of the optical density with respect to the sum of the optical densities of the individual components. Optical path, 1 cm.

The Effect of Riboflavin on the pK_a (6.4)[2] of *o*-Diiodophenols.—As reported above, the association constant for the complex of neutral riboflavin with the binegative anion from 3,5-diiodo-4-hydroxybenzoic acid is 42.8 l. mole^{-1}. The corresponding datum for the un-ionized phenol refers to 3,5-diiodotyrosine, which is easily solubilized by addition of hydrochloric acid. (In the conditions of acidity used there was hardly any protonation of riboflavin.) The equilibrium constant was found to be 50 l. mole^{-1}. That the side chain of the diiodophenol does not influence the equilibrium is suggested by the value 41.3 l. mole^{-1} for the association of riboflavin with the binegative anion from diiodotyrosine. In conclusion, the pK_a of *o*-diiodophenols is not affected by the association with riboflavin.

Experimental

The association constants for the complexes of neutral riboflavin with the undissociated and the dissociated *o*-diiodophenols were determined in connection with other work which is being carried out[3,4] and which will be reported in detail in a later paper.

The apparent equilibrium constant at 25 ± 2° for the complex of anionic riboflavin with the binegative anion from 3,5-diiodo-4-hydroxybenzoic acid was determined spectrophotometrically from the changes that the latter anion produces on the spectrum of the ionized riboflavin. A Beckman DU quartz spectrophotometer and Corex cells of 1 cm. optical path were used. The final volume was 3.0 ml.

Since the isolated components absorb light of the wave length used—riboflavin much more than the partner—the following equation[5] was employed

(1) R. Kuhn and G. Moruzzi, *Ber.*, **67**, 888 (1934).

(2) C. L. Gemmill, *Arch. Biochem. Biophys.*, **54**, 359 (1955).

(3) G. Cilento, "International Biophysics Congress," Stockholm, 1961, Abstracts of Contributed Papers, p. 89.

(4) G. Cilento and M. Berenholc, *J. Am. Chem. Soc.*, **84**, 3968 (1962).

(5) E. Fujimori, *Proc. Natl. Acad. Sci. U. S.*, **45**, 133 (1959).

$$\frac{1}{[\text{binegative anion}]} = K(\epsilon_2 - \epsilon_{\text{rib}})[\text{riboflavin}]_0 \frac{1}{\Delta\text{O.D.}} - K$$

where ΔO.D. represents the change of optical density with respect to the sum of the isolated absorptions. This equation holds for complexes formed in the 1:1 ratio. To secure the data, to 0.5 ml. of a 2.1×10^{-4} *M* aqueous solution of riboflavin, 0.5 to 2.5 ml. of a 2.00×10^{-1} *M* solution of 3,5-diiodo-4-hydroxybenzoic acid in 1.2 *N* sodium hydroxide was added and the volume brought to 3.0 ml. with 1.2 *N* sodium hydroxide solution. Plots for two wave lengths are shown in Fig. 1; the method of least squares was used. Because of the small values of ΔO.D. the observed value of *K*, 10.5 ± 0.6 l. mole^{-1}, can be regarded as reasonably accurate.

Acknowledgment.—We thank the Brazilian "Conselho Nacional de Pesquisas" for research grants and for a fellowship granted to M. B.

THE CATION TRANSFERENCE NUMBER IN AQUEOUS POTASSIUM CHLORIDE AT 70 TO 115°

By Josiah E. Smith, Jr., and Edward B. Dismukes

Southern Research Institute, Birmingham, Alabama

Received November 10, 1962

The moving-boundary method with optical procedures for detecting successive boundary positions has been extensively used for many years in obtaining accurate values of transference numbers in aqueous electrolytes. Recently, moving-boundary studies with certain procedures for determining boundary displacement from electrical resistance effects rather than from optical effects have been described.[1-4] These procedures depend upon the fact that the specific resistance of the solution behind a stable moving boundary is higher than the specific resistance of the solution ahead of the boundary.

To date, there is very little information available on transference numbers in aqueous electrolytes at temperatures above 25°. The existing information at higher temperatures consists mainly of data for sodium chloride and potassium chloride at 35 and 45°.[5,6] However, electrical-resistance procedures for determining boundary displacements might make it possible to obtain data even under high-temperature, high-pressure conditions that would create great difficulties in the use of optical procedures. This communication describes preliminary results from an investigation in which the transference number of potassium ion in approximately 0.1 *N* potassium chloride was determined at temperatures in the range of 70–115°. In this investigation, the electrical-resistance procedure was based upon original work by Fratiello and Kay.[4]

Experimental

The moving-boundary cell contained a silver–silver chloride cathode and a cadmium anode, the latter having been used for creation of an "autogenic" boundary.[7] The principal section of the cell was a vertical 2-mm. bore Pyrex capillary, which was enlarged at the bottom to accommodate the cadmium anode of 4-mm. diameter. At levels of 2.5, 4.0, 11.5, and 13.0 cm. above the anode, platinum wires (probe electrodes a, b, c, and d, respectively) of 0.5-mm. diameter were sealed into the capillary wall with their ends approximately flush with the inner wall. From the upper end of the capillary, a section of glass tubing led to a compartment containing the cathode, which was arranged in such a way that the products formed there during electrolysis did not enter the capillary tubing. Above the cathode compartment, there was a tube open to the atmosphere.

For determinations of transference numbers, the moving-boundary cell was initially filled with potassium chloride solution. A 3-mm. layer of heavy mineral oil was then placed over the aqueous solution in the open tube above the cathode to minimize evaporation of water when the cell was later heated. After the cell was loaded, it was placed in an oil-filled, 4-inch-diameter steel cylinder that was subsequently pressurized with nitrogen at 30 p.s.i.g. (This pressure was in excess of that needed to prevent boiling of the water or formation of bubbles from any dissolved air at elevated temperatures; the pressure used could have produced only a negligible effect on transference numbers.[2])

Current was supplied by batteries and was automatically maintained at a constant value near 2 or 3 ma. by a combination of the devices described by Bender and Lewis[8] and by Lingane.[9] The current was accurately determined periodically during an electrolysis by the potentiometric measurement of the voltage drop across a standard resistor in series with the moving-boundary cell. Immediately after an electrolysis was begun, the voltage drop between the probes a and b was monitored by means of a high-impedance Keithley Model 610 electrometer, and the voltage–time relation was recorded continuously. Before the boundary between the potassium and cadmium chloride solutions reached probe a, the voltage was constant; when the boundary passed probe a, the voltage began to increase linearly with time. The time at which the boundary passed the probe was that obtained from extrapolations of the linear portions of the voltage–time record to a common point. The voltage drop between probes c and d was next monitored to determine the time when the boundary passed probe c. The time Δt required for the boundary to migrate from probe a to probe c was not taken directly from the voltage–time record but from a timer whose action was started roughly 60 sec. after the boundary had passed probe a and stopped about 60 sec. after the boundary had passed probe c. Deflections of the recorder pen were made when the timer was started and stopped. Therefore, delays in operating the timer were determined from the recorder chart and were applied as corrections to the timer reading in order to obtain Δt. The principal source of error in these experiments was thought to arise from the uncertainty in designating the precise instant when a probe electrode was passed by the boundary.

The potassium chloride used in the experiments was Baker and Adamson Reagent Special potassium chloride that was crystallized three times from conductivity water and then carefully dried. The purified salt was dissolved in water that had a negligible specific conductance in comparison with the salt solution. The composition of the solution, in terms of weights *in vacuo*, was 7.419 g. of salt per 1000 g. of water. The exact concentration in equivalents per liter at each temperature was calculated from the density data given in the International Critical Tables.

Results and Discussion

The equation that relates the transference number of potassium ion, t_K, to experimentally determined properties is

$$t_K = \frac{(v + \Delta v)CF}{i\Delta t}$$

Here, v is the volume of the cell (in ml.) between probe electrodes a and c, Δv is a correction term for the gain of aqueous cadmium chloride and the loss of cadmium metal and aqueous potassium chloride below the boundary,[10] C is the concentration of potassium chloride (in equivalents per liter), F is the Faraday constant, i

(1) J. A. Davies and J. P. Butler, *Chem. in Can.*, **6**, No. 5, 39 (1954).
(2) F. T. Wall and S. J. Gill, *J. Phys. Chem.*, **59**, 278 (1955).
(3) J. W. Lorimer, J. R. Graham, and A. R. Gordon, *J. Am. Chem. Soc.*, **79**, 2347 (1957).
(4) A. Fratiello and R. L. Kay, private communication.
(5) R. W. Allgood, D. J. LeRoy, and A. R. Gordon, *J. Chem. Phys.*, **8**, 418 (1940).
(6) R. W. Allgood and A. R. Gordon, *ibid.*, **10**, 124 (1942).
(7) H. P. Cady and L. G. Longsworth, *J. Am. Chem. Soc.*, **51**, 1656 (1929).
(8) P. Bender and D. R. Lewis, *J. Chem. Ed.*, **24**, 454 (1947).
(9) J. J. Lingane, "Electroanalytical Chemistry," 2nd Edition, Interscience Publishers, Inc., New York, N. Y., 1958, p. 503.
(10) D. A. MacInnes and L. G. Longsworth, *Chem. Rev.*, **11**, 171 (1932).

is the current (in milliamperes), and Δt is the time for migration (in seconds) between probes a and c.

The value of v was determined from moving-boundary experiments with the potassium chloride solution at 35°. For this temperature, t_K in the equation above was assigned the value 0.4888 that was previously reported.[5] In four determinations, a mean value of 0.2731 ml., with an average deviation from the mean of 0.0002, was obtained. Calibration experiments at 35° after the cell had been used at higher temperatures indicated that the value remained unchanged. For experiments at higher temperatures, the value of v was corrected for the slight thermal expansion of Pyrex. The value $\Delta v = +0.0003$ ml. was calculated as described[10] for 25°; because it is a small correction term, Δv was not adjusted for its negligible variation with temperature.

Table I gives data for several experiments at temperatures in the range 70–115°. Each temperature shown was that of the thermostat surrounding the cylinder in which the moving-boundary cell was placed. Before electrolysis was begun, ample time was allowed for the inner oil-bath to become equilibrated in temperature with the outer bath. Immediately after electrolysis was begun, the voltage drop in the cell decreased by an amount that corresponded to a 0.5° rise from resistance heating, but thereafter there was no indication of a further temperature rise.

TABLE I

CATION TRANSFERENCE NUMBERS IN AQUEOUS POTASSIUM CHLORIDE

Temp., °C.	Normality	t_K[a]
70	0.09864	0.4834 ± 0.0001
86	.09606	.4818 ± .0001
100	.09512	.4808 ± .0006
115	.09403	.4783

[a] The uncertainty factors are the average deviations from means of two experiments at 70°, two experiments at 86°, and seven experiments at 100°. At each of these temperatures, currents of 2 and 3 ma. were used. A result based upon only one experiment at 115° is given, for reasons indicated in the text.

The excellent agreement shown in Table I for 70 or 86° is actually better than could have been expected from the principal source of error, the determination of Δt, which is subject to an uncertainty of about 0.1%. The scatter at 100° somewhat exceeds the variation expected from errors in Δt. Several experiments were conducted at 115°, but the transference data were scattered much more widely than at 100°. Except in one experiment at 115°, for which the result is given in the table, gas bubbles were detected in the cell when an experiment was concluded and the cell was cooled to room temperature. Throughout the time that the cell was heated, the applied pressure of 30 p.s.i.g. was sufficient to prevent boiling of water or formation of bubbles from dissolved air. It is believed that the bubbles were oxygen formed as the reaction $2H_2O \rightarrow 4H^+ + O_2 + 4e^-$ competed with the expected anode process, $Cd \rightarrow Cd^{+2} + 2e^-$. In preliminary work at room temperature, it was found that electrode gassing definitely occurred unless the anode current density was less than 1 ma./mm.^{2}. Perhaps the anode current density actually used, 0.25 ma./mm.^{2}, was too high to avoid gassing at 115°.

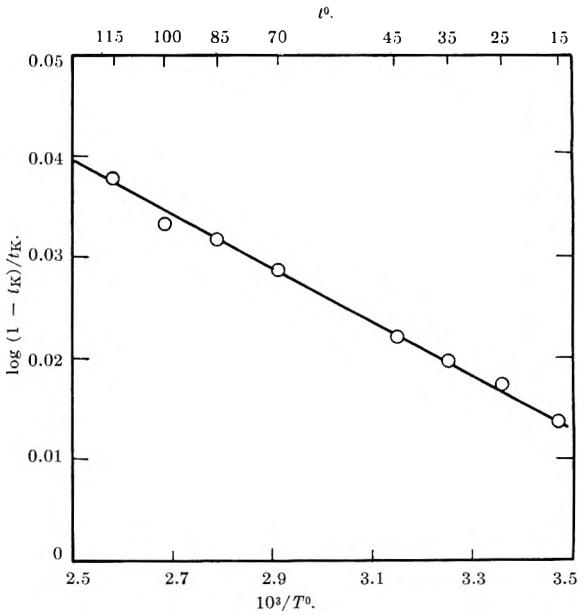

Fig. 1.—Temperature dependence of transference numbers in aqueous KCl, approximately 0.1 N in concentration.

Allgood, LeRoy, and Gordon[5] suggested that $\log (1 - t_K)/t_K$ would be a linear function of $1/T$ (the reciprocal of the absolute temperature) if the activation energies for potassium ion and chloride ion migration differ by an amount that does not depend upon the temperature. Figure 1 presents data from the work of Allgood and co-workers in the range 15–45° and from the present work in the range 70–115°. The data fit a linear relationship with a slope corresponding to an activation energy for chloride ion that is 120 cal. per gram-ion greater than the activation energy for potassium ion. Throughout the range of temperatures for which data are now available, potassium chloride departs from the usual behavior of electrolytes to show transference numbers that become more nearly equal as the temperature increases.

Acknowledgments.—Financial support from the Directorate of Chemical Sciences, Air Force Office of Scientific Research, through Contract AF 49(638)-810, is gratefully acknowledged. Helpful discussions with Professor R. L. Kay of Brown University, particularly with respect to the experimental technique used in this work, also are appreciated.

COMMUNICATION TO THE EDITOR

STUDIES ON THERMOELECTRIC FORCE AND LATTICE DEFECTS AS ACTIVE CENTERS IN PLATINUM CATALYSTS

Sir:

It was proposed[1] recently that the measurement of thermoelectric force (S) of cold-worked metals can be carried out readily with a simple technique and is a very convenient and effective means for the purpose of identifying lattice defects with active centers in metallic catalysts. In this letter, the extension of this method to cold-worked platinum catalysts is given.

(1) S. Kishimoto, *J. Phys. Chem.*, **66**, 2694 (1962).

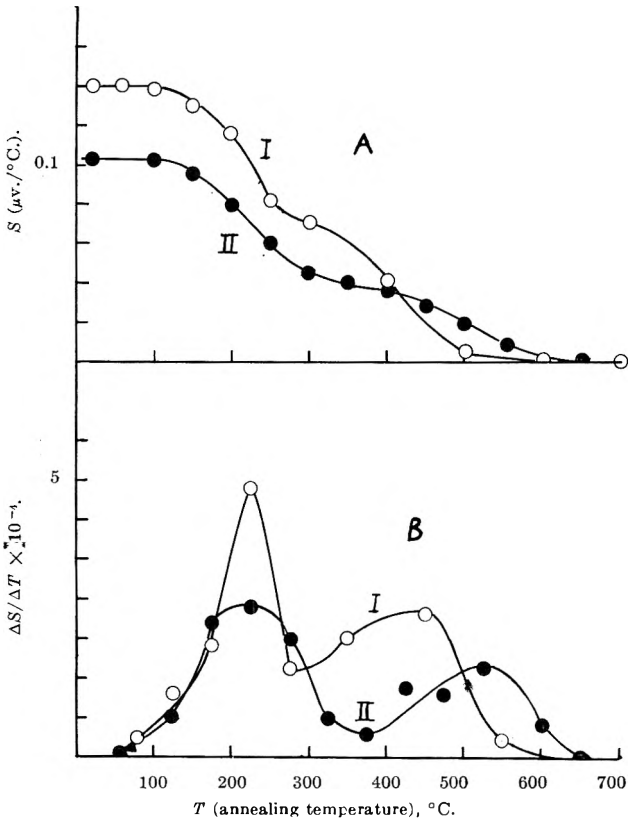

Fig. 1.—Recovery of thermoelectric force (S) of cold-worked platinum by annealing 30 min. at each temperature: (I) 88% compression; (II) 68% compression.

Several investigations[2-6] concerning the annealing of deformed, quenched, and irradiated platinum have been carried out by measuring changes in the physical properties. It was reported by Tammann and Bundel[2,3] that the changes in S and electrical resistivity occur only in the region from 200 and 300° and the decrease in hardness is found at above 600° for cold-worked platinum. Piercy reported[4] that the recovery stages after an extension in liquid nitrogen are observed in the three regions (0–100°, 200–400°, and 400–700°) by the measurements on electrical resistivity, hardness, and X-ray line width, and these stages are attributed to the disappearance of interstitial atoms, vacancies, and to the rearrangement and disappearance of dislocations produced by deformation, respectively.

Since the type of defects and the recovery ranges are markedly affected by the existence of impurities as well as by the nature and degree of working, it is desirable to employ the same specimens for the measurements of both catalytic activity and change in the physical property.[7,8]

The measurement of S was carried out by means of the method previously described.[1] As shown in Fig. 1, the changes in S by annealing for platinum 88 and 68% compressed occur in two distinct regions (150–300°, 350–500° and 150–300°, 450–600°). In Fig. 1(B), the peaks of $\Delta S/\Delta T$ curves are found at 225 and 530° for 68%, and 225 and 450° for 88% compressed specimens, respectively. The second stage is shifted to lower temperature with increase in the degree of compression, while the first stage is not affected by it, in agreement with the observation of Clarebrough and co-workers for cold-worked nickel.[9] On the assumption that the magnitude of S is proportional to the concentration of defects, the activation energy for the migration of lattice defects (Em) can be determined from the isothermal annealing experiments. Em is estimated to be 1.1 to ~1.2 e.v. in the region between 200 and 250°, which agrees well with the value obtained by Piercy at 200–400° (1.1–1.4 e.v.).[4] Making a comparison between the present results and other investigations,[2-6] the two stages are attributed to the disappearance of point defects, probably single or double vacancy (T_V), and to the rearrangement and disappearance of dislocations (T_D), respectively.

The decomposition rate of formic acid was followed between 150 and 250°, using Schwab's apparatus.[10] The catalytic activity of cold-worked platinum (88% compression) decreases suddenly in the two temperature ranges of annealing (200–300° and 400–500°), in a quite analogous manner to that of nickel catalysts for various reactions.[1] These temperature ranges coincide with the recovery temperature of S (T_V and T_D). A large part of activity (about 80%) is lost in the region from 200 to 300°. The activity for the hydrogenation of cinnamic acid (measured volumetrically with Warburg's apparatus at 30°) is lost in the region from 350 to 600°, which is in agreement with T_D. According to the results discussed in a previous paper,[1] the active centers in platinum catalysts may be mainly point defects and rarely the terminations of dislocations at the surface for the former reaction, and only the terminations of dislocations for the latter reaction. In severe deformed metals, the overlapping of T_V and T_D is unavoidable owing to the interaction among lattice defects when their concentration is high, as discussed by Uhara and co-workers.[7,8] Accordingly, the determination of structure of active centers by the annealing experiment is in principle possible only when slightly cold-worked metals are employed and for these purposes the measurement of S is a very effective means.

Acknowledgment.—The author wishes to express sincere thanks to professor I. Uhara for his kind guidance, encouragement, and valuable discussions during this work.

(2) G. Tammann and G. Bundel, *Ann. Physik*, **16**, 120 (1933).
(3) G. Tammann, *Z. Metallk.*, **24**, 220 (1932).
(4) G. R. Piercy, *Phil. Mag.*, **5**, 201 (1960).
(5) F. J. Bradshaw and S. Pearson, *ibid.*, **1**, 812 (1956); **2**, 379 (1957).
(6) G. L. Bacchella, E. Germagnoli, and S. Granata, *J. Appl. Phys.*, **30**, 748 (1957).
(7) I. Uhara, Y. Numata, H. Hamada, and Y. Kageyama, *J. Phys. Chem.*, **66**, 1374 (1962).
(8) I. Uhara, *et al.*, *ibid.*, **67**, 996 (1963).
(9) L. M. Clarebrough, M. E. Hargreaves, M. H. Loretto, and G. W. West, *Acta Metal.*, **8**, 797 (1960).
(10) G. M. Schwab and N. Theophilides, *J. Phys. Chem.*, **50**, 427 (1946).

DEPARTMENT OF CHEMISTRY,
FACULTY OF SCIENCE, S. KISHIMOTO
KOBE UNIVERSITY,
HIGASHINADA-KU, KOBE, JAPAN

RECEIVED FEBRUARY 25, 1963